Theses and Dissertations   Graduate School

2022

Antiviral effects of metalloshielding: Differential antiviral activity of polynuclear platinum and cobalt compounds

Mary Zoepfl

Antiviral effects of metalloshielding: Differential antiviral activity of polynuclear platinum and cobalt compounds

A dissertation submitted in partial fulfillment of the degree requirements for the requirement for the degree of

Doctor of Philosophy

at Virginia Commonwealth University

By

Mary Zoepfl

Bachelor of Science, University of Virginia, 2018

Directors: Dr. Nicholas P. Farrell and Dr. Michael A. McVoy

Professor, Department of Chemistry and Professor, Department of Pediatrics

Virginia Commonwealth University

Richmond, Virginia

April 2022

Table of Contents

List of Figures

List of Tables

Abbreviations

ACE2	Angiotensin-converting enzyme 2
Ad5	Human adenovirus serotype 5
AFM	Atomic Force microscopy
ANP	Acyclic nucleoside phosphonate
aPTT	Activated partial thromboplastin time
AT	Antithrombin
AZT	Azidothymidine
BSL	Bio Safety Level
CAR	Coxsackievirus and adenovirus receptor
CCC	Charged coordination complexes
CD	Circular dichroism spectroscopy
CDC	Center for Disease Control
NIH	National Institutes of Health
COSY	Correlation spectroscopy
COVID-19	Coronavirus viral diease 2019
CPE	Cytopathic effect
CS	Chondroitin sulfate
DDD	Dickerson-Drew Dodecamer
DENV	Dengue fever virus
DFT	Density Functional Theory
dp	Depolymerization
DPP4	Dipeptidyl peptidase four
DS	Dermatan sulfate
dsR/DNA	Double stranded R/DNA
ECM	extracellular matrix
EMCV	Encephalomyocarditis virus
ESI	Electrospray ionization
EtBr	Rthidium bromide
EUA	Emergency use authorization
EV68	enterovirus D68
EV71	enterovirus A71
FDA	US Food and Drug Administration
FGF	Fibroblast growth factor
FIGE	Field-inversion gel electrophoresis
FIV	Feline immunodeficiency virus
FPX	Fondaparinux
Fr	Fraction
FucCS	fucosylated chondroitin sulfate
GAG	Glycosaminoglycans (GAGs)
Gal	Galactose
gB	glycoprotein
GFP	Green fluorescent protein
gH/gL	glycoproteins H and L
GlcN	D-Glucosamine
gM/gN	glycoproteins M and N
GPCMV	Guinea pig CMV (GPCMV)

h	Hour
HA	Hemagglutinin
HBV	Hepatitis B virus
HCII	Heparin cofactor II
HCMV	Human cytomegalovirus
EBV	Epstein-Barr virus
HCoV	Human coronaviruses
HCV	Hepatitis C virus
HIV	Human immunodeficiency virus
HMG	High mobility group
hMPV	Human Metapneumovirus
HPSE	Heparanase
HPV	Human papillomavirus
HRV	Human rhinovirus
HS	Heparan sulfate
HSQC	Heteronuclear single quantum coherence
HSV	Herpes simplex virus
HVEM	Herpes virus entry mediator
IdoA	Iduronic acid
IE	Immediate early proteins
ITC	Isothermal titration calorimetry
IU	International Units
Kbp	Kilo base pairs
kDa	KiloDaltons
LC-MS	Liquid chromatography–mass spectrometry
MB	Methylene blue
MCMV	Mouse cytomegalovirus
MERS-CoV	Middle East respiratory syndrome coronavirus
MMR	Mismatch repair system
MS	Mass spectrometry
MSGs	Marine sulfated glycans
MW	Molecular weight
NA	neuraminidase
NER	nucleotide excision repair system
Neu	Neuraminic acid
NMR	nuclear magnetic resonance (NMR)
NNRTI	non-nucleoside reverse transcriptase inhibitors
NRTI	nucleoside reverse transcriptase inhibitors
PDGFRα	Platelet derived growth factor receptor alpha
PFU	Plaque forming units
PM	Polyoxometalates
PPC	Polynuclear platinum compound
PTD	Protein transduction domains
RBD	Receptor binding domain
RFP	Red fluorescent protein
RFU	Relative fluorescent units
RhCMV	Rhesus cytomegalovirus

RLU	Relative luminescent units
RSV	Respiratory syncytial virus
RuRed	Ruthenium red
SA	Sialic acid
SARS-CoV-1	Severe Acute Respiratory Syndrome coronavirus 1 (emerged 2003)
SARS-CoV-2	Severe Acute Respiratory Syndrome coronavirus 2 (emerged 2019)
SF	Sulfated fucans
SG	Sulfated galactans
SI	Selectivity index
SIV	Simmian immunodeficiency virus
SPR	Surface Plasmon Resonance
ssR/DNA	Single stranded R/DNA
STD	Saturation transfer difference
TEM	Transmission electron microscopy
TF	Tissue factor
TNBC	triple-negative breast cancer
UFH	Unfractionated heparin
VLP	Virus like particle
VOC	variants of concern
VSV	Vesicular stomatitis virus
vWF	von Willebrand factor
VZV	Varicellar zoster virus
WC	Werner's complex

Acknowledgements

Abstract

The majority of antiviral drug development has focused on virus-specific discovery targeting discrete steps in the individual life cycles. Although great strides have been made for a number of clinically relevant diseases such as human immunodeficiency virus, influenza virus, and hepatitis B, broad spectrum antivirals do not exist. Broad spectrum antivirals would offer (1) treatment for viruses without specifically-targeted antivirals, (2) treatment for viruses which have developed resistance to their available treatments, and (3) a rapidly deployable treatment option in viral epidemics. Many viruses including human cytomegalovirus (HCMV), HIV, and SARS-CoV-2. rely on heparan sulfate (HS), a highly sulfated glycosaminoglycan (GAG), to attach and infect cells. Inhibition of the HS-viral interaction therefore has the potential to be of broad-spectrum utility. Substitution-inert polynuclear platinum complexes (PPCs) are known to have both DNA and HS affinity; PPCs metalloshield, or mask, HS to impede a myriad of HS functions including cancer metastasis. In this work, we demonstrate that high-GAG affinity PPCs act as broad-spectrum antivirals by inhibiting virion attachment *via* HS. In extending this concept to charged coordination complexes (CCCs) in general, the Co-containing Werner's complex (WC), maintains DNA and HS affinity and displays antiviral activity. The mechanism of action is not as well-defined as the PPC family and may reflect a hitherto unappreciated relationship between structure, DNA and HS affinity, and biological activity. In summary, this work outlines an extension of glycobiology and medicinal inorganic chemistry in developing broad-spectrum antivirals.

CHAPTER 1: INTRODUCTION

1.1 Impact of viral disease

Broad spectrum antibiotics revolutionized modern medical care. In combatting viral infection, great strides have been made using a "one-bug-one-drug" strategy; effective specifically-targeted antivirals have been developed for a number of clinically relevant diseases such as human immunodeficiency virus (HIV), influenza virus, and hepatitis C virus (HCV) but overall, this strategy offers a small spectrum of coverage and a high cost of drug development.[1] The number and efficacy of broad spectrum antivirals (compounds which inhibit viruses from two or more families) is limited.[2] Antiviral resistance is a growing problem as seen in several clinically relevant viruses; drug resistance management must include drug delivery optimization, the selection of new antiviral therapies based on mechanisms of resistance, and new antiviral development.[3,4] Broad spectrum antivirals would offer (1) treatment for viruses without specifically-targeted antivirals and (2) treatment for viruses which have developed resistance to their specifically-targeted treatments. Additionally, broad spectrum antivirals would offer a rapidly deployable treatment option in viral epidemics. Viral outbreaks such as the 2003 SARS-CoV-1, 2009 H1N1 influenza, and 2013-2015 Ebola cost the global economy billions of US dollars.[5] Enterovirus D68 (EV68) and Dengue fever virus (DENV) have also seen severe outbreaks. As of April 1, 2022, the COVID-19 pandemic (caused by SARS-CoV-2) has infected over 484 million people and caused 6.1 million deaths worldwide. These outbreaks and pandemics emphasize the need for broad-spectrum antivirals.

1.2 Viral replication cycle

Viruses are distinct biological entities; they are infectious, obligate intracellular parasites. Their replication cycle follows six steps: adsorption or attachment, entry or penetration, uncoating, genome replication, protein synthesis, virion assembly, and release (Figure 1.1).

1. Adsorption
Interaction between host receptor molecule and virus ligand (determines host-specificity of the virus)

Lipid envelope
Capsid
Nucleic acid
Virus

6. Release
Complete virus particles are released by budding of host cell membrane (shown here) or disintegration of host cell

Host cell

2. Penetration
Receptor-mediated endocytosis or, in some enveloped viruses, membrane fusion (shown here)

5. Assembly
Assembly of virus components is mediated by host and/or viral enzymes

3. Uncoating
Nucleic acid is liberated from the phagosome (if endocytosed) and/or capsid by complex enzymatic and/or receptor-mediated processes

4. Synthesis
Nucleic acid and protein synthesis are mediated by host and/or viral enzymes. These take place in nucleus or cytoplasm, depending on the specific virus

Figure 1.1: Viral replication cycle. Virus replication relies on host cells and occurs in six steps: adsorption or attachment, penetration or entry, uncoating, genome and protein synthesis, virion assembly, and release of virions from the host cells. Reproduced from virology.ws.

Virion attachment is an interaction between a receptor on the cell surface and a viral glycoprotein or capsid protein. It is generally a non-specific interaction which brings a virion in proximity to its specific cellular receptor, attachment is detailed below. Viral penetration or entry generally depends on whether a virus is enveloped or not. Enveloped viruses enter cells via membrane fusion either with the plasma or an endosomal membrane. In the former, the viral envelope fuses with the cellular plasma membrane and the capsid is released into the cytoplasm. This process is mediated by viral fusion proteins, which have a ligand-triggered conformation change to drive membrane fusion.[6] In the latter, enveloped viruses enter the cell through endocytosis, in which virions attached to the cell surface are engulfed by the cell and the viral envelope fuses with the endosomal membrane. [7] Naked virus cell entry remains poorly understood; either the entire naked virion must cross the plasma membrane or it must undergo conformational changes in order to transfer its genome through the plasma membrane.[8] After entering the cell, the virion must be uncoated, *i.e.,* the capsid must be removed, before viral gene expression or genome replication may begin. Viral uncoating strategies are very diverse, multistep processes dependent on genome type and envelope presence/absence.[9]

Following viral attachment, penetration, and uncoating, the genetic material of the virus directs viral replication, or the production of viral proteins and genomes. Although viruses are classified in families, they are also grouped by genome type in a system devised by David Baltimore (Figure 1.2). Cellular genes are encoded in dsDNA, which are transcribed into mRNA, then further translated into peptides; thus, the flow of information is unidirectional from DNA to RNA to proteins. All viruses must use mRNA to produce proteins but no virus encodes all of the necessary machinery to do so; viruses rely on the translational machinery of the cell. mRNA is defined as a positive sense (+) strand because it is the template for protein synthesis. A strand of DNA of the equivalent sequence is also called the (+) strand. RNA and DNA strands that are complementary to the (+) strand are, of course, called negative (-) strands. Viruses may have double stranded (ds) DNA (**I**), (+) single stranded (ss) DNA (**II**), dsRNA (**III**), (+) RNA (**IV**), (-) ssRNA (**V**), (+) ssRNA (**VI**, or a retrovirus) or a combination of (-) and (+) ssRNA (Figure 1.2). Replication begins with the generation of mRNA through various routes, dependent on viral genome type. For example, HIV utilizes viral reverse transcriptase to transcribe its (+) ssRNA into (-) ssDNA, which is translated and replicated by cellular enzymes into dsDNA, and ultimately transcribed to mRNA. Despite the pathway, viral mRNA generation allows *de novo* viral protein and genome synthesis.[10]
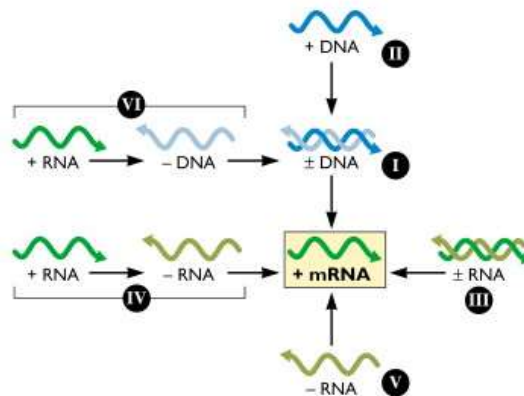
Figure 1.2: The Baltimore scheme. Reproduced from virology.ws.

Virion assembly follows the synthesis of all of the 'building blocks,' *i.e.* viral capsid proteins, accessory proteins, envelope proteins, and viral genomes. It is a genetically programmed, dynamic process which varies widely from virus to virus. However, there are three main strategies: (a) self-assembly, (2) scaffolding protein-assisted assembly, and (3) viral genome-assisted assembly. Regardless of method, capsid assembly is followed by virion release, which, like other parts of the viral replication cycle, varies by virus. There are two methods of virion release: lysis or budding. Cell lysis results in the death of the infected cell. However, enveloped viruses usually exit the cell by budding, by which they gain a viral phospholipid envelope.

1.3 Traditional antiviral targets and their limitations

Before the turn of the century, there were only ten FDA-approved antivirals. Since then, increased research and understanding of the viral replication cycle has led to a number of new antivirals.[11] Roughly 90 antivirals are currently licensed to treat nine viral infections. Twelve antiviral strategies are employed: 5-substituted 2'-deoxyuridines, nucleoside analogs, pyrophosphate analogs, nucleoside reverse transcriptase inhibitors (NRTIs), non-nucleoside reverse transcriptase inhibitors (NNRTIs), protease inhibitors, integrase inhibitors, entry inhibitors, acyclic guanosine analogs, acyclic nucleoside phosphonate analogs, HCV NS5A/NS5B polymerase inhibitors, and influenza virus inhibitors (Figure 1.3).

There are three approved 5-substituted 2'-deoxyuridine analogs: idoxuridine, trifluridine, and brivudine. Idoxuridine and trifluridine must be phosphorylated by cellular kinases to their active forms, which inhibit viral and cellular DNA synthesis, while brivudine is specifically phosphorylated by thymidine kinases of herpes simplex virus (HSV) 1 and VZV, and inhibits viral DNA polymerase.[12–14] While idoxuridine and trifluridine have high toxicity, brivudine has a more favorable safety profile.

Nucleoside analogs, including vidarabine, entecavir, and telbivudine, target viral DNA polymerase. Although vidarabine has high potency against HSV and VZV, it was discontinued because it is barely soluble and rapidly deaminated by adenosine deaminases.[15] Entecavir, approved to treat HBV infections, showed a low rate of resistance but also had modest activity against HIV, thus it has generally not been used to overcome HIV resistance mutations.[16,17] Telbivudine has better suppression of HBV DNA replication with less frequent resistance than lamivudine.[18–20] Due to their low barrier to resistance, telbivudine, lamivudine, and adefovir dipivoxil are not recommended.[21] Orally administered nucleoside analogs with good safety, easy use, and low drug resistance rates are preferred HBV treatments, but high cost limits their use; lamivudine remains first line therapy despite its high rate of resistance.[22]

Foscarnet (trisodium phosphonoformate) is the only approved pyrophosphate analog.[23] Unlike classic antivirals, foscarnet does not need to be phosphorylated before binding to viral DNA polymerase.[24] However, foscarnet is a broad-spectrum antiviral against DNA viruses (HSV-1, HSV-2, VZV, human cytomegalovirus (HCMV), Epstein-Barr virus (EBV), and HBV), but not RNA viruses, except retroviruses (HIV).[25] Yet, foscarnet is exclusively used to treat HCMV or HSV infections which have become resistant to nucleoside analogs; this is likely due to its high level of toxicity in the long term.[26]

Azidothymidine (AZT) was the first approved NRTI in 1985; it targets HIV reverse transcriptase and was later approved to treat HBV as well as HIV. NRTIs, also called 2'3'-dideoxynucleoside analogs, are phosphorylated to the 5'-TP then act as DNA chain terminators.[27,28] They cannot be administered as a monotherapy because of their low barrier to resistance.[29] However, they are regularly administered as a part of highly active antiretroviral therapy, designed to target multiple stages of the HIV replication cycle.[30,31] Most side effects, such as peripheral neuropathy or leukopenia, are reversible.[32]
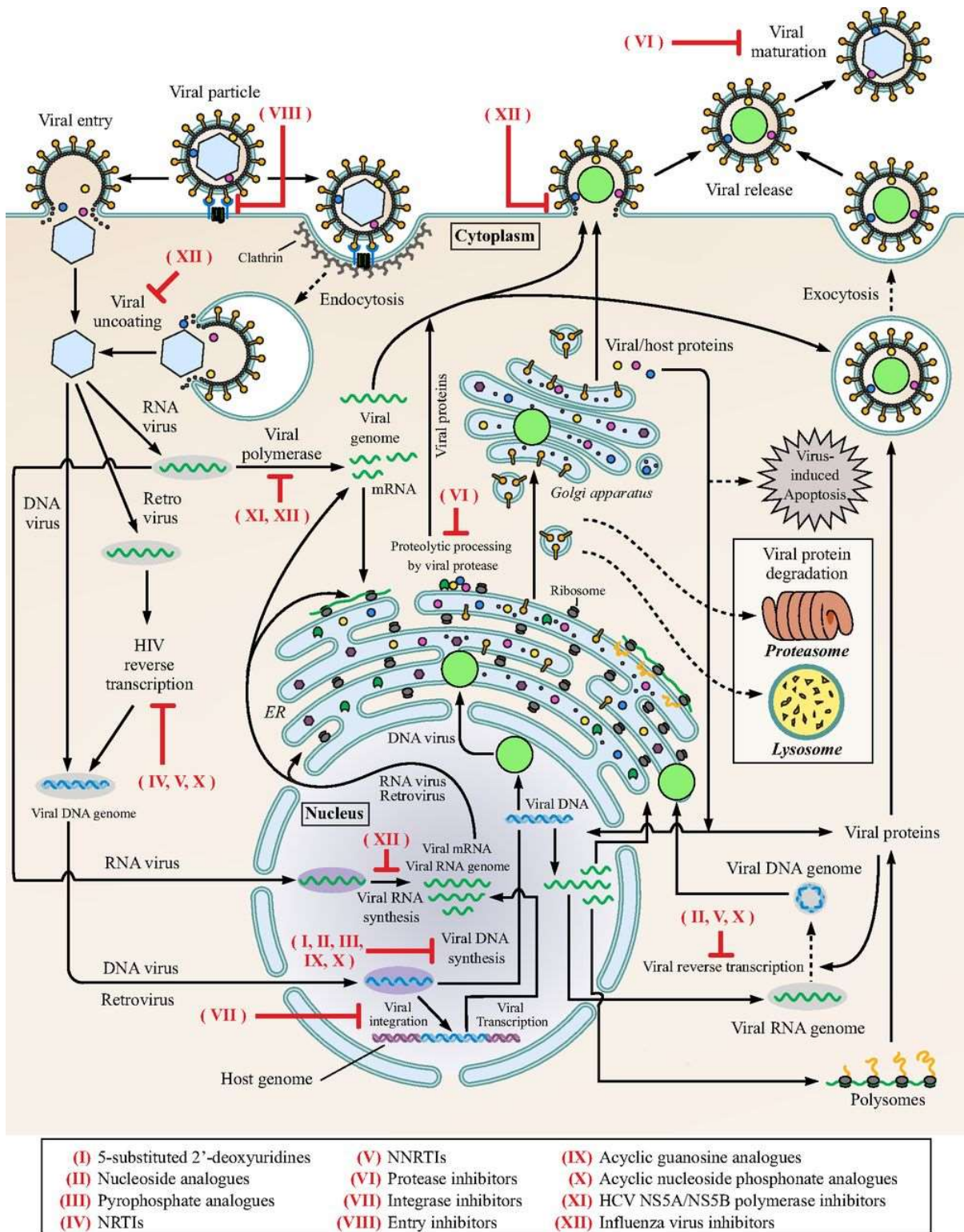
Figure 1.3: Mechanisms of drug actions during the viral life cycle, reproduced from de Clercq 2016.[21]

There are five approved NNRTIs: nevirapine, delavirdine, efavirenz, etravirine, and rilpivirine. Unlike NRTIs, NNRTIs do not need metabolic processing; they bind an allosteric site of HIV-1 RT and cause

a conformational change to impair the catalytic site.[33–36] NNRTIs only treat HIV-1 as structural differences in HIV-2 render it naturally resistant.[37] NNRTIs are common first line agents but resistance and toxicity (central nervous system toxicity and elevated liver enzymatic levels) still occur.[29,32]

Twelve HIV protease inhibitors and seven HCV NS3/4A protease inhibitors are approved.[21] Some viruses, like HIV and HCV, synthesize one large polyprotein from a single gene then cleave it into multiple functional proteins. By targeting a virus's protease and thus inhibiting this cleavage, the virus replication cycle is inhibited. Nine of the ten HIV protease inhibitors are peptidomimetics with an uncleavable hydroxyethylene bond in place of a natural peptide bond; the exception, tipranavir, is built on a coumarin scaffold.[38] Each HIV protease is a competitive inhibitor, they are widely used in HAART but do have side effects as well as resistance mutations.[29,39,40] While HIV has an aspartic protease and HCV has a serine protease, HCV protease inhibitors are similar to HIV protease inhibitors. All seven HCV protease inhibitors are used to treat HCV genotype 1, the most common genotype.[41] Although simeprevir has better response rates and drug interaction profiles than telaprevir and boceprevir, its expense remains a barrier.[21]

HIV integrase inserts viral DNA into the host cell genome in a multistep process; the essential and targeted step is the strand transfer reaction, which covalently links the viral DNA 3' end to the cellular DNA.[42] The Diketo acids target the catalytic site of HIV integrase and inhibit this transfer; they led to the development of raltegravir. Other integrase inhibitors, elviregravir and dolutegravir, are based on 4-quinolone-3-carboxylic acids.[43] Integrase inhibitors are superior to NRTIs, NNRTIs, and protease inhibitors as first line therapies despite the resistance to all three integrase inhibitors.[29,44]

The seven approved entry inhibitors share very little in common structurally. Enfuvirtide is a polypeptide inhibitor of HIV-1, homologous to the heptad repeat region of HIV-1 GP41.[45] However, enfuvirtide has largely become obsolete due to its high cost, subcutaneous administration, and the large number of orally bioavailable HIV drugs.[21] Maraviroc is a chemokine receptor antagonist, targeting CCR5 on the surface of CD4 cells and macrophages.[46] R5-viruses primarily use CCR5 for viral entry while R4-viruses use CXCR4 in later stages of disease progression;[47] as a result, maraviroc is a valuable treatment option for R5-viruses but not R4-viruses.[21,48] Respiratory syncytial virus (RSV) immune globulin-intravenous (RSV-IGIV) is sterile human immunoglobulin isolated from adult plasma with high titer of neutralising antibodies to RSV.[49] Although effective in decreasing the number of hospitalizations and length of hospital stays, the high cost and strict guidelines severely limit RSV-IGIV's use.[21] Palivizumab is a humanized mouse immunoglobulin monoclonal antibody which inhibits the A antigenic site of RSV fusion protein.[50] Palivizumab prophylaxis is effective in infants but the high cost inhibits regular use. VZV immunoglobulin (VZIG) was extracted from the blood of patients with VZV infections; it decreases the risk of complications and clinical illness in immunocompromised patients but was discontinued when VariZIG was approved by the US Food and Drug Administration (FDA) in 2012. VariZIG is detergent-treated, sterile, lyophilized immunoglobulin isolated from human plasma. It offers a postexposure prophylactic option for immunocompromised patients or those unable to be vaccinated for VZV.[21] Finally, docosanol is a 22-carbon, saturated, primary alcohol which inhibits lipid enveloped viruses, including HSV, RSV, HCMV, and VZV *in vitro*.[51] Although its mechanism of action is still debated, it is used clinically as a topical cream to reduce the healing time and duration of symptoms for HSV-1 or HSV-2 infection.[52]

Six approved acyclic guanosine analogs target viral DNA polymerase: acyclovir, ganciclovir, and penciclovir, and their prodrug counterparts valganciclovir, valacyclovir, and famciclovir. Acyclovir, ganciclovir, and penciclovir are phosphorylated first by viral kinases (monophosphorylation), then by host

kinases (di and triphosphorylation), and then compete with natural dGTP. This sequence provides a major component of specificity and safety as the active triphorphorylated forms are not efficiently produced in uninfected cells where viral kinases are absent.[53–55] Acyclovir is the standard of care of HSV infections and famciclovir is widely used for HSV and VZV; resistance mutations are still a concern for all acyclic guanosine analogs.[21]

The ten approved acyclic nucleoside phosphonate (ANP) analogs target viral DNA polymerase and are based on hybridization of (S)-DHPA and phosphonacetic acid, resulting in (S)-HPMPA. (S)-DHPA is the first reported broad-spectrum antiviral and is considered a prototype for ANP analogs.[56–59] ANP analogs inhibit DNA synthesis by terminating the DNA chain due to their phosphonate linkage in place of the natural phosphate linkage. Although ANP analogs require phosphorylation to diphosphates by cellular enzymes, limiting their specificity, they are specifically taken up by lymphocytes, reducing their dose 10-fold and significantly reducing toxicity.[60,61]

Direct acting antivirals for HCV fall into four categories: (1) NS3/4A protease inhibitors, (2) NS5A protein inhibitors, (3) NS5B polymerase inhibitors (either nucleoside or nucleotide), and (4) non-nucleoside NS5B polymerase inhibitors. The four approved HCV NS5A inhibitors bind specifically to the HCV nonstructural protein NS5A, though the exact mechanism of action is unknown.[62–64] Two non-nucleoside NS5B inhibitors function by targeting the allosteric sites of NS5B polymerase.[65,66] Nucleoside NS5B inhibitors use is largely discontinued due to toxicity.

Influenza inhibitors fall into three categories: matrix 2 (M2) inhibitors, neuraminidase (NA) inhibitors, and polymerase inhibitors. Amantadine and rimantadine block H^+ ion transport through M2 proton channels, inhibiting viral uncoating in endosomes.[67,68] Due to widespread resistance, amantadine was abandoned.[69] Four NA inhibitors prevent viral release from the cell.[70] Ribavirin is a nucleoside analog with broad-spectrum antiviral activity against RNA viruses (HCV, RSV, and influenza); it inhibits IMP dehydrodenase, impeding de novo synthesis of GTP.[71,72] Favipiravir is converted intracellularly to its active triphosphate form; it is a broad-spectrum antiviral against RNA viruses.[73–76]

Letermovir, the only antiviral targeting viral DNA packaging, is a 3,4-dihydro-quinazoline-4-yl-acetic acid derivative.[77] It is only active against HCMV; Letermovir does not inhibit other human herpesviruses or even rhesus, mouse, or guinea pig CMV (RhCMV, MCMV, or GPCMV). It was approved in 2018 for treatment of HCMV but resistance mutations have since been reported.[78]

Due to virus genetic diversity and their reliance on cell machinery, there are few antiviral targets specific to viruses that will not interfere with normal cell function. The vast majority of antiviral targets are viral proteins and only work intercellularly (Figure 1.3).[79] Currently, approved antivirals only treat nine viruses, and unfortunately, targeting very few antiviral proteins has resulted in significant antiviral resistance.[3,4] There is an urgent need for new antivirals and new targeting strategies.

1.4 Viral attachment and entry

Many pathogens, including bacteria, viruses, and parasites, rely on glycosaminoglycans (GAGs) in some way. GAGs are linear, negatively charged polysaccharides with repeating disaccharide units of uronic acid (D-glucuronic acid or L-iduronic acid) and amino sugar (D-glucosamine) residues. Unlike other biopolymers (*i.e.*, DNA, proteins), GAGs are not directly encoded by the genome. The sulfation of each monosaccharide, type of monosaccharides in the disaccharide unit, and the geometry of the glycosidic bond within and between disaccharides units differentiate GAGs.[80] GAGs' structural variety leads to a

large diversity of biological roles. Hyaluronic acid, a non-sulfated GAG, has roles in wound healing, cancer progression, and lubricating joints.[80] The sulfation patterns of keratan sulfate determine molecular recognition and cell behavior in essential organs such as the cornea of the eye and central and peripheral nervous system.[81] More broadly, GAGs play essential roles in cell adhesion, growth, differentiation, and signaling, and are implicated in a variety of diseases.

GAGs are ubiquitous across tissue type and are particularly abundant in the extracellular matrix (ECM). Although the human body offers an impressive array of mechanical and physical barriers, once a pathogen has access to the ECM, GAGs, and in particular heparan sulfate (HS) and sialic acid (SA), offer an easy way to attach to cells. The large surface area of the lungs provides ample space area for pathogens like the gram-negative bacterium *Pseudomonas aeruginosa* to attach to cells through HS.[82] Enteric viral and bacterial pathogens can survive the low pH of the stomach and utilize GAGs in the gastrointestinal tract to enter cells. The surface layer of skin does not allow for pathogenic attachment and infection, but if that initial layer is breached, the subcutaneous layer of skin is covered in GAGs which allow viral (HSV), bacterial (*S. aureus*), and parasitic (*Leishmania*) microorganisms to attach, enter, and infect cells.[82] Many of these pathogens, in particular viruses, use HS for attachment (Table 1.1). Though these interactions are not well characterized, the HS-pathogen interaction is believed to mediate initial binding/attachment in a charge dependent manner.[83] Some studies suggest that the viral attachment is dependent on the pattern and level of sulfation as well as the length of HS.[84–86] Once a virus is attached to HS and in proximity to the cell surface, it can initiate entry with its own glycoproteins. The two processes are distinct: (i) attachment is mediated through the generally non-specific, charge-dependent interaction with HS and (ii) entry is often a pathogen-specific protein-mediated event (Figure 1.4A).

Virus Family	Virus	GAG	Genome	Envelope
Adenoviridae	Adenovirus type 2 and 5	HS	dsDNA	No
	Adenovirus type 37	SA		
Bunyaviridae	Rift Valley fever virus	HS	(-) ssRNA	Yes
Caliciviridae	Norovirus genogroup (G) II	HS	(+) ssRNA	No
	Norovirus GII.3 and GII.4	SA		
Coronaviridae	Human CoV-NL63	HS	(+) ssRNA	Yes
	Human CoV-229E	HS		
	SARS-CoV-1	HS		
Flaviviridae	HCV[87]	HS	(+) ssRNA	Yes
	DENV	HS		
Filoviridae	Ebola virus	HS	(-) ssRNA	Yes
Hepadnaviridae	HBV (and delta virus)	HS	ds/ssDNA	Yes
Hepeviridae	Hepatitis E virus	HS	(+) ssRNA	No
Herpesviridae	HSV 1	HS	dsDNA	Yes
	HSV 2	HS		
	HCMV	HS		
	VZV	HS		
	Human herpesvirus 8	HS		
Orthomyxoviridae	Influenza A virus	SA	(-) ssRNA	No
	Influenza B virus	SA		
	Influenza C virus	SA		
Papillomaviridae	Human papillomavirus types 16 and 33	HS	dsDNA	Yes
Paramyxoviridae	RSV	HS	(-) ssRNA	Yes
	Hendra virus	HS		
	Nipah virus	HS		
	Parainfluenza	HS		
	Sendai virus	SA		
Picornaviridae	Coxsackievirus A24	SA	(+) ssRNA	No
	Enterovirus 70	SA		
Polyomaviridae	JC polyomavirus	SA	dsDNA	No
	BK virus	SA		
	Merkel cell virus	SA/HS		
Poxviridae	Vaccinia virus	HS	dsDNA	Yes
Reoviridae	Reovirus type 3	SA	dsRNA	No
Retroviridae	HIV	HS	(-) ssRNA	Yes
Togaviridae	Sindbis virus	HS	(+) ssRNA	Yes

Table 1.1: GAG dependence of viruses. Recreated in part from Cagno et al 2019.[83]
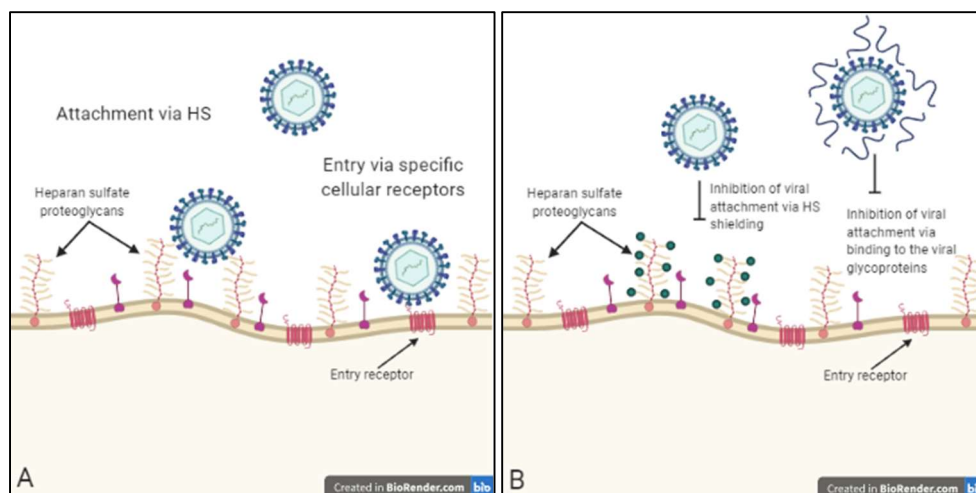
Figure 1.4: Viral attachment and entry and their inhibition. (A) Viral attachment and entry are two distinct events. Attachment relies on non-specific interactions between the virion and HS while viral entry is the result of viral glycoproteins interacting with specific cellular receptors. (B) Viral attachment can be inhibited by either compounds that interact with HS, acting to shield the cell from the virus, or compounds that interact with viral glycoproteins, sequestering the virus from the cell. Created with BioRender.com

There are two strategies to inhibit the HS-viral interaction. The first method targets the viral attachment glycoprotein, essentially acting as neutralizing antibodies (Figure 1.4B).[88] The second method targets cellular HS, shielding the cell from viral attachment. Unlike most previous antiviral targets, HS is (1) a host target and (2) an extracellular structure. Inhibitors with viral targets are likely to develop resistance through the mutational modification of those viral targets. Inhibitors of host targets, like HS, are thus less likely to be susceptible to development resistance. Additionally, as an extracellular structure, HS-targeting further reduces the possibility of mutational change by the virus, as replication within the cell cannot occur. A review of the various approved and experimental inhibitors of the viral-HS interaction follows.

1.4.1 GAG mimetics

Heparin, a structural analog of HS, interacts with the viral particle through its glycoproteins, sequestering the virion, and competitively inhibiting viral attachment.[83] It has broad-spectrum antiviral activity, inhibiting HSV, HCMV, DENV, HIV, human papillomavirus (HPV), RSV, Ebola, human metapneumovirus (hMPV), and many others.[83] Although it is an effective attachment inhibitor, heparin is not an approved antiviral due to its potent anticoagulant activity. Heparin modifications and heparin mimetics have aimed to improve antiviral activity while minimizing anticoagulation activity.

In 1958, Gerber et al. demonstrated anti-mumps and anti-influenza B virus activity of polysaccharides from marine algae and thus introduced marine algae as a source of potential antiviral compounds.[89] In 1988, Baba et al. expanded the potential of sulfated polysaccharides, demonstrating their antiviral activity against enveloped HSV, HCMV, vesicular stomatitis virus (VSV), Sindbis virus, and HIV, but not naked adenovirus, coxsackievirus, poliovirus, and reovirus.[90] These are particularly attractive as drugs as algal polysaccharides are readily available in nature, nontoxic, cheap, and biocompatible.[91]

Carrageenans are anionic sulfated polysaccharides with broad-spectrum antiviral activity; they serve a similar function similar to that of cellulose in plants.[92] Carrageenans are classified into three

groups, λ-, κ-, and ι-carrageenan, based on the existence and location of 3,6-anhydrogalactopyranose and sulfate groups.[93] Carrageenans have demonstrated antiviral activity against HPV,[94] including strains which lead to cervical cancer,[95,96] HSV-1 and HSV-2,[97–101] human rhinovirus (HRV),[102] DENV,[103,104] influenza,[105] and HIV (in a cell free model).[106] In each case, carrageenans inhibit an early stage of viral replication: either viral attachment or virion internalization. While every study identified a target, Yamada et al. noted that antiviral activities of carrageenans correlate with their molecular weight and sulfation, suggesting the importance of both size and charge.[106] Carraguard, a seaweed-derived vaginal gel microbicide, was a very promising inhibitor of HPV and HIV in pre-clinical trials; although it was safe to use, it was ineffective in inhibiting the spread of HIV from males to females in phase III clinical trials.[107–109]

Galactans serve as the main extracellular polysaccharides of red algae; they consist of linear chains of galactoses: a chain of alternating 3-β-D-galactopyranose (G units) and 4-α-D-galactopyranose residues or 4-3,6-anhydrogalactopyranose residues complete their structural backbone with presence of D-series (D unit) in carrageenans and L-series (L unit) in agarans.[110,111] Galactans from various red algae have displayed antiviral activity against HSV-1 and HSV-2,[112,113] DENV,[112] HIV-1 and HIV-2,[114] and hepatitis A virus. Across the board, galactans were not cytotoxic and consistently inhibited viral attachment and/or entry.

Alginates are principal constituents in brown algae cell walls. They are linear anionic polysaccharides, with a backbone of poly-D-glucuronic acid (G blocks) and poly-D-mannuronic acid (M blocks), together with D-guluronic acid and D-mannuronic acid (GM blocks).[115,116] A stand out of this group is a polysaccharide named 911, which has anti-HIV activity in both acute and chronic infection models *in vitro* and *in vivo*. Interestingly, 911 has two mechanisms of action: inhibition of HIV's reverse transcriptase and inhibiting viral attachment. 911 also inhibits hepatitis B virus (HBV) via inhibition of viral DNA polymerase. The sulfated formes of alginate, sulfated polymannuroguluronate (SPMG), has anti-HIV activity via inhibition of viral attachment, preventing the interaction of gp120 and CD4 molecules.[116] Interestingly, there was a correlation between the size of SPMG oligosaccharides and antiviral activity, with the minimal fragment being an octasaccharide.[117,118]

Fucans are high molecular weight sulfated polysaccharides found in the intercellular tissues or mucilaginous matrix of brown algae. Fucan structure varies between algal species but each has a central fucose backbone, mainly bound by glycosidic linkages, forming branching points at every 2-3 fucose residues within the chain.[119] A sulfated fucan from Cladosiphon okamuranus inhibited DENV-2 infection but did not completely inhibit three other serotypes of DENV (DENV-1, DENV-3, and DENV-4). An arginine in the attachment glycoprotein of DENV-2 forms an important interaction with the fucan, suggesting that the sulfation content of the fucan is important for its antiviral activity.[110] Other sulfated fucans from *Dictyota mertensii, Lobophora variegata, Fucus vesiculosus,* and *Spatoglossum schroederi* inhibit HIV infection by inhibiting both attachment and reverse transcriptase. Queiroz et al. noted that sulfate and carboxyl groups were essential for antiviral activity.[120] Other fucans have demonstrated antiviral activity against influenza, HSV-1 and HSV-2 via viral attachment.[121] Fucoidans are a subclass of fucans. Their main skeleton consists of a-1,3-linked sulfated L-fucose, a repeating sequence of alternating a-(1-3)- with the possible a-(1-4)-glycosidic bonds. Fucoidans from *Adenocytis utricularis,*[122] *Undaria pinnatifida* (Mekabu),[123] *Stoechospermum marginatum,*[124] *Undaria pinnatifida,*[125,126] and *Cystoseira indica*[121] have anti-HSV-1 and HSV-2 activity without cytotoxicity. Fucoidans have demonstrated antiviral activity against

HIV, HSV1-2, DENV, and HCMV[127,128] as well as anti-Newcastle disease virus at the initial stages of infection.[129] Consistent with some of the glycans above, an iso fucoidan from *F. vesiculosus* has anti-HIV activity by inhibiting both reverse transcriptase and viral attachment.[119,130]

Other smaller classes of marine glycans have also shown promise as antivirals. Laminaran, linear glycans found in brown algae, is made of β-(1,3)-linked glucose in the central chain, with β-(1,6)-linked side-chain branching.[93,131] Isolated Laminaran inhibits HIV by inhibiting viral attachment and reverse transcriptase.[132] Naviculan is a high molecular weight, sulfated glycan from *Navicula directa*, consisting of galactose, xylose, rhamnose, fucose, and mannose. It has antiviral activity against HSV-1, HSV-2, and HIV by inhibiting viral attachment or fusion.[133] A highly sulfated exopolysaccharide, p-KG03, from *Gyrodinium impudicum* strain KG03 (highly sulfated homopolysaccharide of galactose conjugated with uronic acid and sulfate groups) has incomplete broad spectrum antiviral activity against encephalomyocarditis virus (EMCV) and influenza A (but not influenza B) likely by inhibiting viral attachment or entry.[134,135] Sulfated glycans, A1 and A2, from *Cochlodinium polykrikoides*, are composed of glucose, galactose, mannose, and uronic acid. They inhibit HIV-1, influenza A and B, and RSV A and B; additionally, A1 inhbits HSV-1 and A2 inhibits parainfluenza virus type 2. Importantly, A1 and A2 generate only a weak inhibition of blood coagulation.[136] Calcium Spirulan is isolated from blue-green alga, *Arthrospira platensis*, and is composed of mannose, ribose, fructose, glucose, xylose, galactose, rhamnose, galacturonic acid, glucuronic acid, calcium, and sulfate. It inhibits the virion entry of HSV-1, HCMV, Coxsackie virus, measles, HIV-1, polio, and mumps virus.[137] Like A1 and A2, calcium spirulan exhibits only small anticoagulant activity. Nostoflan, from blue-green alga *Nostoc flagelliforme*, is composed primarily of (4)-β-D-Glcp-()-D-Xylp-(1 and 4)-[β-D-GlcAp-()-]-β-D-Glcp-()-D-Galp-(1). Nostoflan inhibits viral attachment of HSV-1 and HSV-2, and HCMV.[138]

Other GAG or GAG mimetics have been isolated from bacteria. Sulfated derivatives of the K5 capsular polysaccharide from *Escherichia coli* have also shown broad spectrum activity against both enveloped and naked viruses.[139–142] Importantly, these sulfated K5 derivatives lack the toxicity and anticoagulant activity of heparin, which precludes heparin from being a useful antiviral.[143]

GAG mimetic	Viruses inhibited	Reference(s)
Heparin	HSV, HCMV, DENV, HIV, HPV, RSV, Ebola, hMPV, and many others	[83]
polysaccharides obtained from marine algae, *Gclidium cartilagenium* and *Chondrus crispus*	Mumps and influenza B virus	[89]
Sulfated polysaccharides (dextran sulfate, pentosan polysulfate, fucoidan, and carrageenans)	HSV, HCMV, VSV, Sindbis virus, and HIV	[90]
Carrageenans	HPV, HSV-1, HSV-2, HRV, DENV, influenza virus, and HIV	[94,95,104–106,96–103]
Carraguard (seaweed-derived vaginal gel microbicide)	HPV, HIV	[107–109]
Galactans	HSV-1, HSV-2, DENV, HIV-1, HIV-2 and hepatitis A virus	[112–114]
Alginate 911	HIV, HBV	[116]

Fucans	DENV-2, HIV, HSV-1 and HSV-2	[110,120,121]
Fucoidans	HSV-1, HSV-2, HIV, DENV, CMV, Newcastle disease virus	[119,121–130]
Laminaran	HIV	[132]
Naviculan	HSV-1, HSV-2, and HIV	[133]
p-KG03	EMCV, influenza A	[134,135]
Sulfated glycans, A1 and A2, from Cochlodinium polykrikoides	HIV-1, incluenza A and B, RSV A and B, HSV-1, parainfluenza virus type 2	[136]
Calcium Spirulan	HSV-1, HCMV, Coxsackie virus, measles, HIV-1, polio, and mumps virus	[137]
Nostoflan	HSV-1 and HSV-2, and HCMV virus	[138]
Sulfated derivatives of the K5 capsular polysaccharide from *Escherichia coli*	HCMV, DENV, HIV-1, HPV, HSV-1, HSV-2	[139–142]

Table 1.2: Summary of the antiviral activity of GAG mimetics.

With high, variable molecular weights and structural variability, anionic GAG mimetics are poor candidates for therapeutic applications. Although phase I and phase II clinical trials showed several compounds were safe and well tolerated, none of the anionic GAG mimetics were successful in inhibiting viral infection in phase III trials, most likely due to ineffective concentrations in blood and tissue and/or inactivating cleavage by heparanase.[144] Additionally, many GAG mimetics have anticoagulant properties, like heparin, and thus can cause excessive bleeding and thrombocytopenia and require constant patient monitoring and an antidote (proteamine), which makes them poor candidates as antiviral therapies.

1.4.2 Peptide inhibitors

Despite their discovery through a wide variety of methods, the majority of the following antiviral peptides are hydrophobic, amphipathic and have a propensity to bind lipid membranes. This similarity results in a shared mechanism of action – inhibition of viral entry and/or attachment.

A number of peptide inhibitors are fragments of viral entry glycoproteins. CS3 was derived from the "fusion initiation region" of glycoprotein 41 (gp41) and inhibits HIV entry into cells.[145–147] CS3 initiated the development of other gp41-derived peptide inhibitors including enfuvirtide, a 36-residue peptide derived from the C-terminal end of the loop/C-helix heptad repeat (CHR) domain and a portion of the proximal ectodomain region.[148,149] In 2003, the FDA and EMA licensed as an antiviral peptide for HIV, unique in that its mechanism of action did not target reverse transcriptase or HIV protease but HIV entry, though its molecular mechanism is not clear.[148–153] However, it appears that enfuvirtide binds to multiple regions of gp120/gp41 and blocks entry between lipid mixing and opening of the fusion pore.[154] A variant of enfuvirtide, DP178, binds to synthetic membranes and inhibits fusion port formation.[154] A peptide, CP32M, which partially overlaps enfuvirtide, was engineered to be a more ideal amphipathic helix to improve its pharmacological properties.[155] It was a potent inhibitor of many strains of HIV, including those resistant to enfuvirtide.[155,156]

Given the success of enfuvirtide, a similar structure-based approach was used to identify entry inhibitors against other enveloped viruses. Nicol et al. studied a 12-residue peptide, FluPep, for its anti-inflammatory properties, but it also had antiviral activity.[157] FluPep is very hydrophobic, similar to EB; to

increases its solubility it was given the same four N-terminal basic residues (RRKK) as EB, yielding FluPep4. FluPep4 inhibited influenza viruses though direct interaction with the virus.[157]

Graham et al. identified a peptide sequence from RhoA (a small intracellular GTPase), responsible for its interaction with the fusion protein of RSV; this peptide inhibits RSV and HIV *in vitro* due to the interaction with the virus which inhibits cellular binding and entry.[158,159]

Bai at al. identified three peptides which strongly bind to the fusion protein of West Nile virus but only one, P1, inhibited viral infection in vitro. P1 was further engineered to increase activity; the most hydrophobic of the variants, P9, was the most potent inhibitor of West Nile virus. Oddly, when tested against DENV, P1 was more potent than P9, suggesting that the antiviral activity these peprides is highly dependent on the peptide sequence.[160] Interestingly P9 inhibited West Nile virus in a mouse model, was able to cross the blood brain barrier, and increased survival.[160]

Reil et al. hypothesized that inhibition of HIV in patients co-infected with GB virus C (related to hepatitis C) is due to interaction between the glycoprotein E2 of GB virus C and the fusion protein, gp41, of HIV.[161,162] Two peptides derived from E2 inhibited HIV entry *in vitro*; both were aromatic-rich and amphipathic. The peptide's interaction with gp41 alters its conformation and prevents the conformation needed for fusion.

In an effort to develop broad-spectrum antivirals, peptides derived from one virus were screened against multiple. Rapaport et al. developed peptide inhibitors to Sendai virus, Lambert et al. developed peptide inhibitors to RSV, parainfluenza virus, and measles virus, while Lamb et al. developed peptide inhibitors to T-lymphocyte leukemia virus and bovine leukemia virus.[163–165] Melnik et al. derived four peptide inhibitors from the HCMV entry glycoprotein gB, and each demonstrated broad-spectrum within the same family and in other viral families, namely HSV, measles virus, and VSV.[166]

Unfortunately, incomplete broad-spectrum activity is not uncommon in these peptide inhibitors. However, there are successes. Hrobowski et al. identified amphipathic peptides DN59 from DENV and WN83 from West Nile virus; each were derived from viral entry proteins, were effective inhibitors at micromolar concentrations, and inhibited viral entry.[167,168] Interestingly, DN59 and WN83 showed partial cross-reactivity; DN59 was active against DENV and West Nile virus but WN83 was only active against West Nile virus.[169,170]

Similarly, Sainz at al. identified three aromatic-rich peptides derived from the spike protein of SARS-CoV-1, similar to DN59;[171] each of the three peptides inhibited SARS-CoV-1 infection and were hypothesized to inhibit the conformation change of the spike protein required for fusion. Sainz et al. also identified a peptide derived from an analogous portion of the murine hepatitis virus (MHV); although it inhibited both MHV and SARS-CoV-1, the SARS-CoV-1-derived peptide only inhibited SARS-CoV-1, not MHV.[171]

Incomplete broad-spectrum inhibition was also seen for several peptides derived from the Gn fusion protein of Rift Valley Fever virus.[172] The most active peptide, RVFV-6, binds directly to cells and virus and is hypothesized to inhibit the fusion step of viral entry; it is active against Ebola virus and VSV but not the equine encephalitis viruses tested.[172]

Cheng et al. screened 18-residue peptides from the polyprotein of hepatitis C virus; eleven peptides had antiviral activity.[173] C5A, the most potent of the series, forms an amphipathic helix with

strong membrane-binding activity; it interacts directly with hepatitis C viral envelope and is virolytic. C5A was also shown to inhibit HIV due to direct disruption of the viral envelope, and more interestingly, was able to inhibit an established HIV infection.[174] However, C5A was not perfectly broad-spectrum – it did not inhibit VSV or adenovirus; but unlike other compounds which disrupt membranes, C5A does not disrupt mammalian membranes and is non-toxic. C5A's mechanism of action is very similar to DN59, the peptide developed from a DENV protein. Sequence variants did not greatly influence its anti-HCV or anti-HIV activities, suggesting that entry inhibition is not sequence-specific but rather relies on the hydrophobicity or amphipathicity of the peptide.[174]

Of the above peptides, the vast majority are amphipathic and derived from a specific glycoprotein. As a result, they all have similar mechanisms of action: either inhibiting viral attachment, viral entry, or membrane fusion. There are two major weaknesses to using peptides to inhibit viral infection. First, since these peptides are derived from one viral glycoprotein, many fail to be broad-spectrum inhibitors both within a viral family and across viral families. Second, as peptides, all of these inhibitors are subject to inactivating cleavage by proteases.

1.4.3 Inorganic polymers

Like GAG mimetics, inorganic polymers carry a large negative charge and thus were postulated to have similar mechanisms of action (*i.e.*, binding to viral capsids or glycoproteins and sequestering the virion). The simplest inorganic polymers, polyphosphates, are linear polymers of orthophosphate (Pi), occurring naturally in a number of organisms in varying length and amounts. For instance, in *Neisseria meningitidis* and *Neisseria gonorrhoeae* polyphosphates serve as a protective coating on the exterior of the cell.[175,176] Lorenz et al. performed a number of studies to show that polyphosphate chains of four or more phosphates were effective HIV-1 inhibitors and were nontoxic in the concentrations tested.[177] Along with inhibiting syncytium formation, polyphosphates inhibited cell-virus binding but not through the gp120 protein or CD4 receptor, suggesting an inhibition of the HS-viral interaction.

Polyoxometalates (PMs) are discrete metal-oxide cluster anions with a number of similarities to GAG mimetics (high water solubility, a wide variety of structures and size, and highly negative charge).[178] Unlike GAG mimetics, PMs structural variety stems from conformational changes, which depend on their environment, and allow PMs to be exploited as potential therapeutics. Their antiviral activity was first described in 1973 with RNA and DNA viruses *in vivo* as well as the retroviruses Friend leukemia virus and Moloney murine sarcoma virus *in vitro*.[178–180] Jasmin et al. determined that HPA-23 and other PMs inhibited RNA-dependent DNA polymerases of retroviruses; HPA-23 was tested *in vivo* against HIV but was too toxic to be effective in clinical trials.[179,180] However, a number of antiviral PMs have been identified with a different mechanism of action, namely inhibiting viral attachment and/or entry.
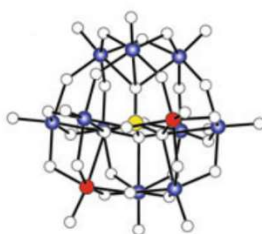
Figure 1.5: Structure of PM-19 as an examples of polyoxometalate structures.

Anionic polyoxotungstate ($K_7[PTi_2W_{10}O_{40}]\cdot6H_2O$; PM-19) is a stand-out of this class (Figure 1.5). *In vitro* assays demonstrated that PM-19 is a potent broad-spectrum inhibitor of herpes viruses including HSV (types 1 and 2, and thymidine kinase-deficient mutants), HCMV, HIV-1, and HIV-2.[181–183] PM-19 outperformed acyclovir (nucleoside analog) but its maximal effect was observed if cells were pretreated rather than when cells were treated after infection; it inhibited viral entry and viral spread without direct interaction with HSV virions.[181,184,185] With this evidence, Dan et al. suggested that PM-19 inhibited viral entry of HSV into cells by disrupting the interaction between HSV envelope glycoprotein D (gD) and its cellular receptor, herpes virus entry mediator (HVEM).[186] As PM-19 inhibits HSV through binding HVEM, it was predicted that PM-19 and other PMs would inhibit viral attachment of enveloped RNA and DNA viruses as well as inhibit the functionality of sialic acid residues of cellular proteins.[186] *In vivo* studies of HSV-1 and HSV-2 revealed that virion attachment inhibition is not PM-19's only mechanism of action; PM-19 also activates macrophages, which engulf virions and increase the immune response.[187,188]

V/W-mixed PMs (PM-43, PM-47, PM-1001, and PM-1002) and Ti/W-mixed PMs (PM-518, PM-520, and PM-523) have broad spectrum antiviral activity against RNA viruses.[189] Titanium substituted PMs were less cytotoxic than their vanadium substituted counterparts, but all were more inhibitory to HIV-1, DENV, influenza virus A, RSV, parainfluenza virus type 2, and canine distemper virus than ribavirin (nucleoside analog) with a few exceptions.[178,189] Ti/W and V/W PMs inhibited SARS-CoV-1, transmissible gastroenteritis virus of swine and feline infectious peritonitis virus; however, there was no apparent relationship between PM structure and antiviral activity.[190,191] Differences in antiviral activity of PMs may depend on the amino acid composition of the viral envelope glycoproteins, as seen in variation in dextran sulfate inhibition.[192]

Yamamoto et al. demonstrated the anti-HIV-1 and simian immunodeficiency virus (SIV) activity of $K_{13}[Ce(SiW_{11}O_{39})2]\cdot26H_2O$ (JM1590) and $K_6[BGa(H_2O)W_{11}O_{39}]\cdot15H_2O$ (JM2766).[193] Both compounds inhibited viral attachment and syncytium formation due to gp120 binding with greater selective indices than those of AZT (NRTI) and dextran sulfate.[90,194,195] *In vivo*, no HIV antigen-specific immune responses were detected, which supports the hypothesis that PMs interact with HIV antigen and suppress viral replication entirely.[178]

While the majority of PMs inhibit viral attachment, PM-523 inhibits membrane fusion between influenza-A envelope and the cellular membrane.[196] Shigeta et al. selected PM-523-resistant influenza-A strains and mutations conferring resistance were found in the interface edges of HA1. This implies that PM-523 binds to the interface of HA trimer and inhibits the opening of the trimers, which prevents the fusion of the viral envelope with cellular membranes.[190] With this mechanism, PM-523 worked synergistically with ribavirin or zanamivir in vitro and in vivo and increased the survival rate of influenza-infected mice significantly, as compared with PM-523 only or ribavirin only controls.[190,197]

The largest issue with antiviral polymers is that the majority of them are not orally bioavailable. While intravenous or intramuscular medication is still useful in a hospital setting, it may not be entirely useful for everyday use. Many PMs have been tested against HIV; however, none have improved in antiviral or cytotoxicity to surpass standards of care, like AZT.[178]

1.4.4 Inorganic small molecules

With the exception of metal complexes of known antivirals, in which an antiviral such as acyclovir is a ligand of the complex, inorganic small molecules have a large structural variety and a corresponding large number of antiviral targets.[198–200] For a broad overview of metal-based antivirals, see de Paiva et al.

(2020).[201] For the purposes of this chapter, we will look at inorganic compounds that act early in the viral replication cycle. Although many compounds do not have a formally defined mechanism of action, the structural similarities, broad-spectrum activities, and timing of inhibition suggest a common antiviral target: HS.

Beginning with simpler metal compounds, Knight et al. screened cobalt (III), nickel (II), and ruthenium (III) amine complexes for anti-Sindbis virus activity.[202] Cobalt hexamine outperformed the nickel and ruthenium complexes, which were more toxic.[202] Importantly, structural modification of cobalt hexamine (*i.e.* macrocyclic, mixed macrocyclic–monodentate, or substitution of a water or chloride for an amine) resulted in either a lack of or sharp decrease in antiviral activity.[202,203] Cobalt hexamine has also been shown to have antiviral activity against adenovirus, HIV, and Ebola virus.[202,204] Cobalt hexamine was well tolerated *in vivo* and significantly improved the survival of mice infected with Ebola virus.[204] Cobalt hexamine's mechanism of action remains unknown; however, it does inhibit an early stage of viral replication.[203] Cobalt hexamine is substitutionally inert, and thus lacks the ability to coordinate and hydrolyze phosphodiester bonds like cisplatin; however, it can form hydrogen bonds with nitrogenous bases of nucleotides of DNA.[205] Thus, it is possible that the ammonia ligands can form analogous hydrogen bonds with HS to inhibit its function in viral attachment.

Further exploration of cobalt (III) compounds revealed several with antiviral properties. The CTC series of compounds are based on a chelating Schiff base and several have broad-spectrum antiviral activity.[206] However, they also have other activities. CTC compounds selectively disrupt the structure and function of zinc fingers, selectively induce myoglobin unfolding, and prevent the progression of type II collagen-induced arthritis in animal models.[207–209] CTC compounds were proven effective as antivirals *in vitro,* and *in vivo* as topical antivirals for herpetic keratitis; CTC-96 was as effective as Viroptic (nucleoside analog) at one-thousandth its effective concentration.[210,211] In much of the initial work, CTC-96 was the most effective and least cytotoxic of the CTC series; its broad-spectrum antiviral activity was then investigated.[203] CTC-96 is an effective antiviral against HSV-1, adenovirus, VSV, and varicella zoster virus (VZV).[211,212] However, CTC-96's broad-spectrum antiviral activity has its limits; it was found to promote, rather than inhibit, papillomavirus wart growth, though the mechanism is unknown.[213] CTC-96's mechanism of action was studied with HSV-1. It targets cell-virus fusion and inhibits cell-to-cell spread and syncytium formation; however the molecular mechanism is unknown.[212] CTC-96 is unlikely to specifically inhibit herpesvirus fusion glycoprotein gD as it also inhibits VZV in a similar manner to HSV, but VZV does not have a gD homologue; this suggests that CTC-96 nonspecifically targets an essential fusogenic apparatus.[212] CTC-96 remains the only cobalt compound which has entered clinical trials as an antiviral.

Other metal complexes are broad-spectrum antivirals; however, most were not as extensively studied as cobalt hexamine or CTC-96. As the role of these metal ions is greatly influenced by their ligands, D-aminosugars were systematically studied to create structure-activity relationships.[214] Interestingly, no complex of zinc, cobalt, or copper with D-aminosugars had virucidal activity.[214] However, $Cu(glucosoxime)_2$ inactivated extracellular virus; Shishkov et al. suggested that it may interfere with viral attachment or membrane fusion.[214] Horton and Varela made copper (II), platinum (II), and palladium (II) complexes of 3-Deoxy-D-erythro-hexos-2-ulose bis(thiosemicarbazone), derived from glucose, and screened them against poliovirus type 1.[215] Each complex had antiviral activity, with the copper(II) complex being the most effective; although no mechanistic studies were performed, their structural similarity to metal-aminosugar complexes would suggest a similar mechanism of action, inhibition of viral attachment or membrane fusion.[215] Metal complexes with amino acids and their derivatives also investigate the role of ligand on antiviral activity. Cobalt (II) complexes with histidine and lysine had no

effect on HSV-1 replication, but cobalt (II) complexes with arginine and serine both inhibited viral attachment.[216] Zinc (II) pinolinate and asparate (Zn(pic)$_2$ and Zn(asp)$_2$) inhibit HSV-1 and VZV to varying degrees. Both appear to inhibit either viral attachment or entry as their antiviral effects are abolished when the complexes are removed from the supernatant.[217,218]

Sodium copper chlorophyllin, a water soluble, semisynthetic green plant pigment chlorophyll derivative, is a common food additive and food colorant.[219,220] It has broad-spectrum antiviral activity against HCV, influenza, HIV, enterovirus A71, and coxsackievirus A16.[221–223] Ito et al. demonstrated that sodium copper chlorophyllin's anti-HIV activity is due to inhibition of viral absorption onto the host cell, and similarly, Liu et al. demonstrated its anti-HCV activity was due to viral attachment inhibition.[221,223] In a mouse model, sodium copper chlorophyllin significantly reduced HCV titers in the lungs and muscles.[223] Interestingly, sodium magnesium chlorophyllin also has broad-spectrum antiviral activity against HSV, VZV, vaccinia virus, influenza A, and Newcastle disease virus.[224] However, unlike sodium copper chlorophyllin, sodium magnesium chlorophyllin has virucidal properties – though its mechanism is unclear.[224]

Simic et al. tested palladium(II) and platinum(II) complexes with 2-(dephenylphosphino)benzaldehyde 1-adamantoylhydrazone against polovirus type 1. However, the Pt(II) complex had some antiviral activity if cells were pretreated and greater antiviral activity if cells were treated after infection, suggesting two mechanisms of action: an inhibition of viral attachment as well as a inhibition of viral replication.[225] The Pd(II) lacked any antiviral activity. Interestingly, not many palladium complexes have antiviral activity.[226,227] However, palladium complexes of bis(thiosemicarbazone) were active against HSV-1 and HSV-2 and were particularly effective against acyclovir-resistant strains.[228] Unfortunately, no mechanistic studies were done. Kovala-Demertzi et al. screened Pd(II) and Pt(II) complexes with pyridine-2-carbaldehyde thiosemicarbazone (HFoTsc) against HSVs. Several compounds were effective against HSV-1 and HSV-2, including strains resistant to acyclovir; inhibition of IE protein expression suggests an inhibition of viral attachment or entry.[229]

1.5 Development of non-traditional platinum drugs

1.5.1 Cisplatin: Platinum's golden boy

In 1844, Michele Peyrone used an excess of ammonia in the synthesis of Magnus' green salt. The resulting mixture was both green and yellow. Peyrone had trouble interpreting his results and assumed the yellow compound was a precursor to Magnus' green salt (Figure 1.6).[230]
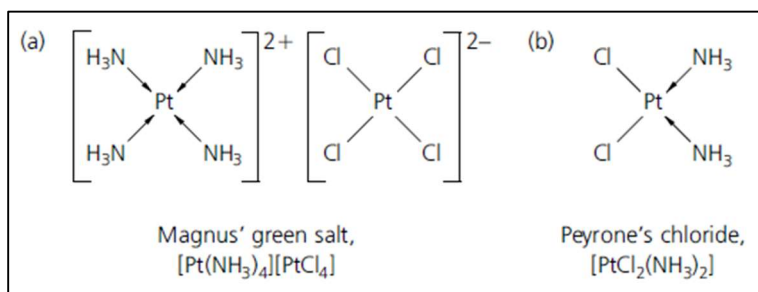
Figure 1.6: Structures of Magnus' green salt and Peyrone's chloride.[230]

Nearly 120 years passed before the biological properties of Peyrone's chloride was investigated. Barnett Rosenburg published the cytostatic activity of group VIIIB transition metal compounds in *E. coli*. Further investigation on his part revealed that the neutral platinum compound, more than the singly or doubly

charged platinum compounds, had little effect on bacterial cell growth but inhibited the ability of the cell to divide.[231] Additionally, the cis isomer was more potent than the trans isomer. Finally, in 1969, Rosenburg demonstrated cisplatin's antitumor properties against sarcoma 180 and leukemia L1210. From that point, Peyrone's salt was rapidly introduced to the clinic as cisplatin and licensed to treat testicular, ovarian, and bladder cancer in 1978.[231] Since then, platinum antitumor agents have become one of the most used chemotherapies. Approximately 20% of all cancer patients receive cisplatin and 50% receive platinum compounds.[231]

Rosenburg discovered the anticancer power of cisplatin but it took a myriad of scientists to define cisplatin's mechanism of action and its consequences. Simply, cisplatin targets cellular DNA to inhibit cell replication. To add detail, the mechanism of action can be divided into four steps: entry into the cell, cisplatin activation, DNA binding, and cellular processing (Figure 1.7).[231]
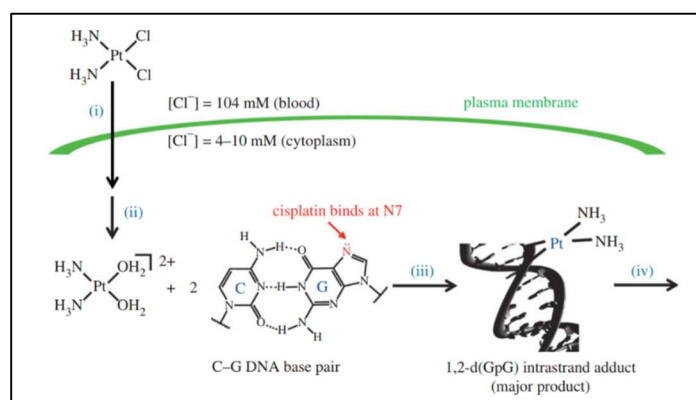
Figure 1.7: Cisplatin's mechanism of action in four steps: entry into the cell, cisplatin activation, DNA binding, and cellular processing, reproduced from Johnstone et al. 2015.[231]

Cellular entry was not easily deciphered. There was debate on whether cisplatin entered via passive diffusion or active transport; the current consensus is that it is a combination. Previously, it was assumed cisplatin could passively cross the cell membrane because it was not charged. This has been disproven with the development of new charged platinum complexes, discussed later in this paper. Copper transporters, like CTR1, have been demonstrated to actively transport cisplatin into cells. Organic cation transports (OCT1 and OCT2) as well as other cell membrane proteins have also been shown to bring cisplatin into cells. However, data in this area continues to be inconsistent and contradictory.[231]

Cisplatin, as it was synthesized by Peyrone, is not the bioactive form. Within a cell, cisplatin undergoes ligand substitution. The ECM has 100 mM chloride while the cytosolic concentration is about 4 mM. This drastic change in chloride concentration precipitates the reaction. Cisplatin is a bifunctional electrophile and its chloride ligands are replaced by nucleophilic water.[232]

Following aquation, cisplatin rapidly binds to B-DNA, either forming intrastand or interstrand cross links. Interstrand and intrastrand cross links differ structurally. Using nuclear magnetic resonance (NMR) spectroscopy, Hopkins et al. demonstrated that interstand cisplatin-DNA crosslinks occur in the minor groove, contrary to the mechanistic explanation, which placed cisplatin in the major groove. The interstrand N7-Pt-N7 linkages imposes bond length and bond angle constraints on DNA, requiring the DNA to alter from the canonical B-DNA structure (PDB ID 1DDP).[233] With cisplatin bound to guanine, cytosine moves to an extrahelical position, leaving guanine without a hydrogen-bonding partner, and the DNA double helix shifts from a right-handed helix to a left-handed helix similar to Z-DNA.[233] The summation of

these changes is a 45° bend of the DNA and an 80° unwinding of the double helix, which cannot be explained by cisplatin in the major groove (Figure 1.8).
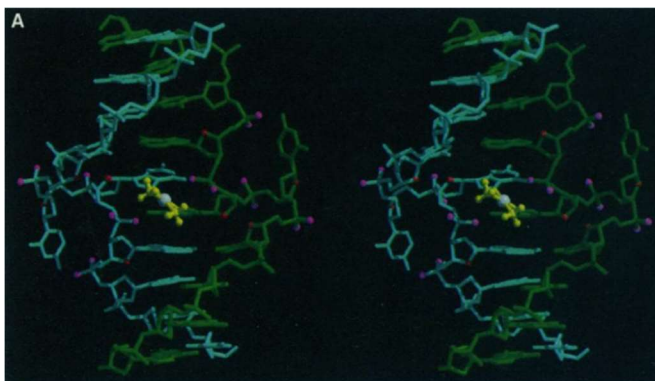
Figure 1.8: Cisplatin-DNA interstrand adduct, reproduced from Huang et al. 1995.[233]

Several interactions may stabilize this complex including: (1) the cross-strand purine-purine stacking of 4A and 5'G, (2) hydrogen bonding between the O4' of 5G's sugar and the base of 7T, and (3) the interaction between the oxyanions of 5G and 5'G with cisplatin's platinum center to form a pseudo-octahedral geometry around the platinum atom. Despite the huge structural deformation to DNA, interstrand cross-links are not particularly cytotoxic as they only account for 3-5% of the cisplatin-DNA adducts.[233]

The intrastand cross-link is more abundant, structurally very different, and thus has graver biological implications. In intrastrand cross links, cisplatin binds to the N7 atoms of purine rings G8 and G9, allowing one amine ligand to hydrogen bond with the one phosphate oxygen of G8.[234] The constraining bond lengths and angles of cisplatin force G8 and G9 to destack and expose their hydrophobic surfaces in the minor groove. HMG1 (high mobility group protein) is a chromatin architectural factor that can recognize the 1,2-d(GpG) and 1,2-d(ApG) DNA intrastrand crosslinks formed by cisplatin.
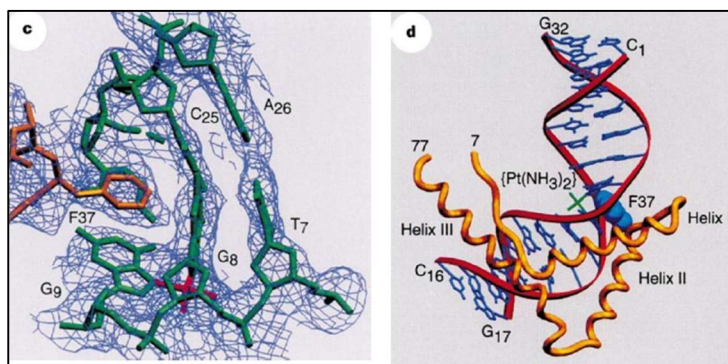
Figure 1.9: Cisplatin-DNA intrastrand adduct complexed with HMG1, reproduced from Ohndorf et al. 1999.[234]

The concave domain of HMG1 binds the minor groove of DNA (Figure 1.9). Since HMG1 itself bends B-DNA when bound, Lippard et al. suggested the HMG-domain proteins bind preferentially to distorted DNA due to the formation of the pre-bent conformation along with the widening of the minor groove.[234] When HMG1 binds the cisplatin-DNA adduct, conformation changes occur at the C-terminus of helix I, the N-terminus of helix II, and the connecting loop. These changes allow Phe37 to intercalation into the DNA (Figure 1.9). The HMG1 Phe37Ala mutant reduces its ability to bind the cisplatin-DNA adduct. The phenyl ring of Phe37 projects into this gap and stacks with G9 base; this increases the angle between the guanine

heterocycles (75°) in comparison to the cisplatin-DNA adduct alone.[234] This complex is lower in free energy and thus more stable. Although there is some variation among HMG-domain proteins at position 37, it is always a hydrophobic residue, capable of serving as "bending wedge." Overall, the DNA-cisplatin-HMG complex, is bent 61° towards the major groove of DNA and the minor groove is expanded to resemble A-DNA.[234]

Following the formation of the cisplatin-DNA intrastrand adduct, cells initiate the DNA damage response. Protein kinases ATM (ataxia-telangiectasia mutated) and ATR (ATM- and Rad3-Related) halt their replication process in the G2 stage. Cells repair their DNA by excising the cisplatin adducts. Several proteins remove a 30-mer oligonucleotide and synthesize a new segment based on the complementary strand. If the cell cannot remove the cisplatin adducts, the cell proceeds through apoptosis.

Targeting DNA makes cisplatin a potent inhibitor of cell replication and growth. However, all cells have DNA and so cisplatin is not naturally selective. Additionally, platinum is a soft acid, meaning it will bind to chloride (a hard base) but would prefer to bind a soft base. In a biological environment, soft bases are numerous; they include sulfur containing molecules like glutathione and methionine.[235] Although these reactions play a role in cisplatin metabolism, they are also responsible for some of the worst complications of cisplatin, including gastrointestinal toxicity, nephrotoxicity, and neurotoxicity. These side effects are dose limiting and so bad that patients would prefer to stop treatment rather than continue cisplatin.

More important than side effects, cisplatin resistance arises in many cancers. Cisplatin resistance cells are able to either more quickly repair damaged DNA or tolerate damaged DNA. Most cisplatin-DNA adducts are removed by the nucleotide excision repair (NER) system, in which enzymes recognize the bend in DNA caused by cisplatin.[235] One of the rate limiting steps of NER is a group of enzymes called ERCC1. An absence of ERCC1 expression has been shown to increase a tumor's sensitivity to cisplatin, indicating its role in DNA repair. Cisplatin resistance can also arise from the mismatch repair (MMR) system. In a healthy cell, the MMR system would attempt to repair insertions and deletions that occur during DNA replication and recombination; if the attempt should fail, the system would transmit a proapoptotic signal. Several mutated or underexpressed MMR proteins, such as MSH2 and MLH1, have been linked to cisplatin resistance.[235] Defects in MMR proteins allow translesion synthesis, which DNA synthesis not blocked by a cisplatin-DNA adduct. Several DNA polymerases can allow translesion synthesis and thus enable cisplatin resistance. Finally, cisplatin interstrand may break both strands of DNA. This damage is repaired in the S phase by the homologous recombination (HR) system. Mutation of BRCA1 and BRCA2 inhibits critical components of the HR system and leaves DNA unfixed.[235]

In response to cisplatin resistance, several derivatives were developed. Currently, there are three approved derivatives in the United States but more are approved for use in Europe and Asia (Figure 1.10).
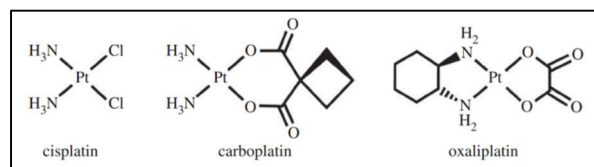
Figure 1.10: Platinum chemotherapies approved for use in the United States

Carboplatin (Figure 1.10 center) was approved in 1989 for the treatment of ovarian cancer and oxaliplatin (Figure 1.10 right) was approved in 2002 for the treatment of advanced colorectal cancer. Both

compounds maintain cisplatin's square planar configuration but replace the chloride leaving groups with a bidentate dicarboxylate ligand that is less reactive. Both compounds have fewer off-target reactions, and therefore lower toxicity. Despite these changes, resistance and toxicity continue to be an issue.

1.5.2 Triplatin DNA binding

In another effort to mitigate cisplatin's resistance, compounds with more than one platinum center were synthesized. This allowed a wider variety of spacing, orientations, and reactivates of platinum centers to form different DNA adducts. The most successful polynuclear platinum compound (PPC) is by far Triplatin (BBR3464) (Figure 1.11).
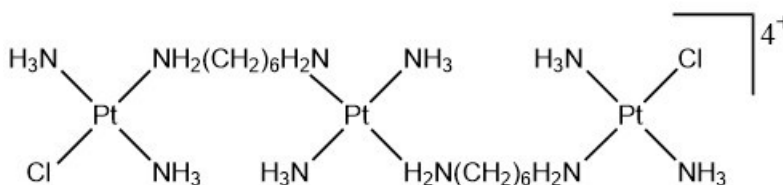
Triplatin

Figure 1.11: Structure of Triplatin. Counterions omitted for clarity.

Like carboplatin and oxaliplatin, Triplatin maintains the square planar configuration of cisplatin as well as the platinum (II) center; Triplatin is two trans-[PtCl(NH$_3$)$_2$] units linked by a tetraamine [trans-Pt(NH$_3$)$_2${H$_2$N(CH$_2$)$_6$NH$_2$}$_2$]$^{2+}$ unit (Figure 1.11). Its overall charge of +4 and the two separate Pt coordination units capable of covalent binding result in DNA binding distinct from that of cisplatin. The high positive charge of Triplatin accelerates DNA binding with a t$_{1/2}$ of ~40 minutes, significantly faster than the neutral cisplatin (t$_{1/2}$ = 240 minutes).[236] The bifunctional DNA binding of Triplatin produces an unwinding angle of 14° in negatively supercoiled pSP73 plasmid DNA with a preference for guanine residues. Approximately 20% of DNA adducts are interstrand crosslinked by Triplatin, while cisplatin is usually 3-5% interstrand crosslinks. Importantly, antibodies raised to cisplatin-adducted DNA do not recognize DNA modified by Triplatin but antibodies raised to transplatin-adducted DNA do.[236] This emphasizes the diverging motif of Triplatin and underlines that Triplatin's different DNA binding may also lead to unique anticancer activity; below are more structural details of Triplatin-DNA binding.
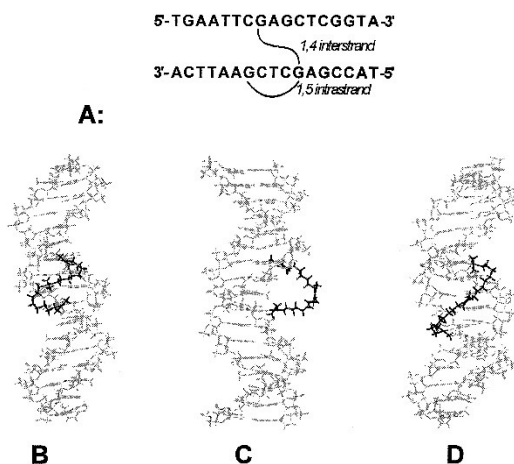
Figure 1.12: Structure of Triplatin-DNA adducts. (A) the schematic of DNA crosslinks. (B) A 1,4 interstrand crosslink with the linker of Triplatin within the major groove. (C) A 1,4 interstrand crosslink with the linker of Triplatin outside of the major groove. (D) A 1,5 intrastrand crosslink. Reprodcued from Brabed et al. 1999.[236]

The incorporation into the linker backbone of charge and hydrogen-bonding capacity dramatically increases the DNA affinity and affects the charge/lipophilicity balance as well as increasing the distance between the two platinum-DNA binding coordination spheres. All of these features may contribute to differentiating DNA binding, cellular uptake, and antitumor activity within the polynuclear platinum family itself.[237,238] The intrastrand crosslinks of Triplatin are analogues of the major adducts of cisplatin, which forms between two neighboring purine residues and results in an unwound duplex with a fixed kink and widened, shallow mine groove.[239] Triplatin intrastrand crosslinks induce a helix bend of 32-34° toward the major groove, a 13° DNA unwinding, disrupt the hydrogen bonding between the 5'-coordinated GC bp, and disort 4-5bp at the site. In comparison, the cisplatin induced 1,3-intrastrand crosslink bends towards the major groove 35° and unwinds DNA by 23°.

DNA altered by platinum adducts attract DNA-binding proteins such as those containing high mobility group (HMG) domains.[234,240,241] HMG binding has been postulated to mediate the anticancer activity of platinum compounds.[234,241] Triplatin-DNA binding results in three unique conformational distortions: 1,2-, 1,3-, and 1,5-intrastrand crosslinks. None of the three results in a stable curvature (directional bending), consistent with the view that these adducts are flexible. The distortion occurs on the 5' side of the crosslink and where applicable, between the platinated G residues. The 1,2-intrastrand crosslink is the structural analog of the most prominent cisplatin-DNA adduct. Due to the distance between platinating centers of Triplatin, it is unlikely to be favored over the longer range intrastrand or interstrand crosslinks. The flexibility of the 1,2-intrastrand crosslink is the monofuntional coordination spheres with only one purine base; Triplatin's linker length as well as its charge and hydrogen-bonding ability enhance its initial DNA recognition but do not appear to greatly contribute to the conformational flexibility. This flexibility is key in the lack of HMG domain recognition in Triplatin-DNA intrastrands crosslinks as the cisplatin-DNA structural motif recognized by HMG domain proteins is stable as described above.[241–243] Thus, the mechanism of anticancer activity of Triplatin does not involve HMG domain proteins recognizing intrastrand crosslinks as a crucial step – this is distinct from cisplatin and its derivatives.

Another cellular mechanism is NER; intrastrand crosslinks of cisplatin are removed by NER, which contributes to cisplatin resistance. The intrastrand crosslinks of Triplatin are readily removed from DNA by NER.[244] The processing of the intrastrand crosslinks of BBR3464 in tumor cells sensitive to this drug may not be relevant to its antitumor effects despite the fact that the trinuclear platinum compound forms on DNA intrastrand crosslinks with a relatively high frequency. NER excision of Triplatin-DNA conformationally flexible adducts results in a greater range of excised fragments compared to sterically rigid adducts produced by cisplatin. It is tempting to speculate that delocalized lesions formed by long range adducts of PPCs may still represent unique challenges for recognition and excision by repair enzymes. However, Triplatin forms more DNA interstrand crosslinks than cisplatin overall. DNA interstrand crosslinks could be even more effective lesions than intrastrand adducts in terminating DNA or RNA synthesis in tumor cells, and thus could be even more likely candidates for the genotoxic lesion relevant to antitumor effects of BBR3464. Additionally, DNA interstrand crosslinks are more difficult to excise and repair because it requires cutting both strands of DNA.

Overall, the DNA binding of Triplatin is distinct from that of cisplatin. While both covalently bind to guanine, Triplatin's two separate platinating moieties extend its DNA distortion and prevent HMG domain protein binding. In phase I clinical trials, Triplatin had a maximum tolerated dose of 0.12 mg/m^2 and a terminal half life of several days, which may explain the higher incidence of neutropenia and

gastrointestinal toxicity.[245] Nausea and vomiting were rare and neuro- and renal toxic effects were not observed. [245] In phase II clincal trials on gastric or gastro-oesophageal adenocarcinoma, plasma protein binding of Triplatin was higher in humans than in mice, and its degradation to an inactive species was more rapid in humans than in mice; although TriplatinNC was generally tolerable at 0.9 mg/m^2, every 21 days, only minimal anti-tumor activity was identified.[246] Similarly in phase II trials on sensitive or refractory small cell lung cancer, 11 patients had disease stabilization, but 23 patients continued to have disease progression at a dose of 0.9 mg/m2 every 21 days.[247] Triplatin remains the only "non-classical" platinum drug to have entered human clinical trials.

1.5.3 TriplatinNC DNA Binding

TriplatinNC is the non-covalent binding analog of Triplatin; in place of the two terminal chlorides, TriplatinNC has two inert hexanediamine, termed dangling amines (Figure 1.13).
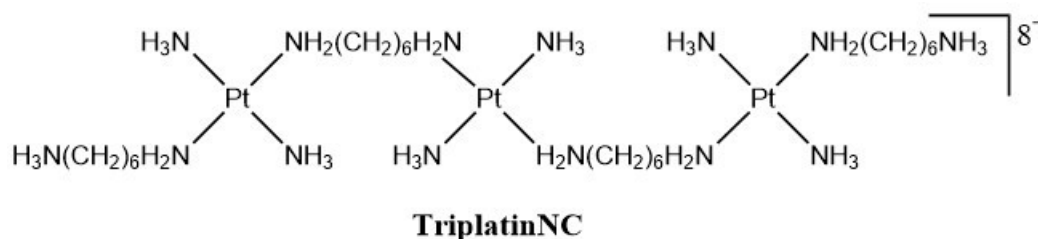
TriplatinNC

Figure 1.13: Structure of TriplatinNC. Counterions omitted for clarity.

Like Triplatin binding, the binding of DNA by TriplatinNC is distinct from cisplatin as TriplatinNC cannot form covalent bonds with DNA, rather it relies on noncovalent interactions. DNA ligands are broken down into intercalators and groove binders. TriplatinNC is neither; it presents a third mode of DNA binding, relying solely on the phosphate backbone. Komeda et al. crystalized TriplatinNC with the Dickerson-Drew Dodecamer (DDD) to ascertain TriplatinNC's mode of DNA binding.[248] TriplatinNC selectively forms hydrogen bonds with phosphate oxygens, forming bidentate NH···O···HN (amine···phosphate···ammine) complexes through hydrogen-bonding interactions. In B-DNA, TriplatinNC selectively binds O2P over O1P, which causes TriplatinNC to track the backbone, link adjacement phosphate groups, and span the minor grove (Figure 1.14). This regular geometric complex, termed phosphate clamps, occur frequently and can be generalized as nucleic acid binding motifs.

s
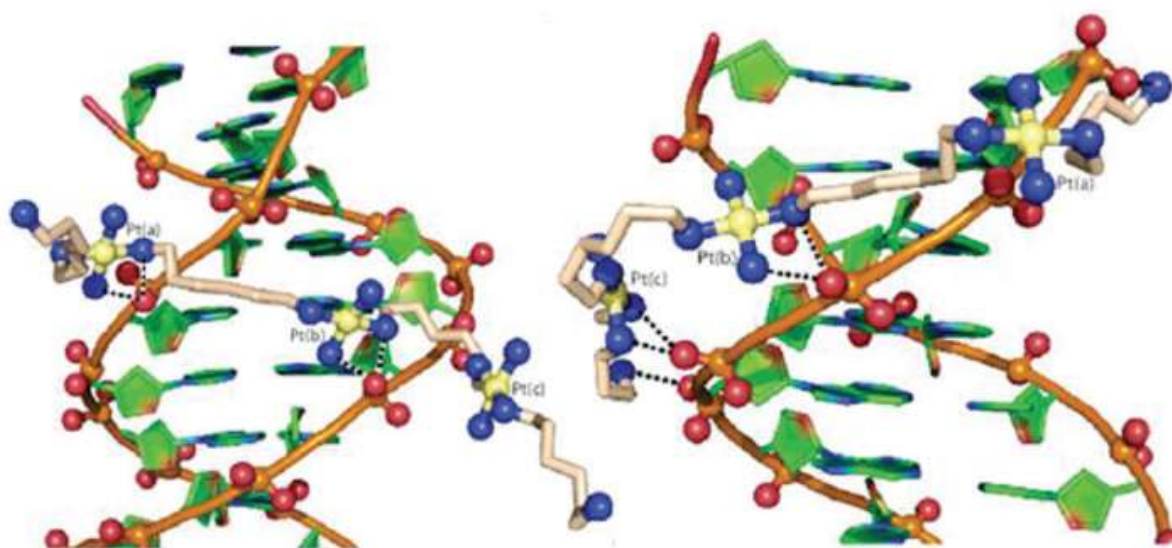
Figure 1.14: Crystal structure of TriplatinNC associated with DDD showing minor-groove spanning (left) and backbone tracking (right), reproduced from Qu et al. 2015.[249]

A phosphate clamp consists of a single OP atom accepting two hydrogen bonds, one each from two am(m)ine ligands of a single platinum (II) center (Figure 1.15). It is cyclic, highly conserved, and requires cis-am(m)ine ligands of platinum (II), as trans ligands are too far apart to form hydrogen bonds and in opposing directions.
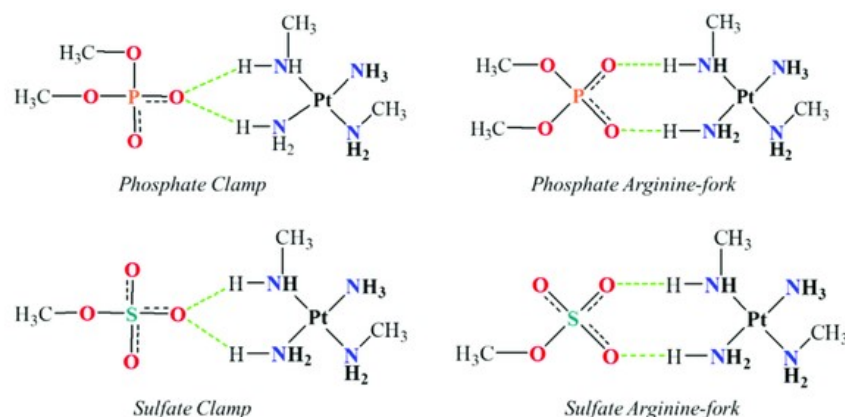
Figure 1.15: Platinum phosphate and sulfate binding as compared phosphate and sulfate arginine-forks.

In Figure 1.16, TriplatinNC forms eight phosphate clamps with eight OPs with each Pt(II) center engaging in at least one phosphate clamp.[248] Phosphate clamps frequency and geometric conservation indicate a favorable stability. In principle, a compound could be designed to take advantage of the predictability and stability of phosphate clamps; for example, varying the linker length between Pt(II) moieties could favor A-DNA over B-DNA or RNA over DNA. The interactions of the amines of TriplatinNC are similar to the interactions of the guanidino group of arginine, which is also phosphate oxygen selective. Arginine displays the ability to form a phosphate clamp, though it was previously described as an arginine fork.

However, an arginine is limited to two clamps while a TriplatinNC's amines can form eight.[248] The bottom line is TriplatinNC forms many noncovalent interactions with DNA, not specific to its sequence.
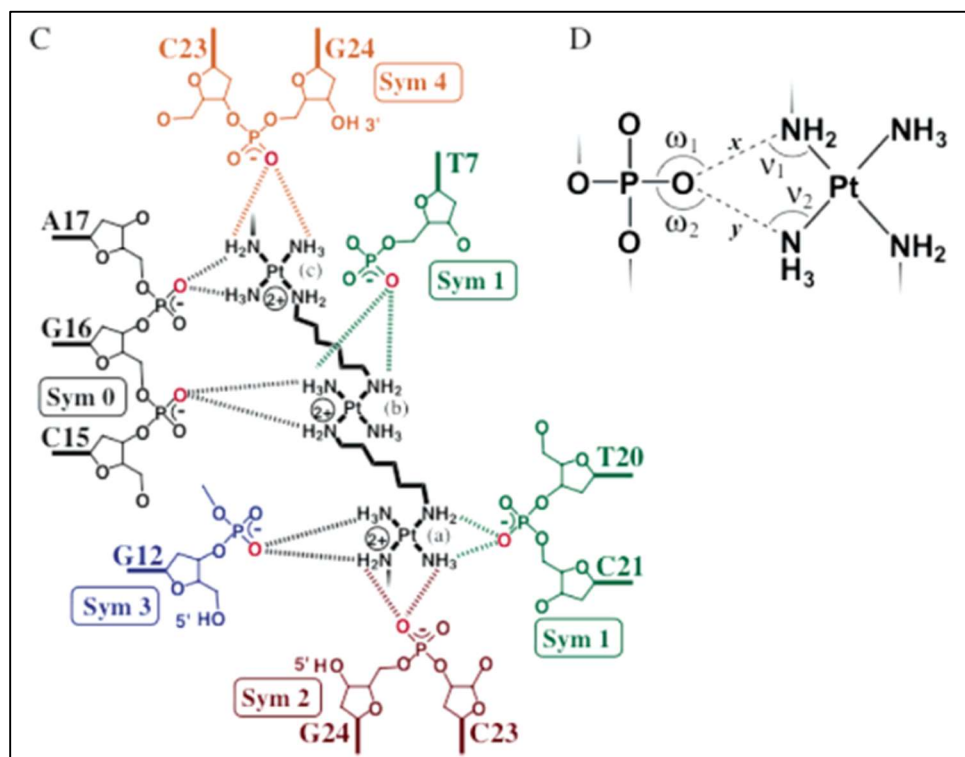
Figure 1.16: Phosphate clamps between TriplatinNC and the DDD. (C) Schematic representation of the seven phosphate clamps formed between TriplatinNC and the DDD; the dangling amines of TriplatinNC are omitted for clarity. (D) Schematic representation of a phosphate clamp illustrating the geometric parameters used to characterize phosphate clamps. Reproduced from Komeda et al. 2005.[248]

Asymmetric neutralization of the phosphate groups, like that resulting from TriplatinNC phosphate clamps, may drive DNA distortion and bending to lead to "phosphate collapse."[250,251] However, the DNA conformation observed in the DDD-TriplatinNC complex differs slightly from the native DDD (NDB entry bdl084).[244] The axial bend is greater in the DDD-TriplatinNC complex and the minor grooved width is modestly impacted. However, the locus of distortion suggests TriplatinNC binding is not the only cause; the substitution of a fully hydrated Mg2+ for a partially dehydrated Na+ in the major groove may also contribute.[248] In native DNA, the Mg^{2+} ion forms hydrogen bonds with DNA bases. Researchers proposed that TriplatinNC, as a highly positively charged molecule, displaces the Mg^{2+} due to electrostatic competition or that the TriplatinNC induced conformational change favors Na^+ over Mg^{2+}.[244] Overall, the conformation changes to DNA are modest in comparison to the changes induced by cisplatin.

The proteins that recognize DNA bending do not register the TriplatinNC-DNA complex. The extreme bend seen in the cisplatin-DNA adduct prove to be cytotoxic, but is easily recognizable by the cell as not natural. TriplatinNC induces a much smaller bend, still cripples DNA replication ability, and thus halts cell growth and replication. TriplatinNC is effective against cisplatin resistance tumors as it bypasses the resistance mechanisms. The structural difference between the two platinum compounds leads to their varying actions and varied bodily responses.

1.5.4 PPC cellular internalization

Cellular internalization of small molecule drugs and macromolecules is critical to their function. For instance, platinum accumulation is reduced in cells that have acquired cisplatin resistance as compared to parental cells.[252] Interestingly, while AH44 (+6) and TriplatinNC (+8) have practically identical DNA binding, their cellular accumulation differs greatly; both have increased accumulation as compared to cisplatin (+4), suggesting that increasing positive charge influences cellular accumulation. In an effort to determine the mechanism of PPC internalization, researchers examined the cellular accumulation of other polycations. Natural and synthetic peptides rely on cationic arginine-rich sequences for cellular uptake and accumulation.[253] Through ionic interactions and hydrogen-binding ability, termed an arginine fork, these sequences, or protein transduction domains (PTDs), bind heparan sulfate proteoglycans (HSPGs) as the first step in their cellular internalization.[254–256] Similarly, HSPGs facilitate the uptake of polyamines. As PTD internalization relies on HS, TAMRA-R9, a fluorescent arginine probe, uptake decreases in GAG-deficient cell lines.[257] TAMRA-R9 has an affinity for heparin typical of receptor-ligand interactions (Kd = 109 nM).[257,258] Conceptualizing PPCs as ''polyarginine mimics,'' the interactions between the amine groups of the triplatinum compounds and the phosphate groups of the DNA backbone are very similar to those of the guanidine groups on arginine (Figure 1.15). As a small molecule analog of the polyarginine motif, TriplatinNC must have a similar affinity, which would suggest that it is likely to engage in similar biological processes, including cellular accumulation.[258] This mechanism of cellular internalization is unique from cisplatin or oxaliplatin.[252,258]

1.6 Heparan Sulfate: A new target for PPCs

1.6.1 GAGs as a target for PPCs

The recognition of GAGs as cellular receptors for positively charged PPCs led the Farrell group to propose a unique HS targeting approach to interfere with HS-protein interaction, termed metalloshielding.[259–261] For substitution-inert complexes such as TriplatinNC, high affinity HS binding is mediated through hydrogen-bonding and electrostatic interactions with the charged sulfates and carboxylates. Density Functional Theory (DFT) showed the formation of 'sulfate clusters', analogous to the phosphate clamp interactions on DNA, but in a more delocalised manner, Figure 1.17.[261]
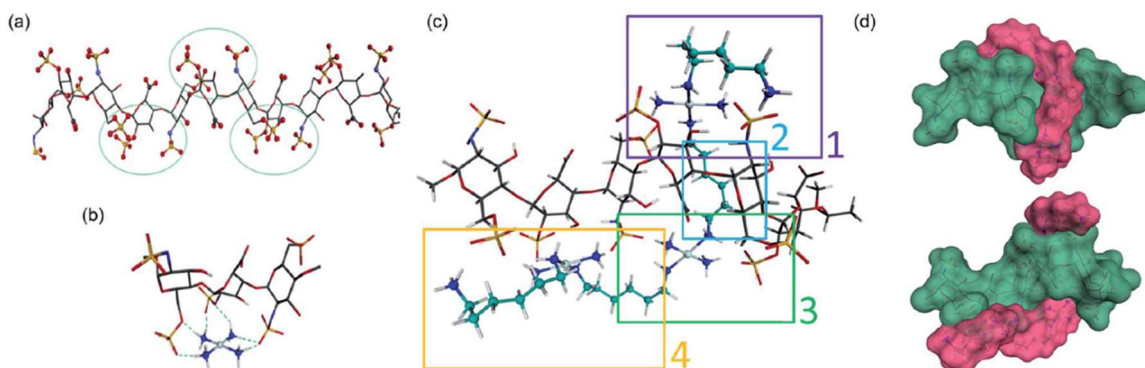
Figure 1.17: TriplatinNC interactions with HS. (a) Structure of the heparin dodecamer comprising dimers of IdoA(2S) (2S0 conformation) and GlcNS(6S) (1HPN). The green circles represent areas of negatively charged sulfate and carboxylate clustering. (b) The optimized structure of [GlcNS(6S)-IdoA(2S)-GlcNS(6S)] trisaccharide modelled with [Pt(NH3)4]2+. (c) Optmized structure of TriplatinNC with a heparin hexamer [IdoA(2S)-GlcNS(6S)]3 showing regions of sulfate clamp interactions (regions 1,3 and 4) and van der Waals contacts between sugar and diamine backbones (region 2). (d) Surface maps showing the relationship of TriplatinNC (magenta) to the heparin hexamer (green). Reproduced from Peterson et al. 2017.[261]

The sulfate moieties are more conformationally flexible than the constrained phosphodiester motif, resulting in greater variability in neighbouring sulfate-sulfate distances compared to the relatively fixed phosphate-phosphate distances in DNA/RNA. The negative charge on the sulfate group is also more dispersed than that of phosphate because of the extra oxygen atom. GAG-protein interfaces are significantly more hydrated than protein–protein interfaces and from a survey of PDB structures, it is estimated that about half of all GAG-protein interactions are water-mediated.[262] The binding affinity of cobalt complexes to GAGs is also shown to be charge-dependent.[263] At the interaction site, each sulfate group interacts with three ammines (a full face) of the octahedral complex (Figure 1.18) – a potentially more effective metalloshielding approach than that observed for the square-planar Pt(amine)$_4$ coordination units of TriplatinNC.[263]
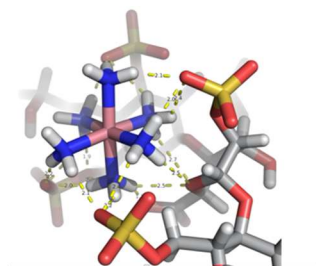
Figure 1.18: Hydrogen bonding observed in the DFT model for the interaction product of [Co(NH$_3$)$_6$]$^{3+}$ with FPX, reproduced from de Paiva et al. 2021.[263]

Several biophysical methods have been used to gauge the strength of M complex-GAG interactions, including use of the competitive inhibitor methylene blue (MB), isothermal titration calorimetry (ITC), and surface plasmon resonance and mass spectrometry. In the next section, TriplatinNC is used as a case study for M-GAG interactions.

Non-covalent interactions: Measuring the strength of PPC-GAG interactions

Direct and indirect assays have been used in heparin-protein assays and in defining the thermodynamic parameters from these interactions.[264,265] An indirect competition assay was developed using the cationic dye MB as reporter to assess M-GAG affinity, Figure 1.19.
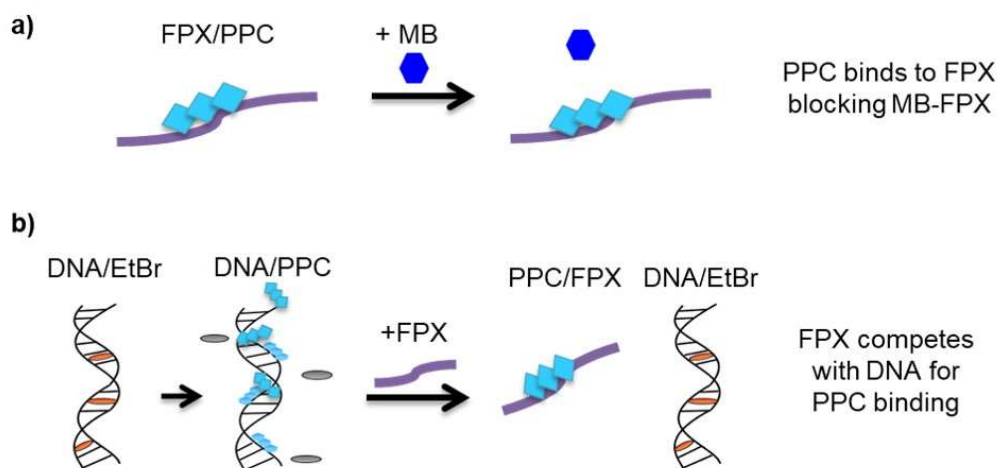
Figure 1.19: Schematic representation of TriplatinNC–FPX binding interaction measured by (a) MB and (b) ethidium bromide reporter assays. TriplatinNC competitively inhibits MB binding to FPX.

The assay is formally analogous to the well-known Ethidium Bromide assay for M-DNA binding. The interaction of MB with GAGs results in a concentration-dependent reduction in its absorbance and the changes can be used to quantify GAG content and calculate affinity constants.[264,266–268] Addition of TriplatinNC to a pre-formed MB-GAG complex releases the dye with concomitant increase in the absorbance of free MB, and the disruption of MB binding can be reported as an IC_{50}, the concentration of complex necessary to give 50% of free dye. By using MB as a reporter for competitive inhibition in a 3-species system, the Kd between TriplatinNC and heparin was calculated to be 66.4 nM, compared with the Kd for the MB-heparin interaction of 351 nM.[269] The latter value is comparable to that measured between MB and chondroitin sulfate (K_d = 578 nM).[264] With Fondaparinux (a model for heparin and HS, FPX) the values of K_d was estimated at 40 nM. In ITC, using a small 3,000 molecular weight (MW) heparin, a one-site model for K_d (TriplatinNC-heparin) gave a value of 33.1 ± 2 nM. In the case of surface plasmon resonance (SPR), the experimental set-up is different to that of ITC since the heparin is immobilized through streptavidin to the dextran sensor surface and the analyte (TriplatinNC) is injected as a continuous flow over the bound heparin. Non-specific binding of TriplatinNC to the negatively-charged surface and streptavidin caused technical issues but a one-site model and 1:1 TriplatinNC/heparin stoichiometry, gave a K_d of 340 ± 30 nM. Since the immobilized heparin in this case had a MW 15,000, it is plausible that there could be multiple binding sites, which may affect the estimated K_d values; SPR data were obtained in presence of 150 mM NaCl confirming that TriplatinNC is capable of binding to heparin at physiologically relevant concentrations of small cations. Care should be taken in comparing affinities across techniques due to the vagaries of each technique; nevertheless, overall results point to a strong interaction.

Non-covalent interactions: PPC-induced modulation of the solution-state HS structure

The detailed interaction of TriplatinNC and FPX was studied by 1D and 2D ^{1}H NMR spectroscopy and mass spectrometry (MS), coupled to DFT calculations and visualization.[270] Conveniently the ^{1}H chemical shifts of the anomeric protons of oligosaccharides fall in the 5-6 ppm region, generally free from interference from the chemical shifts of PPC protons. TriplatinNC (8+) induces major shifts to the anomeric protons of the glucosamine and iduronic acid residues of FPX (rings A, C, D and E of FPX in Figure 1.20).
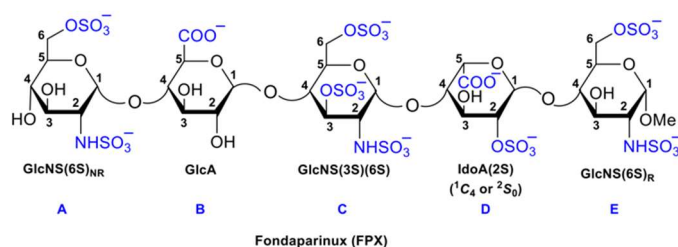
Figure 1.20: Structure of the Heparin template, Fondaparinux (FPX).

Importantly, the significant shifts to the HD1 and HD5 protons of the iduronic acid IdoA(2S) residue indicated potential conformational flexibility around the glycosidic linkage of IdoA(2S) and/or change of its ring conformation, Figure 1.21. The equilibrium ratio of IdoA(2S) conformers can be estimated by calculating the theoretical intra-residue proton-proton three-bond coupling constants of IdoA(2S) (obtained from DFT optimised structures of $^1C_4$ and $^2S_0$ forms) and establishing best agreement between the weighted averages of the theoretical coupling constant data and the corresponding experimental coupling constant data, Figure 1.22.[271–274]
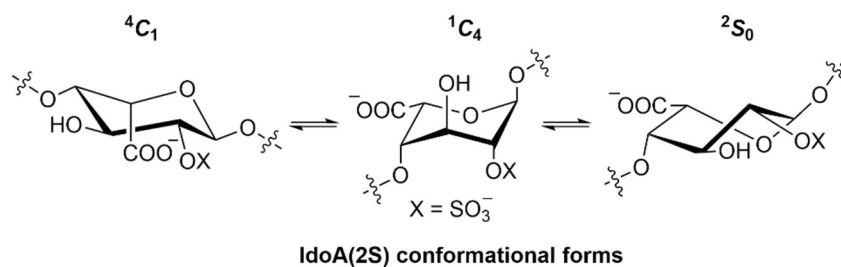
Figure 1.21: The possible chair (4C1 and 1C4) and skew boat (2S0) ring conformations for the iduronic acid (IdoA or IdoA(2S)) residues of HS and heparin.
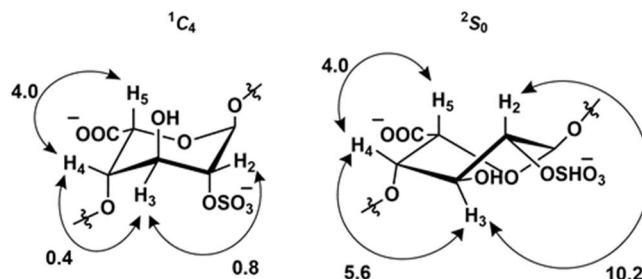
Figure 1.22: Calculated 3JH-C-C-H coupling constants (in Hz) for the IdoA(2S) residue of FPX measured by the torsion angles of the three bonded proton pairs in the fully optimized DFT structures of the 1C4 and 2S0 forms.161 The equilibrium ratio of IdoA(2S) conformers can be estimated by systematically fitting the weighted averages of theoretical coupling constant data against experimental data.

By following this approach, for free FPX, the best fit between the theoretical and experimental coupling constant data was obtained with an IdoA(2S) $^1C_4$:$^2S_0$ conformational ratio of 35:65, consistent with previously published data.[274] In the presence of TriplatinNC this ratio was 75:25 and the $^1C_4$ conformation, which was a minor form in free FPX, is the preferred conformer when FPX is bound by TriplatinNC. These findings were further supported by the analysis of experimental intra-residual NOE cross-peaks of IdoA(2S) protons in free and TriplatinNC bound FPX. Significantly, this study was the first demonstration of a small molecule affecting the conformational ($^1C_4$ /$^2S_0$) ratio of the critical IdoA(2S) moiety on a HS oligosaccharide. Further analysis of the DFT optimized structures showed that the favourable glycosidic linkages between the monosaccharide residues of FPX structure with IdoA(2S) residue in the $^1C_4$ ring conformation orient the sulfate and carboxylate groups for more suitable accommodation of the three square-planar {Pt(am(m)ine)$_4$} coordination units, and provide a better fit than the $^2S_0$ conformation for TriplatinNC binding (Figure 1.23).
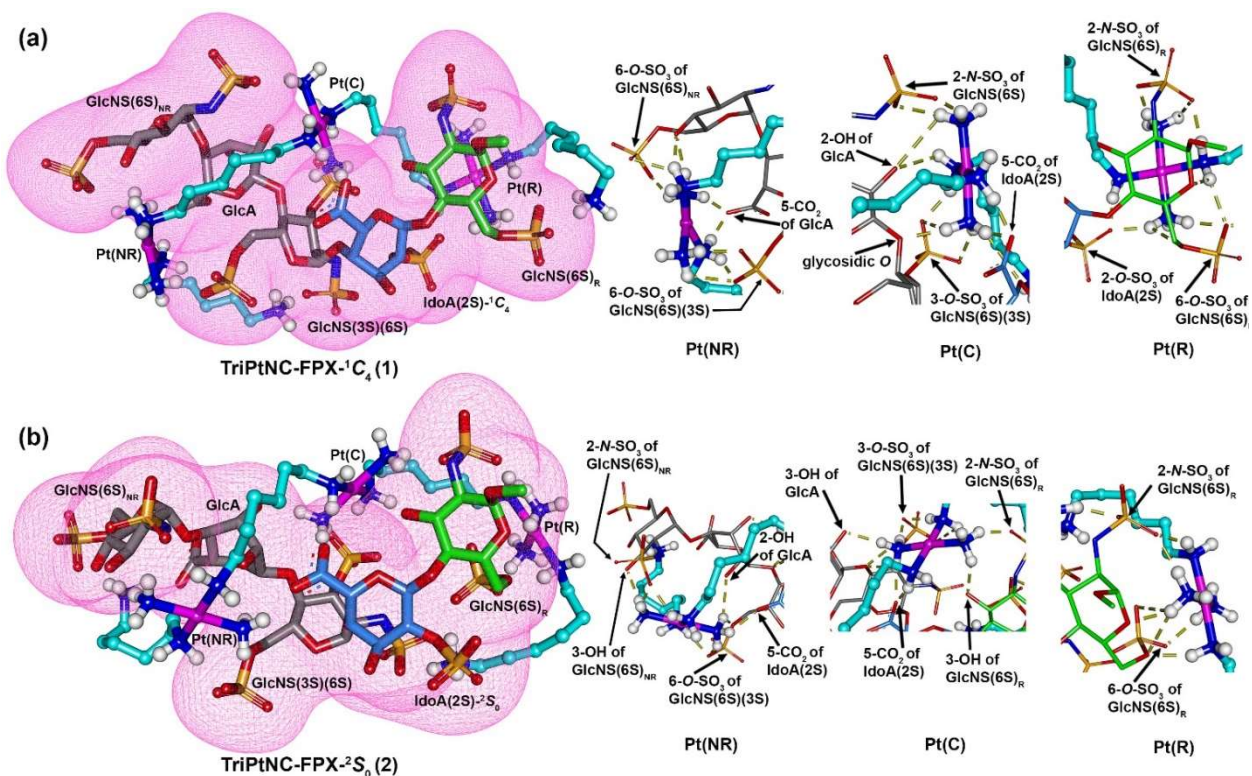
Figure 1.23: DFT optimized structures of TriplatinNC-bound FPX with IdoA(2S) residue of FPX in 1C4 (a) and 2S0 (b) conformations and the corresponding H-bonding networks observed for the three {Pt(amine)4} coordination units of TriplatinNC. the IdoA(2S) rings are shown in blue colour. The reducing end GlcNS(6S)R residue of FPX is shown in green. Reproduced from Gorle et al. 2021.[270]

Investigation of highly sulfated GAGs using MS and MS/MS is generally accompanied by SO_3 loss which competes with glycosidic and through-ring cleavage, limiting the technique's utility for sequence information because the appropriate precursor species is not investigated.[275–277] Use of Na^+ as counter-ion and SO_3 stabilization facilitated the structural determination of FPX by MS/MS.[275] The 1:1 adducts of TriplatinNC with FPX do show the intact precursor, confirming our previously observed metalloshielding on an octasaccharide and protection against sulfate loss in the gas phase.[260] MS/MS studies on FPX showed a cleavage pattern similar to that published,[275] but in the presence of TriplatinNC, the Y ions (Figure 1.24) are not observed suggesting that the adduct is located at that end of the molecule.[270] This method could also be of use to sequence longer-chain oligosaccharides as regions of sulfate clusters could be identified. The binding sites of TriplatinNC linked to an 18-mer ssDNA can be inferred using MS/MS – the adduct forms a block to sequential backbone cleavage.[278]
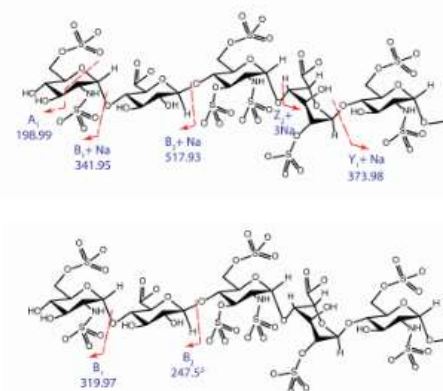
Figure 1.24: Fragmentation patterns of free FPX (top) and TriplatinNC-FPX (bottom) by MS/MS analysis, reproduced from Gorle et al. 2021.[270]

The circular dichroism (CD) spectra of FPX in presence of TriplatinNC shows a significant reduction in the characteristic negative band at approximately 220 nm.[270] It is feasible that neutralization of the heparin can induce condensation, similar to previously observed for DNA.

1.6.2 Covalent interactions: PPC binding with defined mono- and di-saccharide fragments of HS

The cellular chemistry of platinum anticancer agents has emphasized bond-forming reactions with 'soft' *N*- and *S*-donors in metabolism and site of action (*e.g.* histidine, cysteine, methionine protein residues and the purines and pyrimidines of DNA and RNA). A simplified interpretation of the Hard and Soft Acids and Base theory has led to the widespread acceptance that the 'class b' or 'soft' metal ion Pt^{2+} forms only weak bonds with 'hard' oxygen donors and that such complexes are difficult to isolate. Yet, examples abound such as the detailed work of Lippert on simple aqua and hydroxide ligands of cisplatin.[279] Depending on extracellular and intracellular concentrations, presumptive weakly coordinating anions – carboxylate, carbonate, phosphate and sulfate - are potential ligands in the cellular and biological milieu – phosphate has long been known to interfere with kinetic analysis of platinum complex reactions.[280] While these studies emphasize the *O*-base donors as individual ligands, it is plausible that the *O*-donor polyanionic biomolecules such as GAGs present multiple neighboring donors on a more complex polymeric, biomolecular template acting as a 'Lewis base sink'.[280]

2D [^{1}H, ^{15}N] heteronuclear single quantum coherence (HSQC) NMR spectroscopy using the ^{15}N-labelled trinuclear clinical agent Triplatin has detected pre-association, aquation, and covalent binding to DNA.[281,282] Minor groove pre-association of the central $\{PtN_4\}^{2+}$ linker influences the final products of the covalent interaction, notably dictating the formation of the unique $5'-5'$ and antiparallel $3'-3'$ directional isomers of {Pt,Pt} 1,4-interstrand cross-links.[281] In a similar way Triplatin is expected to interact with GAGs through an initial pre-association followed by aquation and then covalent bond formation with the variably substituted *O*-donor groups. The interaction of Triplatin with FPX was investigated by ^{1}H NMR spectroscopy and the initial spectral changes were indicative of pre-association on the oligosaccharide skeleton followed by covalent bond formation through substitution of the Pt-Cl bonds.[261] Changes in the ^{1}H signals of the Triplatin alkanediamine linkers mirrored those observed upon covalent Pt-DNA formation.[281] Similar to our findings with the substitution inert TriplatinNC, Triplatin also showed effective inhibition of physiologically critical HS functions, such as inhibition of growth factor recognition and activity of human (heparanase) and bacterial (heparinase) enzymes on HS.[260,261]

In order to understand the biological influence of Triplatin covalent interaction with HS sequences containing multiple sulfate and carboxylate groups, it is important to understand the kinetics of covalent binding at the monosaccharide level, just as early studies of individual purine and pyrimidine nucleic acid bases contributed to the understanding of the kinetics and thermodynamics of Pt-DNA interactions. [^{1}H, ^{15}N] NMR spectroscopy was used to study the aquation and subsequent covalent binding of ^{15}N labelled Triplatin with three D-glucosamine residues containing varied *O*-sulfate, *N*-sulfate or *N*- acetyl substitutions, which represent monosaccharide fragments present within the repeating disaccharide sequences of HS: GlcNS, GlcNAc(6S) and GlcNS(6S),Figure 1.25.[283]
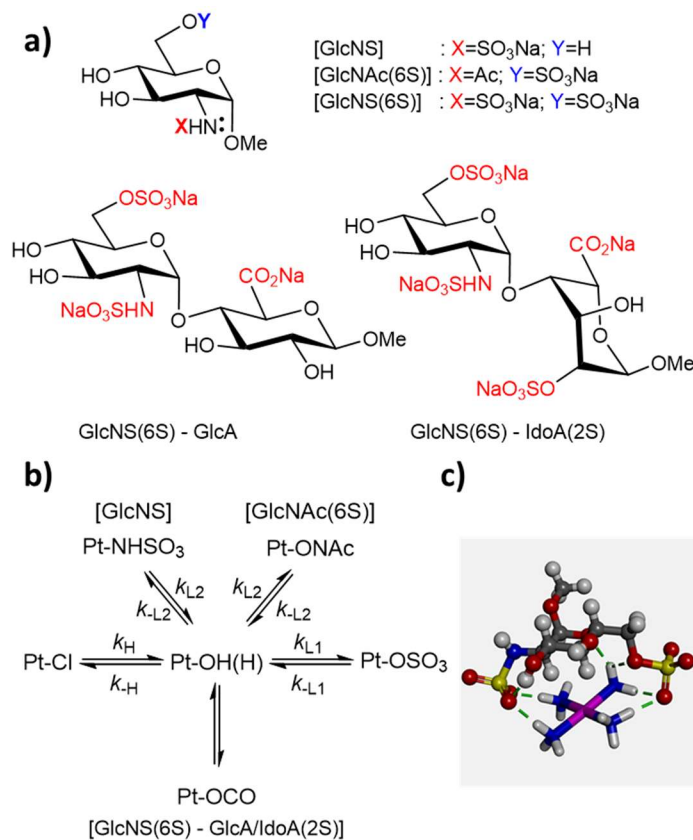
Figure 1.25: [^{1}H,^{15}N] NMR spectroscopy was used to study the aquation and subsequent covalent binding of Triplatin with three D-glucosamine residues containing varied O-sulfate, N-sulfate or N-acetyl substitutions which represent monosaccharide fragments present within the repeating disaccharide sequences of HS.[283] Rate constants obtained from the kinetic model are provided in Table 4. The DFT optimized models for the interaction of [Pt(NH₃)₄]²⁺ (representing the central {PtN₄}²⁺ of Triplatin) with GlcNS(6S) illustrates formation of sulfate clamps involving both 2-N- and 6-O-sulfate. The synthesized disaccharides GlcNS(6S)-GlcA and GlcNS(6S)-IdoA(2S) have also been used for kinetic studies of covalent binding by Triplatin. Reproduced from Gorle et al. 2021.[284]

Analysis of the rate constants for the formation of sulfato species in GlcNS and GlcNAc(6S) shows preferential binding by Triplatin to 2-*N*-sulfate compared to 6-*O*-sulfate, but a more rapid liberation (k_{L1} and k_{-L1} are both 3 times higher for 2-*N*-sulfate than 6-*O*-sulfate). Equilibrium conditions were achieved much more slowly than for disulfated GlcNS(6S) due to covalent binding also to the *N*- and *O*- donors of sulfamate and N-acetyl groups, respectively. These rate constants were 20–40 fold lower than binding to the 2-*N* or 6-*O*-sulfate, but the binding was less reversible. For disulfated GlcNS(6S), covalent binding by Triplatin with either of the two sulfates is significantly lower compared to that with either the 2-*N*-sulfate

of GlcNS or the 6-*O*-sulfate of GlcNAc(6S). Electrostatic interaction between the disulfated monosaccharide (2- charge) and the $\{PtN_4\}^{2+}$ linker, through sulfate clamp formation (Figure 1.25C) would limit covalent binding of the sulfate groups to the terminal Pt-OH$_2$ groups in the aquated Triplatin.[283] Preferential binding to 2-*N*-sulfate may have implications for mediation of PPC cellular accumulation. Notably, accumulation of Triplatin is diminished in the CHO-pgsE-606 mutant,[269] which is 3–5 fold defective in *N*-sulfotransferase activity, resulting in an approximate 2–3 fold reduction of the extent of *N*-sulfation.[285]

GlcNS(6S)-GlcA and GlcNS(6S)-IdoA(2S) were used to extend these studies to disaccharides (Figure 1.25) to include possible covalent interaction with the carboxylate group present at the C-5 position of the GlcA/IdoA residues. In similar [^{1}H,^{15}N] NMR studies, equilibrium conditions were achieved more slowly (65 h) compared to the monosaccharide GlcNAc(6S) (9 h), and carboxy-bound species were the major products at equilibrium.[284]

1.6.3 DNA versus GAG Affinity

For substitution-inert complexes the interactions with both DNA and GAGs will be mediated through hydrogen-bonding and electrostatic interactions. Given the highly anionic nature of both biomolecules, what are the relative affinities of a molecule such as TriplatinNC for DNA, heparin or HS? As mentioned, heparin is considered to have an average of 2.7 sulfate groups *per* disaccharide compared to that of two phosphate groups *per* base pair for DNA. Therefore a number of competitive binding assays were developed to answer this question and to complement the indirect and direct HS-PPC assays. Fluorescence polarization, ethidium bromide, and circular dichroism competition assays can compare the ability of heparin to compete with DNA for binding of charged metal complexes.

DNA Competition Assays. A fluorescence polarization assay measures the tumbling motion of molecules to describe binding events. Typically, the assay incorporates a small fluorescently labelled molecule, such as a DNA oligonucleotide, and an interacting molecule of similar or higher molecular weight, such as a protein. Upon binding, the rotation of the fluorescent molecule decreases, which is measured by emission fluorescence passing through parallel and perpendicular polarized light paths.[286] In this case, researchers examined whether changes in the rotation of a small fluorescently labelled DNA hairpin (DNA-Fl, 23nt, MW 7705) could be detected upon binding of the lower molecular weight metal complex, TriplatinNC (MW 1650). Reproducible saturation binding curves were established with the concentration of drug required for half-maximal binding determined to be EC$_{50}$ = 1.92 µM.[269] When a competitor ligand, for example the same unlabeled DNA hairpin or heparin, is titrated into the reactions, a predictable shift of the curve occurred as competitor ligand competed with labeled DNA for TriplatinNC binding with concomitant increases in apparent EC$_{50}$ values established. The fold-change of the apparent EC$_{50}$ values upon addition of either DNA or heparin were broadly similar, suggesting a similar affinity for TriplatinNC between low molecular weight heparin and DNA substrates. This assay can be extended to any compound – upon competition with heparin, the higher the fold-increase in EC$_{50}$ is a measure of higher heparin affinity, independent of the actual concentrations used for each compound to achieve half-maximal DNA binding. This was also true for other small molecules such as [Co(NH$_3$)$_6$]$^{3+}$; [CoCl(NH$_3$)$_5$]$^{2+}$ and [RuCl(NH$_3$)$_5$]$^{2+}$. While the presence of M-Cl bonds suggest the possibility of covalent binding, the nature of the assays developed, and the kinetic inertness of substitution on Co(III) and Ru(III) centers, suggests that any trends observed across the series of compounds will be most likely due to simple differences in charge. Compared to TriplatinNC, the EC$_{50}$ values of the metal-ammine compounds binding to DNA were

higher (TriplatinNC^{8+} < [Co(NH$_3$)$_6$]$^{3+}$ < [CoCl(NH$_3$)$_5$]$^{2+}$ < [Pt(NH$_3$)$_4$]$^{2+}$ ≈ [RuCl(NH$_3$)$_5$]$^{2+}$), indicating the expected lower binding affinity to DNA.

A second competition assay can be developed by adapting the well-known ethidium bromide (EtBr) fluorescence assay to measure DNA binding affinities of metal complexes. In this case, the fluorescence from intercalator binding to DNA is quenched when the intercalator is displaced upon TriplatinNC–DNA binding. Upon addition of increasing concentrations of heparin or FPX, TriplatinNC is sequestered and the nucleic acid now becomes available to bind the intercalator, with resultant increase in fluorescence (Figure 1.19B). The experiment allows us to define an EC$_{50}$ as the sequestration concentration of heparin required to restore 50% EtBr binding. Since the ability to displace EtBr from DNA differs amongst the complexes themselves, the concentration for any individual PPC ([PPC$_d$]) required to produce an initial 50% decrease in fluorescence was normalized as the modified EtBr-PPC-DNA fluorescence and 100% fluorescence was control EtBr-DNA. This allows a discussion of the EC$_{50}$ as a ratio index of [PPC$_d$]/[FPX$_r$]. The ratio index suggests that above 1, PPCs have more affinity for FPX than DNA, whereas below 1 PPCs have more affinity for DNA than FPX. Thus, AH44 has similar affinities for DNA as FPX with ratio index of 0.97, while MonoplatinNC, DiplatinNC, and TriplatinNC all had slightly higher affinities for FPX than DNA. It is clear that comparison of binding constants or affinities across techniques should be used with caution given the many parameters involved and the complexity across the experiments where the ITC system is a simple 2-species system, heparin-dye reporter assays are 3-species system, and the DNA comparison assays are 4-species systems. Given these caveats, these results are a testament to the relative accuracy of these methods for determining trends of coordination compounds interaction with heparin.

A second relevant example is the use of Ru-polypyridyl fluorophores to quantitate heparin and even detect heparinase activity in cells and determine its substrate specificity.[287,288] The fluorescence of [Ru(phen)$_2$(dppz-idzo)]$^{2+}$ is significantly enhanced in the presence of heparin and may be used to quantitate heparin in the range 0.01-4.87 U mL^{-1}. This "switch-on" assay for heparin, showed good fluorescence selectivity towards heparin over analogs, such as chondroitin sulfate (CS) or hyaluronic acid, which have lower charge density. Notably, the authors state that due to high DNA affinity, the assay should be used in DNA-free biological systems.[287]

The interplay between GAG and DNA affinity may be very relevant in dissecting biological activities of coordination complexes. HS may play a regulatory role by interacting with cationic molecules within the nucleus or by transport of cargo to the nucleus, as observed for cationic antibodies and the polyarginine-based cell-penetrating peptides.[289,290] Notably, GAGs are implicated in cellular uptake of anticancer bleomycin and CS and HS are targeted by the drug.[291] In this respect, this interplay is of broad significance and the analogies previously made between the phosphate clamp and the arginine fork binding mode on DNA become relevant. The interplay of HSPG-mediated cellular accumulation, high-affinity GAG binding, and inherent DNA affinity, needs to be unraveled to identify discrete mechanism of biological action.

Overall, for non-covalent interactions, broadly similar trends for metal-ammine compound interaction with heparin and DNA were observed. In the case of covalent binding, it is more difficult to assess relative strengths of binding when comparing the strength of Pt-O *versus* Pt-N bonds.

1.6.4 Functional consequences of metalloshielding: Anticancer activity

As noted in previous sections, interactions of PPCs have two main consequences with respect to cancer. Firstly, the HSPG-mediated cellular accumulation suggests an approach to selective accumulation into tumor cells and secondly, high-affinity GAG binding is predicted to have *functional* consequences in inhibition and modulation of the physiological response to GAGs. Metalloshielding – or sulfate cluster masking - by PPCs is an effective way to protect HS against the actions of its associated enzymes and growth factor proteins and to modulate the downstream functions of HS.[259–261,270,292]

Growth factors: TriplatinNC (and also Triplatin) inhibits fibroblasat growth factor (FGF) 2 binding to HS *in vitro* whereas cisplatin is completely ineffective.[261] TriplatinNC reduces FGF-2 induced accumulation of phospho-S6 ribosomal protein, a primary initiator of protein synthesis that is activated in response to FGFR phosphorylation and PI3K/Akt/mTOR signaling, in HCT116 cells. A reduction of pS6 is indicative of PPC inhibition of FGF/FGFR signaling. This result emphasizes the relevance of the metalloglycomics approach. FGF-FGFR signaling is modified by cation (Na^+, Ca^2)-heparin polysaccharides.[293] Further, the highly arginine-rich protamine inhibits the angiogenic activity of FGF-2, re-emphasizing our original PPC-polyarginine analogy, but in a different context beyond DNA binding. Metalloshielding prevents growth factor binding and growth factor receptor recruitment with consequent inhibition of FGF-2-induced downstream accumulation of pS6 ribosomal protein in human colon cancer HCT116 cells.[261] Cellular consequences include the inhibition of angiogenesis as measured by the rat aortic ring assay. The efficiency of this inhibition is equivalent to the prototypical oligosaccharide mimetic PI-88.[261]

Heparanase: In biophysical assays, metalloshielding is strong enough to prevent cleavage of FPX by both mammalian heparanase[261] and bacterial heparinase.[292] The enzymatic cleavage of FPX can be studied conveniently using ^{1}H NMR spectroscopy, by monitoring the FPX anomeric protons.[294] When bacterial *P. heparinus* heparinase II is utilised as the FPX cleaving enzyme, FPX is cleaved into a trisaccharide and a double-bond containing disaccharide (Figure 1.26).
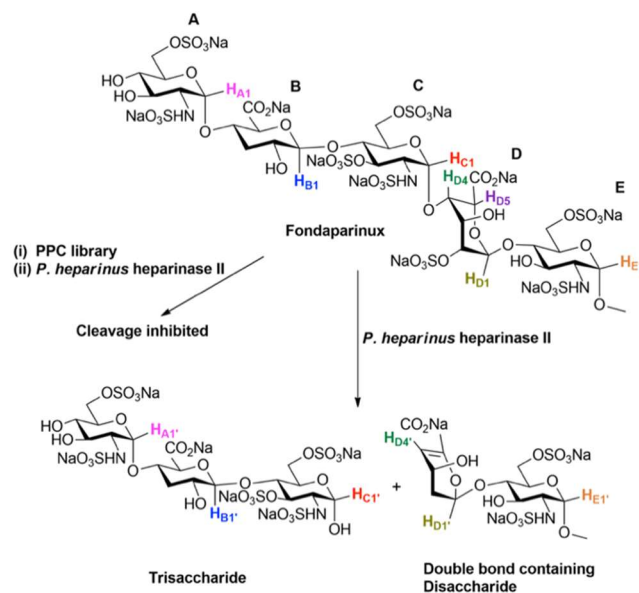
Figure 1.26: Structures of Fondaparinux and cleaved products by bacterial (P. heparinus) heparinase II. In the presence of PPCs, cleavage was completely inhibited. Reproduced from Gorle et al. 2018.[292]

Pre-incubation of FPX with 1 equivalent of TriplatinNC, and a library of other substitution-inert PPCs (Figure 1.27), prior to the addition of the enzyme, completely inhibited the cleavage, with the exception that the mononuclear 2+ charged Pt(tetraammine) complex showed minor cleavage products.[292] Overall, this study showed that PPC positive charge and its dispersion either through Pt coordination spheres or dangling amine groups is essential for the effective metalloshielding of the HS substrate. Notably, FPX cleavage inhibition was observed for the mononuclear complex, MonoplatinNC (4+), highlighting the importance of charge distribution, through dangling amines, for metalloshielding against the enzyme action.
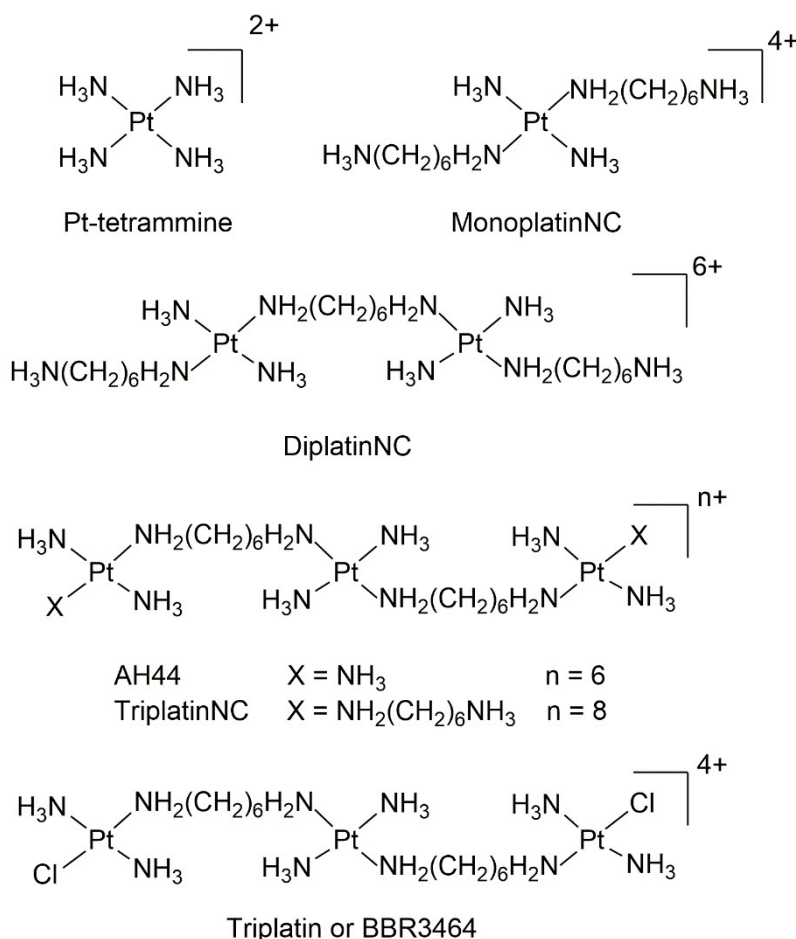
Figure 1.27: Structures of the glycan-interacting polynuclear platinum complexes (PPCs) including the clinically relevant anticancer agent Triplatin/BBR3464. Triplatin also participates in covalent-bond forming interactions through the displacement of Pt-Cl bond. Counterions omitted for clatiry.

The definitive end-point *in vivo* for inhibition of human heparanase enzyme activity and growth factor binding is inhibition of metastasis.[295] Inhibition of HS cleavage in cells has been confirmed recently for TriplatinNC in a cellular assay using triple-negative breast cancer (TNBC) MDA-MB-231 cells.[270] Further, inhibition of metastasis was observed in a syngeneic 4T1 mouse-derived model of TNBC breast cancer metastasis to the lung using a primary tumour resection or "mastectomy" model (Figure 1.28).[270] Pursuit of the consequences of GAG binding has led to this observation of meaningful antimetastatic activity of a non-covalent 8+ platinum complex, a long way from the paradigm of neutral cisplatin.
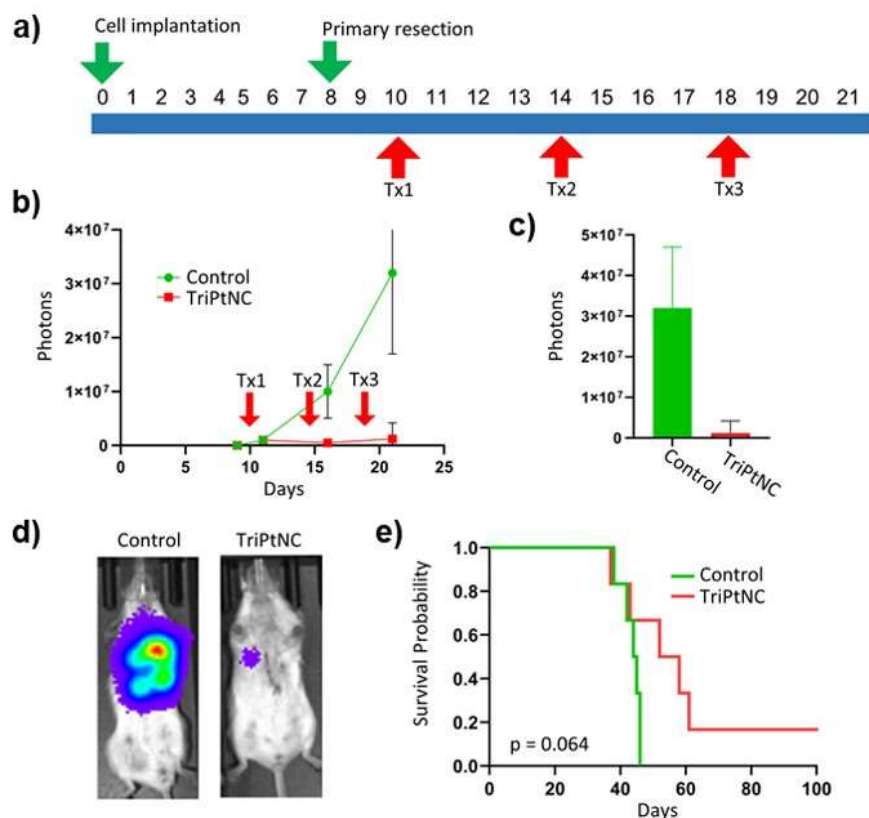
Figure 1.28: Inhibition of metastasis in a syngeneic 4T1 mouse model of triple-negative breast cancer by TriplatinNC. (a). Female BALB/c mice (immune-intact) with 4T1-luc2 murine breast cancer cells were orthotopic-implanted into the mammary fat pad on day 0 and primary tumour resections occurred on day 8. Mice were then treated via i.p. injections of TriplatinNC (25mg/kg), or saline with the dosing scheduled on days 10, 14, and 18 (Tx1, Tx2 and Tx3, respectively). (b),(c) After day 21, TriplatinNC reduced developing metastases. (d). TriplatinNC markedly reduced the tumour load (p = 0.055). E. TriplatinNC had prolonged survival with 1 mouse (out of 7) from treatment surviving over 100 days indicating a cure. Tumours were quantified by bioluminescence using the IVIS. Reproduced from Gorle et al. 2021.[270]

1.7 Antiviral hypothesis

The dual nature of PPCs may enable them to inhibit both DNA function and HS function. PPCs condense DNA, with higher potency than that of conventional DNA condensing agents, and aggregate transfer RNA.[296] TriplatinNC and AH44 were shown to inhibit DNA transcriptional activity and inhibit topoisomerase I-mediated relaxation of supercoiled DNA at lower concentrations than spermine.[296] While PPC-DNA binding inhibits DNA use and leads to apoptosis, we postulated that PPCs would "metalloshield" HS, meaning that PPC-HS binding would inhibit HS's various functions. Indeed, as noted above, PPCs inhibit the enzymatic cleavage of Fondaparinux both by bacterial heparinase and mammalian heparanase,[260,265] and PPC metalloshielding inhibits growth factor binding and growth factor receptor recruitment in human colon HCT116 cells.[261] In this thesis, we will examine the ability of PPCs to inhibit another function of HS, viral attachment, and expand this investigation to less-toxic cobalt complexes.

1.8 References

(1)   Bekerman, E.; Einav, S. Combating Emerging Viral Threats. *Science (80-.).* **2015**, *348* (1), 282–283. https://doi.org/10.1126/science.aaa3778.Combating.

(2)   Norwegian University of Science and Technology. DrugVirus.info.

(3)   Strasfeld, L.; Chou, S. Antiviral Drug Resistance: Mechanims and Clinical Implications. *Infect Dis Clin North Am* **2011**, *24* (2), 413–437. https://doi.org/10.1016/j.idc.2010.01.001.Antiviral.

(4)   Irwin, K. K.; Renzette, N.; Kowalik, T. F.; Jensen, J. D. Antiviral Drug Resistance as an Adaptive Process. *Virus Evol.* **2016**, *2* (1), vew014. https://doi.org/10.1093/ve/vew014.

(5)   Smith, K. M.; Machalaba, C. C.; Seifman, R.; Feferholtz, Y.; Karesh, W. B. Infectious Disease and Economics: The Case for Considering Multi-Sectoral Impacts. *One Heal.* **2019**, *7* (December 2018), 100080. https://doi.org/10.1016/j.onehlt.2018.100080.

(6)   Harrison, S. C. Viral Membrane Fusion. *Nat. Struct. Mol. Biol.* **2008**, *15* (7), 690–698. https://doi.org/10.1038/nsmb.1456.

(7)   Mercer, J.; Schelhaas, M.; Helenius, A. Virus Entry by Endocytosis. *Annu. Rev. Biochem.* **2010**, *79*, 803–833. https://doi.org/10.1146/annurev-biochem-060208-104626.

(8)   Dimitrov, D. S. Virus Entry: Molecular Mechanisms and Biomedical Applications. *Nat. Rev. Microbiol.* **2004**, *2*, 109–122. https://doi.org/10.1038/nrmicro817.

(9)   Kilcher, S.; Mercer, J. DNA Virus Uncoating. *Virology* **2015**, *479–480*, 578–590. https://doi.org/10.1016/j.virol.2015.01.024.

(10)   Rampersad, S.; Tennant, P. Chapter 3: Replication and Expression Strategies of Viruses. In *Viruses: Molecular Biology, Host Interactions, and Applications to Biotechnology*; Tennant, P., Fermin, G., Foster, J. E., Eds.; Academic Press Inc., 2018; pp 55–82. https://doi.org/10.1016/B978-0-12-811257-1.00003-6.

(11)   Clercq, E. De. Strategies in the Design of Antiviral Drugs. *Nat. Rev.* **2002**, *1* (January), 13–25. https://doi.org/10.1038/nrd703.

(12)   Clercq, E. D. E. In Search of a Selective Antiviral Chemotherapy. *Clin. Microbiol. Rev.* **1997**, *10* (4), 674–693.

(13)   Clercq, E. De. Discovery and Development of BVDU (Brivudin) as a Therapeutic for the Treatment of Herpes Zoster. *Biochem. Pharmacol.* **2004**, *68*, 2301–2315. https://doi.org/10.1016/j.bcp.2004.07.039.

(14)   Andrei, G.; Sienaert, R.; Mcguigan, C.; Clercq, E. De; Balzarini, J.; Snoeck, R. Susceptibilities of Several Clinical Varicella-Zoster Virus (VZV) Isolates and Drug-Resistant VZV Strains to Bicyclic Furano Pyrimidine Nucleosides. *Antimicrob. Agents Chemother.* **2005**, *49* (3), 1081–1086. https://doi.org/10.1128/AAC.49.3.1081.

(15)   Mayer, A. M. S.; Glaser, K. B.; Cuevas, C.; Jacobs, R. S.; Kem, W.; Little, R. D.; Mcintosh, J. M.; Newman, D. J.; Potts, B. C.; Shuster, D. E. The Odyssey of Marine Pharmaceuticals: A Current Pipeline Perspective. *Cell* **2010**, *31*, 255–265. https://doi.org/10.1016/j.tips.2010.02.005.

(16)   Tenney, D. J.; Rose, R. E.; Baldick, C. J.; Pokornowski, K. A.; Eggers, B. J.; Fang, J.; Wichroski, M. J.; Xu, D.; Yang, J.; Wilber, R. B.; Colonno, R. J. Long-Term Monitoring Shows Hepatitis B Virus Resistance to Entecavir in Nucleoside-Naive Patients Is Rare Through 5 Years of Therapy. *Hepatology* **2009**, *49* (5), 1503–1514. https://doi.org/10.1002/hep.22841.

(17)   Med, A. I. Entecavir Surprise. *N. Engl. J. Med.* **2007**, *256* (25), 2641–2643.

(18)   Lai, C.-L.; Gane, E.; Liaw, Y.; Hsu, C.-W.; Thongsawat, S.; Wang, Y.; Chen, Y.; Heathcote, E. J.; Rasenack, J.; Bzowej, N.; Naoumov, N. V; Bisceglie, A. M. Di; Zeuzem, S.; Moon, Y. M.; Goodman, Z.; Chao, G.; Constance, B. F.; Brown, N. A. Telbivudine versus Lamivudine in Patients with Chronic Hepatitis B. *N. Engl. J. Med.* **2007**, *357*, 2576–2588.

(19)   Hou, J.; Yin, Y.; Xu, D.; Tan, D.; Niu, J.; Zhou, X.; Wang, Y.; Zhu, L.; He, Y.; Ren, H.; Wan, M.; Chen,

C.; Wu, S.; Chen, Y.; Xu, J.; Wang, Q.; Wei, L.; Chao, G.; Constance, B. F.; Harb, G.; Brown, N. A.; Jia, J. Telbivudine Versus Lamivudine in Chinese Patients with Chronic Hepatitis B: Results at 1 Year of a Randomized, Double-Blind Trial. *Hepatology* **2008**, *47* (2), 447–454. https://doi.org/10.1002/hep.22075.

(20) Lai, C. L.; Leung, N.; Teo, E. N. G. K.; Tong, M.; Wong, F.; Hann, H.-W.; Han, S.; Poynard, T.; Myers, M.; Chao, G.; Lloyd, D.; Brown, N. A.; Group, T. P. I. I. A 1-Year Trial of Telbivudine, Lamivudine, and the Combination in Patients With Hepatitis B e Antigen—Positive Chronic Hepatitis B. *Gastroenterology* **2005**, *129*, 528–536. https://doi.org/10.1053/j.gastro.2005.05.053.

(21) De Clercq, E.; Li, G. Approved Antiviral Drugs over the Past 50 Years. *Clin. Microbiol. Rev.* **2016**, *29* (3), 695–747. https://doi.org/10.1128/CMR.00102-15.

(22) Lok, A. S.-F. Hepatitis B: 50 Years after the Discovery of Australia Antigen. *J. Viral Hepat.* **2016**, *23*, 5–14. https://doi.org/10.1111/jvh.12444.

(23) Helgstrand, E.; Eriksson, B.; Johansson, N. G.; Lannero, B.; Larsson, A.; Misiorny, A.; Noren, J. O.; Sjoberg, B.; Stenberg, K.; Stening, G.; Stridh, S.; Oberg, B. Trisodium Phosphonoformate, a New Antiviral Compound. *Science (80-.).* **1978**, *201*, 819–822.

(24) Tchesnokov, E. P.; Gilbert, C.; Boivin, G.; Gotte, M. Role of Helix P of the Human Cytomegalovirus DNA Polymerase in Resistance and Hypersusceptibility to the Antiviral Drug Foscarnet. *J. Virol.* **2006**, *80* (3), 1440–1450. https://doi.org/10.1128/JVI.80.3.1440.

(25) Oberg, B. Antiviral Effects of Phosphonoformate (PFA, Foscarnet Sodium). *Pharmacol. Ther.* **1989**, *40* (2), 213–285.

(26) Minces, L. R.; Nguyen, M. H.; Mitsani, D.; Shields, R. K.; Kwak, E. J.; Silveira, F. P.; Abdel-Massih, R.; Pilewski, J. M.; Crespo, M. M.; Bermudez, C.; Bhama, J. K.; Toyoda, Y.; Clancy, C. J. Ganciclovir-Resistant Cytomegalovirus Infections among Lung Transplant Recipients Are Associated with Poor Outcomes despite Treatment with Foscarnet-Containing Regimens. *Antimicrob. Agents Chemother.* **2014**, *58* (1), 128–135. https://doi.org/10.1128/AAC.00561-13.

(27) Mitsuya, H.; Weinhold, K. J.; Furman, P. A.; St. Clair, M. H.; Lehrman, S. N.; Gallo, R. C.; Bolognesit, D.; Barry, D. W.; Broder, S. 3'-Azido-3'-Deoxythymidine (BW A509U): An Antiviral Agent That Inhibits the Infectivity and Cytopathic Effect of Human T-Lymphotropic Virus Type III/Lymphadenopathy-Associated Virus in Vitro. *Proceeding Soc. Exp. Biol. Med.* **1985**, *82*, 7096–7100.

(28) Furmant, P. A.; Fyfe, J. A.; St. Clair, M. H.; Weinhold, K.; Rideout, J. L.; Freeman, G. A.; Lehrmant, S. N.; Bolognesi, D. P.; Broder, S.; Mitsuya, H.; Barry, D. W. Phosphorylation of 3'-Azido-3'-Deoxythymidine and Selective Interaction of the 5'-Triphosphate with Human Immunodeficiency Virus Reverse Transcriptase. *Proc. Natl. Acad. Sci. U. S. A.* **1986**, *83*, 8333–8337.

(29) Wensing, A. M.; Calvez, V.; Gunthard, H. F.; Johnson, V. A.; Paredes, R.; Pillay, D.; Shafer, R. W.; Richman, D. D. 2015 Update of the Drug Resistance Mutations in HIV-1. *Top. Antivir. Med.* **2015**, *23* (4), 132–133.

(30) Arts, E. J.; Hazuda, D. J. HIV-1 Antiretroviral Drug Therapy. *Cold Spring Harb Perspect Med* **2012**, *2*, a007161.

(31) Charpentier, C.; Camacho, R.; Ruelle, J.; Eberle, J.; Gurtler, L.; Pironti, A.; Sturmer, M.; Brun-Vezinet, F.; Kaiser, R.; Descamps, D.; Obermeier, M. HIV-2EU — Supporting Resistance Interpretation in Europe: An Update. *Clin. Infect. Dis.* **2015**, *61*, 1346–1347. https://doi.org/10.1093/cid/civ572.

(32) Montessori, V.; Press, N.; Harris, M.; Akagi, L.; Montaner, J. S. G. Adverse Effects of Antiretroviral Therapy for HIV Infection. *CMAJ* **2004**, *170* (2), 229–238.

(33) Tantillo, C.; Ding, J.; Jacobo-Molina, A.; Nanni, R. G.; Boyer, P. L.; Hughes, S. H.; Pauwels, R.; Andries, K.; Janssen, P. A. J.; Arnold, E. Locations of Anti-AIDS Drug Binding Sites and Resistance Mutations in the Three-Dimensional Structure of HIV-1 Reverse Transcriptase: Implications for

Mechanisms of Drug Inhibition and Resistance. *J. Mol. Biol.* **1994**, *243*, 369–387.

(34)   Ding, J.; Das, K.; Moereels, H.; Koymans, L.; Andries, K.; Janssen, P. A. J.; Hughes, S. H.; Arnold, E. Structure of HIV-1 RT/TIBO R 86183 Complex Reveals Similarity in the Binding of Diverse Nonnucleoside Inhibitors. *Nat. Struct. Biol.* **1995**, *2* (5), 407–415.

(35)   Das, K.; Ding, J.; Hsiou, Y.; Clark Jr, A. D.; Moereels, H.; Koymans, L.; Andries, K.; Pauwels, R.; Janssen, P. A. J.; Boyer, P. L.; Clark, P.; Smith Jr, R. H.; Smith, M. B. K.; Michejda, C. J.; Hughes, S. H.; Arnold, E. Crystal Structures of 8-Cl and 9-Cl TIBO Complexed with Wild-Type HIV-1 RT and 8-Cl TIBO Complexed with the Tyr181Cys HIV-1 RT Drug-Resistant Mutant. *J. Mol. Biol.* **1996**, *264*, 1085–1100.

(36)   Cruz, O. J. D.; Uckun, F. M. Dawn of Non-Nucleoside Inhibitor-Based Anti-HIV Microbicides. *J. Antimicrob. Chemother.* **2006**, *57*, 411–423. https://doi.org/10.1093/jac/dki464.

(37)   Tuaillon, E.; Gueudin, M.; Lemee, V.; Gueit, I.; Roques, P.; Corrigan, G. E.; Plantier, J.-C.; Simon, F.; Braun, J. Phenotypic Susceptibility to Nonnucleoside Inhibitors of Virion-Associated Reverse Transcriptase From Different HIV Types and Groups. *J. Acquir. Immune Defic. Syndr.* **2004**, *37* (5), 1543–1549.

(38)   De Clercq, E. Dancing with Chemical Formulae of Antivirals: A Panoramic View (Part 2). *Biochem. Pharmacol.* **2013**, *86* (10), 1397–1410. https://doi.org/10.1016/j.bcp.2013.09.010.

(39)   Wensing, A. M. J.; van Maarseveen, N. M.; Nijhuis, M. Fifteen Years of HIV Protease Inhibitors: Raising the Barrier to Resistance. *Antiviral Res.* **2010**, *85*, 59–74. https://doi.org/10.1016/j.antiviral.2009.10.003.

(40)   François, C.; Hance, A. J. HIV Drug Resistance. *N. Engl. J. Med.* **2004**, *350*, 1023–1035.

(41)   Messina, J. P.; Humphreys, I.; Flaxman, A.; Brown, A.; Cooke, G. S.; Pybus, O. G.; Barnes, E. Global Distribution and Prevalence of Hepatitis C Virus Genotypes. *Hepatology* **2014**, No. Ec 21803, 77–87. https://doi.org/10.1002/hep.27259.

(42)   Hazuda, D. J.; Felock, P.; Witmer, M.; Wolfe, A.; Stillmock, K.; Grobler, J. A.; Espeseth, A.; Gabryelski, L.; Schleif, W.; Blau, C.; Miller, M. D. Inhibitors of Strand Transfer That Prevent Integration and Inhibit HIV-1 Replication in Cells. *Science (80-.).* **2000**, *287*, 646–651.

(43)   Sato, M.; Motomura, T.; Aramaki, H.; Matsuda, T.; Yamashita, M.; Ito, Y.; Kawakami, H.; Matsuzaki, Y.; Watanabe, W.; Yamataka, K.; Ikeda, S.; Kodama, E.; Matsuoka, M.; Shinkai, H. Novel HIV-1 Integrase Inhibitors Derived from Quinolone Antibiotics. *J. Med. Chem.* **2006**, *49*, 1506–1508.

(44)   Messiaen, P.; Wensing, A. M. J.; Fun, A.; Nijhuis, M.; Brusselaers, N.; Vandekerckhova, L. Clinical Use of HIV Integrase Inhibitors: A Systematic Review and Meta-Analysis. *PLoS One* **2013**, *8* (1), e52562. https://doi.org/10.1371/journal.pone.0052562.

(45)   Matthews, T.; Salgo, M.; Greenberg, M.; Chung, J.; DeMasi, R.; Bolognesi, D. Enfuvirtide: The First Therapy to Inhibit the Entry of HIV-1 into Host CD4 Lymphocytes. *Drug Discov.* **2004**, *3* (March), 215–225. https://doi.org/10.1038/nrd1331.

(46)   Kuritzkes, D. R. HIV-1 Entry Inhibitors: An Overview. *Curr. Opin. HIV AIDS* **2009**, *4* (2), 82–87. https://doi.org/10.1097/COH.0b013e328322402e.

(47)   Dolin, R. A New Class of Anti-HIV Therapy and New Challenges. *N. Engl. J. Med.* **2008**, *359*, 1509–1511.

(48)   Raymond, S.; Maillard, A.; Amiel, C.; Peytavin, G.; Trabaud, M. A.; Desbois, D.; Bellecave, P.; Delaugerre, C.; Soulie, C.; Marcelin, A. G.; Descamps, D.; Izopet, J.; Reigadas, S.; Bellecave, P.; Pinson-Recordon, P.; Fleury, H.; Masquelier, B.; Signori-Schmuck, A.; Morand, P.; Bocket, L.; Mouna, L.; André, P.; Tardy, J. C.; Trabaud, M. A.; Descamps, D.; Charpentier, C.; Peytavin, G.; Brun-Vézinet, F.; Haim-Boukobza, S.; Roques, A. M.; Soulié, C.; Lambert-Niclot, S.; Malet, I.; Wirden, M.; Fourati, S.; Marcelin, A. G.; Calvez, V.; Flandre, P.; Assoumou, L.; Costagliola, D.; Morand-Joubert, L.; Delaugerre, C.; Schneider, V.; Amiel, C.; Giraudeau, G.; Maillard, A.; Nicot, F.;

Izopet, J. Virological Failure of Patients on Maraviroc-Based Antiretroviral Therapy. *J. Antimicrob. Chemother.* **2014**, *70* (6), 1858–1864. https://doi.org/10.1093/jac/dkv026.

(49) Robinson, R. F.; Nahata, M. C. Respiratory Syncytial Virus (RSV) Immune Globulin and Palivizumab for Prevention of RSV Infection. *Am. J. Heal. Pharm.* **2000**, *57* (3), 259–267. https://doi.org/10.1093/ajhp/57.3.259.

(50) American Academy of Pediatrics Committee on Infectious Diseases, A. A. of P. B. G. C. Updated Guidance for Palivizumab Prophylaxis Among Infants and Young Children at Increased Risk of Hospitalization for Respiratory Syncytial Virus Infection. *Pediatrics* **2014**, *134* (2), 415–420.

(51) Katz, D. H.; Marcelletti, J. F.; Khalil, M. H.; Pope, L. E.; Katz, L. R. Antiviral Activity of 1-Docosanol, an Inhibitor of Lipid-Enveloped Viruses Including Herpes Simplex. *Proc. Natl. Acad. Sci. U. S. A.* **1991**, *88* (23), 10825–10829. https://doi.org/10.1073/pnas.88.23.10825.

(52) Sacks, S. L.; Thisted, R. A.; Jones, T. M.; Barbarash, R. A.; Mikolich, D. J.; Ruoff, G. E.; Jorizzo, J. L.; Gunnill, L. B.; Katz, D. H.; Khalil, M. H.; Morrow, P. R.; Yakatan, G. J.; Pope, L. E.; Berg, J. E. Clinical Efficacy of Topical Docosanol 10% Cream for Herpes Simplex Labialis: A Multicenter, Randomized, Placebo-Controlled Trial. *J. Am. Acad. Dermatol.* **2001**, *45* (2), P222-230.

(53) Sullivan, V.; Talarico, C. L.; Stanat, S. C.; Davis, M.; Coen, D. M.; Biron, K. K. A Protein Kinase Homologue Controls Phosphorylation of Ganciclovir in Human Cytomegalovirus-Infected Cells. *Nature* **1992**, *358*, 162–164.

(54) Hodge, R. A. V. Famciclovir and Penciclovir. The Mode of Action of Famciclovir Including Its Conversion to Penciclovir. *Antivir. Chem. Chemother.* **1993**, *4* (2), 67–84. https://doi.org/10.1177/095632029300400201.

(55) Elion, G. B.; Furman, P. A.; Fyfe, J. A.; Miranda, P. D. E.; Beauchampt, L.; Schaeffert, H. J. Selectivity of Action of an Antiherpetic Agent, 9-(2-Hydroxyethoxymethyl)Guanine. *Proc. Natl. Acad. Sci. U. S. A.* **1977**, *74* (12), 5716–5720.

(56) De Clercq, E. Antiviral Drug Discovery: Ten More Compounds, and Ten More Stories (Part B). *Med. Res. Rev.* **2009**, *29* (4), 571–610. https://doi.org/10.1002/med.

(57) De Clercq, E.; Holý, A.; Rosenberg, I.; Sakuma, T.; Balzarini, J.; Maudgal, P. C. A Novel Selective Broad-Spectrum Anti-DNA Virus Agent. *Lett. to Nat.* **1986**, *323*, 464–467. https://doi.org/10.1038/323464a0.

(58) De Clercq, E.; Holý, A. Case History: Acyclic Nucleoside Phosphonates: A Key Class of Antiviral Drugs. *Nat. Rev. Drug Discov.* **2005**, *4*, 928–940. https://doi.org/10.1038/nrd1877.

(59) De Clercq, E. The Acyclic Nucleoside Phosphonates (ANPs): Antonín Holý's Legacy. *Med. Res. Rev.* **2008**, *33* (6), 1278–1303. https://doi.org/10.1002/med.

(60) Ray, A. S.; Fordyce, M. W.; Hitchcock, M. J. M. Tenofovir Alafenamide: A Novel Prodrug of Tenofovir for the Treatment of Human Immunodeficiency Virus. *Antiviral Res.* **2016**, *125*, 63–70. https://doi.org/10.1016/j.antiviral.2015.11.009.

(61) Wyatt, C.; Baeten, J. M. Tenofovir Alafenamide for HIV Infection: Is Less More? *Lancet* **2015**, *385*, 2559–2560. https://doi.org/10.1016/S0140-6736(15)60725-5.

(62) Nettles, J. H.; Stanton, R. A.; Broyde, J.; Amblard, F.; Zhang, H.; Zhou, L.; Shi, J.; McBrayer, T. R.; Whitaker, T.; Coats, S. J.; Kohler, J. J.; Schinazi, R. F. Asymmetric Binding to NS5A by Daclatasvir (BMS-790052) and Analogs Suggests Two Novel Modes of HCV Inhibition. *J. Med. Chem.* **2014**, *57*, 10031–10043. https://doi.org/10.1021/jm501291c.

(63) Liu, D.; Ji, J.; Ndongwe, T. P.; Michailidis, E.; Rice, C. M.; Ralston, R.; Sarafianos, S. G. Fast Hepatitis C Virus RNA Elimination and NS5A Redistribution by NS5A Inhibitors Studied by a Multiplex Assay Approach. *Antimicrob. Agents Chemother.* **2015**, *59* (6), 3482–3492. https://doi.org/10.1128/AAC.00223-15.

(64) Berger, C.; Romero-Brey, I.; Radujkovic, D.; Terreux, R.; Zayas, M.; Paul, D.; Harak, C.; Hoppe, S.; Gao, M.; Penin, F.; Lohmann, V.; Bartenschlager, R. Daclatasvir-like Inhibitors of NS5A Block Early

Biogenesis of Hepatitis C Virus-Induced Membranous Replication Factories, Independent of RNA Replication. *Gastroenterology* **2014**, *147*, 1094–1105. https://doi.org/10.1053/j.gastro.2014.07.019.

(65)　De Clercq, E. Current Race in the Development of DAAs (Direct-Acting Antivirals) against HCV. *Biochem. Pharmacol.* **2014**, *89*, 441–452. https://doi.org/10.1016/j.bcp.2014.04.005.

(66)　De Clercq, E. Development of Antiviral Drugs for the Treatment of Hepatitis C at an Accelerating Pace. *Rev. Med. Virol.* **2015**, *25*, 254–267. https://doi.org/10.1002/rmv.

(67)　Liang, R.; Li, H.; Swanson, J. M. J.; Voth, G. A. Multiscale Simulation Reveals a Multifaceted Mechanism of Proton Permeation through the Influenza A M2 Proton Channel. *Proc. Natl. Acad. Sci. U. S. A.* **2014**, *111* (26), 9396–9401. https://doi.org/10.1073/pnas.1401997111.

(68)　Cady, S. D.; Mishanina, T. V.; Hong, M. Structure of Amantadine-Bound M2 Transmembrane Peptide of Influenza A in Lipid Bilayers from Magic-Angle-Spinning Solid-State NMR: The Role of Ser31 in Amantadine Binding. *J. Mol. Biol.* **2009**, *385*, 1127–1141. https://doi.org/10.1016/j.jmb.2008.11.022.

(69)　Razonable, R. R. Antiviral Drugs for Viruses Other than Human Immunodeficiency Virus. *Mayo Clin. Proc.* **2011**, *86* (10), 1009–1026. https://doi.org/10.4065/mcp.2011.0309.

(70)　Russell, R. J.; Haire, L. F.; Stevens, D. J.; Collins, P. J.; Lin, Y. P.; Blackburn, G. M.; Hay, A. J.; Gamblin, S. J.; Skehel, J. J. The Structure of H5N1 Avian Influenza Neuraminidase Suggests New Opportunities for Drug Design. *Nature* **2006**, *443*, 45–49. https://doi.org/10.1038/nature05114.

(71)　Sidwell, R. W.; Huffman, J. H.; Khare, G. P.; Allen, L. B.; Witkowski, J. T.; Robins, R. K. Broad-Spectrum Antiviral Activity of Virazole: 1-β-D-Ribofuranosyl-1,2 ,4-Triazole-3-Carboxamide. *Science (80-.).* **1972**, *177* (4050), 705–706.

(72)　Wray, S. K.; Gilbert, B. E.; Noall, M. W.; Knight, V. Mode of Action of Ribavirin: Effect of Nucleotide Pool Alterations on Influenza Virus Ribonucleoprotein Synthesis. *Antiviral Res.* **1985**, No. 5, 29–37.

(73)　Kiso, M.; Takahashi, K.; Sakai-Tagawa, Y.; Shinya, K.; Sakabe, S.; Le, Q. M.; Ozawa, M.; Furuta, Y.; Kawaoka, Y. T-705 (Favipiravir) Activity against Lethal H5N1 Influenza A Viruses. *Proc. Natl. Acad. Sci. U. S. A.* **2010**, *107* (2), 882–887. https://doi.org/10.1073/pnas.0909603107.

(74)　De Clercq, E. Highlights in Antiviral Drug Research: Antivirals at the Horizon. *Med. Res. Rev.* **2013**, *33* (6), 1215–1248. https://doi.org/10.1002/med.

(75)　Furuta, Y.; Takahashi, K.; Kuno-Maekawa, M.; Sangawa, H.; Uehara, S.; Kozaki, K.; Nomura, N.; Egawa, H.; Shiraki, K. Mechanism of Action of T-705 against Influenza Virus. *Antimicrob. Agents Chemother.* **2005**, *49* (3), 981–986. https://doi.org/10.1128/AAC.49.3.981-986.2005.

(76)　Smee, D. F.; Hurst, B. L.; Egawa, H.; Takahashi, K.; Kadota, T.; Furuta, Y. Intracellular Metabolism of Favipiravir (T-705) in Uninfected and Influenza A (H5N1) Virus-Infected Cells. *J. Antimicrob. Chemother.* **2009**, *64*, 741–746. https://doi.org/10.1093/jac/dkp274.

(77)　Goldner, T.; Hewlett, G.; Ettischer, N.; Ruebsamen-schaeff, H.; Zimmermann, H.; Lischka, P. The Novel Anticytomegalovirus Compound AIC246 (Letermovir) Inhibits Human Cytomegalovirus Replication through a Specific Antiviral Mechanism That Involves the Viral Terminase. *J. Virol.* **2011**, *85* (20), 10884–10893. https://doi.org/10.1128/JVI.05265-11.

(78)　Piret, J.; Boivin, G. Clinical Development of Letermovir and Maribavir: Overview of Human Cytomegalovirus Drug Resistance. *Antiviral Res.* **2019**, *163* (January), 91–105. https://doi.org/10.1016/j.antiviral.2019.01.011.

(79)　Magden, J.; Kaariainen, L.; Ahola, T. Inhibitors of Virus Replication: Recent Developments and Prospects. *Appl Microbiol Biotechnol* **2005**, *66*, 612–621. https://doi.org/10.1007/s00253-004-1783-3.

(80)　Gandhi, N. S.; Mancera, R. L. The Structure of Glycosaminoglycans and Their Interactions with Proteins. *Chem. Biol. Drug Des.* **2008**, *72* (6), 455–482. https://doi.org/10.1111/j.1747-

0285.2008.00741.x.

(81)   Caterson, B.; Melrose, J. Keratan Sulfate , a Complex Glycosaminoglycan with Unique Functional Capability. **2018**, *28* (4), 182–206. https://doi.org/10.1093/glycob/cwy003.

(82)   Aquino, R. S.; Park, P. W. Glycosaminoglycans and Infection. *Front. Biosci.* **2016**, *21*, 1260–1277.

(83)   Cagno, V.; Tseligka, E. D.; Jones, S. T.; Tapparel, C. Heparan Sulfate Proteoglycans and Viral Attachment: True Receptors or Adaptation Bias? *Viruses* **2019**, *11* (7), 1–24. https://doi.org/10.3390/v11070596.

(84)   Hasan, M. H.; Parmar, R.; Liang, Q.; Qiu, H.; Tiwari, V.; Sharp, J. S.; Wang, L.; Tandon, R. The Degree of Polymerization and Sulfation Patterns in Heparan Sulfate Are Critical Determinants of Cytomegalovirus Infectivity. *bioRxiv* **2019**, *prepeint*.

(85)   Liu, L.; Chopra, P.; Li, X.; Wolfert, M. A.; Tompkins, S. M.; Boons, G. J. SARS-CoV-2 Spike Protein Binds Heparan Sulfate in a Length- and Sequence-Dependent Manner. *bioRxiv* **2020**, *preprint*, 1–15.

(86)   Kaltenbach, D. D.; Jaishankar, D.; Hao, M.; Beer, J. C.; Volin, M. V.; Desai, U. R.; Tiwari, V. Sulfotransferase and Heparanase: Remodeling Engines in Promoting Virus Infection and Disease Development. *Front. Pharmacol.* **2018**, *9* (NOV), 1–17. https://doi.org/10.3389/fphar.2018.01315.

(87)   Milewska, A.; Zarebski, M.; Nowak, P.; Stozek, K.; Potempa, J. Human Coronavirus NL63 Utilizes Heparan Sulfate Proteoglycans for Attachment to Target Cells. *J. Virol.* **2014**, *88* (22), 13221–13230. https://doi.org/10.1128/JVI.02078-14.

(88)   Xiao, Y.; Dong, X.; Chen, Y. Neutralizing Antibodies: Mechanism of Neutralization and Protective Activity against HIV-1. *Immunol. Res.* **2002**, *25* (3), 193–200.

(89)   Gerber, P.; Dutcher, J. D.; Adams, E. V.; Sherman, H.; Sherman, J. H. Protective Effect of Seaweed Extracts for Chicken Embryos Infected with Influenza B or Mumps Virus. *Exp. Biol. Med.* **1958**, *99* (3), 590–593.

(90)   Baba, M.; Snoeck, R.; Pauwels, R.; De Clercq, E. Sulfated Polysaccharides Are Potent and Selective Inhibitors of Various Enveloped Viruses, Including Herpes Simplex Virus, Cytomegalovirus, Vesicular Stomatitis Virus, and Human Immunodeficiency Virus. *Antimicrob. Agents Chemother.* **1988**, *32* (11), 1742–1745. https://doi.org/10.1128/AAC.32.11.1742.

(91)   Guo, J.; Skinner, G. W.; Harcum, W. W.; Barnum, P. E. Pharmaceutical Applications of Naturally Occurring Water-Soluble Polymers. *Pharm. Sci. Technol. Today* **1998**, *1* (6).

(92)   Lahaye, M. Developments on Gelling Algal Galactans, Their Structure and Physico-Chemistry. *J. Appl. Phycol.* **2001**, *13*, 173–184.

(93)   Vera, J.; Castro, J.; Gonzalez, A.; Moenne, A. Seaweed Polysaccharides and Derived Oligosaccharides Stimulate Defense Responses and Protection Against Pathogens in Plants. *Mar. Drugs* **2011**, *9*, 2514–2525. https://doi.org/10.3390/md9122514.

(94)   Buck, C. B.; Thompson, C. D.; Roberts, J. N.; Muller, M.; Lowy, D. R.; Schiller, J. T. Carrageenan Is a Potent Inhibitor of Papillomavirus Infection. *PLoS Pathog.* **2006**, *2* (7), e69. https://doi.org/10.1371/journal.ppat.0020069.

(95)   Zeitlin, L.; Whaley, K. J.; Hegarty, T. A.; Moench, T. R.; Cone, R. A. Tests of Vaginal Microbicides in the Mouse Gential Herpes Model. *Contraception* **1997**, *56* (6), 329–335.

(96)   Gonzalez, M. E.; Alarcn, B.; Carrasco, L. Polysaccharides as Antiviral Agents: Antiviral Activity of Carrageenan. *Antimicrob. Agents Chemother.* **1987**, *31* (9), 1388–1393.

(97)   Carlucci, M. J.; Scolaro, L. A.; Damonte, E. B. Herpes Simplex Virus Type 1 Variants Arising After Selection With an Antiviral Carrageenan: Lack of Correlation Between Drug Susceptibility and Syn Phenotype. *J. Med. Virol.* **2002**, *98*, 92–98. https://doi.org/10.1002/jmv.10174.

(98)   Carlucci, M. J.; Pujol, C. A.; Ciancia, M.; Noseda, M. D.; Matulewicz, M. C.; Damonte, E. B.; Cerezo, A. S. Antiherpetic and Anticoagulant Properties of Carrageenans from the Red Seaweed Gigartina

Skottsbergii and Their Cyclized Derivatives: Correlation between Structure and Biological Activity. *Int. J. Biol. Marcomolecules* **1997**, *20*, 97–105.

(99)   Carlucci, M. J.; Scolaro, L. A.; Noseda, M. D.; Cerezo, A. S.; Damonte, E. B. Protective Effect of a Natural Carrageenan on Genital Herpes Simplex Virus Infection in Mice. *Antiviral Res.* **2004**, *64*, 137–141. https://doi.org/10.1016/j.antiviral.2004.07.001.

(100)   de S.F-tischer, P. C.; Talarico, L. B.; Noseda, M. D.; Guimaraes, S. M. P. B.; Damonte, E. B.; Duarte, M. E. R. Chemical Structure and Antiviral Activity of Carrageenans from Meristiella Gelidium against Herpes Simplex and Dengue Virus. *Carbohydr. Polym.* **2006**, *63*, 459–465. https://doi.org/10.1016/j.carbpol.2005.09.020.

(101)   Zacharopoulos, V. R.; Phillips, D. M. Vaginal Formulations of Carrageenan Protect Mice from Herpes Simplex Virus Infection. *Clin. Diagn. Lab. Immunol.* **1997**, *4* (4), 465–468.

(102)   Grassauer, A.; Weinmuellner, R.; Meier, C.; Pretsch, A.; Prieschl-grassauer, E.; Unger, H. Iota-Carrageenan Is a Potent Inhibitor of Rhinovirus Infection. *Virol. J.* **2008**, *5*, 107. https://doi.org/10.1186/1743-422X-5-107.

(103)   Talarico, L. B.; Damonte, E. B. Interference in Dengue Virus Adsorption and Uncoating by Carrageenans. *Virology* **2007**, *363*, 473–485. https://doi.org/10.1016/j.virol.2007.01.043.

(104)   Talarico, L. B.; Noseda, M. D.; Ducatti, D. R. B.; Duarte, M. E. R.; Damonte, E. B. Differential Inhibition of Dengue Virus Infection in Mammalian and Mosquito Cells by Iota-Carrageenan. *J. Gen. Virol.* **2011**, *92*, 1332–1342. https://doi.org/10.1099/vir.0.028522-0.

(105)   Tang, F.; Chen, F.; Li, F. Preparation and Potential in Vivo Anti-influenza Virus Activity of Low Molecular-weight K-carrageenans and Their Derivatives. *J. Appl. Polym. Sci.* **2013**, *127* (3), 2110–2115.

(106)   Yamada, T.; Ogamo, A.; Saito, T.; Watanabe, J.; Uchiyama, H.; Nakagawa, Y. Preparation and Anti-HIV Activity of Low- Molecular-Weight Carrageenans and Their Sulfated Derivatives. *Carbohydr. Polym.* **1997**, *32*, 51–55.

(107)   Sanderson, K. Anti-HIV Gel Trial Fails. *Nature* **2009**. https://doi.org/https://doi.org/10.1038/news.2008.609.

(108)   Marais, D.; Gawarecki, D.; Allan, B.; Ahmed, K.; Altini, L.; Cassim, N.; Gopolang, F.; Hoffman, M.; Ramjee, G.; Williamson, A.-L. The Effectiveness of Carraguard, a Vaginal Microbicide, in Protecting Women against High-Risk Human Papillomavirus Infection. *Antivir. Ther.* **2011**, *16* (8), 1219–1226.

(109)   Skoler-karpoff, S.; Ramjee, G.; Ahmed, K.; Altini, L.; Plagianos, M. G.; Friedland, B.; Govender, S.; De Kock, A.; Cassim, N.; Palanee, T.; Dozier, G.; Maguire, R.; Lahteenmaki, P. Efficacy of Carraguard for Prevention of HIV Infection in Women in South Africa: A Randomised, Double-Blind, Placebo-Controlled Trial. *Lancet* **2008**, *372*, 1977–1987. https://doi.org/10.1016/S0140-6736(08)61842-5.

(110)   Mccandless, E. L.; Craigie, J. S. Sulfated Polysaccharides in Red and Brown Algae. *Ann. Rev. Plant Physiol.* **1979**, *30*, 41–53.

(111)   Delattre, C.; Fenoradosoa, T. A.; Michaud, P. Galactans: An Overview of Their Most Important Sourcing and Applications as Natural Polysaccharides. *Brazilian Achives Biol. Technol.* **2011**, *54* (6), 1075–1092.

(112)   Rodriguez, M.; Merino, E. R.; Pujol, C. A.; Damonte, E. B.; Cerezo, A. S.; Matulewicz, M. C. Galactans from Cystocarpic Plants of the Red Seaweed Callophyllis Variegata (Kallymeniaceae, Gigartinales). *Carbohydr. Res.* **2005**, *340*, 2742–2751. https://doi.org/10.1016/j.carres.2005.10.001.

(113)   Matsuhiro, B.; Conte, A. F.; Damonte, E. B.; Kolender, A. A.; Matulewicz, M. C.; Mejias, E. G.; Pujol, C. A.; Zuniga, E. A. Structural Analysis and Antiviral Activity of a Sulfated Galactan from the Red Seaweed Schizymenia Binderi (Gigartinales , Rhodophyta). *Carbohydr. Res.* **2005**, *340*, 2392–

2402. https://doi.org/10.1016/j.carres.2005.08.004.

(114) Witvrouw, M.; Este, J. A.; Mateu, M. Q.; Reymen, O.; Andrei, G.; Snoeck, R.; Pauwels, R.; Bianchlnl, N. V; Desmyter, J.; De Clercq, E. Activity of a Sulfated Polysaccharide Extracted from the Red Seaweed Aghardhiella Tenera against Human Immunodeficiency Virus and Other Enveloped Viruses. *Antivir. Chem. Chemother.* **1994**, *5* (5), 297–303. https://doi.org/10.1177/095632029400500503.

(115) Mabeau, S.; Kloareg, B. Isolation and Analysis of the Cell Walls of Brown Algae: Fucus Spiralis, F. Ceranoides, F. Vesiculosus, F. Serratus, Bifurcaria Bifurcata and Laminaria Digitata. *J. Exp. Bot.* **1987**, *38* (194), 1573–1580.

(116) Wang, W.; Wang, S.; Guan, H. The Antiviral Activities and Mechanisms of Marine Polysaccharides : An Overview. *Mar. Drugs* **2012**, *10*, 2795–2816. https://doi.org/10.3390/md10122795.

(117) Meiyu, G.; Fuchuan, L.; Xianliang, X.; Jing, L.; Zuowei, Y.; Huashi, G. The Potential Molecular Targets of Marine Sulfated Polymannuroguluronate Interfering with HIV-1 Entry Interaction between SPMG and HIV-1 Rgp120 and CD4 Molecule. *Antiviral Res.* **2003**, *59*, 127–135. https://doi.org/10.1016/S0166-3542(03)00068-8.

(118) Liu, H.; Geng, M.; Xin, X.; Li, F.; Zhang, Z.; Li, J.; Ding, J. Multiple and Multivalent Interactions of Novel Anti-AIDS Drug Candidates, Sulfated Polymannuronate (SPMG)-Derived Oligosaccharides, with Gp120 and Their Anti-HIV Activities. *Glycobiology* **2005**, *15* (5), 501–510. https://doi.org/10.1093/glycob/cwi031.

(119) Patankars, M. S.; Oehningerq, S.; Barnett, T.; Williams, R. L.; Clark, G. F. A Revised Structure for Fucoidan May Explain Some of Its Biological Activities. *J. Biol. Chem.* **1993**, *268* (29), 21770–21776.

(120) Queiroz, K. C. S.; Medeiros, V. P.; Queiroz, L. S.; Abreu, L. R. D.; Rocha, H. A. O.; Ferreira, C. V; Juca, M. B.; Aoyama, H.; L, L. E. Inhibition of Reverse Transcriptase Activity of HIV by Polysaccharides of Brown Algae. **2008**, *62*, 303–307. https://doi.org/10.1016/j.biopha.2008.03.006.

(121) Mandal, P.; Mateu, C. G.; Chattopadhyay, K.; Pujol, C. A.; Damonte, E. B.; Ray, B. Structural Features and Antiviral Activity of Sulphated Fucans from the Brown Seaweed Cystoseira Indica. *Antivir. Chem. Chemother.* **2007**, *18*, 153–162. https://doi.org/10.1177/095632020701800305.

(122) Ponce, N. M. A.; Pujol, C. A.; Damonte, E. B.; Flores, M. L.; Stortz, C. A. Fucoidans from the Brown Seaweed Adenocystis Utricularis: Extraction Methods, Antiviral Activity and Structural Studies. *Carbohydr. Res.* **2003**, *338*, 153–165.

(123) Lee, J.-B.; Hayashi, K.; Hashimoto, M.; Nakano, T.; Hayashi, T. Novel Antiviral Fucoidan from Sporophyll of Undaria Pinnatifida (Mekabu). *Chem. Pharm. Bull.* **2004**, *52* (9), 1091–1094.

(124) Adhikari, U.; Mateu, C. G.; Chattopadhyay, K.; Pujol, C. A.; Damonte, E. B.; Ray, B. Structure and Antiviral Activity of Sulfated Fucans from Stoechospermum Marginatum. *Phytochemistry* **2006**, *67*, 2474–2482. https://doi.org/10.1016/j.phytochem.2006.05.024.

(125) Hemmingson, J. A.; Falshaw, R.; Furneaux, R. H.; Thompson, K. Structure and Antiviral Activity of the Galactofucan Sulfates Extracted from Undaria Pinnatifida (Phaeophyta). *J. Appl. Phycol.* **2006**, *18*, 185–193. https://doi.org/10.1007/s10811-006-9096-9.

(126) Hayashi, K.; Nakano, T.; Hashimoto, M.; Kanekiyo, K.; Hayashi, T. Defensive Effects of a Fucoidan from Brown Alga Undaria Pinnatifida against Herpes Simplex Virus Infection. *Int. Immunopharmacol.* **2008**, *8*, 109–116. https://doi.org/10.1016/j.intimp.2007.10.017.

(127) Hidari, K. I. P. J.; Takahashi, N.; Arihara, M.; Nagaoka, M.; Morita, K.; Suzuki, T. Structure and Anti-Dengue Virus Activity of Sulfated Polysaccharide from a Marine Alga. *Biochem. Biophys. Res. Commun.* **2008**, *376*, 91–95. https://doi.org/10.1016/j.bbrc.2008.08.100.

(128) Witvrouw, M.; De Clercq, E. Sulfated Polysaccharides Extracted from Sea Algae as Potential

Antiviral Drugs. *Gen. Pharmacol.* **1997**, *29* (4), 497–511.

(129) Elizondo-Gonzalez, R.; Cruz-Suarez, L. E.; Ricque-Marie, D.; Mendoza-Gamboa, E.; Rodriguez-padilla, C.; Trejo-Avila, L. M. In Vitro Characterization of the Antiviral Activity of Fucoidan from Cladosiphon Okamuranus against Newcastle Disease Virus. *Virol. J.* **2012**, *9* (307), 1–9.

(130) Leite, E. L.; Medeiros, M. G. L.; Rocha, H. A. O.; Farias, G. G. M.; da Silva, L. F.; Chavante, S. F.; de Abreu, L. D.; Dietrich, C. P.; Nader, H. B. Structure and Pharmacological Activities of a Sulfated Xylofucoglucuronan from the Alga Spatoglossum Schro. *Plant Sci.* **1998**, *132*, 215–228.

(131) Peat, S.; Whelan, W. J.; Lawley, H. G. 141. The Structure of Laminarin. Part I. The Main Polymeric Linkage. *J. Chem. Soc.* **1952**, 724–728.

(132) Muto, S.; Niimura, K.; Oohara, M.; Matsunaga, K.; Hirose, K.; Kakuchi, J.; Furusho, T.; Yoshikumi, C.; Takahashi, M. Polysaccharides and Antiviral Drugs Containing the Smae as Active Ingredient, 1988.

(133) Lee, J.-B.; Hayashi, K.; Hirata, M.; Kuroda, E.; Suzuki, E.; Kubo, Y.; Hayashi, T. Antiviral Sulfated Polysaccharide from Navicula Directa, a Diatom Collected from Deep-Sea Water in Toyama Bay. *Biol. Pharm. Bull.* **2006**, *29* (10), 2135–2139.

(134) Kim, M.; Han, J.; Kim, S.; Kim, H. S.; Lee, W. G.; Kim, S. J.; Kang, P.-S.; Lee, C.-K. In Vitro Inhibition of Influenza A Virus Infection by Marine Microalga-Derived Sulfated Polysaccharide p-KG03. *Antiviral Res.* **2012**, *93*, 253–259. https://doi.org/10.1016/j.antiviral.2011.12.006.

(135) Yim, J. H.; Kim, S. J.; Ahn, S. H.; Lee, C. K.; Rhie, K. T.; Lee, H. K. Antiviral Effects of Sulfated Exopolysaccharide from the Marine Microalga Gyrodinium Impudicum Strain. *Mar. Biotechnol.* **2004**, *6*, 17–25. https://doi.org/10.1007/s10126-003-0002-z.

(136) Hasui, M.; Matsuda, M.; Okutani, K.; Shigeta, S. In Vitro Antiviral Activities of Sulfated Polysaccharides from a Marine Microalga (Cochlodinium Polykrikoides) against Human Immunodeficiency Virus and Other Enveloped Viruses. *Int. J. Biol. Macromol.* **1995**, *17* (5), 293–297.

(137) Hayashi, T.; Hayashi, K. Calcium Spirulan, an Inhibitor of Enveloped Virus Replication, from a Blue-Green Alga Spirulina Platensis Spirulina Platensis. *J. Nat. Prod.* **1996**, *59*, 83–87.

(138) Kanekiyo, K.; Hayashi, K.; Takenaka, H.; Lee, J.-B.; Hayashi, T. Anti-Herpes Simplex Virus Target of an Acidic Polysaccharide, Nostoflan, from the Edible Blue-Green Alga Nostoc Flagelliforme. *Biol. Pharm. Bull.* **2007**, *30* (8), 1573–1575.

(139) Donalisio, M.; Ranucci, E.; Cagno, V.; Civra, A.; Manfredi, A.; Cavalli, R.; Ferruti, P.; Lembo, D. Agmatine-Containing Poly(Amidoamine)s as a Novel Class of Antiviral Macromolecules: Structural Properties and in Vitro Evaluation of Infectivity Inhibition. *Antimicrob. Agents Chemother.* **2014**, *58* (10), 6315–6319. https://doi.org/10.1128/AAC.03420-14.

(140) Mercorelli, B.; Oreste, P.; Sinigalia, E.; Muratore, G.; Lembo, D.; Palù, G.; Loregian, A. Sulfated Derivatives of Escherichia Coli K5 Capsular Polysaccharide Are Potent Inhibitors of Human Cytomegalovirus. *Antimicrob. Agents Chemother.* **2010**, *54* (11), 4561–4567. https://doi.org/10.1128/AAC.00721-10.

(141) Vervaeke, P.; Alen, M.; Noppen, S.; Schols, D.; Oreste, P.; Liekens, S. Sulfated Escherichia Coli K5 Polysaccharide Derivatives Inhibit Dengue Virus Infection of Human Microvascular Endothelial Cells by Interacting with the Viral Envelope Protein E Domain III. *PLoS One* **2013**, *8* (8). https://doi.org/10.1371/journal.pone.0074035.

(142) Rusnati, M.; Vicenzi, E.; Donalisio, M.; Oreste, P.; Landolfo, S.; Lembo, D. Sulfated K5 Escherichia Coli Polysaccharide Derivatives: A Novel Class of Candidate Antiviral Microbicides. *Pharmacol. Ther.* **2009**, *123* (3), 310–322. https://doi.org/10.1016/j.pharmthera.2009.05.001.

(143) Rusnati, M.; Oreste, P.; Zoppetti, G.; Presta, M. Biotechnological Engineering of Heparin/Heparan Sulphate: A Novel Area of Multi-Target Drug Discovery. *Curr. Pharm. Des.* **2005**, *11* (19), 2489–2499. https://doi.org/10.2174/1381612054367553.

(144) Pirrone, V.; Wigdahl, B.; Krebs, F. C. The Rise and Fall of Polyanionic Inhibitors of the Human Immunodeficiency Virus Type 1. *Antiviral Res.* **2011**, *90* (3), 168–182. https://doi.org/10.1016/j.antiviral.2011.03.176.

(145) Qureshi, N. M.; Coy, D. H.; Garry, R. F.; Henderson, L. A. Characterization of a Putative Cellular Receptor for HIV-1 Transmembrane Glycoprotein Using Synthetic Peptides. *AIDS* **1990**, *4*, 553–558.

(146) Garry, R. F.; Russell, W. Fusion Initiation Region in RNA Virus Envelope Proteins, 2005.

(147) Levy, J. A. HIV Pathogenesis: 25 Years of Progress and Persistent Challenges. *AIDS* **2009**, *23*, 147–160. https://doi.org/10.1097/QAD.0b013e3283217f9f.

(148) Fung, H. B.; Guo, Y. Enfuvirtide: A Fusion Inhibitor for the Treatment of HIV Infection. *Clin. Ther.* **2004**, *26* (3), 352–378.

(149) Labonte, J.; Lebbos, J.; Kirkpatrick, P. Enfuvirtide. *Drug Discov.* **2003**, *2* (May), 345–346. https://doi.org/10.1038/nrd1091.

(150) Liu, S.; Niu, J.; Wu, S.; Jiang, S. Different from the HIV Fusion Inhibitor C34 , the Anti-HIV Drug Fuzeon (T-20) Inhibits HIV-1 Entry by Targeting Multiple Sites in Gp41 and Gp120. *J. Biol. Chem.* **2005**, *280* (12), 11259–11273. https://doi.org/10.1074/jbc.M411141200.

(151) Garg, H.; Viard, M.; Jacobs, A.; Blumenthal, R. Targeting HIV-1 Gp41-Induced Fusion and Pathogenesis for Anti-Viral Therapy. *Curr. Top. Med. Chem.* **2011**, *11*, 2947–2958.

(152) Wild, C.; Oast, T.; Mcdanal, C.; Bolognesi, D.; Matthews, T. A Synthetic Peptide Inhibitor of Human Immunodeficiency Virus Replication : Correlation between Solution Structure and Viral Inhibition. *PNAS* **1992**, *89* (November), 10537–10541.

(153) Wild, C.; Greenwell, T.; Matthews, T. Synthetic Peptide from HIV-1 Gp41 Is a Potent Inhibitor of Virus-Mediated Cell-Cell Fusion. *AIDS Res. Hum. Retroviruses* **1993**, *9* (11), 1051–1053.

(154) Kliger, Y.; Gallo, S. A.; Peisajovich, S. G.; Munoz-Barroso, I.; Avkin, S.; Blumenthal, R.; Shai, Y. Mode of Action of an Antiviral Peptide from HIV-1. *J. Biol. Chem.* **2001**, *276* (2), 1391–1397. https://doi.org/10.1074/jbc.M004113200.

(155) He, Y.; Cheng, J.; Lu, H.; Li, J.; Hu, J.; Qi, Z.; Liu, Z.; Jiang, S.; Dai, Q. Potent HIV Fusion Inhibitors against Enfuvirtide-Resistant HIV-1 Strains. *PNAS* **2008**, *105* (42), 16332–16337.

(156) Yao, X.; Chong, H.; Zhang, C.; Qiu, Z.; Qin, B.; Han, R.; Waltersperger, S.; Wang, M.; He, Y.; Cui, S. Structural Basis of Potent and Broad HIV-1 Fusion Inhibitor CP32M. *J. Biol. Chem.* **2012**, *287* (32), 26618–26629. https://doi.org/10.1074/jbc.M112.381079.

(157) Nicol, M. Q.; Ligertwood, Y.; Bacon, M. N.; Dutia, B. M.; Nash, A. A. A Novel Family of Peptides with Potent Activity against Influenza A Viruses. *J. Gen. Virol.* **2012**, *93*, 980–986. https://doi.org/10.1099/vir.0.038679-0.

(158) Budge, P. J.; Graham, B. S. Inhibition of Respiratory Syncytial Virus by RhoA-Derived Peptides: Implications for the Development of Improved Antiviral Agents Targeting Heparin-Binding Viruses. *J. Antimicrob. Chemother.* **2004**, *54*, 299–302. https://doi.org/10.1093/jac/dkh355.

(159) Pastey, M. K.; Crowe, J. E.; Graham, B. S. RhoA Interacts with the Fusion Glycoprotein of Respiratory Syncytial Virus and Facilitates Virus-Induced Syncytium Formation. *J. Virol.* **1999**, *73* (9), 7262–7270. https://doi.org/10.1128/jvi.73.9.7262-7270.1999.

(160) Bai, F.; Town, T.; Pradhan, D.; Cox, J.; Ashish; Ledizet, M.; Anderson, J. F.; Flavell, R. A.; Krueger, J. K.; Koski, R. A.; Fikrig, E. Antiviral Peptides Targeting the West Nile Virus Envelope Protein . *J. Virol.* **2007**, *81* (4), 2047–2055. https://doi.org/10.1128/JVI.01840-06.

(161) Eissmann, K.; Mueller, S.; Sticht, H.; Jung, S.; Zou, P.; Jiang, S.; Gross, A.; Eichler, J.; Fleckenstein, B.; Reil, H. HIV-1 Fusion Is Blocked through Binding of GB Virus C E2D Peptides to the HIV-1 Gp41 Disulfide Loop. *PLoS One* **2013**, *8* (1), e54452. https://doi.org/10.1371/journal.pone.0054452.

(162) Koedel, Y.; Eissmann, K.; Wend, H.; Fleckenstein, B.; Reil, H. Peptides Derived from a Distinct Region of GB Virus C Glycoprotein E2 Mediate Strain-Specific HIV-1 Entry Inhibition . *J. Virol.*

Methods **2011**, *85* (14), 7037–7047. https://doi.org/10.1128/JVI.02366-10.

(163) Rapaport, D.; Ovadia, M.; Shai, Y. L. A Synthetic Peptide Corresponding to a Conserved Heptad Repeat Domain Is a Potent Inhibitor of Sendai Virus-Cell Fusion: An Emerging Similarity with Functional Domains of Other Viruses. *EMBO J.* **1995**, *14* (22), 5524–5531. https://doi.org/10.1002/j.1460-2075.1995.tb00239.x.

(164) Lambert, D. M.; Barney, S.; Lambert, A. L.; Guthrie, K.; Medinas, R.; Davis, D. E.; Bucy, T.; Erickson, J.; Merutka, G.; Petteway, S. R. Peptides from Conserved Regions of Paramyxovirus Fusion (F) Proteins Are Potent Inhibitors of Viral Fusion. *Proc. Natl. Acad. Sci. U. S. A.* **1996**, *93* (5), 2186–2191. https://doi.org/10.1073/pnas.93.5.2186.

(165) Lamb, D.; Schüttelkopf, A. W.; van Aalten, D. M. F.; Brighty, D. W. Highly Specific Inhibition of Leukaemia Virus Membrane Fusion by Interaction of Peptide Antagonists with a Conserved Region of the Coiled Coil of Envelope. *Retrovirology* **2008**, *5* (70), 1–14. https://doi.org/10.1186/1742-4690-5-70.

(166) Melnik, L. I.; Garry, R. F.; Morris, C. A. Peptide Inhibition of Human Cytomegalovirus Infection. *Virol. J.* **2011**, *8* (76), 1–11.

(167) Hrobowski, Y. M.; Garry, R. F.; Michael, S. F. Peptide Inhibitors of Dengue Virus and West Nile Virus Infectivity. *Virol. J.* **2005**, *2* (49), 1–10. https://doi.org/10.1186/1743-422X-2-49.

(168) Lok, S.-M.; Costin, J. M.; Hrobowski, Y. M.; Hoffmann, A. R.; Rowe, D. K.; Kukkaro, P.; Holdaway, H.; Chipman, P.; Fontaine, K. A.; Holbrook, M. R.; Garry, R. F.; Kostyuchenko, V.; Wimley, W. C.; Isern, S.; Rossmann, M. G.; Michael, S. F. Release of Dengue Virus Genome Induced by a Peptide Inhibitor. *PLoS One* **2012**, *7* (11), e50995. https://doi.org/10.1371/journal.pone.0050995.

(169) Schmidt, A. G.; Yang, P. L.; Harrison, S. C. Peptide Inhibitors of Dengue-Virus Entry Target a Late-Stage Fusion Intermediate. *PLoS Pathog.* **2010**, *6* (4), e1000851. https://doi.org/10.1371/journal.ppat.1000851.

(170) Schmidt, A. G.; Yang, P. L.; Harrison, S. C. Peptide Inhibitors of Flavivirus Entry Derived from the E Protein Stem. *J. Virol.* **2010**, *84* (24), 12549–12554. https://doi.org/10.1128/JVI.01440-10.

(171) Sainz, B.; Rausch, J. M.; Gallaher, W. R.; Garry, R. F.; Wimley, W. C. The Aromatic Domain of the Coronavirus Class I Viral Fusion Protein Induces Membrane Permeabilization: Putative Role during Viral Entry. *Biochemistry* **2005**, *44*, 947–958.

(172) Koehler, J. W.; Smith, J. M.; Ripoll, D. R.; Spik, K. W.; Taylor, S. L.; Badger, C. V; Grant, R. J.; Ogg, M. M.; Wallqvist, A.; Guttieri, M. C.; Garry, R. F.; Schmaljohn, C. S. A Fusion-Inhibiting Peptide against Rift Valley Fever Virus Inhibits Multiple , Diverse Viruses. *PLoS Neglected Trop. Dis.* **2013**, *7* (9), e2430. https://doi.org/10.1371/journal.pntd.0002430.

(173) Cheng, G.; Montero, A.; Gastaminza, P.; Whitten-Baur, C.; Wieland, S.; Isogawa, M.; Fredericksen, B.; Selvarajah, S.; Gallay, P. A.; Ghadiri, M. R.; Chisari, F. V. A Virocidal Amphipathic α-Helical Peptide That Inhibits Hepatitis C Virus Infection in Vitro. *PNAS* **2007**, *105* (8), 3088–3093.

(174) Li, G.-R.; He, L.-Y.; Liu, X.-Y.; Liu, A.-P.; Huang, Y.-B.; Qui, C.; Zhang, X.-Y.; Xu, J.-Q.; Yang, W.; Chen, Y.-X. Rational Design of Peptides with Anti-HCV and HIV Activities and Enhanced Specificity. *Chem. Biol. Drug Des.* **2011**, *78*, 835–843.

(175) Tinsley, C. R.; Manjula, B. N.; Gotschlich, E. C. Purification and Characterization of Polyphosphate from Neissenia Meningitidis. *Infect. Immun.* **1993**, *61* (9), 3703–3710.

(176) Noegel, A.; Gotschlich, E. C. Isolation of High Molecular Weight Polyphosphate from Neisseria Gonorrhoeae. *J. Exp. Med.* **1983**, *157*, 2049–2060.

(177) Lorenz, B.; Leuck, J.; Kohl, D.; Muller, W.; Schroder, H. Anti-HIV-1 Activity of Inorganic Polyphosphates. *J. Acquir. Immune Defic. Syndr. Hum. Retrovirology* **1997**, *14*, 110–118.

(178) Muller, W.; Wang, X.; Schroder, H. *Biomedical Inorganic Polymers*; 2013.

(179) Jasmin, C.; Chermann, J.-C.; Herve, G.; Teze, A.; Souchay, P.; Boy-loustau, C.; Raybaud, N.; Sinoussi, F.; Raynaud, M. In Vivo Inhibition of Murine Leukemia and Sarcoma Viruses by the

Heteropoly-Anion 5-Tungsto-2-Antimoniate. *J. Natl. Cancer Inst.* **1974**, *53* (2), 469–474.

(180) Jasmin, C.; Raybaud, N.; Chermann, J.-C.; Haapala, D.; Sinoussi, F.; Boy-Loustau, C.; Bonissol, C.; Kona, P.; Raynaud, M. In Vitro Effects of Silicotungstate on Some RNA Viruses. *Biomedicine* **1973**, *18*, 319–327.

(181) Dan, K.; Miyashita, K.; Seto, Y.; Fujita, H.; Yamase, T. Mechanism of the Protective Effect of Heteropolyoxotungstate against Herpes Simplex Virus Type 2. *Pharmacology* **2003**, *67*, 83–89. https://doi.org/10.1159/000067738.

(182) Fukuma, M.; Seto, Y.; Yamase, T. In Vitro Antiviral Activity of Polyoxotungstate (PM-19) and Other Polyoxometalates against Herpes Simplex Virus. *Antiviral Res.* **1991**, *16*, 327–339.

(183) Take, Y.; Tokutake, Y.; Inouye, Y.; Yoshida, T.; Yamamoto, A.; Yamase, T.; Nakamura, S. Inhibition of Proliferation of Human Immunodeficiency Virus Type 1 by Novel Heteropolyoxotungstates in Vitro. *Antiviral Res.* **1991**, *15*, 113–124.

(184) Dan, K.; Miyashita, K.; Seto, Y.; Fujita, H.; Yamase, T. The Memory Effect of the Heteropolyozotungstate (PM-19) Pretreatment on Infection by Herpes Simplex Virus at the Penetration Stage. *Pharmacol. Res.* **2002**, *46* (4), 2–7. https://doi.org/10.1016/S1043-6618(02)00170-6.

(185) Dan, K.; Miyashita, K.; Seto, Y.; Yamase, T. Quantitation of Herpes Simplex Viral DNA in Vero Cells for Evaluation of an Antiviral Agent Using the Polymerase Chain. *J. Virol. Methods* **1998**, *76*, 73–79.

(186) Dan, K.; Yamase, T. Prevention of the Interaction between HVEM, Herpes Virus Entry Mediator, and GD, HSV Envelope Protein, by a Keggin Polyoxotungstate, PM-19. *Biomed. Pharmacother.* **2006**, *60*, 169–173. https://doi.org/10.1016/j.biopha.2006.02.005.

(187) Ikeda, S.; Nishiya, S.; Yamamoto, A.; Yamase, T.; Nishimura, C.; De Clercq, E. Activity of the Keggin Polyoxotungstate PM-19 Against Herpes Simplex Virus Type 2 Infection in Immunosuppressed Mice: Role of Peritoneal Macrophage Activation. *J. Med. Virol.* **1993**, *41*, 191–195.

(188) Ikeda, S.; Nishiya, S.; Yamase, T.; Nishimura, C.; De Clercq, E. Antiviral Activity of a Keggin Polyoxotungstate PM-19 against Herpes Simplex Virus in Mice. *Antivir. Chem. Chemother.* **1994**, *5*, 47–50. https://doi.org/10.1177/095632029400500107.

(189) Shigeta, S.; Mori, S.; Kodama, E.; Kodama, J.; Takahashi, K.; Yamase, T. Broad Spectrum Anti-RNA Virus Activities of Titanium and Vanadium Substituted Polyoxotungstates. *Antiviral Res.* **2003**, *58*, 265–271. https://doi.org/10.1016/S0166-3542(03)00009-3.

(190) Shigeta, S.; Mori, S.; Yamase, T.; Yamamoto, N.; Yamamoto, N. Anti-RNA Virus Activity of Polyoxometalates. *Biomed. Pharmacother.* **2006**, *60* (5), 211–219. https://doi.org/10.1016/j.biopha.2006.03.009.

(191) Yamase, T. Anti-Tumor, -Viral, and -Bacterial Activities of Polyoxometalates for Realizing an Inorganic Drug. *J. Mater. Chem.* **2005**, *15*, 4773–4782. https://doi.org/10.1039/b504585a.

(192) Hosoya, M.; Balzarini, J. A. N.; Shigeta, S.; De Clercq, E. Differential Inhibitory Effects of Sulfated Polysaccharides and Polymers on the Replication of Various Myxoviruses and Retroviruses, Depending on the Composition of the Target Amino Acid Sequences of the Viral Envelope Glycoproteins. *Antimicrob. Agents Chemother.* **1991**, *35* (12), 2515–2520.

(193) Yamamoto, N.; Schols, D.; De Clercq, E.; Debyser, Z.; Pauwels, R.; Balzarini, J.; Nakashima, H.; Baba, M.; Hosoya, M.; Snoeck, R.; Neyts, J.; Andrei, G.; Murrer, B. A.; Theobald, B.; Bossard, G.; Henson, G.; Abrams, M.; Picker, D. Mechanism of Anti-Human Immunodeficiency Virus Action of Polyoxometalates, a Class of Broad-Spectrum Antiviral Agents. *Mol. Pharmacol.* **1992**, *42*, 1109–1117.

(194) Mitsuya, H.; Looney, D. J.; Kuno, S.; Ueno, R.; Staal, F. W.; Broder, S. Dextran Sulfate Suppression of Viruses in the HIV Family: Inhibition of Virion Binding to CD4+ Cells. *Science (80-.).* **1988**, *240* (4852), 646–649.

(195) Callahan, L. N.; Phelan, M.; Mallinson, M.; Norcross, M. A. Dextran Sulfate Blocks Antibody Binding to the Principal Neutralizing Domain of Human Immunodeficiency Virus Type 1 without Interfering with Gpl20-CD4 Interactions. *J. Virol.* **1991**, *65* (3), 1543–1550.

(196) Shigeta, S.; Mori, S.; Watanabe, J.; Yamase, T.; Schinazi, R. F. In-Vitro Anti Myxovirus Activity and Mechanism of Anti-Influenzavirus Activity of Polyoxometalates PM-504 and PM-523. *Antivir. Chem. Chemother.* **1996**, *7* (6), 346–352. https://doi.org/10.1177/095632029600700608.

(197) Shigeta, S.; Mori, S.; Watanabe, J.; Soeda, S.; Takahashi, K.; Yamase, T. Synergistic Anti-Influenza Virus A (H1N1) Activities of PM-523 (Polyoxometalate) and Ribavirin in Vitro and in Vivo. *Antimicrob. Agents Chemother.* **1997**, *41* (7), 1423–1427. https://doi.org/10.1128/aac.41.7.1423.

(198) Balcarová, Z.; Kasparkova, J.; Žákovská, A.; Nováková, O.; Sivo, M. F.; Natile, G.; Brabec, V. DNA Interactions of a Novel Platinum Drug, Cis-[PtCl(NH3)2(N7-Acyclovir)]+. *Mol. Pharmacol.* **1998**, *53*, 846–855.

(199) Avcioglu, M. V.; Golcu, A. Synthesis of Acyclovir Metal Complexes: Spectral, Electrochemical, Thermal, and DNA Binding. *Synth. React. inorganic, Met. non-metal Chem.* **2015**, *45* (4), 581–590. https://doi.org/10.1080/15533174.2013.831877.

(200) Varadinova, T.; Vilhelmova, N.; Badenas, F.; Terrón, A.; Fiol, J.; Genova, P. Effect of Metal Complexes of Acyclovir and Its Acetylated Derivative on Herpes Simplex Virus 1 and Herpes Simplex Virus 2 Replicaiton. *Acta Virol.* **2005**, *49*, 251–260.

(201) de Paiva, R. E.; Neto, A. M.; Santos, I. A.; Jardim, A. C. G.; Corbi, P. P.; Bergamini, F. What Is Holding Back the Development of Antiviral Metallodrugs? A Literature Overview and Implications for SARS-CoV-2 Therapeutics and Future Viral Outbreaks. *Dalt. Trans.* **2020**, *49*, 16004–16033. https://doi.org/10.1039/D0DT02478C.

(202) Knight, D. A.; Hickey, T. E.; Bongard, J. E.; Thach, D. C.; Yngard, R.; Chang, E. L. Differential Effects of Co (III), Ni (II), and Ru (III) Amine Complexes on Sindbis Virus. *J. Inorg. Biochem.* **2010**, *104*, 592–598. https://doi.org/10.1016/j.jinorgbio.2010.01.012.

(203) Delehanty, J. B.; Bongard, J. E.; Thach, D. C.; Knight, D. A.; Hickey, T. E.; Chang, E. L. Antiviral Properties of Cobalt(III)-Complexes. *Bioorganic Med. Chem.* **2008**, *16*, 830–837. https://doi.org/10.1016/j.bmc.2007.10.022.

(204) Chang, E. L.; Olinger, G. G.; Hensley, L. E.; Lear, C. M.; Scully, C. E.; Mankowski, M. K.; Ptak, R. G.; Thach, D. C.; Knight, D. A. Hexamminecobalt (III) Chloride as Broad Spectrum Antiviral Complex. *Jounral Antivirals Antiretrovir.* **2011**, *3*, 020–027.

(205) Gessner, R. V; Quigley, G. J.; Wang, A. H.; van der Marel, G. A.; van Boom, J. H.; Rich, A. Structural Basis for Stabilization of Z-DNA by Cobalt Hexaammine and Magnesium Cations. *Biochemistry* **1985**, *24*, 237–240. https://doi.org/10.1021/bi00323a001.

(206) Chang, E. L.; Simmers, C.; Knight, D. A. Cobalt Complexes as Antiviral and Antibacterial Agents. *Pharmaceuticals* **2010**, *3* (6), 1711–1728. https://doi.org/10.3390/ph3061711.

(207) Louie, A. Y.; Meade, T. J. A Cobalt Complex That Selectively Disrupts the Structure and Function of Zinc Fingers. *Biochemistry* **1998**, *95*, 6663–6668.

(208) Blum, O.; Haiek, A.; Cwikel, D.; Dori, Z.; Meade, T. J.; Gray, H. B. Isolation of a Myoglobin Molten Globule by Selective Cobalt(III)-Induced Unfolding. *Biochemistry* **1998**, *95*, 6659–6662.

(209) Wooley, P. H.; Whalen, J. D. The Influence of Superoxide Scavenging Compound CTC 23 on Type II Collagen-Induced Arthritis in Mice. *Agents Actions* **1992**, *35*, 273–279.

(210) Asbell, P. A.; Epstein, S. P.; Wallace, J. A.; Epstein, D.; Stewart, C. C.; Burger, R. M. Efficacy of Cobalt Chelates in the Rabbit Eye Model for Epithelial Herpetic Keratitis. *Cornea* **1998**, *17* (5), 550–557.

(211) Epstein, S. P.; Pashinsky, Y. Y.; Gershon, D.; Winicov, I.; Srivilasa, C.; Kristic, K. J.; Asbell, P. A. Efficacy of Topical Cobalt Chelate CTC-96 against Adenovirus in a Cell Culture Model and against Adenovirus Keratoconjunctivitis in a Rabbit Model. *BMC Ophthalmol.* **2006**, *6* (22), 1–11.

https://doi.org/10.1186/1471-2415-6-22.

(212) Schwartz, J. A.; Lium, E. K.; Silverstein, S. J. Herpes Simplex Virus Type 1 Entry Is Inhibited by the Cobalt Chelate Complex CTC-96. *J. Virol.* **2001**, *75* (9), 4117–4128. https://doi.org/10.1128/jvi.75.9.4117-4128.2001.

(213) Ostrow, R. S.; Coughlin, S.; McGlennen, R. C.; Zhanjiang, L.; Zelterman, D.; Faras, A. J. Topical CTC-96 Accelerates Wart Growth in Rabbits Infected with Cottontail Rabbit Papillomavirus. *Antiviral Res.* **1994**, *24*, 27–35.

(214) Shishkov, S.; Varadinova, T.; Panteva, M.; Bontchev, P. Effect of Complexes of Zinc, Cobalt, and Copper with D-Aminosugars on the Replication of Herpes Simplex Virus Type 1 (HSV-1). *Met. Based. Drugs* **1997**, *4* (1), 35–38.

(215) Horton, D.; Varela, O. Cu, Pt, and Pd Complexes of the 3-Deoxy-1, 2-Bis(Thiosemicarbazone) Derived from D-Glucose. *Carbohydr. Res.* **2000**, *328*, 425–429.

(216) Varadinova, T.; Shishkov, S.; Panteva, M.; Bontchev, P. Effect of Complexes of Cobalt with Amino Acids on the Replication of Herpes Simplex Virus Type 1 (HSV-1). *Met. Based. Drugs* **1996**, *3*, 149–154.

(217) Shishkov, S.; Varadinova, T.; Bontchev, P.; Nachev, C.; Michailova, E. Complexes of Zinc Picolinic and Aspartic Acids Inactivate Free Varicella-Zoster Virions. *Met. Based. Drugs* **1996**, *3* (1), 11–14.

(218) Pesheva, M.; Varadinova, T. Zinc (II) Complexes - a New Group of Non-Mutagenic Herpes Simplex Virus Inhibitors. *Met. Based. Drugs* **2000**, *7* (3), 129–131.

(219) Nagini, S. Chemopreventive Potential of Chlorophyllin: A Review of the Mechanisms of Action and Molecular Targets. *Nutr. Cancer* **2015**, *67* (2), 203–211. https://doi.org/10.1080/01635581.2015.990573.

(220) Tumolo, T.; Lanfer-Marquez, U. M. Copper Chlorophyllin: A Food Colorant with Bioactive Properties? *Food Res. Int.* **2012**, *46*, 451–459. https://doi.org/10.1016/j.foodres.2011.10.031.

(221) Ito, A.; Tsuneki, A.; Yoshida, Y.; Ryoke, K.; Kaidoh, T.; Kageyama, S. In Vitro Inhibition of Cytopathic Effect of Influenza Virus and Human Immunodefi- Ciency Virus by Bamboo Leaf Extract Solution and Sodium Copper Chlorophyllin. *Yonago Acta Med.* **2016**, *59*, 61–65.

(222) Ratnoglik, S. L.; Aoki, C.; Sudarmono, P.; Komoto, M.; Deng, L.; Shoji, I.; Fuchino, H.; Kawahara, N.; Hotta, H. Antiviral Activity of Extracts from Morinda Citrifolia Leaves and Chlorophyll Catabolites, Pheophorbide a and Pyropheophorbide a, against Hepatitis C Virus. *Microbiol. Immunol.* **2014**, *58*, 188–194. https://doi.org/10.1111/1348-0421.12133.

(223) Liu, Z.; Xia, S.; Wang, X.; Lan, Q.; Li, P.; Xu, W.; Wang, Q.; Lu, L.; Jiang, S. Sodium Copper Chlorophyllin Is Highly Effective against Enterovirus (EV) A71 Infection by Blocking Its Entry into the Host Cell. *Infect. Dis.* **2020**, *6*, 882–890.

(224) Mekler, L. B.; Bychovsky, A. F.; Krikun, B. L. Electron Microscope Study of the Viricidal Properties of Sodium Magnesium-Ch Lorophyll in Changes in Serum Phospholipids in Male and Female Baboons on a Sucrose Diet. *Nature* **1969**, *222*, 574–575.

(225) Simić, V.; Kolarević, S.; Brčeski, I.; Jeremić, D.; Vuković-Gačić, B. Cytotoxicity and Antiviral Activity of Palladium(II) and Platinum(II) Complexes with 2-(Diphenylphosphino) Benzaldehyde 1-Adamantoylhydrazone. *Turkish J. Biol.* **2016**, *40*, 661–669. https://doi.org/10.3906/biy-1503-23.

(226) Garoufis, A.; Hadjikakou, S. K.; Hadjiliadis, N. Palladium Coordination Compounds as Anti-Viral, Anti-Fungal, Anti-Microbial and Anti-Tumor Agents. *Coord. Chem. Rev.* **2009**, *253*, 1384–1397. https://doi.org/10.1016/j.ccr.2008.09.011.

(227) Visnjevac, A.; Tusek-Bozic, L.; Majeric-Elenkov, M.; Hamersak, Z.; Kooijman, H.; De Clercq, E.; Kojic-Prodic, B. Synthesis, Structural Characterisation and Biological Activity of Zn(II) and Pd(II) Complexes of 3-Substituted 5-(2'-Pyridyl)-1,4-Benzodiazepin-2-One Derivatives.Pdf. *Polyhedron* **2002**, *21*, 2567–2577.

(228) Genova, P.; Varadinova, T.; Matesanz, A. I.; Marinova, D.; Souza, P. Toxic Effects of

Bis(Thiosemicarbazone) Compounds and Its Palladium (II) Complexes on Herpes Simplex Virus Growth. *Toxicol. Appl. Pharmacol.* **2004**, *197*, 107–112. https://doi.org/10.1016/j.taap.2004.02.006.

(229) Kovala-Demertzi, D.; Varadinova, T.; Genova, P.; Souza, P.; Demertzis, M. A. Platinum(II) and Palladium(II) Complexes of Pyridine-2-Carbaldehyde Thiosemicarbazone as Alternative Antiherpes Simplex Virus Agents. *Bioinorg. Chem. Appl.* **2007**, *2007*. https://doi.org/10.1155/2007/56165.

(230) Kauffman, G. B.; Pentimalli, R.; Doldi, S.; Hall, M. D. Michele Peyrone (1813-1883), Discoverer of Cisplatin. *Platin. Met. Rev.* **2010**, *54* (4), 250–256. https://doi.org/10.1595/147106710X534326.

(231) Johnstone, T. C.; Suntharalingam, K.; Lippard, S. J. Third Row Transition Metals for the Treatment of Cancer. *Philos. Trans. R. Soc. A Math. Phys. Eng. Sci.* **2015**, *373* (20140185). https://doi.org/10.1098/rsta.2014.0185.

(232) Ahmad, S. Kinetic Aspects of Platinum Anticancer Agents. *Polyhedron* **2017**, *138*, 109–124. https://doi.org/10.1016/j.poly.2017.09.016.

(233) Huang, H.; Zhu, L.; Reid, B. R.; Drobny, G. P.; Hopkinst, P. B. Solution Structure of a Cisplatin-Induced DNA Interstrand Cross-Link. *Science (80-.).* **1995**, *270* (5243), 1842–1845.

(234) Ohndorf, U.-M.; Rould, M. A.; He, Q.; Pabo, C. O.; Lippard, S. J. Basis for Recognition of Cisplatin-Modified DNA by High Mobility Group Proteins. *Nature* **1999**, *399*, 708–712.

(235) Galluzzi, L.; Senovilla, L.; Vitale, I.; Michels, J.; Martins, I.; Kepp, O.; Castedo, M.; Kroemer, G. Molecular Mechanisms of Cisplatin Resistance. *Oncogene* **2012**, *31*, 1869–1883. https://doi.org/10.1038/onc.2011.384.

(236) Brabec, V.; Kašpárková, J.; Vrána, O.; Nováková, O.; Cox, J. W.; Qu, Y.; Farrell, N. DNA Modifications by a Novel Bifunctional Trinuclear Platinum Phase I Anticancer Agent. *Biochemistry* **1999**, *38* (21), 6781–6790. https://doi.org/10.1021/bi990124s.

(237) Roberts, J. D.; Peroutka, J.; Beggiolin, G.; Manzotti, C.; Piazzoni, L.; Farrell, N. Comparison of Cytotoxicity and Cellular Accumulation of Polynuclear Platinum Complexes in L1210 Murine Leukemia Cell Lines. *J. Inorg. Biochem.* **1999**, *77* (1–2), 47–50. https://doi.org/10.1016/S0162-0134(99)00137-3.

(238) Roberts, J. D.; Peroutka, J.; Farrell, N. Cellular Pharmacology of Polynuclear Platinum Anti-Cancer Agents. *J. Inorg. Biochem.* **1999**, *77* (1–2), 51–57. https://doi.org/10.1016/S0162-0134(99)00147-6.

(239) Jamieson, E. R.; Lippard, S. J. Structure, Recognition, and Processing of Cisplatin–DNA Adducts. *Chem. Rev.* **1999**, *99*, 2467–2498.

(240) Zlatanova, J.; Yaneva, J.; Leuba, S. H. Proteins That Specifically Recognize Cisplatin-damaged DNA: A Clue to Anticancer Activity of Cisplatin. *FASEB J.* **1998**, *12*, 791–799. https://doi.org/10.1096/fasebj.12.10.791.

(241) Zamble, D. B.; Lippard, S. J.; Lippert, B. Cisplatin: Chemistry and Biochemistry of a Leading Anticancer Drug; Wiley-VCH: Weinheim, Germany, 1999; pp 73–110.

(242) Kasparkova, J.; Brabec, V. Recognition of DNA Interstrand Cross-Links of Cis-Diamminedichloroplatinum (II) and Its Trans Isomer by DNA-Binding Proteins. *Biochemistry* **1995**, *34*, 12379–12387.

(243) Brabec, V.; Kelland, L. R.; Farrell, N. P. *Platinum-Based Drugs in Cancer Therapy*; Humana Press Inc: Totowa, NJ, 2000.

(244) Zehnulova, J.; Kasparkova, J.; Farrell, N.; Brabec, V. Conformation, Recognition by High Mobility Group Domain Proteins , and Nucleotide Excision Repair of DNA Intrastrand Cross- Links of Novel Antitumor Trinuclear Platinum Complex BBR3464. *J. Biol. Chem.* **2001**, *276* (25), 22191–22199. https://doi.org/10.1074/jbc.M103118200.

(245) Sessa, C.; Capri, G.; Gianni, L.; Peccatori, F.; Grasselli, G.; Bauer, J.; Zucchetti, M.; Viganò, L.; Gatti,

A.; Minoia, C.; Liati, P.; Can den Bosch, S.; Bernareggi, A.; Camboni, G.; Marsoni, S. Clinical and Pharmacological Phase I Study with Accelerated Titration Design of a Daily Times Five Schedule of BBR3464, a Novel Cationic Triplatinum Complex. *Ann. Oncol.* **2000**, *11*, 977–983. https://doi.org/10.1023/A.

(246) Jodrell, D. I.; Evans, T. R. J.; Steward, W.; Cameron, D.; Prendiville, J.; Aschele, C.; Noberasco, C.; Lind, M.; Carmichael, J.; Dobbs, N.; Camboni, G.; Gatti, B.; De Braud, F. Phase II Studies of BBR3464, a Novel Tri-Nuclear Platinum Complex, in Patients with Gastric or Gastro-Oesophageal Adenocarcinoma. *Eur. J. Cancer* **2004**, *40*, 1872–1877. https://doi.org/10.1016/j.ejca.2004.04.032.

(247) Hensing, T.; Hanna, N. H.; Gillenwater, H. H.; Gabriella Camboni, M.; Allievi, C.; Socinski, M. A. Phase II Study of BBR 3464 as Treatment in Patients with Sensitive or Refractory Small Cell Lung Cancer. *Anticancer. Drugs* **2006**, *17* (6), 697–704.

(248) Komeda, S.; Moulaei, T.; Woods, K. K.; Chikuma, M.; Farrell, N. P.; Williams, L. D. A Third Mode of DNA Binding: Phosphate Clamps by a Polynuclear Platinum Complex. *J. Am. Chem. Soc.* **2006**, *128* (50), 16092–16103. https://doi.org/10.1021/ja062851y.

(249) Qu, Y.; Kipping, R. G.; Farrell, N. P. Solution Studies on DNA Interactions of Substitution-Inert Platinum Complexes Mediated via the Phosphate Clamp. *Dalt. Trans.* **2015**, *44* (8), 3563–3572. https://doi.org/10.1039/C4DT03237C.

(250) Koo, H.-S. S.; Crothers, D. M. Calibration of DNA Curvature and a Unified Description of Sequence-Directed Bending. *Proc. Natl. Acad. Sci. U. S. A.* **1988**, *85* (6), 1763–1767. https://doi.org/10.1073/pnas.85.6.1763.

(251) Rice, J. A.; Crothers, D. M.; Pintot, A. L.; Lippardt, S. J. The Major Adduct of the Antitumor Drug Cis-Diamminedichloroplatinum(II) with DNA Bends the Duplex by Approximately Equal to 40 Degrees toward the Major Groove. *Proc. Natl. Acad. Sci.* **1988**, *85*, 4158–4161.

(252) Hall, M. D.; Okabe, M.; Shen, D. W.; Liang, X. J.; Gottesman, M. M. The Role of Cellular Accumulation in Determining Sensitivity to Platinum-Based Chemotherapy. *Annu. Rev. Pharmacol. Toxicol.* **2008**, *48*, 495–535. https://doi.org/10.1146/annurev.pharmtox.48.080907.180426.

(253) Fuchs, S. M.; Raines, R. T. Internalization of Cationic Peptides: The Road Less (or More?) Traveled. *Cell. Mol. Life Sci.* **2006**, *63* (16), 1819–1822. https://doi.org/10.1007/s00018-006-6170-z.

(254) Belting, M. Heparan Sulfate Proteoglycan as a Plasma Membrane Carrier. *Trends Biochem. Sci.* **2003**, *28* (3), 145–151. https://doi.org/10.1016/S0968-0004(03)00031-8.

(255) Kjellen, L.; Lindahl, U. Proteoglycans: Structures and Interactions. *Annu. Rev. Biochem.* **1991**, *60*, 443–475.

(256) Linhardt, R. J.; Toida, T. Role of Glycosaminoglycans in Cellular Communication. *Acc. Chem. Res.* **2004**, *37*, 431–438.

(257) Fuchs, S. M.; Raines, R. T. Pathway for Polyarginine Entry into Mammalian Cells. *Biochemistry* **2004**, *43* (9), 2438–2444. https://doi.org/10.1021/bi035933x.

(258) Silva, H.; Frézard, F.; Peterson, E. J.; Kabolizadeh, P.; Ryan, J. J.; Farrell, N. P. Heparan Sulfate Proteoglycan-Mediated Entry Pathway for Charged Tri-Platinum Compounds: Differential Cellular Accumulation Mechanisms for Platinum. *Mol. Pharm.* **2012**, *9* (6), 1795–1802. https://doi.org/10.1021/mp300098t.

(259) Farrell, N. P.; Gorle, A. K.; Peterson, E. J.; Berners-Price, S. J. Metalloglycomics. In *Metallo-Drugs: Development and Action of Anticancer Agents*; Sigel, A., Sigel, H., Freisinger, E., Sigel, R. K. O., Eds.; Walter de Gruyter, GmbH: Belrin, Germany, 2018; pp 109–136.

(260) Mangrum, J. B.; Engelmann, B. J.; Peterson, E. J.; Ryan, J. J.; Berners-Price, S. J.; Farrell, N. P. A New Approach to Glycan Targeting: Enzyme Inhibition by Oligosaccharide Metalloshielding. *Chem. Commun.* **2014**, *50* (31), 4056–4058. https://doi.org/10.1039/C3CC49695C.

(261) Peterson, E. J.; Daniel, A. G.; Katner, S. J.; Bohlmann, L.; Chang, C.-W.; Bezos, A.; Parish, C. R.; von Itzstein, M.; Berners-Price, S. J.; Farrell, N. P. Antiangiogenic Platinum through Glycan Targeting. *Chem. Sci.* **2017**, *8* (1), 241–252. https://doi.org/10.1039/C6SC02515C.

(262) Samsonov, S.; Teyra, J.; Pisabarro, M. Docking Glycosaminoglycans to Proteins: Analysis of Solvent Inclusion. *J Comput Aided Mol Des* **2011**, *25*, 477–489.

(263) de Paiva, R. E. F.; Peterson, E. J.; Malina, J.; Zoepfl, M.; Hampton, J. D.; Johnson, W. E.; Graminha, A.; Ourahmane, A.; McVoy, M. A.; Brabec, V.; Berners-Price, S. J.; Farrell, N. P. On the Biology of Werner's Complex. *Angew. Chemie Int. Ed.* **2021**, *60*, 17123–17130. https://doi.org/10.1002/anie.202105019.

(264) Zhang, L.; Li, N.; Zhao, F.; Li, K. Spectroscopic Study on the Interaction between Methylene Blue and Chondroitin 4-Sulfate and Its Analytical Application. *Anal. Chem.* **2004**, *20* (3), 445–450. https://doi.org/10.2116/analsci.20.445.

(265) Gorle, A. K.; Katner, S. J.; Johnson, W. E.; Lee, D. E.; Daniel, A. G.; Ginsburg, E. P.; von Itzstein, M.; Berners-Price, S. J.; Farrell, N. P. Substitution-Inert Polynuclear Platinum Complexes as Metalloshielding Agents for Heparan Sulfate. *Chem. - A Eur. J.* **2018**, *24* (25), 6606–6616. https://doi.org/10.1002/chem.201706030.

(266) Jiao, Q.; Liu, Q.; Sun, C.; He, H. Investigation on the Binding Site in Heparin by Spectrophotometry. *Talanta* **1999**, *48*, 1095–1101.

(267) Tan, L.; Yao, S.; Xie, Q. Electrochemical Determination of Heparin Using Methylene Blue Probe and Study on Competition of Ba2+ with Methylene Blue for Binding Heparin. *Talanta* **2007**, *71*, 827–832.

(268) Chu, H.; Johnson, N. R.; Mason, N. S.; Wang, Y. A [Polycation:Heparin] Complex Releases Growth Factors with Enhanced Bioactivity. *J Control Release* **2011**, *150*, 157–163.

(269) Katner, S. J.; Johnson, W. E.; Peterson, E. J.; Page, P.; Farrell, N. P. Comparison of Metal-Ammine Compounds Binding to DNA and Heparin. Glycans as Ligands in Bioinorganic Chemistry. *Inorg. Chem.* **2018**, *57* (6), 3116–3125. https://doi.org/10.1021/acs.inorgchem.7b03043.

(270) Gorle, A. K.; Haselhorst, T.; Katner, S. J.; Everest-Dass, A. V.; Hampton, J. D.; Peterson, E. J.; Koblinski, J. E.; Katsuta, E.; Takabe, K.; von Itzstein, M.; Berners-Price, S. J.; Farrell, N. P. Conformational Modulation of Iduronic Acid-Containing Sulfated Glycosaminoglycans by a Polynuclear Platinum Compound and Implications for Development of Antimetastatic Platinum Drugs. *Angew. Chemie - Int. Ed.* **2021**, *60* (6), 3283–3289. https://doi.org/10.1002/anie.202013749.

(271) Hricovíni, M.; Driguez, P. A.; Malkina, O. L. NMR and DFT Analysis of Trisaccharide from Heparin Repeating Sequence. *J. Phys. Chem. B* **2014**, *118* (41), 11931–11942. https://doi.org/10.1021/jp508045n.

(272) Hricovíni, M.; Bízik, F. Relationship between Structure and Three-Bond Proton-Proton Coupling Constants in Glycosaminoglycans. *Carbohydr. Res.* **2007**, *342* (6), 779–783. https://doi.org/10.1016/j.carres.2007.01.003.

(273) Hricovíni, M.; Hricovíni, M. Solution Conformation of Heparin Tetrasaccharide. DFT Analysis of Structure and Spin–Spin Coupling Constants. *Molecules* **2018**, *23* (11). https://doi.org/10.3390/molecules23113042.

(274) Hricovíni, M. Solution Structure of Heparin Pentasaccharide: NMR and DFT Analysis. *J. Phys. Chem. B* **2015**, *119* (38), 12397–12409. https://doi.org/10.1021/acs.jpcb.5b07046.

(275) Kailemia, M. J.; Li, L.; Ly, M.; Linhardt, R. J.; Amster, I. J. Complete Mass Spectral Characterization of a Synthetic Ultralow-Molecular- Weight Heparin Using Collision-Induced Dissociation. *Anal. Chem.* **2012**, *84* (13), 5475–5478. https://doi.org/10.1021/ac3015824.

(276) Seo, Y.; Schenauer, M. R.; Leary, J. A. Biologically Relevant Metal-Cation Binding Induces Conformational Changes in Heparin Oligosaccharides as Measured by Ion Mobility Mass

Spectrometry. *Int. J. Mass Spectrom.* **2011**, *303*, 191–198. https://doi.org/10.1038/jid.2014.371.

(277) Staples, G. O.; Zaia, J. Analysis of Glycosaminoglycans Using Mass Spectrometry. *Curr. Proteomics* **2011**, *8* (4), 325–336. https://doi.org/10.2174/157016411798220871.Analysis.

(278) Mangrum, J. B.; Farrell, N. P. Excursions in Polynuclear Platinum DNA Binding. *Chem. Commun.* **2010**, *46* (36), 6640. https://doi.org/10.1039/c0cc01254h.

(279) Lippert, B.; Sanz Miguel, P. J. More of a Misunderstanding than a Real Mismatch? Platinum and Its Affinity for Aqua, Hydroxido, and Oxido Ligands. *Coord. Chem. Rev.* **2016**, *327*, 333–348. https://doi.org/10.1016/j.ccr.2016.03.008.

(280) Gorle, A. K.; Berners-Price, S. J.; Farrell, N. P. Biological Relevance of Interaction of Platinum Drugs with O-Donor Ligands. *Inorganica Chim. Acta* **2019**, *495* (May). https://doi.org/10.1016/j.ica.2019.118974.

(281) Hegmans, A.; Berners-Price, S. J.; Davies, M. S.; Thomas, D. S.; Humphreys, A. S.; Farrell, N. Long Range 1,4 and 1,6-Interstrand Cross-Links Formed by a Trinuclear Platinum Complex. Minor Groove Preassociation Affects Kinetics and Mechanism of Cross-Link Formation as Well as Adduct Structure. *J. Am. Chem. Soc.* **2004**, *126* (7), 2166–2180. https://doi.org/10.1021/ja036105u.

(282) Berners-Price, S.; Ronconi, L.; Sadler, P. J. Insights into the Mechanism of Action of Platinum Anticancer Drugs from Multinuclear NMR Spectroscopy. *rogress Nucl. Magn. Reson. Spectrosc.* **2006**, *49* (1), 65–98.

(283) Gorle, A. K.; Rajaratnam, P.; Chang, C. W.; Von Itzstein, M.; Berners-Price, S. J.; Farrell, N. P. Glycans as Ligands in Bioinorganic Chemistry. Probing the Interaction of a Trinuclear Platinum Anticancer Complex with Defined Monosaccharide Fragments of Heparan Sulfate. *Inorg. Chem.* **2019**, *58* (11), 7146–7155. https://doi.org/10.1021/acs.inorgchem.8b03035.

(284) Gorle, A. K.; Rajaratnam, P.; Chang, C.-W.; von Itzstein, M.; Berners-Price, S. J.; Farrell, N. P. No Title. *Manuscr. Prep.* **2021**.

(285) Bame, K. J.; Esko, J. D. No Title. *J. fo Biol. Chem.* **1989**, *264*, 8059–8065.

(286) Du, X.; Li, Y.; Xia, Y.-L.; Ai, S.-M.; Liang, J.; Sang, P.; Ji, X.-L.; Liu, S.-Q. Insights into Protein-Ligand Interactions: Mechanisms, Models, and Methods. *Int. J. Mol. Sci.* **2016**, *17* (2), 144. https://doi.org/10.3390/ijms17020144.

(287) Cheng, T. T.; Yao, J. L.; Gao, X.; Sun, W.; Shi, S.; Yao, T. M. A New Fluorescence "Switch on" Assay for Heparin Detection by Using a Functional Ruthenium Polypyridyl Complex. *Analyst* **2013**, *138* (12), 3483–3489. https://doi.org/10.1039/c3an00242j.

(288) Yu, Y.; Li, H.; Yang, Y.; Ding, Y.; Wang, Z.; Li, G. Evaluating Tumor-Associated Activity of Extracellular Sulfatase by Analyzing Naturally Occurring Substrate in Tumor Microenvironment of Hepatocellular Carcinoma. *Anal. Chem.* **2016**, *88* (24), 12287–12293. https://doi.org/10.1021/acs.analchem.6b03469.

(289) Stewart, M. D.; Sanderson, R. D. Heparan Sulfate in the Nucleus and Its Control of Cellular Functions. *Matrix Biol.* **2014**, *35*, 56–59. https://doi.org/10.1016/j.matbio.2013.10.009.Heparan.

(290) Naik, R. J.; Chatterjee, A.; Ganguli, M. Different Roles of Cell Surface and Exogenous Glycosaminoglycans in Controlling Gene Delivery by Arginine-Rich Peptides with Varied Distribution of Arginines. *Biochim. Biophys. Acta - Biomembr.* **2013**, *1828* (6), 1484–1493. https://doi.org/10.1016/j.bbamem.2013.02.010.

(291) Li, X.; Lan, Y.; He, Y.; Liu, Y.; Luo, H.; Yu, H.; Song, N.; Ren, S.; Liu, T.; Hao, C.; Guo, Y.; Zhang, L. Heparan Sulfate and Chondroitin Sulfate Glycosaminoglycans Are Targeted by Bleomycin in Cancer Cells. *Cell. Physiol. Biochem.* **2017**, *43* (3), 1220–1234. https://doi.org/10.1159/000481763.

(292) Gorle, A. K.; Zhang, J.; Liu, Q.; Berners-Price, S. J.; Farrell, N. P. Structural Factors Affecting Binding of Platinum Anticancer Agents with Phospholipids: Influence of Charge and Phosphate Clamp Formation. *Chem. - A Eur. J.* **2018**, *24* (18), 4643–4652.

https://doi.org/10.1002/chem.201705822.

(293) Rudd, T. R.; Guimond, S. E.; Skidmore, M. A.; Duchesne, L.; Guerrini, M.; Torri, G.; Cosentino, C.; Brown, A.; Clarke, D. T.; Turnbull, J. E.; Fernig, D. G.; Yates, E. A. Influence of Substitution Pattern and Cation Binding on Conformation and Activity in Heparin Derivatives. *Glycobiology* **2007**, *17* (9), 983–993. https://doi.org/10.1093/glycob/cwm062.

(294) Bohlmann, L.; Chang, C. W.; Beacham, I.; Von Itzstein, M. Exploring Bacterial Heparinase II Activities with Defined Substrates. *ChemBioChem* **2015**, *16* (8), 1205–1211. https://doi.org/10.1002/cbic.201500081.

(295) Levy-Adam, F.; Ilan, N.; Vlodavsky, I. Tumorigenic and Adhesive Properties of Heparanase. *Semin Cancer Biol* **2010**, *20* (3), 153–160. https://doi.org/10.1016/j.semcancer.2010.06.005.Tumorigenic.

(296) Malina, J.; Farrell, N. P.; Brabec, V. Substitution-Inert Trinuclear Platinum Complexes Efficiently Condense/Aggregate Nucleic Acids and Inhibit Enzymatic Activity. *Angew. Chemie - Int. Ed.* **2014**, *53* (47), 12812–12816. https://doi.org/10.1002/anie.201408012.

CHAPTER 2: Platinum structure activity relationships and mechanism of action against HCMV

2.0 Contributions

This chapter is a summary of "Substitution-inert polynuclear platinum compounds inhibit human cytomegalovirus attachment and entry" published in *Antiviral Research*.[1] Preliminary studies (luciferase based $EC_{50}s$ and gene expression assays) were performed by Dr. Amine Ourahmane. Synthesis and methylene blue studies were performed by Dr. Eric Ginsburg. MZ repeated preliminary studies and completed the remaining mechanistic work.

2.1 Background

HCMV, belonging to the beta-herpesviridae family, is an enveloped, double stranded DNA virus. HCMV infects up to 100% of the population.[2] For those fortunate healthy individuals, an HCMV infection may present as a common cold or be asymptomatic. However, in immunocompromised populations, including acquired immunodeficiency syndrome (AIDS) patients and transplant recipients, HCMV infections can result in significant clinical disease.[3–6] Importantly, HCMV can cross the placenta from mother to fetus and cause congenital birth defects characterized by neurodevelopmental delay, sensorineural hearing loss, microcephaly, seizures, intracranial calcifications, cerebral palsy, hepatitis, and chorioretinitis resulting in vision loss.[7–11] Current treatments for HCMV, such as ganciclovir, foscarnet, and cidofovir, target the viral DNA polymerase and halt DNA replication, while letermovir targets the viral terminase and disrupts viral DNA packaging.[2] However, viral resistance to all of these treatments occurs in the clinic and none are approved for use during pregnancy.

As evidenced by HCMV's broad organ tropism, HCMV has a broad cell range within the human body.[12] HCMV replicates in epithelial cells, endothelial cells, fibroblast, smooth muscle cells, dendritic cells, and macrophages. Each of these cell types play their own role in infection; for example, epithelial cells contribute to interhost transmission while endothelial cells and hematopoietic cells contribute to spread within the host.[12] Variations between strains of HCMV cell tropism depend on differences within the *UL128-131* genes, the genes required for cell entry. New treatments should examine viral entry, since HCMV infects a variety of cell types.

Like all herpes viruses, HCMV relies on glycoproteins glycoprotein B(gB) as well as glycoproteins H and L (gH/gL) for viral entry into cells (Figure 2.1). gB, encoded by UL55, interacts with cellular heparan sulfate (HS) and gB-null mutants are able to form viral particles but unable to enter cells without a chemical fusogen.[13,14] A dimer of glycoproteins M and N (gM/gN) also binds heparin immobilized on a column, and neutralizing antibodies target gM/gN.[15–17] Together gM/gN mediate viral attachment via HS but also have intracellular roles.[15,18,19] Through a combination of gB and gM/gN, HCMV virions attach to cellular HS, following which HCMV enters the cell either through endocytosis or membrane fusion. HCMV gH/gL form a heterotrimer with heavily N-glycosylated glycoprotein O, encoded by UL75, UL115, and UL74 respectively. The trimer binds its cellular receptor platelet derived growth factor receptor alpha (PDGFRα).[20–22] However, gO null mutants produce drastically smaller titers in fibroblasts compared to the wild type.[23–26] gH/gL also form a heteropentamer with three small glycoproteins encoded by *UL128-131A*. The *UL128-131A* locus is unstable during passage in fibroblasts, as the pentamer is not essential for fibroblast infection but it is required for the infection of leukocytes, dendritic cells, epithelial cells, and endothelial cells.[27–30] In 2018, neurophilin02 (Nrp2) was identified as the pentamer's receptors though other cellular surface proteins may also function as HCMV receptors.[31,32] Following the interaction of the trimer and/or pentamer with their respective receptors, HCMV enter the cell either by membrane fusion

or endocytosis. Disrupting either the interaction between virions and HS or between the trimer and/or pentamer and their receptors, could block viral entry.
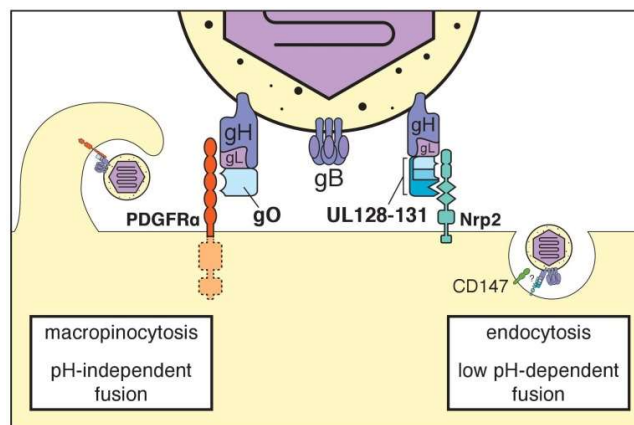
Figure 2.1: Receptors for HCMV gH/gL complexes. HCMV enters cells via two different methods. On the left, the trimer (gH/gL/gO complex) binds PDGFRα to trigger a pH-independent macropinocytosis. On the right, the pentamer (gH/gL/UL128–131 complex) binds Nrp2 to trigger a low pH-dependent endocytosis; CD147 is also required in the latter mode of entry. Reproduced from Nguyen et al. 2015.[32]

Substitution-inert polynuclear platinum compounds (PPCs) are a class of molecules with demonstrated high affinity for HS. Binding is modulated through electrostatic and hydrogen-bonding interactions with anionic sulfates and carboxylates on the HS backbone.[33] This *"metalloshielding"* of critical sulfate receptors by PPCs impedes HS functions in a number of biologically relevant processes, such as growth factor recognition and enzymatic (mammalian heparanase/ bacterial heparinase) cleavage.[34–37] Since HS plays a vital role in viral attachment, mediated through sulfate interactions, electrostatic, and H-bonding interactions,[38] we hypothesized that PPCs would likely interfere with viral attachment. In this study, we extend the reported biological consequences of the PPC/HS interaction to anti-HCMV activity through the use of a small library of PPCs that allowed exploration of the effects of charge, nuclearity (di/tri platinum units), length, and different polyamine linkers on anti-viral activity. We demonstrate that PPCs have anti-viral activity against HCMV in a charge-dependent manner, acting on both epithelial cells and fibroblasts, and act early in the viral replication cycle, consistent with inhibition of viral attachment.

2.2 Rationale for choice of polynuclear platinum compounds

The substitution-inert PPCs were developed from Triplatin, which was originally synthesized to subvert cisplatin resistance in cancer.[39] While Triplatin is useful in targeting cancer, it has labile Pt-Cl bonds, likely to react with any number of biologically relevant nucleophiles. The substitution inert PPC series lack Pt-Cl bonds and instead is based on a $Pt-N_4$ motif. The library used in this study is shown in Figure 2.2. MonoplatinNC (**I**) is the lone mononuclear compound of the series with the smallest positive charge (+4). DiplatinNC (**II**) is one of two dinuclear PPCs with a moderate charge (+6). BBR3571NC (**III**) has an amine in place of the middle platinum moiety of TriplatinNC and has a moderate charge (+7). TriplatinNC (**IV**) is the substitution inert analog of Triplatin with a high positive charge (+8); the rest of the series is based off of **IV**. AH44 (**VI**) maintains the positive charge (+6) of **IV** but has simple ammines on the terminal platinum moieties in place of dangling ammines. With positive charge of +8, three compounds differ only in the length of the alkyldiamine linker: TriplatinNC-but (**VII**), TriplatinNC-pent (**V**), and TriplatinNC-hept (**VIII**). A further two compounds were designed to be prodrugs of IV as acetyl and tert-butyloxycarbonyl protecting (Boc) group are easily cleaved in biological conditions. TriplatinNC-AA (**IX**) has

an acetyl group and TriplatinNC-Boc (**X**) has a Boc group on each of their two terminal dangling ammines, decreasing their charge to (+6). Finally, TetraplatinNC is a tetranuclear PPC with the highest charge of the series (+10). These compounds were chosen to examine variation in overall charge and nuclearity on efficacy on HCMV.
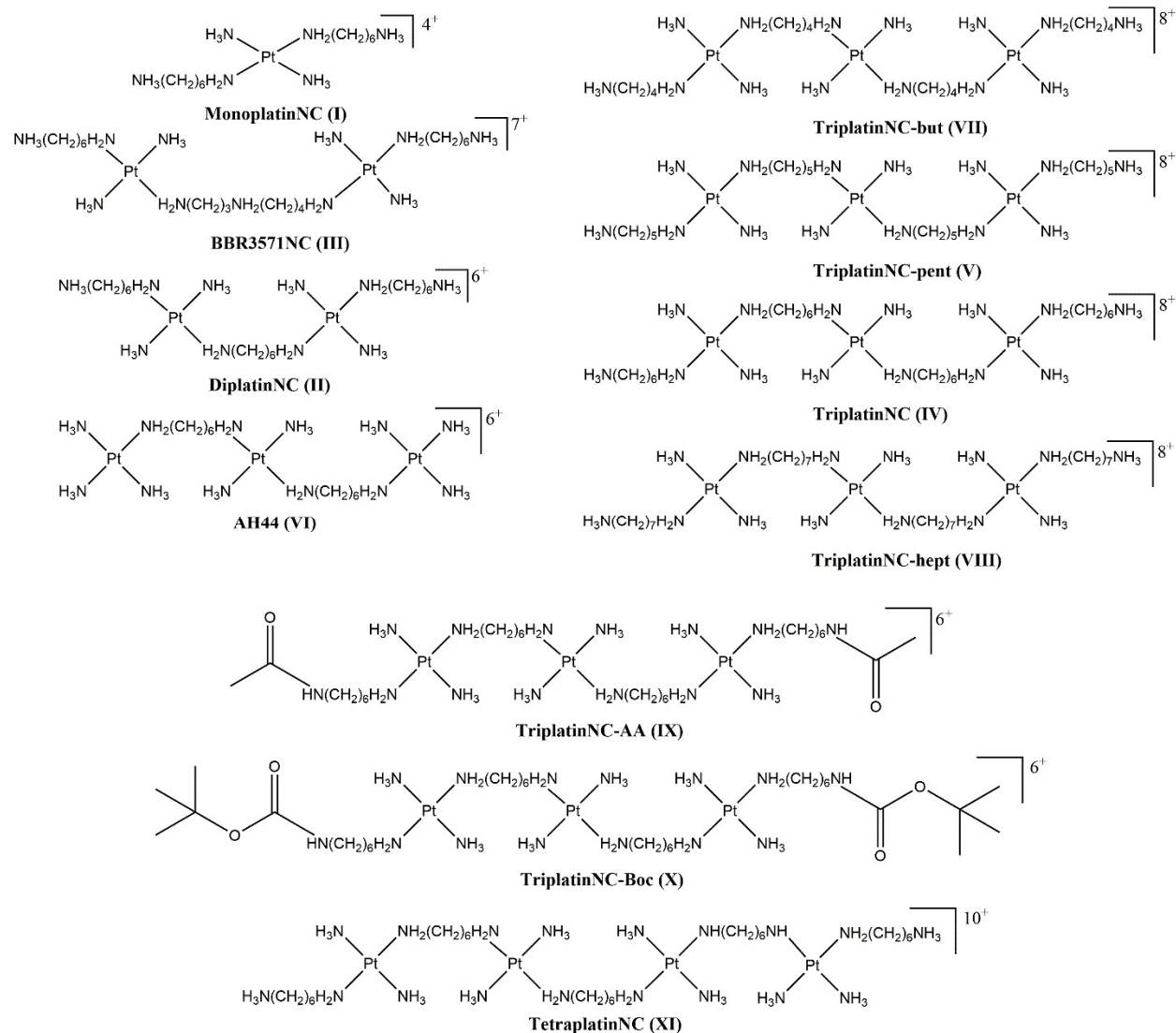
Figure 2.2: The structures of substitution-inert mononuclear and polynuclear platinum complexes. Counterions omitted for clarity.

2.3 Studies of HCMV antiviral activity

The antiviral activity of a compound is quantified by its EC_{50}, the concentration at which 50% of virus replication is inhibited. Cytotoxicity of a compound is quantified by its TC_{50}, the concentration at which 50% of the cells die. To determine EC_{50}s for PPCs, their impact on HCMV yield (production of cell-free infectious virus) was determined using a luciferase-tagged HCMV, while TC_{50}s were simultaneously determined for replicate uninfected cultures using the CellTiter-Glo cell viability assay.[40] Results are shown in Figure 2.3 and summarized in Table 2.1. **I**, although not cytotoxic, exhibited weak antiviral activity and failed to fully repress viral replication at concentrations as high as 200 μM; the dinuclear compounds **II** and **III** exhibited antiviral activities with moderate toxicity; **IV** and **V** exhibited similar antiviral activities,

although **V** was more cytotoxic. Unfortunately, **VI**, **VII**, **VIII**, and **XI** were cytotoxic and their antiviral activity could not be distinguished from their cytotoxicity. Although **X** was not cytotoxic, it also lacked antiviral activity. Finally, **IX** had some antiviral activity but failed to be consistent between trials, leading us to question its stability.

The selectivity index (SI) is the ratio of TC_{50} to EC_{50}. A high SI suggests a favorable safety and efficacy profile of a compound. **III** and **V** had low SIs due to low antiviral activity or high cytotoxicity, respectively, whereas **II** and **IV** had relatively high SIs (Table 2.1). Although **VI** was less cytotoxic than **IV**, it failed to improve on anti-HCMV activity resulting in a low SI. **VII**, **VIII**, **IX**, **X**, and **XI** all had SIs close to 1, meaning their cytotoxicity is approximately equal to their antiviral activity. For this reason, we proceeded with compounds **I-V** for mechanistic studies.

Table 2.1: Activities of PPCs

Structure	Name	Antiviral[a] (EC_{50})	Cytotoxicity[b] (TC_{50})	SI[c]	MB[d] (IC_{50})
I	MonoplatinNC	ND[e]	>200	ND[e]	25.5 ± 0.5
II	DiplatinNC	0.471 ± 0.16	54.31 ± 11.9	115.3	16.6 ± 0.4
III	BBR3571NC	4.066 ± 2.85	63.55 ± 14.4	15.6	17.4 ± 0.8
IV	TriplatinNC	0.338 ± 0.28	24.65 ± 9.53	72.9	10.2 ± 0.4
V	TriplatinNC-pent	0.329 ± 0.19	6.199 ± 3.4	18.8	13.8 ± 0.4
VI*	AH44	6.016	34.50	5.7	13.5 ± 0.5
VII*	TriplatinNC-but	0.8128	1.59	1.9	ND
VIII*	TriplatinNC-hept	6.182	3.969	~1	13.6
IX	TriplatinNC-AA	60.85 ± 11.5	>200	>3.3	12.3 ± 0.4
X*	TriplatinNC-Boc	51.60	~150	2.9	ND
XI*	TetraplatinNC	4.402	4.666	1.0	ND

[a]luciferase-based yield assay
[b]CellTiter-Glo® assay
[c]selectivity index (TC_{50}/EC_{50})
[a,b,d]µM; means of three independent experiments ± standard deviations
[d]inhibition of methylene blue binding to FPX (previously published data, [34])
ND: not determined
*Due to low SI on initial testing and limited quantity available, replicate experiments were not conducted.
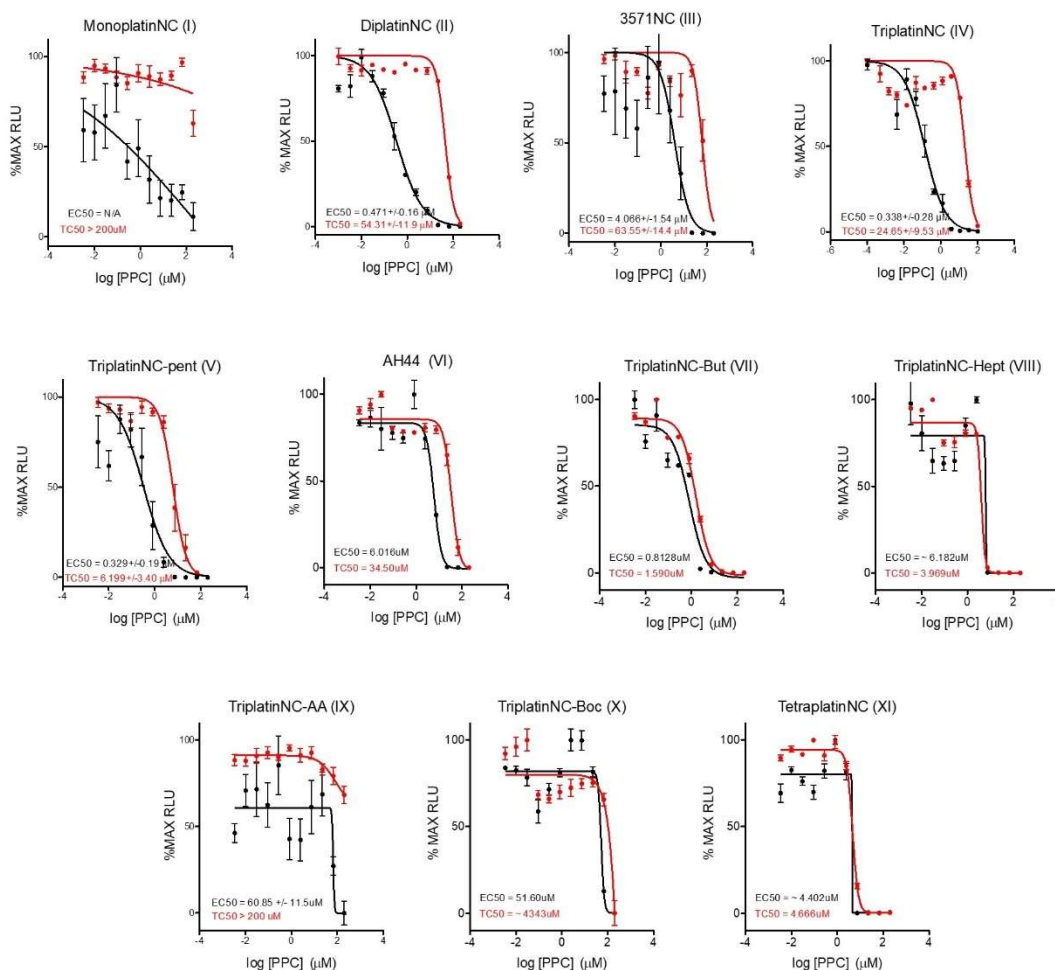
Figure 2.3: Luciferase-based antiviral activities and cytotoxicities of PPCs in fibroblasts. Anti-HCMV activity (black) was measured by incubating MRC-5 fibroblast monolayers in 96-well plates with PPCs for one h, then infecting with luciferase-tagged HCMV RC2626 (125 plaque forming units (PFU)/well). After five days 50 μL of virus-containing culture medium was transferred to fresh MRC-5 cultures and luciferase activities (RLU) in these cultures were measured 48 h later. Cytotoxicity (red) was measured in replicate uninfected cultures treated for five days using the CellTiter-Glo® assay. Data are means of three independent experiments except for compounds VI-VIII and X-XI due to limited quantities.

2.4 Studies of gene expression

The yield-based assay used above measured the impact of PPCs on release of infectious virus progeny. However, our hypothesis predicted that PPCs block viral attachment and entry and therefore should block viral gene expression. We first tested this using a green fluorescent protein (GFP) tagged virus, and as HCMV enters fibroblasts by fusion at the cell surface and epithelial cells by endocytosis,[41,42] we investigated the impact of PPCs on GFP expression in MRC-5 fibroblasts and ARPE-19 epithelial cells.[42] Controls included heparin, known to block HCMV entry,[43] and BAY 38-4766, a terminase inhibitor that acts late in infection and does not impact viral gene expression.[44] When added one h prior to infection, heparin and PPCs **II-V** inhibited GFP expression in both MRC-5 fibroblasts and ARPE-19 epithelial cells, while BAY 38-4766 and PPC **I** did not (Figure 2.4). By contrast, when added one hpi, PPCs **I**, **II**, and **IV** had no impact on GFP expression in either cell type relative to the no inhibitor, heparin, or BAY 38-4766 controls (Figure 2.4).
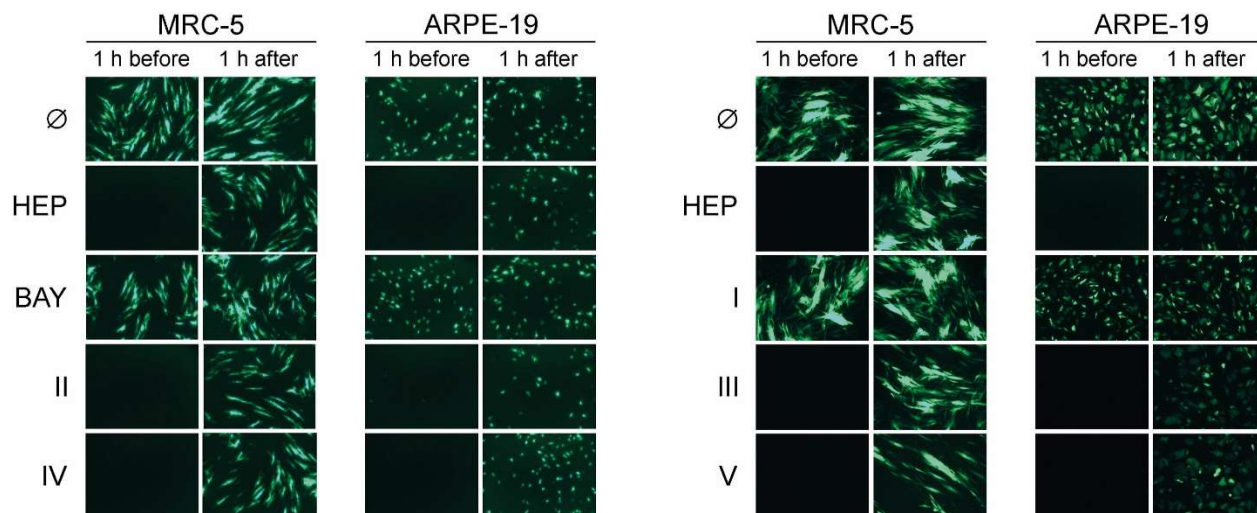
Figure 2.4: PPCs added before infection inhibit expression of a viral marker protein in fibroblasts and epithelial cells. Confluent monolayers of MRC-5 fibroblasts or ARPE-19 epithelial cells in 96-well plates were treated with medium (Ø), 150 µg/ml heparin (HEP), 8 µM BAY 38-4766 (BAY), 20 µM I, 10 µM II, 10 µM III, 5 µM IV, or 1.5 µM V one h before or one h after infection with GFP-tagged HCMV BADr (100 PFU/well). Representative fluorescent micrographs were taken six days post infection.
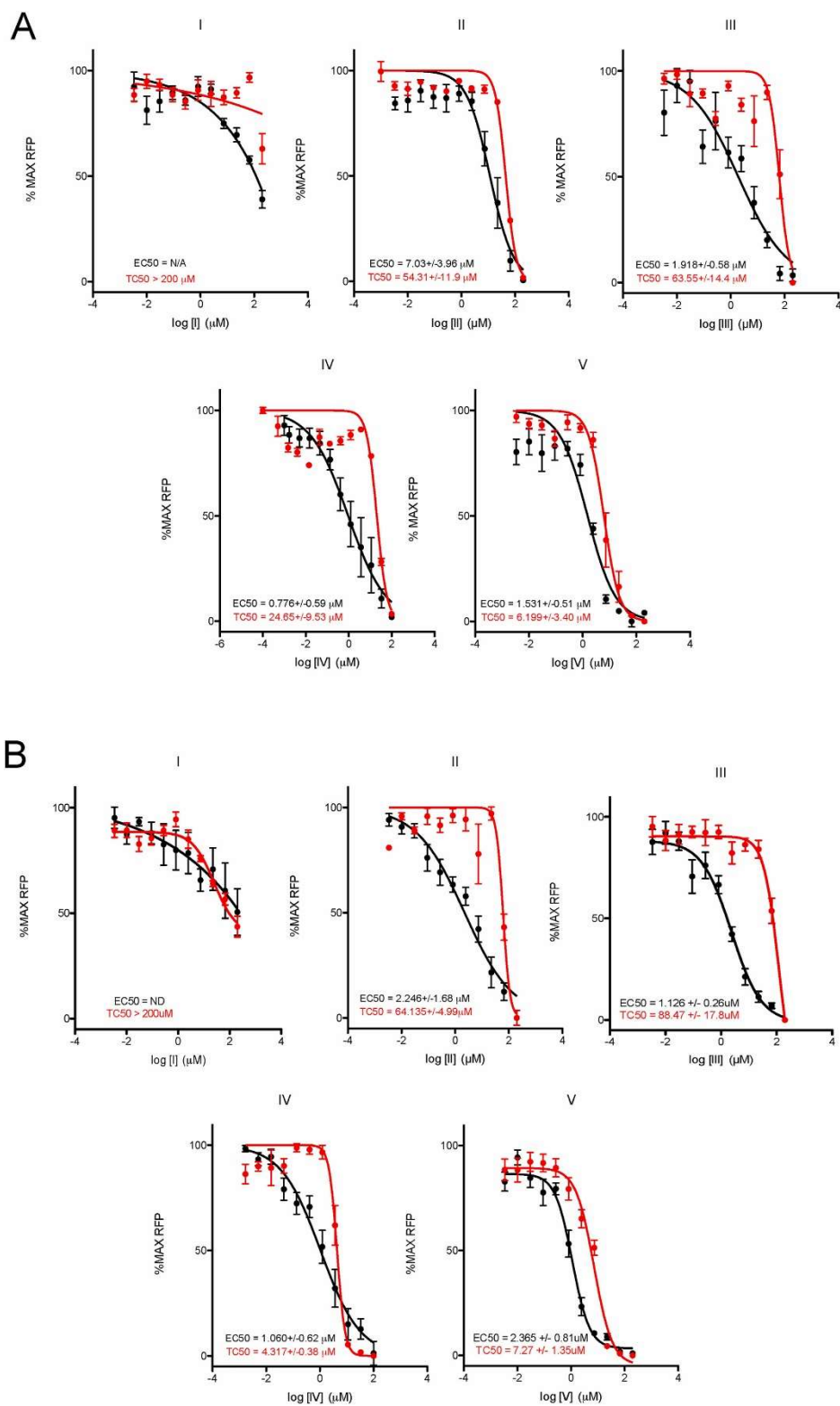
Figure 2.5: GFP-based antiviral activities and cytotoxicities of PPCs in fibroblasts and epithelial cells. Anti-HCMV activity (black) was measured by incubating confluent monolayers of MRC-5 fibroblasts (A) or ARPE-19 epithelial cells (B) with PPCs for one h, then infecting with GFP-tagged HCMV BADr (100 PFU/well) and measuring GFP levels (RFU) six days after infection. Cytotoxicity (red) was measured in replicate uninfected cultures treated for five days using the CellTiter-Glo® assay. Data are means of three independent experiments ± standard deviations.

GFP-based EC$_{50}$s were next determined by quantification of GFP as a marker for viral gene expression (Figure 2.5 and Table 2.2). Similar EC$_{50}$s for the two cell types were obtained for **II-V**, although all appeared less potent in the GFP-based assay compared to the luciferase-based yield assay, and the cytotoxicity of **IV** was higher in ARPE-19s than MRC-5s (Figure 2.5 and Table 2.2). Using the GFP-based assay, **I** again exhibited only partial antiviral activity even at high concentrations (Figure 2.5 and Table 2.2).

Table 2.2. Anti-viral activities determined using GFP-based assays

Structure	MRC-5 *fibroblasts*			ARPE-19 *epithelial cells*		
	Antiviral[a] (EC$_{50}$)	*Cytotoxicity[b] (TC$_{50}$)*	*SI[c]*	*Antiviral[a] (EC$_{50}$)*	*Cytotoxicity[b] (TC$_{50}$)*	*SI[c]*
I	ND[d]	>200	ND[d]	ND[d]	>200	ND[d]
II	7.03 ± 3.96	54.31 ± 11.9	7.7	2.246 ± 1.68	64.135 ± 4.99	29
III	1.918 ± 0.58	63.55 ± 14.4	33.1	1.126 ± 0.26	88.47 ±17.8	78.5
IV	0.776 ± 0.59	24.65 ± 9.53	31.8	1.060 ± 0.62	4.317 ± 0.38	4.1
V	1.513 ± 0.51	6.199 ± 3.4	4.1	2.365 ± 0.81	7.27 ± 1.35	3.1

[a] *GFP-based assay*

[b] *CellTiter-Glo® assay*

[a, b] *µM; means of three independent experiments ± standard deviations*

[c] *selectivity index (TC$_{50}$/EC$_{50}$)*

[d] *not determined*

Based on their ability to inhibit GFP, PPCs must act relatively early in the viral gene expression cascade. We therefore used immunofluorescent staining to determine the impact of PPCs **II** and **IV** on HCMV immediate early (IE) proteins 1 and 2, among the first viral proteins to be expressed within an infected cell, and the late viral protein pp28, which is expressed late in infection and only after viral DNA synthesis. Controls included heparin, an entry inhibitor predicted to block both IE and late protein expression, PFA, a viral DNA polymerase inhibitor predicted to inhibit late but not IE protein expression, and BAY 38-4766, predicted to have no effect on either.[43–45] These controls behaved as expected, while PPCs **II** and **IV**, consistent with inhibition of virion attachment, fully inhibited both IE1/2 and pp28 expression (Figure 2.6).
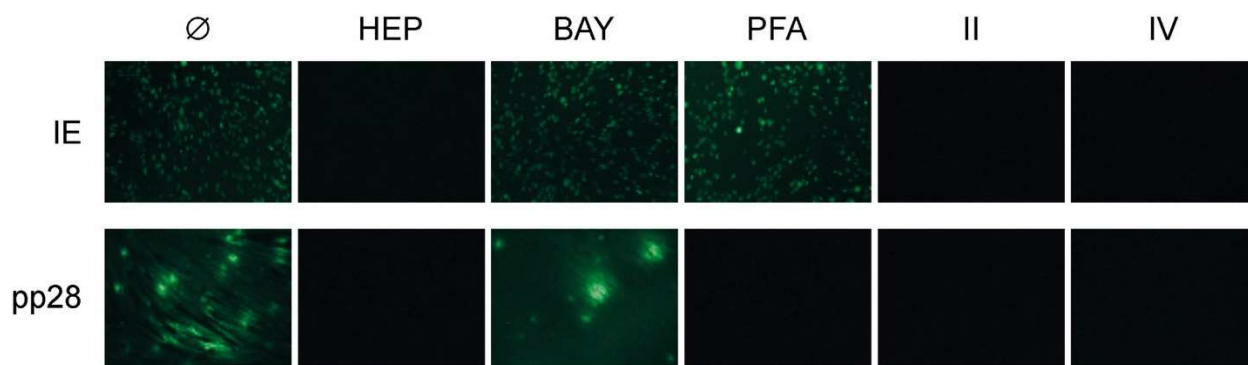
Figure 2.6: PPCs inhibit expression of HCMV IE and pp28 late proteins. MRC-5 fibroblast monolayers were treated with medium (Ø), 150 µg/ml heparin (HEP), 8 µM BAY 38-4766 (BAY), 3.2 mM PFA, 10 µM II, or 5 µM IV one h before infection with HCMV RC2626 (125 PFU/well). Cultures were fixed and fluorescently stained for HCMV IE proteins 48 hpi or for pp28 late protein 120 hpi.

2.5 Time of addition and removal studies

To further define the mechanism of action of PPCs, a time of addition experiment was conducted using a luciferase-based yield assay in which inhibitor was added at different times relative to viral

infection. Unfortunately, consistent results could not be produced. A similar time of addition experiment was conducted using GFP on day six after infection as a measure of viral inhibition after adding inhibitors at different times relative to viral infection. Like heparin, PPCs **II** and **IV** were only active when added within a few hours of adding the virus and lacked antiviral activity if added as early as 12 h after infection (Figure 2.7).
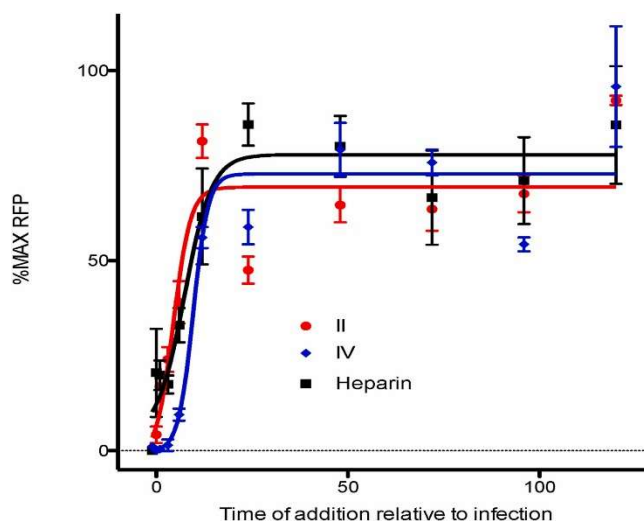
Figure 2.7: Time of addition study. Confluent monolayers of MRC-5 fibroblasts were treated 150 µg/ml heparin, 10 µM II, or 5 µM IV 1 h before, concurrent with, or at various times after infection with GFP-tagged HCMV BADr (100 PFU/well). GFP expression was quantified on day six post infection. Data are means of triplicate wells ± standard deviations.

Treatment/removal experiments were performed to define requirements for PPC interactions with cells or virions. MRC-5 fibroblasts or ARPE-19 epithelial cells were treated with medium or with heparin, **II**, or **IV** for one h, then washed with media prior to infection with GFP-tagged virus BADr. Consistent with heparin acting by binding to virions, pretreatment of cells with heparin and then removal by washing had no effect on subsequent infection (Figure 2.8A). In contrast, pretreatment of either cell type with **II** and **IV** significantly reduced the number of infected GFP+ cells compared to untreated or heparin-treated cells (Figure 2.8A). In the converse experiment virions were incubated with PPCs and then filtered to remove unbound PPCs prior to cell infection. The infectivity of virions treated with **II** or **IV** remained high when used to infect ARPE-19 cells; however, when the same samples were added to MRC-5 cultures their infectivity was significantly reduced (Figure 2.8B). That filtration was effective in reducing the concentrations **II** or **IV** to subinhibitory levels was demonstrated by the unimpaired infectivity of controls in which virions and compounds were filtered separately, then combined prior to infection (Figure 2.8C). While heparin was included as a positive control to demonstrate effective inhibition, it should be noted that heparin is too large to pass through these filters and therefore remained in the retentate with the virions.

These results are consistent with the proposed mode of action in which **II** and **IV** bind to cellular HS and thereby prevent subsequent virion attachment. However, the reduced MRC-5 infectivity of treated virions suggests that **II** and **IV** can also bind to virion components, and that such binding selectively inhibits subsequent MRC-5 but not ARPE-19 infection.
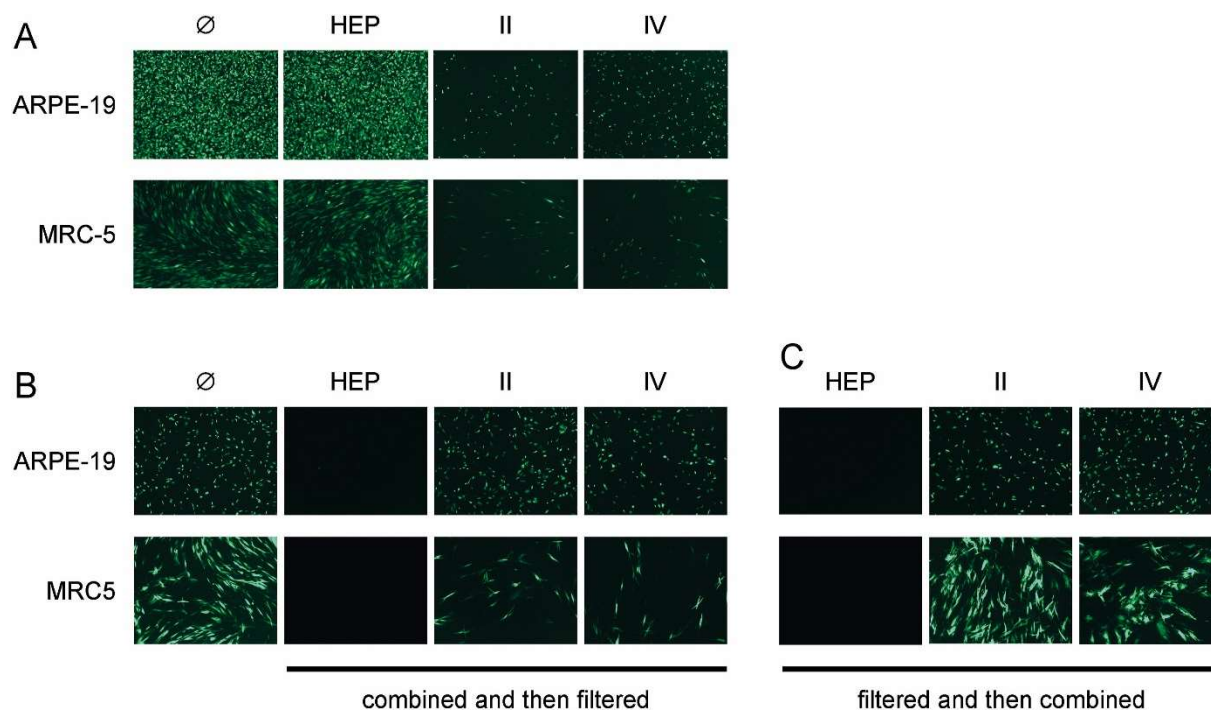
Figure 2.8: Treatment/removal studies. (A) Confluent monolayers of MRC-5 fibroblasts or ARPE-19 epithelial cells in 96-well plates were treated with medium (Ø), 150 µg/ml heparin (HEP), 10 µM II, or 5 µM IV for one h then washed three times with media and infected with GFP-tagged HCMV BADr (100 PFU/well). (B) BADr virions were incubated with medium (Ø), 300 µg/ml heparin, 10 µM II, or 5 µM IV for one h, then filtered to reduce the concentrations of unbound compounds by approximately 100-fold and added to untreated cells. (C) Untreated BADr virions or medium lacking virions but containing 300 µg/ml heparin, 10 µM II, or 5 µM IV were filtered as in (B). The filtered virions were then combined with filtered compounds as indicated and added to untreated cells. Figures show representative fluorescent micrographs taken six days post infection.

Several attempts were made to establish whether or not PPCs block HCMV virion attachment. First, ^{3}H labeled HCMV was produced to quantitatively assess virions attached to the cell surface. Although the viral stock had good radioactivity, *in vitro* experimental data showed that either (1) 3H-thymidine was not incorporated into the virus and thus was washed away, (2) the 3H-thymidine did not efficiently label the virus, or (3) the experiment *in vitro* method was not optimized (Figure 2.9).
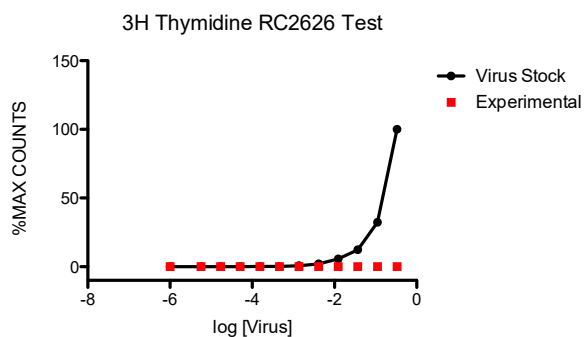
Figure 2.9: 3H thymidine labeled RC2626 test. MRC5 cells were infected with RC2626 in the presence of 3H thymidine in order to make a labeled viral stock. This stock was serially diluted and MRC5 cells were harvested 48 hpi. The amount of 3H thymidine was measured by a scintillator.

The HCMV pp65 protein is an abundant component of the virion tegument.[46] Upon infection, virion-associated pp65 is deposited first into the cytoplasm and subsequently localizes to the nucleus.[47] Consequently, pp65 staining shortly after infection serves to indicate virion attachment.[48] To determine if PPCs inhibit pp65 deposition, MRC-5 fibroblasts were untreated or treated for one h with heparin, **II**, or **IV**, then infected with BADr and incubated six h before fixation and immunofluorescent staining with an antibody to pp65. The pp65 signal could be readily detected in the untreated control culture, whereas treatment with heparin, **II**, or **IV** each eliminated the pp65 signal (Figure 2.10). This result indicates that, like heparin, **II** and **IV** inhibit virion attachment to cells.

Figure 2.10: PPCs inhibit cellular deposition of tegument protein pp65. MRC-5 fibroblast monolayers were treated with medium (∅), 150 µg/ml heparin (HEP), 10 µM II, or 5 µM IV for one h and then incubated with HCMV BADr (200 PFU/well) for one h at 4°C. Cultures were then shifted to 37°C and incubated for six hours before being fixed and fluorescently stained for the HCMV tegument protein pp65.

2.6 Discussion

Most current treatments for HCMV (ganciclovir, its orally available prodrug valganciclovir, cidofovir, and foscarnet) target the viral DNA polymerase (UL54). Letermovir is unique in that it inhibits viral DNA packaging. Unfortunately, all suffer from acquired resistance and the DNA polymerase inhibitors cause dose-limiting side effects.[45]

Like all herpesviruses, HCMV relies on envelope glycoproteins for virion entry into cells. gB and the gM/gN heterodimer are believed to interact with HS on the cell surface to initiate attachment.[43,49] Unlike most anti-viral targets, HS is an extracellular non-viral structure. Thus, antivirals targeting virion/HS binding are presumably less prone to develop resistance, as the virus would have to mutate to acquire mechanisms of entry that no longer rely on HS. The HS/viral interaction has been the focus of antiviral research as disrupting the interaction has the potential to inhibit infection of any HS-dependent virus.

As well-defined substitution-inert coordination compounds, PPCs are not as easily subject to the enzymatic degradation that diminish the efficacy of antiviral activity of heparin and other HS mimetics. Further, their substitution-inert nature means they are not susceptible to metabolic degradation by thiol-containing substances such as glutathione, which are considered to deactivate the anticancer agent cisplatin.[50] In this study, we examined the antiviral activities of five PPCs, which we predicted would prevent viral entry by virtue of metalloshielding of HS. Consistent with this hypothesis, we found that antiviral activities of PPCs loosely correlate with their GAG affinity (Table 2.1). **I** is the only mononuclear compound of the series studied and did not display effective antiviral activity. This is consistent with a relatively small positive charge (+4) and the lowest GAG affinity of the PPCs studied.[34] The dinuclear compounds (**II** and **III**) were among the least cytotoxic of the series with good anti-HCMV activity. In agreement with their GAG affinity, **II** outperformed **III** across the board, suggesting an increase in length is not advantageous; however, inhibition of attachment may be charge-dependent. The trinuclear compounds, **IV** and **V**, possess the same overall charge, but the alkyldiamine chain linking the platinum centers varies. **IV** and **V** have nearly identical antiviral activities, outperforming the dinuclear compounds,

but the higher cytotoxicity of **V** reduces its selectivity index (Table 2.1). Other compounds, such as **IX** and **X**, had protecting groups on the terminal dangling amines and had reduced antiviral activity, suggesting that either increased bulk or decreased charge are unfavorable.

Following attachment of HCMV virions, a trimeric complex of glycoproteins H, L, and O (gH/gL/gO) is required for entry into fibroblasts, while entry into epithelial and endothelial cells requires in addition a pentameric complex consisting of gH/gL complexed with UL128, UL130, and UL131A.[51] However, as HCMV presumably relies on HS for attachment in either case, inhibitors of virion/HS interaction should be active despite cell type. As seen with **II** through **V**, PPCs inhibit HCMV in both fibroblasts and epithelial cells, although EC$_{50}$s varied between cell type (Table 2.2).

In agreement with the proposed molecular mechanism of inhibiting virion attachment, **II** and **IV** blocked cellular deposition of pp65 as well as downstream events of viral immediate early and late gene expression. Also consistent with a block to attachment, antiviral activity depended on their presence prior to or very soon after addition of virus. Indeed, in these respects the PPC phenotype closely paralleled that of heparin, a known attachment inhibitor.[43] Unlike heparin, however, PPCs are not predicted to interact with virions, but instead are proposed to function through metalloshielding of HS, precluding virion attachment. This is supported by treatment/removal experiments demonstrating that PPCs **II** and **IV** act by binding to cells while heparin does not. However, both **II** and **IV** also exhibited inhibition when bound to virions, although surprisingly this activity was selective for fibroblast but not epithelial cell infection. This suggests that PPCs bind to virion factors that are important for fibroblast entry but dispensable for epithelial cell entry.

Collectively, our findings suggest that targeting HS merits consideration as a strategy to block viral attachment, which should be less subject to development of viral resistance than current treatments. Cisplatin exhibits activity against herpes simplex II infections but its cytotoxicity would preclude its use as an antiviral agent.[52] The advantage of the substitution-inertness of the PPCs discussed here, acting through only molecular recognition motifs of hydrogen bonding and electrostatic interactions, is that they are less cytotoxic than covalently binding cisplatin. The concept is further extendable to other substitution-inert charged coordination compounds with considerable scope for enhancing selectivity index for antiviral applications.

2.7 Conclusion

Our study demonstrates the utility of the metalloglycomics concept – the study of the interaction of metal ions and coordination compounds with biologically relevant oligosaccharides and, in particular, GAGs and proteoglycans – in design of new antiviral chemotypes.[39] Exploitation of the high PPC-HS affinity gives effective HCMV inhibitors, with the potential for broad spectrum antiviral activity. *In vivo*, GAGs are associated with aquated metal ions such as Na$^+$, Ca^{2+} and Zn^{2+}. The inherent ability of coordination compounds to alter oxidation state, coordination number and geometry, as well as substitution lability of coordinated ligands will allow systematic modulation to produce a wide range of chemotypes for refinement of structure-activity relationships, and in this case therapeutic selectivity. Unlike heparin mimetics and small peptides, the ability of PPCs to withstand enzymatic cleavage and/or thiol degradation offers a potential enhancement over these approaches.[53] New alternative strategies to exploit glycans in general as targets for medical and clinical use are still needed and therapeutic intervention of glycan function remains an understudied area compared to approaches for DNA and proteins.[39] To our knowledge, this is the first demonstration of direct interaction of a coordination compound with a virion, opening new areas for exploration in bioinorganic chemistry. This proof-of-concept of the utility of HS metalloshielding thus suggests potential for a broad-spectrum class of agents acting on both RNA and DNA viruses. In summary, inhibition of viral attachment to GAGs is an attractive yet still underexploited

target and these results blend the two areas of glycan targeting and medicinal inorganic chemistry into a new innovative field of high clinical relevance, expanding both areas of research into hitherto unexplored territory.

2.7 Experimental methods

2.7.1 Cell and viral culture

Human MRC-5 fetal lung fibroblasts (ATCC CCL-171) and human APRE-19 epithelial cells (derived from retinal pigment epithelium) (ATCC CRL-2302) were purchased from American Type Culture Collection. MRC-5 and APRE-19 cells were cultured at 37°C in a 5% CO_2 atmosphere using Dulbecco's Modified Eagle Medium supplemented with 10% fetal bovine serum, 50 U/mL penicillin, 50 mg/mL streptomycin, and 29.2 mg/mL L-glutamine (DMEM, all from Life Technologies).

Virus BAD*r*UL131-Y4 (BADr), a gift from Dai Wang and Thomas Shenk, is a variant of HCMV strain AD169 that is epithelial tropic due to repair of a mutation in *UL131A* and contains a green-fluorescent protein (GFP) reporter cassette.[54] Virus RC2626 is a variant of HCMV strain Towne that contains an expression cassette for firefly luciferase.[55] RC2626 and BADr were propagated in MRC-5 and ARPE-19 cells, respectively. Virus stocks were derived from infected cell culture supernatants, adjusted to 0.2 M sucrose, and stored in liquid nitrogen. Viral titers were determined using MRC-5s as described.[56]

2.7.2 Compounds and compound synthesis

BAY 38-4766 was a gift from Bayer Pharmaceuticals, foscarnet (phosphonoformic acid, PFA) was purchased from InvivoGen, and heparin sodium was purchased from Acros Organics (Lot # B0146868). MonoplatinNC, DiplatinNC, TriplatinNC, AH44, TriplatinNC-pent, TriplatinNC-hept, TriplatinNC-Boc, and TetraplatinNC were prepared according to published methods.[34,57,58] BBR3571NC was synthesized through adaptation of published procedures.[1,59] TripaltinNC-but was synthesized through the adaption of TriplatinNC-hept and -pent procedures.[60] The complexes were characterized by C, H, N elemental analysis, and ^{1}H and [195]Pt nuclear magnetic spectroscopy.

TriplatinNC-AA:[61] TriplatinNC (1mmol) was dissolved in water, and DIPEA (2.2 mmol) was added. After 30 minutes, acetic anhydride was added dropwise over a period of 1 h. The reaction was then heated at 50°C for 48 hours and filtered through celite to remove any unreacted starting materials and reduced platinum. The volume of the filtrate was reduced to almost dryness and acetone was added to force the precipitation of the product. The precipitate was filtered off then washed with acetone. Further purification, as needed, was achieved by recrystallization in water. Yield- 84% 1H NMR (D2O): δ 3.08 (t,4H), 2.56 (t, 12H), 1.90 (s, 6H), 1.55 (m, 12H), 1.42 (m 4H), 1.24 (m,16H). Elemental analysis calculatedd for C28,H85,N20,O20,Pt3 - C 20.92, H 5.33, N 17.43. Obtained: C 20.90, H 5.27, N 17.38.

BAY 38-4766, PFA, MonoplatinNC, DiplatinNC, BBR3571NC, TriplatinNC, and TriplatinNC-pent were dissolved in water at a stock concentration of 10 mM. Heparin was dissolved in water at a stock concentration of 1000 µg/mL.

2.7.3 Luciferase-based yield assay of antiviral activity

Eleven three-fold serial dilutions of **I-XI** were prepared in DMEM. Final concentrations ranged from 200 µM to 3.4 nM for **I-III** and **V-XI** and from 100 µM to 1.7 nM for TriplatinNC. Black-wall/clear-bottom 96-well plates with confluent monolayers of MRC-5 cells were treated with different concentrations of each test compound in triplicate. After one h incubation cells were infected with RC2626 (125 PFU/well). Infected and uninfected wells without compound served as controls. Following incubation for five days 100 µL of culture media was removed from each well and transferred to wells of a fresh 96-well plate containing confluent uninfected MRC-5 cells. Following an additional two-day incubation luciferase activity was measured by removing 100 µL of media and adding 100 µL of Steady-Glo® luciferase substrate (Promega), incubating ten minutes at room temperature, and measuring relative luminosity units (RLU) using a BioTek Synergy HT Multi-Mode Microplate reader. Prism 5 software (Graphpad) was used to determine 50% effective concentration (EC_{50}) values as the inflection points of best-fit four-

parameter curves for RLU (means of triplicate data) versus log inhibitor concentration. Graphical representations were normalized to % maximum RLU.

2.7.4 GFP-based assay of antiviral activity

Confluent monolayers of MRC-5 or ARPE-19 cells in 96-well plates were prepared and treated with compound dilutions as described in *2.7.3* above. After one h of incubation cells were infected with virus BADr (100 PFU/well). Following incubation for six days, relative fluorescence units (RFU) of GFP fluorescence were quantified by BioTek Synergy HT Multi-Mode Microplate reader and EC_{50} values were determined as described in *2.7.3*. Graphical representations were normalized to % maximum RFU.

2.7.5 Cytotoxicity

Replicate MRC-5 or ARPE-19 cell cultures were prepared simultaneously with those described in *2.7.3* and *2.7.4* but were not infected. After incubation of five days cell viability was determined by removing 100 µL of culture media from each well, adding 100 µL of CellTiter-Glo® reagent (Promega), incubation for ten minutes at room temperature, and measuring RLU using a BioTek Synergy HT Multi-Mode Microplate reader. 50% cytotoxicity concentrations (TC_{50}) were calculated as inflection points of four-parameter curves as described in *2.3*. Graphical representations were normalized to % maximum RLU.

2.7.6 Inhibition of GFP fluorescence

Inhibition of GFP expression was evaluated by treating confluent monolayers of MRC-5 or ARPE-19 cells in black-wall/clear-bottom 96-well plates with compounds for one h before addition of 100 PFU/well virus BADr. Six days after infection representative micrographs were taken with a Nikon Eclipse TS100 Inverted UV microscope.

2.7.7 Detection of viral proteins by immunofluorescence (IFA)

Confluent monolayers of MRC-5 cells in 16-well Nunc™ Lab-Tek™ glass chamber slides (ThermoFisher) were treated with compounds and one h later infected with RC2626 (125 PFU/well). Cells were fixed and stained for detection of HCMV immediate early (IE) proteins 48 h post infection (hpi) or for pp28 late protein 120 hpi. Culture medium was removed and monolayers were fixed with 1% formaldehyde in PBS for 30 min., washed three times with PBS, permeabilized by incubation on ice for 20 minutes with 0.5% Triton-X100 in PBS, washed three times with PBS, then incubated 30 minutes at room temperature in blocking buffer (20% fetal bovine serum in PBS). Fixed cells were then incubated one h at room temperature with primary antibodies to HCMV IE1 and IE2 proteins (MAB810, Millipore Sigma) or to pp28 (CH19, Virusys) diluted 1:600 in blocking buffer. After washing three-four times with blocking buffer, cells were incubated in the dark for one h at room temperature with secondary goat anti-mouse IgG conjugated to Alexa Fluor 488 (Life Technologies) diluted 1:200 in blocking buffer, then washed three-four times with PBS and imaged with a Nikon Eclipse TS100 Inverted UV microscope. A similar protocol was used to detect the HCMV tegument protein pp65 except that MRC-5 cells in chamber slides were treated with compounds for one h, infected at 4°C with BADr (200 PFU/well) for one h, then shifted to 37°C and fixed at six hpi. Detection used anti-pp65 primary antibody (CA003-100, Virusys) with secondary goat anti-mouse IgG conjugated to Alexa Fluor 594 (Life Technologies) and imaged with a Zeiss Axio Imager 2 and 89-North PhotoFluor LM-75.

2.7.8 Time of addition and treatment/removal studies

Confluent monolayers of MRC-5 cells in black-wall/clear-bottom 96-well plates were infected with BADr (100 PFU/well). A single inhibitory concentration of each compound (150 µg/ml heparin, 10 µM **II**, or 5 µM **IV**) was added to triplicate wells one h before, at the time of, and 3, 6, 12, 24, 48, 72, 96, or 120 hpi. Infected or uninfected wells not treated with compounds served as controls. Following incubation for

six days, GFP fluorescence was quantified using a BioTek Synergy HT Multi-Mode Microplate reader. Percent maximum RFUs were plotted versus time of compound addition (relative to infection) using Prism 5 software.

To determine if PPCs act by interacting with cells or with virions, 10 μM DiplatinNC, 5 μM TriplatinNC, or 300 μg/mL heparin were incubated for one h with either BADr virions or with confluent monolayers of MRC-5 or ARPE-19 cells in black-wall/clear-bottom 96-well plates. Compounds were then removed from cells by three washes with DMEM or from virions by filtration using Vivaspin 20 centrifugal concentrators (Sartorius Stedim; MWCO 50,000). Matching solutions of DiplatinNC, TriplatinNC, or heparin, each lacking virions, as well as virions incubated with DMEM, were similarly filtered and combined after filtration to serve as controls. Treated/washed cells were infected with 100 PFU/well untreated BADr, or untreated confluent monolayers of MRC-5 or ARPE-19 cells were infected with treated/filtered BADr virions or control mixtures. Six days after infection representative micrographs were taken with a Nikon Eclipse TS100 Inverted UV microscope.

2.7.9 ^{3}H Thymidine Labeled Virus

Confluent MRC5 cells were infected with RC2626 at a low MOI in media containing 250μCuries of ^{3}H labeled thymidine. Following a 10-day incubation, virus was harvested, adjusted to sucrose, and stored in liquid nitrogen.

To titer the labeled virus, confluent monolayers of MRC5 cells were infected with serially diluted 3H-thymidine RC2626. Following a 2-hour incubation, cells were harvested using a PhD Cell-Harvester; the cells, not the culture media, were transferred onto filter paper. The radioactive virus on the filter paper was quantified with a scintillation counter. Viral stock was also quantified with a scintillation counter. Counts were graphed using Prism.

2.8 References

(1) Shoup, M.; Ourahmane, A.; Ginsburg, E. P.; Farrell, N. P.; Mcvoy, M. A. Substitution-Inert Polynuclear Platinum Compounds Inhibit Human Cytomegalovirus Attachment and Entry. *Antiviral Res.* **2020**, *184*, 104957.

(2) Hodowanec, A. C.; Pikis, A.; Komatsu, T. E.; Sampson, M. R.; Younis, I. R.; Rear, J. J. O.; Singer, M. E. Treatment and Prevention of CMV Disease in Transplant Recipients : Current Knowledge. *J. Clin. Pharmacol.* **2019**, *59* (6), 784–798. https://doi.org/10.1002/jcph.1363.

(3) Arvin, A. M.; Fast, P.; Myers, M.; Plotkin, S.; Rabinovich, R. Vaccine Development to Prevent Cytomegalovirus Disease: Report from the National Vaccine Advisory Committee. *Clin. Infect. Dis.* **2004**, *39*, 233–239. https://doi.org/10.1086/421999.

(4) Bonaros, N.; Mayer, B.; Schachner, T.; Laufer, G.; Kocher, A. CMV-Hyperimmune Globulin for Preventing Cytomegalovirus Infection and Disease in Solid Organ Transplant Recipients: A Meta-Analysis. *Clin. Transplant.* **2008**, *22*, 89–97. https://doi.org/10.1111/j.1399-0012.2007.00750.x.

(5) Cannon, M. J.; Schmid, D. S.; Hyde, T. B. . Review of Cytomegalovirus Seroprevalence and Demographic Characteristics Associated with Infection. *Rev. Med. Virol.* **2010**, *20*, 202–213. https://doi.org/10.1002/rmv.

(6) Steininger, C.; Puchhammer-Stöckl, E.; Popow-Kraupp, T. Cytomegalovirus Disease in the Era of Highly Active Antiretroviral Therapy (HAART). *J. Clin. Virol.* **2006**, *37*, 1–9. https://doi.org/10.1016/j.jcv.2006.03.005.

(7) Demmler-Harrison, G. J. Congenital Cytomegalovirus: Public Health Action towards Awareness, Prevention, and Treatment. *J. Clin. Virol.* **2009**, *46S*, S1–S5. https://doi.org/10.1016/j.jcv.2009.10.007.

(8) Kenneson, A.; Cannon, M. J. Review and Meta-Analysis of the Epidemiology of Congenital Cytomegalovirus (CMV) Infection. *Rev. Med. Virol.* **2007**, *17*, 253–276. https://doi.org/10.1002/rmv.

(9) Manicklal, S.; Emery, V. C.; Lazzarotto, T.; Boppana, S. B.; Gupta, R. K. The "Silent" Global Burden of Congenital Cytomegalovirus. *Clin. Microbiol. Rev.* **2013**, *26* (1), 86–102. https://doi.org/10.1128/CMR.00062-12.

(10) Nyholm, J. L.; Schleiss, M. R. Prevention of Maternal Cytomegalovirus Infection: Current Status and Future Prospects. *Int. J. Womens. Health* **2010**, *2*, 23–35. https://doi.org/10.2147/ijwh.s5782.

(11) Swanson, E. C.; Schleiss, M. R. Congenital Cytomegalovirus Infection: New Prospects for Prevention and Therapy. *Pediatr. Clin. North Am.* **2013**, *60*, 335–349. https://doi.org/10.1016/j.pcl.2012.12.008.

(12) Sinzger, C.; Digel, M.; Jahn, G. Cytomegalovirus Cell Tropism. In *Current Topics in Microbiology and Immunology: Human Cytomegalovirus*; Shenk, T. E., Stinski, M. F., Eds.; Springer: Heidelberg, Germany, 2008; pp 63–84.

(13) Boyle, K. A.; Compton, T. Receptor-Binding Properties of a Soluble Form of Human Cytomegalovirus Glycoprotein B. *J. Virol.* **1998**, *72* (3), 1826–1833.

(14) Isaacson, M. K.; Compton, T. Human Cytomegalovirus Glycoprotein B Is Required for Virus Entry and Cell-to-Cell Spread but Not for Virion Attachment, Assembly, or Egress. *J. Virol.* **2009**, *83* (8), 3891–3903. https://doi.org/10.1128/jvi.01251-08.

(15) Kari, B.; Gehrz, R. A Human Cytomegalovirus Glycoprotein Complex Designated GC-II Is a Major Heparin-Binding Component of the Envelope. *J. Virol.* **1992**, *66* (3), 1761–1764.

(16) Kari, B.; Gehrz, R. Structure, Composition and Heparin Binding Properties of a Human Cytomegalovirus Glycoprotein Complex Designated GC-II. *J. Gen. Virol.* **1993**, *74* (2), 255–264. https://doi.org/10.1099/0022-1317-74-2-255.

(17) Mach, M.; Kropff, B.; Kryzaniak, M.; Britt, W. Complex Formation by Glycoproteins M and N of Human Cytomegalovirus: Structural and Functional Aspects. *J. Virol.* **2005**, *79* (4), 2160–2170. https://doi.org/10.1128/JVI.79.4.2160.

(18) Krzyzaniak, M.; Mach, M.; Britt, W. J. The Cytoplasmic Tail of Glycoprotein M (GpUL100) Expresses Trafficking Signals Required for Human Cytomegalovirus Assembly and Replication. *J. Virol.* **2007**, *81* (19), 10316–10328. https://doi.org/10.1128/jvi.00375-07.

(19) Mach, M.; Osinski, K.; Kropff, B.; Schloetzer-Schrehardt, U.; Krzyzaniak, M.; Britt, W. The Carboxy-Terminal Domain of Glycoprotein N of Human Cytomegalovirus Is Required for Virion Morphogenesis. *J. Virol.* **2007**, *81* (10), 5212–5224. https://doi.org/10.1128/jvi.01463-06.

(20) Kabanova, A.; Marcandalli, J.; Zhou, T.; Bianchi, S.; Baxa, U.; Tsybovsky, Y.; Lilleri, D.; Silacci-Fregni, C.; Foglierini, M.; Fernandez-Rodriguez, B. M.; Druz, A.; Zhang, B.; Geiger, R.; Pagani, M.; Sallusto, F.; Kwong, P. D.; Corti, D.; Lanzavecchia, A.; Perez, L. Platelet-Derived Growth Factor-α Receptor Is the Cellular Receptor for Human Cytomegalovirus GHgLgO Trimer. *Nat. Microbiol.* **2016**, *1* (8), 1–8. https://doi.org/10.1038/nmicrobiol.2016.82.

(21) Wu, Y.; Prager, A.; Boos, S.; Resch, M.; Brizic, I.; Mach, M.; Wildner, S.; Scrivano, L.; Adler, B. Human Cytomegalovirus Glycoprotein Complex GH/GL/GO Uses PDGFR-α as a Key for Entry. *PLoS Pathog.* **2017**, *13* (4), 1–24. https://doi.org/10.1371/journal.ppat.1006281.

(22) Stegmann, C.; Hochdorfer, D.; Lieber, D.; Subramanian, N.; Stöhr, D.; Laib Sampaio, K.; Sinzger, C. A Derivative of Platelet-Derived Growth Factor Receptor Alpha Binds to the Trimer of Human Cytomegalovirus and Inhibits Entry into Fibroblasts and Endothelial Cells. *PLoS Pathog.* **2017**, *13* (4), 1–27. https://doi.org/10.1371/journal.ppat.1006273.

(23) Dunn, W.; Chou, C.; Li, H.; Hai, R.; Patterson, D.; Stolc, V.; Zhu, H.; Liu, F. Functional Profiling of a Human Cytomegalovirus Genome. *Proc. Natl. Acad. Sci. U. S. A.* **2003**, *100* (SUPPL. 2), 14223–14228. https://doi.org/10.1073/pnas.2334032100.

(24) Hobom, U.; Brune, W.; Messerle, M.; Hahn, G.; Koszinowski, U. H. Fast Screening Procedures for Random Transposon Libraries of Cloned Herpesvirus Genomes: Mutational Analysis of Human Cytomegalovirus Envelope Glycoprotein Genes. *J. Virol.* **2000**, *74* (17), 7720–7729. https://doi.org/10.1128/jvi.74.17.7720-7729.2000.

(25) Jiang, X. J.; Adler, B.; Sampaio, K. L.; Digel, M.; Jahn, G.; Ettischer, N.; Stierhof, Y.-D.; Scrivano, L.; Koszinowski, U.; Mach, M.; Sinzger, C. UL74 of Human Cytomegalovirus Contributes to Virus Release by Promoting Secondary Envelopment of Virions. *J. Virol.* **2008**, *82* (6), 2802–2812. https://doi.org/10.1128/jvi.01550-07.

(26) Wille, P. T.; Knoche, A. J.; Nelson, J. A.; Jarvis, M. A.; Johnson, D. C. A Human Cytomegalovirus GO-Null Mutant Fails To Incorporate GH/GL into the Virion Envelope and Is Unable To Enter Fibroblasts and Epithelial and Endothelial Cells. *J. Virol.* **2010**, *84* (5), 2585–2596. https://doi.org/10.1128/jvi.02249-09.

(27) Hahn, G.; Revello, M. G.; Patrone, M.; Percivalle, E.; Campanini, G.; Sarasini, A.; Wagner, M.; Gallina, A.; Milanesi, G.; Koszinowski, U.; Baldanti, F.; Gerna, G. Human Cytomegalovirus UL131-128 Genes Are Indispensable for Virus Growth in Endothelial Cells and Virus Transfer to Leukocytes. *J. Virol.* **2004**, *78* (18), 10023–10033. https://doi.org/10.1128/jvi.78.18.10023-10033.2004.

(28) Adler, B.; Scrivano, L.; Ruzcics, Z.; Rupp, B.; Sinzger, C.; Koszinowski, U. Role of Human Cytomegalovirus UL131A in Cell Type-Specific Virus Entry and Release. *J. Gen. Virol.* **2006**, *87* (9), 2451–2460. https://doi.org/10.1099/vir.0.81921-0.

(29) Patrone, M.; Secchi, M.; Fiorina, L.; Ierardi, M.; Milanesi, G.; Gallina, A. Human Cytomegalovirus UL130 Protein Promotes Endothelial Cell Infection through a Producer Cell Modification of the Virion. *J. Virol.* **2005**, *79* (13), 8361–8373. https://doi.org/10.1128/jvi.79.13.8361-8373.2005.

(30) Gerna, G.; Percivalle, E.; Lilleri, D.; Lozza, L.; Fornara, C.; Hahn, G.; Baldanti, F.; Revello, M. G.

Dendritic-Cell Infection by Human Cytomegalovirus Is Restricted to Strains Carrying Functional UL131-128 Genes and Mediates Efficient Viral Antigen Presentation to CD8+ T Cells. *J. Gen. Virol.* **2005**, *86* (2), 275–284. https://doi.org/10.1099/vir.0.80474-0.

(31) Martinez-Martin, N.; Marcandalli, J.; Huang, C. S.; Arthur, C. P.; Perotti, M.; Foglierini, M.; Ho, H.; Dosey, A. M.; Shriver, S.; Payandeh, J.; Leitner, A.; Lanzavecchia, A.; Perez, L.; Ciferri, C. An Unbiased Screen for Human Cytomegalovirus Identifies Neuropilin-2 as a Central Viral Receptor. *Cell* **2018**, *174* (5), 1158-1171.e19. https://doi.org/10.1016/j.cell.2018.06.028.

(32) Nguyen, C. C.; Kamil, J. P. Pathogen at the Gates: Human Cytomegalovirus Entry and Cell Tropism. *Viruses* **2018**, *10* (104). https://doi.org/10.3390/v10120704.

(33) Farrell, N. P. Multi-Platinum Anti-Cancer Agents. Substitution-Inert Compounds for Tumor Selectivity and New Targets. *Chem. Soc. Rev.* **2015**, *44* (24), 8773–8785. https://doi.org/10.1039/C5CS00201J.

(34) Gorle, A. K.; Katner, S. J.; Johnson, W. E.; Lee, D. E.; Daniel, A. G.; Ginsburg, E. P.; von Itzstein, M.; Berners-Price, S. J.; Farrell, N. P. Substitution-Inert Polynuclear Platinum Complexes as Metalloshielding Agents for Heparan Sulfate. *Chem. - A Eur. J.* **2018**, *24* (25), 6606–6616. https://doi.org/10.1002/chem.201706030.

(35) Katner, S. J.; Johnson, W. E.; Peterson, E. J.; Page, P.; Farrell, N. P. Comparison of Metal-Ammine Compounds Binding to DNA and Heparin. Glycans as Ligands in Bioinorganic Chemistry. *Inorg. Chem.* **2018**, *57* (6), 3116–3125. https://doi.org/10.1021/acs.inorgchem.7b03043.

(36) Mangrum, J. B.; Engelmann, B. J.; Peterson, E. J.; Ryan, J. J.; Berners-Price, S. J.; Farrell, N. P. A New Approach to Glycan Targeting: Enzyme Inhibition by Oligosaccharide Metalloshielding. *Chem. Commun.* **2014**, *50* (31), 4056–4058. https://doi.org/10.1039/c3cc49695c.

(37) Peterson, E. J.; Daniel, A. G.; Katner, S. J.; Bohlmann, L.; Chang, C. W.; Bezos, A.; Parish, C. R.; Von Itzstein, M.; Berners-Price, S. J.; Farrell, N. P. Antiangiogenic Platinum through Glycan Targeting. *Chem. Sci.* **2016**, *8* (1), 241–252. https://doi.org/10.1039/c6sc02515c.

(38) Cagno, V.; Tseligka, E. D.; Jones, S. T.; Tapparel, C. Heparan Sulfate Proteoglycans and Viral Attachment: True Receptors or Adaptation Bias? *Viruses* **2019**, *11* (7), 1–24. https://doi.org/10.3390/v11070596.

(39) Farrell, N. P.; Gorle, A. K.; Peterson, E. J.; Berners-Price, S. J. Metalloglycomics. In *Metallo-Drugs: Development and Action of Anticancer Agents*; Sigel, A., Sigel, H., Freisinger, E., Sigel, R. K. O., Eds.; Walter de Gruyter, GmbH: Belrin, Germany, 2018; pp 109–136.

(40) Bhave, S.; Elford, H.; McVoy, M. A. Ribonucleotide Reductase Inhibitors Hydroxyurea, Didox, and Trimidox Inhibit Human Cytomegalovirus Replication in Vitro and Synergize with Ganciclovir. *Antiviral Res.* **2013**, *100* (1), 151–158. https://doi.org/10.1016/j.antiviral.2013.07.016.

(41) Wang, D.; Shenk, T. Human Cytomegalovirus Virion Protein Complex Required for Epithelial and Endothelial Cell Tropism. *PNAS* **2005**, *102* (50), 18153–18158.

(42) Ryckman, B. J.; Jarvis, M. A.; Drummond, D. D.; Nelson, J. A.; Johnson, D. C. Human Cytomegalovirus Entry into Epithelial and Endothelial Cells Depends on Genes UL128 to UL150 and Occurs by Endocytosis and Low-PH Fusion. *J. Virol.* **2006**, *80* (2), 710–722. https://doi.org/10.1128/JVI.80.2.710.

(43) Compton, T.; Nowlin, D. M.; Cooper, N. R. Initiation of Human Cytomegalovirus Infection Requires Initial Interaction with Cell Surface Heparan Sulfate. *Virology* **1993**, *193* (2), 834–841. https://doi.org/10.1006/viro.1993.1192.

(44) Reefschlaeger, J.; Bender, W.; Hallenberger, S.; Weber, O.; Eckenberg, P.; Goldmann, S.; Haerter, M.; Buerger, I.; Trappe, J.; Herrington, J. A.; Haebich, D.; Ruebsamen-Waigmann, H. Novel Non-Nucleoside Inhibitors of Cytomegaloviruses (BAY 38-4766): In Vitro and in Vivo Antiviral Activity and Mechanism of Action. *J. Antimicrob. Chemother.* **2001**, *48*, 757–767. https://doi.org/10.1093/jac/48.6.757.

(45)   Meesing, A.; Razonable, R. R. New Developments in the Management of Cytomegalovirus Infection After Transplantation. *Drugs* **2018**, *78* (11), 1085–1103. https://doi.org/10.1007/s40265-018-0943-1.

(46)   Varnum, S. M.; Streblow, D. N.; Monroe, M. E.; Smith, P.; Auberry, K. J.; Pas, L.; Wang, D.; Ii, D. G. C.; Rodland, K.; Wiley, S.; Britt, W.; Shenk, T.; Smith, R. D.; Nelson, J. A. Identification of Proteins in Human Cytomegalovirus (HCMV) Particles: The HCMV Proteome. *J. Virol.* **2004**, *78* (20), 10960–10966. https://doi.org/10.1128/JVI.78.20.10960.

(47)   Duan, Y.; Miao, L.; Ye, H.; Yang, C.; Fu, B.; Schwartz, P. H.; Rayner, S.; Fortunato, E. A.; Luo, M. A Faster Immunofluorescence Assay for Tracking Infection Progress of Human Cytomegalovirus. *Acta Biochim Biophys Sin* **2012**, *44*, 597–605. https://doi.org/10.1093/abbs/gms041.Advance.

(48)   Ibig-rehm, Y.; Götte, M.; Gabriel, D.; Woodhall, D.; Shea, A.; Brown, N. E.; Compton, T.; Feire, A. L. High-Content Screening to Distinguish between Attachment and Post-Attachment Steps of Human Cytomegalovirus Entry into Fibroblasts and Epithelial Cells. *Antiviral Res.* **2011**, *89*, 246–256. https://doi.org/10.1016/j.antiviral.2011.01.007.

(49)   Vanarsdall, A. L.; Johnson, D. C. Human Cytomegalovirus Entry into Cells. *Curr. Opin. Virol.* **2012**, *2* (1), 37–42. https://doi.org/10.1016/j.coviro.2012.01.001.

(50)   Benedetti, B. T.; Peterson, E. J.; Kabolizadeh, P.; Mart??nez, A.; Kipping, R.; Farrell, N. P. Effects of Noncovalent Platinum Drug-Protein Interactions on Drug Efficacy: Use of Fluorescent Conjugates as Probes for Drug Metabolism. *Mol. Pharm.* **2011**, *8* (3), 940–948. https://doi.org/10.1021/mp2000583.

(51)   Liu, J.; Jardetzky, T. S.; Chin, A. L.; Johnson, D. C.; Vanarsdall, L. The Human Cytomegalovirus Trimer and Pentamer Promote Sequential Steps in Entry into Epithelial and Endothelial Cells at Cell Surfaces and Endosomes. *J. Virol.* **2018**, *92* (21), 1–15.

(52)   Snyder, M. B.; Saravolatz, L. D.; Markowitz, N.; Pohlod, D.; Taylor, R. C.; Ward, S. G. The In-Vitro and in-Vivo Efficacy of Cisplatin and Analogues in the Treatment of Herpes Simplex Virus-II Infections. *J. Antimicrob. Chemother.* **1987**, *19*, 815–822.

(53)   Farrell, N. P. New Perspectives and Targets for the Periodic Table. In *Advances in Inorganic Chemistry*; van Eldik, R., Sadler, P., Eds.; 2020.

(54)   Wang, D.; Shenk, T. Human Cytomegalovirus UL131 Open Reading Frame Is Required for Epithelial Cell Tropism. *J. Virol.* **2005**, *79* (16), 10330–10338. https://doi.org/10.1128/jvi.79.16.10330-10338.2005.

(55)   McVoy, M. A.; Mocarski, E. S. Tetracycline-Mediated Regulation of Gene Expression within the Human Cytomegalovirus Genome. *Virology* **1999**, *258* (2), 295–303. https://doi.org/10.1006/viro.1999.9724.

(56)   Cui, X.; Adler, S. P.; Davison, A. J.; Smith, L.; Habib, E. S. E.; McVoy, M. A. Bacterial Artificial Chromosome Clones of Viruses Comprising the Towne Cytomegalovirus Vaccine. *J. Biomed. Biotechnol.* **2012**, *2012*, 428498. https://doi.org/10.1155/2012/428498.

(57)   Harris, A. L.; Yang, X.; Hegmans, A.; Povirk, L.; Ryan, J. J.; Kelland, L.; Farrell, N. P. Synthesis, Characterization, and Cytotoxicity of a Novel Highly Charged Trinuclear Platinum Compound. Enhancement of Cellular Uptake with Charge. *Inorg. Chem.* **2005**, *44* (26), 9598–9600. https://doi.org/10.1021/ic051390z.

(58)   Prisecaru, A.; Molphy, Z.; Kipping, R. G.; Peterson, E. J.; Qu, Y.; Kellett, A.; Farrell, N. P. The Phosphate Clamp: Sequence Selective Nucleic Acid Binding Profiles and Conformational Induction of Endonuclease Inhibition by Cationic Triplatin Complexes. *Nucleic Acids Res.* **2014**, *42* (22), 13474–13487. https://doi.org/10.1093/nar/gku1157.

(59)   Qu, Y.; Moniodis, J.; Harris, A.; Yang, X.; Hegmans, A.; Povirk, L.; Berners-Price, S. J.; Farrell, N. . Solution Behavior of the Phosphate Clamp. DNA Binding By a Non-Covalent Polynuclear Platinum Compound. In *Polyamine Drug Discovery*; Woster, P. M., Casero, R., Eds.; 2011; pp 191–204.

https://doi.org/10.1039/9781849733090-00191.

(60)   Prisecaru, A.; Molphy, Z.; Kipping, R. G.; Peterson, E. J.; Qu, Y.; Kellett, A.; Farrell, N. P. The Phosphate Clamp: Sequence Selective Nucleic Acid Binding Profiles and Conformational Induction of Endonuclease Inhibition by Cationic Triplatin Complexes. *Nucleic Acids Res.* **2014**, *42* (22), 13474–13487. https://doi.org/10.1093/nar/gku1157.

(61)   Ginsburg, E. P. Heparan Sulfate. A Ligand for Coordination Compounds., University of Virginia, 2020.

CHAPTER 3: Broad-spectrum antiviral activity of PPCs

3.0 Contributions

This chapter, in part, summarizes the draft paper "Substitution-inert polynuclear platinum compounds selectively inhibit heparan-sulfate dependent viruses" to be submitted to *Antiviral Research*. Ralph Kipping and Eric Ginsburg synthesized and performed methylene blue assays for the series of PPCs. Anton Chestukhin produced transfection-grade plasmid DNAs and soluble ACE2. MZ performed all antiviral studies.

3.1 Background

In the previous chapter, we established the anti-HCMV activity of PPCs and their mechanism of action – inhibition of viral attachment via metalloshielding of heparan sulfate. Given that many viruses rely on HS for cellular attachment, PPCs should have broad-spectrum antiviral activity against HS-dependent viruses. We endeavored to explore their activity against both enveloped and nonenveloped viruses with either DNA or RNA genomes.

Following our demonstration of PPCs' antiviral activity against HCMV, our Australian collaborators (the Berners-Price group) investigated their activity against enterovirus A71 (EV71) and human metapneumovirus (hMPV).[1,2] Briefly, EV71 is a non-enveloped RNA virus, which causes hand, foot, and mouth disease in children; however, enteroviruses can also cause encephalitis, myocarditis, poliomyelitis, acute heart failure, and sepsis.[3] hMPV is an enveloped RNA virus, that causes pneumonia in infants and the elderly.[4] Discovered in 2001, hMPV is the major etiological agent responsible for about 5% to 10% of hospitalizations of children suffering from acute respiratory tract infections; it can cause severe bronchiolitis and pneumonia with symptoms indistinguishable from those caused by human respiratory syncytial virus.[5] There are no vaccines for either EV71 or hMPV and treatment of these infections is largely supportive or centered on relieving the symptoms.[3,5] Both EV71 and hMPV rely on HS for cellular attachment.[4,6]

MonoplatinNC, DiplatinNC, and TriplatinNC each had micromolar activities against EV71, as did the control, suramin, an EV71 capsid binding inhibitor (Table 3.1).[7–9] The anti-EV71 activity of these PPCs correlated with their charge and nuclearity, similar to their anti-HCMV activity.[1] The higher selectivity index of TriplatinNC led to its use in the subsequent studies.

Compound	$IC_{50}{}^{a}$ (µM)	$CC_{50}{}^{b}$ (µM)	SI^{c}
MonoplatinNC	>50	>500	>10
DiplatinNC	28 ± 0.48	>500	>17.9
TriplatinNC	5.35 ± 1.47	327.35 ± 137.39	61.2
Suramin	20.78 ± 1.33	>500	>24

Table 3.1: Anti-EV71 activity of PPCs and Suramin. (^{a}) Inhibitory activity of PPCs and suramin against EV71 infection of RD cells (values are mean IC_{50} ± SD, n = 3). (^{b}) Cytotoxicity of PPCs towards RD cells in the conditions of dose–response experiments (values are mean CC_{50} ± SD, n = 2). (^{c}) Selectivity index, SI = CC_{50}/IC_{50}.[2]

To establish TriplatinNC's mechanism of action against EV71, a number of studies were performed. A time of addition experiment illustrated that TriplatinNC inhibited EV71 replication only if cells were treated prior to infection, similar to suramin which blocks virus binding and entry (Figure 3.1).[9]
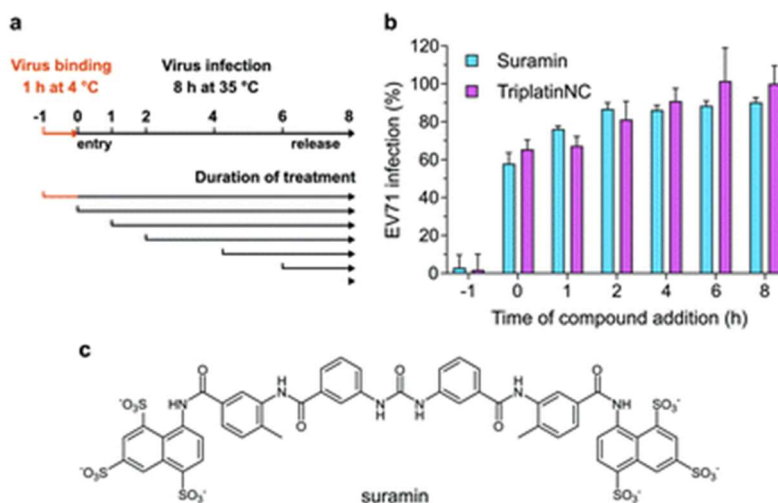
Figure 3.1: Time of addition-dependent activity of TriplatinNC and suramin against EV71 infection of RD cells. (a) Time of addition and duration of treatment by suramin or TriplatinNC during a single round of virus replication. (b) EV71 infection of RD cells as a function of the time of addition of suramin or TriplatinNC. Cells were incubated with EV71 for 1 h at 4 °C (t_{-1}) after which monolayers were washed with fresh media and transferred at 35 °C for 8 h (t_0). Compounds (200 µM suramin or 100 µM TriplatinNC) were applied at indicated time points. Infection was measured by in situ ELISA, using an anti-EV71 VP1 primary antibody. Bars represent the average of duplicate measurements, ± SD. (c) Structure of suramin. Reproduced from Bailly et al. 2021.[2]

To assess whether TriplatinNC could inhibit viral-HS binding, cells were preincubated with compound and washed prior to infection (Figure 3.2). As suramin binds the EV71 capsid rather than a cellular component, preincubation with suramin does not inhibit infection; however, preincubation with TriplatinNC maintains antiviral activity, albeit with a decreased EC50, perhaps explained by the shortened exposure time (1 h vs 24 h exposure). These data suggest that TriplatinNC inhibits EV71 by binding a cellular component, consistent with this mechanism of action against HCMV.[1] This was further confirmed with hMPV infection, demonstrating TriplatinNC's activity against both enveloped and naked viruses (Figure 3.2).
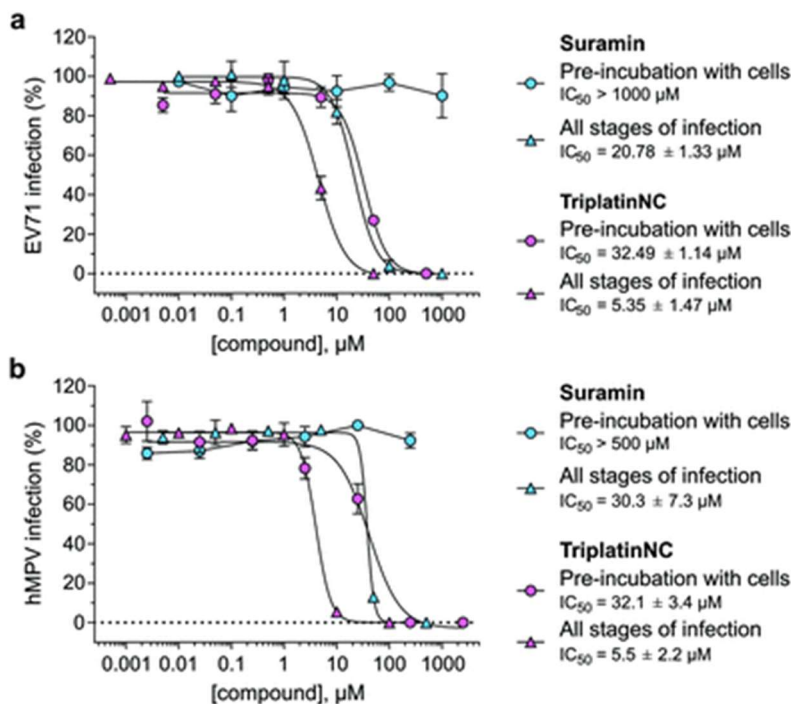
Figure 3.2: Dose-dependent activity of TriplatinNC and suramin against EV71 and hMPV in vitro *infection when applied at different stages of infection. (a) EV71 infection of RD cells; (b) hMPV infection of LLC-MK2 cells. Compounds were either present at all stages of infection or pre-incubated with cells for 1 h at 4 °C before a 24 h or 72 h infection for EV71 or hMPV, respectively. Infection was measured by* in situ *ELISA using anti-EV71 VP1 or anti-hMPV N primary antibodies. Data points represent the average of 3 independent experiments, ± SD (n = 3). Reproduced from Bailly et al. 2021.[2]*

As TriplatinNC had a higher potency when present for the duration of the viral infection, a secondary mode of action was investigated via competition saturation transfer difference (STD) NMR.[2] Whole EV71 virions were incubated with TriplatinNC, then FPX was added to compete with the first. If TriplatinNC binds to the virus, the saturation would transfer to the TriplatinNC protons, which would be observed from free to bound states; adding FPX would affect saturation of TriplatinNC, provided both compounds bind competitively. As seen in Figure 3.3, TriplatinNC does bind the viral capsid as saturation signals increase both when FPX is added. Interestingly, there is evidence of a trimeric complex between TriplatinNC, FPX, and the EV71 viral capsid, as additional TriplatinNC induced chemical shifts in the anomeric protons of FPX indicative of a 1:1 TriplatinNC:FPX adduct.[2]

The five-fold axis of the EV71 capsid pentamer, composed of VP1, is positively charged, and comprises the predicted binding region for GAGs; other regions of the capsid are composed of negatively charged VP2 and mixed charge VP3. Anionic FPX was predicted to bind to the GAG-binding 5-fold axis region while cationic TriplatinNC was expected to bind the negatively charged VP2 region. However, the TriplatinNC:FPX adduct is of mixed charge and likely to bind both the VP1 and VP2; this is supported by the increase in STD signal intensities of FPX or TriplatinNC upon addition of the second compound that may suggest that virus:FPX and virus:TriplatinNC adducts may be stabilized upon addition of the second compound and formation of the ternary complex. In whole, these data suggest that TriplatinNC can bind to HS on the cell surface, inhibiting attachment, as well as to the viral capsid, sequestering the virus-like neutralizing antibodies.
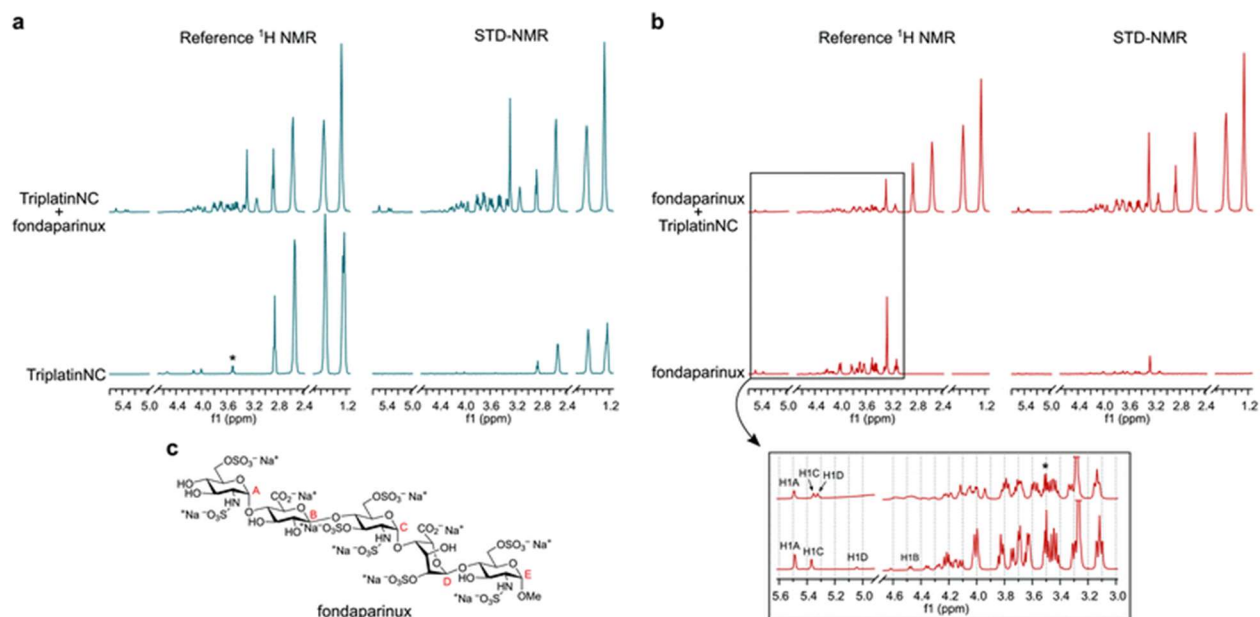
Figure 3.3: Competition STD-NMR experiment of fondaparinux (FPX) and TriplatinNC in the presence of EV71 particles. ^{1}H and STD-NMR spectra, in the presence of purified virus, of TriplatinNC before and after addition of FPX (a), and of FPX before and after addition of TriplatinNC (b). Experiments were carried out in the presence of 2.2 mM of compound. Reference off-resonance proton (^{1}H) and Saturation Transfer Difference (STD) NMR intensities are respectively comparable. STD peak intensities are representative of the relative binding of ligand protons to the EV71 capsid. *: contaminant. (c) Structure of FPX. The position of the anomeric protons is indicated in red (A–E). Reproduced from Bailly et al. 2021.[2]

Given TriplatinNC's broad-spectrum antiviral activity against HCMV, EV71, and hMPV, we endeavored to further explore PPCs antiviral activity against other clinically relevant viruses. In the following section, we examine the activities of TriplatinNC and DiplatinNC against GPCMV, adenovirus, SARS-CoV-2, SARS-CoV-1, MERS-CoV, and influenza virus. Each set of data will be preceded by brief background on the virus.

3.2 Studies of anti-GPCMV

Human CMV cannot infect animals due to the species-specificity of CMV. Unlike mouse or other small animal CMVs, GPCMV can cross the placenta and infect the fetus, like HCMV. Guinea pigs also have a long gestational period and hemochorial placenta; it is structurally and histologically similar to the human placenta. Finally, congenitally infected guinea pigs display similar symptoms as infected human infants, namely intrauterine growth retardation, brain involvement, and sensorineural hearing loss.[10] In an effort to find a suitable animal model, DiplatinNC and TriplatinNC were evaluated for anti-GPCMV (Figure 3.4). The potency of DiplatinNC and TriplatinNC inhibition of GPCMV replication was similar to their activities against HCMV, but unfortunately, both were cytotoxic to guinea pig cells, precluding separation of antiviral activity from toxicity. Thus, GPCMV is not a viable option for an animal testing.
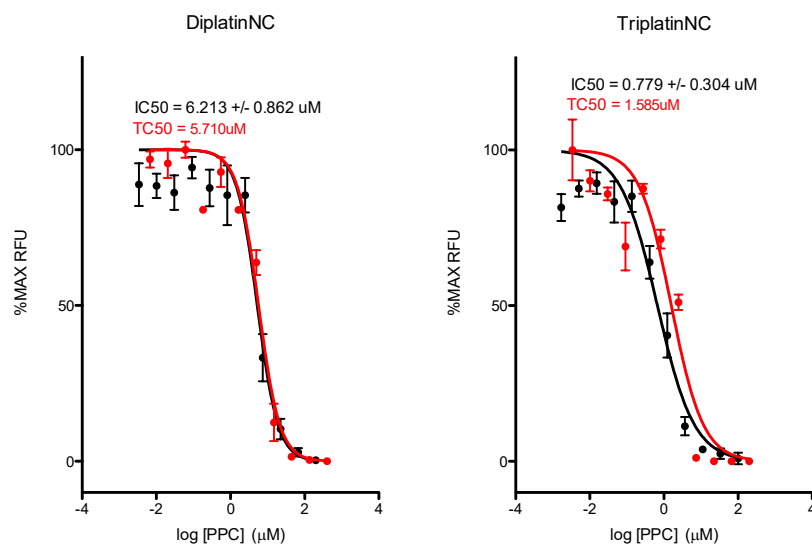
Figure 3.4: Red fluorescent protein (RFP)-based anti-GPCMV activity of DiplatinNC and TriplatinNC. Confluent GLF cells were treated with serially diluted compounds for one h, then infected with RFP-tagged GPCMV (100 PFU/well). Six days post infection, RFP expression was quantified and graphed (black line). Identical non-infected cells were tested for cytotoxicity (red line).

3.3 Studies of anti-adenovirus activity

Adenoviruses are naked, double-stranded DNA viruses. The 57 adenoviruses are classified into seven species (A-G) based on hemagglutination properties, DNA homology, and oncogenicity in rodents. There is an imperfect correlation between species and tissue tropism (Table 3.2).[11] Human adenovirus infections are generally self-limited in the respiratory, genitourinary, and gastrointestinal tracts and the ocular surface. Children, people living in close quarters, and immunocompromised patients are most at risk for adenovirus infection. Though there is an adenovirus vaccine for those in the military, there is not a vaccine for the civilian community, nor is there an FDA-approved antiviral for adenovirus infection.[12] Prospective treatments include antivirals already available for other viruses. Cidofovir, a phosphonyl acyclic nucleotide, inhibits viral DNA polymerase and is approved for HCMV infection. However, cidofovir has a narrow efficacy/toxicity ratio and is associated with lachrymal canalicular blockage.[12] Ribavirin inhibits inosine monophosphate dehydrogenase and is approved for treating respiratory syncytial virus and hepatitis C virus infections.[12] Other prospects are being investigated but all have intercellular targets. New treatments may consider extracellular targets to avoid resistance and toxicities.

Species	Serotype	Major site of infection
A	12, 18, 31, 61	Gastrointestinal (GI) tract
B	3, 7, 11, 14, 16, 21, 34, 35, 50, 55, 66	Respiratory, urinary
C	1, 2, 5, 6, 57	Respiratory
D	8-10. 13, 15, 17, 19, 20, 22-30, 32, 33, 36-39, 42-29	Eye, GI tract
E	4	Respiratory
F	40, 41	GI tract
G	52	GI tract

Table 3.2: Infection associated with adenovirus species and serotype (recreated) [11].

As there are so many adenoviruses, there are a variety of receptors. Generally, attachment through a primary receptor is followed by interaction with a second receptor, responsible for internalization.[13] All adenoviruses, except those in species B, begin infection when the knob of the fiber protein binds the 42-kDa glycoprotein receptor called coxsackievirus and adenovirus receptor (CAR) (Figure 3.5).[14] Following fiber-CAR binding, the penton base binds α_v integrins through the Arg-Gly-Asp (RGD) sequence, which triggers endocytosis. CAR is not the only receptor for adenoviruses.[13] HS mediates CAR-independent attachment and infection by adenovirus 2 and 5.[14,15] The basic amino acid motifs in adenovirus's capsid proteins allow protein recognition of HS and mutations within the proximal fiber shaft modifies adenovirus 5 tropism *in vivo*.[16,17] Although it is unknown whether other adenoviruses use HS, the HS binding site is conserved in all group C adenoviruses.
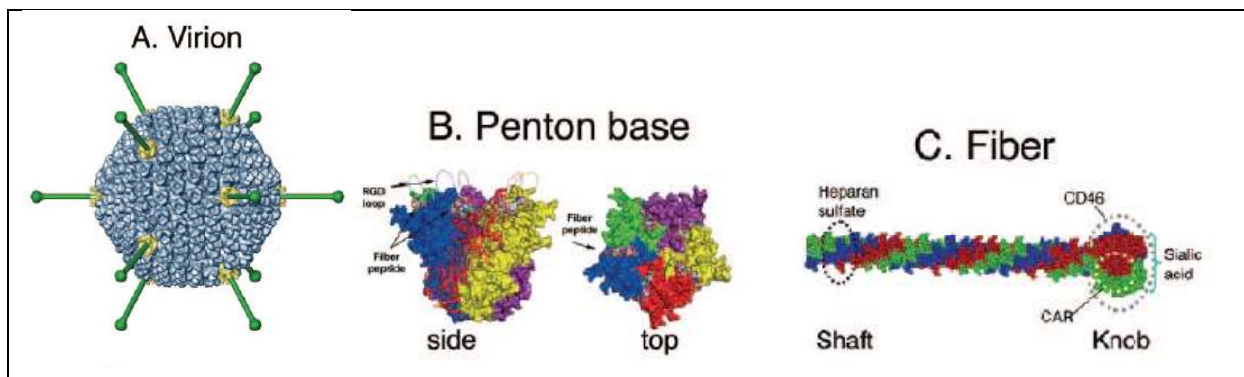
Figure 3.5: Adenovirus structure: (A) Virion structure in which the hexon trimer is in blue, the pentameric penton base is in yellow, and the fiber is in green. (B) Penton base with side and top views. Reproduced from Zhang et al. 2015.[13]

3.3.1 GFP-based antiviral activity

DiplatinNC and TriplatinNC were previously shown to have antiviral activity against HCMV. Here, we utilized a GFP-tagged adenovirus to assess activity against a naked, HS-dependent virus.
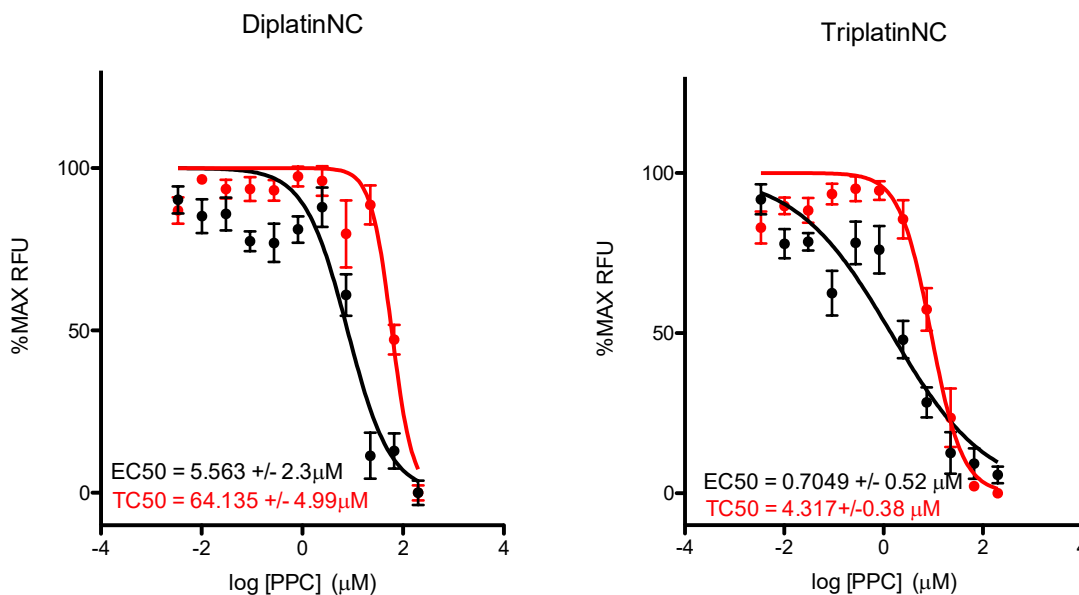
Figure 3.6: Adenovirus antiviral and cytotoxicity in ARPE-19. Confluent ARPE-19 epithelial cells were treated with serially diluted compounds for one h, then infected with GFP-tagged adenovirus (100 PFU/well). Five days post infection, GFP expression was quantified and graphed (black line). Cytotoxicity (red) was measured in replicate uninfected cultures treated for five days using

the CellTiter-Glo® assay. Prism was used to produce the best-fit four parameter curves for %maximum RLU vs the log of the drug concentration. Data points represent the average of nine replicates and error bars are the standard deviation.

	GFP based IC50	ARPE-19 TC50	SI
DiplatinNC	5.563 +/- 2.28	64.13 +/- 4.99	11.5
TriplatinNC	0.705 +/- 0.52	4.32 +/- 0.38	6.1

Table 3.3: Adenovirus IC50 and TC50 mean values (μM) derived from three separate cytotoxicity and antiviral assays, each with three replicates.

DiplatinNC and TriplatinNC had anti-adenovirus activity to some extent in epithelial cells. Both compounds have less activity against adenovirus as compared to HCMV (Figure 3.6 and Table 3.3). However, since adenovirus can enter cells without binding HS, infection may be able to occur through CAR even in the presence of metalloshielding by PPCs.

3.3.2 Mechanistic studies

Assuming PPCs have the same mechanism of action in adenovirus infection as they do in HCMV infection, PPCs should block viral attachment and entry and therefore should block viral gene expression. We utilized a GFP-tagged virus to assess the impact of PPCs on GFP expression in ARPE-19 epithelial cells. Controls included heparin, which is known to block adenovirus entry.[15] When added one h prior to infection, heparin and PPCs inhibited GFP expression. In contrast, when added one hpi, heparin and PPCs had no impact on GFP expression (Figure 3.7).
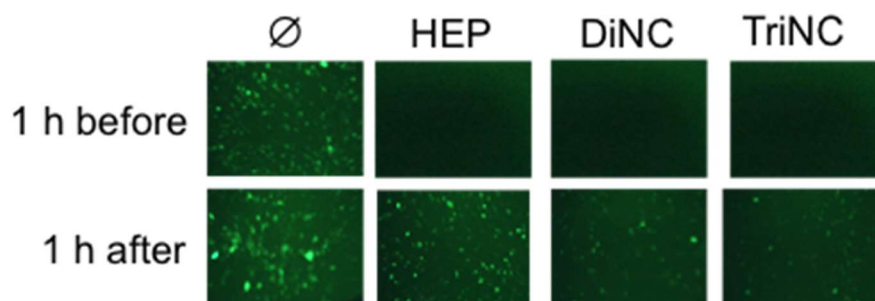
*Figure 3.7: **PPCs added before infection inhibit expression of a viral marker protein in epithelial cells.** Confluent monolayers of ARPE-19 epithelial cells in 96-well plates were treated with medium (Ø), 150 µg/ml heparin (HEP), 10 µM DiNC, or 5 µM TriNC one h before or one h after infection with GFP-tagged adenovirus (100 PFU/well). Representative fluorescent micrographs were taken five days post infection.*

Similarly, a GFP-based time of addition was conducted to determine the timing of inhibition of the viral replication cycle. Inhibitor were added at different times relative to viral infection. As in the experiments with HCMV, heparin as well as DiplatinNC and TriplatinNC were only active when added within a few hours of adding the virus, and lacked antiviral activity if added as early as 1 h after infection (Figure 3.8).
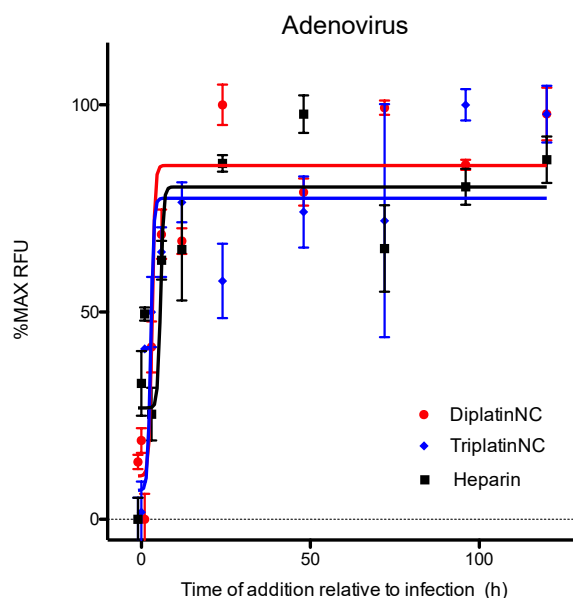
*Figure 3.8: **Time of addition study for adenovirus**. Confluent monolayers of ARPE-19 epithelial cells were treated with 150 µg/ml heparin, 10 µM DiNC, or 5 µM TriNC 1 h before, concurrent with, or at various times after infection with GFP-tagged adenovirus (100 PFU/well). GFP expression was quantified on day five post infection. Data are means of triplicate wells ± standard deviations.*

3.4 Coronaviruses

In light of SARS-CoV-2, we became interested in coronaviruses. Coronaviruses are enveloped, ssRNA viruses with large genomes of 27-34kbp. There are seven human coronaviruses (HCoV), four of which cause common colds and the other three are well-known epidemic and pandemic viruses. Limited research was done on coronaviruses following the 2003 SARS-CoV-1 and 2015 MERS epidemics. Since the outbreak of SARS-CoV-2, there has been a considerable amount of research dedicated to anti-coronavirals and vaccines.

Host specificity entry by coronavirus relies on the spike (S) glycoprotein, which is not well conserved between HCoVs. As a result, coronaviruses use a wide variety of cellular proteins as entry receptors (Table 3.4).

Coronavirus	Cellular receptor
HCoV-229E*	Aminopeptidase N
HCoV-NL63*	Angiotensin-converting enzyme 2
HCoV-OC43	N-acetyl-9-O-acetylneuraminic acid
HCoV-HKU1	N-acetyl-9-O-acetylneuraminic acid
SARS-CoV-1*	Angiotensin-converting enzyme 2
MERS-CoV*	Dipeptodyl peptidase 4
SARS-CoV-2*	Angiotensin-converting enzyme 2

Table 3.4: Coronaviruses and their cellular receptors. (*) denotes HS-dependent viruses.

However, there are common themes in spike protein-receptor interactions. Like many other viruses, HCoV-229E and HCoV-NL63 are HS-dependent; there is some evidence that SARS-CoV-1 is also HS-dependent.[18–20] All three of the HCoVs that rely on human angiotensin-converting enzyme 2 (ACE2) interact with the same non-catalytic site of ACE2.[21–23] All three have a high concentration of tyrosine in

their receptor binding domains, which contributes to both hydrogen bonding and hydrophobic interactions. All three also rely on a large number of polar interactions and hydrogen bonds, specifically with histidine-34, aspartic acid-30, and tyrosine-41 on human ACE2. HCoV-OC43 and HCoV-HKU1 bind the same cellular receptor as the influenza virus (N-acetyl-9-O-acetylneuraminic acid).[24] Both share a conserved receptor binding domain which contains a sulfate ion hydrogen bonded to lysine-81 and threonine-83. The carboxylate moiety of N-acetyl-9-O-acetylneuraminic acid binds to and recognizes this sulfate and that polar interaction allows the 5-N-acyl and 5-N-glycolyl moieties to interact with an adjacent hydrophobic pocket.[24] Across the board, HCoVs rely on a combination of polar interactions, hydrogen bonds, and hydrophobic interactions. Disrupting these amphipathic interactions could impede viral entry and infection. The PPC chemotype is capable of significant modulation for structure-activity relationships. We can target, by suitable chemistry, a broader range of polar interactions, perhaps encompassing both HS and sialic acid dependent viruses.

Efforts to work with the two BSL-2 HS-dependent HCoVs, HCoV-229E and HCoV-NL63, proved challenging, and given the greater clinical relevance of SARS-CoV-1, SARS-CoV-2, and MERS-CoV, we chose to utilize pseudotyped lentivirus particles to study these BSL-3 viruses under BSL-2 conditions.

3.4.1 Pseudotyping lentiviruses

Many clinically relevant viruses are dangerous to work with and require additional procedures for protection and safety. The Center for Disease Control (CDC) and National Institutes of Health (NIH) published *Biosafety in Microbiological and Biomedical Laboratories (BMBL)* to define biosafety levels (BSL) 1 through 4, which describe the environment and laboratory conditions required to work with any particular pathogen. Pathogens are divided into BSL categories based on their risk of disease as well as the availability of preventive and therapeutic treatments. Pathogens such as SARS-CoV-2 require a BSL-3 laboratory and procedures. However, pseudotyping a BSL-3 virus onto a safer non-replicative viral particle enables them to be worked with under BSL-2 conditions.

A pseudovirus is an enveloped recombinant viral particle with one or more of its structural proteins not encoded in its genome.[26] Pseudoviruses are commonly modified to produce a surface protein from another virus instead of its own. Importantly, psuedoviruses may infect susceptible cells, but cannot replicate in infected host cells; this difference enables BSL-3 and 4 viruses to be studied under BSL-2 conditions. Pseudoviruses usually carry reporter genes such as GFP or luciferase for easy quantitative analysis as the fluorescence or chemiluminescent signal should be directly proportional to the number of pseudovirus-infected cells.[27] As such, pseudoviruses are used to study cellular tropism, receptor recognition, and viral entry inhibition. While pseudoviruses can attach and enter in the manner of the target virus, they cannot replicate and may not induce pathogenesis like the wild-type target virus; thus, pseudotyping systems should eventually be validated against authentic virus-based assays.

Several packaging systems have been developed for producing pseudotyped virus-like particles, those based on lentiviruses (HIV, SIV, or FIV), murine leukemia virus, and the vesicular stomatitis virus (VSV). Each have their advantages: the VSV packaging system is less selective for envelope proteins, lentiviral vectors are highly efficiently packaging systems, and MLV can be more efficient than lentiviral vectors depending on the conditions and cell type.[27] Each of these systems maintain the genetic sequences required for viral transcription and packaging but do not include those required for envelope proteins; a plasmid with the target virus' envelope protein is used instead. While the packaging system

can affect pseudovirus yield, the envelope protein localization and expression, as well as the cell line and packaging conditions, are significant factors; most pseudotyping systems require optimization.[27]

In this chapter, we utilize an HIV-based lentiviral pseudotyping system for SARS-CoV-2 optimized and published by Crawford et al..[28] HIV-1 derived lentiviral particles are created by transfecting HEK-293T cells with a plasmid comprising a lentiviral RNA genome encoding either GFP or luciferase as a reporter protein, a plasmid encoding SARS-CoV-2 spike glycoprotein, and plasmids encoding structural lentiviral proteins required for viral particle assembly (Figure 3.9). These SARS-CoV-2 lentiviruses may infect permissive cells expressing the SARS-CoV-2 cellular receptor, ACE2. Later in this chapter, we will adapt this system by exchanging the plasmid for SARS-CoV-2 spike glycoprotein with plasmids encoding entry glycoproteins from other viruses.
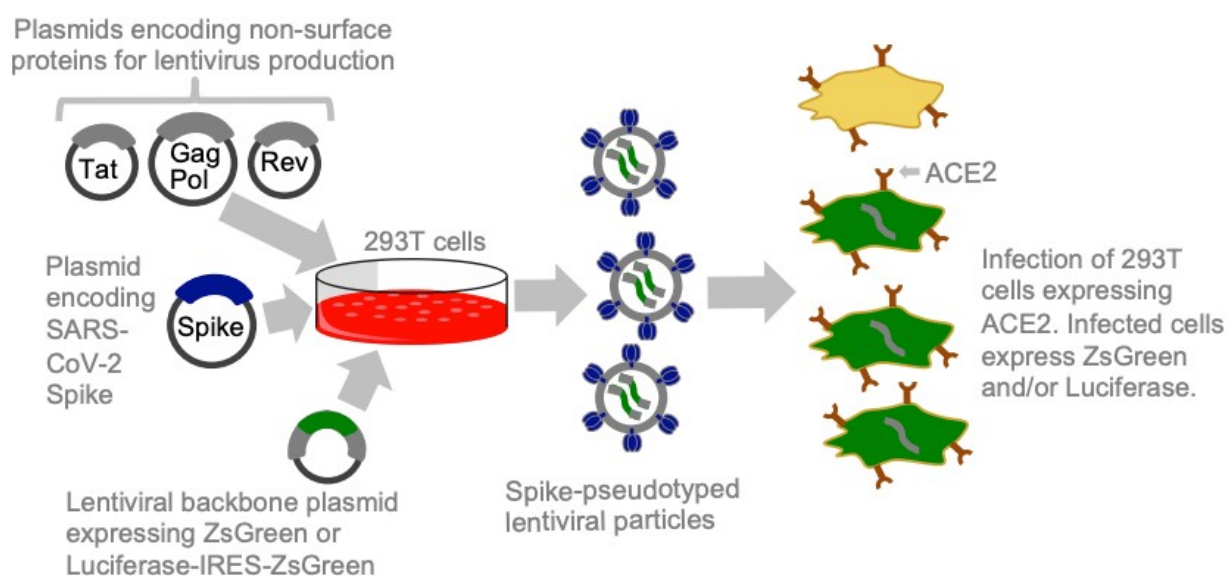
Figure 3.9: Schematic of pseudotyping lentivirus. HEK-293T cells are transfected with plasmids encoding non-surface proteins for lentivirus production, lentiviral backbone expressing GFP or luciferase, and a viral glycoprotein, such as SARS-CoV-2 spike protein. Lentiviral particles expressing the viral glycoptieins are harvested from the culture supernatants of transfected cells; these pseudotyped lentiviruses may enter cells that express appropriate cellular receptor, such as ACE2, resulting in transduction that can be detected by subsequent expressing either GFP or luciferase. Reproduced from Crawford et al. 2020.[28]

3.4.2 SARS-CoV-2

Severe acute respiratory syndrome coronavirus 2 (SARS-CoV-2), the causative agent of coronavirus disease 2019 (COVID-19), emerged in late 2019. SARS-CoV-2 is a β-coronavirus with large RNA genome, encoding 28 proteins: four structural, sixteen nonstructural, and eight accessory proteins.[29,30] Like other HCoVs, SARS-CoV-2 is zoonotic. The closest relative of SARS-CoV-2 is a bat coronavirus from *Rhinolophus affinis* RaTG13 (96.2%). However, the degree of divergence suggests a gap of more than 20 years of evolution, meaning that one of the known bat coronaviruses may be the evolutionary precursor, but is not the direct progenitor of SARS-CoV-2.[31] Guangdong pangolin coronaviruses also exhibit high sequence similarity to SARS-CoV-2 (92.4%), and more importantly, they share all five essential residues for receptor binding.[32] In contrast, the Guangxi pangolin coronavirus only shares one amino acid required for receptor binding and 85% of its spike sequence.[33,34] Unlike bats, which can carry coronaviruses without symptoms, pangolins show clinical signs such as pneumonia.[34] Thus, pangolins are unlikely to be the direct

reservoir and more likely have acquired CoVs after spillover from the natural bat hosts.[32] The zoonotic origins of SARS-2 and its intermediate hosts remain elusive, though monitoring of bat and pangolin coronaviruses is merited in light of the previous pandemics.

Following droplet transmission, SARS-CoV-2 binds to its cellular receptor, ACE2, and infects two types of cells in the lungs: mucus producing goblet cells and ciliated epithelial cells.[30] It later infects other cells expressing ACE2 found in the lungs, heart, kidneys, and intestines.[30] The SARS-CoV-2 spike protein determines its tropism; it is 1,273 amino acids, longer than that of SARS-CoV-1 (1,255 amino acids) and has two subunits, S1 and S2. S1 contains the receptor binding domain (RBD) at its C terminus and is responsible for virion attachment; it is also the target for neutralizing antibodies.[35] S2 mediates fusion of viral and cellular membranes at its C terminus.[36] Following S1 binding to ACE2, S2 brings the virion in proximity to the cellular membrane so that fusion occurs, inducing conformational changes. Spike protein is cleaved during endocytosis at the S1/S2 boundary, which contains a S2' polybasic furin cleavage site, resulting in formation of a viral fusion peptide.[30,36] The insertion of a polybasic furin cleavage cite is unique; it enables S1/S2 cleavage by furin or other host proteases including transmembrane protease serine protease 2 (TMPRSS2) and cathepsin L.[32,37] This feature is not seen in other human coronaviruses but is seen in bat coronaviruses.[32]

Numerous studies reveal how the RBD of SARS-CoV-2 binds ACE2.[30] The RBD of SARS-CoV-2 spike includes residues 437-507, which differs from SARS-CoV-1 in five residues critical for ACE2 binding: Y455L, L486F, N493Q, D494S, and T501N. Both viruses bind the same site of ACE2.[38] Additionally, four residues of the receptor binding motif (AA 482-485: GVEG) results in a more compact conformation in the ACE2 binding than SARS-CoV-1 and better contact with the N-terminus of ACE2.[22] The strong interactions between spike and ACE2 results in very efficient entry into host cells.[30,32] There is some speculation that the insertion of this site increased the transmission ability of SARS-2 compared to SARS-1.[32]

Like many viruses, SARS-CoV-2 relies on heparan sulfate for initial cellular attachment; it then binds ACE2, as described above to enter the cell. The receptor binding domain of S1 binds HS as well as ACE2. The binding of HS to the receptor binding domain in S1 shifts it into the open conformation needed to bind ACE2.[35,39,40] The putative binding site for HS is adjacent to the ACE2-binding site; it contains a group of positively charged amino acids, namely R346, R355, K444, R466, and possibly R509 (Figure 3.10).[41,42] Amino acids F347, S349, N354, G447, Y449, and Y451 may also contribute to HS binding through hydrogen bonds and hydrophobic interactions.[41,42] The majority of the amino acids in the SARS-CoV-2 HS-binding site are conserved from SARS-CoV-1 with the exception of N354, which is replaced with a negatively charged glutamate; the sequence of spike RBD is 73% identical between the two (Figure 3.10).[41,42]
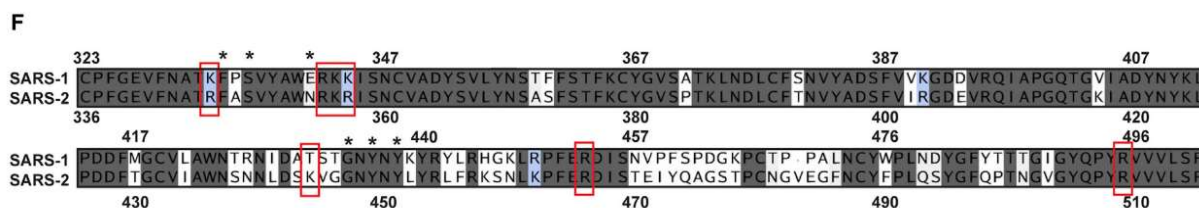
Figure 3.10: SARS-CoV-1 and SARS-CoV-2 sequence alignment for the receptor binding domain of Spike glycoprotein. Red boxes indicate amino acids contributing to the electropositive region where heparan sulfate binds. Identical residues are in grey, conservative substitution are in blue and non-conserved residues are in white. Reproduced from Clausen et al. 2020.[42]

This change together with R444K suggests that SARS-CoV-2 may have an enhanced interaction with HS compared to SARS-CoV-1. There is also some data to suggest that the sulfation pattern of HS can alter the HS-spike binding; however, an ideal pattern has not been identified.[41] Inhibition of SARS-CoV-2 attachment by heparin has been well established.[41,43] Overall, the spike protein of SARS-CoV-2 engages both HS and ACE2 and HS binding may enhance ACE2 binding and therefore infection.

Ultimately, SARS-CoV-2 infection results in COVID-19. In SARS-CoV-2 pathogenesis, the virion enters lung cells via ACE2 and uses host cell machinery to replicate. As the host cell loses the ability to maintain homeostasis, apoptosis occurs and the dead cells and debris accumulate in the lungs, causing a number of respiratory symptoms. The immune system overreacts to lung damage and causes further damage, eventually leading to respiratory failure and death.[44] As of April 1, 2022, there have been over 486 million cases of COVID-19 and over 6.1 million deaths worldwide. COVID-19 presents a range of severity with some patients asymptomatically infected, some with mild respiratory disease, and some with severe disease requiring hospitalization. Generally, patients present with fever, myalgia, loss of smell, headache, and respiratory symptoms. [45] Additionally, some patients have symptoms extending well beyond viral infection, termed "Long COVID-19". The primary route of transmission for SARS-CoV-2 is respiratory droplets. A number of host factors influence the severity of disease such as age, cardiovascular disease, diabetes, cancer, and obesity.[45] A number of laboratory markers are also indicative of more severe cases: neutrophilia/lymphopenia, raised ferritin, raised IL-6, raised ACE2, or D-dimer over 1 µg/mL.[45]

While a number of vaccines have been successfully developed, antivirals are still a critical need. There are several antiviral targets to inhibit SARS-CoV-2 (Figure 3.11). Furin inhibitors focus on preventing spike cleavage and thus entry.[30] Clathrin-mediated endocytosis inhibitors and cathepsin inhibitors inhibit well-established cellular pathways.[30] TMPR22 inhibitors prevent SARS-CoV-2's entry via inhibition of a serine protease.[46] Endosomal acidification inhibitors, such a chloroquine, influence the virus cycle process and immune response.[47] PLpro inhibitors, such as ribavirin and chloramphenicol, fit into the active site of the enzyme and inhibit its deubiquitinase activity, improving the host immune response.[48] 3CLpro inhibitors bind the active site of 3CLpro, the main protease of SARS-CoV-2.[49–51] Helicase inhibitors inhibit the formation of double-stranded RNA and thus inhibit viral replication.[30] RNA-dependent RNA polymerase inhibitors, such as Remdesivir, have been used against a number of viruses; they inhibit viral RNA synthesis.[30,52] CYP inhibitors prevent extreme increases in cytokine levels which are indicative of poor patient outcomes. Membrane bound RNA synthesis inhibitors prevent the formation of double membrane vesicles, decreasing SARS-CoV-2's ability to replicate.[53,54]
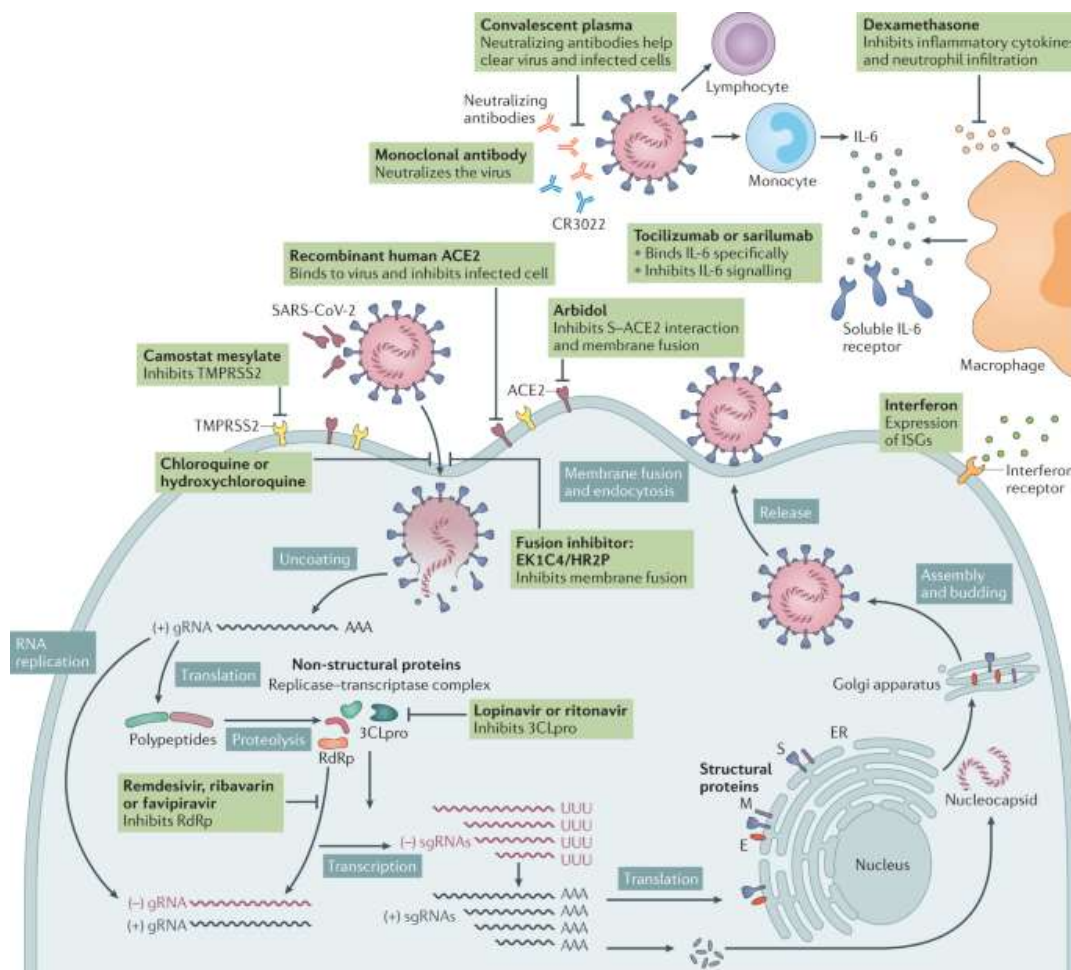
Figure 3.11: Antiviral targets of SARS-CoV-2 and where they would inhibit viral replication. Reproduced from Hu et al. 2021.[32]

Currently the FDA has granted an emergency use authorization for Pfizer's Paxlovid, which is a combination of Nirmatrelvir and ritonavir.[55] Nimatrelvir is a protease inhibitor while ritonavir slows the breakdown of Nirmatrelvir. The FDA has also granted Merck's Molnupiravir an emergency use authorization.[56] Molnupiravir is a small-molecule ribonucleoside prodrug of N-hydroxycytidine that acts by increasing the frequency of mutations in the viral RNA genome and thereby impairs SARS-CoV-2 replication.[57]

3.4.2.1 Proof of concept

As our SARS-CoV-2 pseudoviruses contain both luciferase and GFP, we first tested two compounds, TriplatinNC and DiplatinNC, and screened them using both tags. EC_{50}s were determined using the luciferase- and GFP-tagged SARS-CoV-2 VLPs, while TC_{50}s were simultaneously determined for replicate uninfected cultures using the CellTiter-Glo cell viability assay.[58] Results are shown in Figure 3.12 and Figure 3.13. DiplatinNC and TriplatinNC's luciferase-based EC_{50}s and their GFP-based EC_{50}s were nearly equal. This is consistent with each tag being under the same promotor as well as the published assay, which measures infection rather than spread or viral production.[28] Moving forward, we utilized the GFP-based assay to avoid using the expensive reagents required for the luciferase-based assay.
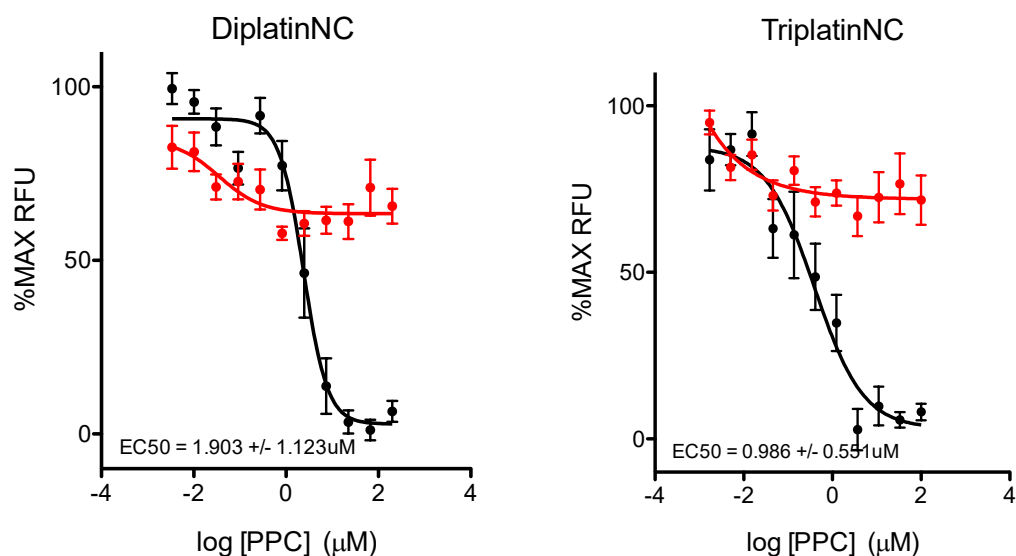
Figure 3.12: GFP-based anti-pseudotyped SARS-CoV-2 activity of DiplatinNC and TriplatinNC. Confluent HEK-293T-ACE2 cells were treated with serially diluted compound for one hour then infected with pseudotyped SARS-CoV-2. Two days post infection, GFP expression was quantified and graphed (black line). Identical non-infected cells were tested for cytotoxicity (red line).
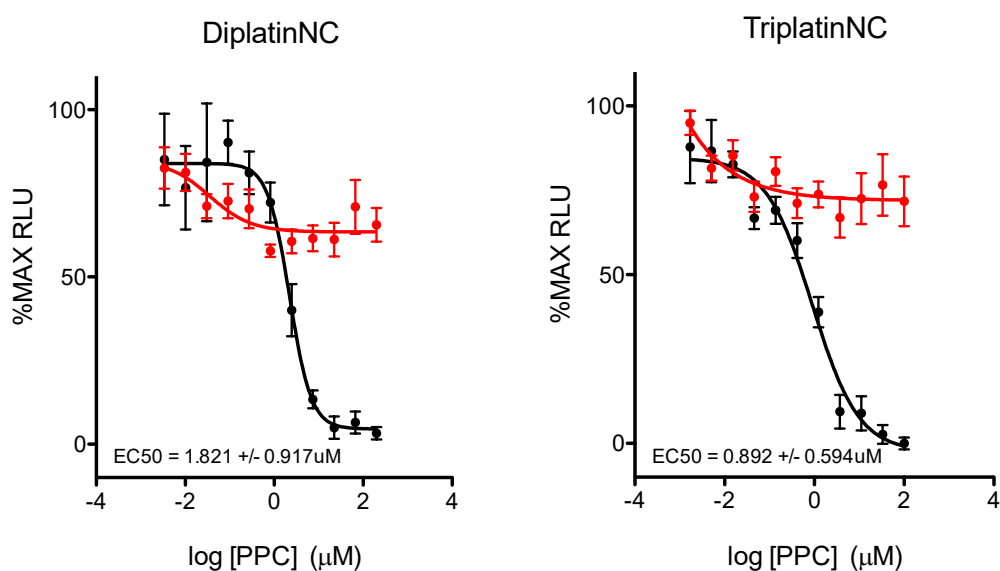
Figure 3.13: Luciferase-based anti-pseudotyped SARS-CoV-2 activity of DiplatinNC and TriplatinNC. Confluent HEK-293T-ACE2 cells were treated with serially diluted compound for one hour then infected with pseudotyped SARS-CoV-2. Two days post infection, 50uL of supernatant was replaced with 50uL of SteadyGlo. Luciferase activity was quantified and graphed (black line). Identical non-infected cells were tested for cytotoxicity (red line).

3.4.2.2 Selection of compounds

Substitution-inert PPCs were developed from covalently binding Triplatin, which was originally synthesized to subvert cisplatin resistance in cancer.[59] While Triplatin is useful in targeting cancer, it has labile Pt-Cl bonds, likely to react with any number of biologically relevant nucleophiles. The substitution

inert PPC series lack Pt-Cl bonds and instead is based on a Pt-N$_4$ motif, therefore reducing potential for off-target toxicity. The library used in this study is shown in Figure 3.14.
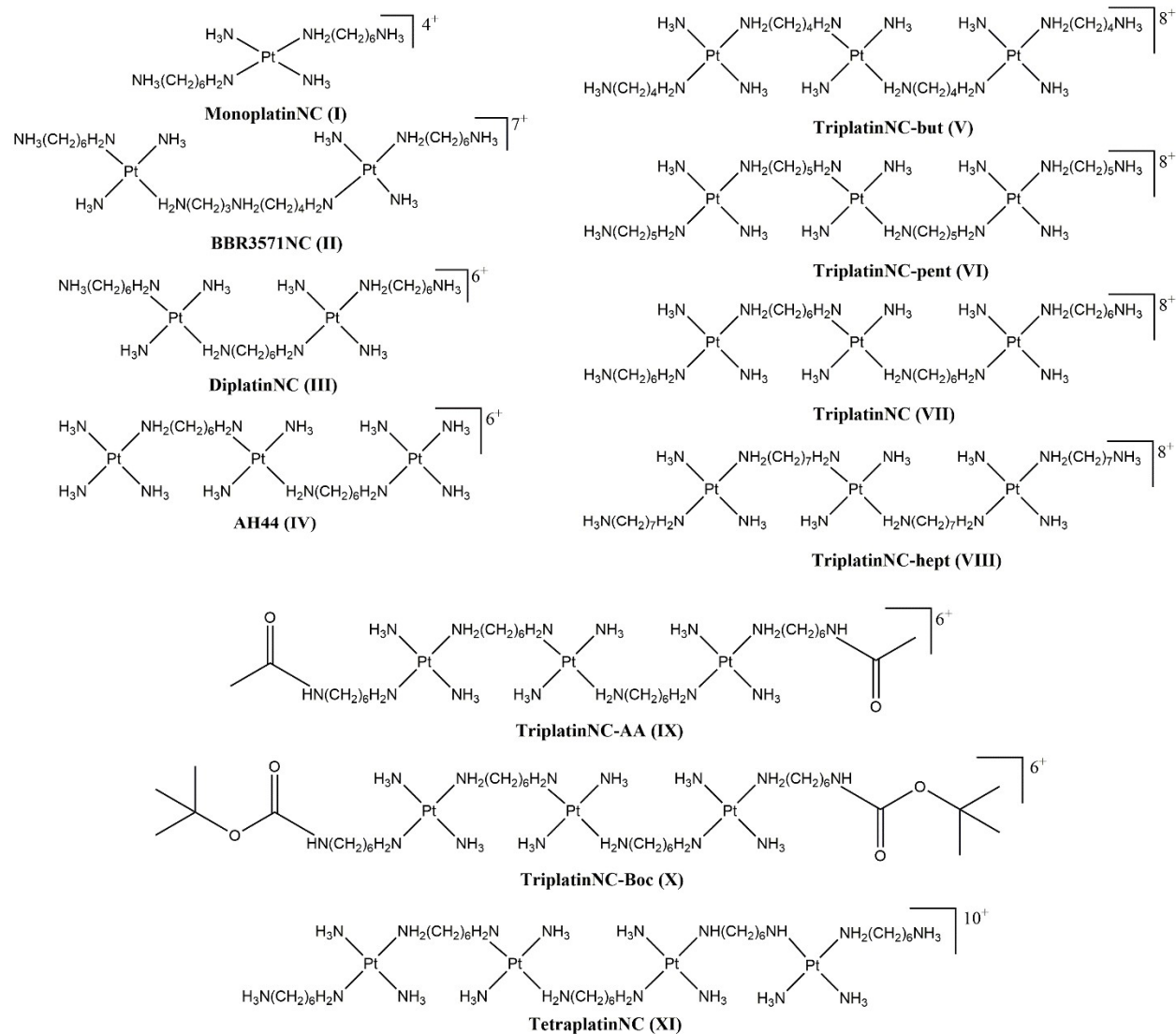
Figure 3.14: The structures of substitution-inert polynuclear platinum complexes. Counterions omitted for clarity.

MonoplatinNC (**I**) is the lone mononuclear compound of the series with the smallest positive charge (+4). DiplatinNC (**II**) is one of two dinuclear PPCs with a moderate charge (+6). BBR3571NC (**III**) has an amine in place of the middle platinum moiety of TriplatinNC and has a moderate charge (+7). TriplatinNC (**VII**) is the substitution inert analog of Triplatin with a high positive charge (+8); the rest of the series is based off of **VII**. AH44 (**IV**) has a positive charge (+6) but has simple ammines on the terminal platinum moieties in place of dangling ammines of **VII**. With positive charge of +8, three compounds differ only in the length of the alkyldiamine linker: TriplatinNC-but (**V**), TriplatinNC-pent (**VI**), and TriplatinNC-hept (**VIII**). A further two compounds were designed to be prodrugs of **VII** as the acetyl and tert-butyloxycarbonyl protecting (Boc) groups are easily cleaved in biological conditions; TriplatinNC-AA (**IX**) has an acetyl group and TriplatinNC-Boc (**X**) has a Boc group on each of their two terminal dangling

ammines, decreasing their charge to (+6). Finally, TetraplatinNC (**XI**) is a tetranuclear PPC with the highest charge of the series (+10).

All compounds were screened for anti-HCMV activity. Mononuclear **I** lacked HCMV activity up to 200µM but polynuclear compounds **II**, **III**, **VI**, and **VII** had µM activities.[1] Other compounds were either too cytotoxic or their antiviral activity could not be separated from their cytotoxicity (data shown in Chapter 2). Given the shorter assay time using pseudotyped lentiviral particles (two days verses five days), the entire library was screened against SARS-CoV-2 to examine variation in overall charge and nuclearity on efficacy on antiviral activity.

3.4.2.3 Structure-activity relationships

The antiviral activity of a compound is quantified by its EC_{50}, the concentration at which 50% of virus replication is inhibited. Cytotoxicity of a compound is quantified by its TC_{50}, the concentration at which 50% of the cells die. To determine EC_{50}s for PPCs, their impact on SARS-CoV-2 entry was determined using a GFP-tagged pseudotyped lentivirus, while TC_{50}s were simultaneously determined for replicate uninfected cultures using the CellTiter-Glo cell viability assay.[28,58] Results are shown in Figure 3.15 and summarized in Table 3.5. **I** is the only mononuclear compound of the series and it did not have anti-SARS-CoV-2 activity; this aligns with previous results in which **I** did not have anti-HCMV or anti-EV61 activity. The two dinuclear compounds (**II** and **III**) had good anti-SARS-CoV-2 activity but were outperformed by all but one trinuclear and tetranuclear compounds. **IV** was least active of the trinuclear series, but has both a decreased charge and length. **VII** and those differing only in the length of the linker (**V**, **VI**, and **VIII**) were not significantly different, indicating that the length of the linker has little effect on anti-SARS-CoV-2 activity. However, adding a protecting group to the dangling amines of **VII**, as seen with **IX** and **X**, decreased their anti-SARS-CoV-2 activity; this may be due to a decrease in charge or an increase in bulk. Finally, **XI** had the best anti-SARS-CoV-2 activity, indicating once again that increasing positive charge or length/nuclearity improved antiviral activity. The anti-SARS-CoV-2 activity of the PPC series loosely correlated with HS affinity, as measured by the MB assay.
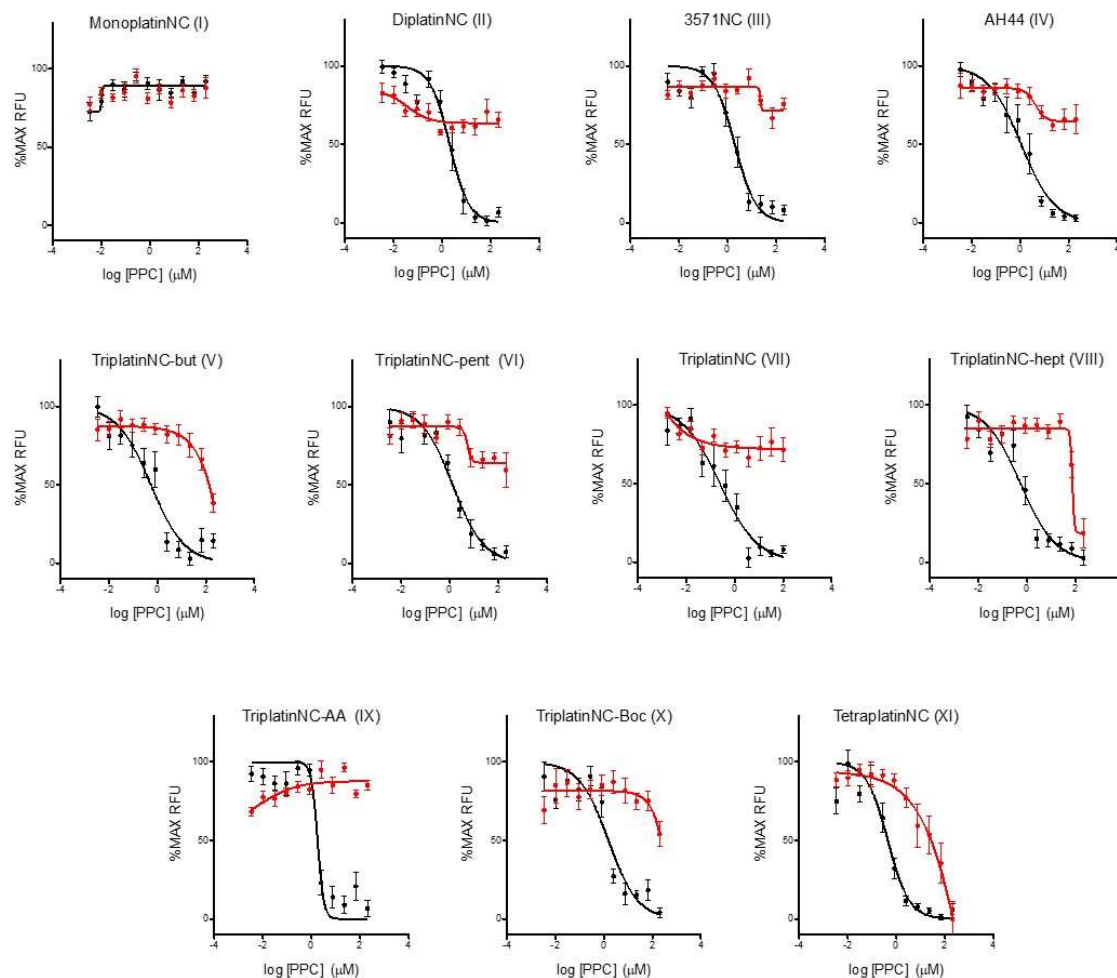
Figure 3.15: **Antiviral activity of PPCs against pseudotyped SARS-CoV-2.** *Anti-SARS-CoV-2 activity (black) was measured by incubating HEK-293T-hACE2 cell monolayers in 384-well plates with PPCs for one h, infecting with GFP-tagged pseudovirus (125 transducing units/well), and measuring GFP levels (RFU) two days after infection. Cytotoxicity (red) was measured in replicate uninfected cultures treated for two days using the CellTiter-Glo® assay. Data are means of three independent experiments ± standard deviations.*

Structure	Name	Antiviral[a] (EC$_{50}$)	Cytotoxicity[b] (TC$_{50}$)	SI[c]	MB[d] (IC$_{50}$)
I	MonoplatinNC	Not active	>200	N/A	25.5 ± 0.5
II	DiplatinNC	1.812 ± 0.35	>200	>110.4	16.6 ± 0.4
III	BBR3571NC	2.266 ± 0.51	>200	>88.3	17.4 ± 0.8
IV	AH44	3.708 ± 0.74	>200	>53.9	13.5 ± 0.5
V	TriplatinNC-but	0.885 ± 0.51	~200	~225.9	ND
VI	TriplatinNC-pent	1.825 ± 0.66	>200	>109.6	13.8 ± 0.4
VII	TriplatinNC	0.986 ± 0.55	>200	>202.8	10.2 ± 0.4
VIII	TriplatinNC-hept	0.603 ± 0.41	183.95 ± 22.69	305.3	13.6 *
IX	TriplatinNC-AA	1.913 ± 0.44	>200	104.5	12.3 ± 0.4
X	TriplatinNC-Boc	1.749 ± 0.41	~175	~100.1	ND
XI	TetraplatinNC	0.511 ± 0.34	110.19 ± 19.78	215.5	ND

Table 3.5: Anti-SARS-CoV-2 Activities of PPCs. [a]GFP-based assay. [b]CellTiter-Glo® assay. [c]selectivity index (TC$_{50}$/EC$_{50}$). [a,b,d]μM; means of three independent experiments ± standard deviations. [d]inhibition of methylene blue binding to Fondaparinux (previously published data, [60]). ND: not determined. (*) denotes single data point.

The selectivity index (SI) is the ratio of TC_{50} to EC_{50}. A high SI suggests a favorable safety and efficacy profile of a compound. In contrast with previous work, the PPC series was less cytotoxic (Table 3.5), presumably due at least in part to the shorter time of PPC exposure needed for these assays. The majority of compounds did not have significant cytotoxicity up to 200 μM, though **VIII**, **X**, and **XI** were slightly toxic at high concentrations and the decreased cytotoxicity greatly improved the therapeutic indices. All compounds, apart from the inactive **I** as well as **III** and **IV**, had therapeutic indices of above 100, indicating a promising safety profile. We selected **III** and **VII** to evaluate the broad-spectrum activity of PPCs and to confirm their mechanism of action. Although some compounds outperformed **III** and **VII** in anti-SARS-CoV-2 activity or therapeutic index, **III** and **VII** were chosen to continue in mechanistic studies and broad-spectrum activity studies due to limited quantities of other PPCs.

3.4.2.4 Mechanistic studies

To assess the mechanism of action of PPCs, we treated cells at various time points before and after infection of SARS-CoV-2. As seen in Figure 3.16, **III** and **VII** inhibit GFP expression only when present prior to infection, similar to heparin. Likewise, a time of addition assay with SARS-CoV-2 revealed that **III** and **VII** only inhibit viral GFP expression when cells are pretreated, indicative of entry and attachment inhibitors (Figure 3.17). We also pretreated cells then washed with media prior to infecting to assess whether PPCs bind a cellular factor to inhibit virion attachment; as DiplatinNC and TriplatinNC remained active at inhibiting the majority of GFP expression after washing, we conclude that both bind a cellular component, likely HS, to inhibit viral attachment (Figure 3.16).
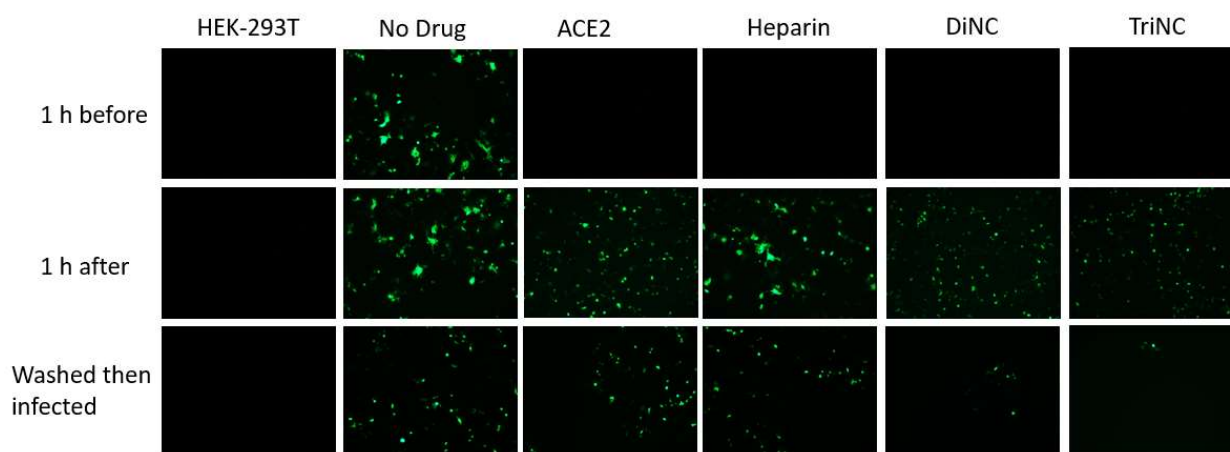
Figure 3.16: PPCs inhibit GFP expression resulting from SARS-CoV-2 pseudovirus transduction. Confluent monolayers of HEK-293T (left column) or HEK-293T-ACE2 cells (all other columns) in 96-well plates were treated with medium (Ø), 150 μg/ml heparin (HEP), 300 μg/ml soluble ACE2, 10 μM DiNC, or 5 μM TriNC one h before (top) or one h after (bottom) infection with GFP-tagged pseudovirus (100 transducing units/well). Alternatively, cells were washed after compound treatment but prior to infection. Representative fluorescent micrographs were taken two days post infection.
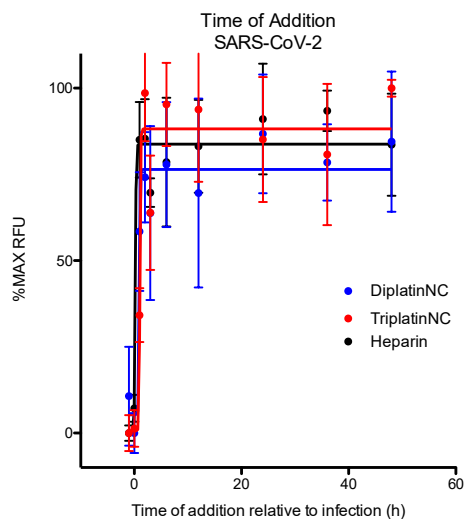
Figure 3.17: Time of addition study for SARS-CoV-2. Confluent monolayers of HEK-293T-ACE2 cells were treated with 150 µg/ml heparin, 10 µM DiNC, or 5 µM TriNC 1 h before, concurrent with, or at various times after infection with GFP-tagged pseudovirus (100 transducing units/well). GFP expression was quantified on day two post infection. Data are means of triplicate wells ± standard deviations.

3.4.3 SARS-CoV-1

Severe acute respiratory syndrome coronavirus 1 (SARS-CoV-1), the causative agent of SARS, emerged in late 2002. SARS-CoV-1 infected 8,456 people and caused 809 deaths.[61,62] Like SARS-CoV-2, SARS-CoV-1 is a zoonotic virus. Approximately one third of the early cases of SARS-CoV-1 were animal or food handlers and 13% of asymptomatic animal handlers in Guangdong province have antibodies against SARS-CoV-1 compared to 1-3% in control groups, emphasizing an animal-derived virus.[63,64] Additionally, healthy Himalayan masked palm civets, Chinese ferret badgers, and racoon dogs harbor SARS-like coronaviruses with 99% identity in the spike protein compared to SARS-CoV-1.[65] SARS-CoV-1 originated from bats and palm civets and have been established as the natural reservoir.[62]

SARS-CoV-1 spread primarily through respiratory droplets but there is also evidence of aerosol, fomite, and fecal-oral transmission.[62] There is no evidence of SARS-CoV-1 transmission prior to symptom onset of asymptomatic transmission.[66] Rather SARS-CoV-1 transmission is greatest from severely ill patients, normally in the second week of illness.[62] This differs greatly from SARS-CoV-2 and limited the spread of SARS-CoV-1 as evident from its low reproductive number of R0.[67,68]

SARS-CoV-1 infection presents with fever, chills, malaise, headache, cough, dyspnea, pneumonia, and diarrhea.[62] It is generally less aggressive in children compared to adults.[62,69] There is no evidence for an effective vaccine or antiviral for SARS-CoV-1. Ribavirin was used clinically but lacked *in vitro* efficacy; subsequent reports failed to identify any benefit from ribavirin.[61,62] For now, treatment of SARS-CoV-1 is limited to supportive care.[62] However, like SARS-CoV-2, SARS-CoV-1 depends on HS for attachment and ACE2 for cell entry, suggesting that targeting virion attachment or entry could inhibit both viruses.

SARS-CoV-1 infection begins with HS attachment. Although the interaction is less well characterized than the SARS-CoV-2 interaction, SARS-CoV-1 infection is inhibited by HS-binding lactoferrin.[19] Following attachment, SARS-CoV-1 binds the same site of ACE2 as SARS-CoV-2. The SARS-CoV-1 spike protein binds one of the two lobes of ACE2 and does not bind or occlude the peptidase active site.[21] The receptor binding

domain of SARS-CoV-1 spike is approximately 193 residues, in which seven cysteines are essential for ACE2 binding and residues 424-494 anchor the core interaction.[70] Six tyrosines present both polar hydroxyl group and hydrophobic aromatic rings.[21] Mutations at glutamic acid 452 or aspartic acid 454 severely decrease or abolish the ACE2 interaction.[70] The receptor binding domain of SARS-CoV-1 spike and palm civet coronavirus spike differ at 479 and 487, resulting in binding human ACE2 103-104 times more tightly.[71] In palm civet CoV, residue 479 is lysine and 487 is serine, whereas in SARS-CoV-1, these residues are asparagine and threonine, respectively.[21] Overall, the SARS-CoV-1 attaches to cells via HS and enters cells through ACE2-interaction, which relies on a network of hydrophilic interactions and hydrogen bonding.[21]

3.4.3.1 Studies of anti-SARS-CoV-1 activity

III and **VII** each had micromolar anti-SARS-CoV-1 activity with **VII** outperforming **III** (Figure 3.18 and Table 3.7). As SARS-CoV-1 infects the same cells as SARS-CoV-2, **III** and **VII** maintain their low cytotoxicity and thus have very good therapeutic indices of 105.1 and 202.8 respectively.
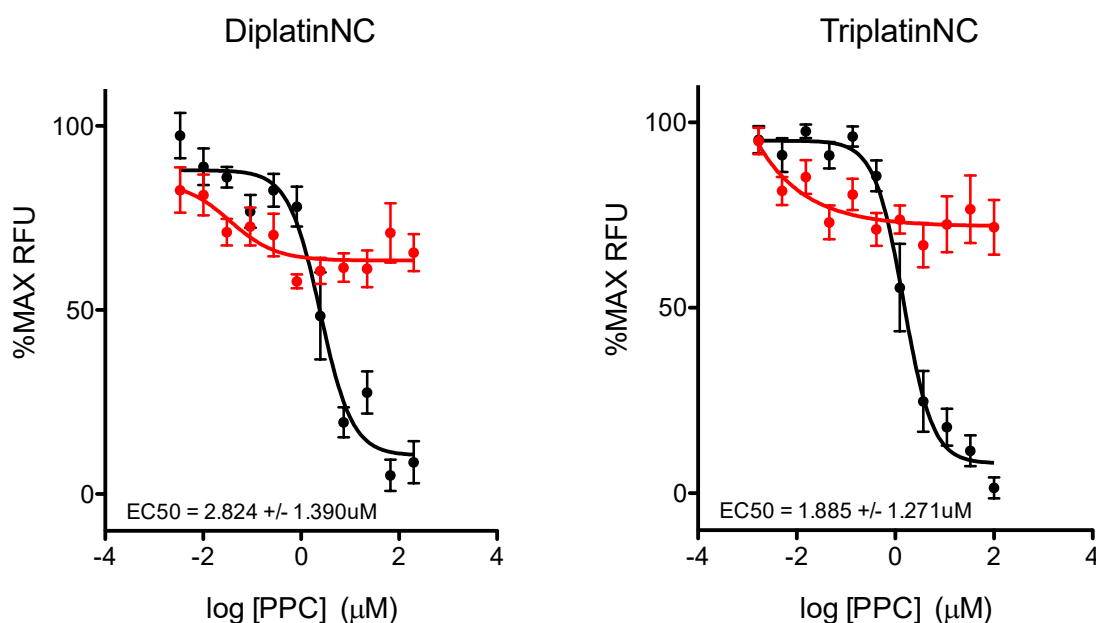
Figure 3.18: GFP-based anti-pseudotyped SARS-CoV-1 activities of DiplatinNC and TriplatinNC. Confluent HEK-293T-ACE2 cells were treated with serially diluted compound for one hour then infected with pseudotyped SARS-CoV-1. Two days post infection, GFP expression was quantified and graphed (black line). Identical non-infected cells were tested for cytotoxicity (red line).

3.4.3.2 Mechanistic studies

To confirm that PPCs inhibit SARS-CoV-1 attachment, we performed a number of gene expression assays. In Figure 3.19, **III** and **VII** only inhibited GFP expression of SARS-CoV-1 when cells were pretreated, similar to heparin; GFP was also inhibited if cells were treated ad washed prior to infection, indicating that PPCs bind a cellular component to inhibit virion attachment. Likewise, in Figure 3.20, **III** and **VII** only inhibited SARS-CoV-1 if cells were treated in the initial hours; adding inhibitors three to 48 hours after infection had no effect on GFP, indicating an early-acting mechanism.
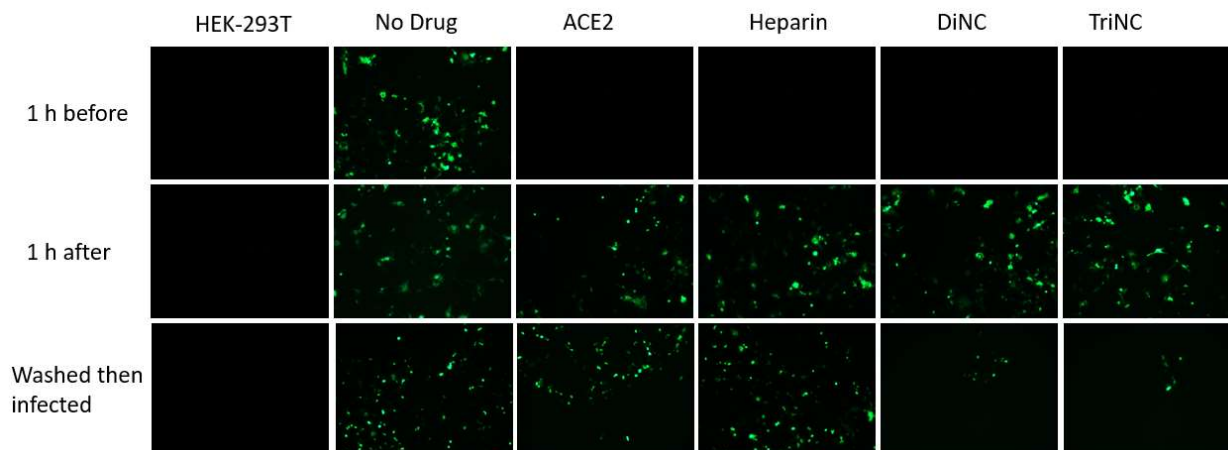
Figure 3.18: PPCs inhibit GFP expression resulting from SARS-CoV-1 pseudovirus transduction. Confluent monolayers of HEK-293T (left column) or HEK-293T-ACE2 cells (all other columns) in 96-well plates were treated with medium (Ø), 150 μg/ml heparin (HEP), 300 μg/ml soluble ACE2, 10 μM DiNC, or 5 μM TriNC one h before (top) or one h after (middle) infection with GFP-tagged pseudovirus (100 transducing units/well). Alternatively, cells were washed after compound treatment but prior to infection (bottom). Representative fluorescent micrographs were taken two days post infection.
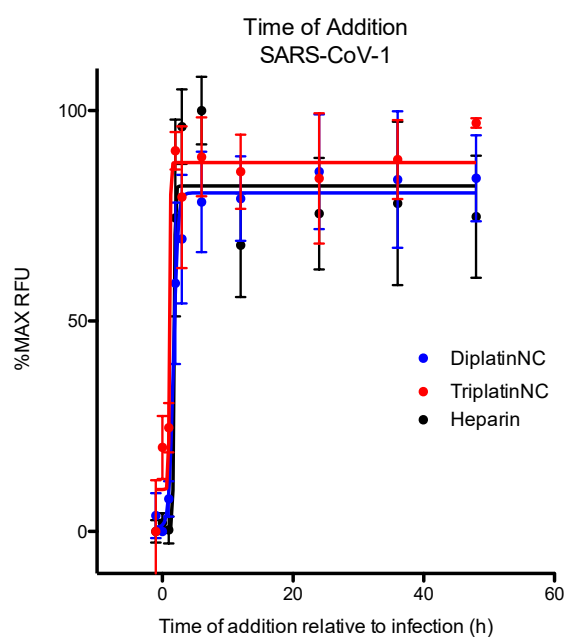
*Figure 3.19: **Time of addition study for SARS-CoV-1**. Confluent monolayers of HEK-293T-ACE2 cells were treated with medium (Ø), 150 μg/ml heparin, 10 μM DiNC, or 5 μM TriNC 1 h before, concurrent with, or at various times after infection with GFP-tagged pseudotyped virus (100 transducing units/well). GFP expression was quantified on day two post infection. Data are means of triplicate wells ± standard deviations.*

3.4.4 MERS-CoV

Middle East Respiratory Syndrome coronavirus (MERS-CoV) emerged in September 2012. It causes sporadic cases of severe acute respiratory infection.[72] Since its identification, MERS-CoV has infected 2,583 people and caused 889 deaths, with a roughly 34% case fatality rate.[73,74] Like other coronaviruses, MERS-CoV is a zoonotic virus. It is most closely related to *Tylonycteris* and *Pipistrellus* bat

CoVs HKU4 and HKU5, respectively; additionally, phylogenetic analysis revealed that MERS-CoV is distantly related to African bat coronavirus. suggesting that it originated from bat coronaviruses.[75] However, bats are unlikely to be a source of direct bat-to-human transmission as bats are uncommon in the Middle East. In screening endemic animals, dromedary camels were the only animals positive for anti-MERS-CoV antibody, suggesting they are the probable source for zoonotic transmission of the virus.[73,76] Surprisingly, camel serum samples from 1982 were positive for MERS-CoV antibodies, which raises the question: why was human MERS-CoV infection not detected prior to 2012?

MERS-CoV transmission from camels to humans is unclear but likely multifaceted.[76] Although the exact mode of human transmission is unknown, there is evidence of health-care associated transmission and limited non-sustained human-to-human transmission, likely through droplet or contact transmission.[72] MERS-CoV is less transmissible than other coronaviruses with an R_0 factor of 0.7, significantly lower than an R_0 of 1, a mark of epidemic potential.[77]

MERS-CoV infection has a range of clinical presentations. While some patients are asymptomatically infected, others present with mild respiratory illness to severe acute pneumonia, leading to death.[76] Most commonly MERS-CoV infection manifests with flu-like symptoms such as fever, sore throat, non-productive cough, chills/rigors, chest pain, headache, myalgia, shortness of breath, and dyspnea.[76]

There are no approved vaccines or antiviral treatments for MERS-CoV.[73,76] Clinical studies administered type I interferons and ribavirin early in MERS-CoV infection; while one study found that treatment enhanced the survival of critically ill patients, another found there was no effect on patient mortality.[78,79] Lopinavir, an HIV protease inhibitor, was also used in MERS patients but its efficacy has not been proved.[76] Supportive care remains the only treatment for MERS-CoV.

Unlike SARS-CoV-1 and 2, MERS-CoV relies on sialic acid for attachment and dipeptidyl peptidase four (DPP4) for cell entry.[80] Sialic acids are not GAGs; they are derivatives of neuraminic acid and like GAGs, they are ubiquitous carbohydrates with a number of cellular roles, including viral attachment. The MERS-CoV spike proteins binds sialic acids rather than HS. Interestingly MERS-CoV spike binds a site distinct from the site used by HCoV-OC43 spike in complex with 9-O-acetyl sialylated receptors despite the close similarity of these proteins.[24,81] There is some debate on the selectively of MERS-CoV spike; there is evidence for both a α2,3-linked and α2,6-linked glycan preference as well as *N*-glycolylneuraminic (Neu4Gc) and Neu5Ac preference.[82,83] Regardless of specificity, MERS-CoV attachment relies on sialic acids, depending on a network of electrostatic, hydrophobic and van der Walls interactions; however, there is also evidence for sialic acid-independent MERS-CoV cell attachment and entry.[82,83]

MERS-CoV spike protein binds DPP4, which does not share any sequence or structural similarity to other coronavirus receptors, namely ACE2 or aminopeptidase N (APN).[84,85] Therefore, it follows that MERS-CoV spike binding differs greatly from SARS-COV-1 and 2 spike binding. MERS-CoV spike receptor binding domain (E367 to Y606) relies on E382-C585 to bind to S39-P766 of the DPP4 extracellular domain; importantly the binding cite is not close to the hydrolase domain and does not inhibit its function, consistent with DPP4 inhibitors not blocking MERS-CoV entry.[80,85] Like SARS-CoV-1 and 2 spike, MERS-CoV receptor binding domain contains a core subdomain and a receptor-binding subdomain, which relies on a number of essential cysteines. At the spike-DPP4 interface, 14 MERS-CoV residues contact 15 DPP4 residues.[85] Point mutations in these residues revealed that hydrogen bonding between MERS-CoV Y499 and DPP4 R336, between MERS-CoV E536, D537, and D539 and DPP4 K267, hydrophobic interactions with

MERS-CoV L506. W553, and V555, as well as the salt-bridge between MERS-CoV D510 and DPP4 R317 are essential for viral entry.[85]

3.4.4.1 Studies of anti-MERS-CoV activity

III and **VII** lacked anti-MERS-CoV activity up to 200 µM but had moderate cytotoxicity in HeLa-DPP4 cells (Figure 3.21). This was further demonstrated by gene expression assays (Figure 3.22). As MERS-CoV is a sialic acid-dependent and not an HS-dependent virus, these data suggest that PPCs have specificity in their mechanism of action. Controls were HeLa cells not expressing DPP4, which should not allow pseudovirus entry, heparin, which does not inhibit MERS-CoV except at very high concentrations (Chapter 5.4), and soluble ACE2, which inhibits SARS-CoV-1 and 2 entry but not MERS-CoV entry.
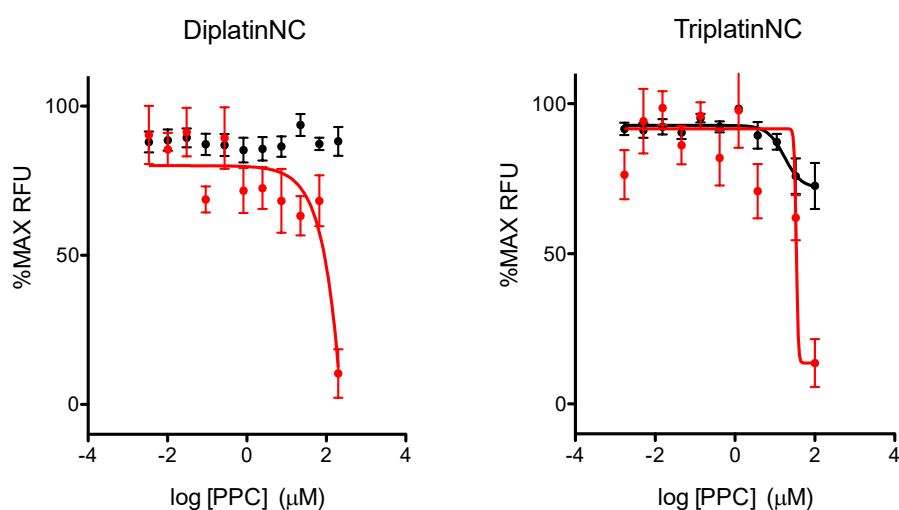
Figure 3.20: ***Antiviral activity of DiplatinNC (III) and TriplatinNC (VII) against pseudotyped MERS-CoV.*** *Anti-MERS activity (black) was measured by incubating HeLa-DPP4 cell monolayers in 384-well plates with PPCs for one h, infecting with GFP-tagged pseudovirus (125 transducing units/well), and measuring GFP levels (RFU) two days after infection. Cytotoxicity (red) was measured in replicate uninfected cultures treated for two days using the CellTiter-Glo® assay. Data are means of three independent experiments ± standard deviations.*
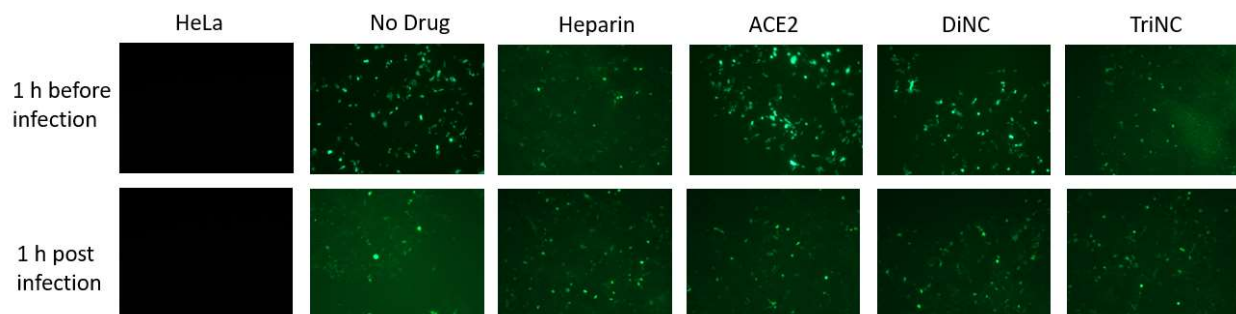
Figure 3.21: ***PPCs do not inhibit GFP expression resulting from MERS-CoV pseudovirus transduction.*** *Confluent monolayers of HeLa (left column) HeLa-DPP4 cells (all other columns) in 96-well plates were treated with medium (Ø), 150 µg/ml heparin (HEP), 300 µg/ml soluble ACE2, 10 µM DiNC, or 5 µM TriNC one h before or one h after infection with GFP-tagged pseudotyped virus (100 infectious units/well). Representative fluorescent micrographs were taken two days post infection.*

3.5 Influenza virus

Influenza viruses belong to the Orthomyxoviridae family of RNA viruses, separated into four types: A, B, C, and D.[86,87] Influenza virus is an enveloped virus with eight segments of (-)ssRNA, encoding ten viral

proteins: the three subunits of viral-specific RNA polymerase, hemagglutinin (HA), neuraminidase (NA), nucleoprotein, matrix protein, proton channel protein M2, and two nonstructural proteins.[86,88] Influenza infection causes respiratory symptoms along with fever, muscle aches, headache, and general weakness; it can lead to pneumonia and death, with the highest infection rates among young people and the highest mortality rates among older adults.[89] Transmission routes are through respiratory droplets, fomites, and aerosols.[90,91] In an average year in the US, influenza is seasonal and infects approximately 25 to 50 million people and causes 20,000 deaths.[92] However, due to its segmented genome and high rates of reassortment (often between animal- and human- type influenza viruses), antigenic shift is frequent and causes epi- and pandemics, the most notable of which was in 1918, followed by the 1957 H2N2, the 1968 H3N2, and the 2009 H1N1 pandemics.[89,93,94]

The best public health intervention is influenza vaccination.[95] There are also four approved antivirals, three of which target NA (oseltamivir, zanamivir, peramivir) to prevent new virions from exiting infected cells.[86,96] However, resistance to all three NA inhibitors has become a critical issue, particularly following the H1N1 pandemic in which resistance to oseltamivir was 27%, compared to 3% for seasonal influenza H3N2.[86,97] Resistance is limited against baloxavir, which targets the endonuclease subunit of the influenza virus polymerase complex.[98] Other influenza inhibitors (amantadine and rimantadine), which targeted the M2 ion channel protein of influenza, have been discontinued due to a high degree of resistance.[99,100] Due to the limitations of the available antivirals, new strategies are needed.

Influenza enters susceptible cells much like other enveloped viruses. It relies on hemagglutinin (HA), which is the viral glycoprotein responsible for both attachment to the cell surface via α-sialic acid and virion entry via membrane fusion.[86,88,101] HA trimers bind to a terminal α-sialic acid linked to saccharides on the cell surface. The C-terminus of HA is embedded in the viral matrix protein layer while the sialic-acid binding site is within a surface depression on the top of trimeric HA.[88] As many HA trimers are on the virion surface, attachment is proposed to be a multivalent process that collectively forms a strong interaction.[102,103] Specifically, two aromatic residues (Tyr98 and Trp153) sit on top of the sialic acid using strong hydrophobic interactions, while four functional groups further strengthen HA-sialic acid binding: the carboxyl group of sialic acid forms hydrogen bonds with Gln226, the amide in the acetylamido group forms hydrogen bonds with a main chain carbonyl group, the methyl group in the acetylamido group forms van der Waals interactions with Trp153, and two hydroxyl groups of the glycerol moiety forms hydrogen bonds with Gln226 and Glu190 as well as a main chain carbonyl group.[88,104] These interactions form the basis of HA-sialic acid recognition, although there are variations between subtypes. Overall, human influenza A HA prefers α2,6 glycosidic linkages; however, influenza B has a slightly different binding site and prefers α2,3 glycosidic linkage,[88] while influenza C HA greatly differs, and in fact utilizes 9-O-acetylsialic acid, not αsialic acid, for attachment. Regardless of preference, the role of HA-sialic acid binging is not entirely clear and there is evidence of sialic acid independent entry, suggesting another possible primary receptor.[88,105] Following attachment, the influenza virion is endocytosed. In the late endosome, when the pH is below 5, HA undergoes cleavage and conformational changes that drive membrane fusion and release of the capsid into the cytoplasm.[88,106]

3.5.1 Anti-Influenza activity

Unlike the SARS-CoV-1 and SARS-CoV-2, influenza virus relies on sialic acid, not HS, to attach to the cell surface. To further demonstrate the selectively of PPCs, we tested **III** and **VII** against influenza virus, using the pseudotyping system described above (Figure 3.23). Interestingly, neither **III** or **VII** inhibited pseudotyped influenza virus or GFP expression, indicating their selective mechanism of action: inhibition

of viral attachment via HS (Figure 3.23 and Figure 3.24). These results are similar to those described above for MERS-CoV, which is also reported to utilize sialic acid and not HA for attachment.
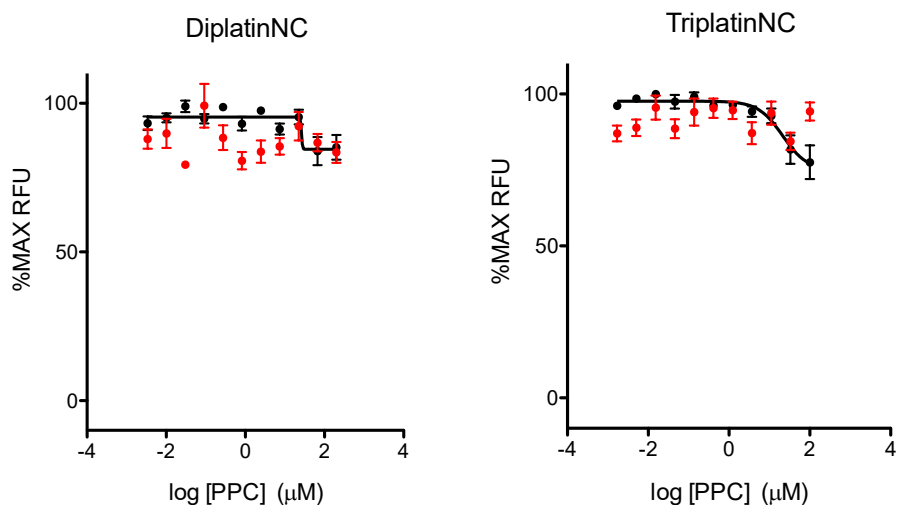
Figure 3.22: GFP-based anti-pseudotyped influenza activity of DiplatinNC and TriplatinNC. Confluent HEK-293T cells were treated with serially diluted compounds for one hour, then infected with HA pseudotyped particles. Two days post infection, GFP expression was quantified and graphed (black line). Identical non-infected cells were tested for cytotoxicity (red line).
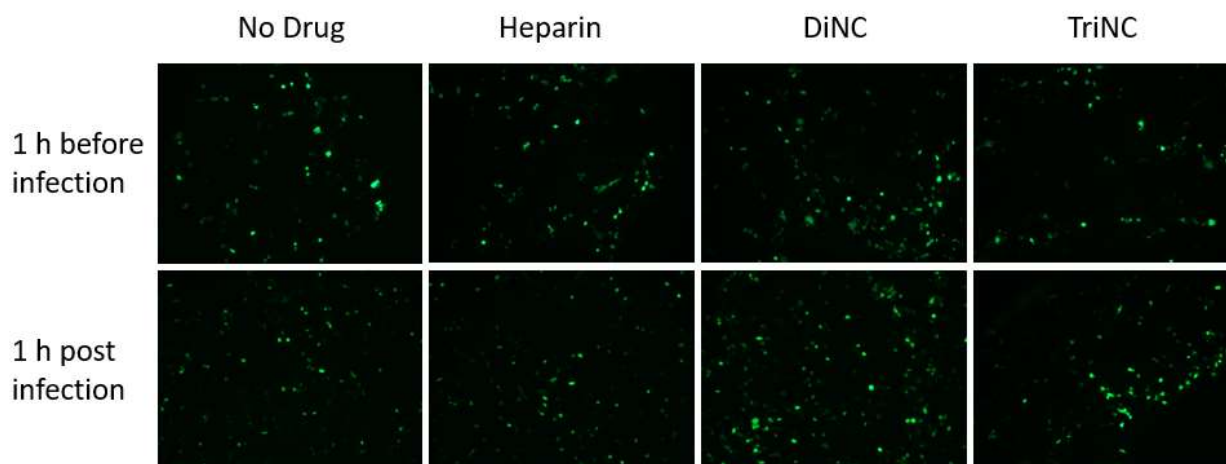
*Figure 3.23: **PPCs do not inhibit GFP expression following transduction with HA-pseudoviruses.** Confluent monolayers of HEK-293T cells in 96-well plates were treated with medium (Ø), 150 µg/ml heparin (HEP), 10 µM DiNC, or 5 µM TriNC one h before or one h after infection with GFP-tagged HA-pseudotyped virus (100 transducing units/well). Representative fluorescent micrographs were taken two days post infection.*

3.5 Ruthenium Red

As we developed antiviral PPC structure-activity relationships and defined their HS-selective mechanism, we endeavored to further detail the effects of inorganic compounds on viral attachment. Ruthenium Red (RuRed, Figure 3.25) is a polycationic coordination compound. RuRed has been used to study cellular mechanism as it is known to non-specifically bind and inhibit several proteins such as mammalian ion channels,[107,108] plant ion channels,[109] and Ca^{2+} binding proteins. RuRed is also a well-known

dye for sialic acid, as well as pectins and mucliages in plants.[110] As such, RuRed has been used in electron microscopy for increased resolution and contrast in animal materials.[110–112] RuRed also inhibits neurotransmission through interaction with sialic acids.[109,113]
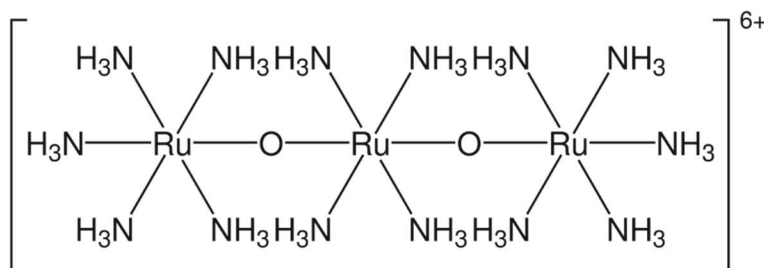
Figure 3.24: Structure of Ruthenium Red. Counterions omitted for clarity.

With a charge of +6, RuRed is equal to both DiplatinNC and Werner's complex (discussed in chapter 4). As a positively charged compound, we predicted that RuRed may bind HS and prevent the infection by HS-dependent viruses. However, given its ability to stain sialic acids, it predicted that it could potentially inhibit sialic-acid dependent viruses such as MERS-CoV and influenza virus.

3.5.1 Antiviral activity of RuRed

We tested RuRed against SARS-CoV-2, SARS-CoV-1, MER-CoV, and influenza virus, using the pseudotyping system described above (Figure 3.26 and Table 3.6). Interestingly, RuRed lacked antiviral activity against both HS-dependent viruses, but had μM activities against sialic-acid dependent MERS-CoV and influenza virus. Similar to PPCs, RuRed inhibited GFP expression in influenza virus only if cells were pretreated, suggesting that it inhibits viral attachment/entry (Figure 3.27).
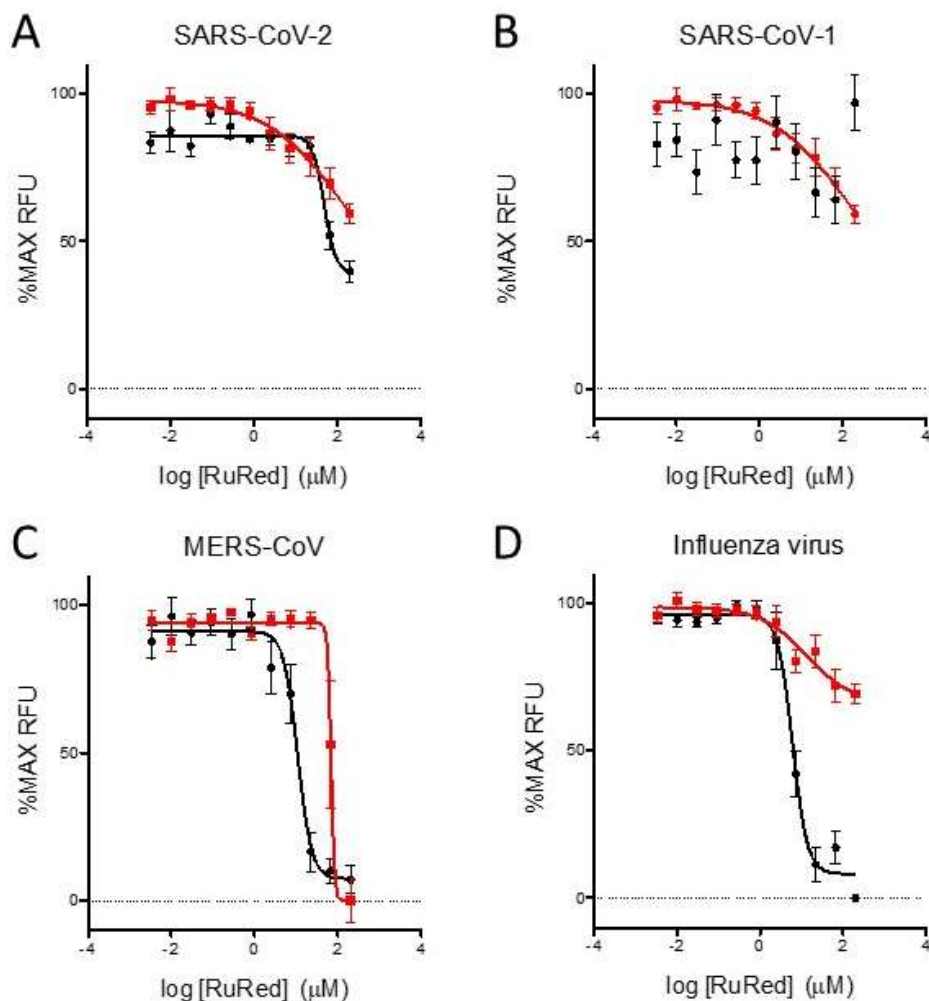
Figure 3.25: Antiviral activity of RuRed. GFP-based anti-SARS-CoV-2 (A), SARS-CoV-1 (B), MERS-CoV (C) or influenza virus (D). Confluent HEK-293T-ACE2 (A, B), HeLa-DPP4 (C), or HEK-293T (D) cells were treated with serially diluted RuRed for one hour then infected with pseudotyped viruses. Two days post infection, GFP expression was quantified and graphed (black line). Identical non-infected cells were treated for two days and tested for cytotoxicity (red line).

Virus	Antiviral^a (EC$_{50}$)	Cytotoxicity^b (TC$_{50}$)	SI^c
SARS-CoV-2	Not active	>200	N/A
SARS-CoV-1	Not active	>200	N/A
MERS-CoV	11.763 ± 3.27	67.80 ± 8.27	5.8
Influenza virus	6.136 ± 1.11	>200	>32.6

Table 3.6: Antiviral activity of RuRed. a GFP-based assay. b CellTiter-Glo® assay. c selectivity index (TC50/EC50). a,b µM; results are means of three independent experiments ± standard deviations.
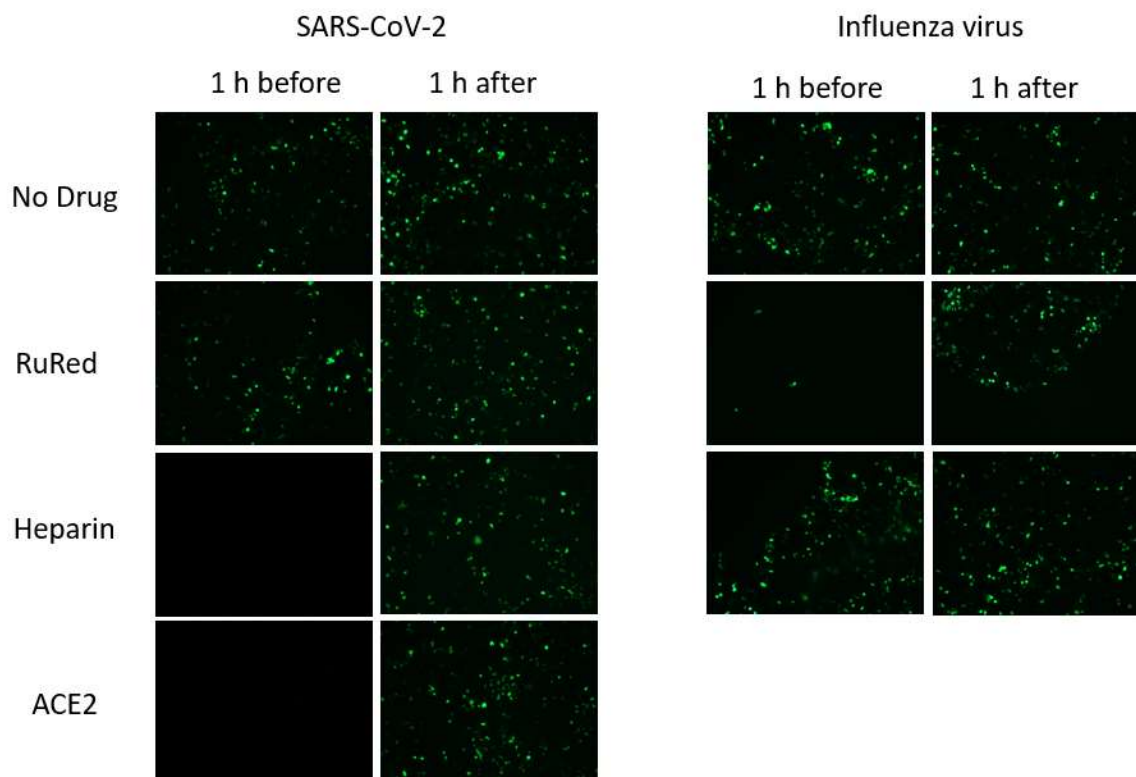
Figure 3.26: RuRed inhibit GFP expression following transduction with influenza (right) but not SARS-CoV-2 (left) pseudoviruses. Confluent monolayers of HEK-293T-ACE2 (left) or HEK-293T (right) cells in 96-well plates were treated with medium (Ø), 150 µg/ml heparin (HEP), 300 µg/ml soluble ACE2, or 100 µM RuRed one h before or one h after infection with GFP-tagged pseudotyped viruses (100 transducing units/well). Representative fluorescent micrographs were taken two days post infection.

3.6 Discussion

Current medical interventions for emerging viruses are extremely limited. Vaccines are an essential protective measure in viral epi- and pandemics however their development is time-consuming and often exacerbated by viral genome mutations leading to antigenic drift and loss of vaccine efficacy.[94,95,114] Effective treatments for viral infection are also difficult as many emerging viruses are zoonotic by nature or are the result of mutations in existing viruses.[115] Repurposing existing approved drugs aides in discovery of new treatments; however, drug repurposing often identifies candidates that may or may not work well *in vivo*.[115] Ultimately, treatments for emerging viral disease are often limited to immune modulation and supportive care.

Broad-spectrum antivirals, or compounds which inhibit viruses from more than one viral family, offer a potential solution to this problem. Broad-spectrum antivirals must target a commonality between viruses. Previously, broad-spectrum antivirals have targeted viral polymerases, an intercellular target which allows for mutations giving rise to resistance.[116] Importantly, these polymerase inhibitors have incomplete broad-spectrum activity. For instance, ribavirin inhibits a number of RNA viruses (RSV, hepatitis C, influenza A and B, parainfluenza viruses, hepatitis E, and metapneumovirus) but largely failed to inhibit SARS-CoV-1 during its epidemic.[116]

Entry inhibitors may have more success as they may be less subject to resistance mutations. Many viruses use HS, a glycosaminoglycan, or sialic acids to attach to the cell surface before using more specific interactions between their entry protein and cellular receptor to enter cells. This makes HS or SA uniquely qualified to be a broad-spectrum target. Thus far HS has been largely targeted by small peptide or HS mimetics with varying degrees of success, as reviewed in Chapter 1. Considering our previous work, we hypothesized that PPCs would avoid previously seen issues, such as excessive bleeding, and maintain an HS-targeting strategy to inhibit HS-dependent viruses, including SARS-CoV-2 and perhaps sialic acid dependent viruses.

In this work, we demonstrated the anti-SARS-CoV-2 activity of the PPC series (Table 3.5). The structure-activity relationships reinforced and built on those with HCMV and EV71, which emphasized the importance of charge and nuclearity. In comparing the mononuclear, dinuclear, trinuclear, and tetranuclear compounds, it is clear that increasing nuclearity improves anti-SARS-CoV-2 activity. Mononuclear **I** lacked antiviral activity and dinuclear **II** and **III** were consistently outperformed by trinuclear compounds and the lone tetranuclear compound (**XI**). Although nuclearity is closely related to length and charge, it is evident that a minimum of two platinum centers is required for measurable antiviral activity, but the difference between three and four platinum centers does not greatly increase antiviral activity. Mononuclear **I**, with the smallest positive charge of the series (+4), lacked antiviral activity; dinuclear **III** and trinuclear **IV** both have a charge of +6 and good antiviral activity though these were both outperformed by compounds with greater positive charge, suggesting that a minimum of +6 is required for robust anti-SARS-CoV-2 activity. This is of particular interest given that RuRed also has a charge of +6 but lacks SARS-CoV-2 activity, clearly demonstrating that the charge of the coordination compound alone is not the determining factor of antiviral activity.

In modifying **VII**'s structure, we observed a number of structure-activity relationships. Replacing the terminal dangling amines with simple amines (**IV**) decreases antiviral activity, implying that the additional length is important for activity; this is supported by the structural-activity relationship seen in MB assays, in which HS affinity decreases with the removal of the dangling amines. Varying the length of the diamineakyl linker (**V**, **VI**, **VII**, and **VIII**) did not significantly affect the antiviral activity, indicating that it is nuclearity or charge rather than length that influences antiviral activity. The addition of protecting groups on the dangling amines (**IX** and **X**) decreased charge and antiviral activity; this may be due to a number of structural features. First, it demonstrates once again that charge is important, as both **IX** and **X** have a decreased charge comparted to **VII**. It also implies that increasing bulk may impede PPCs ability to adequately bind and shield HS. Overall, this structure-activity study reveals that (i) a minimum of two platinum centers and a positive charge of +6 charge are required for antiviral activity; (ii) dangling amines perform better than simple amines, (ii); the length of the diamineakyl linker does not affect antiviral activity; and (iv) protecting groups on dangling amines decreases antiviral activity.

More in-depth work with **III** and **VII** unveiled a number of important revelations. As hypothesized, PPCs inhibit a broad-spectrum of viruses, regardless of genome type, envelope, or viral glycoprotein (Table 3.7). Their micromolar activity against pandemic SARS-CoV-2 and epidemic SARS-CoV-1, as well as adenovirus, underline their potential utility as broad-spectrum viral inhibitors. Mechanistic work illustrated that PPCs maintain their mechanism of action across these viruses: inhibition of viral attachment presumably via blocking HS. Their inhibition of viral GFP expression only if added prior to infection indicates a mechanism of action that is prior to viral gene expression. Similarly, in time of addition experiments, PPCs inhibit only when added prior to or in the very early hours of infections, similar

to heparin, a well-known entry inhibitor. Compound removal studies revealed that PPCs bind a cellular component, hypothesized to be HS, in order to inhibit virion attachment. Collectively, these data build on those with HCMV, EV71, and human metapneumovirus and highlight PPCs' inhibition of attachment.

Virus	DiplatinNC			TriplatinNC		
	EC50	TC50	SI	EC50	TC50	SI
HCMV[1]	0.471 ± 0.16	54.31 ± 11.9	115.3	0.338 ± 0.28	24.65 ± 9.53	72.9
Adenovirus	5.563 ± 2.3	61.34 ± 4.99	11	0.709 ± 0.52	4.317 ± 0.38	6
hMPV[2]	N/A	N/A	N/A	5.5 ± 2.2	146 ± 6.6	26.5
EV71[2]	28 ± 0.48	>500	17.9	5.35 ± 1.47	327.25 ± 137.4	61.2
SARS-CoV-2	1.812 ± 0.35	>200	110.4	0.986 ± 0.551	>200	202.8
SARS-CoV-1	2.556 ± 0.58	>200	78.2	1.502 ± 0.72	>200	133.2
influenza	Not active	>200	N/A	Not active	>200	N/A
MERS-CoV	Not active	~120	N/A	Not active	~120	N/A

Table 3.7: Summary table for the broad-spectrum antiviral activity of TriplatinNC and DiplatinNC. All values are reported in micromolar (μM).

Finally, and perhaps most interestingly, PPCs do not inhibit influenza virus or MERS-CoV. Influenza virus and MERS-CoV each attach to host cells via sialic acids, a class of alpha-keto acid sugars with a nine-carbon backbone that are less sulfated than HS. Given the structural differences from HS, sialic acids are generally less negatively charged. This may suggest that PPCs have a lower affinity for SA as compared to HS, impeding PPCs ability to inhibit SA-dependent viruses; this is supported by data which state that sulfates are essential in PPC-HS binding. It also suggests that PPCs have a selective mechanism of action for HS-dependent virion attachment.

The results for RuRed also indicate that more than charge that determines a compound's antiviral activity. RuRed is well-known to bind to sialic acids. Interestingly, RuRed does not inhibit HS-dependent SARS-CoV-1 or 2, but it does inhibit sialic acid-dependent influenza virus and MERS-CoV. This is particularly of note as RuRed has the same charge (6+) as DiplatinNC, yet the two compounds are opposite in their activities, emphasizing the importance of structure over charge. Besides differing in their metal centers, DiplatinNC has square planar geometry, while RuRed has octahedral geometry. As discussed in Section 1.6, an octahedral face of three ammines could potentially be more effective in metalloshielding than the square planar structure of PPCs.[117] However, in this case, it did not improve the antiviral activity against HS-dependent viruses.

The inhibition of HS- over SA-dependent viruses may also reflect the varied structures of the glycans. Sialic acids are most commonly N-acetylneuraminic acid, which caps N- or O-glycans and glycolipids; a number of positions (C4, C5, and C7-9) may be modified (Figure 3.27).
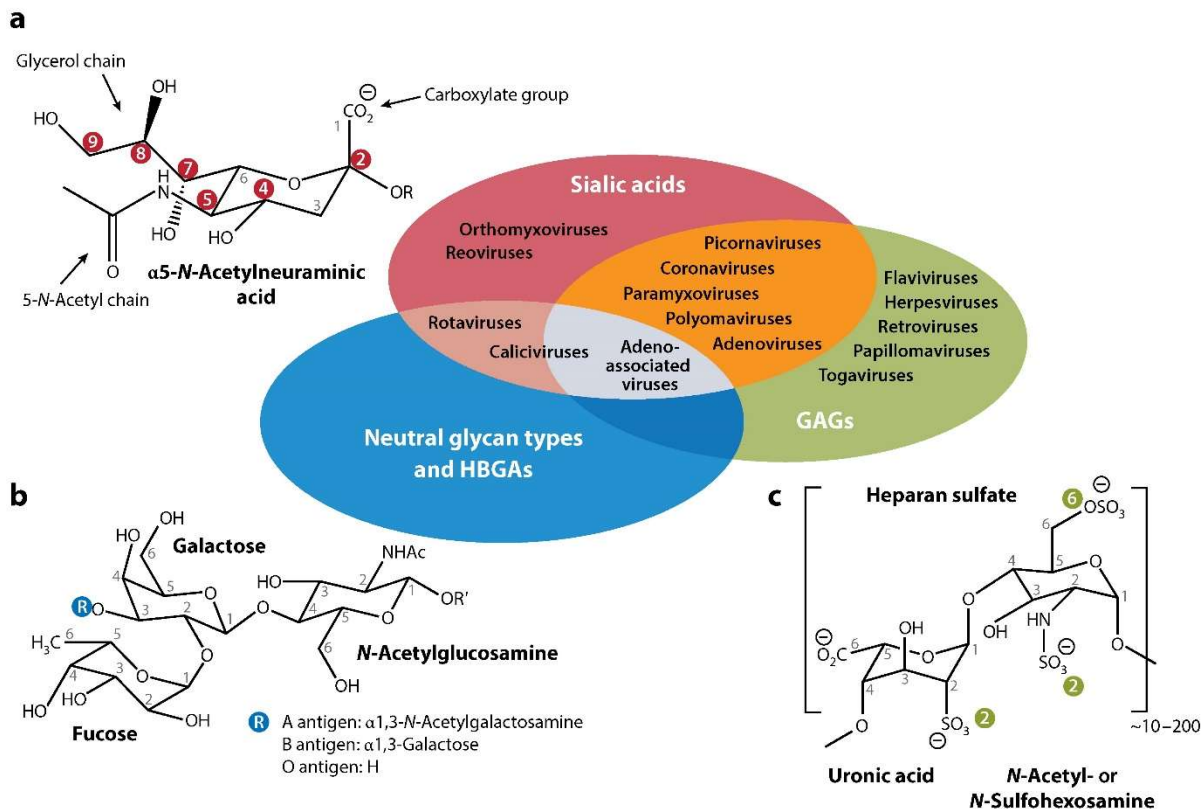
Figure 3.27: Glycans as viral receptors.[118] Viruses may use (a) sialic acids, (b) neutral oligosaccharides, or (c) GAGs for attachment and/or entry. The Venn diagram depicts examples of viruses which use the respective glycans. Reproduced from Stroh and Stehle 2014.

Compared to HS, sialic acid has a regular structure; despite this, viruses employ a number of strategies to engage sialic acids. While polyomaviruses SV40, BKPyV, and JCPyV bind Neu5Ac in the same orientation and in a similar manner, polyomaviruses MCPyV, MPyV, and LPyV each employ a different strategy and orientation to bind Neu5Ac.[118] This theme is continued across a number of sialic acid binding viruses including MERS-CoV and influenza virus as described above. Similarly, HS has a large structural variety; it consists of a nonbranching, repeating disaccharides of hexosamine and uronic acid (iduronic or glucuronic acid); it is often modified at C2 or hexosamine by N-sulfation or acetylation, and at C2 and C6 of uronic acid by hexosamine. Due to its heterogeneous nature, it is difficult to study virion-HS binding.[119] With that said, there are a few structural descriptions of these interactions. Picornavirus engages HS in a surface-exposed groove and SARS-CoV-2 binds HS via amphipathic interactions with its spike protein.[118] However, other studies, like those with human papillomavirus and AAV, only report low-resolution interactions, which preclude atomic analysis.[118] Clouding things further, many of these studies were performed with heparin, a structural analog of HS, and thus only hold so much weight.

The current knowledge of how viruses bind glycans at the atomic level is incomplete, which hinders an in-depth analysis of the inhibitors of these interactions.[118,119] When comparing HS and sialic acids, it is clear that a virus may favor binding one over the other, and thus it is plausible that an inhibitor

would exhibit a similar preference. On one hand, the observation that PPCs inhibit HS dependent viruses while RuRed inhibits sialic acid dependent viruses may provide insight into their interactions with glycans. On the other hand, these compounds may be more useful in deciphering the interactions between virion and glycan. It is difficult to say which portion of HS is essential to viral binding and which groups should be shielded for antiviral effect. But if we could identify the mode of RuRed-sialic acid binding, we could extrapolate sialic acid-virion binding. Likewise, with PPCs and HS-dependent viruses.

3.7 Conclusion

The HS-virion interaction has been described as non-specific and charge-dependent with ongoing research looking to identify the structural groups essential for viral attachment. Inorganic inhibitors of viral attachment had unclear structure-activity relationships and their mechanisms were also unclear. In this chapter, we continued to investigate antiviral activities of PPCs. Increasing the charge, length, and nuclearity of PPCs improved their anti-SARS-CoV-2 activity, in line with the trends identified with HCMV and EV71.[1,2] DiplatinNC and TriplatinNC inhibit additional HS-dependent viruses via a cellular component but do not inhibit sialic-acid dependent viruses, in contrast to RuRed. With this observation we established that the PPC mechanism of action is specific, in contrast to the prior dogma. Moving forward, additional studies on sialic acid affinity are crucial but ultimately the goal should be to examine options for an animal model. The most common objection to inorganic treatments, particularly those containing platinum, is the possibility for off-target toxicity. While we have established that PPCs bind non-covalently and thus should have minimal toxicity, it is important to assuage concerns through thorough investigation. Once that is established, we believe that PPCs, and charged coordination compounds in general, will be positioned to contribute to antiviral development and mechanistic inquiry of virion-glycan binding.

3.8 Experimental methods

3.8.1 Cell and viral culture

Human APRE-19 epithelial cells (derived from retinal pigment epithelium) (ATCC CRL-2302), guinea pig lung fibroblast cells (GPL) (ATCC-CCL158), and human adenocarcinoma epithelial cells (HeLa cells) (ATTC CCL-2) were purchased from American Type Culture Collection. Human Embryonic Kidney Cells (HEK-293T) and HEK-293T expressing human angiotensin-converting enzyme 2 (HEK-293T-hACE2; NR-52511) cells were purchased from BEI Resources. HeLa cells expression dipeptidyl peptidase 4 (HeLa-DPP4) were a gift from David Namazee. APRE-19, HeLa, HeLa-DPP4, HEK-293T, and HEK-293T-hACE2 cells were cultured at 37 °C in a 5% CO_2 atmosphere using Dulbecco's Modified Eagle Medium supplemented with 10% fetal bovine serum, 50 U/mL penicillin, 50 mg/mL streptomycin, and 29.2 mg/mL L-glutamine (DMEM, all from Life Technologies).

Guinea pig CMV (GPCMV) with a red fluorescent tag (N13R10r129-TurboFP635) was derived from BAC N13R10r129-TurboFP635; it was propagated in GPLs.[120] Virus stocks were derived from infected cell culture supernatants, adjusted to 0.2 M sucrose, and stored in liquid nitrogen. Viral titers were determined using GPLs as described.[121] Stocks of GFP-tagged adenovirus, provided by Dr. Daniel Conway at Virginia Commonwealth University, were produced using the pAdeasy adenovirus-packaging system as described.[122,123]

3.8.2 Compounds and compound synthesis

MonoplatinNC, DiplatinNC, TriplatinNC, AH44, TriplatinNC-pent, TriplatinNC-hept, TriplatinNC-Boc, and TetraplatinNC were prepared according to published methods.[60,124,125] BBR3571NC was synthesized through adaptation of published procedures.[1,126] TripaltinNC-but was synthesized through the adaption of TriplatinNC-hept and -pent procedures.[127] The complexes were characterized by C, H, N elemental analysis, and ^{1}H and [195]Pt nuclear magnetic spectroscopy.

TriplatinNC-AA:[128] TriplatinNC (1 mmol) was dissolved in water, and DIPEA (2.2 mmol) was added. After 30 minutes, acetic anhydride was added dropwise over a period of 1 h. The reaction was then heated at 50 °C for 48 h and filtered through celite to remove any unreacted starting materials and reduced platinum. The volume of the filtrate was reduced to almost dryness and acetone was added to force the precipitation of the product. The precipitate was filtered off then washed with acetone. Further purification, as needed, was achieved by recrystallization in water. Yield- 84% 1H NMR (D2O): δ 3.08 (t,4H), 2.56 (t, 12H), 1.90 (s, 6H), 1.55 (m, 12H), 1.42 (m 4H), 1.24 (m,16H). Elemental analysis calculated for C28,H85,N20,O20,Pt3 - C 20.92, H 5.33, N 17.43. Obtained: C 20.90, H 5.27, N 17.38.

All PPCs were dissolved in water at a stock concentration of 10 mM. Heparin sodium purchased from Acros Organics (Lot # B0146868) and dissolved in water at a stock concentration of 1 mg/mL.

3.8.3 Pseudotyping lentivirus

SARS-CoV-2 pseudotyped lentiviruses were prepared as outlined in Crawford et al.[151] SARS-CoV-1, MERS-CoV, and influenza virus were prepared by adapting the procedure. Briefly, transfection quality plasmid DNA of the following plasmids were prepared:

- pHAGE-CMV-Luc2-IRES-ZsGreen-W (BEI catalog number NR-52516): Lentiviral backbone plasmid that uses a CMV promoter to express luciferase followed by an IRES and ZsGreen.
- HDM-Hgpm2 (BEI catalog number NR-52517): lentiviral helper plasmid expressing HIV Gag-Pol under a CMV promoter.

- HDM-tat1b (NR-52518): Lentiviral helper plasmid expressing HIV Tat under a CMV promoter.
- pRC-CMV-Rev1b (NR-52519): Lentiviral helper plasmid expressing HIV Rev under a CMV promoter.

All plasmid DNA preparations were purified by double CeCl banding and kindly provided by Dr. Anton Chestukhin. HEK-293T cells were seeded into 6-well plates overnight to produce 50%–70% confluency at the time of transfection. Cells were transfected using BioT (Bioland Sci entific LLC) following the manufacturer's instructions. Each well received the following plasmid mix: 1 µg of pHAGE-CMV-Luc2-IRES-ZsGreen-W (NR-52516), 0.22 µg each of plasmids HDM-Hgpm2 (NR-52517), HDM-tat1b (NR-52518), and pRC-CMV-Rev1b (NR-52519), and 0.34 µg of viral glycoprotein encoding plasmid (either SARS-CoV-2 Spike (pGBW-m4137383; Addgene_149541), SARS-CoV-1 spike (pcDNA3.3_CoV1_D28; Addgene #170447),[162] influenza HA (pNAHA; Addgene #44169),[163] or MERS-CoV spike (pCDNA3.3_MERS_D12; Addgene #170448)[162]). Media was changed 18 to 24 h post-transfection. Pseudoviruses were harvested by filtering the supernatant with a 0.45 µm SFCA low protein-binding filter 60 h post transfection and stocks were stored either 4°C for immediate use or frozen long-term at -80 °C. Titers of pseudotyped lentiviruses were determined after a single freeze-thaw. Serially diluted stock was applied to HEK-293T-ACE2 cells and two days post infection, cells were also visually assessed to quantitate the titer of the stock (the lowest dilution with GFP positive cells).

3.8.4 Luciferase-based yield assay of antiviral activity

Eleven three-fold serial dilutions of DiplatinNC and TriplatinNC were prepared in DMEM. Final concentrations ranged from 200 µM to 3.4 nM for DiplatinNC, and 100 µM to 1.7 nM for TriplatinNC. Black-wall/clear-bottom 96-well plates with confluent monolayers of HEK-293T-ACE2 cells were treated with different concentrations of each test compound in triplicate. After one h of incubation cells were infected with pseudotyped SARS-CoV-2. Infected and uninfected wells without compound served as controls. Following a two-day incubation, luciferase activity was measured by removing 100 µL of media and adding 100 µL of Steady-Glo® luciferase substrate (Promega), incubating ten minutes at room temperature, and measuring relative luminosity units (RLU) using a BioTek Synergy HT Multi-Mode Microplate reader. Prism 5 software (Graphpad) was used to determine 50% effective concentration (EC$_{50}$) values as the inflection points of best-fit four-parameter curves for RLU (means of triplicate data) versus log inhibitor concentration. Graphical representations were normalized to % maximum RLU.

3.8.5 GFP-based assay of antiviral activity

For pseudotyped viruses: Confluent monolayers of HEK-293T-ACE2 or HEK-293T cells in 384-well plates were prepared and treated with compound dilutions as described in *3.8.4* above. After one h of incubation cells were infected with pseudotyped SARS-CoV-1, SARS-CoV-2, MERS-CoV, or influenza virus. Following incubation for two days, relative fluorescence units (RFU) of GFP fluorescence were quantified by BioTek Synergy HT Multi-Mode Microplate reader and EC$_{50}$ values were determined as described in *3.8.4*. Graphical representations were normalized to % maximum RFU.

For adenovirus: Confluent monolayers of ARPE-19 cells in 96-well plates were prepared and treated with compound dilutions as described in *3.8.4* above. After one h of incubation cells were infected with GFP-tagged adenovirus (100 PFU/well). Following incubation for five days, relative fluorescence units (RFU) of GFP fluorescence were quantified by BioTek Synergy HT Multi-Mode Microplate reader and EC$_{50}$ values were determined as described in *3.9.4*. Graphical representations were normalized to % maximum RFU.

For GPCMV: Confluent monolayers of guinea pig lung fibroblasts (GLFs) in 96-well plates were prepared and treated with compound dilutions as described in *3.9.4* above. After one h of incubation cells were infected with RFP-tagged GPCMV (100 PFU/well). Following incubation for five days, relative fluorescence units (RFU) of RFP fluorescence were quantified by BioTek Synergy HT Multi-Mode Microplate reader and EC_{50} values were determined as described in *3.9.4*. Graphical representations were normalized to % maximum RFU.

3.8.6 Cytotoxicity

Replicate HEK-293T-ACE2 or HEK-293T cell cultures were prepared simultaneously with those described in *3.9.4* and *3.9.5* but were not infected. After incubation of two days cell viability was determined by removing 50 μL of culture media from each well, adding 50 μL of CellTiter-Glo® reagent (Promega), incubation for ten minutes at room temperature, and measuring RLU using a BioTek Synergy HT Multi-Mode Microplate reader. 50% cytotoxicity concentrations (TC_{50}) were calculated as inflection points of four-parameter curves as described in *3.9.4*. Graphical representations were normalized to % maximum RLU. A similar procedure was repeated for ARPE-19 and GLF cells but the incubation period lasted five days.

3.8.7 Inhibition of GFP fluorescence

Inhibition of GFP expression was evaluated by treating confluent cell monolayers in black-wall/clear-bottom 96-well plates with compounds for one h before addition of 100 PFU/well virus adenovirus. Five days after infection representative micrographs were taken with a Nikon Eclipse TS100 Inverted UV microscope.

3.8.8 Time of addition

Confluent cell monolayers in black-wall/clear-bottom 96-well plates were infected with adenovirus (100 PFU/well). A single inhibitory concentration of each compound was added to triplicate wells one h before, at the time of, and 3, 6, 12, 24, 48, 72, 96, or 120 hpi. Infected or uninfected wells not treated with compounds served as controls. Following incubation for five days, GFP fluorescence was quantified using a BioTek Synergy HT Multi-Mode Microplate reader. Percent maximum RFUs were plotted versus time of compound addition (relative to infection) using Prism 5 software.

3.9 References

(1)   Shoup, M.; Ourahmane, A.; Ginsburg, E. P.; Farrell, N. P.; Mcvoy, M. A. Substitution-Inert Polynuclear Platinum Compounds Inhibit Human Cytomegalovirus Attachment and Entry. *Antiviral Res.* **2020**, *184*, 104957.

(2)   Bailly, B.; Gorle, A. K.; Dirr, L.; Malde, A. K.; Farrell, N. P.; Berners-Price, S. J.; von Itzstein, M. Platinum Complexes Act as Shielding Agents against Virus Infection. *Chem. Commun.* **2021**, *57* (38), 4666–4669. https://doi.org/10.1039/D1CC01593A.

(3)   Lugo, D.; Krogstad, P. Enteroviruses in the Early 21st Century: New Manifestations and Challenges. *Curr. Opin. Pediatr.* **2016**, *28* (1), 107–113. https://doi.org/10.1038/s41395-018-0061-4.

(4)   Chang, A.; Masante, C.; Buchholz, U. J.; Dutch, R. E. Human Metapneumovirus (HMPV) Binding and Infection Are Mediated by Interactions between the HMPV Fusion Protein and Heparan Sulfate. *J. Virol.* **2012**, *86* (6), 3230–3243. https://doi.org/10.1128/jvi.06706-11.

(5)   Panda, S.; Mohakud, N. K.; Pena, L.; Kumar, S. Human Metapneumovirus: Review of an Important Respiratory Pathogen. *Int. J. Infect. Dis.* **2014**, *25*, 45–52. https://doi.org/10.1016/j.ijid.2014.03.1394.

(6)   Earley, D. F.; Bailly, B.; Maggioni, A.; Kundur, A. R.; Thomson, R. J.; Chang, C. W.; Von Itzstein, M. Efficient Blocking of Enterovirus 71 Infection by Heparan Sulfate Analogues Acting as Decoy Receptors. *ACS Infect. Dis.* **2019**, *5* (10), 1708–1717. https://doi.org/10.1021/acsinfecdis.9b00070.

(7)   Nishimura, Y.; McLaughlin, N. P.; Pan, J.; Goldstein, S.; Hafenstein, S.; Shimizu, H.; Winkler, J. D.; Bergelson, J. M. The Suramin Derivative NF449 Interacts with the 5-Fold Vertex of the Enterovirus A71 Capsid to Prevent Virus Attachment to PSGL-1 and Heparan Sulfate. *PLoS Pathog.* **2015**, *11* (10), 1–19. https://doi.org/10.1371/journal.ppat.1005184.

(8)   Ren, P.; Zheng, Y.; Wang, W.; Hong, L.; Delpeyroux, F.; Arenzana-Seisdedos, F.; Altmeyer, R. Suramin Interacts with the Positively Charged Region Surrounding the 5-Fold Axis of the EV-A71 Capsid and Inhibits Multiple Enterovirus A. *Sci. Rep.* **2017**, *7* (January), 1–11. https://doi.org/10.1038/srep42902.

(9)   Ren, P.; Zou, G.; Bailly, B.; Xu, S.; Zeng, M.; Chen, X.; Shen, L.; Zhang, Y.; Guillon, P.; Arenzana-Seisdedos, F.; Buchy, P.; Li, J.; Von Itzstein, M.; Li, Q.; Altmeyer, R. The Approved Pediatric Drug Suramin Identified as a Clinical Candidate for the Treatment of EV71 Infection - Suramin Inhibits EV71 Infection in Vitro and in Vivo. *Emerg. Microbes Infect.* **2014**, *3* (9), e62. https://doi.org/10.1038/emi.2014.60.

(10)   Schleiss, M. R.; McVoy, M. A. Guinea Pig Cytomegalovirus: A Model for the Prevention and Treatment of Maternal-Fetal Cytomegalovirus Transmission. *Future Virol.* **2010**, *5* (2), 207–217. https://doi.org/10.2217/fvl.10.8.

(11)   Ison, M.; Hayden, R. Adenovirus. *Microbiol. Spectr.* **2016**, *4* (4), 1–16. https://doi.org/10.1128/microbiolspec.

(12)   Kinchington, P. R.; Romanowski, E. G.; Gordon, Y. J. Prospects for Adenovirus Antivirals. *J. Antimicrob. Chemother.* **2005**, *55*, 424–429. https://doi.org/10.1093/jac/dki057.

(13)   Zhang, Y.; Bergelson, J. M. Adenovirus Receptors. *J. Virol.* **2005**, *79* (19), 12125–12131. https://doi.org/10.1128/JVI.79.19.12125.

(14)   Dechecchi, M. C.; Melotti, P.; Bonizzato, A.; Santacatterina, M.; Chilosi, M.; Cabrini, G. Heparan Sulfate Glycosaminoglycans Are Receptors Sufficient To Mediate the Initial Binding of Adenovirus Types 2 and 5. *J. Virol.* **2001**, *75* (18), 8772–8780. https://doi.org/10.1128/jvi.75.18.8772-8780.2001.

(15)   Dechecchi, M. C.; Tamanini, A.; Bonizzato, A.; Cabrini, G. Heparan Sulfate Glycosaminoglycans Are

Involved in Adenovirus Type 5 and 2-Host Cell Interactions. *Virology* **2000**, *268* (2), 382–390. https://doi.org/10.1006/viro.1999.0171.

(16) Smith, T. A. G.; Iverson, W. O.; Sherer, A. D.; Markovits, J. E.; Lyons, R. M.; Kaleko, M.; Stevenson, S. C.; Idamakanti, N.; Marshall-Neff, J.; Rollence, M. L.; Wright, P.; Kaloss, M.; King, L.; Mech, C.; Dinges, L. Receptor Interactions Involved in Adenoviral-Mediated Gene Delivery after Systemic Administration in Non-Human Primates. *Hum. Gene Ther.* **2003**, *14* (17), 1595–1604. https://doi.org/10.1089/104303403322542248.

(17) Smith, T. A. G.; Idamakanti, N.; Rollence, M. L.; Marshall-Neff, J.; Kim, J.; Mulgrew, K.; Nemerow, G. R.; Kaleko, M.; Stevenson, S. C. Adenovirus Serotype 5 Fiber Shaft Influences in Vivo Gene Transfer in Mice. *Hum. Gene Ther.* **2003**, *14* (8), 777–787. https://doi.org/10.1089/104303403765255165.

(18) Cagno, V.; Tseligka, E. D.; Jones, S. T.; Tapparel, C. Heparan Sulfate Proteoglycans and Viral Attachment: True Receptors or Adaptation Bias? *Viruses* **2019**, *11* (7), 1–24. https://doi.org/10.3390/v11070596.

(19) Lang, J.; Yang, N.; Deng, J.; Liu, K.; Yang, P.; Zhang, G.; Jiang, C. Inhibition of SARS Pseudovirus Cell Entry by Lactoferrin Binding to Heparan Sulfate Proteoglycans. *PLoS One* **2011**, *6* (8). https://doi.org/10.1371/journal.pone.0023710.

(20) Milewska, A.; Zarebski, M.; Nowak, P.; Stozek, K.; Potempa, J. Human Coronavirus NL63 Utilizes Heparan Sulfate Proteoglycans for Attachment to Target Cells. *J. Virol.* **2014**, *88* (22), 13221–13230. https://doi.org/10.1128/JVI.02078-14.

(21) Li, F.; Li, W.; Farzan, M.; Harrison, S. C. Structure of SARS Coronavirus Spike Receptor-Binding Domain Structure of SARS Coronavirus Spike Receptor-Binding Domain Complexed with Receptor. *Science (80-.).* **2005**, *309*, 1864–1868. https://doi.org/10.1126/science.1116480.

(22) Yan, R.; Zhang, Y.; Guo, Y.; Xia, L.; Zhou, Q. Structural Basis for the Recognition of the 2019-NCoV by Human ACE2. *Science (80-.).* **2020**. https://doi.org/10.1101/2020.02.19.956946.

(23) Hofmann, H.; Pyrc, K.; Hoek, L. Van Der; Geier, M.; Berkhout, B.; Po, S. Human Coronavirus NL63 Employs the Severe Acute Respiratory Syndrome Coronavirus Receptor. *PNAS* **2005**, *102* (22), 7988–7993.

(24) Hulswit, R. J. G.; Lang, Y.; Bakkers, M. J. G.; Li, W.; Li, Z.; Schouten, A.; Ophorst, B.; Van Kuppeveld, F. J. M.; Boons, G. J.; Bosch, B. J.; Huizinga, E. G.; De Groot, R. J. Human Coronaviruses OC43 and HKU1 Bind to 9-O-Acetylated Sialic Acids via a Conserved Receptor-Binding Site in Spike Protein Domain A. *Proc. Natl. Acad. Sci. U. S. A.* **2019**, *116* (7), 2681–2690. https://doi.org/10.1073/pnas.1809667116.

(25) Klaiber, N.; Mcvoy, M. A.; Zhao, W. Susceptibility of Enterovirus-D68 to RNAi-Mediated Antiviral Knockdown. *Antiviral Res.* **2019**, *170*, 104565. https://doi.org/10.1016/j.antiviral.2019.104565.

(26) Sanders, D. A. No False Start for Novel Pseudotyped Vectors. *Curr. Opin. Biotechnol.* **2002**, *13* (5), 437–442. https://doi.org/10.1016/S0958-1669(02)00374-9.

(27) Li, Q.; Liu, Q.; Huang, W.; Li, X.; Wang, Y. Current Status on the Development of Pseudoviruses for Enveloped Viruses. *Rev. Med. Virol.* **2018**, *28*, e1963. https://doi.org/10.1002/rmv.1963.

(28) Crawford, K. H. D. K. H. D.; Eguia, R.; Dingens, A. S. A. S.; Loes, A. N. A. N. A. N.; Malone, K. D. K. D.; Wolf, C. R. C. R.; Chu, H. Y. H. Y.; Tortorici, M. A. A.; Veesler, D.; Murphy, M.; Pettie, D.; King, N. P. N. P.; Balazs, A. B. A. B.; Bloom, J. D. J. D. Protocol and Reagents for Pseudotyping Lentiviral Particles with SARS-CoV-2 Spike Protein for Neutralization Assays. *Viruses* **2020**, *12* (5), 513. https://doi.org/10.3390/v12050513.

(29) Srinivasan, S.; Cui, H.; Gao, Z.; Liu, M.; Lu, S.; Mkandawire, W.; Narykov, O.; Sun, M.; Korkin, D. Structural Genomics of SARS-COV-2 Indicates Evolutionary Conserved Functional Regions of Viral Proteins. *Viruses* **2020**, *12*, 360. https://doi.org/10.3390/v12040360.

(30) Haque, S. K. M.; Ashwaq, O.; Sarief, A.; Azad John Mohamed, A. K. A Comprehensive Review

about SARS-CoV-2. *Future Virol.* **2020**, *15* (9), 625–648. https://doi.org/10.2217/fvl-2020-0124.

(31)   Zhang, Y. Z.; Holmes, E. C. A Genomic Perspective on the Origin and Emergence of SARS-CoV-2. *Cell* **2020**, *181* (2), 223–227. https://doi.org/10.1016/j.cell.2020.03.035.

(32)   Hu, B.; Guo, H.; Zhou, P.; Shi, Z.-L. Characteristics of SARS-CoV-2 and COVID-19. *Nat. Rev. Microbiol.* **2021**, *19* (3), 141–154. https://doi.org/10.1038/s41579-020-00459-7.

(33)   Lam, T. T. Y.; Jia, N.; Zhang, Y. W.; Shum, M. H. H.; Jiang, J. F.; Zhu, H. C.; Tong, Y. G.; Shi, Y. X.; Ni, X. B.; Liao, Y. S.; Li, W. J.; Jiang, B. G.; Wei, W.; Yuan, T. T.; Zheng, K.; Cui, X. M.; Li, J.; Pei, G. Q.; Qiang, X.; Cheung, W. Y. M.; Li, L. F.; Sun, F. F.; Qin, S.; Huang, J. C.; Leung, G. M.; Holmes, E. C.; Hu, Y. L.; Guan, Y.; Cao, W. C. Identifying SARS-CoV-2-Related Coronaviruses in Malayan Pangolins. *Nature* **2020**, *583* (7815), 282–285. https://doi.org/10.1038/s41586-020-2169-0.

(34)   Xiao, K.; Zhai, J.; Feng, Y.; Zhou, N.; Zhang, X.; Zou, J. J.; Li, N.; Guo, Y.; Li, X.; Shen, X.; Zhang, Z.; Shu, F.; Huang, W.; Li, Y.; Zhang, Z.; Chen, R. A.; Wu, Y. J.; Peng, S. M.; Huang, M.; Xie, W. J.; Cai, Q. H.; Hou, F. H.; Chen, W.; Xiao, L.; Shen, Y. Isolation of SARS-CoV-2-Related Coronavirus from Malayan Pangolins. *Nature* **2020**, *583* (7815), 286–289. https://doi.org/10.1038/s41586-020-2313-x.

(35)   Walls, A. C. A. C.; Park, Y. J. Y. J.; Tortorici, M. A. A.; Wall, A.; McGuire, A. T. A. T.; Veesler, D. Structure, Function, and Antigenicity of the SARS-CoV-2 Spike Glycoprotein. *Cell* **2020**, *181*, 281–292. https://doi.org/10.1101/2020.02.19.956581.

(36)   Belouzard, S.; Millet, J. K.; Licitra, B. N.; Whittaker, G. R. Mechanisms of Coronavirus Cell Entry Mediated by the Viral Spike Protein. *Viruses* **2012**, *4* (6), 1011–1033. https://doi.org/10.3390/v4061011.

(37)   Coutard, B.; Valle, C.; de Lamballerie, X.; Canard, B.; Seidah, N. G.; Decroly, E. The Spike Glycoprotein of the New Coronavirus 2019-NCoV Contains a Furin-like Cleavage Site Absent in CoV of the Same Clade. *Antiviral Res.* **2020**, *176*, 104742.

(38)   Wan, Y.; Shang, J.; Graham, R.; Baric, R. R. S.; Li, F. Receptor Recognition by the Novel Coronavirus from Wuhan: An Analysis Based on Decade-Long Structural Studies of SARS Coronavirus. *J. Virol.* **2020**, *94* (7), e00127-20.

(39)   Kirchdoerfer, R. N.; Wang, N.; Pallesen, J.; Wrapp, D.; Turner, H. L.; Cottrell, C. A.; Corbett, K. S.; Graham, B. S.; McLellan, J. S.; Ward, A. B. Stabilized Coronavirus Spikes Are Resistant to Conformational Changes Induced by Receptor Recognition or Proteolysis. *Sci. Rep.* **2018**, *8*, 15701.

(40)   Wrapp, D.; Wang, N.; Corbett, K. S.; Goldsmith, J. A.; Hsieh, C. L.; Abiona, O.; Graham, B. S.; McLellan, J. S. Cryo-EM Structure of the 2019-NCoV Spike in the Prefusion Conformation. *Science (80-.).* **2020**, *367*, 1260–1263.

(41)   Kim, S. Y.; Jin, W.; Sood, A.; Montgomery, D. W.; Grant, O. C.; Fuster, M. M.; Fu, L.; Dordick, J. S.; Woods, R. J.; Zhang, F.; Linhardt, R. J. Characterization of Heparin and Severe Acute Respiratory Syndrome-Related Coronavirus 2 (SARS-CoV-2) Spike Glycoprotein Binding Interactions. *Antiviral Res.* **2020**, *181*, 104873.

(42)   Clausen, T. M.; Sandoval, D. R.; Spliid, C. B.; Pihl, J.; Perrett, H. R.; Painter, C. D.; Narayanan, A.; Majowicz, S. A.; Kwong, E. M.; McVicar, R. N.; Thacker, B. E.; Glass, C. A.; Yang, Z.; Torres, J. L.; Golden, G. J.; Bartels, P. L.; Caradonna, T. M.; Kellman, B. P.; Martino, C.; Gordts, P. L. S. M.; Chanda, S. K.; Schmidt, A. G.; Godula, K.; Leibel, S. L.; Jose, Jo.; Corbett, K. D.; Ward, A. B.; Carlin, A. F.; Esko, J. D. SARS-CoV-2 Infection Depends on Cellular Heparan Sulfate and ACE2. *Cell* **2020**, *183*, 1–15. https://doi.org/10.1016/j.cell.2020.09.033.

(43)   Tandon, R.; Sharp, J. S.; Zhang, F.; Pomin, V. H.; Ashpole, N. M.; Mitra, D.; McCandless, M. G.; Jin, W.; Liu, H.; Sharma, P.; Linhardt, R. J. Effective Inhibition of SARS-CoV-2 Entry by Heparin and Enoxaparin Derivatives. *Virology* **2021**, *95*, e01987-20.

(44)   Kim, D. E.; Min, J. S.; Jang, M. S.; Lee, J. Y.; Shin, Y. S.; Park, C. M.; Song, J. H.; Kim, H. R.; Kim, S.;

Jin, Y. H.; Kwon, S. Natural Bis-Benzylisoquinoline Alkaloids-Tetrandrine, Fangchinoline, and Cepharanthine, Inhibit Human Coronavirus Oc43 Infection of Mrc-5 Human Lung Cells. *Biomolecules* **2019**, *9* (11). https://doi.org/10.3390/biom9110696.

(45) Cevik, M.; Kuppalli, K.; Kindrachuk, J.; Peiris, M. Virology, Transmission, and Pathogenesis of SARS-CoV-2. *BMJ* **2020**, *371*, m3862. https://doi.org/10.1136/bmj.m3862.

(46) Hoffmann, M.; Kleine-Weber, H.; Schroeder, S.; Krüger, N.; Herrler, T.; Erichsen, S.; Schiergens, T. S.; Herrler, G.; Wu, N. H.; Nitsche, A.; Müller, M. A.; Drosten, C.; Pöhlmann, S. SARS-CoV-2 Cell Entry Depends on ACE2 and TMPRSS2 and Is Blocked by a Clinically Proven Protease Inhibitor. *Cell* **2020**, *181* (2), 271-280.e8. https://doi.org/10.1016/j.cell.2020.02.052.

(47) Devaux, C. A.; Rolain, J. M.; Colson, P.; Raoult, D. New Insights on the Antiviral Effects of Chloroquine against Coronavirus: What to Expect for COVID-19? *Int. J. Antimicrob. Agents* **2020**, *55* (5), 105938. https://doi.org/10.1016/j.ijantimicag.2020.105938.

(48) Wu, C.; Liu, Y.; Yang, Y.; Zhang, P.; Zhong, W.; Wang, Y.; Wang, Q.; Xu, Y.; Li, M.; Li, X.; Zheng, M.; Chen, L.; Li, H. Analysis of Therapeutic Targets for SARS-CoV-2 and Discovery of Potential Drugs by Computational Methods. *Acta Pharm. Sin. B* **2020**, *10* (5), 766–788. https://doi.org/10.1016/j.apsb.2020.02.008.

(49) Yang, H. Design of Wide-Spectrum Inhibitors Targeting Coronavirus Main Proteases. *PLoS Biol.* **2005**, *3* (10), 1742–1752.

(50) Pillaiyar, T. An Overview of Severe Acute Respiratory Syndrome-Coronavirus (SARS-CoV) 3CL Protease Inhibitors: Peptidomimetics and Small Molecule Chemotherapy. *J. Med. Chem.* **2016**, *59* (14), 6595–6628.

(51) Chen, Y. W. Prediction of the SARS-CoV-2 (2019-NCoV) 3C-like Protease (3CLpro) Structure: Virtual Screening Reveals Velpatasvir, Ledipasvir, and Other Drug Repurposing Candidates. *F1000Research* **2020**, *9*, 129.

(52) Gordon, C. J. The Antiviral Compound Remdesivir Potently Inhibits RNA-Dependent RNA Polymerase from Middle East Respiratory Syndrome Coronavirus. *J. fo Biol. Chem.* **2020**, *295* (15), 4773–4779.

(53) Lundin, A.; Dijkman, R.; Bergström, T.; Kann, N.; Adamiak, B.; Hannoun, C.; Kindler, E.; Jónsdóttir, H. R.; Muth, D.; Kint, J.; Forlenza, M.; Müller, M. A.; Drosten, C.; Thiel, V.; Trybala, E. Targeting Membrane-Bound Viral RNA Synthesis Reveals Potent Inhibition of Diverse Coronaviruses Including the Middle East Respiratory Syndrome Virus. *PLoS Pathog.* **2014**, *10* (5), e1004166.

(54) Suliman, K. Emergence of a Novel Coronavirus, Severe Acute Respiratory Syndrome Coronavirus 2: Biology and Therapeutic Options. *J. Clin. Microbiol.* **2020**, *58* (5), 300187–20.

(55) FDA. Coronavirus (COVID-19) Update: FDA Authorizes First Oral Antiviral for Treatment of COVID-19 https://www.fda.gov/news-events/press-announcements/coronavirus-covid-19-update-fda-authorizes-first-oral-antiviral-treatment-covid-19#:~:text=Today%2C the U.S. Food and,of age and older weighing.

(56) FDA. Coronavirus (COVID-19) Update: FDA Authorizes Additional Oral Antiviral for Treatment of COVID-19 in Certain Adults https://www.fda.gov/news-events/press-announcements/coronavirus-covid-19-update-fda-authorizes-additional-oral-antiviral-treatment-covid-19-certain#:~:text=Today%2C the U.S. Food and,progression to severe COVID-19%2C.

(57) Kabinger, F.; Stiller, C.; Schmitzová, J.; Dienemann, C.; Kokic, G.; Hillen, H. S.; Höbartner, C.; Cramer, P. Mechanism of Molnupiravir-Induced SARS-CoV-2 Mutagenesis. *Nat. Struct. Mol. Biol.* **2021**, *28* (9), 740–746. https://doi.org/10.1038/s41594-021-00651-0.

(58) Bhave, S.; Elford, H.; McVoy, M. A. Ribonucleotide Reductase Inhibitors Hydroxyurea, Didox, and Trimidox Inhibit Human Cytomegalovirus Replication in Vitro and Synergize with Ganciclovir. *Antiviral Res.* **2013**, *100* (1), 151–158. https://doi.org/10.1016/j.antiviral.2013.07.016.

(59) Galluzzi, L.; Senovilla, L.; Vitale, I.; Michels, J.; Martins, I.; Kepp, O.; Castedo, M.; Kroemer, G.

Molecular Mechanisms of Cisplatin Resistance. *Oncogene* **2012**, *31*, 1869–1883. https://doi.org/10.1038/onc.2011.384.

(60) Gorle, A. K.; Katner, S. J.; Johnson, W. E.; Lee, D. E.; Daniel, A. G.; Ginsburg, E. P.; von Itzstein, M.; Berners-Price, S. J.; Farrell, N. P. Substitution-Inert Polynuclear Platinum Complexes as Metalloshielding Agents for Heparan Sulfate. *Chem. - A Eur. J.* **2018**, *24* (25), 6606–6616. https://doi.org/10.1002/chem.201706030.

(61) Demmler, G. J.; Ligon, B. L. Severe Acute Respiratory Syndrome (SARS): A Review of the History, Epidemiology, Prevention, and Concerns for the Future. *Semin. Pediatr. Infect. Dis.* **2003**, *14* (3), 240–244. https://doi.org/10.1016/S1045-1870(03)00056-6.

(62) Skowronski, D. M.; Astell, C.; Brunham, R. C.; Low, D. E.; Petric, M.; Roper, R. L.; Talbot, P. J.; Tam, T.; Babiuk, L. Severe Acute Respiratory Syndrome (SARS): A Year in Review. *Annu. Rev. Med.* **2005**, *56*, 357–381. https://doi.org/10.1146/annurev.med.56.091103.134135.

(63) Zhong, N. S.; Zheng, B. J.; Li, Y. M.; Poon, L. L. M.; Xie, Z. H.; Chan, K. H.; Li, P. H.; Tan, S. Y.; Chang, Q.; Xie, J. P.; Liu, X. Q.; Xu, J.; Li, D. X.; Yuen, K. Y.; Peiris, J. S. M.; Guan, Y. Epidemiology and Cause of Severe Acute Respiratory Syndrome (SARS) in Guangdong, People's Republic of China, in February, 2003. *Lancet* **2003**, *362*, 1353–1358. https://doi.org/10.1016/S0140-6736(03)14630-2.

(64) He, J.; Xu, R.; Yu, D.; Peng, G.; Liu, Y.; Liang, W.; Li, L.; Guo, R.; Fang, Y.; Zhang, X.; Zheng, H.; Luo, H.; Lin, J. Severe Acute Respiratory Syndrome in Guangdong Province of China: Epidemiology and Control Measures. *Chinese J. Prev. Med.* **2003**, *37* (4), 227–232.

(65) Guan, Y.; Zheng, B. J.; He, Y. Q.; Liu, X. L.; Zhuang, Z. X.; Cheung, C. L.; Luo, S. W.; Li, P. H.; Zhang, L. J.; Guan, Y. J.; Butt, K. M.; Wong, K. L.; Chan, K. W.; Lim, W.; Shortridge, K. F.; Yuen, K. Y.; Peiris, J. S. M.; Poon, L. L. M. Isolation and Characterization of Viruses Related to the SARS Coronavirus from Animals in Southern China. *Science (80-.).* **2003**, *302*, 276–278. https://doi.org/10.1126/science.1087139.

(66) Peiris, J. S. M.; Yuen, K. Y.; Osterhaus, A. D. M. E.; Stöhr, K. The Severe Acute Respiratory Syndrome. *N. Engl. J. Med.* **2004**, *349*, 2431–2441. https://doi.org/10.1097/01.idc.0000129853.80250.2c.

(67) Lipsitch, M.; Cohen, T.; Cooper, B.; Robins, J. M.; Ma, S.; James, L.; Gopalakrishna, G.; Chew, S. K.; Tan, C. C.; Samore, M. H.; Fisman, D.; Murray, M. Transmission Dynamics and Control of Severe Acute Respiratory Syndrome. *Science (80-.).* **2003**, *300* (5627), 1966–1970. https://doi.org/10.1126/science.1086616.

(68) Riley, S.; Fraser, C.; Donnelly, C. A.; Ghani, A. C.; Abu-Raddad, L. J.; Hedley, A. J.; Leung, G. M.; Ho, L. M.; Lam, T. H.; Thach, T. Q.; Chau, P.; Chan, K. P.; Lo, S. V.; Leung, P. Y.; Tsang, T.; Ho, W.; Lee, K. H.; Lau, E. M. C.; Ferguson, N. M.; Anderson, R. M. Transmission Dynamics of the Etiological Agent of SARS in Hong Kong: Impact of Public Health Interventions. *Science (80-.).* **2003**, *300*, 1961–1966. https://doi.org/10.1126/science.1086478.

(69) Hon, K. L. E.; Leung, C. W.; Cheng, W. T. F.; Chan, P. K. S.; Chu, W. C. W.; Kwan, Y. W.; Li, A. M.; Fong, N. C.; Ng, P. C.; Chiu, M. C.; Li, C. K.; Tam, J. S.; Fok, T. F. Clinical Presentations and Outcome of Severe Acute Respiratory Syndrome in Children For Personal Use . Only Reproduce with Permission from The Lancet Publishing Group . *Lancet* **2003**, 3–5.

(70) Wong, S. K.; Li, W.; Moore, M. J.; Choe, H.; Farzan, M. A 193-Amino Acid Fragment of the SARS Coronavirus S Protein Efficiently Binds Angiotensin-Converting Enzyme 2. *J. Biol. Chem.* **2004**, *279* (5), 3197–3201. https://doi.org/10.1074/jbc.C300520200.

(71) Li, W.; Zhang, C.; Sui, J.; Kuhn, J. H.; Moore, M. J.; Luo, S.; Wong, S.-K.; Huang, I.-C.; Xu, K.; Vasilieva, N.; Murakami, A.; He, Y.; Marasco, W. A.; Guan, Y.; Choe, H.; Farzan, M. Receptor and Viral Determinants of SARS-Coronavirus Adaptation to Human ACE2. *EMBO J.* **2005**, *24*, 1634–1643.

(72) Al-Tawfiq, J. A. Middle East Respiratory Syndrome-Coronavirus Infection: An Overview. *J. Infect.*

Public Health **2013**, *6*, 319–322.

(73)   Ramadan, N.; Shaib, H. Middle East Respiratory Syndrome Coronavirus (MERS-COV): A Review. *Germs* **2019**, *9*, 35–42. https://doi.org/10.18683/germs.2019.1155.

(74)   de Groot, R. J.; Baker, S. C.; Baric, R. S.; Brown, C. S.; Drosten, C.; Enjuanes, L.; Fouchier, R. A. M.; Galiano, M.; Gorbalenya, A. E.; Memish, Z. A.; Perlman, S.; Poon, L. L. M.; Snijder, E. J.; Stephens, G. M.; Woo, P. C. Y.; Zaki, A. M.; Zambon, M.; Ziebuhr, J. Commentary: Middle East Respiratory Syndrome Coronavirus (MERS-CoV): Announcement of the Coronavirus Study Group. *J. Virol.* **2013**, *87* (14), 7790–7792. https://doi.org/10.1128/jvi.01244-13.

(75)   Corman, V. M.; Ithete, N. L.; Richards, L. R.; Schoeman, M. C.; Preiser, W.; Drosten, C.; Drexler, J. F. Rooting the Phylogenetic Tree of Middle East Respiratory Syndrome Coronavirus by Characterization of a Conspecific Virus from an African Bat. *J. Virol.* **2014**, *88* (19), 11297–11303. https://doi.org/10.1128/jvi.01498-14.

(76)   Fehr, A. R.; Channappanavar, R.; Perlman, S. Middle East Respiratory Syndrome: Emergence of a Pathogenic Human Coronavirus. *Annu. Rev. Med.* **2017**, *68*, 387–399. https://doi.org/10.1146/annurev-med-051215-031152.

(77)   Poletto, C.; Pelat, C.; Lévy-Bruhl, D.; Yazdanpanah, Y.; Boëlle, P. Y.; Colizza, V. Assessment of the Middle East Respiratory Syndrome Coronavirus (MERS-CoV) Epidemic in the Middle East and Risk of International Spread Using a Novel Maximum Likelihood Analysis Approach. *Eurosurveillance* **2014**, *19* (23), 20699. https://doi.org/10.2807/1560-7917.ES2014.19.23.20824.

(78)   Omrani, A. S.; Saad, M. M.; Baig, K.; Bahloul, A.; Abdul-Matin, M.; Alaidaroos, A. Y.; Almakhlafi, G. A.; Albarrak, M. M.; Memish, Z. A.; Albarrak, A. M.; Lancet. Ribavirin and Interferon Alfa-2a for Severe Middle East Respiratory Syndrome Coronavirus Infection: A Retrospective Cohort Study. *Lancet Infect. Dis.* **2014**, *12*, 1090–1095.

(79)   Al-tawfiq, J. A.; Momattin, H.; Dib, J.; Memish, Z. A. Ribavirin and Interferon Therapy in Patients Infected with the Middle East Respiratory Syndrome Coronavirus: An Observational Study. *Int. J. Infect. Dis.* **2014**, *20*, 42–46.

(80)   Raj, V. S.; Mou, H.; Smits, S. L.; Dekkers, D. H. W.; Müller, M. A.; Dijkman, R.; Muth, D.; Demmers, J. A. A.; Zaki, A.; Fouchier, R. A. M.; Thiel, V.; Drosten, C.; Rottier, P. J. M.; Osterhaus, A. D. M. E.; Bosch, B. J.; Haagmans, B. L. Dipeptidyl Peptidase 4 Is a Functional Receptor for the Emerging Human Coronavirus-EMC. *Nature* **2013**, *495*, 251–254. https://doi.org/10.1038/nature12005.

(81)   Alejandra Tortorici, M.; Walls, A. C.; Lang, Y.; Wang, C.; Li, Z.; Koerhuis, D.; Boons, G. J.; Bosch, B. J.; Rey, F. A.; de Groot, R. J.; Veesler, D. Structural Basis for Human Coronavirus Attachment to Sialic Acid Receptors. *Nat. Struct. Mol. Biol.* **2019**, *26* (6), 481–489. https://doi.org/10.1038/s41594-019-0233-y.

(82)   Li, W.; Hulswit, R. J. G.; Widjaja, I.; Raj, V. S.; McBride, R.; Peng, W.; Widagdo, W.; Tortorici, M. A.; Van Dieren, B.; Lang, Y.; Van Lent, J. W. M.; Paulson, J. C.; De Haan, C. A. M.; De Groot, R. J.; Van Kuppeveld, F. J. M.; Haagmans, B. L.; Bosch, B. J. Identification of Sialic Acid-Binding Function for the Middle East Respiratory Syndrome Coronavirus Spike Glycoprotein. *Proc. Natl. Acad. Sci. U. S. A.* **2017**, *114* (40), E8508–E8517. https://doi.org/10.1073/pnas.1712592114.

(83)   Park, Y. J.; Walls, A. C.; Wang, Z.; Sauer, M. M.; Li, W.; Tortorici, M. A.; Bosch, B. J.; DiMaio, F.; Veesler, D. Structures of MERS-CoV Spike Glycoprotein in Complex with Sialoside Attachment Receptors. *Nat. Struct. Mol. Biol.* **2019**, *26* (12), 1151–1157. https://doi.org/10.1038/s41594-019-0334-7.

(84)   Yeager, C. L.; Ashmun, R. A.; Williams, R. K.; Cardellichio, C. B.; Shapiro, L. H.; Look, A. T.; Holmes, K. V. Human Aminopeptidase N Is a Receptor for Human Coronavirus 229E. *Nature* **1992**, *357* (6377), 420–422. https://doi.org/10.1038/357420a0.

(85)   Wang, N.; Shi, X.; Jiang, L.; Zhang, S.; Wang, D.; Tong, P.; Guo, D.; Fu, L.; Cui, Y.; Liu, X.; Arledge, K. C.; Chen, Y. H.; Zhang, L.; Wang, X. Structure of MERS-CoV Spike Receptor-Binding Domain

Complexed with Human Receptor DPP4. *Cell Res.* **2013**, *23* (8), 986–993. https://doi.org/10.1038/cr.2013.92.

(86) Javanian, M.; Barary, M.; Ghebrehewet, S.; Koppolu, V.; Vasigala, V. K. R.; Ebrahimpour, S. A Brief Review of Influenza Virus Infection. *J. Med. Virol.* **2021**, *93* (8), 4638–4646. https://doi.org/10.1002/jmv.26990.

(87) Paules, C.; Subbarao, K. Influenza. *Lancet* **2017**, *12* (390), 697–708.

(88) Luo, M. Influenza Virus Entry. *Adv. Exp. Med. Biol.* **2012**, *726*, 201–221. https://doi.org/10.1007/978-1-4614-0980-9_9.

(89) Moghadami, M. A Narrative Review of Influenza: A Seasonal and Pandemic Disease. *Iran. J. Med. Sci.* **2017**, *42* (1), 2–13.

(90) Cowling, B. J.; Ip, D. K. M.; Fang, V. J.; Suntarattiwong, P.; Olsen, S. J.; Levy, J.; Uyeki, T. M.; Leung, G. M.; Malik Peiris, J. S.; Chotpitayasunondh, T.; Nishiura, H.; Mark Simmerman, J. Aerosol Transmission Is an Important Mode of Influenza A Virus Spread. *Nat. Commun.* **2013**, *4*, 1935. https://doi.org/10.1038/ncomms2922.

(91) Killingley, B.; Greatorex, J.; Digard, P.; Wise, H.; Garcia, F.; Varsani, H.; Cauchemez, S.; Enstone, J. E.; Hayward, A.; Curran, M. D.; Read, R. C.; Lim, W. S.; Nicholson, K. G.; Nguyen-Van-Tam, J. S. The Environmental Deposition of Influenza Virus from Patients Infected with Influenza A(H1N1)Pdm09: Implications for Infection Prevention and Control. *J. Infect. Public Health* **2016**, *9* (3), 278–288. https://doi.org/10.1016/j.jiph.2015.10.009.

(92) Clayville, L. R. Influenza Update, a Review of Currently Available Vaccines. *P T* **2011**, *36* (10), 659–668.

(93) Kim, H.; Webster, R. G.; Webby, R. J. Influenza Virus: Dealing with a Drifting and Shifting Pathogen. *Viral Immunol.* **2018**, *31* (2), 174–183. https://doi.org/10.1089/vim.2017.0141.

(94) Morens, D. M.; Taubenberger, J. K. Making Universal Influenza Vaccines: Lessons from the 1918 Pandemic. *J. Infect. Dis.* **2019**, *219*, S5–S13. https://doi.org/10.1093/infdis/jiy728.

(95) Paules, C. I.; Fauci, A. S. Influenza Vaccines: Good, but We Can Do Better. *J. Infect. Dis.* **2019**, *219* (Suppl 1), S1–S4. https://doi.org/10.1093/infdis/jiy633.

(96) Kosik, I.; Yewdell, J. W. Influenza Hemagglutinin and Neuraminidase: Yin–Yang Proteins Coevolving to Thwart Immunity. *Viruses*. 2019. https://doi.org/10.3390/v11040346.

(97) Stephenson, I.; Democratis, J.; Lackenby, A.; McNally, T.; Smith, J.; Pareek, M.; Ellis, J.; Bermingham, A.; Nicholson, K.; Zambon, M. Neuraminidase Inhibitor Resistance after Oseltamivir Treatment of Acute Influenza A and B in Children. *Clin. Infect. Dis.* **2009**, *48* (4), 389–396.

(98) Todd, B.; Tchesnokov, E. P.; Gotte, M. The Active Form of the Influenza Cap-Snatching Endonuclease Inhibitor Baloxavir Marboxil Is a Tight Binding Inhibitor. *J. fo Biol. Chem.* **2021**, *296*, 100486.

(99) Jalily, P. H.; Duncan, M. C.; Fedida, D.; Wang, J.; Tietjen, I. Put a Cork in It: Plugging the M2 Viral Ion Channel to Sink Influenza. *Antiviral Res.* **2020**, *178*, 10.

(100) Wang, J.; Li, F.; Ma, C. Recent Progress in Designing Inhibitors That Target the Drug-Resistant M2 Proton Channels from the Influenza A Viruses. *Biopolymers* **2015**, *104* (4), 291–309.

(101) Schauer, R. Sialic Acids as Regulators of Molecular and Cellular Interactions. *Curr. Opin. Struct. Biol.* **2009**, *19* (5), 507–514. https://doi.org/10.1016/j.sbi.2009.06.003.

(102) Hanson, J.; Sauter, N.; Skehel, J.; Wiley, D. Proton Nuclear Magnetic Resonance Studies of the Binding of Sialosides to Intact Influenza Virus. *Virology* **1992**, *189* (2), 525–533.

(103) Sauter, N. K.; Bednarski, M. D.; Wurzburg, B. A.; Hanson, J. E.; Whitesides, G. M.; Skehel, J. J.; Wiley, D. C. Hemagglutinins from Two Influenza Virus Variants Bind to Sialic Acid Derivatives with Millimolar Dissociation Constants: A 500-MHz Proton Nuclear Magnetic Resonance Study. *Biochemistry* **1989**, *28* (21), 8388–8396.

(104) Lin, T.; Wang, G.; Li, A.; Zhang, Q.; Wu, C.; Zhang, R.; Cai, Q.; Song, W.; Yuen, K. Y. The

Hemagglutinin Structure of an Avian H1N1 Influenza A Virus. *Virology* **2009**, *392* (1), 73–81. https://doi.org/10.1016/j.virol.2009.06.028.

(105) Nicholls, J. M.; Chan, R. W. Y.; Russell, R. J.; Air, G. M.; Peiris, J. S. M. Evolving Complexities of Influenza Virus and Its Receptors. *Trends Microbiol.* **2008**, *16* (4), 149–157.

(106) Lakadamyali, M.; Rust, M. J.; Zhuang, X. Endocytosis of Influenza Viruses. *Microbes Infect* **2004**, *6* (10), 929–936. https://doi.org/10.1016/j.micinf.2004.05.002.Endocytosis.

(107) Ma, Z.; Siebert, A. P.; Cheung, K. H.; Lee, R. J.; Johnson, B.; Cohen, A. S.; Vingtdeux, V.; Marambaud, P.; Foskett, J. K. Calcium Homeostasis Modulator 1 (CALHM1) Is the Pore-Forming Subunit of an Ion Channel That Mediates Extracellular Ca2+ Regulation of Neuronal Excitability. *Proc. Natl. Acad. Sci. U. S. A.* **2012**, *109* (28). https://doi.org/10.1073/pnas.1204023109.

(108) Dreses-Werringloer, U.; Vingtdeux, V.; Zhao, H.; Chandakkar, P.; Davies, P.; Marambaud, P. CALHM1 Controls the Ca2+-Dependent MEK, ERK, RSK and MSK Signaling Cascade in Neurons. *J. Cell Sci.* **2013**, *126* (5), 1199–1206. https://doi.org/10.1242/jcs.117135.

(109) Simonneau, M.; Tauc, L. Transmitter Release: Ruthenium Red Used to Demonstrate a Possible Role of Sialic Acid Containing Substrates. *J. Physiol.* **1979**, *291*, 161–178.

(110) Colombo, P. M.; Rascio, N. Ruthenium Red Staining for Electron Microscopy of Plant Material. *J. Ultrasructure Res.* **1977**, *60* (2), 135–139. https://doi.org/10.1016/S0022-5320(77)80060-9.

(111) Shirahama, T.; Cohen, A. S. The Role of Mucopolysaccharides in Vesicle Architecture and Endothelial Transport: An Electron Microscope Study of Myocardial Blood Vessels. *J. Cell Biol.* **1972**, *52* (1), 198–206. https://doi.org/10.1083/jcb.52.1.198.

(112) Luft, J. Electron Microscopy of Cell Extraneous Coats as Revealed by Ruthenium Red Staining. *J. Cell Biol.* **1964**, *23*, 54A.

(113) Wieraszko, A. Evidence That Ruthenium Red Disturbs the Synaptic Transmission in the Rat Hippocampal Slices through Interacting with Sialic Acid Residues. *Brain Res.* **1986**, *378* (1), 120–126. https://doi.org/10.1016/0006-8993(86)90292-1.

(114) Ramesh, S.; Govindarajulu, M.; Parise, R. S.; Neel, L.; Shankar, T.; Patel, S.; Lowery, P.; Smith, F.; Dhanasekaran, M.; Moore, T. Emerging SARS-CoV-2 Variants: A Review of Its Mutations, Its Implications and Vaccine Efficacy. *Vaccines* **2021**, *9*, 1195.

(115) Shyr, Z. A.; Cheng, Y. S.; Lo, D. C.; Zheng, W. Drug Combination Therapy for Emerging Viral Diseases. *Drug Discov. Today* **2021**, *26* (10), 2367–2376. https://doi.org/10.1016/j.drudis.2021.05.008.

(116) Adalja, A.; Inglesby, T. Broad-Spectrum Antiviral Agents: A Crucial Pandemic Tool. *Expert Rev. Anti. Infect. Ther.* **2019**, *17* (7), 467–470. https://doi.org/10.1080/14787210.2019.1635009.

(117) de Paiva, R. E. F.; Peterson, E. J.; Malina, J.; Zoepfl, M.; Hampton, J. D.; Johnson, W. E.; Graminha, A.; Ourahmane, A.; McVoy, M. A.; Brabec, V.; Berners-Price, S. J.; Farrell, N. P. On the Biology of Werner's Complex. *Angew. Chemie Int. Ed.* **2021**, *60*, 17123–17130. https://doi.org/10.1002/anie.202105019.

(118) Ströh, L. J.; Stehle, T. Glycan Engagement by Viruses: Receptor Switches and Specificity. *Annu. Rev. Virol.* **2014**, *1*, 285–306. https://doi.org/10.1146/annurev-virology-031413-085417.

(119) Sorin, M. N.; Kuhn, J.; Stasiak, A. C.; Stehle, T. Structural Insight into Non-Enveloped Virus Binding to Glycosaminoglycan Receptors: A Review. *Viruses* **2021**, *13*, 800. https://doi.org/10.3390/v13050800.

(120) Bierle, C. J.; Anderholm, K. M.; Wang, B. J.; McVoy, M. A.; Schleiss, M. R. Targeted Mutagenesis of Guinea Pig Cytomegalovirus Using CRISPR/ Cas9-Mediated Gene Editing. *J. Virol.* **2016**, *90* (15), 6989–6998. https://doi.org/10.1128/JVI.00139-16.Editor.

(121) Cui, X.; Adler, S. P.; Davison, A. J.; Smith, L.; Habib, E. S. E.; McVoy, M. A. Bacterial Artificial Chromosome Clones of Viruses Comprising the Towne Cytomegalovirus Vaccine. *J. Biomed. Biotechnol.* **2012**, *2012*, 428498. https://doi.org/10.1155/2012/428498.

(122) Xiao, K.; Allison, D. F.; Buckley, K. M.; Kottke, M. D.; Vincent, P. A.; Faundez, V.; Kowalczyk, A. P. Cellular Levels of P120 Catenin Function as a Set Point for Cadherin Expression Levels in Microvascular Endothelial Cells. *J. Cell Biol.* **2003**, *163* (3), 535–545. https://doi.org/10.1083/jcb.200306001.

(123) He, T.-C.; Zhou, S.; da Costa, L. T.; Yu, J.; Kinzler, K. W.; Vogelstein, B. A Simplified System for Generating Recombinant Adenoviruses. *PNAS* **1998**, *95* (March), 2509–2514.

(124) Harris, A. L.; Yang, X.; Hegmans, A.; Povirk, L.; Ryan, J. J.; Kelland, L.; Farrell, N. P. Synthesis, Characterization, and Cytotoxicity of a Novel Highly Charged Trinuclear Platinum Compound. Enhancement of Cellular Uptake with Charge. *Inorg. Chem.* **2005**, *44* (26), 9598–9600. https://doi.org/10.1021/ic051390z.

(125) Prisecaru, A.; Molphy, Z.; Kipping, R. G.; Peterson, E. J.; Qu, Y.; Kellett, A.; Farrell, N. P. The Phosphate Clamp: Sequence Selective Nucleic Acid Binding Profiles and Conformational Induction of Endonuclease Inhibition by Cationic Triplatin Complexes. *Nucleic Acids Res.* **2014**, *42* (22), 13474–13487. https://doi.org/10.1093/nar/gku1157.

(126) Qu, Y.; Moniodis, J.; Harris, A.; Yang, X.; Hegmans, A.; Povirk, L.; Berners-Price, S. J.; Farrell, N. . Solution Behavior of the Phosphate Clamp. DNA Binding By a Non-Covalent Polynuclear Platinum Compound. In *Polyamine Drug Discovery*; Woster, P. M., Casero, R., Eds.; 2011; pp 191–204. https://doi.org/10.1039/9781849733090-00191.

(127) Prisecaru, A.; Molphy, Z.; Kipping, R. G.; Peterson, E. J.; Qu, Y.; Kellett, A.; Farrell, N. P. The Phosphate Clamp: Sequence Selective Nucleic Acid Binding Profiles and Conformational Induction of Endonuclease Inhibition by Cationic Triplatin Complexes. *Nucleic Acids Res.* **2014**, *42* (22), 13474–13487. https://doi.org/10.1093/nar/gku1157.

(128) Ginsburg, E. P. Heparan Sulfate. A Ligand for Coordination Compounds., University of Virginia, 2020.

(129) Rogers, T. F.; Zhao, F.; Huang, D.; Beutler, N.; Burns, A.; He, W.; Limbo, O.; Smith, C.; Song, G.; Woehl, J.; Yang, L.; Abbott, R. K.; Callaghan, S.; Garcia, E.; Hurtado, J.; Parren, M.; Peng, L.; Ramirez, S.; Ricketts, J.; Ricciardi, M. J.; Rawlings, S. A.; Wu, N. C.; Yuan, M.; Smith, D. M.; Nemazee, D.; Teijaro, J. R.; Voss, J. E.; Wilson, I. A.; Andrabi, R.; Briney, B.; Landais, E.; Sok, D.; Jardine, J. G.; Burton, D. R. Isolation of Potent SARS-CoV-2 Neutralizing Antibodies and Protection from Disease in a Small Animal Model. *Science (80-.).* **2020**, *369* (6506), 956–963.

(130) Patel, M.; Giddings, A. M.; Sechelski, J.; Olsen, J. C. High Efficiency Gene Transfer to Airways of Mice Using Influenza Hemagglutinin Pseudotyped Lentiviral Vectors. *J Gene Med* **2017**, *15* (1), 51–62. https://doi.org/10.1002/jgm.2695.High.

Chapter 4: Antiviral activity of Werner's complex and its mechanism of action in HCMV

4.0 Contributions

This chapter is, in part, a summary of "On the Biology of Werner's Complex" published in *Angewandte Chemie International Edition*.[1] Dr Nicholas P. Farrell, Erica J. Peterson, J. David Hampton, Angelica Graminha, and Wyatt E Johnson performed the cellular accumulation and GAG interactions. Raphael E.F. de Paiva and Susan J. Berners-Price carried out the NMR binding experiments; enzymatic cleavage assays and DFT calculations. Jaroslav Malina and Viktor Brabec performed the DNA and tRNA binding assays. Preliminary antiviral studies (luciferase based EC50s and gene expression assays) were performed by Amine Ourahmane. MZ repeated preliminary work and performed all additional mechanistic antiviral studies, including spectrum of activity, time of addition, FIGE, and TEM.

This chapter is also, in part, a summary of a paper draft on mononuclear cobalt compounds. Jessica Christian performed methylene blue and ethidium bromide assays with Miriam Hanna. Eric Ginsburg performed synthesis with Eduardo Pancheo. Erica Peterson and James D Hampton performed heparanase and Matrigel assays with Dylan Ward. Wyatt E. Johnson performed synthesis as well as MS and NMR studies. MZ performed all antiviral assays including luciferase- and GFP-based EC50s as well as gene expression assays.

4.1 Background

4.1.1 Alfred Werner and Coordination Chemistry

Alfred Werner is the undisputed father of coordination chemistry, however widespread opposition meant his stereochemical beliefs were not accepted for some time.[2] Werner had a strong background in stereochemistry beginning in his doctoral work in which he noted that the stereochemistry of nitrogen is a tetrahedron and thus should allow for optical isomers.[3] This was demonstrated experimentally ten years later by Pope and Peachey.[4]

Werner's stereochemical insights later extended into inorganic chemistry; his theory of coordination chemistry was based on data gathered by Sophus Mads Jorgensen. Jorgensen interpreted the structure of chromium, cobalt, rhodium, and platinum coordination complexes using the chain theory: ammonia molecules can be linked in a chain ($-NH_3-$) analogous to hydrocarbon ($-CH_2-$) chains (Figure 1).[5]
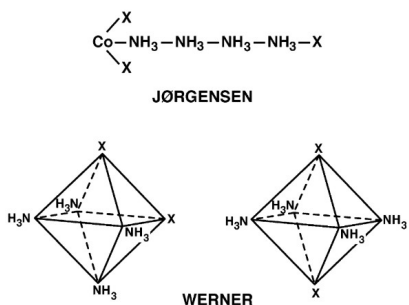
Figure 4.1: Changing Coordination chemistry. (Top) The Blomstrand–Jørgensen model for cobalt amine complexes of [Co(NH$_3$)$_4$X$_3$] with pentavalent nitrogen atoms. (Bottom): Illustration of octahedral cis and trans isomers of the same complex, [Co(NH$_3$)$_4$X$_2$]$^+$. Reproduced from Ernst et al. 2011.[2]

Werner rejected the pentavalent nitrogen proposed by Jorgensen; instead, he introduced the concept of coordination number, the number of atoms or ions immediately surrounding a central atom in a complex or crystal, and proposed that this arrangement allows for stereoisomers. Given this, Werner believed that the *croceo* and *violeo* salts, studied by many chemists of the day, were the cis and trans isomers of an octahedral cobalt coordination complex (Figure 4.1). Unlike the Jorgensen-Bloomstrand model, Werner's model explained why $[Co(NH_3)_4Cl_2]$ did not form a precipitate upon treatment with silver ions.[6–9] Using this theory, Werner deduced the complete chemistry of polynuclear cobalt (III) amine complexes with bridging groups such as NH_2, OH, SO_4, NO_2, and O_2, and correctly predicted their structures.[2,10]

Due to famous and vocal opposition form Jorgenson and others,[11] Werner's theory was not accepted for many years. Werner and his group began to work to demonstrate proof of chirality, which would confirm his model. Chiral compounds are asymmetric in such a way that the structure and its mirror image are not superimposable; chiral compounds are optically active, meaning they rotate plane-polarized light. At this time, organic compounds were well studied and their chirality was established. Inorganic compounds, by the current model, could not be chiral, but by Werner's theory, they should be. Ten years after Werner's proposal, Perkin, Pope, and Wallach delivered proof of optical activity in a chiral compound without an asymmetric carbon.[12] For his work in coordination chemistry, Werner received the Nobel Prize in 1913. Following this success, Werner's group demonstrated the optical activity of more than 40 inorganic chiral compounds. These included a chiral tetranuclear cobalt complex, first synthesized by Jorgensen, which does not include a single carbon; it later became known as Werner's Hexol or Werner's complex (WC) (Figure 4.2).[13]
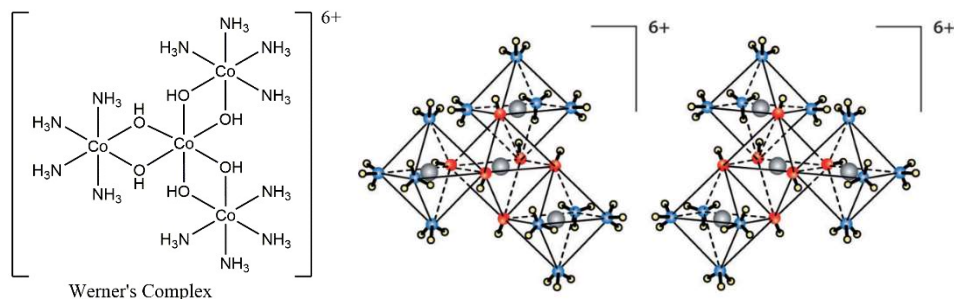
Figure 4.2: Structure of Werner's complex (Left) and a depiction of its enantiomers (right). Reproduced from Ernst et al. 2011.[2]

4.1.2 The biology of Werner's Complex

Despite its fame in inorganic chemistry, little is known about WC's biological properties, which are of interest for two reasons: WC is chiral and it is inorganic. As a chiral compound, WC's enantiomers have the same physical (*i.e.* boiling point or melting point) and chemical properties (*i.e.* oxidation states, flammability, or acidity) but may not have the same biological properties. The differences between enantiomers are commonly exploited in the pharmaceutical industry. For example, Warfin, a widely prescribed anticoagulant, is marketed as a racemic mixture; however (S)-warfin is more potent than (R)-warfin and each enantiomer is metabolized by different enzymatic pathways.[14] Second, like the PPCs described in Chapter 2, WC is *formally* substitution inert, meaning that its hydrogen-bonding and electrostatic interactions dictate its affinity for biomolecules and their conformation and function.[15] Analogous to PPCs, WC's inability to covalently bond provides a larger therapeutic window with noncytotoxic effects. It should be noted that WC has not been studied in a biological medium; it is possible that WC may generate covalent bonds if its metabolites are capable of forming covalent bonds.

As a highly charged cation, we predicted that WC would behave similarly to PPCs and bind to anionic molecules, like GAGs and DNA. PPCs bind both GAGs and DNA, relying heavily on charge and amine hydrogen bonding, and impact their function. We assumed that WC, as a charged amine-based complex, would share their inherent dual function activity.[16,17] The following data are part of an effort to define this iconic compound's biological activity and therapeutic potential.

4.1.2.1 Biophysical Assays with Fondaparinux

The methylene blue competition assay (described in Chapter 2) quantifies a compound's HS affinity as an IC_{50}. Using heparin as an HS model the IC_{50} of WC was 41.1 µM, using heparin as compared to 3.1 ± 0.1 µM for TriplatinNC (3.1 ± 0.1 µM) and lower than cobalt hexamine (16.9 ± 0.4 µM).[15,17] Using fondaparinux, (FPX), WC has an IC_{50} of 41.4 µM as compared to 10.2 ± 0.4 µM for TriplatinNC and 64.5 µM for cobalt hexamine; this suggests that there is a dependence of affinity on oligosaccharide and complex structure.[15,18] H1 nuclear magnetic resonance (NMR) with WC and FPX demonstrated a charge-dependent interaction. ESI-MS with FPX revealed that while cobalt hexamine forms 1:1 and 2:1 adducts, WC forms a unique 2:2 stoichiometry. The lack of any sulfate peaks confirm that WC can metalloshield FPX.[15]

Density functional theory (DFT) was used to propose binding models in which both cobalt hexamine ($[Co(NH_3)_6]_{3+}$) and WC have extensive hydrogen bonding networks with sulfate groups of HS (Figure 4.3).[15] Cobalt hexamine sits between the C and D rings of FPX; at each interaction site, a sulfate groups interacts with three ammines (a full face) of the octahedral complex. This is potentially a more effective metalloshielding approach than the square-planar Pt(amine) coordination units of TriplatinNC.[19] WC wraps the D ring of FPX, inducing a more compact and folded conformation. The steric effects of the formally tetranuclear species produce a more varied set of interactions compared to the mononuclear $[Co(NH_3)_6]^{3+}$. The combined data confirm the strong affinity of Co^{3+} compounds for GAGs and FPX.
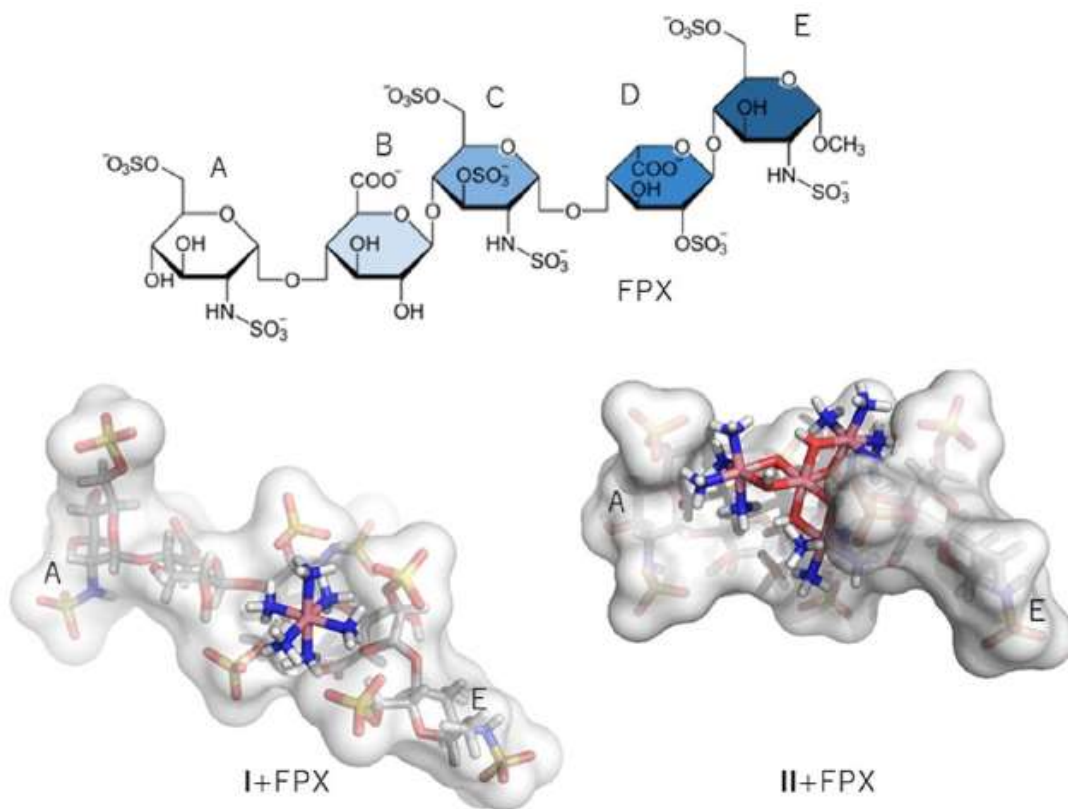
Figure 4.3: Cobalt-Fondaparinux (FPX) interactions. (Top) Structure of FPX; counterions omitted for clarity. (Bottom) DFT-optimized adducts between cobalt hexamine (Left, I) or WC (Right, II) with FPX. Reproduced from de Paiva et al. 2021.[1]

4.1.2.2 Biological assays related to heparan sulfate

WC's affinity for FPX predicted an inhibition of HS function. HSPGs are known to mediate cellular accumulation of cationic protein domains.[20,21] The HSPG binding and internalization of polyarginine TAMRA-R9 (a nonarginine peptide (R9) coupled to the TAMRA fluorescent label 5-(6) carboxytetramethylrhoamine) may be visualized by fluorescence microscopy.[15] While cobalt hexamine had little effect on TAMRA-R9 CHO cell entry, WC was effective in inhibiting is entry into CHO cells, suggesting that WC binds HSPGs in place of TAMRA-R9 and implies that WC uses HSPGs to enter cells (Figure 4.4). This was confirmed by repeating the experiment with GAG-deficient A745 CHO K1 cells (deficient in xylosyl transferase XYLT2 gene) and in pgs E606-mutant cells (HS-N-sulfotransferase defective).[15] Antiproliferative effects of WC (measured by MTT assay) correlated with cellular accumulation, indicated by IC50s of 36, 70, and 86 for wt CHO, CHO K1, and pgs E606 cells, respectively (Figure 4.4). These results confirm that HSPGs play a role in cellular accumulation of charged coordination compounds and metal cations, extending beyond platinum.[15,22]
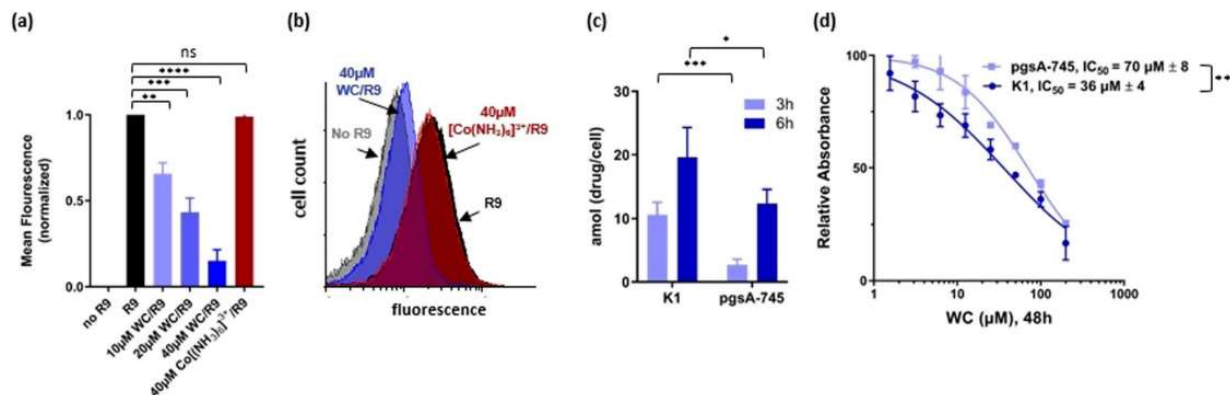
Figure 4.4: The cellular entry of Werner's Complex is GAG-dependent. a, b) TAMRA-R9 (R9) competition assay; CHO-K1 cells were treated with the indicated concentrations of compounds for 10 min, followed by treatment with 1 mM TAMRA-R9 for 1h at 37 ℃. The cells were harvested with trypsin, collected, washed and analyzed at 488–585 nm by flow cytometry. c) Cobalt cellular accumulation assay; CHO-K1 and CHO-pgsA745 cells were treated with 10 mM WC for the indicated time, harvested, and washed. Cell pellets were digested with nitric acid and cobalt levels measured using inductively coupled plasma mass spectrometry. d) Cell proliferation (MTT) assay; CHO-K1 and CHO-pgsA745 cells were treated with the indicated concentrations of WC for 48 h. MTT reagent was added for 3h, removed, and precipitates were dissolved in DMSO. Relative absorbance was determined as treated/untreated controls x100. Reproduced from de Paiva et al. 2021.[1]

4.1.2.3 Functional consequences of GAG binding

The enzymatic cleavage of GAGs initiates angioneogensis and growth factor/growth factor receptor binding and recruitment.[23,24] The metalloshielding of HS has functional consequences (*i.e.* inhibition of enzymatic cleavage and/or diminished growth factor recognition). Using a colorimetric assay for heparinase cleavage and FPX, WC inhibited FPX cleavage with greater effect than cobalt hexamine and had an IC$_{50}$ comparable to TriplatinNC (Figure 4.5).[17,25,26] These data were confirmed by NMR-based assays with FPX where WC inhibited both heparanase and heparinase activity, while cobalt hexamine did not.[27–29]

Cellular invasion of the extracellular matrix relies on the cleavage of GAGS and the release of growth factors. In a Boyden-Chamber assay, WC and cobalt hexamine were equally effective at inhibiting high HPSE expression MDA-MB-231 triple negative breast cancer cells from invading through a Matrigel membrane.[15] A wound assay in which an "wound" is inflicted in HUVEC cells, assessed WC's ability to halt cell mobility; WC significantly inhibited wound healing while cobalt hexamine did not (Figure 4.5).
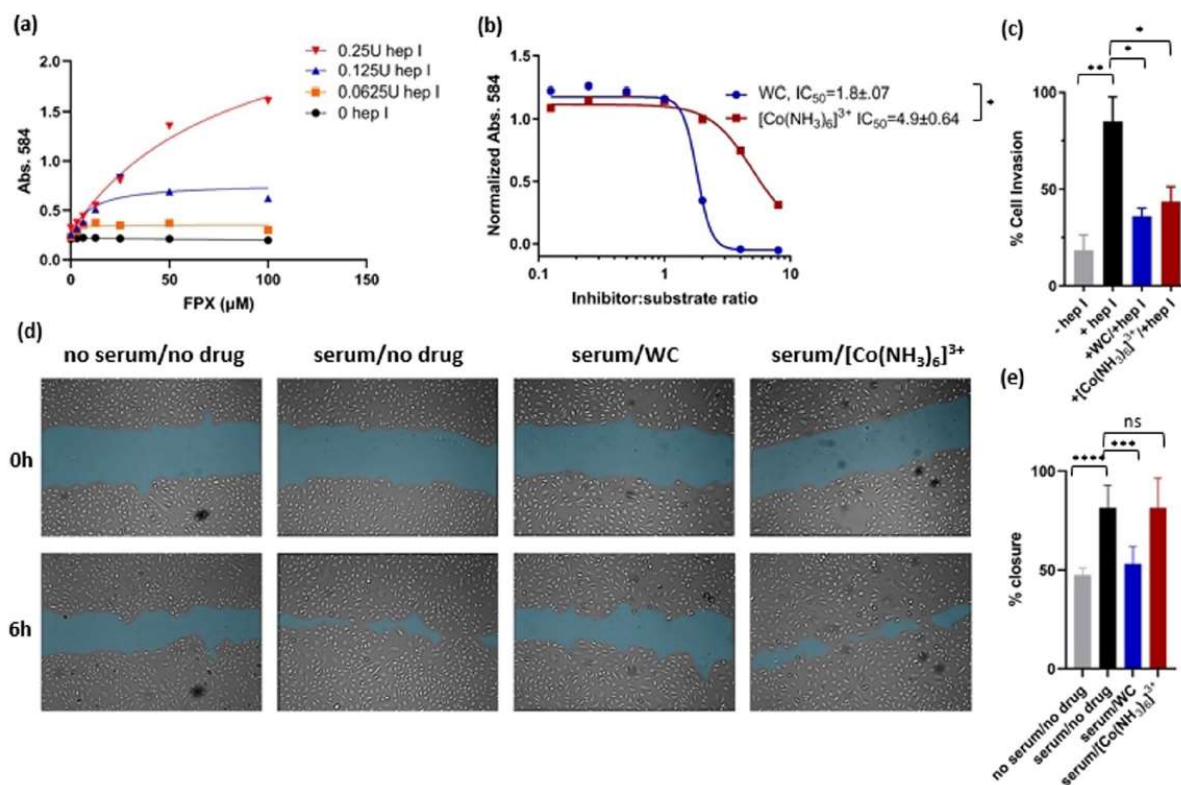
Figure 4.5: Werner's Complex inhibits the function of GAG-interacting proteins. a) Hep I activity assay (FPX cleavage); FPX was incubated for 1 h with hep I. Reactions were stopped by adding 100 μL 1.69 mM WST-1, plates heated to 60 ℃ for 1 h, and absorbance readings measured at 584 nm. b) Various concentrations of compound were incubated for 15 minutes at 37 ℃ with 50 mM FPX in buffer. After addition of 0.25 U hep I for 1 h, reactions were stopped by adding 100 μL 1.69 mM WST-1, plates heated to 60 ℃ for 1 h, and absorbance readings measured at 584 nm. c) Hep I activity assay (HS cleavage); Growth factor-reduced matrigel in a Boyden chamber was treated with either PBS or equimolar amounts (50 mM) of the indicated compounds for 1 h, followed by treatment with additional PBS or 0.3 units of hep I for 16 h. After extensive washes, inserts were filled with media containing 0.2% FBS, and placed into wells containing media containing 10% FBS. Serum-starved MDA-MB-231 cells were seeded onto matrigel or control inserts without matrigel. After 12 h, cells which had invaded through matrigel were fixed and stained using methanol/crystal violet. Percent invasion was determined by dividing the number of cells invaded through matrigel to cells that migrated through the control insert. d) Serum-induced cell migration assay; HUVECs were grown to approximately 90% confluence in each well of a 24-well plate containing endothelial media. The cell monolayer was scratched with a p200 pipette tip. The media was removed and replaced with unsupplemented media, or supplemented media with equimolar doses (100 mM) of the indicated compound. The closure of the scratch was monitored by light microscopy. e) Photographs of (d) at time 0 and 6 h were analyzed with Image J. Reproduced from de Paiva et al. 2021.[1]

4.1.2.4 DNA binding effects

Assuming WC has a dual nature like PPCs, its DNA binding was also assessed with a number of methods. The DNA binding of cobalt hexamine is well studied, especially its ability to induce B→Z DNA conformational changes in DNA sequences.[30,31] Via a gel retardation assay, WC is better able than cobalt hexamine to bind and condense DNA, thus preventing migration of plasmid psP73 and tRNA down the gel. Since cobalt hexamine is well known DNA condenser,[32] we examined WC's ability to condense DNA with total light scattering (Figure 4.6).[33–35] This method is based on the measurement of the intensity of the light scattered by the diluted DNA and RNA solutions due to the formation of condensed DNA and RNA particles upon addition of condensing agents. An EC_{50} describes the concentration of a compound needed to induce 50% condensation of nuclear DNA. WC condenses DNA as well as TriplatinNC.[33–35]
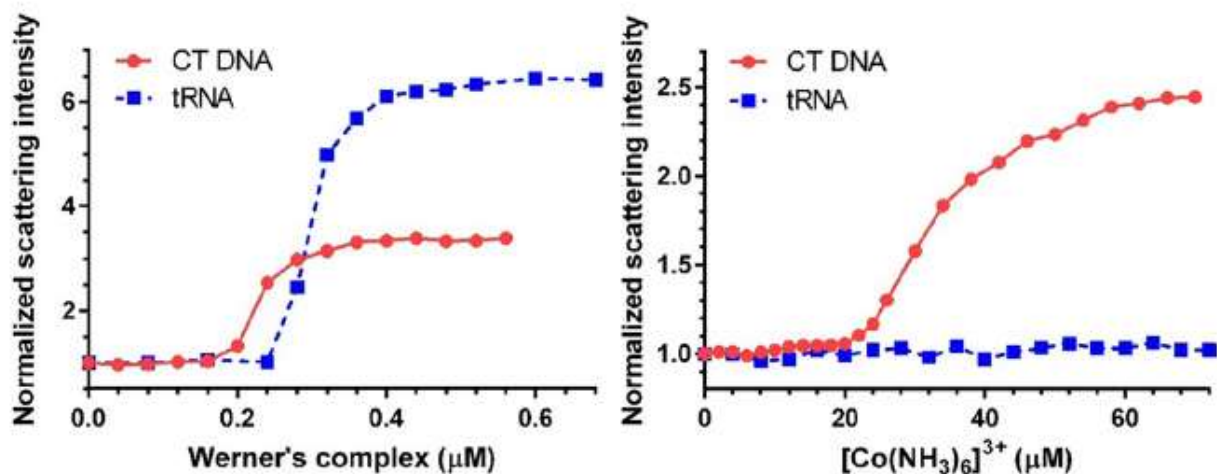
Figure 4.6: DNA and RNA condensation by WC and cobalt hexamine. Plots of the scattered light intensity versus the concentration of WC (left panel) or [Co(NH3)6]3+ (right panel) in the presence of calf thymus (CT) DNA (red) or tRNA (blue). The calculated EC50 values (µM) are 0.23:0.01 and 0.31:0.02 for WC DNA and tRNA condensation, respectively. For [Co(NH3)6]3+, the equivalent values are 35.4 and >70 for CT DNA and tRNA, respectively. Reproduced from de Paiva et al. 2021.[1]

DNA and RNA condensation were also visualized using atomic force microscopy (AFM). WC induced the formation of large (several micrometers in diameter) multimolecular condensates of DNA molecules at the concentration as low as 1.56 mM (Figure 4.7). WC in combination with tRNA molecules generated densely packed particles at the concentration of 12.5 µM. In both these cases, WC was much more effective than the simple polyamine spermine. Much higher concentrations of $[Co(NH_3)_6]_{3+}$ (up to 400 µM) were needed to observe DNA condensation while the compound did not condense tRNA at concentrations up to 1.6 mM. Thus, while clearly more effective than the mononuclear 3+ compound, the similarity in efficiency of DNA and tRNA compaction between WC and linear TriplatinNC emphasizes that despite the superficially different structural types, charge density and the geometrical fit between negatively charged phosphates and the positively charged coordination compounds are important parameters for efficient DNA collapse.[35]
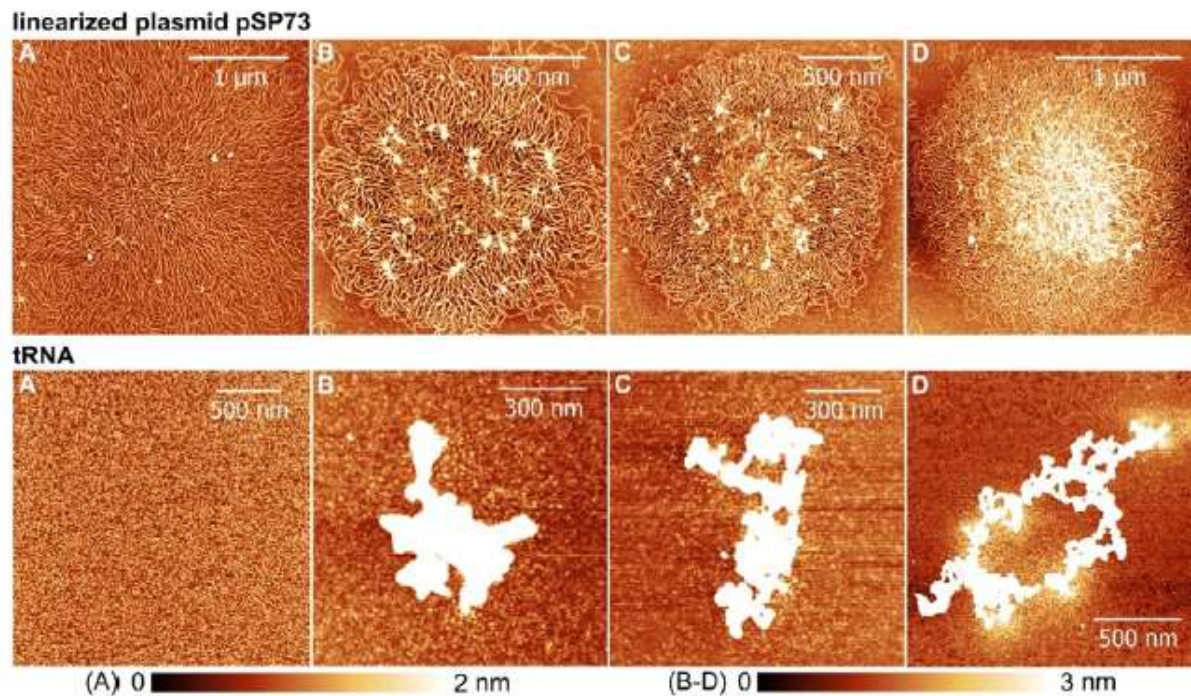
Figure 4.7: Condensation of DNA and tRNA observed by AFM. Top: Representative AFM images of linearized plasmid pSP73 DNA in the presence of WC at A) 1.56, B,C) 3.125, or D) 6.25 μM. Bottom: Representative AFM images of tRNA in the presence of WC at A) 6.25 and B–D) 12.5 mm. The protocol followed published procedures.[34–36] Reproduced from de Paiva et al. 2021.[1]

Condensation of DNA and RNA molecules can affect important DNA-related enzymatic activities including DNA replication and transcription.[37] WC fully inhibited the transcriptional activity of DNA at 30 μM concentration, whereas 1 mM $[Co(NH_3)_6]_{3+}$ was insufficient for full inhibition of RNA polymerase activity (Figure 4.8). Overall, charge does appear to be a more important factor in efficiency of transcription inhibition—WC has similar efficiency to the 6+ PPC DiplatinNC whereas only low μM concentrations (approx. 4 μM) are needed for the 8+ TriplatinNC.[34,35] Nevertheless, WC is much more effective than the commonly used spermine, which affects transcriptional activity in a concentration-dependent manner, and whose inhibitory action is also affected by DNA morphology.[38] Inhibition of topoisomerase I (topo 1) catalysis depends on the properties of DNA aggregates.[34,35] Relaxation of negatively supercoiled pSP73 KB plasmid DNA by Topoisomerase I is inhibited by increasing concentrations of WC and $[Co(NH_3)_6]_{3+}$. At concentrations of 200 μM supercoiled and relaxed DNA (corresponding to supercoiled and relaxed forms of plasmid DNA), WC and $[Co(NH_3)_6]_{3+}$ begin to inhibit Topoisomerase I DNA relaxation at 32 μM and 6 μM concentrations, respectively. Thus, the impact of DNA condensation by WC can be seen in inhibition of transcriptional activity and Topoisomerase I catalyzed relaxation of negatively supercoiled DNA; these effects are also seen with TriplatinNC.[39]
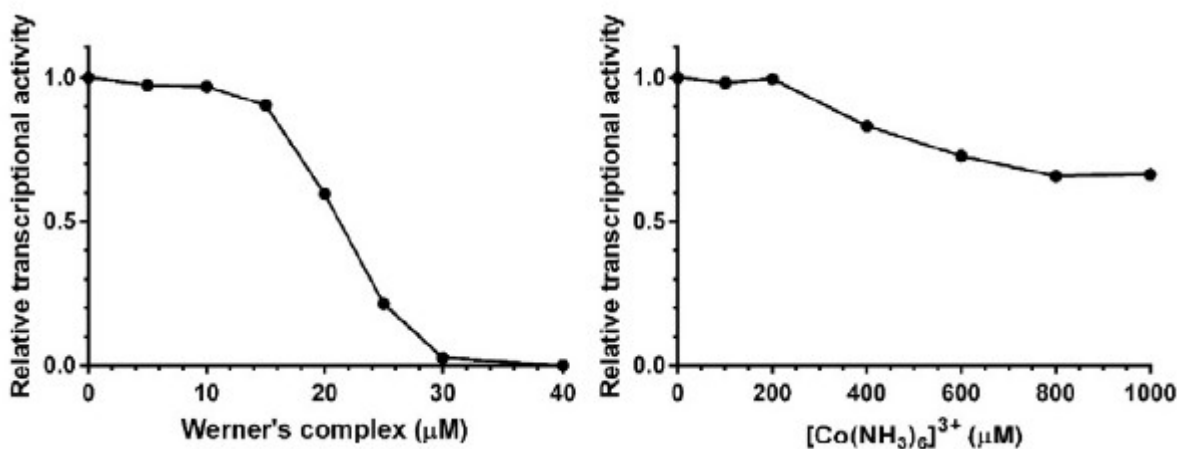
Figure 4.8: Plots of the relative transcriptional activity of pBR322 plasmid DNA as a function of cobalt complex concentrations. Reproduced from de Paiva et al. 2021.[1]

4.1.3 Antiviral Hypothesis

The study of non-covalent interactions of PPCs suggested that these should be general for charged coordination complexes. As WC is a highly positively charged coordination complex with high GAG and DNA affinity, we predicted WC would also possess broad-spectrum antiviral activity by inhibiting the HS-viral interaction. These results would expand the biological role of cobalt complexes. The redox and magnetic properties of Co coordination complexes suggest possibilities for their use in imaging, diagnostics, and therapy.[40] Earlier studies had examined briefly the use of Co complexes as analytical probes for sulfated GAG content,[41–45] but no effects on function were examined. In the following section, we aim to expand the antiviral chemotype to cobalt coordination compounds with a focus on WC.

4.2 Studies of anti-HCMV activity

The antiviral activity of a compound is quantified by its EC_{50}, the concentration at which 50% of virus replication is inhibited. Cytotoxicity of a compound is quantified by its TC_{50}, the concentration at which 50% of the cells die. To determine the EC_{50} of WC, its impact on HCMV yield (production of cell-free infectious virus) was determined using a luciferase-tagged HCMV, while the TC_{50} was simultaneously determined for replicate uninfected cultures using the CellTiter-Glo cell viability assay.[46] Results are shown in Figure 9 and summarized in Table 1. WC is less toxic than PPCs such as TriplatinNC and DiplatinNC, but maintains µM antiviral activity. The selectivity index (SI) is the ratio of TC_{50} to EC_{50}. A high SI suggests a favorable safety and efficacy profile of a compound. Given WC's minimal cytotoxicity, its SI is favorable.
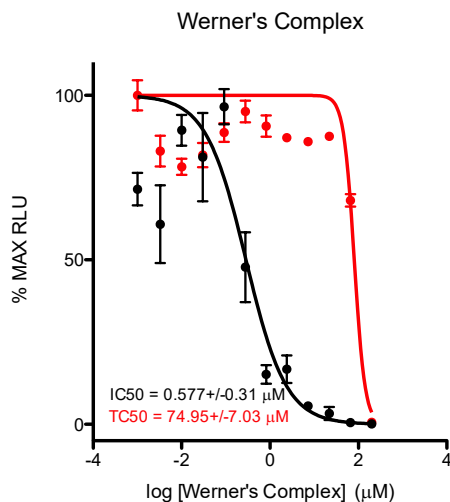
Figure 4.9: Luciferase-based antiviral activity and cytotoxicity of WC in fibroblasts. Anti-HCMV activity (black) was measured by incubating MRC-5 fibroblast monolayers in 96-well plates with WC for one h, then infecting with luciferase-tagged HCMV RC2626 (125 PFU/well). After five days 50 μL of virus-containing culture medium was transferred to fresh MRC-5 cultures and luciferase activities (RLU) in these cultures were measured 48 h later. Cytotoxicity (red) was measured in replicate uninfected cultures treated for five days using the CellTiter-Glo® assay. Data are means of three independent experiments.

Table 4.1 Anti-HCMV activity of WC

Antiviral[a] (EC_{50})	Cytotoxicity[b] (TC_{50})	SI^c	MB^d (IC_{50})
0.577 ± 0.31	74.95 ± 7.03	129.9	41.4

Table 4.1: Anti-HCMV activity of WC. [a]luciferase-based yield assay. [b]CellTiter-Glo® assay. [c]selectivity index (TC_{50}/EC_{50}). [a,b,d]μM; means of three independent experiments ± standard deviations. [d]inhibition of methylene blue binding to Fondaparinux (previously published data, [1])

4.3 WC does not inhibit viral attachment like PPCs

The yield-based assay used above measured the impact of WC on release of infectious virus progeny. However, our hypothesis predicted that WC, like PPCs, would block viral attachment and entry and therefore should block viral gene expression. First, we tested this using a GFP-tagged HCMV. Controls included heparin, known to block HCMV entry,[47] and BAY 38-4766, a terminase inhibitor that acts late in infection and does not impact viral gene expression. When added one h prior to infection, heparin inhibited GFP expression while BAY 38-4766 and WC did not. When added one hpi, neither WC, heparin, or BAY 38-4766 had an impact on GFP expression (Figure 11). When cells were treated with WC then washed, GFP expression was not inhibited, unlike PPCs which reduce GFP expression when cells are washed.[48] Interestingly, even a higher concentration of WC (25 μM) did not impact GFP expression regardless of when cells were treated. All of these data indicate that unlike PPCs, WC does not inhibit viral attachment or entry.
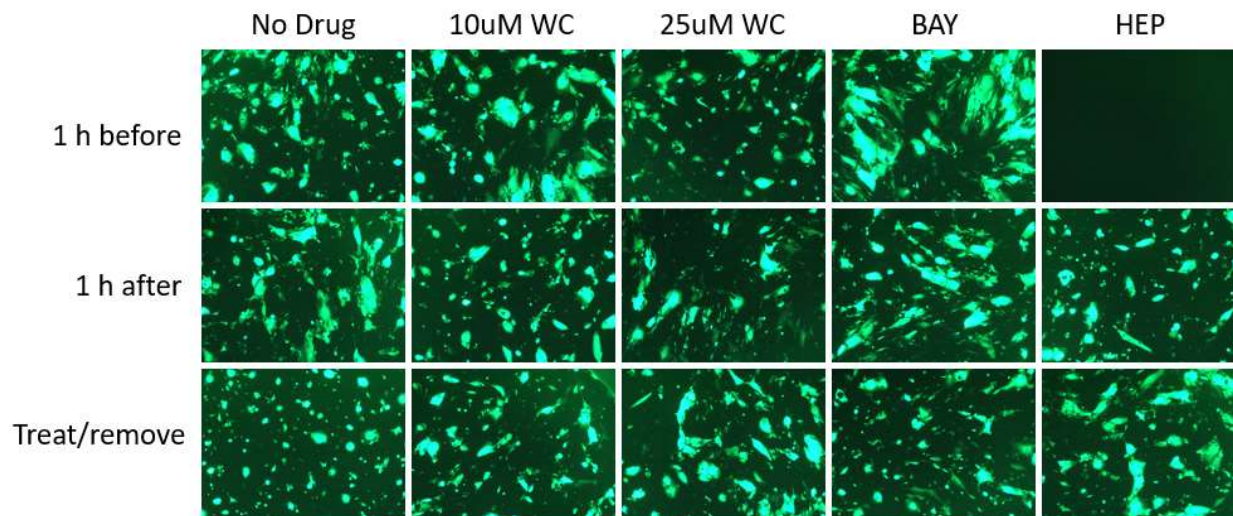
Figure 4.10: WC does not inhibit expression of a viral marker protein independent of time of addition. GFP based mechanistic studies for WC. (Top) Confluent monolayers of MRC-5 fibroblasts in 96-well plates were treated with medium, 150 µg/ml heparin (HEP), 10 µM WC, 25 µM WC, or 8 µM BAY 38-4766 (BAY) for one h then infected with GFP-tagged HCMV BADr (100 PFU/well). (Middle) Confluent monolayers of MRC-5 fibroblasts in 96-well plates were infected with BADr (100 PFU/well) for 1 h then treated with medium, 150 µg/ml heparin (HEP), 10 µM WC, 25 µM WC, or 8 µM BAY. (Bottom) Confluent monolayers of MRC-5 fibroblasts in 96-well plates were treated with medium, 150 µg/ml heparin (HEP), 10 µM WC, 25 µM WC, or 8 µM BAY for one h then washed three times with media and infected with GFP-tagged HCMV BADr (100 PFU/well). Six days after infection representative micrographs were taken with a Nikon Eclipse TS100 Inverted UV microscope.

To further investigate the WC mechanism of action, we used immunofluorescent staining to determine the impact of WC on HCMV immediate early (IE) proteins 1 and 2, among the first viral proteins to be expressed within an infected cell, or the late viral protein pp28, which is expressed late in infection and only after viral DNA synthesis. BAY 38-4766 was a control; as a packaging inhibitor, it should not inhibit either GFP, IE, or pp28 expression.[47,49,50] These controls behaved as expected, while WC failed to inhibit either IE1/2 and pp28 expression (Figure 12). This suggests a mechanism of action after viral DNA synthesis.
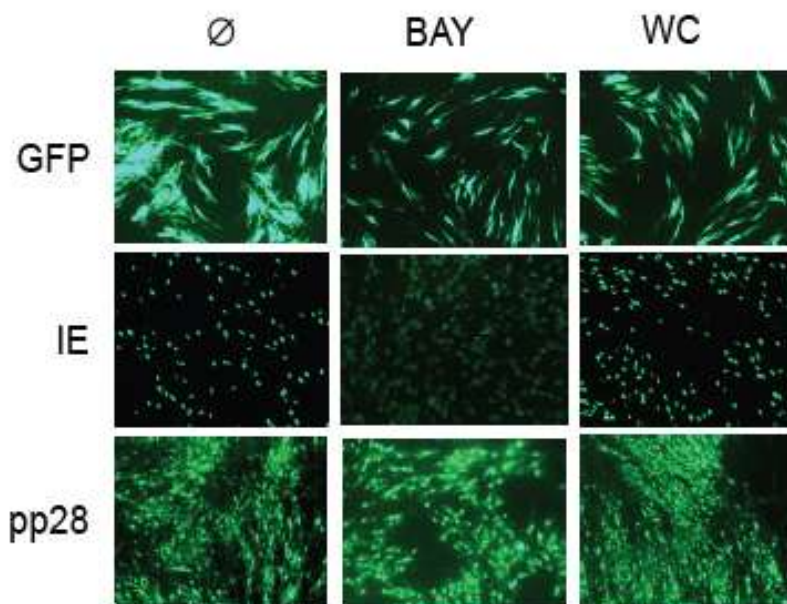
Figure 4.11: WC does not inhibit expression of HCMV IE protein or pp28 late protein. MRC-5 fibroblast monolayers were treated with medium (Ø), 8 µM BAY 38-4766 (BAY), or 25 µM WC one h before infection with HCMV RC2626 (125 PFU/well). Cultures were imaged for GFP or fixed and fluorescently stained for HCMV IE proteins 48 hpi or for pp28 late protein 120 hpi.

To further define the mechanism of action of WC, a time of addition experiment was conducted using a luciferase-based yield assay in which inhibitor was added at different times relative to viral infection. Heparin was only active when added within a few hours of adding the virus and lacked antiviral activity if added as early as 12 h after infection (Figure 13). WC and BAY 38-4766 were active if added 48 h after infection.
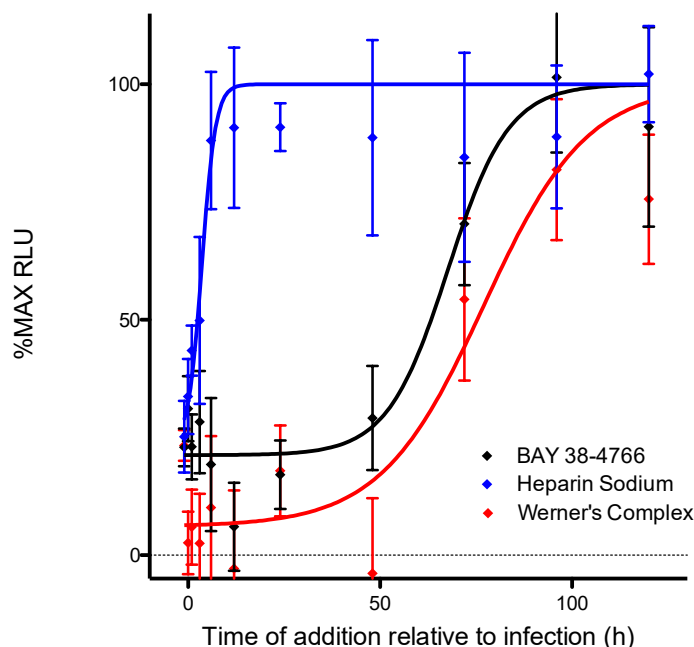
Figure 4.12: Time of addition study. Confluent monolayers of MRC-5 fibroblasts were treated with 150 μg/ml heparin, or 25 μM WC, or 8 μM BAY 38-4766 (BAY) 1 h before, concurrent with, or at various times after infection with luciferase-tagged HCMV RC2626 (125 PFU/well). After five days 50 μL of virus-containing culture medium was transferred to fresh MRC-5 cultures and luciferase activities (RLU) in these cultures were measured 48 h later. Data are means of triplicate wells ± standard deviations.

4.4 WC has a late acting mechanism

From our preliminary studies using HCMV we conclude that WC does not impact HCMV viral attachment, entry, or viral gene expression, but appears to act at later times, coincident with capsid assembly, DNA packaging, virion morphogenesis, or egress. HCMV replication begins with circularizing its genome, then it employs a rolling circle mechanism to produce concatemers (Figure 14). Prior to packaging, pro-capsids are assembled with internal scaffold proteins. One end of a concatemer docks with the pro-capsid and as DNA enters the scaffold proteins are proteolytically cleaved and somehow exit the capsid. After a full-length genome has entered the capsid, the concatemer is cleaved leaving the monomer inside the C-capsid and releasing a slightly shorter concatemer.[51] Viral DNA packaging results in three types of HCMV capsids: empty A-capsids, B-capsids that contain scaffold proteins, and DNA-filled C-capsids (Figure 15).[52] B-capsids contain proteolytically-processed scaffold fragments but no DNA and are thought to result from spontaneous scaffold proteolysis in the absence of DNA packaging. A-capsids are thought to arise from unstable C-capsids that have spontaneously ejected their DNA. Thus, DNA packaging inhibitors, such as letermovir, prevent formation of normal genome length DNA monomers from and result in abnormal ratios of A-, B-, and C-capsids (fewer A- and C-capsids, more B-capsids).
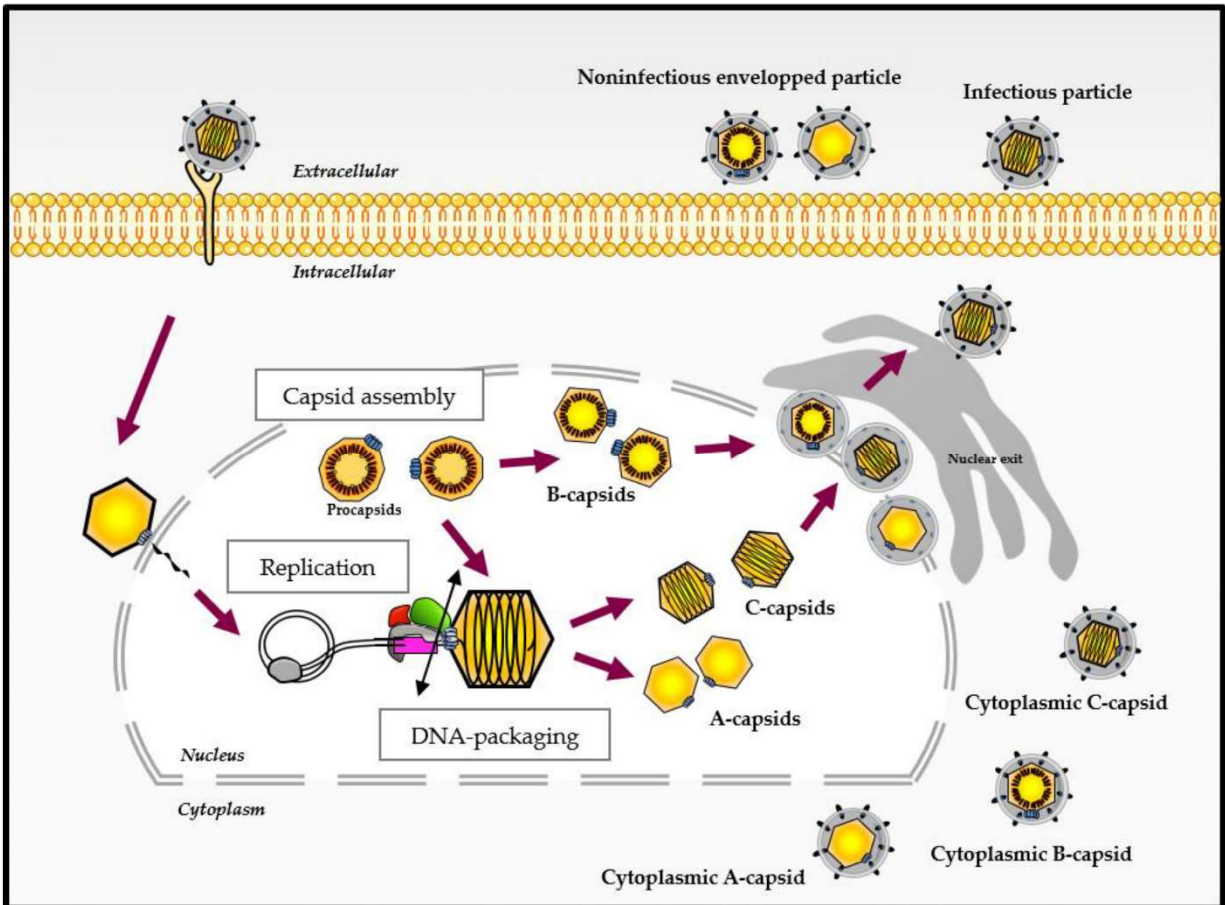
Figure 4.13: Overview of herpesvirus replication.[53] *Following attachment and host cell entry, the viral capsid docks at a nuclear pore and delivers its DNA into the nucleus. After genome replication via a rolling circle mechanism, the ends of the concatemers dock on the pore of a viral capsid and a monomer of DNA enters and is cleaved. Different capsids are present in an infected cell, detailed in the next figure. Finally, capsids exit the nucleus, gain their tegument proteins and envelope and leave the cell. Reproduced from Muller et al. 2021.*
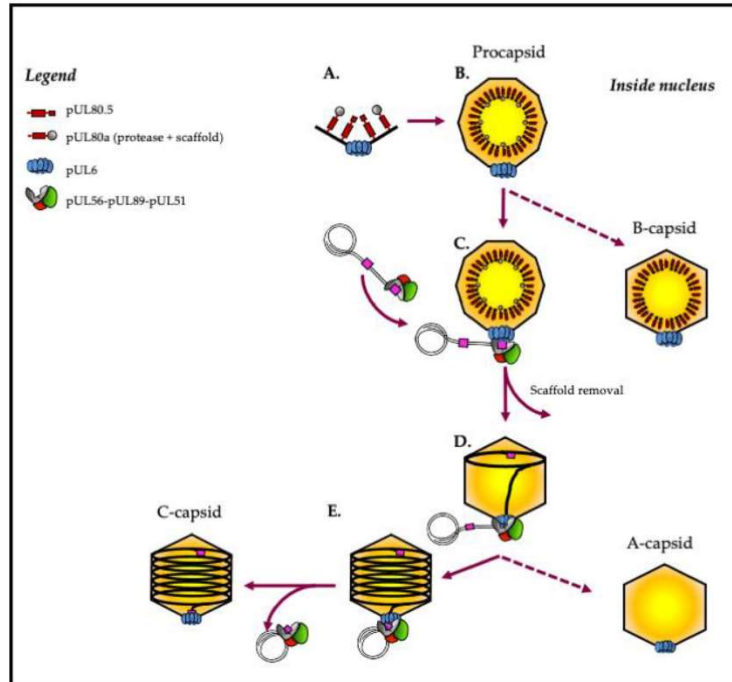
Figure 4.14: Herpesvirus capsid formation and DNA packaging.[53] (A, B) Intranuclear capsid formation is initiated by the assembly of major capsid protein (black), small capsid protein (black), portal protein (blue), and scaffold proteins (red and grey). (C) The terminase complex of pUL56, pUL89, and pUL51 recognizes 'pac' motifs ('cis-acting DNA packaging signals', pink) and performs an initial cleavage of viral DNA. (D) Utilizing its ATPase activity terminase inserts a genome monomer of DNA into the capsid. At the same time the maturational protease cleaves scaffold, which exits the capsid. (E) Terminase performs a final cleavage of DNA to release the viral DNA and disassociate from the filled C-capsid. Spontaneous cleavage of scaffolding proteins can also result in B-capsids lacking viral DNA but containing scaffold fragments, and spontaneous loss of DNA can result in A-capsids that lack both scaffolding and DNA. Reproduced from Muller et al. 2021.

4.4.1 Field-inversion gel electrophoresis

In standard gel electrophoresis, a constant current runs through an agarose gel in order to separate DNA fragments by size, with shorter segments traveling faster than longer segments. However, DNA fragments over ~ 15-20 kb in length do not resolve by standary gel electrophoresis. This is believed to be due to the propensity of larger DNA molecules to get entangled on agarose fibers. Field-inversion gel electrophoresis (FIGE) is a DNA separation technique which has better resolution and band separation than standard gel electrophoresis, particularly for DNA molecules larger than 20 kb. In FIGE, the polarity of the electrical current inverts periodically, moving the DNA forward for a time and then backwards, which presumably allows the DNA to untangle from agarose fibers and reorient. Larger molecules require more time than smaller molecules to reorient their migration as the current changes direction. While the forward time is longer than the backward time, in order to move the DNA down the gel, the ratio of forward to backward pulse times and the total length of each cycle can be varied. As such, shorter segments of DNA travel farther than longer segments, as in standard gel electrophoresis, but the more time provided for each current direction, the larger the size range of DNA molecules that can be separated by FIGE.[54] Thus, FIGE can be used to separate large DNA molecules, such as the 235-kb HCMV genome.[51]

To assess the cleavage of HCMV concatemer DNA, we performed FIGE of HCMV-infected cells cultured in inhibitory concentrations of WC, the DNA packaging inhibitors BAY 38-4766 and letermovir, or media-only control. If WC does not inhibit concatemer cleavage, we will see a DNA specie corresponding to 235 kb, representing monomeric HCMV genomes, as in the media-only control. If WC inhibits concatemer cleavage, we will see a reduction in 235-kb DNA, similar to the impact of letermovir or BAY-

38-4766.
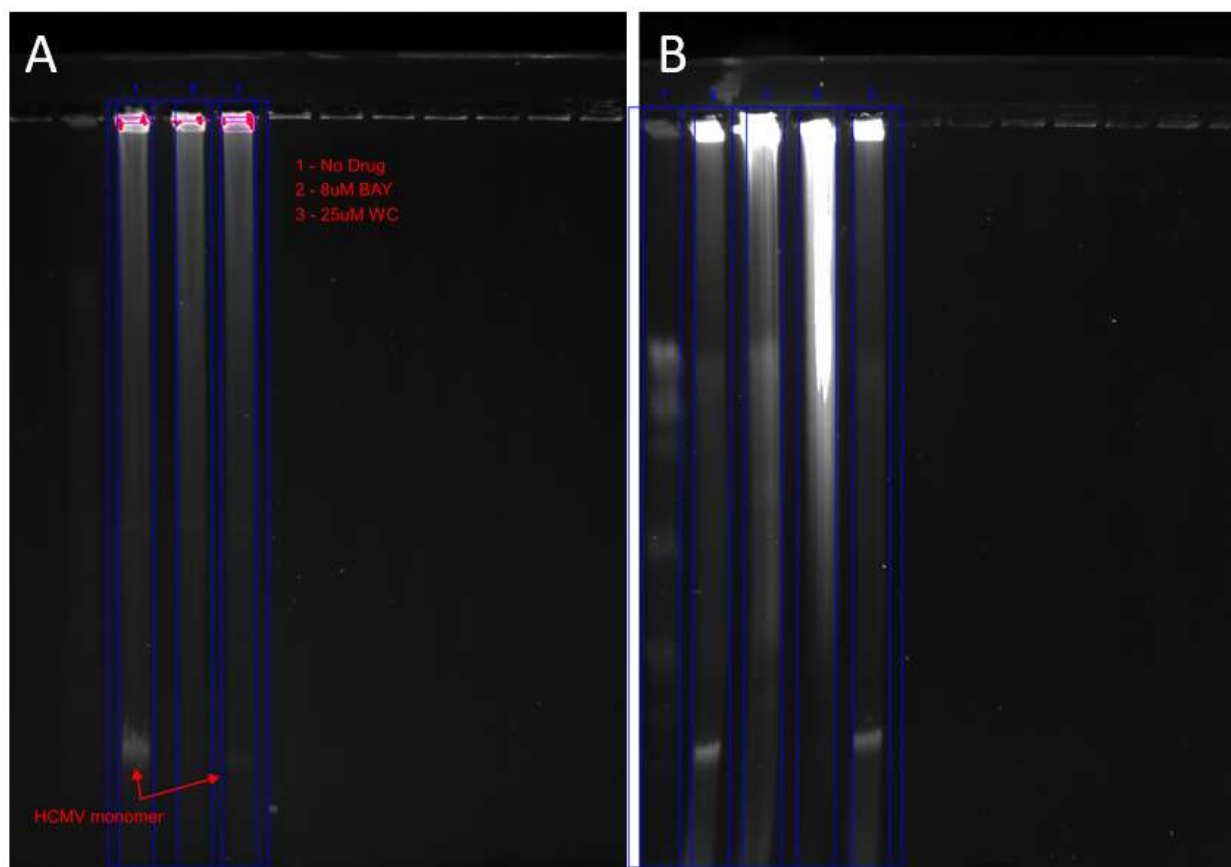
Figure 4.15: FIGE analysis of DNA species in WC-treated HCMV-infected cells. (A) MRC5 fibroblasts were untreated or treated 8 μM BAY 38-4766 (BAY) or 25 μM WC for 1 h then infected with HCMV strain AD169 at a MOI of 5. Five days post infection, cell-associated DNA was isolated, separated by FIGE, and visualized by GelRed staining and UV light . Lanes from left to right: MW markers, no drug (1), BAY 38-4766 (2), and WC (3). (B) MRC5 fibroblasts were untreated or treated with 10 μM Letermovir, 8 μM 38-4766 (BAY), or 25 μM WC for 1 h then infected with HCMV strain AD169 at high MOI. Five days post infection, cell-associated DNA was processed as above. Lanes from left to right: MW markers (1), no drug (2), BAY 38-4766 (3), Letermovir(4), and WC (5).

The results shown in Figure 15A indicate that WC decreases but does not elimiate monomeric HCMV DNA in comparison to the media-only control, suggesting a possible mechanism involving inhibition of DNA packaging. However, as the MOI of this experiment was not sufficient to initially infect all the cells in the culture, it is possible that the observed decrease in monomeric DNA is an indirect effect of WC inhibiting secondary spread to cells that were initially not infected. This interpretation was supported by a repeat experiment conducted at higher multiplicity of infection in which WC did not significantly decrease the amount of monomeric DNA when compared to the control (Figure 15B). Thus, while it is possible that WC may have a minor effect on monomer formation, it appears that inhibition of DNA monomer formation is not the primary mechanism of action.

4.4.2 Transmission electron microscopy

Transmission electron microscopy (TEM) is the only imaging technique capable of the direct visualization of viruses. As TEM uses electrons rather than light to magnify images, it is only limited by the wavelength of an electron, while light microscopy is limited by the comparatively large wavelength of light. Thus, TEM can create more magnified images at a higher resolution. TEM has a long history of viral

research; in 1938, the first electron micrograph of poxvirus was published and in the 1940s, smallpox and chickenpox infections were diagnosed via TEM.[55] In the 1970s and 1980s, TEM contributed to the discovery of adeno-, entero-, paramyxo-, and reoviruses.[56] Today, TEM is still used to identify infectious agents during disease outbreaks and in routine diagnosis to characterize infections not diagnosed by molecular assays.[55,56] TEM is also used in basic science research to investigate the viral replication cycle and the structure of an infected cell as well as to determine a compound's impact on viral replication.[57]

To assess the mechanism of action of WC, we performed TEM to visualize HCMV viral packaging and observed the number and ratio of viral capsids in the nucleus. Confluent cell monolayers were treated with nontoxic but inhibitory concentrations of WC for one hour with a media-only control then infected with HCMV at a high multiplicity of infection for five days. Following fixing with 2.5% glutaraldehyde in 0.1M sodium cacodylate buffer and staining with 2% osmium tetroxide, TEM micrographs were taken of nuclei, where viral DNA packaging occurs. If WC, like letermovir, inhibits viral DNA packaging, the number of C-capsids will be reduced and B-capsids will be more abundant.[58] In initial TEM experiments, WC-treated cells displayed an odd phenotype – C-capsids with dark half-moons rather than full circles (Figure 16). Additionally, there was a lack of B capsids but an appropriate number of A-capsids. This phenotype has not been observed in HCMV-infected cells previously. It could indicate a unique alteration of viral DNA packaging.
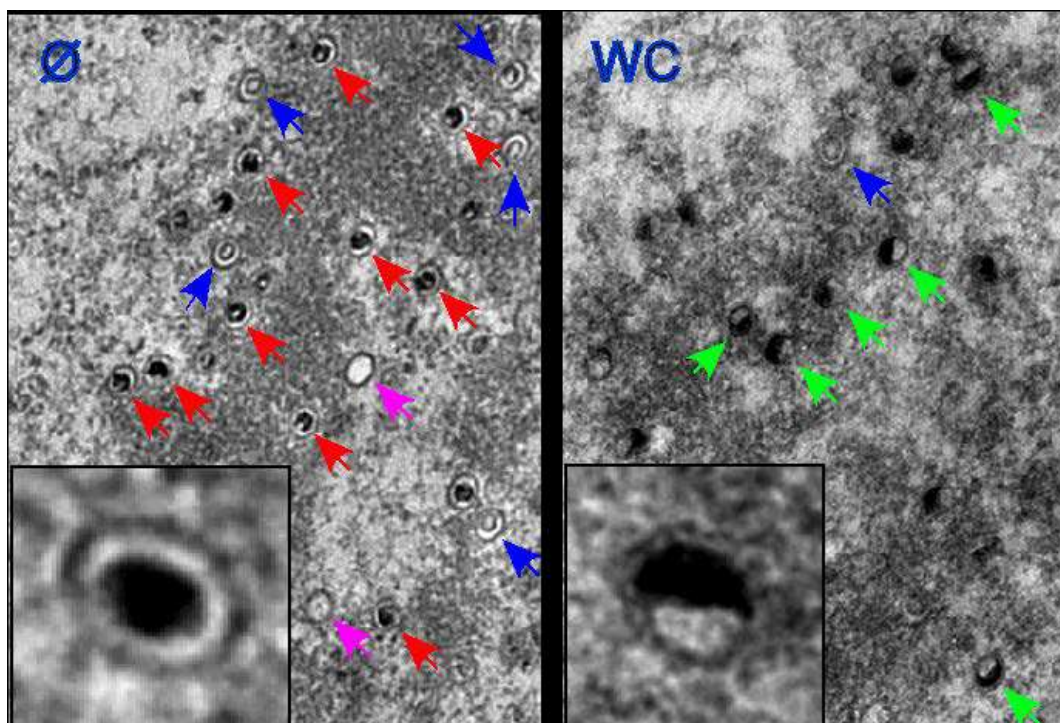
Figure 4.16. Novel half-moon capsids in WC-treated cells. TEMs of fibroblasts infected with HCMV strain AD169 six days post infection in the absence (Ø) or presence of 25μM WC. Arrows indicate A-capsids (magenta), B-capsids (blue), normal C-capsids (red), or half-moon C-capsids (green). Insets show representative normal and halfmoon C-capsids at higher magnification.

4.5 Antiviral-spectrum activity of WC

We also evaluated the spectrum of antiviral activity of WC. First, we assessed the anti-GPCMV activity via an RFP-based yield assay. Unfortunately, GPCMV was not inhibited by WC except at a toxic concentration (Figure 4.17 Left). The anti-adenoviral activity of WC was measured using a GFP-based

assay; although WC may have partial inhibitory at very high concentrations (>200uM), it is difficult to separate its antiviral activity from its cytotoxicity (Figure 4.17 Middle). Finally, we examined WC's anti-SARS-CoV-2 activity using GFP-tagged pseudotyped-lentiviruses. WC has anti-SARS-CoV-2 activity at very high concentrations (Figure 4.17 Right). The results for adenovirus and SARS-CoV-2 suggest the possibility that, like the PPCs, WC can metalloshied HS to inhibit viral attachment, but only at very high concentrations, emphasizing the relationship between DNA and HS affinity with biological activity.
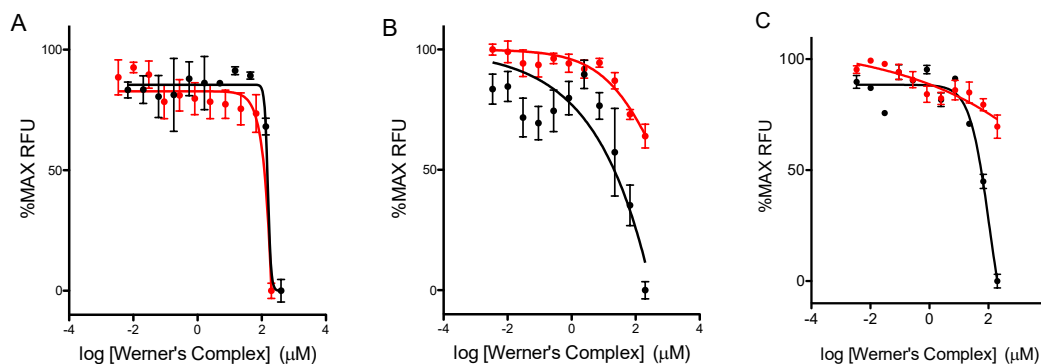
Figure 4.17: Broad-spectrum antiviral activity of WC. (A) Guinea pig lung fibroblasts were treated with serially diluted WC for 1 h then infected with a RFP-tagged GPCMV. RFP signal was read 6 days post infection. (B) ARPE-19 cells were treated with serially diluted WC for 1 h then infected with GFP-tagged adenovirus; GFP signal was read 5 days post infection. (C) HEK-293T-ACE2 cells were treated with serially diluted WC for 1 h then infected with SARS-CoV-2 pseudotyped lentivirus; GFP signal was quantitated two days post infection. Cytotoxicity (red) was measured in replicate uninfected cultures treated for two or five days using the CellTiter-Glo® assay. Data are means of three independent experiments.

4.6 Cobalt structure activity relationships

PPCs inhibit HCMV cellular attachment and entry through inhibition of HS-virus interactions, as shown in section 2. 5. The 6+ Werner's Complex, in contrast, is also an effective antiviral agent but its mechanism of action is still not clear and may be more "DNA-centered" than "HS-centered". It is therefore of interest to examine whether we can delineate between these two mechanisms of antiviral activity. Given the demonstrated effect on HS-related functions such as heparinase cleavage and cellular invasion, we chose a small library of charged coordination complexes (CCCs) varying in charge and nuclearity to investigate structure-activity relationships.

4.6.1 Selection of compounds

To develop structure-activity relationships in HS-affinity and antiviral activity, we tested a series of cobalt compounds (Figure 4.18). Each of the cobalt compounds in this series are mononuclear and have a small positive charge (less than +3), with the exception of the dinuclear 4+ Taube dimer (**G**). Hexamminecobalt (III)), ([Co(NH$_3$)$_6$]$^{3+}$, (**B**) has a moderate positive charge (+3) and multiple ammine groups with the potential for hydrogen bonding. Tris(ethylenediamine)cobalt (III) ([Co(en)$_3$]$^{3+}$, (**C**) has increased bulk and lipophilicity but maintains the charge of **B**. Like WC, **C** is also chiral; as enantiomers are known to differ in their biological activities, we tested **C** as a racemic mixture and also as its + (D) and - (E) enantiomers. The effect of planar ligands and diminished hydrogen-bonding were examined using tris(2,2'-bipyridine)cobalt (III) (**F**). The possible effect of covalent bond formation was examined with a series of compounds; pentaamminechlorocobalt (III) (**H**); tetraamminecarbonatocobalt (II) (**J**); and Dichlorobis(ethylenediamine) cobalt (III) (**I**) which replaces one ethylenediamine ligand with two chloride

ligands. Finally, we tested a synthetic intermediate of Werner's Complex (WC), the Taube dimer (**G**), which has the highest charge of the group and the only dinuclear compound of the series.
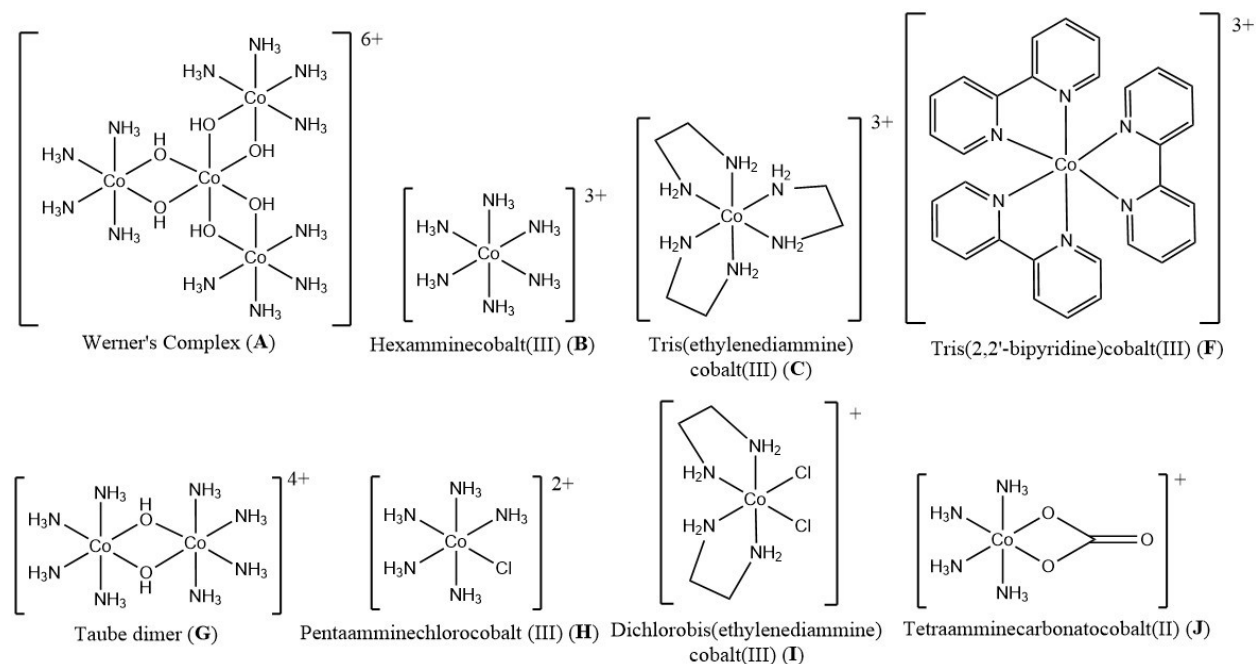
Figure 4.18: The structures of substitution-inert mononuclear and polynuclear cobalt complexes. Counterions omitted for clarity. Enantiomers of C are not depicted but both + and - enantiomers were isolated and tested.

4.6.2 Additional Background

4.6.2.1 Biophysical studies

Methylene Blue and Ethidium Bromide Competitive Inhibition Assays: Methylene blue (MB) has been used to quantify sulfate content on heparin chains and to examine heparin binding interactions; it is described in section 1.6.1. The association constant between FPX and MB was previously calculated using a Scatchard plot (4.1×10^4 M^{-1}). Results are summarized in Table 1. Although all compounds have some affinity for FPX, all have lower affinity when compared to PPCs. However, PPCs are polynuclear with much higher charges. A trend of charge is also supported by WC (**A**) with the highest affinity but one within this series, as well as the strongest charge. **F** also has affinity for FPX, which interesting as it is the only compound with aromatic ligands. Also of note, the covalently binding compounds (**H-J**) have low affinity for FPX, although the assay is designed to measure non-covalent interactions only.

Compound	Charge	MB-FPX IC$_{50}$^{a} (μM)	EtBr-DNA EC$_{50}$^{b} (μM)
A	6+	41.1 ± 0.7*	104 ± 2
B	3+	64.5 ± 1.1*	689 ± 17*
C	3+	71.0 ± 2.9	156 ±4
D	3+	72.0 ± 0.8	154 ± 5
E	3+	63 ± 0.2	159 ± 3
F	3+	36.4 ± 0.9	N/A
G	4+	52.8 ± 0.5	124 ± 6
H	2+	75.6 ± 1.2	>1000*

	1+	116.1 ± 1.6	N/A
I			
J	1+	>75	N/A

Table 4.2: IC50 and EC50 values of cobalt compounds for FPX and DNA affinity as measured by ethidium bromide and methylene blue reporter assays. Compounds are listed with their overall charge. (a) The MB-FPX IC50 value was determined as the concentration of complex required for half-maximal inhibition of MB binding to FPX. (b) The EtBr-FPX EC50 is the concentration of FPX required to restore 50% EtBr binding. (*) denotes previously published data [15,59].

Ethidium bromide competition assay assesses the strength of non-covalent FPX-compound interactions; it is described in section 1.6.3. The cobalt results are summarized in Table 1. Once again, all compounds have a marked decrease in affinity as compared to PPCs although they do maintain some affinity. WC (**A**) maintains the best affinity, emphasizing the importance of charge or nuclearlity once again; this is underlined by **G**, the dinuclear synthetic intermediate of WC with a charge of 4+. **C** as well as its isolated enantiomers **D** and **E** have strong affinity for FPX and the three are not markedly different. Finally, **B** the simplest of the series and a standard to cobalt interactions, had very low affinity, despite having the same charge of **E**, suggesting the FPX interaction requires more than simple ammines.

Mass Spectrometry: Negative mode electrospray ionization (ESI) is commonly used for identification and analysis of heparin. We have previously shown through ESI-MS studies that FPX undergoes sulfate loss in the gas phase. Analysis regarding the retention of labile sulfate groups on the heparin backbone has shown metal cations stabilize sulfate groups. In the present work we examine the stoichiometry of cobalt complexes bound to FPX and their ability to protect against sulfate loss. We again compare the difference in covalent and non-covalent interactions.

Non-Covalent Substitution-inert Complexes. We compared **C** with previous studies on **B**. We further separated the enantiomers to examine possible enantiospecific effects. Using the MB-FPX system, preliminary studies on FPX using showed very little difference amongst the compounds for both FPX and DNA binding. ESI-MS showed peaks corresponding to a 1:1 adduct between **C** and FPX (*m/z* 3 state). Peaks were also observed corresponding to a retained sodium ion at 440.2640 *m/z* (4-) and loss of one sulfate at 414.7801 *m/z* (4-). Peaks were observed attributable to a 1:2 Co:FPX stoichiometry at 755.1908 *m/z* (1+). The [59]Co NMR spectrum of **B** with D-glucosamine showed a shift of approximately 60 ppm from the parent peak with the appearance of two peaks suggesting some enantiomeric selectivity between the racemate and the sugar.[60]

Covalently Binding Complexes. The monodentate $[CoCl(NH_3)_5]^{2+}$, **H**, and bidentate $[CoCl_2(en)_2]^+$ have the ability to interact both covalently and non-covalently. For **H**, peaks attributable to both covalent and non-covalent interactions were observed for the 2-, 3-, and 4- charge states. A 1:1 binding interaction was observed covalently at 823.0062 *m/z* (2-) and 548.3354 *m/z* (3-) along with loss of one sulfate at 521.6825 *m/z* (3-), and 410.9996 *m/z* (4-). The non-covalent interaction was also observed with a coordinated water molecule at 832.0118 *m/z* (2-), 554.3389 *m/z* (3-), and 415.5021 *m/z* (4-). The [59]Co chemical shift of $[CoCl(NH_3)_5]^{2+}$ shifts by -1983 ppm in the presence of glucosamine-6-O-sulfate, while the peak assigned to the aquated Co species is also easily observed.

Both covalent and non-covalent interactions were observed for **I** in the 2- and 3- charge states. Water may also coordinate one of the free ligand sites, still allowing a covalent interaction between cobalt and FPX. The covalent 1:1 binding interaction was observed at 560.0038 *m/z* (3-) and 840.5086 *m/z* (2-) and also associated with one coordinated water at 566.0074 *m/z* (3-) and 849.5138 *m/z* (2-). Peaks attributable to a non-covalent interaction were observed at 571.9964 *m/z* (3-) and 858.5203 *m/z* (2-),

again associated with 2 coordinated waters. Loss of one sulfate was also observed at 533.3511 *m/z* (3-) with no coordinated water. Significant loss of sulfates from parent FPX was also observed. A 2:1 binding stoichiometry of Co:FPX was observed at 928.2545 *m/z* (2-) including a loss of two sulfates at 849.5138 *m/z* (2-). A 1:2 covalent binding interaction was also observed at 695.1204 *m/z* (1+), while a 1:1 non-covalent binding interaction was observed at 507.2612 *m/z* (1-) with no dissociated chlorides.

In summary, mass spectrometry and NMR confirmed the formation of Co-FPX adducts both through non-covalent interactions as well as direct Co-FPX bond formation. Non-covalent interactions appear to protect more sulfates as compared to covalent interactions, likely due to the more dispersed nature of non-covalent interactions having a greater ability to "metalloshield", in contrast to more localized protection afforded by the covalent interactions.

4.6.2.2 Biological effects of cobalt complexes: Inhibition of enzyme activity on FPX by mononuclear cobalt compounds

A principal function of HS is cleavage by mammalian heparanase. Cellular invasion through the extracellular matrix (ECM) requires degradation of the matrix by HPSE, and cell motility in response to growth factors. We have used FPX as a substrate for both mammalian heparanase and bacterial heparinase (Hep1). The cleavage patterns of FPX by bacterial heparinase (often used as a model for the mammalian enzyme) are shown in Figure 4.19. Colorimetric assays for enzymatic activity and inhibitor screening have been developed.[26] Using this previously described colorimetric assay, inhibition of heparinase cleavage is very effective for the pentaammine complex with only weak inhibition seen for **C** and **I** in Figure 4.19.
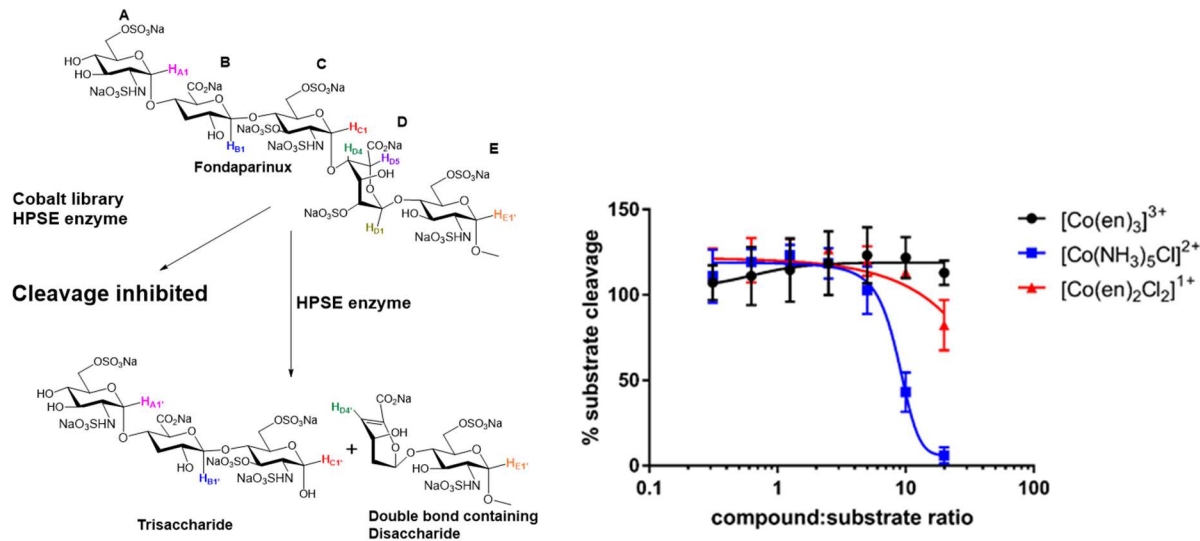
Figure 4.19: Heparanase inhibition. Left – Structure of fondaparinux and cleavage products by F. heparinum heparinase I/P. heparinus heparinase II. Lettering denotes anomeric hydrogens. Right - H inhibits heparinase I cleavage of fondaparinux more effectively than I or C.

The ability of the Co complexes to inhibit cell invasion through matrigel basement membrane was assayed using a Boyden-chamber assay.[61] Serum-starved cells were seeded into the top chamber onto a matrigel membrane with or without heparinase I. Compounds were added to the top chamber in serum-free media. The bottom chamber was filled with media containing 10% serum. In Figure 4.20, we see that

the 50 μM pentammine complex was very effective in inhibiting cellular invasion of matrigel by MDA-MB-231 (triple-negtaive breast cancer) cells. Covalent binding appears to enhance the inhibition and both **H** and **I** are more effective than **C**. These results contrast with weak inhibition seen for **B**, and the inhibitory concentrations, especially for **H**, are comparable to those previously observed for the 6+ WC. The results of the two heparinase cleavage assays clearly demonstrate that **H** exhibits an interesting effect on heparinase and growth factor function.
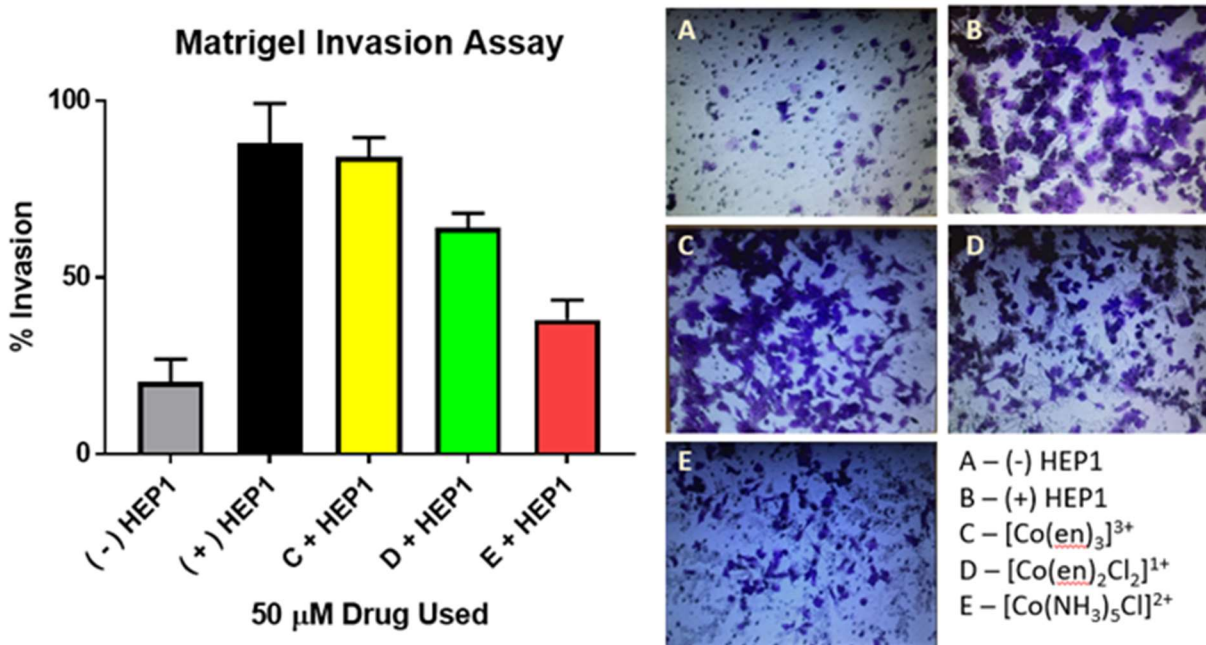
Figure 4.20: H inhibits the heparinase I induced invasion of matrigel by MDA-MB231 cells more than I or C. Left: Growth factor reduced Matrigel was treated with either PBS or equimolar amounts of cobalt compound (50 μM) for 1 h, followed by treatment with additional PBS or 0.3 units of heparinase I. Matrigel chambers incubated at 37 °C for 16 h to allow digestion of Matrigel. Wells were washed 10× times with PBS to remove remaining enzyme or compound. Inserts were filled with media containing 0.2 % FBS and placed into wells with media containing 10 % FBS. 8×10⁴ serum-starved MDA-MB-231 cells were seeded onto Matrigel or control inserts without Matrigel. After 12 h, cells that invaded through Matrigel were fixed and stained using methanol and crystal violet. % invasion was determined by dividing the number of cells that invaded through Matrigel by the number that migrated through the inserts without Matrigel. Right: Representative light microscopy images of crystal violet stained cells that invaded Matrigel.

4.6.3 Antiviral activities. Charges greater than 3+ are required for measurable antiviral activity as measured through a luciferase-based yield assay or a GFP-based spread assay.

The anti-HCMV activity of the cobalt series was measured by the luciferase-based yield and GFP-based spread assays previously described (sections 2.3 and 2.4). Although none of the mononuclear cobalt compounds were cytotoxic, none had antiviral activity against HCMV up to 200 μM by either assay, indicating they do not inhibit the formation and release of new virions into culture media or the cell-to-cell spread of viral infection (Figure 2 and Figure 3). However, **G** was also non-cytotoxic and appeared to have some antiviral activity at high concentrations; it is dinuclear and has the highest charge of the series. There was some concern about the solubilty of G; experiments were repeated with a different counterion but G lacked antiviral activity (Figure 4.23). These data suggest that mononuclear compounds do not

sufficiently shield HS in a maner necessary to block viral entry, either due to their charge or size, and thus do not have antiviral activity.
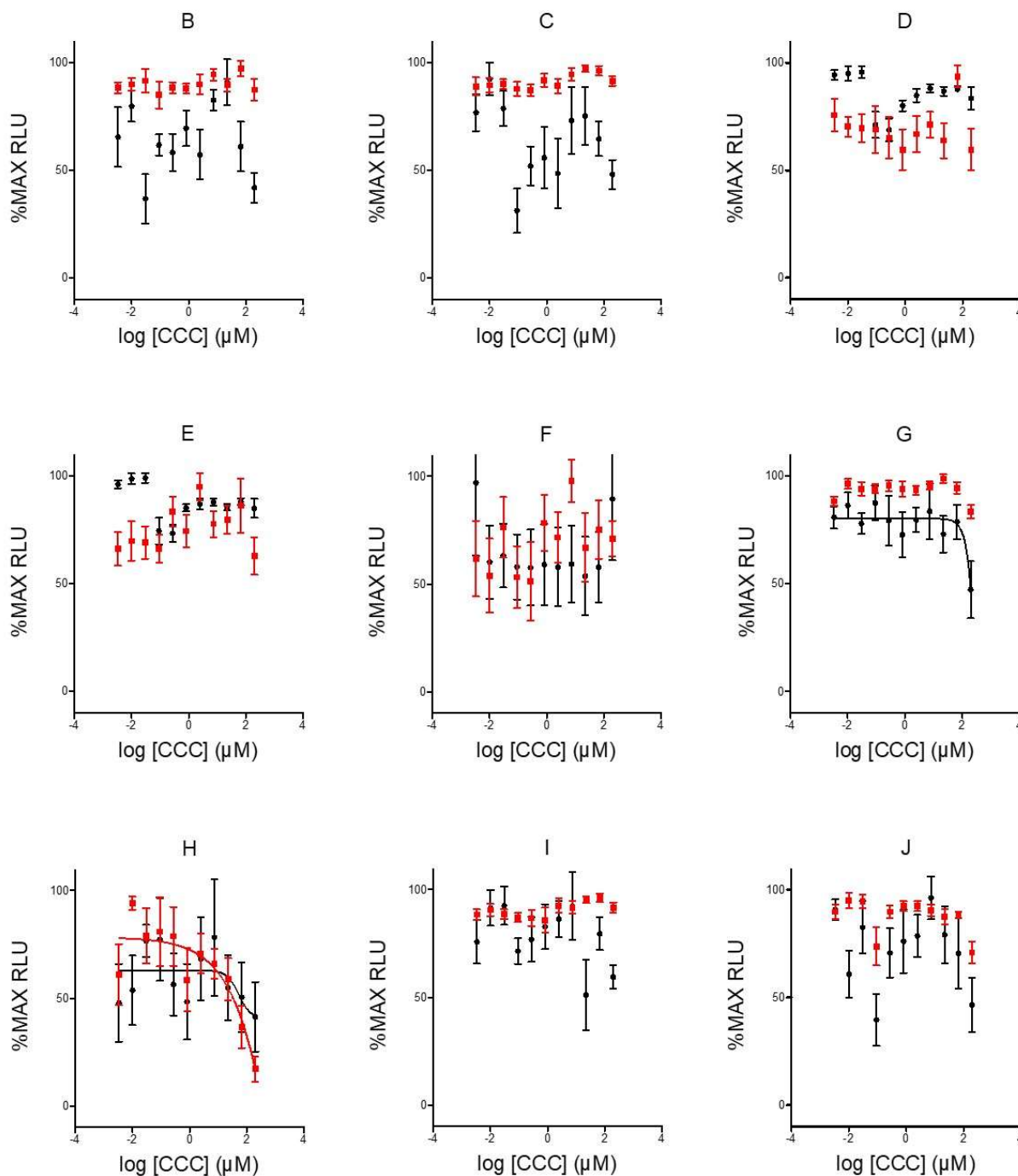
Figure 4.21: Luciferase-based HCMV antiviral activities and cytotoxicities of cobalt compounds in fibroblasts. Anti-HCMV activity (black) was measured by incubating MRC-5 fibroblast monolayers in 96-well plates with compounds for one h, then infecting with luciferase-tagged HCMV RC2626 (125 PFU/well). After five days 50 µL of virus-containing culture medium was transferred to fresh MRC-5 cultures and luciferase activities (RLU) in these cultures were measured 48 h later. Cytotoxicity (red) was measured in replicate uninfected cultures treated for five days using the CellTiter-Glo® assay. Data are means of three independent experiments ± standard deviations.
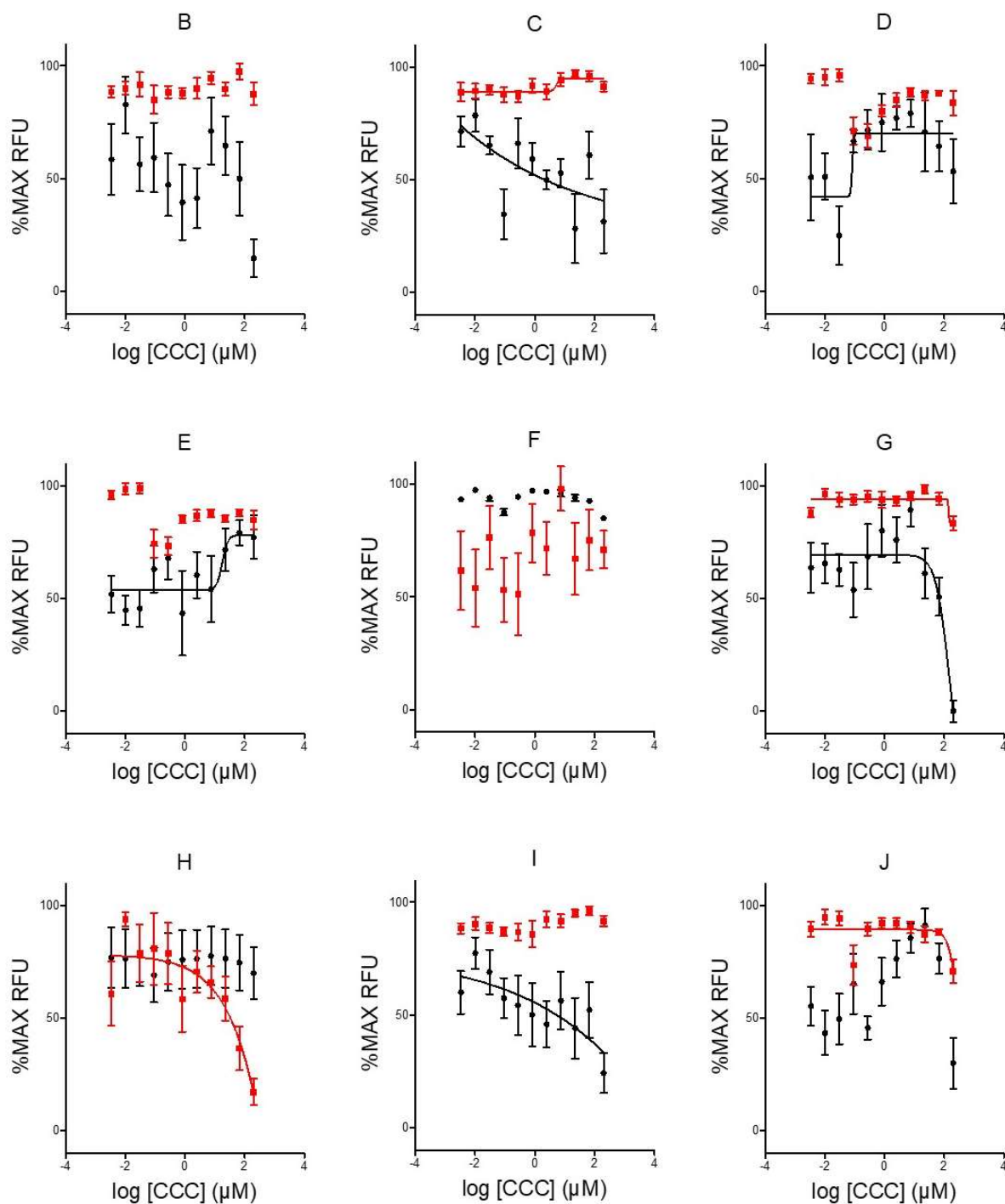
Figure 4.22: GFP-based HCMV antiviral activities and cytotoxicities of cobalt compounds in fibroblasts. Anti-HCMV activity (black) was measured by incubating confluent monolayers of MRC-5 fibroblasts with CCCs for one h, then infecting with GFP-tagged HCMV BADr (100 PFU/well) and measuring GFP levels (RFU) six days after infection. Cytotoxicity (red) was measured in replicate uninfected cultures treated for five days using the CellTiter-Glo® assay. Data are means of three independent experiments ± standard deviations.
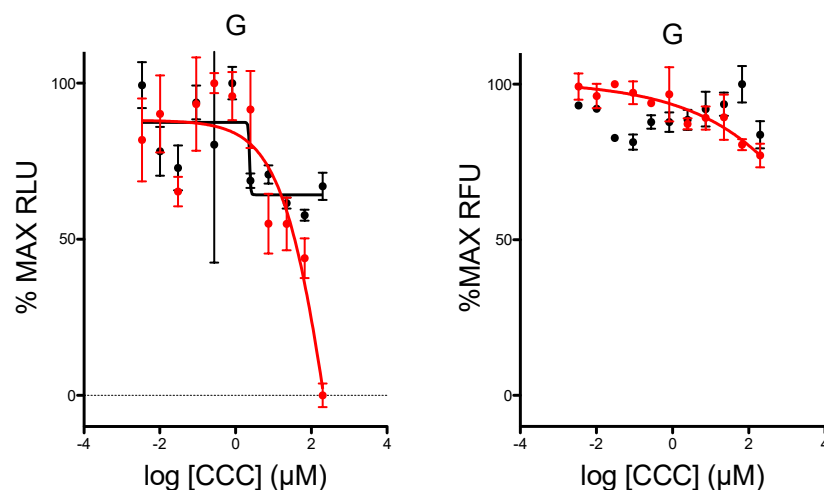
Figure 4.23:Repeated luciferase and GFP-based HCMV antiviral activity of cobalt dimer (G) in fibroblasts. (Left) Anti-HCMV activity (black) was measured by incubating MRC-5 fibroblast monolayers in 96-well plates with compounds for one h, then infecting with luciferase-tagged HCMV RC2626 (125 PFU/well). After five days 50 μL of virus-containing culture medium was transferred to fresh MRC-5 cultures and luciferase activities (RLU) in these cultures were measured 48 h later. (Right) Anti-HCMV activity (black) was measured by incubating confluent monolayers of MRC-5 fibroblasts with CCCs for one h, then infecting with GFP-tagged HCMV BADr (100 PFU/well) and measuring GFP levels (RFU) six days after infection. Cytotoxicity (red) was measured in replicate uninfected cultures treated for five days using the CellTiter-Glo® assay. Data are single replicates.

4.6.4 Mononuclear cobalt compounds do not inhibit viral GFP expression.

Gene expression and entry assays signal the timing of viral inhibition. Heparin, a well-known viral attachment inhibitor, inhibits viral GFP expression only if cells are treated prior to infection. This cobalt series failed to inhibit viral GFP expression if cells are pretreated or treated after infection, indicating they do not inhibit viral attachment or entry, unlike heparin or PPCs (Figure 4.25).
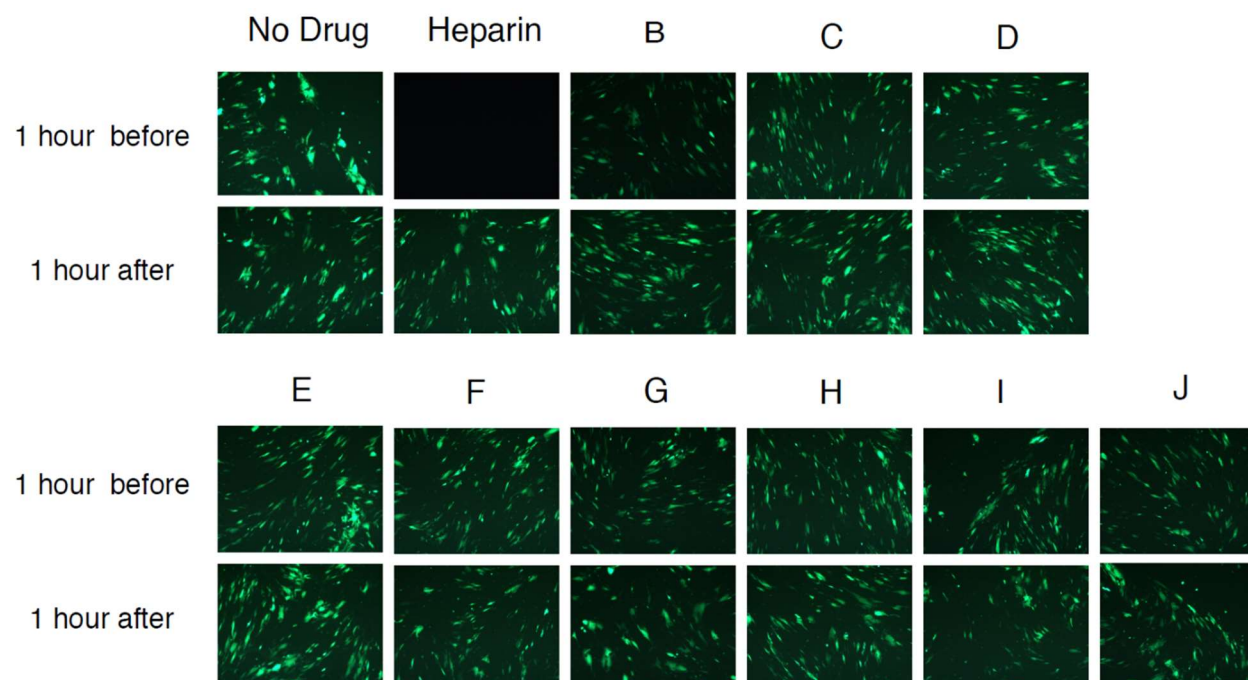
Figure 4.25: CCCs do not inhibit expression of a viral marker protein. Confluent monolayers of MRC-5 fibroblasts in 96-well plates were treated with medium (Ø), 150 µg/ml heparin (HEP), or 25 µM A-G one h before or one h after infection with GFP-tagged HCMV BADr (100 PFU/well). Representative fluorescent micrographs were taken six days post infection.

The mononuclear Co compounds, independent of covalent binding ability varied from 1+ to 3+. In the case of HCMV antiviral activity, we conclude that regardless of covalent binding ability, antiviral activity is not seen even at 4+ or higher charge for Taube's dimer (**G**).

4.6.5 Discussion

Cobalt compounds have a long history of antiviral activity.[62–64] The simplest compound, cobalt hexammine, is well known to have broad spectrum antiviral activity against Sindbis virus, adenovirus, HIV, and Ebola virus but at high millimolar concentrations.[64,65] Importantly, structural modification of cobalt hexammine (*i.e.* macrocyclic, mixed macrocyclic–monodentate, or substitution of a water or chloride for an amine) results in either a lack of or a sharp decrease in its antiviral activity.[65,66] Cobalt hexammine was well tolerated *in vivo and significantly* improved the survival of mice infected with Ebola virus.[67] Cobalt hexammine's mechanism of action remains unknown; however, it does inhibit an early stage of viral replication.[66]

The CTC series of Co compounds are based on a chelating Schiff base and demonstrate broad-spectrum antiviral activity, best demonstrated by CTC-96 (Figure 4.26).[66] CTC-96 is an effective antiviral against HSV-1, adenovirus, vesicular stomatitis virus, and varicella zoster virus.[68,69] CTC-96 targets cell-virus fusion and inhibits cell-to-cell spread and syncytium formation; however, the molecular mechanism is unknown.[68] Importantly, CTC-96 is unlikely to specifically inhibit herpes virus fusion glycoprotein gD as it also inhibits VZV in a similar manner to HSV, yet VZV does not have a gD homologue; this suggests that CTC-96 nonspecifically targets an essential fusogenic apparatus.[68] CTC-96 (Doxovir™) remains the only cobalt compound that has entered clinical trials as an antiviral.[69]
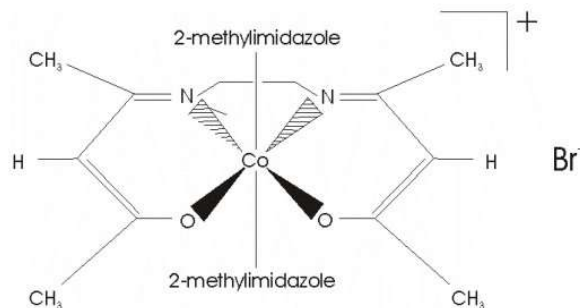
Figure 4.26: Structure of CTC-96.[69]

Consideration of GAGs as targets and receptors for CCCs has led to the description here of the unexpected ability of Co(pentammine) to inhibit heparinase cleavage of FPX (a model for HS) along with associated downstream functions such as inhibition of cellular invasion. In assessing potential antiviral activity, HS is an attractive target but, in the compounds studied here, incipient activity at reasonable concentrations is only seen beginning with the 6+ WC. This series of compounds may lack sufficient charge and length for HS affinity and thus be unable to inhibit viral attachment. Nevertheless, these studies indicate a systematic structure activity study to optimize activity, including polynuclear CCC, is warranted.

4.7 Discussion

The study of WC as well as the mononuclear cobalt series expanded the CCC chemotype. Although the mononuclear series was not active against HCMV, WC has micromolar antiviral activity. Diverging from PPCs, WC does not impact viral attachment, entry, or viral gene expression. WC appears to act at later times, coincident with HCMV capsid assembly, DNA packaging, virion morphogenesis, or egress. Preliminary findings suggest that WC may alter viral DNA packaging, displaying a novel phenotype of half-moon capsids. These conclusions are consistent with the effects produced on DNA by WC, especially with respect to the very efficient nucleic acid condensation and its consequences. However, these conclusions are at odds with late protein expression (pp28 expression), which indicates that there is no significant impact on DNA or its replication to the extent that RNA transcription or protein translation are affected, as seen in previous biophysical assays.[15]

It is possible that WC is inhibiting DNA relaxation by topoisomerase I or decatenation by topoisomerase II, both of which are essential in viral replication.[70] Topoisomerase II cleaves both strands of DNA to alleviate torsional strain produced by replication; HCMV infections induced expression of cellular topoisomerase II, suggesting it as an antiviral target.[71] A number of topoisomerase II inhibitors halt HCMV replication, only some allowed late protein expression.[72–74] Likewise, topoisomerase I cleaves a single strand of DNA to allow for untangling and supercoiling in replication; topoisomerase I inhibitors block viral replication including that of HCMV.[70,72] It is possible that WC inhibits topoisomerase I or II, as some of these inhibitors also inhibit late gene expression.

Still, WC's mechanism of action appears to be more 'DNA-centered' rather than 'HS-centered,' like that of PPCs.[48] Given that the number of half-moon "C" capsids is not decreased compared to the control, it seems unlikely that WC inhibits the any mechanism or enzyme effecting the ability of DNA to enter the capsids. WC may also induce DNA condensation specific to the capsid environment. However, the fact that WC does not inhibit GPCMV and capsid DNA condensation would seem to be a generic

herpesvirus mechanism. This may be an indication that WC is specific for HCMV and not for other herpesviruses; if that is the case, it would have major implications as to its mechanism of action.

Although half-moon capsids seen in TEM are fascinating, there is a concern that the half-moon capsids could be an artifact of cobalt interacting with the fixing or staining agents. Cobalt has been used to stain the nerve cell body in vertebrates and invertebrates in TEM.[75–77] To rule out possible staining artifacts, we plan to perform additional TEM experiments: (1) MRC5 fibroblasts infected one hour after WC treatment, (2) MRC5 fibroblasts infected one hour after cobalt hexammine treatment, (3) infected MRC5 fibroblasts treated with WC two hours prior to fixation, and (4) infected MRC5 fibroblasts treated with cobalt hexammine two hours prior to fixation. As cobalt hexammine does not have anti-HCMV activity and is formally substitution-inert, any observed effect by cobalt hexammine (*e.g.,* half-moon capsids) would not be due to an antiviral activity and would indicate an artifact resulting from interaction between cobalt hexammine and the fixing or staining agents. In the same vein, cells treated with either WC or cobalt hexammine two hours prior to fixing and staining should not contain half-moon capsids as the compounds were not present for the majority of the viral replication cycle. Observation of abnormal capsids would again suggest an artifact of staining rather than an antiviral mechanism.

If the control TEM experiments do not suggest half-moon capsids are a staining artifact, additional experiments can be performed to detail WC's mechanism of action. For example, we can determine if the half-moon C capsids can exit the nucleus and mature into infectious virions. Maribavir, a HCMV antiviral in phase III clinical trials, inhibits UL97, a protein kinase that is required for capsid nuclear egress [78]. In the same TEM experiment as above, with maribavir as a control, nuclear and cytoplasmic capsids can be counted. If WC, like maribavir, inhibits nuclear egress, there will be a marked decrease in capsids in the cytoplasm and an accumulation of capsids in the nucleus.

4.8 Conclusion

It is possible that WC has two independent mechanisms of action: a late-acting MOA apparent at low concentrations, as seen for HCMV, and an early-acting charge-dependent mechanism of action impacting attachment at higher concentrations, as may be the case for adenovirus or SARS-CoV-2. The distinction between the two limiting mechanisms of action (HS or DNA-centered) could reflect an intriguing balance between extracellular (GAG) and intracellular (DNA) binding effects and affinities.[79] In this respect, this aspect is of broad significance and the analogies we have previously made between the phosphate clamp and the arginine fork binding mode on DNA become relevant.[80–82] HS may play a regulatory role by interacting with cationic molecules within the nucleus or by transport of cargo to the nucleus. Precedence for the latter concept comes from studies on cationic antibodies and the polyarginine-based cell penetrating peptides.[83] The interplay of HSPG-mediated cellular accumulation, high-affinity GAG binding, and inherent DNA affinity, and indeed potential virus particle binding, needs to be unraveled to identify long-term approaches to broad spectrum antiviral molecules with specific modes of action. The detailed chemical nature of WC reactions in biological media remains to be elucidated in further studies. Regardless, our considerations of the importance of "noncovalent" interactions (rather than the covalent binding reactions of, for example, cisplatin) in dictating biological effects has expanded the potential for therapeutic applications and demonstrated further unusual properties of formally substitution-inert charged coordination complexes, with hitherto underappreciated but exciting biological activities.

Future work should focus on further detailing WC's mechanism of action, namely the novel packaging phenotype and viral DNA replication. Additionally, WC is a chiral compound and therefore should be examined as its separated enantiomers. Many approved drugs are chiral and some enantiomers are more active than their counterparts. With that in mind, both the anti-HCMV activity and mechanism of action of each enantiomer should be compared to that of racemic mixture. Finally, WC should be evaluated in an animal model. As WC's cytotoxicity is much lower than that of PPCs, it may be a more attractive candidate for *in vivo* study. HCMV cannot infect animals due to the species-specificity of CMV. WC was not active against guinea pig CMV, eliminating its use as an animal model for HCMV. Rhesus macaque (*Macaca mulatta*) CMV (RhCMV) can infect a fetus via transplacental infection and disease progression is similar to that in HCMV, however the expense of rhesus macaques is prohibitive. Mouse CMV is a more viable option; unlike GPCMV and RhCMV, mouse CMV does not cross the placenta to infect the fetus. However, newborn mice brain development corresponds to that of a human fetus in the second trimester thus, infection of newborn mice can model fetal infection and its effect on the central nervous system.[84,85] Although less ideal GPCMV or RCMV, MCMV is a viable option for an animal model for WC.

4.9 Experimental methods

4.9.1 Cell and viral culture

Human MRC-5 fetal lung fibroblasts (ATCC CCL-171), human APRE-19 epithelial cells (derived from retinal pigment epithelium) (ATCC CRL-2302), guinea pig lung fibroblast cells (GPL) (ATCC-CCL158), and human adenocarcinoma epithelial cells (HeLa cells) (ATTC CCL-2) were purchased from American Type Culture Collection. Human Embryonic Kidney Cells (HEK-293T) and HEK-293T expressing human angiotensin-converting enzyme 2 (HEK-293T-hACE2; NR-52511) cells were purchased from BEI Resources. HeLa cells expressing dipeptidyl peptidase 4 (HeLa-DPP4) were a gift from David Namazee. MRC-5, APRE-19, HeLa, HeLa-DPP4, HEK-293T, and HEK-293T-hACE2 cells were cultured at 37°C in a 5% CO_2 atmosphere using Dulbecco's Modified Eagle Medium supplemented with 10% fetal bovine serum, 50 U/mL penicillin, 50 mg/mL streptomycin, and 29.2 mg/mL L-glutamine (DMEM, all from Life Technologies).

Virus BAD*r*UL131-Y4 (BADr), a gift from Dai Wang and Thomas Shenk, is a variant of HCMV strain AD169 that is epithelial tropic due to repair of a mutation in *UL131A* and contains a green-fluorescent protein (GFP) reporter cassette.[86] Virus RC2626 is a variant of HCMV strain Towne that contains an expression cassette for firefly luciferase.[87] RC2626 and BADr were propagated in MRC-5 and ARPE-19 cells, respectively. Guinea pig CMV (GPCMV) with a red fluorescent tag (N13R10r129-TurboFP635) was derived from BAC N13R10r129-TurboFP635; it was propagated in GPL cells.[88] Virus stocks were derived from infected cell culture supernatants, adjusted to 0.2 M sucrose, and stored in liquid nitrogen. Viral titers were determined using MRC-5, ARPE-19, or GPFs as described.[89] Stocks of GFP-tagged adenovirus, provided by Dr. Daniel Conway at Virginia Commonwealth University, were produced using the pAdeasy adenovirus-packaging system as described.[90,91]

4.9.2 Compounds and compound synthesis

BAY 38-4766 was a gift from Bayer Pharmaceuticals, foscarnet (phosphonoformic acid, PFA) was purchased from InvivoGen, and heparin sodium was purchased from Acros Organics (Lot # B0146868). Werner's complex was prepared according to published methods.[92] Letermovir was a gift from Merck & Co., Inc.. BAY 38-4766, PFA, and WC were dissolved in water at a stock concentration of 10 mM. Heparin was dissolved in water at a stock concentration of 1000 μg/mL.

Pentaamminechlorocobalt(III) chloride and hexaamminecobalt(III) chloride were purchased from Sigma-Aldrich (USA). Tris(2,2'-bipyridine)cobalt(III) tris(hexafluorophosphate) was purchased from TCI America (USA). Tris(ethylenediamine)cobalt(III) chloride, *t*-dichlorobis(ethylenediamine)cobalt(III) chloride, and potassium hexacyanocobaltate(III) were synthesized according to published methods.[93–95]

Taube dimer synthesis: This synthesis was adapted from published methods.[96,97] 7.0 grams of ammonium carbonate was dissolved in 20 mL of water. Then 20.0 mL of NH3OH was added. In a separate beaker, 5.0 grams of cobalt (II) sulfate heptahydrate was dissolved in 10 mL of water. With stirring, the ammonium carbonate solution was poured into the beaker containing the cobalt solution. 3 mL of 30% H_2O_2 was slowly added with stirring, and the solution was evaporated to 30-35 mL on a hot plate. The solution should not be heated to boiling. Throughout evaporation 2 g of ammonium carbonate was added in small amounts. The hot solution was vacuum filtered then cooled in an ice bath. Red product crystals were removed with vacuum filtration and washed with a small amount of filtrate. 2.0 grams of the red product crystals were dissolved in 55 mL of 0.3 M H_2SO_4 and CO_2 gas bubbled off. 20-25 mL of EtOH was added in small portions. The precipitate was filtered off, washed with 50% EtOH until free from acid (checked with litmus paper), and air dried. A solution was prepared with the dried precipitate and a small

amount of water. NH$_3$OH was added until pH 8, checked with a pH probe. Then, small portions of EtOH was added until precipitate stopped forming. The solid was collected, and dried in an oven at 110 °C.

4.9.3 Luciferase-based yield assay of anti-HCMV activity

Eleven three-fold serial dilutions of compound were prepared in DMEM; final concentrations ranged from 200 µM to 3.4 nM. Black-wall/clear-bottom 96-well plates with confluent monolayers of MRC-5 cells were treated with different concentrations of each test compound in triplicate. After one h of incubation cells were infected with RC2626 (125 PFU/well). Infected and uninfected wells without compound served as controls. Following incubation for five days 100 µL of culture media was removed from each well and transferred to wells of a fresh 96-well plate containing confluent uninfected MRC-5 cells. Following an additional two-day incubation luciferase activity was measured by removing 100 µL of media and adding 100 µL of Steady-Glo® luciferase substrate (Promega), incubating ten min. at room temperature, and measuring relative luminosity units (RLU) using a BioTek Synergy HT Multi-Mode Microplate reader. Prism 5 software (Graphpad) was used to determine 50% effective concentration (EC$_{50}$) values as the inflection points of best-fit four-parameter curves for RLU (means of triplicate data) versus log inhibitor concentration. Graphical representations were normalized to % maximum RLU.

4.9.4 GFP-based assay of antiviral activity

For HCMV: Confluent monolayers of MRC-5 fibroblasts in 96-well plates were prepared and treated with compound dilutions as described in *4.8.3* above. After one h of incubation cells were infected with virus BADr (100 PFU/well). Following incubation for six days, relative fluorescence units (RFU) of GFP fluorescence were quantified by BioTek Synergy HT Multi-Mode Microplate reader and EC$_{50}$ values were determined as described in *4.8.3*. Graphical representations were normalized to % maximum RFU.

For adenovirus: Confluent monolayers of ARPE-19 cells in 96-well plates were prepared and treated with compound dilutions as described in *4.8.3* above. After one h of incubation cells were infected with GFP-tagged adenovirus (100 PFU/well). Following incubation for five days, relative fluorescence units (RFU) of GFP fluorescence were quantified by BioTek Synergy HT Multi-Mode Microplate reader and EC$_{50}$ values were determined as described in *4.8.3*. Graphical representations were normalized to % maximum RFU.

For GPCMV: Confluent monolayers of GPFs in 96-well plates were prepared and treated with compound dilutions as described in *4.8.3* above. After one h of incubation cells were infected with RFP-tagged GPCMV (100 PFU/well). Following incubation for five days, relative fluorescence units (RFU) of RFP fluorescence were quantified by BioTek Synergy HT Multi-Mode Microplate reader and EC$_{50}$ values were determined as described in *4.8.3*. Graphical representations were normalized to % maximum RFU.

For pseudotyped viruses: Confluent monolayers of HEK-293T-ACE2 or HEK-293T cells in 384-well plates were prepared and treated with compound dilutions as described in *4.8.3* above. After one h of incubation cells were infected with pseudotyped SARS-CoV-2. Following incubation for two days, relative fluorescence units (RFU) of GFP fluorescence were quantified by BioTek Synergy HT Multi-Mode Microplate reader and EC$_{50}$ values were determined as described in *4.8.3*. Gaphical representations were normalized to % maximum RFU.

4.9.5 Cytotoxicity

Replicate MRC-5, ARPE-19, GPFs, or HEK-293T-ACE2 cell cultures were prepared simultaneously with those described in *4.8.3* and *4.8.4* but were not infected. After incubation of five or two days cell viability was determined by removing 100 µL of culture media from each well, adding 100 µL of CellTiter-

Glo® reagent (Promega), incubation for ten minutes at room temperature, and measuring RLU using a BioTek Synergy HT Multi-Mode Microplate reader. 50% cytotoxicity concentrations (TC$_{50}$) were calculated as inflection points of four-parameter curves as described in *4.8.3*. Graphical representations were normalized to % maximum RLU.

4.9.6 Inhibition of GFP expression

Inhibition of GFP expression was evaluated by treating confluent monolayers of MRC-5 cells in black-wall/clear-bottom 96-well plates with compounds for one h before addition of 100 PFU/well virus BADr. Six days after infection representative micrographs were taken with a Nikon Eclipse TS100 Inverted UV microscope.

4.9.7 Detection of viral proteins by immunofluorescence (IFA)

Confluent monolayers of MRC-5 cells in 16-well Nunc™ Lab-Tek™ glass chamber slides (ThermoFisher) were treated with compounds and one h later infected with RC2626 (125 PFU/well). Cells were fixed and stained for detection of HCMV immediate early (IE) proteins 48 h post infection (hpi) or for pp28 late protein 120 hpi. Culture medium was removed and monolayers were fixed with 1% formaldehyde in PBS for 30 min., washed three times with PBS, permeabilized by incubation on ice for 20 minutes with 0.5% Triton-X100 in PBS, washed three times with PBS, then incubated 30 minutes at room temperature in blocking buffer (20% fetal bovine serum in PBS). Fixed cells were then incubated one h at room temperature with primary antibodies to HCMV IE1 and IE2 proteins (MAB810, Millipore Sigma) or to pp28 (CH19, Virusys) diluted 1:600 in blocking buffer. After washing three-four times with blocking buffer, cells were incubated in the dark for one h at room temperature with secondary goat anti-mouse IgG conjugated to Alexa Fluor 488 (Life Technologies) diluted 1:200 in blocking buffer, then washed three-four times with PBS and imaged with a Zeiss Axio Imager 2 and 89-North PhotoFluor LM-75.

4.9.8 Time of addition and treatment/removal studies

Confluent monolayers of MRC-5 cells in black-wall/clear-bottom 96-well plates were infected with RC2626 (100 PFU/well). A single inhibitory concentration of each compound (150 µg/ml heparin, or 25 µM WC, or 8 µM BAY 38-4766) was added to triplicate wells one h before, at the time of, and 3, 6, 12, 24, 48, 72, 96, or 120 hpi. Infected or uninfected wells not treated with compounds served as controls. Following incubation for five days 100 µL of culture media was removed from each well and transferred to wells of a fresh 96-well plate containing confluent uninfected MRC-5 cells. Following an additional two day incubation luciferase activity was measured by removing 100 µL of media and adding 100 µL of Steady-Glo® luciferase substrate (Promega), incubating ten minutes at room temperature, and measuring relative luminosity units (RLU) using a BioTek Synergy HT Multi-Mode Microplate reader. Percent maximum RFUs were plotted versus time of compound addition (relative to infection) using Prism 5 software.

To determine if PPCs act by interacting with cells or with virions, confluent monolayers of MRC-5 fibroblasts were treated with 10 or 25 µM WC, or 300 µg/mL heparin in black-wall/clear-bottom 96-well plates. Compounds were then removed from cells by three washes with DMEM. Treated/washed cells were infected with 100 PFU/well untreated BADr. Six days after infection representative micrographs were taken with a Nikon Eclipse TS100 Inverted UV microscope.

4.9.9 Tandem FIGE and TEM

Field-inversion Gel electrophoresis: Confluent monolayers of MRC-5 fibroblasts in 100 mm dishes were treated with 25 µM WC, 8 µM BAY, or no inhibitor, then infected with HCMV strain AD169 (10^6 PFU). Six

days post infection, cells were washed twice with chilled TE (4°C) then scraped into a conical tube with 5 mL of TE. Cells were pelleted by low speed centrifugation, resuspended in melted (52°C) 1% Seaplaque, and quickly injected into plug molds. After plugs solidified they were removed from the molds, placed in a conical tube with TE, and refrigerated at 4°C. To remove proteins, the TE buffer was decanted and replaced with 1 mg/mL proteinase K in SE buffer (0.5 M EDTA, 1% Sarkosy) and incubated at 52°C for 48 hours. SE buffer was decanted and replaced with TE. The TE buffer was replaced two additional times with a minimum of 1 h 4°C incubations between replacements. Plugs were stored in TE at 4°C.

Plugs were cast into 15 cm x 15 cm 1% Seakem agarose (FMC) gels in 0.5x TBE buffer with precast yeast chromosome MW markers (BioRad DNA Size standards S. cerevisiae; CAT#170-3605). FIGE was performed in a standard gel box with 0.5x TBE buffer circulating through a refrigerated water bath set to stabilize buffer temperature in the gel box at 14°C. The power supply and FIGE controller were set to the following parameters: 120V; starting pulse time = 5 seconds; ending pulse time = 60 seconds; forward to backward ratio = 3:1; run time = 36 hours. At completion, the gel was stained with GelRed according to standard protocol and imaged using UV light.

Transmission electron microscopy: Confluent monolayers of MRC-5 fibroblasts in 100 mm dishes were treated with 25 μM WC, 8 μM BAY, or no inhibitor then infected with AD169 (10^6 PFU). Six days post infection, cells are harvested pelleted in PBS, and fixed at room temperature with the primary fixative (2.5% glutaraldehyde in 0.1M sodium cacodylate buffer). Following initiral fixation, samples are submitted to VCU's microscopy core. Samples are then rinsed with 0.1M cacodylate buffer and undergo an additional fixation with 2% osmium tetroxide in 0.1M cacodylate buffer for one hour. Samples are dehydrated in a graded ethanol series (50%, 70%, 80%, 95% for 5-10 minutes each then 100% ethanol for 10-15 minutes three times) and treated with propylene oxide three times for 10–15 minutes each. Finally samples are infiltrated with 50/50 mix of propylene oxide and EMbed 812 resin mix – 4-6 hours or overnight, infiltrated with pure EMbed 812 resin (Electron Microscopy Sciences, Inc.) mix – 6-8 hours or overnight, and embed in molds, place in 60˚C oven for 2 days.

To image the samples, specimen blocks are sectioned with the Leica EM UC6i Ultramicrotome (Leica Microsystems Inc., Buffalo Grove, IL). A00-900A thick sections on grids, stained with 5% Uranyl acetate and Reynold's Lead Citrate. Samples are viewed with the JEOL JEM-1400 TEM (JEOL USA, Inc.) and imaged with the Gatan OneView digital camera (Gatan Inc, Pleasanton, CA).

4.9.10 Pseudotyping lentivirus

SARS-CoV-2 pseudotyped lentiviruses were prepared as outlined in Crawford et al.[98]

- pHAGE-CMV-Luc2-IRES-ZsGreen-W (BEI catalog number NR-52516): Lentiviral backbone plasmid that uses a CMV promoter to express luciferase followed by an IRES and ZsGreen.
- HDM-Hgpm2 (BEI catalog number NR-52517): lentiviral helper plasmid expressing HIV Gag-Pol under a CMV promoter.
- HDM-tat1b (NR-52518): Lentiviral helper plasmid expressing HIV Tat under a CMV promoter.
- pRC-CMV-Rev1b (NR-52519): Lentiviral helper plasmid expressing HIV Rev under a CMV promoter.

All plasmid DNA preparations were purified by double CeCl banding and kindly provided by Dr. Anton Chestukhin. HEK-293T cells were seaded into 6-well plates overnight to proudce 50%–70% confluency at the time of transfection. Cells were transfected using BioT (Bioland Sci entific LLC) following the

manufacturer's instructions. Each well received the following plasmid mix: 1 µg of pHAGE-CMV-Luc2-IRES-ZsGreen-W (NR-52516), 0.22 µg each of plasmids HDM-Hgpm2 (NR-52517), HDM-tat1b (NR-52518), and pRC-CMV-Rev1b (NR-52519), and 0.34 µg of Spike protein encoding pladmid (SARS-CoV-2 Spike (pGBW-m4137383; Addgene_149541)). Media was changed 18 to 24 h post-transfection. Pseudoviruses were harvested by filtering   the supernatant with a 0.45 µm SFCA low protein-binding filter 60 h post transfection and stocks were stored either 4°C for immediate use or frozen long-term at -80°C. Titers of pseudotyped lentiviruses were determined after a single freeze-thaw. Serially diluted stock was applied to HEK-293T-ACE2 cells and two days post infection, cells were also visually assessed to quantitate the titer of the stock (the lowest dilution with GFP positive cells).

4.10 References

(1)   Paiva, R. E. F.; Peterson, E. J.; Malina, J.; Zoepfl, M.; Hampton, J. D.; Johnson, W. E.; Graminha, A.; Ourahmane, A.; McVoy, M. A.; Brabec, V.; Berners-Price, S. J.; Farrell, N. P. On the Biology of Werner's Complex. *Angew. Chemie Int. Ed.* **2021**, *60* (31), 17123–17130. https://doi.org/10.1002/anie.202105019.

(2)   Ernst, K. H.; Wild, F. R. W. P.; Blacque, O.; Berke, H. Alfred Werner's Coordination Chemistry: New Insights from Old Samples. *Angewandte Chemie - International Edition*. November 11, 2011, pp 10780–10787. https://doi.org/10.1002/anie.201104477.

(3)   Ramberg, P. J. *P. J. Ramberg, Chemical Structure, Spatial Arrangement. The Early History of Stereochemistry 1874 – 1914*; Ashgate Pub.: Burlington, USA, 2003.

(4)   Pope, W. J.; Peachey, S. J. CXIV.—Asymmetric Optically Active Nitrogen Compounds. Dextro- and Lævo-α-Benzylphenylallylmethylammonium Iodides and Bromides.Pdf. *J. Chem. Soc. Transs* **1899**, *57*, 1127.

(5)   Bailar, Jr., J. C. Historical Introduction. In *Coordination Chemistry, ACS Monograph 168*; Martell, A. E., Ed.; Van Nostrand Reinhold: New York, 1971; pp ix–xv.

(6)   Werner, A.; Miolati, A. No Title. *Z. Phys. Chem.* **1893**, *12*, 35–55.

(7)   Werner, A.; Miolati, A. No Title. *Z. Phys. Chem.* **1894**, *14*, 506–521.

(8)   Werner, A.; Miolati, A. No Title. *Z. Phys. Chem.* **1896**, *21*, 225–238.

(9)   Kauffman, G. B. Alfred Werner's Research on Polynuclear Coordination Compounds. *Coord. Chem. Rev.* **1972**, *9*, 339–363.

(10)   Spingler, B.; Scanavy-Grigorieff, M.; Werner, A.; Berke, H.; Lippard, S. J. Crystal Structure Determination of a (μ-Amido)(μ-Hydroxo)(μ-Superoxo)Dicobalt(III) Complex from the Werner Collection.Pdf. *Inorg. Chem.* **2001**, *40*, 1054–1066.

(11)   Kauffman, G. B. Sophus Mads Jorgesen (1837-1914): A Chapter in Coordination Chemistry History. *J. Chem. Educ.* **1959**, *36* (10), 521–527. https://doi.org/10.1021/ed036p521.

(12)   Perkin, W. H.; Pope, W. J.; Wallach, O. CXCVIII.—Optically Active Substances Containing No Asymmetric Atom. 1-Methylcyclohexylidene -4-Acetic Acid. *Trans. Chem. Soc.* **1909**, No. 95, 1789–1802.

(13)   Werner, A. No Title. *Ber. Dtsch. Chem. Ges.* **1914**, *47*, 3087–3094.

(14)   Nguyen, L. A.; He, H.; Pham-Huy, C. Chiral Drugs: An Overview. *Int. J. Biomed. Sci.* **2006**, *2* (2), 85–100.

(15)   de Paiva, R. E. F.; Peterson, E. J.; Malina, J.; Zoepfl, M.; Hampton, J. D.; Johnson, W. E.; Graminha, A.; Ourahmane, A.; McVoy, M. A.; Brabec, V.; Berners-Price, S. J.; Farrell, N. P. On the Biology of Werner's Complex. *Angew. Chemie Int. Ed.* **2021**, *60*, 17123–17130. https://doi.org/10.1002/anie.202105019.

(16)   Farrell, N. P. Medicinal Inorganic Chemistry. New Perspectives and Targets for the Periodic Table. In *Adv. Inorg. Chem. (AINC), Vol. 75. A thematic volume devoted to 'Medicinal Chemistry';* van Eldik, R., Sadler, P. J., Eds.; 2020; pp 57-86.

(17)   Gorle, A. K.; Katner, S. J.; Johnson, W. E.; Lee, D. E.; Daniel, A. G.; Ginsburg, E. P.; von Itzstein, M.; Berners-Price, S. J.; Farrell, N. P. Substitution-Inert Polynuclear Platinum Complexes as Metalloshielding Agents for Heparan Sulfate. *Chem. - A Eur. J.* **2018**, *24* (25), 6606–6616. https://doi.org/10.1002/chem.201706030.

(18)   Peterson, E. J.; Daniel, A. G.; Katner, S. J.; Bohlmann, L.; Chang, C.-W.; Bezos, A.; Parish, C. R.; von Itzstein, M.; Berners-Price, S. J.; Farrell, N. P. Antiangiogenic Platinum through Glycan Targeting. *Chem. Sci.* **2017**, *8* (1), 241–252. https://doi.org/10.1039/C6SC02515C.

(19)   Gorle, A. K.; Haselhorst, T.; Katner, S. J.; Everest-Dass, A. V.; Hampton, J. D.; Peterson, E. J.; Koblinski, J. E.; Katsuta, E.; Takabe, K.; von Itzstein, M.; Berners-Price, S. J.; Farrell, N. P.

Conformational Modulation of Iduronic Acid-Containing Sulfated Glycosaminoglycans by a Polynuclear Platinum Compound and Implications for Development of Antimetastatic Platinum Drugs. *Angew. Chemie - Int. Ed.* **2021**, *60* (6), 3283–3289. https://doi.org/10.1002/anie.202013749.

(20) Belting, M. Heparan Sulfate Proteoglycan as a Plasma Membrane Carrier. *Trends Biochem. Sci.* **2003**, *28* (3), 145–151. https://doi.org/10.1016/S0968-0004(03)00031-8.

(21) Fuchs, S. M.; Raines, R. T. Pathway for Polyarginine Entry into Mammalian Cells. *Biochemistry* **2004**, *43* (9), 2438–2444. https://doi.org/10.1021/bi035933x.

(22) Silva, H.; Frézard, F.; Peterson, E. J.; Kabolizadeh, P.; Ryan, J. J.; Farrell, N. P. Heparan Sulfate Proteoglycan-Mediated Entry Pathway for Charged Tri-Platinum Compounds: Differential Cellular Accumulation Mechanisms for Platinum. *Mol. Pharm.* **2012**, *9* (6), 1795–1802. https://doi.org/10.1021/mp300098t.

(23) Chiodelli, P.; Bugatti, A.; Urbinati, C.; Rusnati, M. Heparin/Heparan Sulfate Proteoglycans Glycomic Interactome in Angiogenesis: Biological Implications and Therapeutical Use. *Molecules* **2015**, *20* (4), 6342–6388. https://doi.org/10.3390/molecules20046342.

(24) Weiss, R. J.; Esko, J. D.; Tor, Y. Targeting Heparin– and Heparan Sulfate–Protein Interactions. *Org Biomol Chem* **2018**, *15* (27), 5656–5668. https://doi.org/10.1039/c7ob01058c.Targeting.

(25) Zoepfl, M.; Dwivedi, R.; Taylor, M. C.; Pomin, V. H.; McVoy, M. A. Antiviral Activities of Four Marine Sulfated Glycans against Adenovirus and Human Cytomegalovirus. *Antiviral Res.* **2021**, *190* (April), 105077. https://doi.org/10.1016/j.antiviral.2021.105077.

(26) Hammond, E.; Li, C. P.; Ferro, V. Development of a Colorimetric Assay for Heparanase Activity Suitable for Kinetic Analysis and Inhibitor Screening. *Anal. Biochem.* **2010**, *396*, 112–116.

(27) Farrell, N. P.; Gorle, A. K.; Peterson, E. J.; Berners-Price, S. J. Metalloglycomics. In *Metallo-Drugs: Development and Action of Anticancer Agents*; Sigel, A., Sigel, H., Freisinger, E., Sigel, R. K. O., Eds.; Walter de Gruyter, GmbH: Belrin, Germany, 2018; pp 109–136.

(28) Bohlmann, L.; Chang, C. W.; Beacham, I.; Von Itzstein, M. Exploring Bacterial Heparinase II Activities with Defined Substrates. *ChemBioChem* **2015**, *16* (8), 1205–1211. https://doi.org/10.1002/cbic.201500081.

(29) Bohlmann, L.; Tredwell, G. D.; Yu, X.; Chang, C. W.; Haselhorst, T.; Winger, M.; Dyason, J. C.; Thomson, R. J.; Tiralongo, J.; Beacham, I. R.; Blanchard, H.; Von Itzstein, M. Functional and Structural Characterization of a Heparanase. *Nat. Chem. Biol.* **2015**, *11* (12), 955–957. https://doi.org/10.1038/nchembio.1956.

(30) Subramani, V. K.; Ravichandran, S.; Bansal, V.; Kim, K. K. Chemical-Induced Formation of BZ-Junction with Base Extrusion. *Biochem. Biophys. Res. Commun.* **2019**, *508* (4), 1215–1220. https://doi.org/10.1016/j.bbrc.2018.12.045.

(31) Thiyagarajan, S.; Rajan, S. S.; Gautham, N. Cobalt Hexammine Induced Tautomeric Shift in Z-DNA: The Structure of d(CGCGCA).d(TGCGCG) in Two Crystal Forms. *Nucleic Acids Res.* **2004**, *32* (19), 5945–5953. https://doi.org/10.1093/nar/gkh919.

(32) Kankia, B. I.; Buckin, V.; Bloomfield, V. A. Hexamminecobalt(III)-Induced Condensation of Calf Thymus DNA: Circular Dichroism and Hydration Measurements. *Nucleic Acids Res.* **2001**, *29* (13), 2795–2801. https://doi.org/10.1093/nar/29.13.2795.

(33) Malina, J.; Farrell, N. P.; Brabec, V. Substitution-Inert Polynuclear Platinum Complexes Act as Potent Inducers of Condensation/Aggregation of Short Single- and Double-Stranded DNA and RNA Oligonucleotides. *Chem. - A Eur. J.* **2019**, *25* (12), 2995–2999. https://doi.org/10.1002/chem.201806276.

(34) Malina, J.; Farrell, N. P.; Brabec, V. Substitution-Inert Trinuclear Platinum Complexes Efficiently Condense/Aggregate Nucleic Acids and Inhibit Enzymatic Activity. *Angew. Chemie - Int. Ed.* **2014**, *53* (47), 12812–12816. https://doi.org/10.1002/anie.201408012.

(35) Malina, J.; Farrell, N. P.; Brabec, V. DNA Condensing Effects and Sequence Selectivity of DNA Binding of Antitumor Noncovalent Polynuclear Platinum Complexes. *Inorg. Chem.* **2014**, *53* (3), 1662–1671. https://doi.org/10.1021/ic402796k.

(36) Malina, J.; Cechova, K.; Brabec, V.; Farrell, N. P. Substitution-Inert Polynuclear Platinum Complexes with Dangling Amines: Condensation/Aggregation of Nucleic Acids and Inhibition of DNA-Related Enzymatic Activitiesˊ. *Inorg. Chem.* **2019**, *58*, 6804–6810. https://doi.org/10.1021/acs.inorgchem.9b00254.

(37) Bloomfield, V. A. DNA Condensation. *Curr. Opin. Struct. Biol.* **1996**, *6* (3), 334–341.

(38) Lucke, F.; Kubo, K.; Tsumoto, K.; Yoshikawa, K. Enhancement and Inhibition of DNA Transcriptional Activity by Spermine: A Marked Difference between Linear and Circular Templates. *FEBS Lett.* **2005**, *579*, 1873–3468.

(39) Peterson, E. J.; Menon, V. R.; Gatti, L.; Kipping, R.; Dewasinghe, D.; Perego, P.; Povirk, L. F.; Farrell, N. P. Nucleolar Targeting by Platinum: P53-Independent Apoptosis Follows RRNA Inhibition, Cell-Cycle Arrest, and DNA Compaction. *Mol. Pharm.* **2015**, *12* (1), 287–297. https://doi.org/10.1021/mp5006867.

(40) Renfrew, A. K.; O'Neill, E. S.; Hambley, T. W.; New, E. J. Harnessing the Properties of Cobalt Coordination Complexes for Biological Application. *Coord. Chem. Rev.* **2018**, *375*, 221–233. https://doi.org/10.1016/j.ccr.2017.11.027.

(41) Bykchov, S.; Kharlamova, V. Study of Complexes of Sulfoglycosoamnioglycans with Hexamine Cobalt(III). *Bull. Exper. Biol. Med.* **1974**, *78*, 28–31.

(42) Vouras, M.; Schubert, M. The Outer Sphere Association of Chondroitin Sulfate with Polyvalent Complex Cations. *J. Am. Chem. Soc.* **1957**, *79* (4), 792–795. https://doi.org/10.1021/ja01561a004.

(43) Farber, S. J.; Schubert, M.; Schuster, N. The Binding of Cations by Chondroitin Sulfate. *J. Clin. Invest.* **1957**, *36*, 1715–1722.

(44) Graham, H.; Williams, J. Quantitative Aspects of the Interaction of Carrageenan and Other Hydrocolloids with Polyvalent Cobalt Complexes. *J. Food Sci.* **1966**, *31*, 362-372.

(45) Parada, J.; Larrazábal, G.; Aguirre, P.; Zolezzi, S.; Vega, C.; Garrido, C. The Stereoselective Synthesis of the Werner Complex with Substoichiometric Sugars. *J. Chil. Chem. Soc.* **2008**, *53* (1), 1390–1392. https://doi.org/10.4067/S0717-97072008000100012.

(46) Bhave, S.; Elford, H.; McVoy, M. A. Ribonucleotide Reductase Inhibitors Hydroxyurea, Didox, and Trimidox Inhibit Human Cytomegalovirus Replication in Vitro and Synergize with Ganciclovir. *Antiviral Res.* **2013**, *100* (1), 151–158. https://doi.org/10.1016/j.antiviral.2013.07.016.

(47) Compton, T.; Nowlin, D. M.; Cooper, N. R. Initiation of Human Cytomegalovirus Infection Requires Initial Interaction with Cell Surface Heparan Sulfate. *Virology* **1993**, *193* (2), 834–841. https://doi.org/10.1006/viro.1993.1192.

(48) Shoup, M.; Ourahmane, A.; Ginsburg, E. P.; Farrell, N. P.; Mcvoy, M. A. Substitution-Inert Polynuclear Platinum Compounds Inhibit Human Cytomegalovirus Attachment and Entry. *Antiviral Res.* **2020**, *184*, 104957.

(49) Reefschlaeger, J.; Bender, W.; Hallenberger, S.; Weber, O.; Eckenberg, P.; Goldmann, S.; Haerter, M.; Buerger, I.; Trappe, J.; Herrington, J. A.; Haebich, D.; Ruebsamen-Waigmann, H. Novel Non-Nucleoside Inhibitors of Cytomegaloviruses (BAY 38-4766): In Vitro and in Vivo Antiviral Activity and Mechanism of Action. *J. Antimicrob. Chemother.* **2001**, *48*, 757–767. https://doi.org/10.1093/jac/48.6.757.

(50) Meesing, A.; Razonable, R. R. New Developments in the Management of Cytomegalovirus Infection After Transplantation. *Drugs* **2018**, *78* (11), 1085–1103. https://doi.org/10.1007/s40265-018-0943-1.

(51) Mcvoy, M. A.; Adler, S. P. Human Cytomegalovirus DNA Replicates after Early Circularization by Concatemer Formation, and Inversion Occurs within the Concatemer. *J. Virol.* **1994**, *68* (2), 1040–

1051.

(52)   Tandon, R.; Mocarski, E. S.; Conway, J. F. The A, B, Cs of Herpesvirus Capsids. *Viruses* **2015**, *7*, 899–914. https://doi.org/10.3390/v7030899.

(53)   Muller, C.; Alain, S.; Baumert, T. F.; Ligat, G.; Hantz, S. Structures and Divergent Mechanisms in Capsid Maturation and Stabilization Following Genome Packaging of Human Cytomegalovirus and Herpesviruses. *Life* **2021**, *11*, 150. https://doi.org/10.3390/life11020150.

(54)   Birren, B.; Lai, E. *Pulsed Field Gel Electrophoresis: A Practical Guide*; Academic Press Inc.: San Diego, CA, 1993.

(55)   Hazelton, P. R.; Gelderblom, H. R. Electron Microscopy for Rapid Diagnosis of Emerging Infectious Agents. *Emerg. Infect. Dis.* **2003**, *9* (3), 294–303. https://doi.org/10.3201/eid0903.020327.

(56)   Roingeard, P.; Raynal, P. I.; Eymieux, S.; Blanchard, E. Virus Detection by Transmission Electron Microscopy: Still Useful for Diagnosis and a plus for Biosafety. *Rev. Med. Virol.* **2019**, *29* (1), 1–9. https://doi.org/10.1002/rmv.2019.

(57)   Risco, C.; De Castro, I. F.; Sanz-Sánchez, L.; Narayan, K.; Grandinetti, G.; Subramaniam, S. Three-Dimensional Imaging of Viral Infections. *Annu. Rev. Virol.* **2014**, *1* (1), 453–473. https://doi.org/10.1146/annurev-virology-031413-085351.

(58)   Goldner, T.; Hewlett, G.; Ettischer, N.; Ruebsamen-schaeff, H.; Zimmermann, H.; Lischka, P. The Novel Anticytomegalovirus Compound AIC246 (Letermovir) Inhibits Human Cytomegalovirus Replication through a Specific Antiviral Mechanism That Involves the Viral Terminase. *J. Virol.* **2011**, *85* (20), 10884–10893. https://doi.org/10.1128/JVI.05265-11.

(59)   Katner, S. J.; Johnson, W. E.; Peterson, E. J.; Page, P.; Farrell, N. P. Comparison of Metal-Ammine Compounds Binding to DNA and Heparin. Glycans as Ligands in Bioinorganic Chemistry. *Inorg. Chem.* **2018**, *57* (6), 3116–3125. https://doi.org/10.1021/acs.inorgchem.7b03043.

(60)   Borer, L. L.; Russell, J. G.; Settlage, R. E.; Bryant, R. G. Experiments with Tris(Ethylenediamine)Cobalt(III) Compounds: 59Co NMR and the Resolution of Enantiomeric [Co(En)3] 3+ Ion and Analysis by Formation of Diastereomeric Ion Pairs. *J Chem Ed* **2002**, *79* (4), 494.

(61)   Hulett, M. D.; Freeman, C.; Hamdorf, B. J.; Baker, R. T.; Harris, M. J.; Parish, C. R. Cloning of Mammalian Heparanase , an Important Enzyme in Tumor Invasion and Metastasis. *Nat. Med.* **1999**, *5* (7), 803–809.

(62)   de Paiva, R. E.; Neto, A. M.; Santos, I. A.; Jardim, A. C. G.; Corbi, P. P.; Bergamini, F. What Is Holding Back the Development of Antiviral Metallodrugs? A Literature Overview and Implications for SARS-CoV-2 Therapeutics and Future Viral Outbreaks. *Dalt. Trans.* **2020**, *49*, 16004–16033. https://doi.org/10.1039/D0DT02478C.

(63)   Hutchinson, D. W. Metal Chelators as Potential Antiviral Agents. *Antiviral Res.* **1985**, *5*, 193–205.

(64)   Chang, E. L.; Simmers, C.; Knight, D. A. Cobalt Complexes as Antiviral and Antibacterial Agents. *Pharmaceuticals* **2010**, *3* (6), 1711–1728. https://doi.org/10.3390/ph3061711.

(65)   Knight, D. A.; Hickey, T. E.; Bongard, J. E.; Thach, D. C.; Yngard, R.; Chang, E. L. Differential Effects of Co (III), Ni (II), and Ru (III) Amine Complexes on Sindbis Virus. *J. Inorg. Biochem.* **2010**, *104*, 592–598. https://doi.org/10.1016/j.jinorgbio.2010.01.012.

(66)   Delehanty, J. B.; Bongard, J. E.; Thach, D. C.; Knight, D. A.; Hickey, T. E.; Chang, E. L. Antiviral Properties of Cobalt(III)-Complexes. *Bioorganic Med. Chem.* **2008**, *16*, 830–837. https://doi.org/10.1016/j.bmc.2007.10.022.

(67)   Chang, E. L.; Olinger, G. G.; Hensley, L. E.; Lear, C. M.; Scully, C. E.; Mankowski, M. K.; Ptak, R. G.; Thach, D. C.; Knight, D. A. Hexamminecobalt (III) Chloride as Broad Spectrum Antiviral Complex. *Jounral Antivirals Antiretrovir.* **2011**, *3*, 020–027.

(68)   Schwartz, J. A.; Lium, E. K.; Silverstein, S. J. Herpes Simplex Virus Type 1 Entry Is Inhibited by the Cobalt Chelate Complex CTC-96. *J. Virol.* **2001**, *75* (9), 4117–4128.

https://doi.org/10.1128/jvi.75.9.4117-4128.2001.

(69) Epstein, S. P.; Pashinsky, Y. Y.; Gershon, D.; Winicov, I.; Srivilasa, C.; Kristic, K. J.; Asbell, P. A. Efficacy of Topical Cobalt Chelate CTC-96 against Adenovirus in a Cell Culture Model and against Adenovirus Keratoconjunctivitis in a Rabbit Model. *BMC Ophthalmol.* **2006**, *6* (22), 1–11. https://doi.org/10.1186/1471-2415-6-22.

(70) Packard, J. E.; Dembowski, J. A. HSV-1 DNA Replication—Coordinated Regulation by Viral and Cellular Factors. *Viruses* **2021**, *13*, 1–15.

(71) Benson, J. D.; Huang, E. S. Human Cytomegalovirus Induces Expression of Cellular Topoisomerase II. *J. Virol.* **1990**, *64* (1), 9–15. https://doi.org/10.1128/jvi.64.1.9-15.1990.

(72) Maschera, B.; Ferrazzi, E.; Rassu, M.; Toni, M.; Palu, G. Evaluation of Topoisomerase Inhibitors as Potential Antiviral Agents. *Antivir. Chem. Chemother.* **1993**, *4* (2), 85–91. https://doi.org/10.1177/095632029300400202.

(73) Huang, E.-S.; Benson, J. D.; Huong, S.; Wilson, B.; van der Horst, C. Irreversible Inhibition of Human Cytomegalovirus Replication by Topoisomerase II Inhibitor, Etoposide: A New Strategy for the Treatment of Human Cytomegalovirus Infection. *Antiviral Res.* **1992**, *17* (1), 17–32.

(74) Benson, J. D.; Huang, E. S. Two Specific Topoisomerase II Inhibitors Prevent Replication of Human Cytomegalovirus DNA: An Implied Role in Replication of the Viral Genome. *J. Virol.* **1988**, *62* (12), 4797–4800. https://doi.org/10.1128/jvi.62.12.4797-4800.1988.

(75) Pittman, R. M.; Cohen, C. D.; Tweedle, M. J. Branching of Central Neurons: Intracellular Cobalt Injection for Light and Electron Microscopy. *Science (80-.).* **1972**, *176* (4033), 412–414.

(76) Hausen, K.; Wolburg-Buchholz, K. An Improved Cobalt Sulfide-Silver Intensification Method for Electron Microscopy. *Brain Res.* **1980**, *187* (2), 462–466.

(77) Antal, M. The Application of Cobalt Labelling to Electron Microscopic Investigations of Serial Sections. *J. Neurosci. Methods* **1984**, *12* (1), 69–77.

(78) Piret, J.; Boivin, G. Clinical Development of Letermovir and Maribavir: Overview of Human Cytomegalovirus Drug Resistance. *Antiviral Res.* **2019**, *163* (January), 91–105. https://doi.org/10.1016/j.antiviral.2019.01.011.

(79) Stewart, M. D.; Sanderson, R. D. Heparan Sulfate in the Nucleus and Its Control of Cellular Functions. *Matrix Biol.* **2014**, *35*, 56–59. https://doi.org/10.1016/j.matbio.2013.10.009.Heparan.

(80) Komeda, S.; Moulaei, T.; Woods, K. K.; Chikuma, M.; Farrell, N. P.; Williams, L. D. A Third Mode of DNA Binding: Phosphate Clamps by a Polynuclear Platinum Complex. *J. Am. Chem. Soc.* **2006**, *128* (50), 16092–16103. https://doi.org/10.1021/ja062851y.

(81) Komeda, S.; Qu, Y.; Mangrum, J. B.; Hegmans, A.; Williams, L. D.; Farrell, N. P. The Phosphate Clamp as Recognition Motif in Platinum–DNA Interactions. *Inorganica Chim. Acta* **2016**, *452*, 25–33. https://doi.org/10.1016/j.ica.2016.04.052.

(82) Calnan, B. J.; Tidor, B.; Biancalana, S.; Hudson, D.; Frankel, A. D. Arginine-Mediated RNA Recognition: The Arginine Fork. *Science (80-.).* **1991**, *252* (5009), 1167–1171.

(83) Naik, R. J.; Chatterjee, A.; Ganguli, M. Different Roles of Cell Surface and Exogenous Glycosaminoglycans in Controlling Gene Delivery by Arginine-Rich Peptides with Varied Distribution of Arginines. *Biochim. Biophys. Acta - Biomembr.* **2013**, *1828* (6), 1484–1493. https://doi.org/10.1016/j.bbamem.2013.02.010.

(84) Reddehase, M. J.; Lemmermann, N. A. W. Mouse Model of Cytomegalovirus Disease and Immunotherapy in the Immunocompromised Host: Predictions for Medical Translation That Survived the "Test of Time." *Viruses* **2018**, *10* (12), 693. https://doi.org/10.3390/v10120693.

(85) Fisher, M. A.; Lloyd, M. L. A Review of Murine Cytomegalovirus as a Model for Human Cytomegalovirus Disease—Do Mice Lie? *Int. J. Mol. Sci.* **2021**, *22* (1), 1–19. https://doi.org/10.3390/ijms22010214.

(86) Wang, D.; Shenk, T. Human Cytomegalovirus UL131 Open Reading Frame Is Required for

Epithelial Cell Tropism. *J. Virol.* **2005**, *79* (16), 10330–10338. https://doi.org/10.1128/jvi.79.16.10330-10338.2005.

(87) McVoy, M. A.; Mocarski, E. S. Tetracycline-Mediated Regulation of Gene Expression within the Human Cytomegalovirus Genome. *Virology* **1999**, *258* (2), 295–303. https://doi.org/10.1006/viro.1999.9724.

(88) Bierle, C. J.; Anderholm, K. M.; Wang, B. J.; McVoy, M. A.; Schleiss, M. R. Targeted Mutagenesis of Guinea Pig Cytomegalovirus Using CRISPR/ Cas9-Mediated Gene Editing. *J. Virol.* **2016**, *90* (15), 6989–6998. https://doi.org/10.1128/JVI.00139-16.Editor.

(89) Cui, X.; Adler, S. P.; Davison, A. J.; Smith, L.; Habib, E. S. E.; McVoy, M. A. Bacterial Artificial Chromosome Clones of Viruses Comprising the Towne Cytomegalovirus Vaccine. *J. Biomed. Biotechnol.* **2012**, *2012*, 428498. https://doi.org/10.1155/2012/428498.

(90) Xiao, K.; Allison, D. F.; Buckley, K. M.; Kottke, M. D.; Vincent, P. A.; Faundez, V.; Kowalczyk, A. P. Cellular Levels of P120 Catenin Function as a Set Point for Cadherin Expression Levels in Microvascular Endothelial Cells. *J. Cell Biol.* **2003**, *163* (3), 535–545. https://doi.org/10.1083/jcb.200306001.

(91) He, T.-C.; Zhou, S.; da Costa, L. T.; Yu, J.; Kinzler, K. W.; Vogelstein, B. A Simplified System for Generating Recombinant Adenoviruses. *PNAS* **1998**, *95* (March), 2509–2514.

(92) Bernal, I.; Cetrullo, J.; Berhane, S. The Crystal and Molecular Structures of Two Derivatives of Werner's Hexol Cluster Cation: [Co{(OH)2Co(NH3)4}3](NO3)5 (OH) · 4H2O(I) and [Co{(OH)2Co(NH3)4}3](NO3)6 · 2H2O(II). *J. Coord. Chem.* **2000**, *52* (2), 185–205. https://doi.org/https://doi.org/10.1080/00958970008022586.

(93) Broomhead, J. A.; Dwyer, F. P.; Hogarth, J. W. *Inorganic Synthesis*; McGraw–Hill: New York, 1960; Vol. 6.

(94) Bailar, Jr., J. C. *Inorganic Synthesis, Vol. 2*; 1946.

(95) Poskozim, P. S. The Preparation of Potassium Hexacyanocobaltate(III). *J. Chem. Educ.* **1969**, *46*, 384–385.

(96) Greenway, A.; Lancashine, R. Cobalt (III) Ammines- "Werner" Complexes. *J. Chem. Educ.* **1892**, *59* (5), 419–420.

(97) Hoffman, A.; Taube, H. The Reduction of Some U-Hydroxo-Cobaltammines. *Inorg. Chem.* **1968**, *7* (5), 903–908.

(98) Crawford, K. H. D. K. H. D.; Eguia, R.; Dingens, A. S. A. S.; Loes, A. N. A. N. A. N.; Malone, K. D. K. D.; Wolf, C. R. C. R.; Chu, H. Y. H. Y.; Tortorici, M. A. A.; Veesler, D.; Murphy, M.; Pettie, D.; King, N. P. N. P.; Balazs, A. B. A. B.; Bloom, J. D. J. D. Protocol and Reagents for Pseudotyping Lentiviral Particles with SARS-CoV-2 Spike Protein for Neutralization Assays. *Viruses* **2020**, *12* (5), 513. https://doi.org/10.3390/v12050513.

CHAPTER 5: Flipping the Coin: Broad-spectrum antiviral activity and mechanism of action for marine sulfated glycans

5.0 Contributions

This chapter is a summary of two published papers and a draft paper. The contributions are as follows:

Antiviral activities of four marine sulfated glycans against adenovirus and human cytomegalovirus by Mary Zoepfl, Rohini Dwivedi, Maggie C. Taylor, Vitor H. Pomin, and Michael A. McVoy.[1] RH and MT isolated and purified the marine sulfated glycans. MZ performed antiviral studies.

Fractionation of sulfated galactan from the red alga Botryocladia occidentalis separates its anticoagulant and anti-SARS-CoV-2 properties by Seon Beom Kim, Mary Zoepfl, Priyanka Samanta, Fuming Zhang, Ke Xia, Reena Thara, Robert J. Linhardt, Robert J. Doerksen, Michael A. McVoy, and Vitor H. Pomin.[2] SBK undertook most of the work by extracting, purifying, and depolymerizing BoSG, fractionated BoSG oligos, conducted all NMR experiments, and performed the anticoagulant assays. PS performed the computational analysis. FZ performed the SPR analysis. KX performed the top-down analysis. RT assisted SBK in almost all experiments. MZ conducted antiviral studies.

Draft paper: "Selective antiviral inhibition by marine sulfated glycans." Dr. Vitor Pomin and his lab performed all isolation, purification, and structural analysis on the marine sulfated glycans. Anton Chestukhin provided all plasmids and the soluble ACE2. MZ performed antiviral studies.

5.1 General Background

Targeting either cellular HS or viral glycoproteins will disrupt the HS-viral interaction and prevent infection. A variety of compounds have been used to bind to HS and shield cells from viral attachment including polycationic peptides, small organic molecules, and inorganic molecules; however, none have cleared clinical trials. As detailed in the previous chapters, we have developed a series of inorganic small molecules which target HS to inhibit viral attachment with broad-spectrum activity. Alternatively a compound may bind surface viral glycoproteins, effectively sequestering the virions away from the cell and acting like neutralizing antibodies.[3] The majority of these compounds are HS mimetics, many of which have broad spectrum antiviral activity. The largest issue of these mimetics is anticoagulant activity or related side effects and *in vivo* half-life.

This chapter details a collaboration with Dr. Vitor H. Pomin from University of Mississippi. Dr. Pomin has studied the structure and biological functions of marine glycans for two decades; specifically, he has developed advanced structure-activity relationships for the anticoagulant effects of marine glycans. In this collaboration, we aimed to test marine glycans for antiviral activity, determine their mechanism of action, and develop structure-activity relationships to balance the anticoagulation effects and antiviral activity.

5.1.1 Coagulation and Heparin

Hemostasis, the arrest of bleeding, is in a constant balance of pro- and anticoagulation as both uncontrolled bleeding and uncontrolled clotting are fatal. Coagulation can generally be separated into a physical process, which leads to the formation of a platelet plug, and a chemical process, which leads to the formation of fibrin polymers (Figure 5.1).[4]
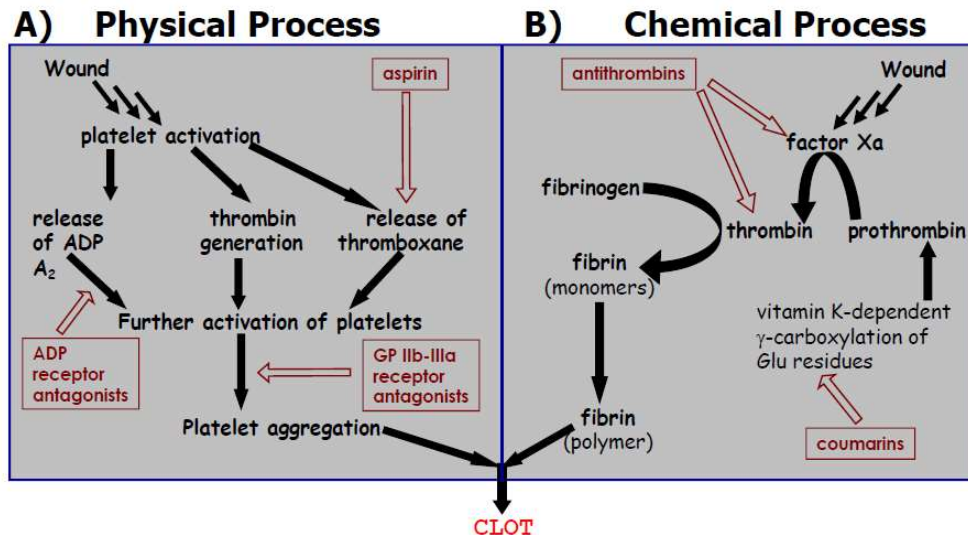
Figure 5.1: Overview of coagulation.[4] The physical process of clotting (A) begins with platelet activation and leads to their aggregations into a platelet plug. The chemical process (B) ultimately leads to the activation of factor Xa and formation of fibrin polymers. Together, these processes lead to the formation of a clot. Reproduced from Desai et al. 2004.

Briefly, platelet plug formation, or primary coagulation, begins with platelet adhesion following a vascular injury; von Willebrand factor (vWF), a glycoprotein, binds collagen from damaged endothelial cells and the platelet glycoprotein complex I receptor on the platelet, forming a bridge. This triggers a morphological change in the platelet which becomes irregular. Activated platelets then release α granules, containing P-selectin, fibrinogen, fibronectin, factor V, factor VIII, platelet factor IV, platelet-derived growth factor and tumor growth factor-α (TGF-α), and δ granules or Dense granules containing adenosine triphosphate (ATP), adenosine diphosphate (ADP), calcium (Ca^{2+}), serotonin, histamine and epinephrine. Activated platelets also release thromboxane A2, further promoting platelet aggregation and ultimately forming the platelet plug to temporarily seal the vascular injury.[5]

The chemical process, or secondary coagulation, can be separated into intrinsic and extrinsic pathways, both of which converge on factor X activation (Figure 5.2). The extrinsic pathway is activated by extracellular tissue factor (TF); under normal physiological conditions, TF is expressed in endothelial cells and would not come into contact with plasma procoagulation factors. TF activates factor VII then factor VIIa with calcium activate factor X. The intrinsic pathway runs parallel and begins with the activation of factor XII by HMW kininogen. Factor XIIa activates factor XI and in turn, factor XIa activates factor IX. Concurrently, factor VIII is activated by factor IIa (thrombin). The combination of IXa, calcium, and VIIIa activate factor X. Factor Xa catalyzes the activation of factor II (prothrombin) to factor IIa (thrombin). Thrombin generation promotes the activation of fibrinogen to fibrin monomers and also activates XIII (fibrin stabilization factor), which covalently links fibrins monomers to polymers and strengthens the platelet plug. Numerous positive feedback loops amplify this cascade and continuously promote the binding of thrombin and platelets.[5]
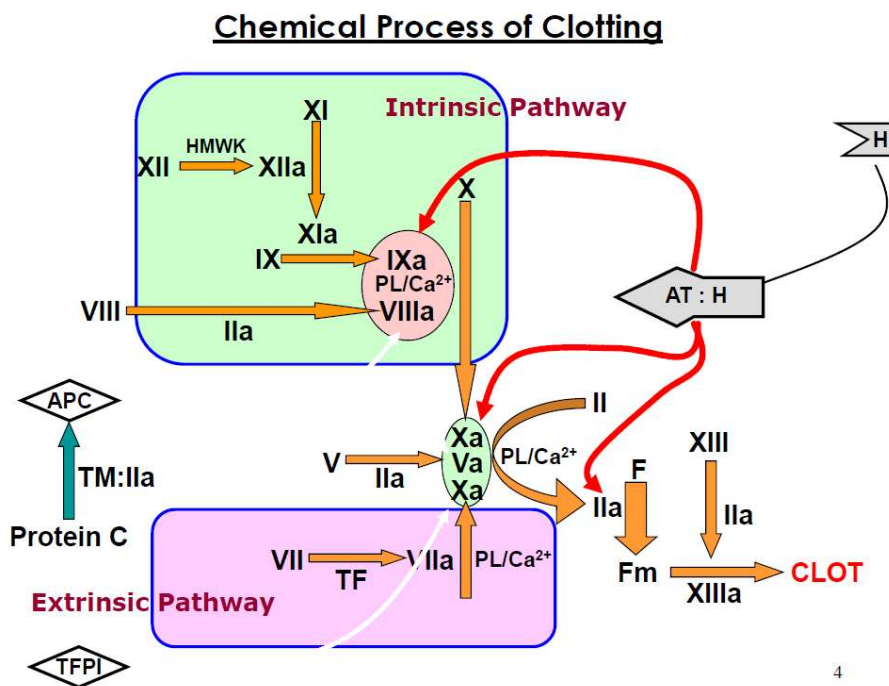
Figure 5.2: Chemical process of clotting.[4] Abbreviations are as follows: Antithrombin (AT), heparin (H), tissue factor (TF), tissue Factor Pathway Inhibitor (TFPI), activated protein C (APC), fibrin (F), Thrombomodulin (TM), and anticoagulation factors are denoted by their numerals; an "a" indicates they have been activated. Reproduced from Desai et al. 2004.

When properly balanced, coagulation seals wounds and saves lives. However, when improperly balanced, either due to a genetic disorder or traumatic injury, either excessive bleeding or clotting can be fatal. The human body has natural anticoagulation factors. The TF plasminogen inhibitor slows the extrinsic pathway by inhibiting TF from binding factor VIIa. The protein C pathway contains a series of proteins which inhibit factor Va, VIIIa, and IIa (thrombin). Antithrombin, however, is the main inhibitor of factor IIa (thrombin) and factor Xa; it is a serine protease inhibitor, catalyzed by heparin. Heparin is a heterogenous polysaccharide, existing in low quantities *in vivo* but also isolated from pigs and licensed by the FDA (Figure 5.3).[6] A pentasaccharide sequence within heparin binds specifically to antithrombin and is the only segment with anticoagulant activity. In two distinct mechanisms, the heparin-antithrombin complex inhibits factor Xa and IIa (thrombin). When the pentasaccharide sequence binds antithrombin, antithrombin undergoes a conformational change that is better recognized by factor Xa.[4] Thrombin inhibition, while aided by the conformational change, also requires the full-length heparin to serve as a bridge to increase binding.[4] These pathways provide the balance of hemostasis. Just as any medication can affect metabolism, a therapeutic drug can also shift the balance of hemostasis and therefore it is essential to consider a compound's pro- or anticoagulant activity along with its desired effect.
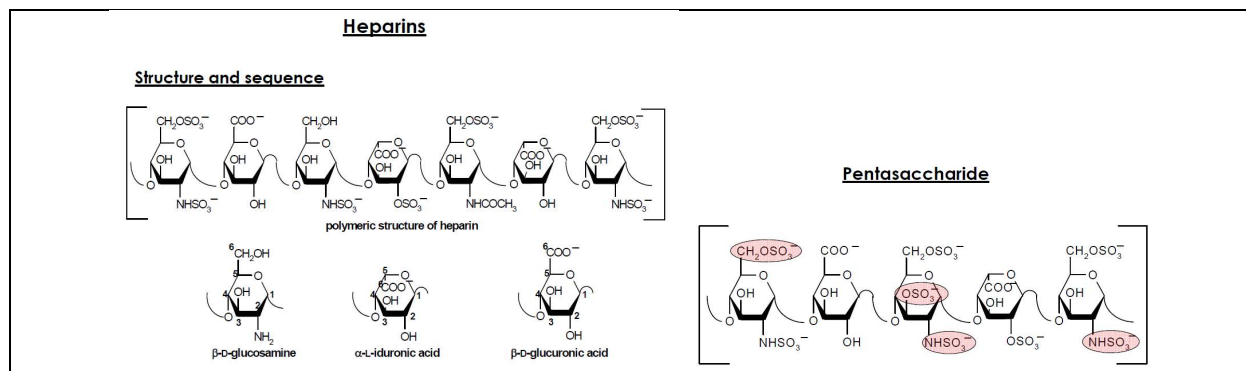
Figure 5.3: Heparin and the pentasaccharide.[4]

5.1.2 Structural and functional characterization of marine sulfated glycans

Like the algal glycans described in Chapter 1, marine glycans are naturally polyanionic, which allows them to electrostatically interact with important proteins and other biomolecules. Also similar to algal glycans, they are nontoxic, inexpensive, and biocompatible.[7] Unlike algal glycans, marine glycans tend to have more regular structures, allowing the development of structure-activity relationships. Although much of their interactions are due to electrostatic interactions in which sulfation content is the largest determinant, the overall structural features of marine glycans (*i.e.* pattern of sulfation glycosylation, anomeric and enantiomeric configurations, glycosidic linkage position, monosaccharide type and composition) are more influential.[8] Pomin et al. have characterized and described the structures of approximately 20 new sulfated galactans (SGs), sulfated fucans (SFs), and GAGs and screened many for anticoagulant effects.[8–15] Curiously, sulfation level did not correlate with anticoagulant activities; SGs and SFs with near equal sulfation level but a different pattern had different anticoagulation activity, suggesting that charge density alone is not the structural determinant for the anticoagulation activity of glycans. With further investigation of regularly-structured marine glycans, Pomin et al. determined that certain structural combinations of sulfation and glycosylation are required for anticoagulant effects.[8,16,17]

Marine glycans are structurally distinct from their mammalian counterparts, resulting in differing activities. For instance, dermatan sulfate (DS) from ascidian species *Styela plicata* (SpDS) is composed of [→4)-α-L-IdoA-(2R1,3R2)-(1→3)-β-D-GalNAc-(4R3,6R4)-(1→]n where the R1, R2, R3, and R4 are sulfate groups at 66, < 5, 94, and 6 percent, respectively.[18] SpDS is mostly 2-sulfated at the IdoA unit but largely 4-sulfated at the GalNAc unit, whereas mammalian DS sulfation is primarily at 2-sulfated IdoA units together with occasional C4 sulfation at GalNAc units. Similarly, fucosylated chondroitin sulfate (FucCS) isolated from sea-cucumbers is composed of {→3)-β-D-GalNAc-(1→4)-[α-L-Fucp-(1→3)]-β-D-GlcA-(1→}n, in which the branching Fucp unit can be sulfated at the 2, and/or 3, and/or 4-positions within different percentages according to the species of occurrence.[14] Mammalian CS is composed of [→4)-β-D-GlcA-(1→3)-β-D-GalNAc-(1→]n, in which the GalNAc units can be either mostly 4-sulfated (CS-A) or predominantly 6-sulfated (CS-C).[19] Differing structures allows for different biological activities.

As described above, procoagulation proteases (*i.e.,* factor IIa and Xa) are inhibited by serpins (serine protease inhibitors, *e.g.* antithrombin and heparin cofactor II). Heparin's anticoagulation properties are serpin-dependent. Like heparin, the majority of the marine glycans studied by Pomin and others exhibit serpin-dependent anticoagulation effects depending on their structural features: the ascidian DS,[18,20,21] the sea-cucumber FucCS,[10,22] the algal SFs and SGs,[10,23,24] and the invertebrate SFs and SGs.[16,17,23] Exceptions exist: FucCS from the sea-cucumber *Ludwigothurea grisea* (LgFucCS) and the SG from the red alga *Botryocladia occidentalis* (BoSG) exhibit a serpin-independent anticoagulant mechanism.[25,26] LgFucCS and BoSG inhibit the formation of blood cofactor complexes at the cell surface,

preventing factor Xa and IIa generation by inhibiting the activation of tenase and prothrombinase complexes, which activate factor X and II respectively.[25,26] This mechanism of action has also been observed in other SGs but clear structure-activity relationships have yet to be established.[27]

Serpin-dependent anticoagulation structure-activity relationships have been established; they rely on sugar type, sulfation percentage and stereospecificity, and branching. SF from *Strongylocentrotus franciscanus* (SfSF) and the SG from *Echinometra lucunter* (ElSG) are homopolysaccharides that differ only on sugar type (Fucp or Galp respectively) with the same 2-sulfation pattern, anomeric, and glycoside linkages.[28] However, ElSG exhibits significant anticoagulant activity (20 IU mg, ten-fold less than unfractionated heparin) as compared to SfSF (~2 IU/mg) as measured by the activated partial thromboplastin time (aPTT) method.[15] In partial explanation, SfSF exclusively inhibits the factor Xa/antithrombin system while ElSG inhibits both the factor Xa/antithrombin and the factor IIa/HCII systems, suggesting that biological effect is dependent on sugar-type.[29] Similarly, algal SGs from the red algae *Botryocladia occidentalis* (BoSG) and *Gelidium crinale* (GcSG) have identical backbones and differ only in their sulfation pattern.[24,30] However, they have a 30% difference in anticoagulant activity, indicating the anticoagulant activity is proportional to their sulfation content. The stereospecificity of marine glycans is important for anticoagulant activity.[8,10,11] The site of sulfation has an essential influence on anticoagulant activity as demonstrated by 2,4-disulfated units in 3-link α-L-fucans which amplify antithrombin-mediated anticoagulant activity. This is also seen in 4-sulfation, which enhances HCII inhibition of factor IIa while 2-sulfation decreases this activity.[10] Similarly, ascidian DS from *Styela plicata* and *Halocynthia pyriformis* with 94 and 99% 4-O-sulfated GalNac sulfation and 66 and 70% of 2-sulfation IdoA have significant anticoagulant activities (aPTT = 11 and 8 IU/mg, respectively), while bovine DS, which is largely 2-sulfation at IdA and minimally 4-sulfated at GalNac, lacks anticoagulant activity.[18] This reinforces the importance of 4-sulfation in anticoagulant activity. Finally, in sea-cucumber FucCS, when sulfated fucosyl branches are removed, their anticoagulant activity is eliminated, indicating they are essential.[14] In addition to branching itself, the 1,2-disulfaction of the fucosyl branches is important for anticoagulant activity, consistent with 3-linked α-L-fucans described above.[31]

Overall, the regular well-defined structures of marine invertebrate glycans enable SAR development. The structural combinations necessary for anticoagulant activities are as follows: 2-sulfation in α-L-SGs, the 2,4-di-sulfation in α-L-fucopyranosyl units in SFs, or increased sulfation of homogeneous SGs. Additionally, 4-sulfation enhanced the inhibition of thrombin via heparin cofactor-II by invertebrate SFs.[29]

5.2 *Antiviral activities of four marine sulfated glycans against adenovirus and human cytomegalovirus*

5.2.1 Introduction

Glycosaminoglycans (GAGs) are linear polysaccharides of repeating disaccharide units containing an amino sugar (either N-acetylglucosamine or N-acetylgalactosamine) and a uronic acid (either glucuronic acid and/or iduronic acid) or the neutral sugar, galactose. As a result of their structural diversity, GAGs have a variety of biological roles, including cell signaling, growth, and wound repair.[32] GAGs are ubiquitous on cell surfaces where they serve as receptors and signals for cellular and pathogenic processes. The sulfation of GAGs presents a net negative charge at cell surfaces that viral or other pathogens can bind electrostatically to initiate entry either by membrane fusion or endocytosis.[33] Virion attachment through GAG binding and subsequent entry are often independent events in which attachment is thought to be largely nonspecific and charge-dependent, while entry is mediated by highly

specific protein-protein interactions. In particular, interactions with heparan sulfate (HS), a highly sulfated GAG, is a common requirement for infection by many viruses, and consequently, inhibitors targeting virion-HS interactions have potential as broad-spectrum antivirals that could exert a major impact on global health.

A variety of compounds have been used to bind to HS and thereby shield cells from viral attachment, including polycationic peptides, small organic compounds, and inorganic molecules.[34–37] Alternatively, inhibitors may bind virion components to sequester and inactivate virions in a manner similar to neutralizing antibodies.[3] The majority of the latter inhibitors are HS mimetics and many have broad spectrum antiviral activity. Here we describe the antiviral activities of four sulfated marine glycans and compare them to heparin, a commonly used HS-mimetic composed primarily of disaccharide repeating units of [-4)-N,6-disulfated-glucosamine-(α1-4)-2-sulfated-iduronic acid-(α1-] (Figure 5.4A). The marine sugars include: (i) a sulfated galactan isolated from the red algae *Botryocladia occidentalis* (BoSG) composed of the disaccharide repeating unit [-3)-2,4-disulfated-galactose-(α1-4)-2,3-disulfated-galactose-(β1-] in which sulfation patterns may vary in percentage but never in position (Figure 5.4B);[29] (ii) a fucosylated chondroitin sulfate isolated from the sea cucumber *Isostichopus badionotus* (IbFucCS) composed of the trisaccharide-repeating unit {-4)-[fucose-(α1-3)]-glucuronic acid-(β1-3)-N-acetylgalactosamine-(β1-} in which sulfation patterns may vary in percentage but never in position (Figure 5.4C);[38] (iii) a sulfated fucan isolated from the sea urchin *Lytechinus variegatus* (LvSF) composed of the tetrasaccharide-repeating unit of [-3)-4-sulfated-fucose-(α1-3)-2,4-disulfated-fucose-(α1-3)-2-sulfated-fucose-(α1-3)-2-sulfated-fucose-(α1] (Figure 5.4D);[29] and (iv) a sulfated fucan also isolated from *Isostichopus badionotus* (IbSF) composed of the tetrasaccharide-repeating unit of [-3)-fucose-(α1-3)-2,4-disulfated-fucose-(α1-3)-2-sulfated-fucose-(α1-3)-2-sulfated-fucose-(α1] (Figure 5.4E).[39]

In contrast to heparin and the red algae-derived BoSG, which are heterogeneous in terms of sulfation pattern (although BoSG is a homopolymer of galactose, while heparin is composed of more than one sugar in the backbone), the other three invertebrate-derived sulfated glycans exhibit chemically defined structures with more uniform distribution of sulfation and sugar composition.[12,40,41] In addition, and again in contrast to heparin and other GAG mimetics that are highly hemorrhagic, no bleeding effects have been reported for the marine sulfated sugars BoSG, LvSF, and IbSF.[27,42] Therefore, this set of well-defined and structurally distinct sulfated glycans provides a unique opportunity to identify through structure-activity studies those structure(s) associated with optimal antiviral activities or undesirable biological effects. These unique chemical and biological properties make the marine sugars promising molecular tools in antiviral research.
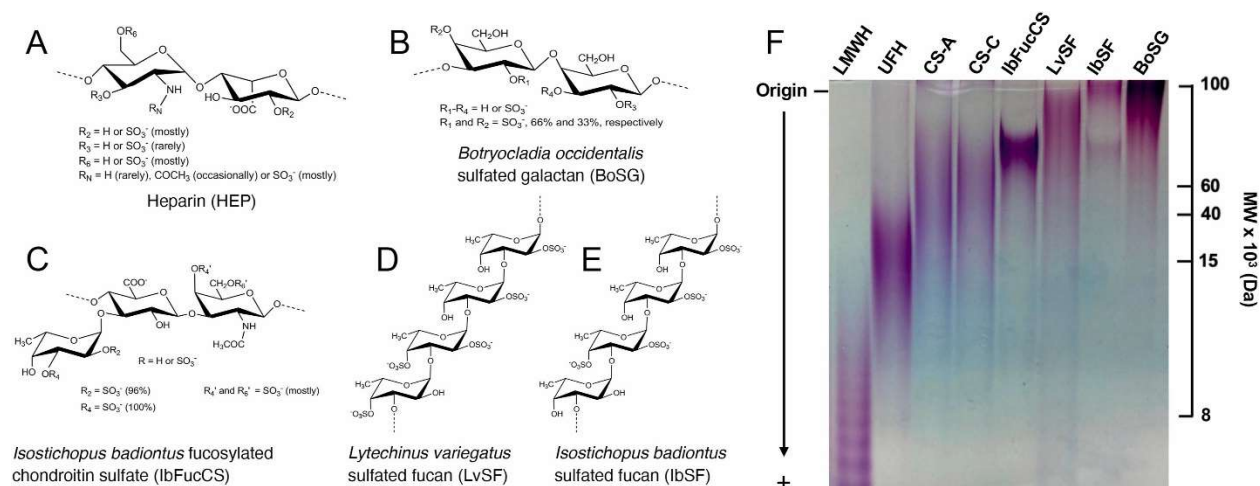
Figure 5.4: Structures and size characterization of the marine sulfated glycans. (A–E) Structures are shown for heparin and the four marine sulfated glycans (counterions and carbon-bonded hydrogens omitted for clarity). (F) The indicated sulfated glycans (10 µg) were separated by polyacrylamide gel electrophoresis and stained with toluidine blue. To the right are indicated MWs of standard compounds LMWH (7.5 kDa), UFH (15 kDa), CS-A, (40 kDa), and CS-C (60 kDa)

5.2.2 Results

5.2.2.1 Structures and size characterization of marine sulfated glycans

Structures for heparin and the four marine sulfated glycans are shown in Figure 5.4A-E. While most sulfated glycans have a polydisperse nature, each exhibits a characteristic size range and an average MW. To better define the average and range of MWs for the four marine sulfated glycans, IbSF, IbFucCS, BoSG, and LvSF were analyzed by polyacrylamide gel electrophoresis and compared with known standards (Figure 5.4F). Approximate average MWs were 75, 90, and 100 kDa for IbFucCS, LvSF, and IbSF, respectively, and >100 kDa for BoSG. Samples have shown no residual solvent contamination, and specific signal patterns consistent to each sugar type. See Santos et al.[43] for heparin, Farias et al.[24] for BoSG, Chen et al. 2012[39] for IbSF, Pomin et al.[44] and Chen et al.[38] for IbFucCS.

5.2.2.2 Studies of anti-HCMV and anti-adenovirus activity

Our hypothesis predicts that marine sulfated glycans may act as HS-mimetics to inhibit viral infection by disrupting virion-HS interactions. If so, they should block entry and subsequent gene expression of viruses that enter cells through HS-dependent mechanisms. To test this hypothesis we evaluated the four marine glycans for inhibition of two HS-dependent DNA viruses: human cytomegalovirus (HCMV), an enveloped herpesvirus, and human adenovirus serotype 5 (Ad5), a non-enveloped virus. In both cases genetically modified viruses containing GFP reporter cassettes were used so that successful infection could be detected and quantified using GFP. Human MRC-5 fibroblasts or ARPE-19 epithelial cells were pretreated for one h with increasing concentrations of BoSG, LvSF, IbSF, or IbFucCS, while heparin was used as a positive control as it is known to block infection of both HCMV and Ad5.[45,46] GFP-tagged HCMV variant BADr was then added to MRC-5 cultures and GFP-tagged Ad5 was added to ARPE-19 cultures and after six days total GFP fluoresence was measured. As shown in Figure 5.5, heparin and all four marine glycans reduced GFP expression in HCMV- and Ad5-infected cultures in a dose-dependent manner, while all compounds were non-toxic up to the highest concentration tested (400 µg/mL).

To compare relative antiviral potencies the 50% effective concentration (EC_{50}) for each compound was determined as the concentration at which GFP levels were reduced by half. Cytotoxicities were determined by measuring cell viability in replicate uninfected cultures. As cell viability with all compounds remained over 50% at concentrations up to and including the highest tested (400 µg/mL), 50% cytotoxicity concentrations (TC_{50}) were reported as > 400 µg/mL. A high TC_{50} to EC_{50} ratio, or selectivity index (SI), suggests a favorable safety and efficacy profile. Table 5.1 and Table 5.2 summarize these quantitative data as derived from the experiments shown in Figure 5.5. As toxicity of all four marine glycans was > 400 µg/mL, SIs were approximated by assigning TC_{50} 400 µg/mL. The resulting high SIs imply potentially favorable safety profiles.

Table 5.1. *Anti-HCMV activities of marine sulfated glycans*

Structure	HCMV Antiviral[a] (EC_{50})	Cytotoxicity (TC_{50})[b]	Selectivity index (SI)[c]
BoSG	1.719 ± 1.028	> 400	232.7
LvSF	1.369 ± 0.477	> 400	292.1
IbSF	0.662 ± 0.450	> 400	603.6
IbFucCS	0.422 ± 0.349	> 400	947.5
Heparin	0.331 ± 0.106	> 400	1211.1

[a]GFP-based assay. [b]Luciferase-based cytotoxicity assay . [a,b]µg/mL; means of three independent experiments ± standard deviations. [c]SI = TC_{50}/EC_{50} (TC_{50} = 400 for these calculations)

Table 5.2. *Anti-Adenovirus activities of marine sulfated glycans*

Structure	Adenovirus Antiviral[a] (EC_{50})	Cytotoxicity (TC_{50})[b]	Selectivity index (SI)[c]
BoSG	1.738 ± 0.201	> 400	230.1
LvSF	0.229 ± 0.129	> 400	1742.4
IbSF	0.237 ± 0.116	> 400	1685.6
IbFucCS	0.124 ± 0.034	> 400	3238.9
Heparin	1.815 ± 0.719	> 400	220.4

[a]GFP-based assay. [b]Luciferase-based cytotoxicity assay. [a,b]µg/mL; means of three independent experiments ± standard deviations. [c]SI = TC_{50}/EC_{50} (TC_{50} = 400 for these calculations)
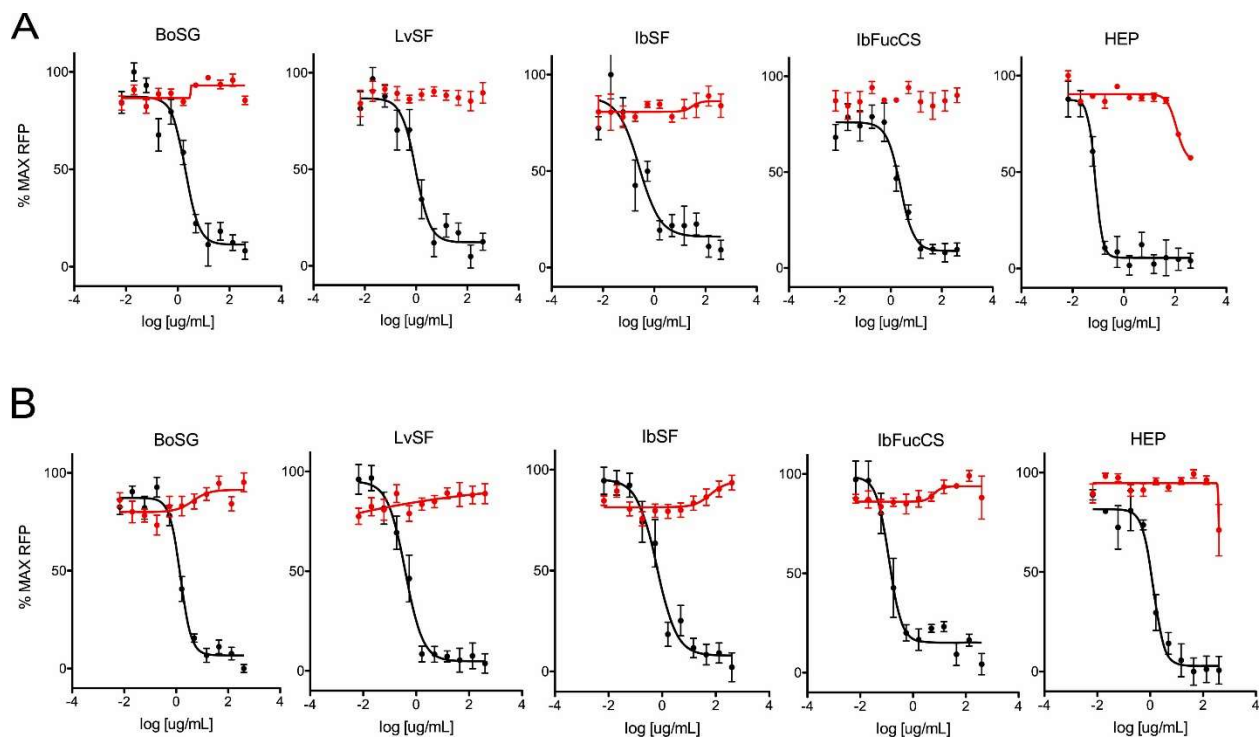
Figure 5.5: GFP-based HCMV and adenovirus antiviral activities and cytotoxicities of marine sulfated glycans. (A) Anti-HCMV activity (black) was measured by incubating MRC-5 fibroblast monolayers in 96-well plates with a compound for one h, then infecting with GFP-tagged HCMV BADr (100 PFU/well). (B) Anti-adenovirus activity (black) was measured by incubating ARPE-19 epithelial cell monolayers in 96-well plates with a compound for one h, then infecting with GFP-tagged adenovirus (100 PFU/well). After six days GFP activities (RFU) in these cultures were measured. Cytotoxicity (red) was measured in replicate uninfected cultures treated for five days using the CellTiter-Glo® assay. Data are means of triplicate wells ± standard deviations.

5.2.2.3 Time of addition studies indicate an early-acting mechanism of action

If marine glycans act by blocking virion attachment or entry, they should be ineffective if added after viral entry is complete. To address this question, a single inhibitory concentration (150 µg/mL) of BoSG, LvSF, IbSF, IbFucCS, or heparin was added to cells one h before or one h after infection with GFP-tagged HCMV or Ad5 and GFP expression was visualized by fluoresence microscopy. When added to cells prior to adding the virus, heparin and all four marine glycans greatly reduced or eliminated GFP expression in both HCMV- and Ad5-infected cultures. In contrast, no inhibition of GFP expression was observed if heparin or the four marine glycans were added 1 h after cells were exposed to either virus (Figure 5.6).
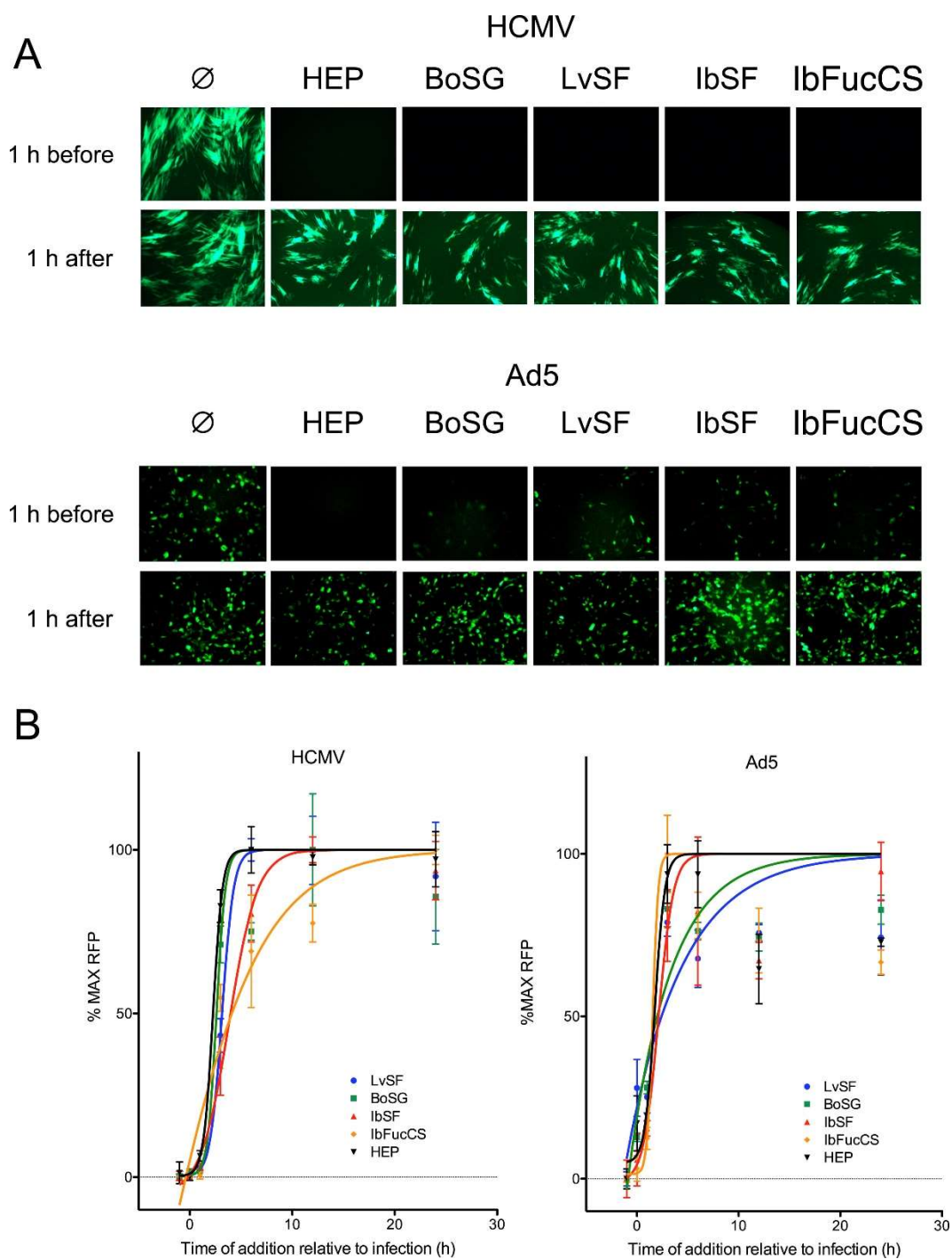
Figure 5.6: Marine sulfated glycans inhibit viral-encoded GFP expression when present prior to HCMV or Ad5 infection. (A) Confluent monolayers of MRC-5 fibroblasts or ARPE-19 epithelial cells in 96-well plates were treated with medium (Ø) or with 150 μg/mL BoSG, LvSF, IbSF, IbFucCS, or heparin (HEP) either 1 h before or 1 h after infection with GFP-tagged HCMV BADr (100 PFU/well) or GFP-tagged Ad5 (100 PFU/well). Representative fluorescent micrographs were taken six days post infection. (B) Confluent monolayers of MRC-5 fibroblasts or ARPE-19 epithelial cells were treated as above either 1 h before, concurrent with, or 1, 3, 6, 12, or 24 h after infection with GFP-tagged HCMV BADr (100 PFU/well) or GFP-tagged Ad5 (100 PFU/well). GFP expression was quantified on day six days post infection. Data are means of triplicate wells ± standard deviations.

To more precisely and quantitatively define the kinetics of inhibition, a time of addition experiment was conducted in which cells were treated with compounds before, during, or after infection and GFP was measured on day six post infection. Consistent with the qualitative results described above, heparin and the four marine glycans were only active in inhibiting HCMV or Ad5 GFP expression if present prior to or within the first 1 h post infection, while addition of compounds three or more h after infection had no effect on GFP levels (Figure 5.6).

5.2.2.4 Marine sulfated glycans inhibit HCMV immediate early gene expression and cellular deposition of virion-associated tegument protein pp65

The earliest *de novo* gene expression events during HCMV replication result in production of the viral Immediate Early 1 and 2 (IE1/2) proteins. To determine if marine glycans block IE1/2 expression, cells were pretreated with heparin or the four marine glycans prior to infection with HCMV variant RC2626 (which does not express GFP), and the IE1/2 proteins were detected by immunofluorescence 48 h after infection. Again, consistent with inhibition of virion attachment or entry, IE1/2-positive cells were undetectable in cultures pretreated with heparin, BoSG, LvSF, IbSF, or IbFucCS (Figure 5.7).

The HCMV pp65 protein is an abundant component of the virion tegument[47] that is deposited into the cytoplasm upon infection and subsequently localizes to the nucleus.[48] Consequently, detection of pp65 shortly after infection indicates virion attachment.[49] To determine if marine glycans block attachment of HCMV virions to cells, deposition of pp65 was similarly assessed by immunofluorescence 6 h after HCMV infection. Again, heparin and the four marine glycans eliminated pp65 deposition onto cells, consistent with inhibition of virion attachment (Figure 5.7).
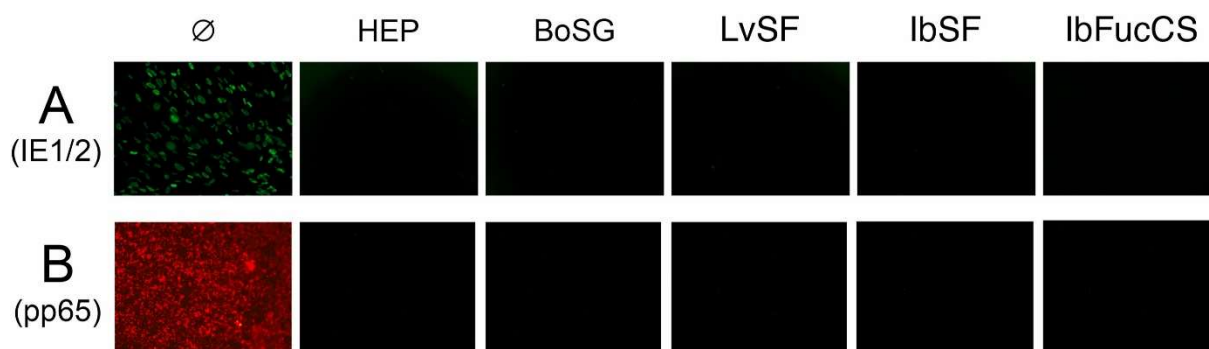
Figure 5.7: Marine sulfated glycans inhibit expression of HCMV IE1/2 proteins and deposition of tegument protein pp65. (A) MRC-5 fibroblast monolayers were treated for 1 h with medium (Ø) or 150 µg/mL heparin (HEP), BoSG, LvSF, IbSF, or IbFucCS, then infected with HCMV RC2626 (125 PFU/well). Cultures were fixed and fluorescently stained for HCMV IE1/2 proteins 48 h post infection. (B) MRC-5 fibroblast monolayers were treated as above but incubated with HCMV BADr (200 PFU/well) for 1 h at 4°C. Cultures were then shifted to 37°C and incubated for 6 h before being fixed and fluorescently stained for the HCMV tegument protein pp65.

5.2.2.5 Sulfated marine glycans appear to target virion rather than cellular factors

To further define the potential virion target(s) of BoSG, LvSF, IbSF, and IbFucCS, cells were pretreated with each glycan for 1 h and then washed three times with media prior to infection with GFP-tagged HCMV or Ad5 viruses. Detection of GFP by fluorescence microscopy six days after infection demonstrated that cells exposed to heparin or the four marine glycans remained susceptible to HCMV or Ad5 infection as pretreatment and removal failed to significantly inhibit GFP expression (Figure 5.8). These results indicate that heparin and the marine glycans do not act by binding to cellular components, but more likely interact with virion components and thereby disrupt the ability of virions to attach to cells.
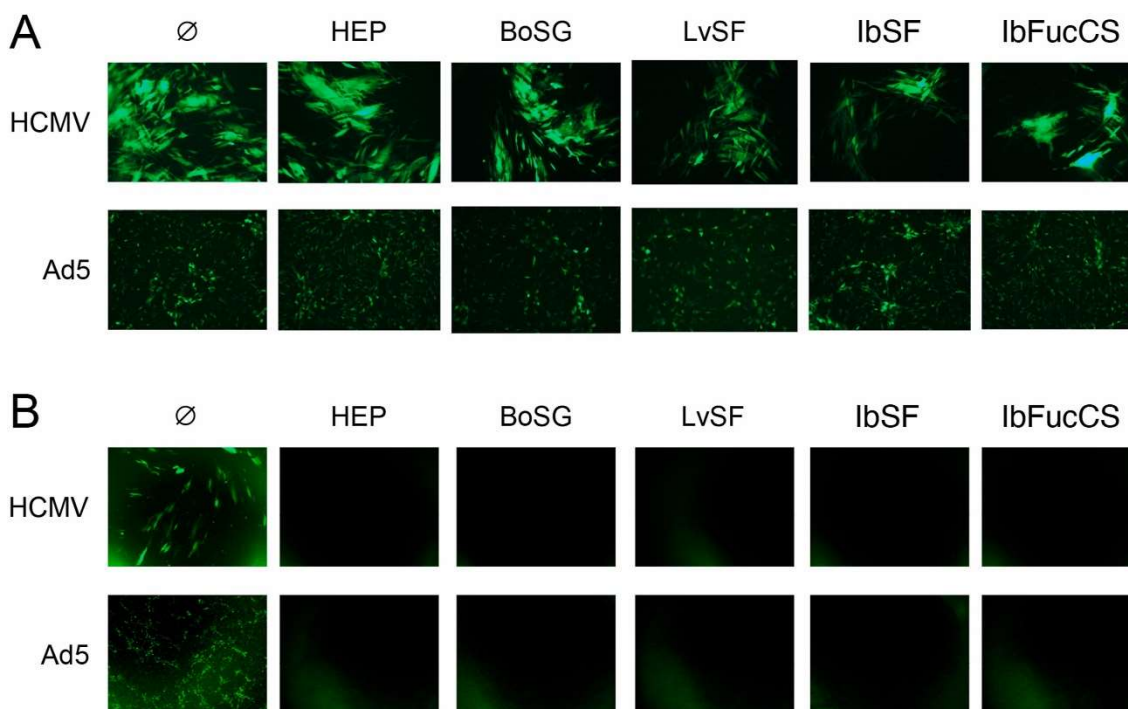
Figure 5.8: Treatment/removal studies. (A) Confluent monolayers of MRC-5 fibroblasts (top) or ARPE-19 epithelial cells (bottom) in 96-well plates were treated with medium (Ø) or 150 µg/mL heparin (HEP), BoSG, LvSF, IbSF, or IbFucCS for 1 h then cells were washed three times with medium and infected with GFP-tagged HCMV BADr (100 PFU/well) or GFP-tagged Ad5 (100 PFU/well). (B) HCMV BADr or adenovirus virions were incubated with sulfated glycans as in (A) for 1 h, then diluted 10,000-fold with culture medium to a non-inhibitory concentration (15 ng/mL). Virions with sulfated glycans were then added to MRC-5 fibroblasts (top) or ARPE-19 epithelial cells (bottom) in 96-well plates. Representative fluorescent micrographs were taken six days post infection.

5.2.3 Discussion and Conclusion

In 2018 the World Health Organization released a list of priority pathogens to direct research and development. These pathogens were chosen based on their epidemic potential and/or lack of effective countermeasures (*i.e.*, antivirals or vaccines). As of Fall 2020 there are eleven viruses on the list, namely SARS-CoV-1, SARS-CoV-2, MERS, Crimean-Congo hemorrhagic fever virus, Ebola virus, Marburg virus, Lassa fever virus, Nipah virus, henipavirus, and Rift Valley fever virus. Of these, seven are HS-dependent and one is speculated to be HS-dependent.[50,51] An inhibitor targeting virion-HS interactions could potentially prevent infections by many or all of these viruses.

Compounds targeting virion-HS interactions have seen moderate success as broad spectrum antivirals *in vitro*. Polycationic peptides, like polyarginine, associate with HS and have broad spectrum antiviral activity[35,52] but are subject to inactivation by proteolytic cleavage. Organic small molecules such as N,N'-bisheteryl derivatives of dispirotripiperazine inhibit the attachment of several viruses, including strains resistant to traditional specifically-targeted treatments.[53–55] Inorganic compounds take advantage of the natural affinity between metal cations and GAGs, which *in vivo* are associated with physiologically relevant cations.[56] Inorganic polymers and small molecules have both demonstrated broad-spectrum antiviral activity although none have progressed beyond the clinical evaluation phase or been licensed.[36,37,57]

Alternatively, compounds that disrupt virion-HS interactions by targeting viral glycoproteins can also be broad-spectrum but have a number of issues that preclude their general use as antivirals. Although

polystyrene sulfonate demonstrated activity against HIV-1, HSV-1, HSV-2, and influenza A virus, high concentrations are needed, which increases the likelihood of non-specific binding and reduces effectiveness.[58–62] Suramin inhibits viral attachment but is also bound by plasma proteins, which reduces its efficacy *in vivo.*[63–65]

A large number of compounds modeled after HS inhibit viral infection by sequestering virions. Heparin is a well-known viral entry inhibitor that electrostatically interacts with viral glycoproteins and competitively inhibits virion attachment.[50,66–69] However, heparin is also an effective anticoagulant and as such common side effects of heparin include excessive bleeding and thrombocytopenia, requiring constant patient monitoring and, if needed, use of an antidote (protamine).[70] In an effort to circumvent these issues, a number of other GAGs or HS-mimetics have been tested for antiviral activity. Dextran sulfate inhibits viral attachment but suffers from similar issues as heparin.[66–68,71] Carrageenans (sulfated polysaccharides from red seaweeds) inhibit enveloped DNA and RNA viruses but do not inhibit non-enveloped viruses, suggesting that enveloped viruses may be more susceptible to GAG mimetic antivirals.[72–75] Carraguard failed Phase III clinical trials due to a large number of adverse events.[76] Sulfated derivatives of the K5 polysaccharide from *E. coli* have also shown broad-spectrum antiviral activity.[77,78] Cellulose sulfate is active against a number of viruses and bacteria, including HSV-1, HSV-2, HPV, HIV-1, *Neisseria gonorrhoeae*, and *Chlamydia trachomatis,* but failed to show efficacy in phase two clinical trials.[58,79–82]

The anticoagulant properties of the marine sugars used in this work have been previously described. BoSG and IbFucCS exhibit strong anticoagulant activities of 93 and 183 international units (IU)/mg, respectively, as determined by the activated partial thromboplastin time method, whereas the two sulfated fucans LvSF and IbSF exhibit negligible activities of 3 and 9 IU/mg, respectively.[13,39] From the current work both sulfated fucans have sub-µM EC_{50}s against HCMV and Ad5 with no evident cytotoxicity at 400 µg/mL (Figure 5.5, Table 5.1, and Table 5.2). These features make these sulfated fucans promising candidates for further evaluation and development as potential antivirals.

IbSF shows the lowest density of charge due to the presence of lower sulfation content as compared to the other polysaccharides tested here (Figure 5.4). From the structure-activity relationship standpoint achieved by exploiting the marine sugars of defined structures, it was interesting to see that LvSF and IbSF presented similar antiviral activities against both viruses (Table 5.1, and Table 5.2), although slightly better for IbSF. We note that LvSF and IbSF are comparatively similar in terms of structure with regard to monosaccharide composition of glycosidic bonds, anomericity, and sulfation positions and sequencing. However, IbSF is less sulfated than LvSF as the 4-sulfated-fucose in LvSF is replaced by a non-sulfated fucose in IbSF (Figure 5.4). These observations suggest that a non-anticoagulant sulfated glycan can still present antiviral effects and that activity is not merely due to a consequence of sulfation content and negative charge density but also due to the potential conformational shapes of these carbohydrates in solution and upon interaction with their protein partners. Such conformational differences might lead to different affinities for the viral proteins, ultimately resulting in different antiviral actions. Recently Pomin et al. showed by NMR and computational simulations the 3D structure of LvSF in solution,[83] PDB ID 7KS6. Pomin et al. are currently investigating through the same methods the conformational view of IbSF. Data from these two works concerned with the structural biology of the invertebrate-derived sulfated fucans may help to elucidate the antiviral activities of these two sugars as reported here.

Our studies demonstrate the antiviral activities of marine sulfated glycans against two very different DNA viruses, one enveloped (HCMV) and one non-enveloped (Ad5). All four compounds had μg/mL activities, suggesting that structure and sulfation of the glycans did not have a large influence on antiviral activity. Unlike previously studied GAG mimetics and heparin, BoSG, LvSF, IbSF, and IbFucCS have homogenous structures; their sulfation levels vary but the pattern of saccharide units is consistent. However, BoSG and IbFucCS have anticoagulant activities which, like other GAG mimetics, would presumably preclude their general use as antivirals. Consistent with the similarity of their structures, LvSF and IbSF have similar antiviral activities, and as both lack anticoagulant activity, they merit further study as antivirals. Conformational differences, studied trough NMR and computational simulations, may help to explain differences in antiviral and anticoagulant activities of these glycans.

5.3 *Fractionation of sulfated galactan from the red alga Botryocladia occidentalis separates its anticoagulant and anti-SARS-CoV-2 properties*

5.3.1 Introduction

A global pandemic caused by the severe acute respiratory syndrome coronavirus (SARS-CoV-2) or coronavirus disease-19 (Covid-19) was declared by the World Health Organization in March 2020.[84] The virus has rapidly spread to more than 222 countries since February 2020. SARS-CoV-2 is a zoonotic beta coronavirus primarily transmitted from person-to-person through respiratory droplets.[85,86] During the pandemic, global pharmaceutical companies started manufacturing vaccines, some of which have been approved by the US Food and Drug Administration under the Emergency Use Authorization. Vaccines have prevented many patients from becoming critically ill or dying and assisted in controlling the pandemic. Oral treatments of Covid-19, Molnupiravir and Paxlovid, have recently been issued an Emergency Use Authorization and are currently awaiting full approval by the FDA.[87,88] Nevertheless, discovery of new anti-SARS-CoV-2 agents is urgently needed, especially for treating infections by highly transmittable variants.[89,90]

The cell entry mechanism of SARS-CoV-2 has been well studied. The receptor binding domain (RBD) in the S1 subunit of the spike-protein (S-protein) recognizes the heparan sulfate (HS) chains in cell surface proteoglycans and the human angiotensin-converting enzyme 2 (hACE2).[91–95] Structural analyses have revealed the mechanisms behind interactions between the SARS-CoV S-protein RBD and its host receptor hACE2.[96,97] A heparin binding site has been identified in the SARS-CoV-2 S-protein and the interaction with HS has been shown to be essential for hACE2 binding.[95]

Since SARS-CoV-2 S-protein depends on cellular HS for cell binding, several recent studies have proposed anti-SARV-CoV-2 effects of exogenous sulfated glycans such as unfractionated heparin (UFH), non-anticoagulant heparin, or HS-based molecules derived from lung and other tissues, in order to block virus binding.[98–100] However, heparin and derivatives may present severe side effects or complications such as hemorrhage,[101,102] thrombocytopenia,[103,104] osteoporosis,[105,106] hypersensitivity reactions,[107] and hypoaldosteronism.[108] Hence, reports showing potential non-heparin anti-SARS-CoV-2 sulfated glycans, including unique molecules from marine sources, have recently appeared in the literature.[109–113] However, these recent reports have studied the actions of the sulfated polysaccharides only against the Wuhan SARS-CoV-2 strain (wild type) and not the mutated variants, including those of more infectious potency.

Viral mutation is naturally generated by multiple viral replications.[114] RNA viruses are frequently and randomly mutated at higher frequency than DNA viruses because RNA polymerases lack exonuclease proofreading activity.[115] Among all RNA viruses, coronaviruses mutate less frequently due to an enzyme

that corrects errors during viral replication.[115] Nonetheless, the number of variants of SARS-CoV-2 are increasing, mainly because of the pandemic. Variants have been identified worldwide, and a few such variants have been considered variants of concern (VOC) based on their harmful impact on human health. Such VOC may exhibit greater transmissibility, virulence, or immune escape mutations.[116]

The N501Y mutation that emerged among the Alpha variants and improves S-protein binding to cellular receptors and enhances virulence.[117] Current SARS-CoV-2 VOC include Alpha (B.1.1.7), Beta (B.1.351), Gamma (P.1), Delta (B.1.617.2), and Omicron (B.1.1.529).[117] The N501Y mutation located in the RBD is found in all the VOCs except Delta. This N501Y mutation is associated with the highest transmissibility and has given rise to other lineages with additional mutations in the S-protein RBD.[118] The emergence of a triple-mutated variant (K417T, E484K, N501Y, B.1.1.28), referred to as Gamma SARS-CoV-2, has been reported in Brazil.[119–122] The Gamma variant has shown high transmissible rates, inherent immune escape from neutralizing antibodies,[123–125] and increased propensity of reinfection.

The main sulfated glycan isolated from the red alga *Botryocladia occidentalis*, a sulfated galactan (BoSG), has been well-characterized to possess not only antiviral activity,[1,126] but also antimalarial,[127] anticoagulant,[30,128–130] and antithrombotic activities.[27,129,131] BoSG is structurally homogeneous in terms of its backbone, composed of the disaccharide repeating unit [→4)-α-$_D$-Gal-(1→3)-β-$_D$-Gal-(1→], but very heterogenous in terms of sulfation pattern (Figure 5.9A). The anticoagulant and antithrombotic properties of BoSG have been widely studied and strong responses have been observed in these systems.[132–134] Studies regarding mechanism of action have indicated activity towards heparin cofactor II (HCII) and antithrombin (AT), and dependency of molecular weight (MW) on these activities.[24]
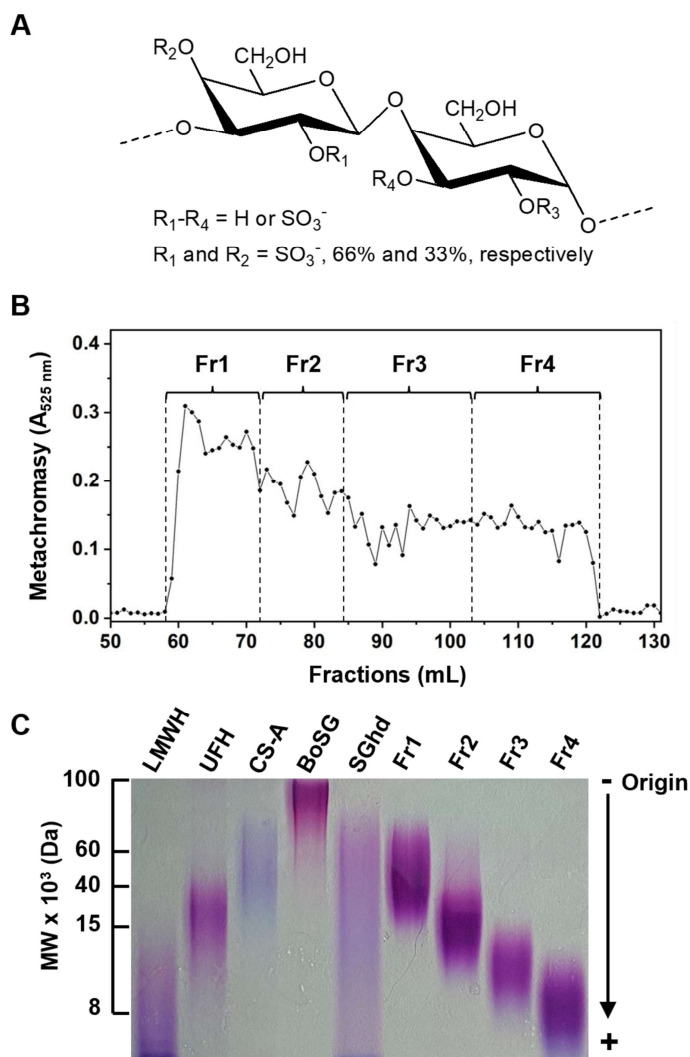
Figure 5.9: **Structure of BoSG, size fractionation, and MW estimation of low MW derivatives.** *(A) BoSG is composed of a repeating disaccharide unit of the following structure [3-β-Gal2R14R2-(1→4)-α-Gal2R3R-(1→)]n, in which R = SO3⁻ or OH, R1 and R2 = 66% and 33% sulfation, respectively. (B) Oligosaccharides were produced by mild acid hydrolysis, fractionated by SEC using a Bio-Gel P-10 column, and detected by metachromasy using DMB (●). Fractions Fr1-Fr4 are indicated. (C) The MW distribution of BoSG, hydrolyzed unfractionated BoSG (SGhd), and the four low MW fractions (Fr1-Fr4) were analyzed by PAGE along with the following molecular markers: low MW heparin (LMWH, ~8kDa), unfractionated heparin (UFH, ~15 kDa), and chondroitin sulfate A (CS-A, ~40 kDa). Samples (10 µg/each) were separated by 22% PAGE and stained with toluidine blue.*

Here, we analyze the structural, anti-SARS-CoV-2, anticoagulant, and S-protein binding properties of BoSG and its low MW derivatives. For this, a multifaceted approach was used through multiple analytical and biophysical techniques, including liquid-chromatography, electrophoresis, nuclear magnetic resonance (NMR), mass spectrometry (MS), surface plasmon resonance (SPR), computational docking, and assays measuring inhibitory activities against blood cofactors or cellular entry by SARS-CoV-2. Our results demonstrate that we can generate sulfated oligosaccharides from a marine alga with low residual of anticoagulant activity while retaining anti-SARS-CoV-2 activity.

5.3.2 Results

5.3.2.1 Purification of BoSG

Crude polysaccharides were obtained from the body wall of the red alga *B. occidentalis* through nonspecific proteolytic digestion using papain followed by ethanol precipitation, as previously described.[24,135,136] The crude polysaccharides were subjected to anion-exchange chromatography on a DEAE Sephacel column and eluted with a linear NaCl gradient up to 3M concentration. The fractions obtained by this chromatography were monitored by metachromasia using 1,9-dimethylmethylene blue (DMB).[137] The peak corresponding to the *B. occidentalis*-derived sulfated galactan (BoSG) started to elute at 0.9 M NaCl. After pooling the fractions belonging to this peak and desalination, the structural integrity of the BoSG preparation was confirmed by 1D ^{1}H NMR, demonstrating a spectral pattern similar to previous work.[24]

5.3.2.2 Depolymerization of BoSG

Mild acid hydrolysis is routinely used for depolymerization of sulfated glycans, especially those for which specific digestive enzymes are unknown.[44,138,139] The choice of 0.1 M hydrochloric acid and 60°C temperature was based on previous reports.[129,131] To produce low MW derivatives from the above BoSG preparation that could be suitable for further fractionation by size-exclusion chromatography (SEC), different hydrolysis times (1, 3, 5, 7, 9, and 11h) were evaluated. The MW distributions of the derivatives obtained were analyzed by polyacrylamide gel electrophoresis (PAGE). Large-scale production of BoSG oligosaccharides was then made by 7 h of hydrolysis, since this time yielded a suitable MW range of medium-sized oligosaccharides to be filtered through the Bio-Gel P-10 column.

5.3.2.3 Production of low MW BoSG derivatives

Approximately 30 mg of BoSG were employed for production of oligosaccharides. The SEC column of choice was based on previous work.[44,138–141] The Bio-Gel P-10 column has been reported to be effective for fractionation of medium- and/or small-sized sulfated oligosaccharides. Figure 5.9B shows the chromatographic profile of fractionation of BoSG derivatives monitored by metachromasy. Although no resolved peaks indicative of size-defined oligosaccharides were evident, four fractions (Fr1-Fr4) were randomly pooled. As analyzed by PAGE (Figure 5.9C), oligosaccharides with different MW distributions were generated. The polydisperse nature of all four fractions indicated a complex and heterogeneous mixture of oligosaccharide chains within the samples.

5.3.2.4 Structural analyses of the BoSG low MW derivatives

NMR spectroscopy has been extensively used in structural characterization of BoSG.[24] The 4-linked α-Gal unit can be 2,3-*O*-disulfated with an anomeric NMR ^{1}H signal between 5.45 and 5.65 ppm, or 2-*O*-mono or 3-*O*-monosulfated with an anomeric NMR ^{1}H signal between 5.10 and 5.45 ppm (Figure 5.10A and Table 5.3).[24] The ^{1}H chemical shift of the non-sulfated α-Gal unit of BoSG resonates within the same region as the ^{1}H chemical shifts of the monosulfated region (Figure 5.10A and Table 5.3). The ^{1}H NMR spectra of the oligosaccharide fractions (Fr1-Fr4) clearly show a profile similar to the spectral profile of native BoSG. The major ^{1}H peaks seen in the spectra of the fragments are clearly in the monosulfated and/or non-sulfated region of δ_H at 5.1-5.45 ppm. Hence, desulfation seems to occur during formation of the low MW derivatives produced by mild acid hydrolysis of BoSG. The characterization of the desulfation units was confirmed by the correlation of the ^{1}H-^{1}H correlation spectroscopy (COSY) spectra and ^{1}H-^{13}C heteronuclear single quantum coherence (HSQC) (Figure 5.10B) spectra of Fr4 compared with reference δ_H and δ_C values.[142,143]
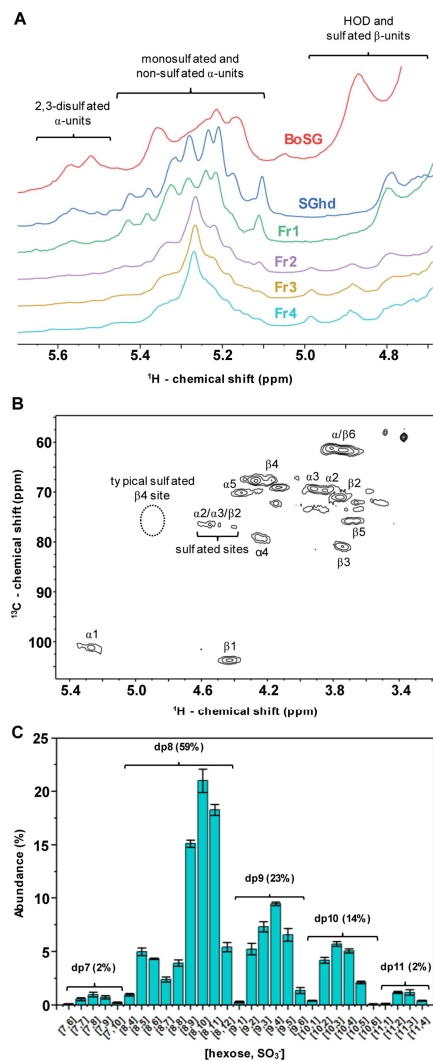
*Figure 5.10: **1D ¹H NMR, 2D ¹H-¹³C HSQC and top-down LC-MS analyses of BoSG fragments.** (A) 1D ¹H NMR spectra of native BoSG (red), hydrolyzed unfractionated SGhd (royal blue), Fr1 (green), Fr2 (purple), Fr 3 (yellow), and Fr4 (cyan). (B) 2D ¹H-¹³C HSQC spectrum of Fr4 recorded in D2O at 50 °C on a 500 MHz Bruker NMR instrument. Chemical shifts are referenced to trimethylsilylpropionic acid to 0 ppm for ¹H and methanol for ¹³C. ¹H chemical shift ranges related to disulfated, monosulfated, and non-sulfated α and β units are indicated accordingly in the 1D ¹H spectra in panel A. ¹H-¹³C pairs of α and β units are labeled in the 2D cross-peaks of panel B using Greek letters denoting the anomeric (ring) unit followed by a number of the ¹H-¹³C pair of the galactose ring. The typical region of the ¹H4-¹³C4 cross-peak of a 4-sulfated β-galactose unit is indicated in the HSQC spectrum with dashed circle. (C) Percentage distribution of oligosaccharides of Fr4 according to their degrees of polymerization (dp) and sulfation number.*

Carbohydrate	Unit	¹H and ¹³C chemical shift (ppm)ᵃ					
		H1/C1	H2/C2	H3/C3	H4/C4	H5/C5	H6/C6
Fr4	→4)-α-D-Gal-3(SO₃⁻)-(1→	5.27/102.7	4.02/68.6	**4.61/77.8**	-	-	-
	→3)-β-D-Gal-2(SO₃⁻)-(1→	4.44/105.3	**4.59/78.1**	*4.26/80.6*	-	-	-
BoSG	→4)-α-D-Gal-2,3(SO₄)-(1→	5.62/100.5	**4.73/74.5**	**4.58/78.2**	-	-	-
	→4)-α-D-Gal-2(SO₄)-(1→	5.27	4.59	4.05	-	-	-
Desulfated BoSG	→4)-α-D-Gal-(1→	5.29/102.9	3.85/71.5	3.95/70.9	*4.22/80.9*	4.16/73.9	3.78/63.0
	→3)-β-D-Gal-(1→	4.40/105.3	3.78/72.3	*3.75/82.7*	4.12/70.4	3.73/77.5	3.78/63.0
Sulfated galactan from *Gigartina skottsbergii*	→4)-α-D-Gal-2(SO₃⁻)-(1→	5.45/94.7	**4.52/75.9**	4.11	-	-	-
Sulfated galactan from *Styela plicata*	→4)-α-D-Gal-3(SO₃⁻)-(1→	5.21/101.2	4.16/68.1	**4.65/76.9**	*4.51/77.4*	4.36/72.7	3.79/60.3
Sulfated galactan from *Glyptocidaris cremularis*	→3)-β-D-Gal-2(SO₃⁻)-(1→	4.94/104.1	**4.52/80.2**	*4.11/81.8*	4.37/70.5	4.02/74.3	3.82/62.5
	→3)-β-D-Gal-(1→	4.73/107.2	3.87/72.0	*3.90/83.5*	4.24/69.1	3.75/77.0	3.82/62.5
Desulfated galactan from *G. crenularis*	→3)-β-D-Gal-(1→	4.79/103.5	3.90/69.9	*3.93/81.9*	4.29/68.3	3.82/74.8	3.87/60.5
Sulfated galactan from *Codium isthmocladum*	→3)-β-D-Gal-4(SO₃⁻)-(1→	4.84/103.1	3.71/71.9	*4.16/77.6*	**4.94/77.8**	3.95/74.8	3.96,3.86/60.4
Desulfated galactan from *C. isthmocladum*	→3)-β-D-Gal-(1→	4.81/102.6	3.64/73.8	*3.92/82.9*	4.39/67.1	3.86/75.2	3.94,3.85/60.3
Sulfated galactan from *Meretrix petechialis*	→3)-β-D-Gal-2(SO₃⁻)-(1→	4.83	**4.45**	3.97	-	-	-
Native galactan from *Echinometra lucunter*	→3)-α-D-Gal-2(SO₃⁻)-(1→	5.47/97.2	**4.65/76.1**	*4.23/75.9*	4.35/73.9	NR/73.9	3.82/63.8
Desulfated galactan from *E. lucunter*	→3)-α-D-Gal-(1→	5.26/98.1	4.08/73.5	*4.14/77.2*	4.32/69.5	4.24/68.5	3.82/63.9

Table 5.3: 1H and 13C chemical shifts of α- and β-galactose units with different linkages, anomericities, and sulfation patterns. ᵃChemical shifts are referenced to external trimethylsilylpropionic acid at 0 ppm for 1H and methanol for 13C. Values in bold indicate sulfate position; those in italics indicate glycosylated positions.

The chemical shifts of sulfated units allowed identification of the 3-*O*-monosulfated α-Gal unit by the ¹H/¹H (5.27/4.02 ppm) and ¹H2/¹H3 (4.02/4.61 ppm) ¹H-¹H COSY correlation as a [→4)-α-D-Gal-3(SO₃⁻)-(1→)] unit and of the 2-*O*-monosulfated β-Gal unit by the ¹H1/¹H2 (4.44/4.59 ppm) and ¹H2/¹H3 (4.59/4.26 ppm) ¹H-¹H correlation as a [→3)-β-D-Gal-2(SO₃⁻)-(1→] unit. Selective desulfation has already been observed from mild acid hydrolysis of other marine sulfated glycans[44,138,144] and should not be unexpected for the case of BoSG in this work.
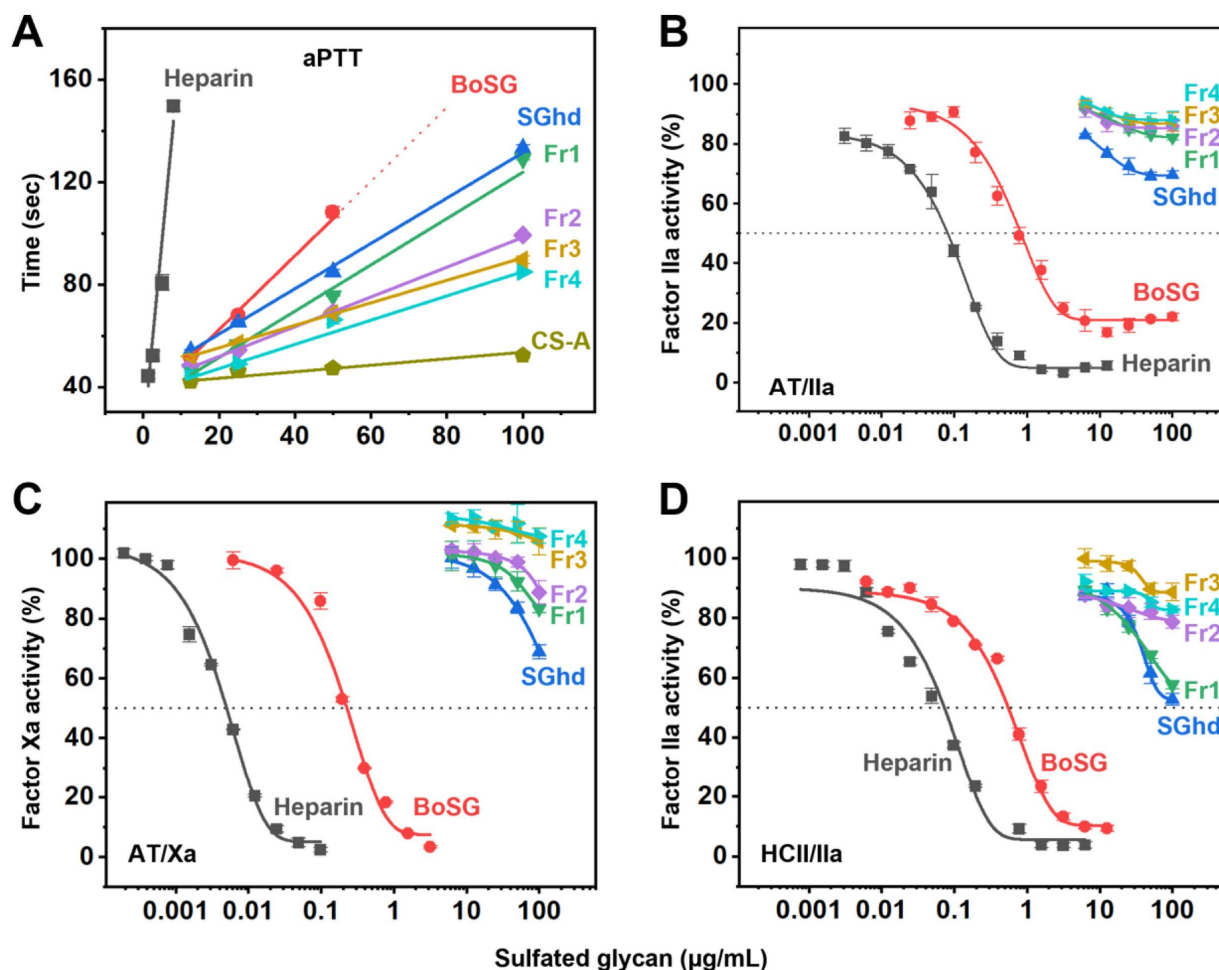
*Figure 5.11: **Anticoagulant activity-concentration curves of BoSG and derivatives.** (A) aPTT, (B) AT-mediated factor IIa inhibition, (C) AT-mediated factor Xa inhibition, and (D) HCII-mediated factor IIa inhibition. Sulfated glycans tested were unfractionated heparin (UFH, black), native BoSG (red), hydrolyzed unfractionated SGhd (royal blue), Fr1 (green), Fr2 (purple), Fr3 (yellow), and Fr4 (cyan). Concentrations of coagulation (co)factors were 10 nM of AT or HCII and 2 nM of factors IIa or Xa.*

Further analyses were conducted through a combination of 2D ^{1}H-^{13}C HSQC spectrum (Figure 5.10B) and top-down liquid chromatography LC-MS (Figure 5.10C) to assess more structural details of the low MW derivatives of BoSG after mild acid hydrolysis. Taking into account that Fr4 showed the most homogeneous 1D ^{1}H NMR profile (Figure 5.10A), and is also the fragment of the lowest MW distribution and potentially with the most structural modifications caused by the reaction, this fraction was chosen for these analyses.

From the assignments of the ^{1}H-^{13}C HSQC and ^{1}H-^{1}H COSY cross-peaks related to the sulfated sites, and comparison of chemical shifts with references in the literature, we were able to clearly identify the presence of 3-*O*-sulfated α-Gal units and 2-*O*-sulfated β-Gal units in Fr4 (Figure 5.10B). This can be seen from the cluster of ^{1}H-^{13}C HSQC and ^{1}H-^{1}H COSY cross-peaks related to monosulfated sites, $δ_H$-$δ_C$ from 4.40-74.5 to 4.73-80.2 ppm (Figure 5.10B and Table 5.3). Note that there is clearly no ^{1}H4-^{13}C4 signal in the typical region of 4-sulfation for the β-Gal unit ($δ_H$-$δ_C$ at 4.94-77.8 ppm) in the HSQC spectrum (Figure 5.10B and Table 5.3). This demonstrates the absence of 4-sulfation in the β-Gal units of Fr4. The ^{1}H-^{13}C HSQC spectrum also showed clear absence of the ^{1}H1-^{13}C1 cross-peak of the native 2,3-*O*-sulfated unit with typical $δ_H$-$δ_C$ at 5.62-100.5 ppm (Figure 5.10B and Table 5.3).

The presence of only two sets of anomeric ^{1}H-^{13}C peaks, one with δ_H-δ_C at 5.27-102.7 ppm belonging to the α-Gal unit and one with δ_H-δ_C of 4.40-78.6 ppm belonging to the β-Gal unit (Figure 5.10B and Table 5.3), as opposed to at least four anomeric HSQC cross-peaks seen in the native BoSG,[30] indicates more homogeneous composition for Fr4 than for the native BoSG. From the NMR spectra (Figure 5.10A and 2B), this increased structural homogeneity in Fr4 can be attributed to the occasional desulfations that can occur on the disulfated Gal units during mild acid hydrolysis. The 1D ^{1}H NMR spectra of fractions Fr2 and Fr3 (purple and yellow lines, respectively) as well as Fr4 (cyan line) in Figure 5.10A are very similar to each other, indicating similar homogeneity. In contrast, both the hydrolyzed unfractionated BoSG sample (royal blue line) and the fraction of highest MW (Fr1, green line) still showed some 2,3-O-disulfated α-Gal units, as in the native BoSG spectrum (in red). This can be seen from the presence of ^{1}H peaks at the downfield region of the 1D spectra (Figure 5.10A).

Figure 5.10C shows the percentage of the composing oligosaccharides in Fr4 obtained by the top-down LC-MS analysis. The bars indicate the oligosaccharide composition according to their number of hexoses along with their number of sulfate groups. More than half of the composing oligosaccharides in Fr4 have a degree of depolymerization (dp) equal to 8. This indicates a great portion of Fr4 as octasaccharide components. Two additional dp fractions also observed in Fr4 were dp9 and dp10. The major peaks of dp9 and dp10 (23% and 14% of the total content) show even lower numbers of sulfate groups/hexose units. This indicates the presence of mono- or non-sulfated units in dp9 and dp10. The numbers of sulfate groups in the bars with the highest abundance in the dp8 fraction showed 9-11 sulfates/8 monosaccharide units, indicating therefore great abundance of monosulfated (and fewer disulfated) units in the dp8 fraction. These data corroborate well with the observation of the dominant presence of monosulfated units in Fr4 as seen through the 1D ^{1}H (Figure 5.10A) and 2D ^{1}H-^{13}C NMR spectra (Figure 5.10B).

5.3.2.5 Anticoagulant activities of BoSG and derivatives

The ideal anti-SARS-CoV-2 marine sulfated glycan would be devoid of anticoagulant effects.[145] The native BoSG, a hydrolyzed unfractionated BoSG sample (SGhd), and the four fractions of different MWs derived from BoSG (Fr1-Fr4) were subjected to *in vitro* anticoagulant assays to investigate the impact of MW on the anticoagulant action of BoSG. The methods employed were the activated partial thromboplastin time (aPTT) (Figure 5.11A), and protease inhibition assays using purified serpins, AT (Figure 5.11B and C) and HCII (Figure 5.11D), over the blood factors IIa (Figure 5.11B and D) and Xa (Figure 5.11C). Unfractionated heparin (UFH) with anticoagulant activity of 180 IU/mg was used in all experiments as a control. Anticoagulant activities of the six BoSG samples obtained from the aPTT curves (Figure 5.11A) as well as the half-maximal inhibitory concentration (IC$_{50}$) values obtained from the catalytic inhibitory curves (Figure 5.11B-D) are displayed in Table 5.4.

Sulfated glycan	aPTT (IU/mg)[a]	AT/IIa	AT/Xa	HCII/IIa
		IC$_{50}$ (μg/mL)		
UFH	180.00	0.08	0.0050	0.07
BoSG	21.09	0.82	0.23	0.55
SGhd	15.91	ND	ND	ND
Fr1	13.19	ND	ND	ND
Fr2	9.80	ND	ND	ND
Fr3	7.54	ND	ND	ND
Fr4	8.64	ND	ND	ND

From the data shown in Figure 5.11, anticoagulant properties can be seen for native BoSG (red curves), although it is significantly less active than UFH (black curves). BoSG is active in all anticoagulant systems. However, upon depolymerization, the anticoagulant properties of BoSG were significantly reduced. Loss of activity begins with the hydrolyzed unfractionated SGhd derivative (Figure 5.11, royal blue curves). The fractionated derivatives with different MWs showed reduced activity as the MW decrease (Figure 5.11 and Table 5.4). These results confirm that the anticoagulant action of BoSG is MW-dependent and that native MW is ideal for maximizing its anticoagulant action. Depolymerization of BoSG to produce lower MW fragments provides an efficient strategy to mitigate the anticoagulant properties of this marine carbohydrate.

5.3.2.6 Anti-SARS-CoV-2 activities of BoSG and derivatives

The anti-SARS-CoV-2 activities of UFH, BoSG, and derivatives (SGhd and Fr1-Fr4) were determined by measuring reduction in green fluorescent protein (GFP) expression following transduction of hACE2-expressing HEK293T cells with a lentivirus pseudotyped with SARS-CoV-2 S-protein (Wuhan strain) (Figure 5.12). Half-maximal effective concentration (EC_{50}) values obtained from curves of GFP vs. polysaccharide concentration are shown in Table 5.5. Complete inhibition could be achieved with all samples but in a concentration-dependent fashion (Figure 5.12). Similar anti-SARS-CoV-2 activities were observed for BoSG and UFH, while anti-SARS-CoV-2 action of SGhd, and Fr1-Fr4 were slightly less active than native BoSG (Table 5.5). All polysaccharides (UFH, BoSG, SGhd and Fr1-Fr4) had no cytotoxicity at any tested concentration (red curves, Figure 5.12). These results indicate that, although somewhat less active than native BoSG, low MW BoSG derivatives retain potent anti-SARS-CoV-2 activity.
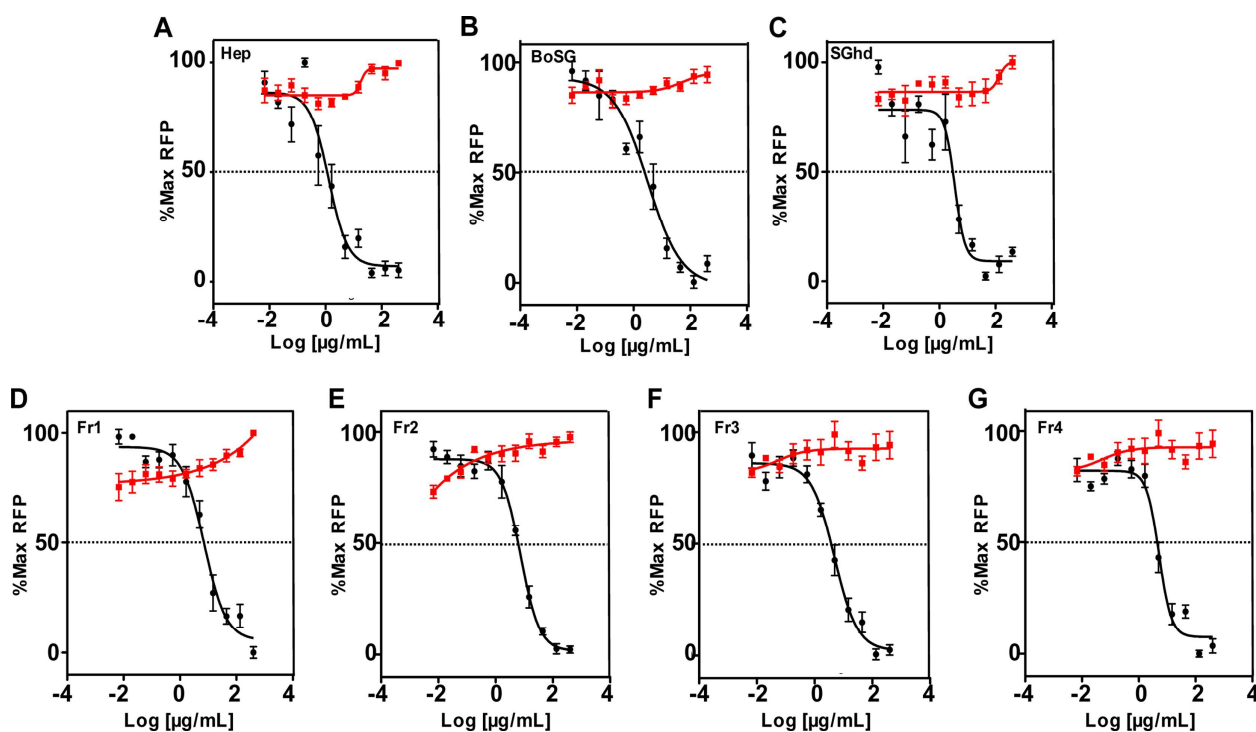
Figure 5.12: **Anti-SARS-CoV-2 activities of BoSG and derivatives.** *Confluent monolayers of HEK-293T-HACE2 cells in 384-well plates were treated with increasing concentrations of unfractionated heparin (A), native BoSG (B), hydrolyzed unfractionated*

SGhd (C), Fr1 (D), Fr2 (E), Fr3 (F), or Fr4 (G). After one hour of incubation cells were transduced with a lentivirus pseudotyped with SARS-CoV-2 (Wuhan strain) S-protein. Following incubation for 48 h, GFP fluorescence in each well was measured as RFU. Cell viability (red) was measured using the CellTiter-Glo® assay as RLU produced from replicate uninfected HEK-293T-HACE2 cell cultures treated in parallel for 48 h. All values were normalized to % of maximum RFUs or RLUs. Data shown are means of three independent experiments ± standard deviations

Sulfated glycan	SARS-CoV-2[a]
Heparin	2.11 ± 1.44
BoSG	2.00 ± 0.79
SGhd	3.55 ± 1.28
Fr1	6.59 ± 1.48
Fr2	6.34 ± 2.68
Fr3	6.29 ± 1.59
Fr4	5.51 ± 1.74

Table 5.5: EC_{50} values of heparin, BoSG, and derivatives in SARS-CoV-2 inhibition. [a]EC_{50} (µg/mL) for inhibition of pseudotyped SARS-CoV-2 entry.

5.3.2.7 Binding properties of BoSG and derivatives with blood cofactors and S-proteins

Competitive SPR using heparin immobilized on a streptavidin (SA)-coated sensor chip was used to investigate the binding of UFH, BoSG, and low MW derivatives with blood coagulation factors IIa (Figure 5.13A), AT (Figure 5.13B), and HCII (Figure 5.13C), and four S-protein RBDs, including wild type (Figure 5.13D), Alpha N501Y (Figure 5.13E), Delta L452R (Figure 5.13F), and Gamma K417T/E484K/N501Y (Figure 5.13E). Binding activities were normalized to the protein alone (black bars). Competitive IC_{50} values between the native BoSG and UFH are shown in Table 5.4. Based on these results, BoSG has strong affinity for IIa and HCII but low affinity for AT, as expected based on previous reports.[24,131] All low MW derivatives of BoSG (SGhd and Fr1-Fr4) showed no significant binding to the blood (co)-factors (Figure 5.13A-C). This observation is consistent with the MW-dependence of anticoagulant activity of BoSG derivatives seen in Figure 5.11.
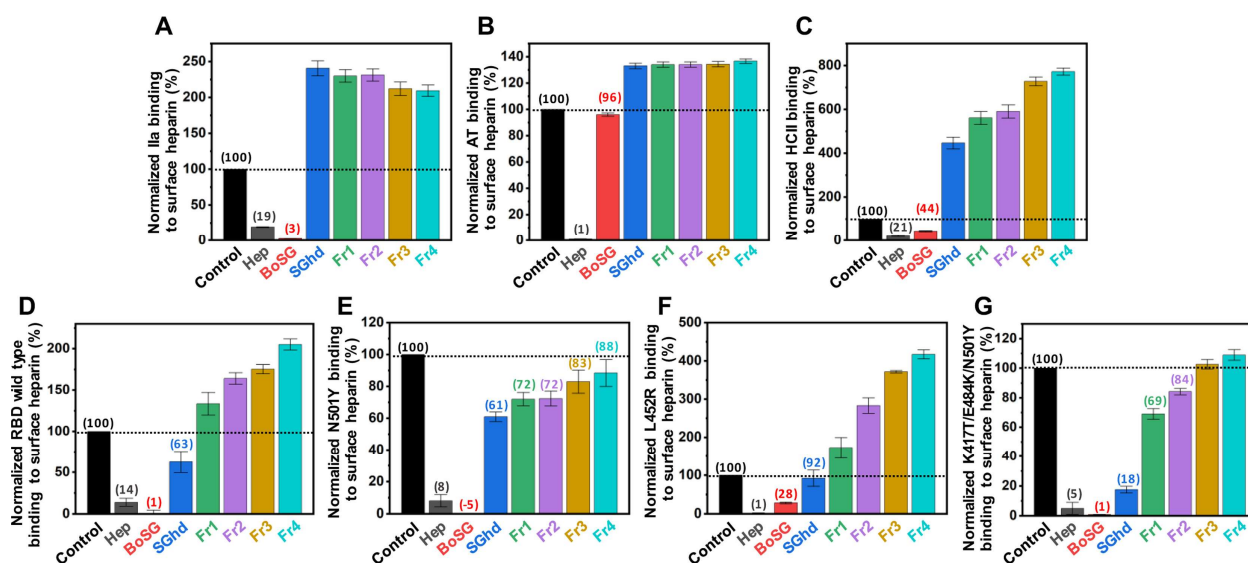
*Figure 5.13: **SPR evaluation of protein–heparin binding and inhibition by BoSG and derivatives.** Bar graphs indicate normalized binding of IIa (A), AT (B), or HCII (C), or S-protein RBDs of wild type Wuhan strain (D), or N501Y (E), L452R (F), or K417T/E484K/N501Y mutants (G) to surface-immobilized heparin. Inhibition of binding by sulfated glycans is shown for no-glycan*

control (black), UFH (grey), native BoSG (red), hydrolyzed unfractionated SGhd (royal blue), Fr1 (green), Fr2 (purple), Fr3 (yellow), and Fr4 (cyan). Dashed lines represent the control level in all panels. Numbers above bars indicate average inhibitory values.

Proteins	BoSG (µg/mL)	Heparin (µg/mL)
Thrombin	18.6 ± 0.7	41.6 ± 1.4
Antithrombin	ND	14.6 ± 0.8
HC Ⅱ	83.4 ± 5.5	44.5 ± 4.5
RBD wild type	9.0 ± 1.9	8.5 ± 1.7
RBD N501Y	4.4 ± 0.9	9.1 ± 1.4
RBD L452R	10.8 ± 4.0	6.1 ± 2.5
RBD K417T/E484K/N501Y	4.4 ± 0.8	7.7 ± 1.2

Table 5.6: IC$_{50}$ values for inhibition of binding by coagulation factors or S-proteins to immobilized heparin. ^{a} Means ± standard deviations from three independent experiments. ^{b} Not determined.

The binding of native BoSG (red bars) to the four S-protein RBDs was in general very similar to that observed for heparin (grey bars) (Figure 5.13D-G). This is consistent with the anti-SARS-CoV-2 data in Figure 5.12. Curiously, the BoSG low MW fragments showed very interesting and distinct binding properties among the RBD mutants. SGhd (royal blue bars) was able to interact with all RBDs but with different levels of affinity (Figure 5.13D-G). The best affinity was observed for the triple mutant (Figure 5.13G). Fractions Fr1-Fr4 showed strong binding affinity for the Alpha N501Y variant (Figure 5.13E), some affinity for the Gamma K417T/E484K/N501Y variant (Figure 5.13G,) and weak binding to wild type (Figure 5.13D) and the Delta L452R variant (Figure 5.13F). These results indicate that the BoSG derivatives have strong affinity for the RBDs that contain the N501Y substitution. In addition, through the competitive SPR assay (Table 5.4), it was further demonstrated that the native BoSG has stronger binding affinities for the N501Y-containing RBDs than for the single L452R variant or wild type RBD. The binding affinities of BoSG to the Alpha and Gamma variants (N501Y-containing strains) were approximately two-fold higher than those of UFH (Table 5.4).

5.3.2.8 Molecular docking of BoSG-derived disaccharide constructs to N501Y RBD

To define the contributions of different BoSG sulfation patterns to binding with the S-protein RBD, four possible BoSG (monosulfated/monosaccharide) disaccharides were constructed and computationally docked to the binding site close to the N501Y substitution in Alpha S-protein, which had the highest affinity observed by SPR. A heparin disaccharide was also constructed and docked for comparison. The binding site examined in this study was the same one previously used for the holothurian sulfated glycans in binding analyses to the wild type and the N501Y mutant S-protein RBDs.[145] The docking data are shown in Figure 5.14 and docking scores of the best-scored docked poses for the heparin disaccharide and the four BoSG disaccharides obtained from AutoDock Vina are shown in Figure 5.14F. The best-scoring docked pose of the heparin disaccharide to the N501Y mutant S-protein RBD indicated that its IdoA is oriented towards R408 and its O3 and O4 hydroxyl groups interact with D405 and R408, respectively (Figure 5.14A). Heparin binding to the N501Y variant lacked any interaction with Y501. A similar binding mode was observed for the BoSG [4S-3S] disaccharide (Figure 5.14B). However, some residues such as D405, R408 and Y505 were not seen to be interacting with the BoSG [4S-3S] disaccharide, resulting in a slight worsening of the docking score as compared to that of the heparin disaccharide (Figure 5.14F).
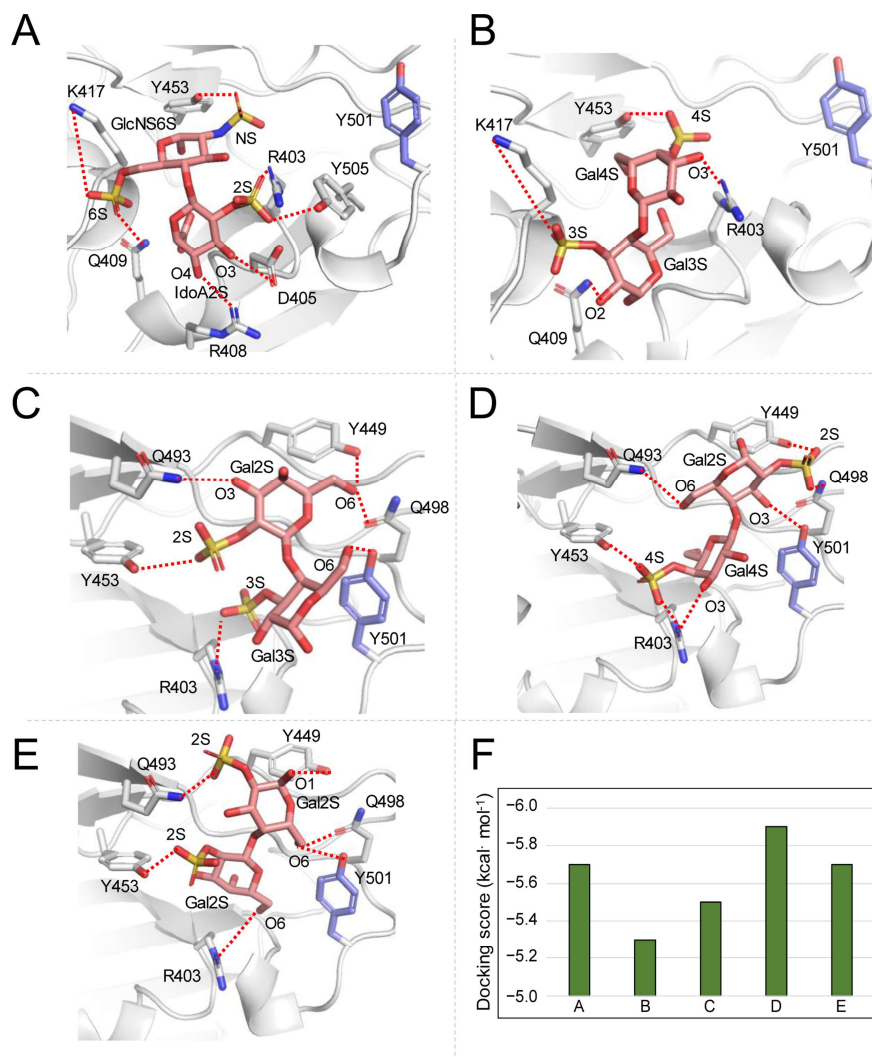
Figure 5.14: ***Predicted binding poses of heparin and BoSG (monosulfated/monosaccharide) disaccharides bound to N501Y of SARS-CoV2 S-protein RBD.*** *Docked (A) heparin, (B) BoSG [4S-3S], (C) BoSG [2S-3S], (D) BoSG [4S-2S], and (E) BoSG [2S-2S] disaccharides in N501Y variant. Selected neighboring interacting residues and the variant residue are shown in gray and purple, respectively. Dashed lines indicate polar interactions between the RBD and glycan atoms. (F) Docking scores of the top-scored docked poses as obtained from AutoDock Vina.*

The other three BoSG disaccharides [2S-3S], [4S-2S], and [2S-2S], showed a similar overall binding mode (Figure 5.14C–E), but one that differs significantly from the heparin and BoSG [4S-3S] disaccharide binding modes. In the BoSG [2S-3S] disaccharide, Y501 forms a polar interaction with O6 of its reducing end Gal unit which contains the 3-sulfation (Figure 5.14C). An electrostatic interaction between the 3-sulfation of the reducing end and R403 was additionally observed. Four residues, Y449, Y453, Q493, and Q498, formed polar interactions with O6, 2S, and O3 groups of the non-reducing end Gal unit of the BoG [2S-3S] disaccharide. Curiously, the Y453 residue showed significant interaction with one sulfate group of the non-reducing end Gal unit in each BoSG disaccharide (4S in Figure 5.14B and 6D; and 2S in Figure 5.14C and 6E).

In the BoSG [4S-2S] disaccharide, the 2S in the reducing end Gal unit forms two polar interactions with Y449 and Q498 (Figure 5.14D). The altered residue, Y501, and Q493 form polar interactions with O3 and O6 of the reducing moiety, respectively. Similar to what was found for the BoSG [2S-3S] disaccharide

(Figure 5.14C), R403 formed an electrostatic interaction with the 4S group of the [4S-2S] disaccharide (Figure 5.14D). An additional polar interaction was observed between R403 and the O3 group of the non-reducing end unit of this disaccharide.

Finally, for the BoSG homogeneously 2-sulfated disaccharide (Figure 5.14E), the O1 and 2S groups of the reducing end unit formed polar interactions with residues Y449 and Q493, respectively. The O6 group of the reducing end showed polar interactions with Y501. The non-reducing end of this BoSG disaccharide showed two key polar interactions of the 2S and O6 groups with residues Y453 and R403, respectively. For the two BoSG disaccharides containing 2-sulfation in the reducing end (Figure 5.14D and E), the overall binding orientation of the glycan was similar, with the sub-pocket containing residue Y449 being occupied by the reducing end of the sugar. Overall, from the docking poses of the RBD–BoSG disaccharides, it could be seen that residues Y501, Y449, Q498, R403, Q493 and Y453 play key roles in binding with the S-protein RBD N501Y mutant.

5.3.3 Discussion and Conclusion

Structural and functional investigations on the sulfated galactan from the red alga *B. occidentalis* (BoSG) are usually complex in nature. This polysaccharide, although highly potent in anticoagulation[24,26,27,131,146,147] and antithrombosis[27,129,148] can also show potential effects towards other systems,[126,127,147] including virus-associated pathologies.[126] In addition, the structure of BoSG is somewhat heterogeneous, not with regard to its highly homogeneous backbone (composed of repeating disaccharides with alternating 4-linked α-Gal and 3-linked β-Gal units), but in terms of sulfation patterns. Sulfation can occur at different sites of this molecule (C2 and C4 positions of the β-Gal unit and C2 and C3 positions of the α-Gal unit), and at different degrees (Figure 5.9A). This makes structural investigations and consequent structure-activity relationships of BoSG laborious and complex.

Here we decided to follow the strategy of depolymerizing BoSG for production of oligosaccharides to diminish the above-mentioned complexities regarding the structural and functional features of BoSG. Specific enzymes capable to cleave this marine polysaccharide (galactanases) are not widely known. Since chemical hydrolysis based on acidic digestive methods are well-established and commonly used for other marine sulfated glycans, such as sulfated fucans,[44,83,138,139,141] and also previously reported for BoSG,[131] we opted to use mild acid for depolymerization of BoSG. The optimal conditions established were 0.1 M HCl at 60°C for 7 h.

BoSG was properly depolymerized, giving rise to polydisperse oligosaccharide-based content with different MWs (SGhd, Figure 5.9C). The MW of this digested material ranged roughly from 80 kDa to 2 KDa and size fractionation (Figure 5.9B) led to a broad profile with no clearly defined peaks, indicating a lack of size- or structurally-defined oligosaccharide digestion products. This observation indicates nonspecific cleavage of glycosidic bonds of BoSG during the mild acid hydrolysis. In addition, desulfation specially at the C4 position of the β-Gal units was observed during the chemical depolymerization, as concluded from our analyses using 1D ^{1}H, 2D ^{1}H-^{1}H COSY, ^{1}H-^{13}C NMR and LC-MS (Figure 5.10). Desulfation of BoSG during formation of low MW fragments by mild acid hydrolysis was not unexpected since selective desulfation (at the C2 position) has been reported during mild acid hydrolysis of other marine sulfated glycans.[44,138]

From the undefined SEC profile (Figure 5.9B), four random fractions of BoSG oligosaccharides were pooled: Fr1 (MW ∼ 80-15 kDa), Fr2 (MW ∼ 40-10 kDa), Fr3 (MW∼15-8 kDa) and Fr4 (MW ∼10-2

kDa), as roughly estimated based on PAGE (Figure 5.9C). From the 1D ^{1}H NMR spectra the three lowest MW fragments (Fr2-Fr4) showed very similar spectra, in which the α-anomeric ^{1}H region has a dominant peak of δ_H at 5.27 ppm (purple, yellow, and cyan lines in Figure 5.10A). This signal was further characterized through the use of the ^{1}H-^{13}C HSQC and ^{1}H-^{1}H COSY spectrum of Fr4, indicating a monosulfated α-Gal unit. The ^{1}H chemical shift of the ^{1}H1 of all the 3-*O*-sulfated α-Gal units is very close in the spectrum (Table 5.3). The clear absence of the ^{1}H4-^{13}C4 signal of the 4-*O*-sulfated β-Gal unit was noted in the ^{1}H-^{13}C HSQC spectrum, indicating a lack of sulfation at the C4 of this 3-linked unit. Results from LC-MS (Figure 5.10C) indicated three major conclusions: (i) dp8 (octasaccharide) is the major oligosaccharide component of Fr4; (ii) the formation of oligosaccharides with odd and even dp numbers indicates random cleavage of the glycosidic linkages of BoSG; and (iii) the major components of Fr4 are monosulfated/monosaccharides. From the set of structural results we were able to demonstrate the structural heterogeneity of the BoSG fragments. For instance, Fr4 is composed of more than 20 different oligosaccharides (from dp7 to dp11, also with different sulfation contents per dp) (Figure 5.10C). Further purification based on size and charge might be needed in future work concerning the actual development of a structurally defined BoSG-derived oligosaccharide as an anti-SARS-CoV-2 drug.

Previous reports have shown that BoSG is active in the coagulation cascade by enhancing the inhibitory activities of AT over factors IIa and Xa, and HCII over factor IIa.[30,130,131] Here we investigated these anticoagulant systems using the BoSG low MW derivatives (Figure 5.11 and Table 5.4). We observed a clear dependence on the MW of BoSG in anticoagulation. In our studies only the native BoSG was capable of significant inhibition of coagulation activities in assays based on purified proteins (Figure 5.11C-D). The BoSG derivatives showed moderate activity in the aPTT system (Figure 5.11A). Since these fragments were observed to be very inactive on the serpin-dependent mechanism (Figure 5.11B-D), the residual activity observed through aPTT is very likely due to the residual serpin-independent anticoagulant action of BoSG, as reported previously.[26,27,128]

Although the residual anticoagulant action of low MW BoSG fragments is very weak, prophylactic monitoring of anticoagulant side effects should be carried out in case these fragments move on to clinical trials and use in human patients. The weak residual anticoagulant action of sulfated glycans used as antiviral therapeutics can be neutralized, if necessary, by administration of protamine sulfate, as performed for UFH, but this is much less likely to be necessary since the administered doses will be very low in the case of BoSG oligosaccharides. It is known that LMWH does not change aPTT very much and does not present bleeding risk as a side effect. As opposed to UFH, which requires constant monitoring, LMWH-based treatment does not require monitoring. We hypothesize that the BoSG fragments may behave like LMWH given their low aPTT values. However, future *in vivo* studies must be made to confirm such a hypothesis.

A previous report explained the reasons for the necessity of longer chains of BoSG to achieve the serpin-dependent anticoagulant action.[131] Results have indicated that the template mechanism is more dominant than the allosteric mechanism in serpin-dependent thrombin inactivation and that longer BoSG chains are likely capable to hold multiple serpins (AT or HCII) and proteases (IIa or Xa) together. Decrease in the length of this polysaccharide has the indicated impact on its activity over the coagulation factors, with consequential reduction of the serpin-dependent anticoagulant action.[131] Here, we demonstrate again that reduction in MW of BoSG decreases its anticoagulant effect, at least through the serpin-dependent mechanism.

In contrast, reduction of the MW of BoSG did not significantly impact anti-SARS-CoV-2 activity (Figure 5.12 and Table 5.5). For instance, although ~three-fold less active than native BoSG, Fr4, which is mostly composed of octasaccharides and generally monosulfated per monosaccharide, was very active in inhibiting entry of SARS-CoV-2 S-protein-pseudotyped lentivirus, while SGhd and Fr1-Fr3 were only 1.5 and 3-fold, respectively, less active than native BoSG. This data suggests that a medium-sized BoSG oligosaccharide would be sufficient for inhibition of S-protein RBD interaction with HS or hACE2. Our SPR-based binding results have confirmed that reduction of MW of BoSG can significantly impact the anticoagulant outcome but not the anti-SARS-CoV-2 effect (Figure 5.5).

One might question the impact of sulfation versus chain length on the biological systems, since besides MW reduction we also observe desulfation during mild acid hydrolysis of BoSG. The contributions of these two structural features (sulfation and MW) can be deduced by comparing the results obtained from PAGE (Figure 5.9C), the 1D ^{1}H NMR spectra of the BoSG derivatives, and the inhibitory curves (Figure 5.11C-D and Figure 5.12). As can be seen, desulfation is dominant in Fr2-Fr4 since these derivatives showed the most modified 1D ^{1}H NMR spectra as compared to the native BoSG, especially regarding the changes on the downfield ^{1}H signals of the 2,3-disulfated α-Gal units (Figure 5.10A). Based on our analysis, disulfated α-Gal units are still significantly present in the SGhd (royal blue line in Figure 5.10A) and Fr1 (green line in Figure 5.10A). Hence, these fragments show chemical changes more with respect to MW than to sulfation (Figure 5.9C versus Figure 5.10A). The MW reduction from native BoSG (≥ 100 kDa, (Figure 5.9C) to the polydisperse MW distribution of SGhd (below 90 kDa) was, however, enough to significantly abolish the serpin-dependent anticoagulant property (red and royal blue curves in Figure 5.11B-C and Table 5.2), but not significantly impact anti-SARS-CoV-2 activity (Figure 5.12B and C and Table 5.5). This indicates a primary dependence on MW for the anticoagulation capability.

The anti-SARS-CoV-2 activities of SGhd and Fr1 (more sulfated molecules) as compared to Fr2-F4 (in which structural changes in these fractions are primarily MW reduction rather than desulfation, see Figure 5.10A) were nearly equal (Figure 5.12 and Table 5.5). This suggests little impact of MW or desulfation on anti-coronaviral activity. In contrast, the anticoagulant effect of BoSG requires longer glycan chains to achieve the template serpin-dependent anticoagulant mechanism seen in the tertiary serpin-protease-glycan complex. In addition, longer BoSG chains can enable interaction and inactivation of multiple blood proteases by the same glycan chain. As opposed to the anticoagulant effect, SPR data (Figure 5.13) indicates that inhibition of heparin binding by S-protein RBD containing the N501Y mutation can be accomplished just by medium-sized oligomeric lengths in order to achieve effective molecular interactions and consequent viral inhibition (Figure 5.12).

Docking of the BoSG disaccharides to the N501Y mutant S-protein helped predict the overall poses of the BoSG derivatives in the binding site close to the 501Y residue and indicated the various possible pairwise mutant–BoSG polar interactions. This will identify all the possibly important S-protein RBD residues for potential modification to modulate glycan binding. Negative docking scores of the sulfated glycans indicated that the binding to the site close to the 501Y residue was favorable.

Docking analysis (Figure 5.14) has shown that heparin and the BoSG [4S-3S] disaccharide can interact with the S-protein N501Y RBD with similar binding poses between them (Figure 5.14A and B), but with different poses as compared with the three other BoSG disaccharides, which showed similar binding poses between them (Figure 5.14C-F). For the former two disaccharides, atomic interactions were observed between residues K417 and Q409 with the reducing end monosaccharide units (Figure 5.14A

and B). For the latter three BoSG disaccharides, atomic interactions were observed between residues Y501, Y449, Q498, R403, Y453, and Y449 and the disaccharides. The studied BoSG disaccharides containing 2-sulfation at the 4-linked α-Gal unit at the reducing end ([2S-2S] and [4S-2S]) had the best docking scores although just slightly better than the other three studied disaccharides. In summary, sulfation and monosaccharide composition impact the binding properties of heparin and BoSG to the S-protein RBD sites near the 501Y residue.

In this work, we were able to successfully produce a set of different oligosaccharide fractions from the structurally complex sulfated galactan from the red alga B. occidentalis (BoSG). Native BoSG shows both significant anticoagulant and anti-SARS-CoV-2 actions. The ideal anticoronaviral sulfated glycans would be those lacking activity on coagulation. This would make the polysaccharide more specific towards its antiviral action. Through a strategy of depolymerization we were able to virtually abolish the anticoagulant action of the BoSG-derived oligosaccharides but still retain the anti-SARS-CoV-2 action. Here, we also noticed great selectivity of the BoSG and low MW derivatives towards the SARS-CoV-2 variants that express the N501Y mutation in their S-protein RBD. In conclusion, the absence of anticoagulant effects associated with specific anti-SARS-CoV-2 effects indicates the important and selective properties of the red algal sulfated glycan studied here.

5.4 Selective antiviral inhibition by marine sulfated glycans

5.4.1 Introduction

Emerging viruses are an increasingly large issue. In the past 20 years, we have seen the emergence of three coronaviruses (SARS-CoV-1 in 2003, MERS-CoV in 2015, and SARS-CoV-2 in 2019) and two influenza viruses (H1N1 in 2009 and H7N9 in 2013), not to mention emerging viruses from the 20th century.[149] With each new virus, we face the challenge of developing new vaccines and therapeutics. Broad-spectrum antivirals have the potential to ameliorate this problem; if they were ready for rapid deployment, we could then focus on the development of new specifically targeted treatments.

Previously, viral entry and attachment have been a target for potential broad-spectrum antivirals. A large number of viruses utilize glycans, including HS, a highly sulfated glycosaminoglycan, and sialic acids, to attach to the cell surface, and then use specific cellular receptors for entry. Peptides, small molecules, and glycan mimetics have been used to inhibit viral attachment. As reviewed in Chapter 1, GAG mimetics are often plagued with anticoagulant activity, making it difficult to rationalize their use as antivirals.

Here, we test the antiviral activity of five marine sulfated glycans (MSGs) against SARS-CoV-1, SARS-CoV-2, MERS-CoV, and influenza virus, and compare them to heparin, a commonly used HS-mimetic composed primarily of disaccharide repeating units of [-4)-N,6-disulfated-glucosamine-(α1-4)-2-sulfated-iduronic acid-(α1-] (Figure 5.15A). A sulfated galactan isolated from the red alga *Botryocladia occidentalis* (BoSG) is composed of the disaccharide repeating unit [-3)-2,4-disulfated-galactose-(α1-4)-2,3-disulfated-galactose-(β1-] in which sulfation patterns may vary in percentage but never in position (MW >100 kDa) (Figure 5.15B).[29] A fucosylated chondroitin sulfate isolated from the sea cucumber *Isostichopus badionotus* (IbFucCS) is composed of the trisaccharide-repeating unit {-4)-[fucose-(α1-3)]-glucuronic acid-(β1-3)-N-acetylgalactosamine-(β1-} in which sulfation patterns may vary in percentage but never in position (MW ~75 kDa) (Figure 5.15C).[38] A sulfated fucan isolated from the sea urchin *Lytechinus variegatus* (LvSF) is composed of the tetrasaccharide-repeating unit of [-3)-4-sulfated-fucose-(α1-3)-2,4-disulfated-fucose-(α1-3)-2-sulfated-fucose-(α1-3)-2-sulfated-fucose-(α1] (MW ~90 kDa) (Figure 5.15D).[29]

A sulfated fucan also isolated from *Isostichopus badionotus* (IbSF) is composed of the tetrasaccharide-repeating unit of [-3)-fucose-(α1-3)-2,4-disulfated-fucose-(α1-3)-2-sulfated-fucose-(α1-3)-2-sulfated-fucose-(α1] (MW ~100 kDa) (Figure 5.15E).[39] A fucosylated chondroitin sulfate (FucCS) from the sea cucumber *Pentacta pygmaea* (PpFucCS) is composed of {$\rightarrow$3)-β-GalNAcX-(1$\rightarrow$4)-β-GlcA-[(3$\rightarrow$1)Y]-(1$\rightarrow$}, where X = 4S (80%), 6S (10%) or nonsulfated (10%), Y = α-Fuc2,4S (40%), α-Fuc2,4S-(1$\rightarrow$4)-α-Fuc (30%), or α-Fuc4S (30%), and S = SO_3^- (MW ~10–60 kDa) (Figure 5.15F).[145] Overall BoSG and PpFucCS are heterogenous in sulfation pattern while LvSF, IbSF, and IbFucCS have chemically defined structures with more uniform sulfation and saccharide composition.[12,40,41,145] This series of MSGs should allow an investigation of the relationships between structure and antiviral activity.
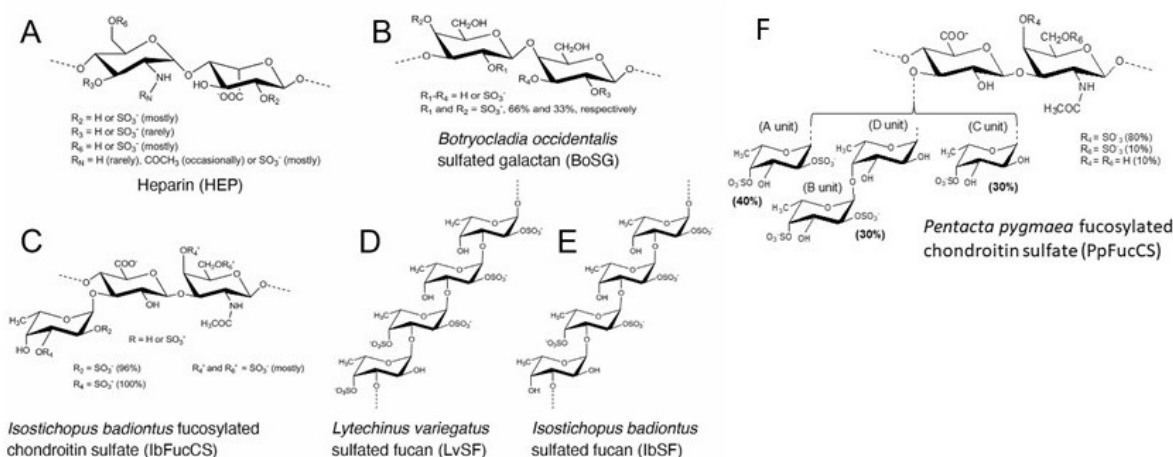
Figure 5.15: Structures and size characterization of the marine sulfated glycans and heparin (counterions and carbon-bonded hydrogens omitted for clarity).

5.4.2 Results

5.4.2.1 Marine sulfated glycans inhibit SARS-CoV-1 and SARS-CoV-2

The antiviral activity of a compound is quantified by its EC_{50}, the concentration at which 50% of virus replication is inhibited. Cytotoxicity of a compound is quantified by its TC_{50}, the concentration at which 50% of the cells die. To determine EC_{50}s for MSGs, their impact on viral entry was determined using GFP-tagged pseudotyped lentiviruses, while TC_{50}s were simultaneously determined for replicate uninfected cultures using the CellTiter-Glo cell viability assay.[150,151] Results are shown in Figure 5.16 and Table 5.7.

The selectivity index (SI) is the ratio of TC_{50} to EC_{50}. A high SI suggests a favorable safety and efficacy profile of a compound. The MSGs did not have any cytotoxicity up to 400 µg/mL and as such, have large selectivity indices (Table 5.7, and Table 5.8)
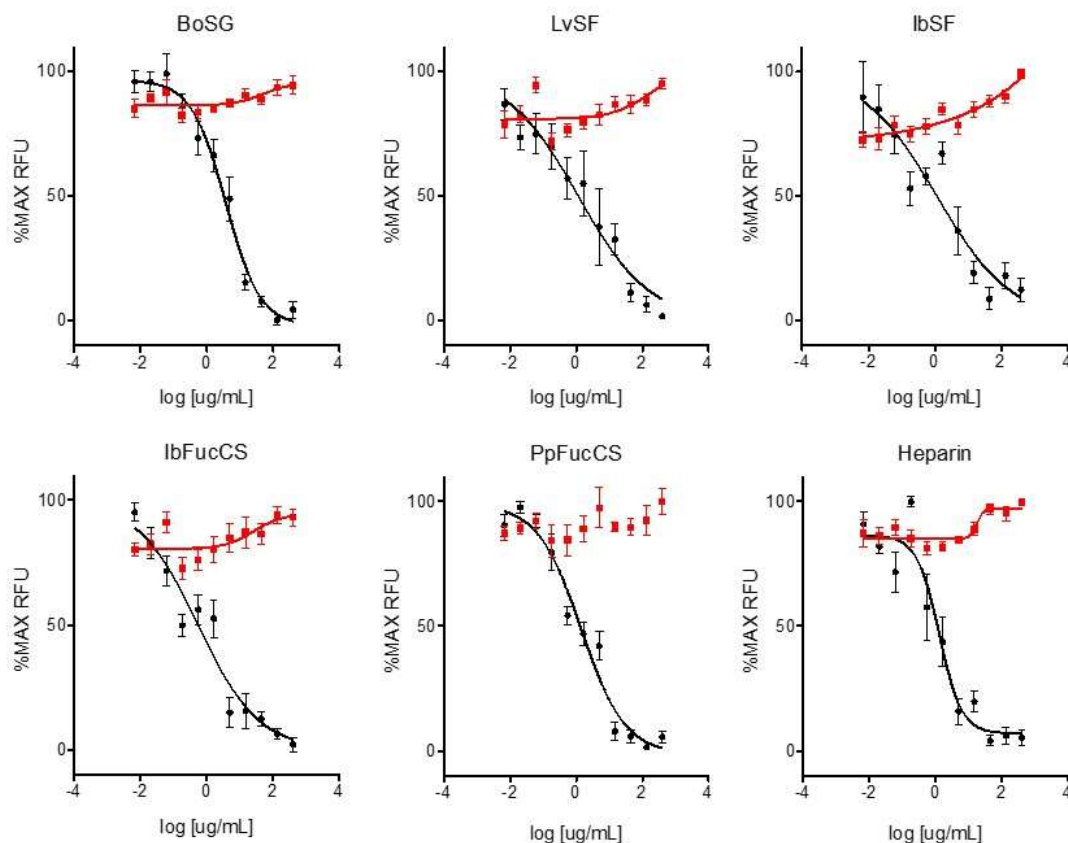
Figure 5.16: Antiviral activity of MSGs against pseudotyped SARS-CoV-2. Anti-SARS-CoV-2 activity (black) was measured by incubating HEK-293T-hACE2 cell monolayers in 384-well plates with MSGs for one h, infecting with GFP-tagged pseudovirus (125 transducing units/well), and measuring GFP levels (RFU) two days after infection. Cytotoxicity (red) was measured in replicate uninfected cultures treated for two days using the CellTiter-Glo® assay. Data are means of three independent experiments ± standard deviations.

Table 5.7: Anti-SARS-CoV-2 activities of MSGs.

MSG	Antiviral[a] (EC_{50})	Cytotoxicity[b] (TC_{50})	SI[c]
Heparin	2.11 ± 1.44	>400	>189.6
BoSG	2.00 ± 0.79	>400	>200
LvSF	3.99 ± 0.54	>400	>100.3
IbSF	3.75 ± 0.87	>400	>106.7
IbFucCS	1.07 ± 0.85	>400	>373.8
PpFucCS	1.64 ± 0.78	>400	>243.9

[a]*GFP-based assay.* [b]*CellTiter-Glo® assay.* [c]*selectivity index (TC_{50}/EC_{50}).* [a,b,d]*µg/mL; means of three independent experiments ± standard deviations.*

Likewise, MSGs were screened for anti-SARS-CoV-1 activity using pseudotyped lentiviruses (Figure 5.17 and Table 5.8). All MSGs maintained low EC_{50}s, lacked cytotoxicity up to 400 µg/mL, and had favorable selectivity indices.

*Figure 5.17: **Antiviral activity of MSGs against pseudotyped SARS-CoV-1.** Anti-SARS-CoV-1 activity (black) was measured by incubating HEK-293T-hACE2 cell monolayers in 384-well plates with MSGs for one h, infecting with GFP-tagged pseudovirus (125 transducing units/well), and measuring GFP levels (RFU) two days after infection. Cytotoxicity (red) was measured in replicate uninfected cultures treated for two days using the CellTiter-Glo® assay. Data are means of three independent experiments ± standard deviations.*

Table 5.8: Anti-SARS-CoV-1 activities of MSGs.

MSG	Antiviral[a] (EC_{50})	Cytotoxicity[b] (TC_{50})	SI^c
Heparin	1.672 ± 0.21	>400	>239.3
BoSG	2.504 ± 0.39	>400	>159.7
LvSF	3.131 ± 0.81	>400	>127.8
IbSF	3.358 ± 0.94	>400	>119.1
IbFucCS	3.373 ± 0.99	>400	>118.6
PpFucCS	3.499 ± 0.77	>400	>114.3

[a]GFP-based assay. [b]CellTiter-Glo® assay. [c]selectivity index (TC_{50}/EC_{50}). [a,b,d]µg/mL; means of three independent experiments ± standard deviations.

5.4.2.2 MSGs inhibit entry of SARS-CoV-2 and SARS-CoV-1

To assess the mechanism of action of MSGs, we treated cells at various time points before and after infection of SARS-CoV-1 or 2 pseudotyped lentiviruses. As seen in Figure 5.18 and Figure 5.19, MSGs inhibited GFP expression only if cells were treated prior to infection, similar to heparin. Likewise, a time of addition assay with SARS-CoV-1 or -2 revealed that MSGs only inhibit viral GFP expression if cells were pretreated, indicative of entry or attachment inhibitors (Figure 5.20). Finally, we treated cells with compounds, washed with media, then infected the cells to assess whether MSGs bind a cellular or viral

component to inhibit attachment; as MSGs did not significantly inhibit most GFP expression after washing, we can conclude that they bind a viral component (Figure 5.21and Figure 5.22).
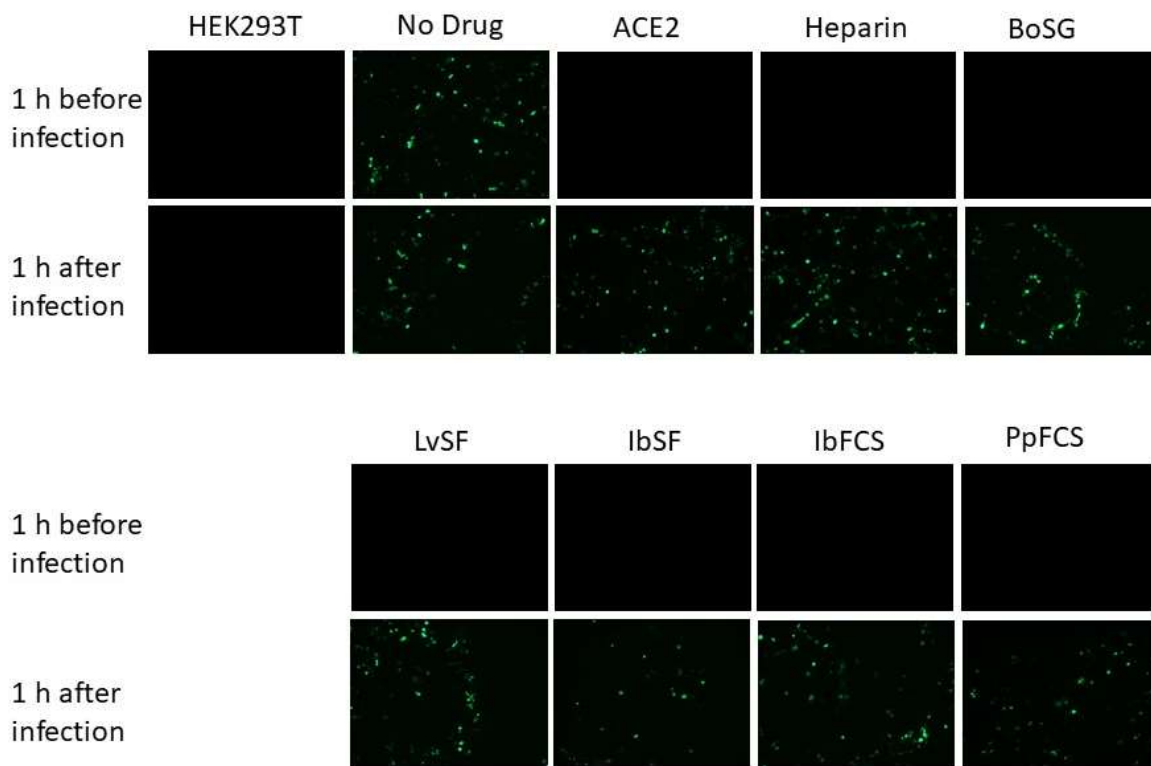
Figure 5.18: MSGs inhibit GFP expression resulting from transduction of SARS-CoV-2 pseudoviruses. Confluent monolayers of HEK-293T (top, left column) or HEK-293T-ACE2 (all other columns) cells in 96-well plates were treated with medium (Ø), 150 µg/ml heparin, BoSG, LvSF, IbSF, IbFucCS, or PpFucCS, or 300 µg/ml soluble ACE2 one h before (top) or one h after (bottom) infection with GFP-tagged SARS-CoV-2 pseudovirus (100 transducing units/well).
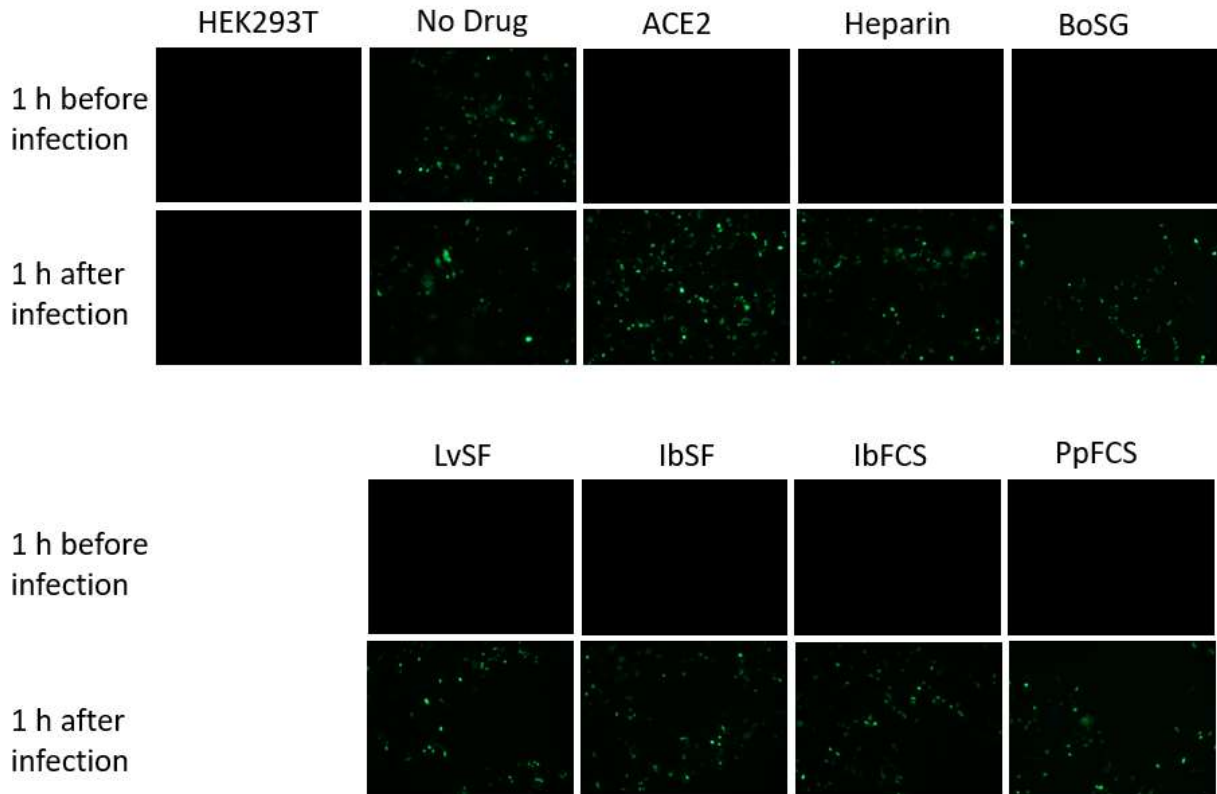
Figure 5.19: MSGs inhibit GFP expression resulting from transduction of SARS-CoV-1. Confluent monolayers of HEK-293T (top, left column) or HEK-293T-ACE2 cells (all other columns) in 96-well plates were treated with medium (Ø), 150 μg/ml heparin, BoSG, LvSF, IbSF, IbFucCS, or PpFucCS, or 300 μg/ml soluble ACE2 one h before (top) or one h after (bottom) infection with GFP-tagged SARS-CoV-1 pseudovirus (100 transducing units/well).
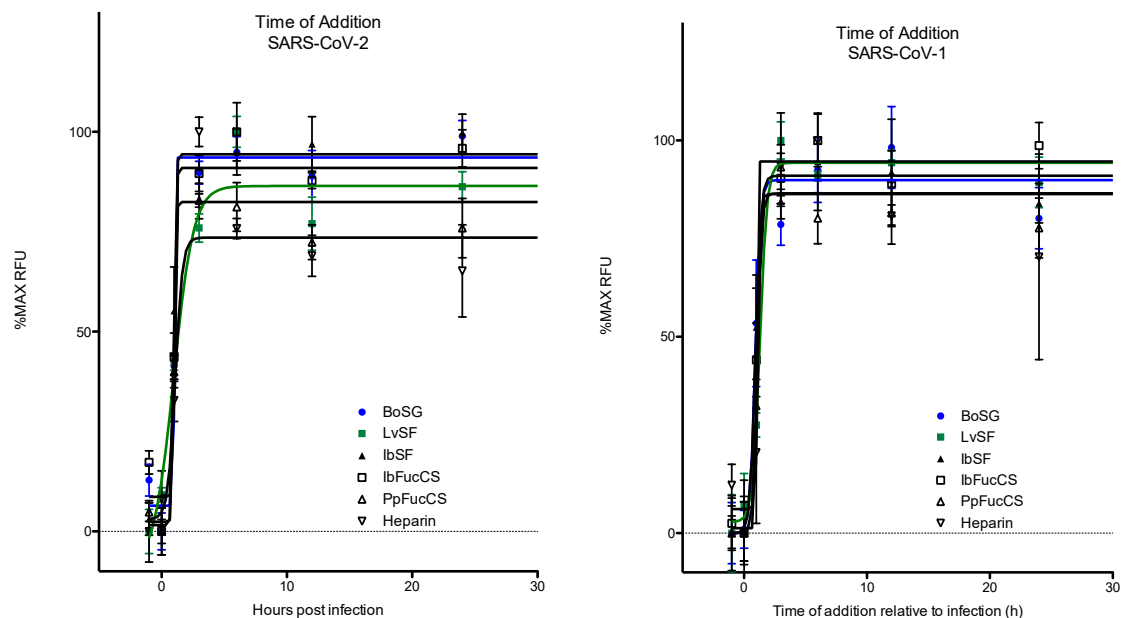
Figure 5.20: Time of addition study for MSG inhibition of SARS-CoV-2 (Left) or SARS-CoV-1 (Right). Confluent monolayers of HEK-293T-ACE2 cells were treated with 150 μg/ml heparin, BoSG, LvSF, IbSF, IbFucCS, or PpFucCS 1 h before, concurrent with, or at

various times after infection with GFP-tagged pseudoviruses (100 transducing units/well). GFP expression was quantified on day two post infection. Data are means of triplicate wells ± standard deviations.
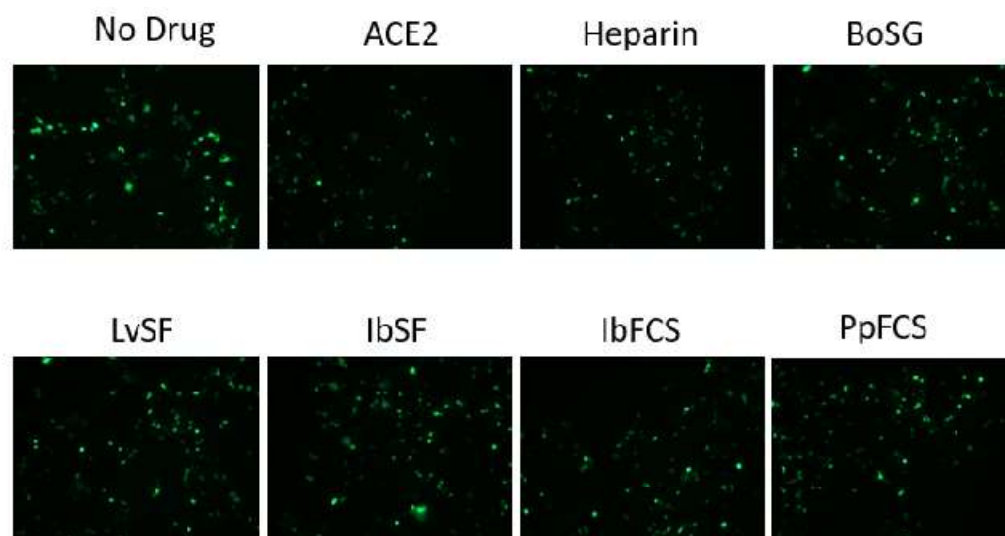
Figure 5.21: MSGs bind a viral component to inhibit SARS-CoV-2. Confluent monolayers of HEK-293T-ACE2 cells in 96-well plates were treated with medium (Ø), 150 μg/ml heparin, BoSG, LvSF, IbSF, IbFucCS, or PpFucCS, or 300 μg/ml soluble ACE2 for one h then washed thoroughly prior to infection with GFP-tagged SARS-CoV-2 pseudovirus (100 transducing units/well). Representative fluorescent micrographs were taken two days post infection.
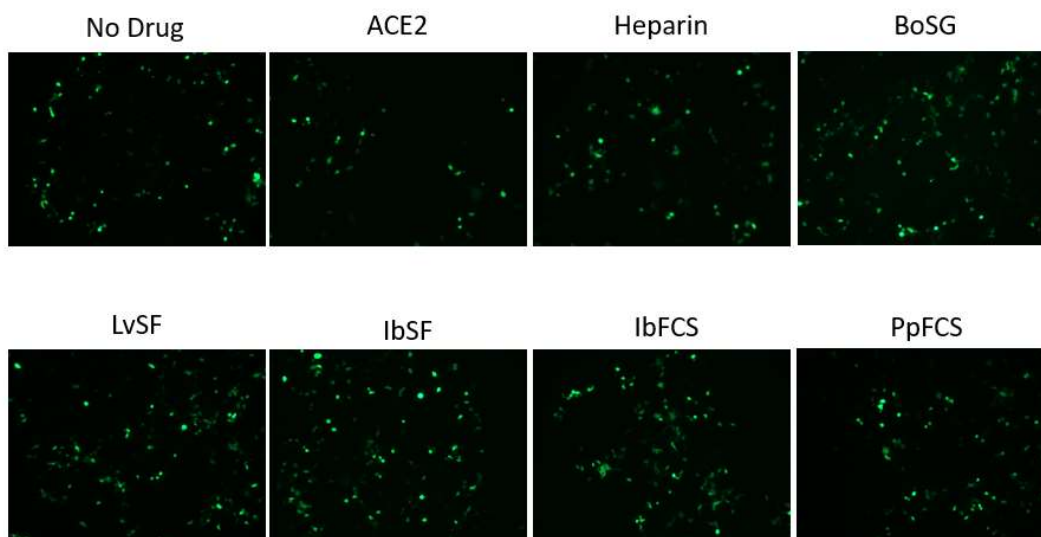
Figure 5.22: MSGs bind a viral component to inhibit SARS-CoV-1. Confluent monolayers of HEK-293T-ACE2 cells in 96-well plates were treated with medium (Ø), 150 μg/ml heparin, BoSG, LvSF, IbSF, IbFucCS, or PpFucCS, or 300 μg/ml soluble ACE2 for one h then washed thoroughly prior to infection with GFP-tagged SARS-CoV-1 pseudovirus (100 transducing units/well). Representative fluorescent micrographs were taken two days post infection.

5.4.2.3 MSGs inhibit MERS-CoV

The anti-MERS-CoV activity of MSGs was assessed with the pseudotyped lentivirus system. Results are shown in Figure 5.23 and Table 5.9. MSGs were more potent than heparin but were considerably less potent against MERS-CoV in comparison to their activities against SARS-CoV-1 and 2 (Figure 5.16 and Figure 5.17). Their selectivity indices remain high as they were not cytotoxic to HeLa-DPP4 cells.

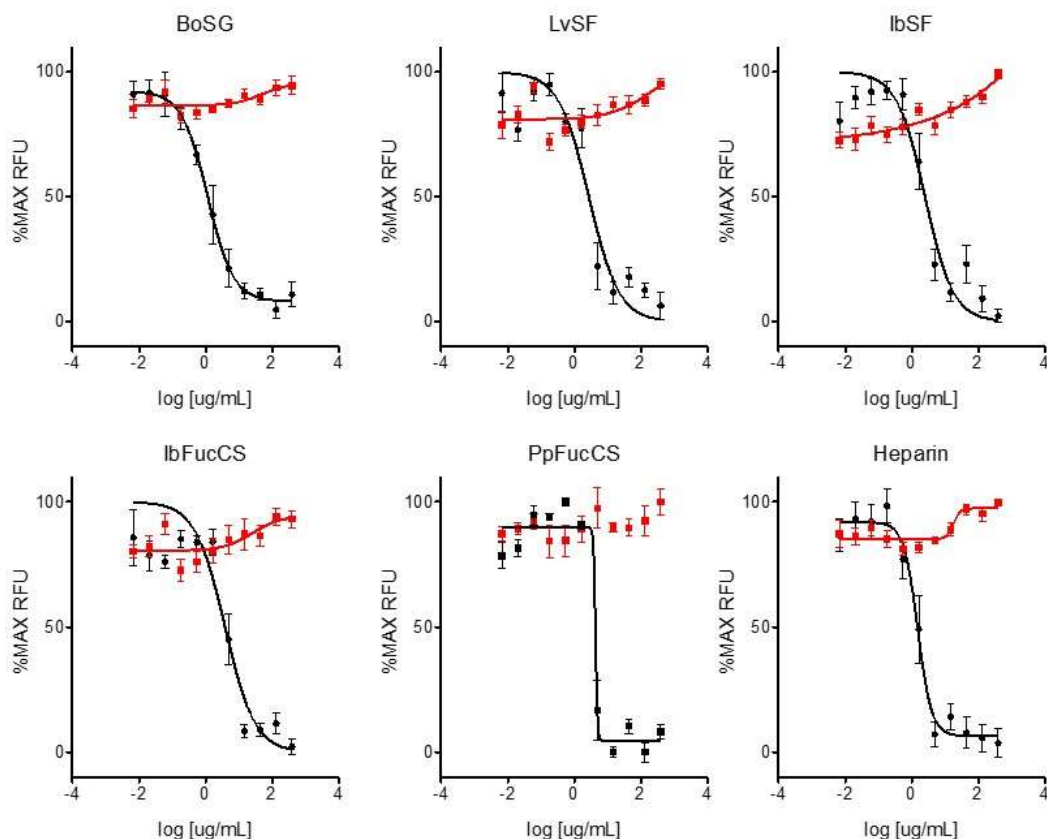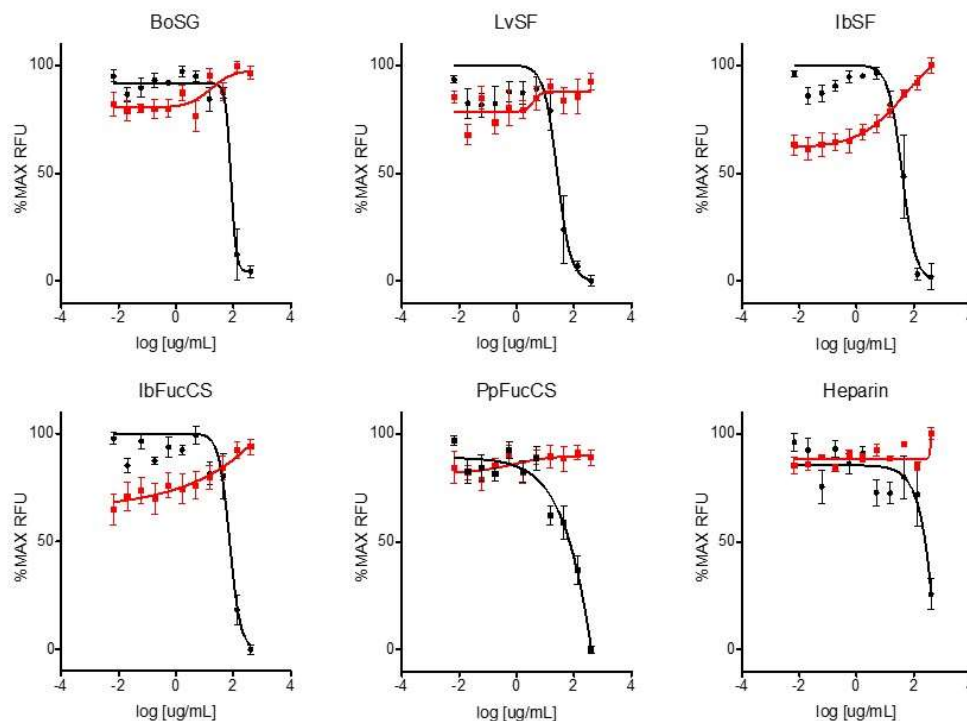*Figure 5.23: **Antiviral activity of MSGs against pseudotyped MERS-CoV.** Anti-MERS-CoV activity (black) was measured by incubating HeLa-DPP4 cell monolayers in 384-well plates with PPCs for one h, infecting with GFP-tagged pseudovirus (100 transducing units/well), and measuring GFP levels (RFU) two days after infection. Cytotoxicity (red) was measured in replicate uninfected cultures treated for two days using the CellTiter-Glo® assay. Data are means of three independent experiments ± standard deviations.*

Table 5.9: Anti-MERS-CoV activities of MSGs.

MSG	Antiviral^a (EC$_{50}$)	Cytotoxicity^b (TC$_{50}$)	SI^c
Heparin	~400	>400	>1
BoSG	83.89 ± 14.1	>400	>4.7
LvSF	35.46 ± 9.4	>400	>11.2
IbSF	44.64 ± 9.1	>400	>8.9
IbFucCS	86.72 ± 11.2	>400	>4.6
PpFucCS	123.01 ± 19.7	>400	>3.3

^{a}GFP-based assay. ^{b}CellTiter-Glo® assay. ^{c}selectivity index (TC$_{50}$/EC$_{50}$). ^{a,b,d}µg/mL; means of three independent experiments ± standard deviations.

5.4.2.4 MSGs do not inhibit influenza virus

The impact of MSGs on influenza virus entry was determined using a GFP-tagged lentivirus pseudotyped with influenza HA, while TC$_{50}$s were simultaneously determined for replicate uninfected cultures using the CellTiter-Glo cell viability assay.[150,151] Results are shown in Figure 5.24; MSGs were not active against influenza virus up to 400 µg/mL.
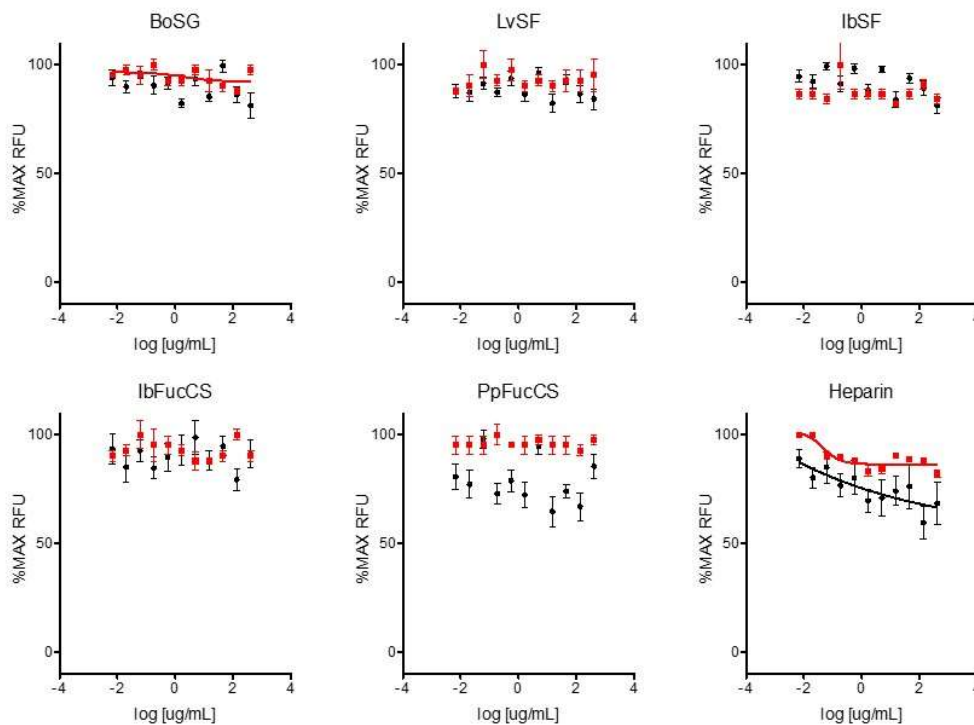
Figure 5.24: Antiviral activity of MSGs against influenza HA pseudotyped lentiviruses. Anti-influenza virus activity (black) was measured by incubating HEK-293T cell monolayers in 384-well plates with MSGs for one h, infecting with GFP-tagged HA pseudoviruses (100 transducing units/well), and measuring GFP levels (RFU) two days after infection. Cytotoxicity (red) was measured in replicate uninfected cultures treated for two days using the CellTiter-Glo® assay. Data are means of three independent experiments ± standard deviations.

5.4.3 Discussion and Conclusion

Emerging viruses such as SARS-CoV-1, MERS-CoV, influenza virus, and SARS-CoV-2 pose a current and future threat to public health. Each of these viruses has been shown to be dependent on glycans, either HS or sialic acid, for attachment and/or entry. As such, glycan mimetics have been shown to inhibit their replication. With high and variable molecular weights and structural variability, anionic GAG mimetics are poor candidates for therapeutic applications. However, the structures of MSGs are more regular than their mammalian counterparts; additionally marine and algal polysaccharides are readily available in nature, nontoxic, inexpensive, and biocompatible, making them a more reasonable option for use as antiviral inhibitors.[7]

The anti-SARS-CoV-2 activity of BoSG, LvSF, IbFucCS, IbSF, and PpFucCS have been previously described using pseudotyped baculoviral system.[145] Here, the FucCSs (IbFucCS and PpFucCS) were the most active, followed by BoSG, heparin, and IbSF, which were approximately equal; LvSF had the lowest activity (Table 5.7). This echoes what was previously reported, albeit with different EC_{50}s, which is reasonable considering the two different pseudotyping systems. Likewise, the antiviral activities were similar to those in SARS-CoV-1 activity (Table 5.8). PpFucCS was the most active and LvSF was the least. Considering the similarities between SARS-CoV-1 and 2 spike proteins, this is also reasonable.[95,152] However, the entire series of MSGs was much less active against MERS-CoV but more active than heparin (Table 5.9). This may be consistent with MERS-CoV spike's affinity for HS, which is reduced compared to that of SARS-CoV-1 and 2.[152] This is also in line with the differing glycan dependence between the three

coronaviruses. However it may also indicate that high sulfation is not favored for anti-MERS-CoV activity. Finally, none of the MSGs were active against influenza virus up to 440 ug/mL. Given that this is the only non-coronavirus tested, it is possible that the structural requirement for the glycan differs too much between coronavirus Spike and influenza virus hemagglutinin.[153] However, it may also be an incomplete broad-spectrum antiviral activity as seen previously. For instance, a highly sulfated exopolysaccharide, p-KG03, from *Gyrodinium impudicum* strain KG03 (highly sulfated homopolysaccharide of galactose conjugated with uronic acid and sulfate groups) has incomplete broad spectrum antiviral activity against encephalomyocarditis virus (EMCV) and influenza A, but not influenza B.[154,155] This was also seen with sulfated polysaccharides studied by Baba et al. which were active against HSV, HCMV, VSV, Sindbis virus, and HIV, but not against adenovirus, coxsackievirus, poliovirus, and reovirus.[72]

Across the three coronaviruses, MSGs maintained their mechanism of action, as described in HCMV and adenovirus.[1] MSGs inhibit GFP expression of pseudotyped SARS-CoV-1 and -2 as well as MERS-CoV only if cells were treated prior to infection. Time of addition revealed that these viruses were only inhibited if MSGs were present prior to or at the time of infection. Finally, washing experiments indicated that MSGs bind a viral component to inhibit attachment. Presumably, MSGs are binding coronavirus spike protein, which is supported by published surface plasmon resonance and molecular modeling.[2,145]

In terms of structure-activity relationships, the molecular weights of MSGs are directly related to their activity.[44,129,131] In these data, PpFucCS had the best anti-SARS-CoV-2 activity but it has the lowest molecular weight. This was also seen by Dwivedi et al., who postulated that PpFucCS may have special structure features that compensates for its shorter backbone; the terminal α-Fuc-2,4S unit is the major feature of PpFucCS and may serve in this role.[145] The sulfation level and monosaccharide type pattern has been suggested to determine viral-glycan binding.[50] Interestingly, PpFucCS and IbFucCS had similar antiviral activity despite their structural differences. Of note, BoSG was only slightly less active than the FucCSs despite its larger sulfation content and different monosaccharide type. Both sulfated fucans (IbSF and LvSF) were less active than the other MSGs, but had similar antiviral activities to each other. Although both are homopolymers of α-Fuc units, they have different sulfation papers in their repeating tetrasaccharide; LvSF is 4-sulfated, where IbSF is unsulfated in the α-Fuc units, giving LvSF a slightly higher negative charge.[39,83]

While heparin and its derivatives have excellent antiviral activities against a number of viruses, heparin has potent anticoagulant activity and is associated with hemorrhage and heparin-induced thrombocytopenia.[50,104] MSGs have variable anticoagulant activity in comparison. FucCSs are well known anticoagulants, targeting serpins HCII and AT as well as tenase complex; PpFucCS has moderate anticoagulant activity, less than both heparin and IbFucCS.[145,156,157] BoSG has strong anticoagulant activity, however its anti-SARS-COV-2 activity has been separated from anticoagulant activity through fractionation (Section 5.4).[2] Both sulfated fucans have negligible anticoagulant activity.[13,39]

In this study, we demonstrated the incomplete broad-spectrum antiviral activity of MSGs. While this series of MSGs have similar antiviral activity against both SARS-CoV-1 and -2, they have significantly decreased activity against MERS-CoV; this may indicate the drastic difference between the spike proteins of these coronaviruses and merits further study. None of the MSGs were active against influenza virus, perhaps illustrating influenza's dependence on sialic acids. That being said, these MSGs still balance antiviral activity with anticoagulant activity. In this series, the sulfated fucans had the lowest anticoagulant

activity but maintained good antiviral activity, making them candidates for further study for the development of broad-spectrum antivirals.

5.5 Materials and Methods

5.5.1 Cell and viral culture

Human MRC-5 fetal lung fibroblasts (ATCC CCL-171), human APRE-19 epithelial cells (derived from retinal pigment epithelium) (ATCC CRL-2302), and human adenocarcinoma epithelial cells (HeLa cells) (ATTC CCL-2) were purchased from American Type Culture Collection. Human Embryonic Kidney Cells (HEK-293T) and HEK-293T expressing human angiotensin-converting enzyme 2 (HEK-293T-hACE2; NR-52511) cells were purchased from BEI Resources. HeLa cells expressing dipeptidyl peptidase 4 (HeLa-DPP4) were a gift from David Namazee (Scripps). APRE-19, HeLa, HeLa-DPP4, HEK-293T, and HEK-293T-hACE2 cells were cultured at 37°C in a 5% CO_2 atmosphere using Dulbecco's Modified Eagle Medium supplemented with 10% fetal bovine serum, 50 U/mL penicillin, 50 mg/mL streptomycin, and 29.2 mg/mL L-glutamine (DMEM, all from Life Technologies).

Virus BAD*r*UL131-Y4 (BADr), a gift from Dai Wang and Thomas Shenk (Princeton University), is a variant of HCMV strain AD169 that is epithelial tropic due to repair of a mutation in *UL131A* and contains a green-fluorescent protein (GFP) reporter cassette.[158] Virus RC2626 is a variant of HCMV strain Towne that contains an expression cassette for firefly luciferase.[159] RC2626 and BADr were propagated in MRC-5 and ARPE-19 cells, respectively. Virus stocks were derived from infected cell culture supernatants, adjusted to 0.2 M sucrose, and stored in liquid nitrogen. Viral titers were determined using MRC-5s as described.[160] Stocks of GFP-tagged adenovirus, provided by Dr. Daniel Conway at Virginia Commonwealth University, were produced using the pAdeasy adenovirus-packaging system as described.[161,162]

5.5.2 Compounds and compound synthesis

BAY 38-4766 was a gift from Bayer Pharmaceuticals, foscarnet (phosphonoformic acid, PFA) was purchased from InvivoGen, and heparin sodium was purchased from Acros Organics (Lot # B0146868). BAY 38-4766, PFA, and MonoplatinNC were dissolved in water at a stock concentration of 10 mM. Heparin was dissolved in water at a stock concentration of 1000 µg/mL.

Purification of BoSG, LvSF, and PpFucCS were conducted as previously described [24,145,163]. Sea cucumber *Isostichopus badionotus* was obtained from Gulf Specimen Lab (Gulf of Mexico, Florida keys). Polysaccharides IbSF and IbFucCS were isolated from *Isostichopus badionotus* following a slightly modified protocol reported earlier [38,39]. BoSG, LvSF, IbSF, PpFucCS, and IbFucCS were dissolved in water at a stock concentration of 3 mg/mL.

5.5.3 Luciferase-based yield assay of antiviral activity

Eleven three-fold serial dilutions of MSGs were prepared in DMEM. Final concentrations ranged from 400 µg/mL to 6.7 ng/mL. Black-wall/clear-bottom 96-well plates with confluent monolayers of MRC-5 cells were treated with different concentrations of each test compound in triplicate. After one h of incubation cells were infected with RC2626 (125 PFU/well). Infected and uninfected wells without compound served as controls. Following incubation for five days 100 µL of culture media was removed from each well and transferred to wells of a fresh 96-well plate containing confluent uninfected MRC-5 cells. Following an additional two-day incubation luciferase activity was measured by removing 100 µL of media and adding 100 µL of Steady-Glo® luciferase substrate (Promega), incubating ten minutes at room temperature, and measuring relative luminosity units (RLU) using a BioTek Synergy HT Multi-Mode Microplate reader. Prism 5 software (Graphpad) was used to determine 50% effective concentration (EC_{50})

values as the inflection points of best-fit four-parameter curves for RLU (means of triplicate data) versus log inhibitor concentration. Graphical representations were normalized to % maximum RLU.

5.5.4 GFP-based assay of antiviral activity

For HCMV: Confluent monolayers of MRC-5 cells in 96-well plates were prepared and treated with compound dilutions as described in *5.6.3* above. After one h of incubation cells were infected with virus BADr (100 PFU/well). Following incubation for six days, relative fluorescence units (RFU) of GFP fluorescence were quantified by BioTek Synergy HT Multi-Mode Microplate reader and EC_{50} values were determined as described in *5.5.3*. Graphical representations were normalized to % maximum RFU.

For Adenovirus: Confluent monolayers of ARPE-19 cells in 96-well plates were prepared and treated with compound dilutions as described in *5.6.3* above. After one h of incubation cells were infected with GFP-tagged adenovirus (100 PFU/well). Following incubation for five days, relative fluorescence units (RFU) of GFP fluorescence were quantified by BioTek Synergy HT Multi-Mode Microplate reader and EC_{50} values were determined as described in *5.6.3*. Graphical representations were normalized to % maximum RFU.

For pseudotyped virus: Confluent monolayers of HEK-293T-ACE2, HeLa-DPP4, or HEK-293T cells in 384-well plates were prepared and treated with compound dilutions as described in *5.5.3* above. After one h of incubation cells were infected with GFP-tagged pseudovirus (100 transducing units/well). Following incubation for two days, relative fluorescence units (RFU) of GFP fluorescence were quantified by BioTek Synergy HT Multi-Mode Microplate reader and EC_{50} values were determined as described in *5.5.3*. Graphical representations were normalized to % maximum RFU.

5.5.5 Cytotoxicity

Replicate MRC-5, ARPE-19, HEK-293T-ACE2, HeLa-DPP4, or HEK-293T cell cultures were prepared simultaneously with those described in *5.5.3* and *5.5.4* but were not infected. After incubation for five days cell viability was determined by removing 100 µL of culture media from each well, adding 100 µL of CellTiter-Glo® reagent (Promega), incubation for ten minutes at room temperature, and measuring RLU using a BioTek Synergy HT Multi-Mode Microplate reader. 50% cytotoxicity concentrations (TC_{50}) were calculated as inflection points of four-parameter curves as described in *5.5.3*. Graphical representations were normalized to % maximum RLU.

5.5.6 Inhibition of GFP fluorescence

For HCMV: Inhibition of GFP expression was evaluated by treating confluent monolayers of MRC-5 cells in black-wall/clear-bottom 96-well plates with compounds for one h before addition of 100 PFU/well virus BADr. Six days after infection representative micrographs were taken with a Nikon Eclipse TS100 Inverted UV microscope.

For adenovirus: Inhibition of GFP expression was evaluated by treating confluent monolayers of ARPE-19 cells in black-wall/clear-bottom 96-well plates with compounds for one h before addition of 100 PFU/well adenovirus. Five days after infection representative micrographs were taken with a Nikon Eclipse TS100 Inverted UV microscope.

For pseudovirus: Inhibition of GFP expression was evaluated by treating confluent monolayers of HEK-293T-ACE2, HeLa-DPP4, or HEK-293T cells in black-wall/clear-bottom 96-well plates with compounds

for one h before addition of 100 transducing units/well pseudoviruses. Two days after infection representative micrographs were taken with a Nikon Eclipse TS100 Inverted UV microscope.

5.5.7 Detection of viral proteins by immunofluorescence (IFA)

Confluent monolayers of MRC-5 cells in 16-well Nunc™ Lab-Tek™ glass chamber slides (ThermoFisher) were treated with compounds and one h later infected with RC2626 (125 PFU/well). Cells were fixed and stained for detection of HCMV immediate early (IE) proteins 48 h post infection (hpi) or for pp28 late protein 120 hpi. Culture medium was removed and monolayers were fixed with 1% formaldehyde in PBS for 30 minutes, washed three times with PBS, permeabilized by incubation on ice for 20 minutes with 0.5% Triton-X100 in PBS, washed three times with PBS, then incubated 30 minutes at room temperature in blocking buffer (20% fetal bovine serum in PBS). Fixed cells were then incubated one h at room temperature with primary antibodies to HCMV IE1 and IE2 proteins (MAB810, Millipore Sigma) or to pp28 (CH19, Virusys) diluted 1:600 in blocking buffer. After washing three-four times with blocking buffer, cells were incubated in the dark for one h at room temperature with secondary goat anti-mouse IgG conjugated to Alexa Fluor 488 (Life Technologies) diluted 1:200 in blocking buffer, then washed three-four times with PBS and imaged with a Nikon Eclipse TS100 Inverted UV microscope. A similar protocol was used to detect the HCMV tegument protein pp65 except that MRC-5 cells in chamber slides were treated with compounds for one h, infected at 4°C with BADr (200 PFU/well) for one h, then shifted to 37°C and fixed at six hpi. Detection used anti-pp65 primary antibody (CA003-100, Virusys) with secondary goat anti-mouse IgG conjugated to Alexa Fluor 594 (Life Technologies) and imaged with a Zeiss Axio Imager 2 and 89-North PhotoFluor LM-75.

5.5.8 Time of addition and treatment/removal studies

Confluent monolayers of MRC-5 cells in black-wall/clear-bottom 96-well plates were infected with BADr (100 PFU/well). A single inhibitory concentration of each compound (150 µg/ml heparin or MSGs) was added to triplicate wells one h before, at the time of, and 3, 6, 12, 24, 48, 72, 96, or 120 hpi. Infected or uninfected wells not treated with compounds served as controls. Following incubation for six days, GFP fluorescence was quantified using a BioTek Synergy HT Multi-Mode Microplate reader. Percent maximum RFUs were plotted versus time of compound addition (relative to infection) using Prism 5 software. This procedure was adapted for adenovirus and pseudoviruses by changing the cell type and/or time of addition.

To determine if MSGs act by interacting with cells or with virions, MRC-5 cells were treated with 150 µg/mL heparin or MSGs for 1 h, washed three times with media, then infected with 100PFU/well BADr. Six days after infection representative micrographs were taken with a Nikon Eclipse TS100 Inverted UV microscope. This procedure was adapted for adenovirus and pseudoviruses by changing the cell type.

5.5.9 Production of pseudotyped lentiviruses
SARS-CoV-2 pseudotyped lentiviruses were prepared as outlined in Crawford et al.[151] SARS-CoV-1, MERS-CoV, and influenza virus were prepared by adapting the procedure.

- pHAGE-CMV-Luc2-IRES-ZsGreen-W (BEI catalog number NR-52516): Lentiviral backbone plasmid that uses a CMV promoter to express luciferase followed by an IRES and ZsGreen.
- HDM-Hgpm2 (BEI catalog number NR-52517): lentiviral helper plasmid expressing HIV Gag-Pol under a CMV promoter.
- HDM-tat1b (NR-52518): Lentiviral helper plasmid expressing HIV Tat under a CMV promoter.

- pRC-CMV-Rev1b (NR-52519): Lentiviral helper plasmid expressing HIV Rev under a CMV promoter.

All plasmid DNA preparations were purified by double CeCl banding and kindly provided by Dr. Anton Chestukhin. HEK-293T cells were seeded into 6-well plates overnight to produce 50%–70% confluency at the time of transfection. Cells were transfected using BioT (Bioland Sci entific LLC) following the manufacturer's instructions. Each well received the following plasmid mix: 1 μg of pHAGE-CMV-Luc2-IRES-ZsGreen-W (NR-52516), 0.22 μg each of plasmids HDM-Hgpm2 (NR-52517), HDM-tat1b (NR-52518), and pRC-CMV-Rev1b (NR-52519), and 0.34 μg of viral glycoprotein encoding plasmid (either SARS-CoV-2 Spike (pGBW-m4137383; Addgene_149541), SARS-CoV-1 spike (pcDNA3.3_CoV1_D28; Addgene #170447),[164] influenza HA (pNAHA; Addgene #44169),[165] or MERS-CoV spike (pCDNA3.3_MERS_D12; Addgene #170448)[164]). Media was changed 18 to 24 h post-transfection. Pseudoviruses were harvested by filtering the supernatant with a 0.45 μm SFCA low protein-binding filter 60 h post transfection and stocks were stored either 4°C for immediate use or frozen long-term at -80°C. Titers of pseudotyped lentiviruses were determined after a single freeze-thaw. Serially diluted stock was applied to HEK-293T-ACE2, HEK-293T, or HeLa-DPP4 cells and two days post infection, cells were also visually assessed to quantitate the titer of the stock (the lowest dilution with GFP positive cells).

5.6 References

(1)   Zoepfl, M.; Dwivedi, R.; Taylor, M. C.; Pomin, V. H.; McVoy, M. A. Antiviral Activities of Four Marine Sulfated Glycans against Adenovirus and Human Cytomegalovirus. *Antiviral Res.* **2021**, *190* (April), 105077. https://doi.org/10.1016/j.antiviral.2021.105077.

(2)   Kim, S. B.; Zoepfl, M.; Samanta, P.; Zhang, F.; Xia, K.; Thara, R.; Linhardt, R. J.; Doerksen, R. J.; McVoy, M. A.; Pomin, V. H. Fractionation of Sulfated Galactan from the Red Alga Botryocladia Occidentalis Separates Its Anticoagulant and Anti-SARS-CoV-2 Properties. *J. Biol. Chem.* **2022**, *Accepted M*. https://doi.org/10.1016/j.jbc.2022.101856.

(3)   Xiao, Y.; Dong, X.; Chen, Y. Neutralizing Antibodies: Mechanism of Neutralization and Protective Activity against HIV-1. *Immunol. Res.* **2002**, *25* (3), 193–200.

(4)   Desai, U. R. New Antithrombin-Based Anticoagulants. *Med. Res. Rev.* **2004**, *24* (2), 151–181. https://doi.org/10.1002/med.10058.

(5)   Palta, S.; Saroa, R.; Palta, A. Overview of the Coagulation System. *Indian J. Anaesth.* **2014**, *58* (5), 515–523. https://doi.org/10.1016/B978-0-323-60984-5.00062-7.

(6)   Lever, R.; Mulloy, B.; Page, C. P. *Heparin - A Century of Progress*; Lever, R., Mulloy, B., Page, C. P., Eds.; Springer International Publishing: New York, NY, 2012.

(7)   Guo, J.; Skinner, G. W.; Harcum, W. W.; Barnum, P. E. Pharmaceutical Applications of Naturally Occurring Water-Soluble Polymers. *Pharm. Sci. Technol. Today* **1998**, *1* (6).

(8)   Pomin, V. H. Review: An Overview about the Structure-Function Relationship of Marine Sulfated Homopolysaccharides with Regular Chemical Structures. *Biopolymers* **2009**, *91* (8), 601–609. https://doi.org/10.1002/bip.21200.

(9)   Vieira, R. P.; Mourão, P. A. S. Occurrence of a Unique Fucose-Branched Chondroitin Sulfate in the Body Wall of a Sea Cucumber. *J. Biol. Chem.* **1988**, *263* (34), 18176–18183.

(10)   Mourao, P. A. S. Use of Sulfated Fucans as Anticoagulant and Antithrombotic Agents: Future Perspectives. *Curr. Pharm. Des.* **2004**, *10*, 967–981. https://doi.org/10.2174/1381612043452730.

(11)   Pomin, V. H.; Mourão, P. A. S. Structure, Biology, Evolution, and Medical Importance of Sulfated Fucans and Galactans. *Glycobiology* **2008**, *18* (12), 1016–1027. https://doi.org/10.1093/glycob/cwn085.

(12)   Pomin, V. H. Fucanomics and Galactanomics: Marine Distribution , Medicinal Impact, Conceptions, and Challenges. *Mar. Drugs* **2012**, *10*, 793–811. https://doi.org/10.3390/md10040793.

(13)   Pomin, V. H. Fucanomics and Galactanomics: Current Status in Drug Discovery, Mechanisms of Action, and Role of the Well-de Fi Ned Structures. *Biochim. Biophys. Acta* **2012**, *1820*, 1971–1979. https://doi.org/10.1016/j.bbagen.2012.08.022.

(14)   Pomin, V. H. Holothurian Fucosylated Chondroitin Sulfate. *Mar. Drugs* **2014**, *12*, 232–254. https://doi.org/10.3390/md12010232.

(15)   Pomin, V. H. How to Analyze the Anticoagulant and Antithrombotic Mechanisms of Action in Fucanome and Galactanome? *Glycoconj. J.* **2014**, *31*, 89–99. https://doi.org/10.1007/s10719-013-9509-3.

(16)   Pereira, M. S.; Melo, F. R.; Mourão, P. A. S. Is There a Correlation between Structure and Anticoagulant Action of Sulfated Galactans and Sulfated Fucans? *Glycobiology* **2002**, *12* (10), 573–580. https://doi.org/10.1093/glycob/cwf077.

(17)   Pomin, V. H. *Structure-Function Relationship of Anticoagulant and Antithrombotic Well-Defined Sulfated Polysaccharides from Marine Invertebrates*, 1st ed.; Elsevier Inc., 2012; Vol. 65. https://doi.org/10.1016/B978-0-12-416003-3.00012-3.

(18)   Pavão, M. S. G.; Aiello, K. R. M.; Werneck, C. C.; Silva, L. C. F.; Valente, A. P.; Mulloy, B.; Colwell, N. S.; Tollefsen, D. M.; Mourão, P. A. S. Highly Sulfated Dermatan Sulfates from Ascidians: Structure versus Anticoagulant Activity of These Glycosaminoglycans. *J. Biol. Chem.* **1998**, *273*

(43), 27848–27857. https://doi.org/10.1074/jbc.273.43.27848.

(19)   Pomin, V. H.; Mourão, P. A. de S. Structure versus Anticoagulant and Antithrombotic Actions of Marine Sulfated Polysaccharides. *Brazilian J. Pharmacogn.* **2012**, *22* (4), 921–928. https://doi.org/10.1590/S0102-695X2012005000068.

(20)   Vicente, C. P.; He, L.; Pavão, M. S. G.; Tollefsen, D. M. Antithrombotic Activity of Dermatan Sulfate in Heparin Cofactor II-Deficient Mice. *Blood* **2004**, *104* (13), 3965–3970. https://doi.org/10.1182/blood-2004-02-0598.

(21)   Kozlowski, E. O.; Pavao, M. S. G.; Borsig, L. Ascidian Dermatan Sulfates Attenuate Metastasis, Inflammation and Thrombosis by Inhibition of P-Selectin. *J. Thromb. Haemost.* **2011**, *9*, 1807–1815. https://doi.org/10.1111/j.1538-7836.2011.04401.x.

(22)   Mourao, P. A. S.; Pereira, M. S.; Pavao, M. S. G.; Mulloy, B.; Tollefsen, D. M.; Mowinckel, M. C.; Abildgaard, U. Structure and Anticoagulant Activity of a Fucosylated Chondroitin Sulfate from Echinoderm. Sulfated Fucose Branches on the Polysaccharide Account for Its High Anticoagulant Action. *J. Biol. Chem.* **1996**, *271* (39), 23973–23984. https://doi.org/10.1074/jbc.271.39.23973.

(23)   Pereira, M. S.; Mulloy, B.; Mourão, P. A. S. Structure and Anticoagulant Activity of Sulfated Fucans: Comparison between the Regular, Repetitive, and Linear Fucans from Echinoderms with the More Heterogenous and Branched Polymers from Brown Algae. *J. Biol. Chem.* **1999**, *274* (12), 7656–7667. https://doi.org/10.1074/jbc.m002422200.

(24)   Farias, W. R. L.; Valente, A.-P.; Pereira, M. S.; Mourão, P. A. S. Structure and Anticoagulant Activity of Sulfated Galactans. Isolation of a Unique Sulfated Galactan from the Red Algae Botryocladia Occidentalis and Comparison of Its Anticoagulant Action with That of Sulfated Galactans from Invertebrates. *J. Biol. Chem.* **2000**, *275* (38), 29299–29307. https://doi.org/10.1074/jbc.M002422200.

(25)   Glauser, B. F.; Pereira, M. S.; Monteiro, R. Q.; Mourão, P. A. S. Serpin-Independent Anticoagulant Activity of a Fucosylated Chondroitin Sulfate. *Thromb. Haemost.* **2008**, *100* (3), 420–428. https://doi.org/10.1160/TH08-04-0210.

(26)   Glauser, B. F. B. F.; Rezende, R. M. R. M. R. M.; Melo, F. R. F. R. F. R.; Pereira, M. S. M. S.; Francischetti, I. M. B. I. M. B.; Monteiro, R. Q. R. Q.; Rezaie, A. R. A. R. A. R.; Mourão, P. A. S. P. A. S. Anticoagulant Activity of a Sulfated Galactan: Serpin-Independent Effect and Specific Interaction with Factor Xa. *Thromb. Haemost.* **2009**, *102* (6), 1183–1193. https://doi.org/10.1160/TH09-04-0273.

(27)   A.-L.G, Q.; Santos, G. R. C. R. C.; Oliveira, S.-N. M. C. G. N. M. C. G.; Glauser, B. F. F.; Fontes, B. P. P.; Queiroz, I. N. L. N. L.; Benevides, N. M. B. M. B.; Pomin, V. H. H.; Mourão, P. A. S.; Quindere, A. L. G.; Santos, G. R. C. R. C.; Oliveira, S.-N. M. C. G. N. M. C. G.; Glauser, B. F. F.; Fontes, B. P. P.; Queiroz, I. N. L. N. L.; Benevides, N. M. B. M. B.; Pomin, V. H. H.; Mourao, P. A. S.; A.-L.G, Q.; Santos, G. R. C. R. C.; Oliveira, S.-N. M. C. G. N. M. C. G.; Glauser, B. F. F.; Fontes, B. P. P.; Queiroz, I. N. L. N. L.; Benevides, N. M. B. M. B.; Pomin, V. H. H.; Mourão, P. A. S. Is the Antithrombotic Effect of Sulfated Galactans Independent of Serpin? *J. Thromb. Haemost.* **2014**, *12*, 43–53. https://doi.org/10.1111/jth.12448.

(28)   Pereira, M. S.; Vilela-Silva, A. C. E. S.; Valente, A. P.; Mourão, P. A. S. A 2-Sulfated, 3-Linked α-L-Galactan Is an Anticoagulant Polysaccharide. *Carbohydr. Res.* **2002**, *337*, 2231–2238. https://doi.org/10.1016/S0008-6215(02)00215-X.

(29)   Pomin, V. H.; Mourão, P. A. S. Specific Sulfation and Glycosylation — a Structural Combination for the Anticoagulation of Marine Carbohydrates. *Front. Cell. Infect. Microbiol.* **2014**, *4* (33), 1–8. https://doi.org/10.3389/fcimb.2014.00033.

(30)   Pereira, M. G. M. G.; Benevides, N. M. B. N. M. B.; Melo, M. R. S. M. R. S. M. R. S.; Valente, A. P. A. P.; Melo, F. R. F. R. F. R.; Mourão, P. A. S. P. A. S. Structure and Anticoagulant Activity of a Sulfated Galactan from the Red Alga, Gelidium Crinale. Is There a Specific Structural Requirement

for the Anticoagulant Action? *Carbohydr. Res.* **2005**, *340*, 2015–2023. https://doi.org/10.1016/j.carres.2005.05.018.

(31) Fonseca, R. J. C.; Santos, G. R. C.; Mourão, P. A. S. Effects of Polysaccharides Enriched in 2,4-Disulfated Fucose Units on Coagulation, Thrombosis and Bleeding: Practical and Conceptual Implications. *Thromb. Haemost.* **2009**, *102* (5), 829–836. https://doi.org/10.1160/TH08-11-0773.

(32) Gandhi, N. S.; Mancera, R. L. The Structure of Glycosaminoglycans and Their Interactions with Proteins. *Chem. Biol. Drug Des.* **2008**, *72* (6), 455–482. https://doi.org/10.1111/j.1747-0285.2008.00741.x.

(33) Aquino, R. S.; Park, P. W. Glycosaminoglycans and Infection. *Front. Biosci.* **2016**, *21*, 1260–1277.

(34) Hao, C.; Yu, G.; He, Y.; Xu, C.; Zhang, L.; Wang, W. Marine Glycan–Based Antiviral Agents in Clinical or Preclinical Trials. *Rev. Med. Virol.* **2019**, *29*, e2043. https://doi.org/10.1002/rmv.2043.

(35) Badani, H.; Garry, R. F.; Wimley, W. C. Peptide Entry Inhibitors of Enveloped Viruses: The Importance of Interfacial Hydrophobicity. *Biochim. Biophys. Acta* **2014**, *1838* (9), 2180–2197. https://doi.org/10.1016/j.bbamem.2014.04.015.

(36) Muller, W.; Wang, X.; Schroder, H. *Biomedical Inorganic Polymers*; 2013.

(37) de Paiva, R. E.; Neto, A. M.; Santos, I. A.; Jardim, A. C. G.; Corbi, P. P.; Bergamini, F. What Is Holding Back the Development of Antiviral Metallodrugs? A Literature Overview and Implications for SARS-CoV-2 Therapeutics and Future Viral Outbreaks. *Dalt. Trans.* **2020**, *49*, 16004–16033. https://doi.org/10.1039/D0DT02478C.

(38) Chen, S.; Xue, C.; Yin, L.; Tang, Q.; Yu, G.; Chai, W. Comparison of Structures and Anticoagulant Activities of Fucosylated Chondroitin Sulfates from Different Sea Cucumbers. *Carbohydr. Polym.* **2011**, *83* (2), 688–696. https://doi.org/10.1016/j.carbpol.2010.08.040.

(39) Chen, S.; Hu, Y.; Ye, X.; Li, G.; Yu, G.; Xue, C.; Chai, W. Sequence Determination and Anticoagulant and Antithrombotic Activities of a Novel Sulfated Fucan Isolated from the Sea Cucumber Isostichopus Badionotus. *Biochim. Biophys. Acta - Gen. Subj.* **2012**, *1820* (7), 989–1000. https://doi.org/10.1016/j.bbagen.2012.03.002.

(40) Pomin, V. H. Marine Non-Glycosaminoglycan Sulfated Glycans as Potential Pharmaceuticals. *Pharmaceuticals* **2015**, *8*, 848–864. https://doi.org/10.3390/ph8040848.

(41) Pomin, V. H. Antimicrobial Sulfated Glycans: Structure and Function. *Curr. Top. Med. Chem.* **2017**, *17* (3), 319–330. https://doi.org/10.2174/15680266156661506051.

(42) Vasconcelos, A. A. A. A.; Sucupira, I. D. I. D. I. D.; Guedes, A. L. A. L.; Queiroz, I. N. I. N.; Frattani, F. S. F. S.; Fonseca, R. J. R. J.; Pomin, V. H. V. H. V. H. Anticoagulant and Antithrombotic Properties of Three Structurally Correlated Sea Urchin Sulfated Glycans and Their Low-Molecular-Weight Derivatives. *Mar. Drugs* **2018**, *16* (9), 304. https://doi.org/10.3390/md16090304.

(43) Santos, G. R. C.; Tovar, A. M. F.; Capillé, N. V. M.; Pereira, M. S.; Pomin, V. H.; Mourão, P. A. S. Structural and Functional Analyses of Bovine and Porcine Intestinal Heparins Confirm They Are Different Drugs. *Drug Discov. Today* **2014**, *19* (11), 1801–1807. https://doi.org/10.1016/j.drudis.2014.07.004.

(44) Pomin, V. H. V. H.; Pereira, M. S. M. S.; Valente, A.-P. A. P. A.-P.; Tollefsen, D. M. D. M.; Pavão, M. S. G. M. S. G.; Mourão, P. A. S. P. A. S. Selective Cleavage and Anticoagulant Activity of a Sulfated Fucan: Stereospecific Removal of a 2-Sulfate Ester from the Polysaccharide by Mild Acid Hydrolysis, Preparation of Oligosaccharides, and Heparin Cofactor II-Dependent Anticoagulant Activity. *Glycobiology* **2005**, *15* (4), 369–381. https://doi.org/10.1093/glycob/cwi021.

(45) Compton, T.; Nowlin, D. M.; Cooper, N. R. Initiation of Human Cytomegalovirus Infection Requires Initial Interaction with Cell Surface Heparan Sulfate. *Virology* **1993**, *193* (2), 834–841. https://doi.org/10.1006/viro.1993.1192.

(46) Dechecchi, M. C.; Melotti, P.; Bonizzato, A.; Santacatterina, M.; Chilosi, M.; Cabrini, G. Heparan Sulfate Glycosaminoglycans Are Receptors Sufficient To Mediate the Initial Binding of Adenovirus

Types 2 and 5. *J. Virol.* **2001**, *75* (18), 8772–8780. https://doi.org/10.1128/jvi.75.18.8772-8780.2001.

(47) Varnum, S. M.; Streblow, D. N.; Monroe, M. E.; Smith, P.; Auberry, K. J.; Pas, L.; Wang, D.; Ii, D. G. C.; Rodland, K.; Wiley, S.; Britt, W.; Shenk, T.; Smith, R. D.; Nelson, J. A. Identification of Proteins in Human Cytomegalovirus (HCMV) Particles: The HCMV Proteome. *J. Virol.* **2004**, *78* (20), 10960–10966. https://doi.org/10.1128/JVI.78.20.10960.

(48) Duan, Y.; Miao, L.; Ye, H.; Yang, C.; Fu, B.; Schwartz, P. H.; Rayner, S.; Fortunato, E. A.; Luo, M. A Faster Immunofluorescence Assay for Tracking Infection Progress of Human Cytomegalovirus. *Acta Biochim Biophys Sin* **2012**, *44*, 597–605. https://doi.org/10.1093/abbs/gms041.Advance.

(49) Ibig-rehm, Y.; Götte, M.; Gabriel, D.; Woodhall, D.; Shea, A.; Brown, N. E.; Compton, T.; Feire, A. L. High-Content Screening to Distinguish between Attachment and Post-Attachment Steps of Human Cytomegalovirus Entry into Fibroblasts and Epithelial Cells. *Antiviral Res.* **2011**, *89*, 246–256. https://doi.org/10.1016/j.antiviral.2011.01.007.

(50) Cagno, V.; Tseligka, E. D.; Jones, S. T.; Tapparel, C. Heparan Sulfate Proteoglycans and Viral Attachment: True Receptors or Adaptation Bias? *Viruses* **2019**, *11* (7), 1–24. https://doi.org/10.3390/v11070596.

(51) Liu, L.; Chopra, P.; Li, X.; Wolfert, M. A.; Tompkins, S. M.; Boons, G. J. SARS-CoV-2 Spike Protein Binds Heparan Sulfate in a Length- and Sequence-Dependent Manner. *bioRxiv* **2020**, *preprint*, 1–15.

(52) Qureshi, A.; Thakur, N.; Tandon, H.; Kumar, M. AVPdb: A Database of Experimentally Validated Antiviral Peptides Targeting Medically Important Viruses. *Nucleic Acids Res.* **2014**, *42* (D1), 1147–1153. https://doi.org/10.1093/nar/gkt1191.

(53) Paeschke, R.; Woskobojnik, I.; Makarov, V.; Schmidtke, M.; Bogner, E. DSTP-27 Prevents Entry of Human Cytomegalovirus. *Antimicrob. Agents Chemother.* **2014**, *58* (4), 1963–1971. https://doi.org/10.1128/AAC.01964-13.

(54) Schmidtke, M.; Karger, A.; Meerbach, A.; Egerer, R.; Stelzner, A.; Makarov, V. Binding of a N,N'-Bisheteryl Derivative of Dispirotripiperazine to Heparan Sulfate Residues on the Cell Surface Specifically Prevents Infection of Viruses from Different Families. *Virology* **2003**, *311* (1), 134–143. https://doi.org/10.1016/S0042-6822(03)00166-1.

(55) Selinka, H.-C.; Florin, L.; Patel, H. D.; Freitag, K.; Schmidtke, M.; Makarov, V. A.; Sapp, M. Inhibition of Transfer to Secondary Receptors by Heparan Sulfate-Binding Drug or Antibody Induces Noninfectious Uptake of Human Papillomavirus. *J. Virol.* **2007**, *81* (20), 10970–10980. https://doi.org/10.1128/jvi.00998-07.

(56) Stevic, I.; Parmar, N.; Paredes, N.; Berry, L. R.; Chan, A. K. C. Binding of Heparin to Metals. *Cell Biochem. Biophys.* **2011**, *59*, 171–178. https://doi.org/10.1007/s12013-010-9129-5.

(57) Shoup, M.; Ourahmane, A.; Ginsburg, E. P.; Farrell, N. P.; Mcvoy, M. A. Substitution-Inert Polynuclear Platinum Compounds Inhibit Human Cytomegalovirus Attachment and Entry. *Antiviral Res.* **2020**, *184*, 104957.

(58) Anderson, R. A.; Zaneveld, L. J. D.; Usher, T. C. Cellulose Sulfate for Use as Antimicrobial and Contraceptive Agent, 2000.

(59) Neurath, A. R.; Strick, N.; Li, Y. Y. Anti-HIV-1 Activity of Anionic Polymers: A Comparative Study of Candidate Microbicides. *BMC Infect. Dis.* **2002**, *2* (27), 1–11. https://doi.org/10.1186/1471-2334-2-27.

(60) Herold, B. C.; Bourne, N.; Marcellino, D.; Kirkpatrick, R.; Strauss, D. M.; Zaneveld, L. J. D.; Waller, D. P.; Anderson, R. A.; Chany, C. J.; Barham, B. J.; Stanberry, L. R.; Cooper, M. D. Poly(Sodium 4-Styrene Sulfonate): An Effective Candidate Topical Antimicrobial for the Prevention of Sexually Transmitted Diseases. *J. Infect. Dis.* **2000**, *181* (2), 770–773. https://doi.org/10.1086/315228.

(61) Zaneveld, L. J. D.; Waller, D. P.; Anderson, R. A.; Chany, C.; Rencher, W. F.; Feathergill, K.; Diao, X.

H.; Doncel, G. F.; Herold, B.; Cooper, M. Efficacy and Safety of a New Vaginal Contraceptive Antimicrobial Formulation Containing High Molecular Weight Poly(Sodium 4-Styrenesulfonate). *Biol. Reprod.* **2002**, *66* (4), 886–894. https://doi.org/10.1095/biolreprod66.4.886.

(62)   Mauck, C. K.; Weiner, D. H.; Ballagh, S. A.; Creinin, M. D.; Archer, D. F.; Schwartz, J. L.; Pymar, H. C.; Lai, J.; Rencher, W. F.; Callahan, M. M. Single and Multiple Exposure Tolerance Study of Polystyrene Sulfonate Gel: A Phase I Safety and Colposcopy Study. *Contraception* **2004**, *70*, 77–83. https://doi.org/10.1016/j.contraception.2004.02.016.

(63)   Yao, X. J.; Wainberg, M. A.; Richard, M.; Pollak, M. The Ability of Suramin to Block CD4-Gp120 Binding Is Reversed in the Presence of Albumin. *Antimicrob. Agents Chemother.* **1991**, *35* (12), 2636–2638. https://doi.org/10.1128/AAC.35.12.2636.

(64)   De Clercq, E. Suramin - a Potent Inhibitor of the Reverse Transcriptase of RNA Tumor Viruses. *Cancer Lett.* **1979**, *8* (1), 9–22.

(65)   De Clercq, E. Suramin in the Treatment of AIDS - Mechanism of Action. *Antiviral Res.* **1987**, *7* (1), 1–10.

(66)   De Clercq, E. Antiviral Therapy for HIV Infections.Pdf. *Clin. Microbiol. Rev.* **1995**, *8* (2), 200–239.

(67)   Astrup, T.; Galsmar, I. On the Anticoagulant Acitivty of Heparin and Synthetic Polysaccharide Sulfuric Acids. *Acta Physiol. Scand.* **1944**, *8* (4), 361–364.

(68)   Busso, M. E.; Resnick, L. Anti-Human Immunodeficiency Virus Effects of Dextran Sulfate Are Strain Dependent and Synergistic or Antagonistic When Dextran Sulfate Is given in Combination with Dideoxynucleosides. *Antimicrob. Agents Chemother.* **1990**, *34* (10), 1991–1995. https://doi.org/10.1128/AAC.34.10.1991.

(69)   Ito, M.; Baba, M.; Sato, A.; Pauwels, R.; De Clercq, E.; Shigeta, S. Inhibitory Effect of Dextran Sulfate and Heparin on the Replication of Human Immunodeficiency Virus (HIV) in Vitro. *Antiviral Res.* **1987**, *7* (6), 361–367.

(70)   Oduah, E. I.; Linhardt, R. J.; Sharfstein, S. T. Heparin: Past , Present, and Future. *Pharmaceuticals* **2016**, *9* (38), 1–12. https://doi.org/10.3390/ph9030038.

(71)   Mitsuya, H.; Looney, D. J.; Kuno, S.; Ueno, R.; Staal, F. W.; Broder, S. Dextran Sulfate Suppression of Viruses in the HIV Family: Inhibition of Virion Binding to CD4+ Cells. *Science (80-.).* **1988**, *240* (4852), 646–649.

(72)   Baba, M.; Snoeck, R.; Pauwels, R.; De Clercq, E. Sulfated Polysaccharides Are Potent and Selective Inhibitors of Various Enveloped Viruses, Including Herpes Simplex Virus, Cytomegalovirus, Vesicular Stomatitis Virus, and Human Immunodeficiency Virus. *Antimicrob. Agents Chemother.* **1988**, *32* (11), 1742–1745. https://doi.org/10.1128/AAC.32.11.1742.

(73)   Gerber, P.; Dutcher, J. D.; Adams, E. V.; Sherman, H.; Sherman, J. H. Protective Effect of Seaweed Extracts for Chicken Embryos Infected with Influenza B or Mumps Virus. *Exp. Biol. Med.* **1958**, *99* (3), 590–593.

(74)   Ehresmann, D. W.; Deig, E. F.; Hatch, M. T.; DiSalco, L. H.; Verdos, N. A. Antiviral Substances from California Marine Algae. *J. Phycol.* **1976**, *13* (1), 37–40.

(75)   Nakashima, H.; Kido, Y.; Kobayashi, N.; Motoki, Y.; Neushul, M.; Yamamoto, N. Antiretroviral Activity in a Marine Red Alga: Reverse Transcriptase Inhibition by an Aqueous Extract of Schizymenia Pacifica. *J. Cancer Res. Clin. Oncol.* **1987**, *113*, 413–416.

(76)   Skoler-karpoff, S.; Ramjee, G.; Ahmed, K.; Altini, L.; Plagianos, M. G.; Friedland, B.; Govender, S.; De Kock, A.; Cassim, N.; Palanee, T.; Dozier, G.; Maguire, R.; Lahteenmaki, P. Efficacy of Carraguard for Prevention of HIV Infection in Women in South Africa: A Randomised, Double-Blind, Placebo-Controlled Trial. *Lancet* **2008**, *372*, 1977–1987. https://doi.org/10.1016/S0140-6736(08)61842-5.

(77)   Donalisio, M.; Ranucci, E.; Cagno, V.; Civra, A.; Manfredi, A.; Cavalli, R.; Ferruti, P.; Lembo, D. Agmatine-Containing Poly(Amidoamine)s as a Novel Class of Antiviral Macromolecules: Structural

Properties and in Vitro Evaluation of Infectivity Inhibition. *Antimicrob. Agents Chemother.* **2014**, *58* (10), 6315–6319. https://doi.org/10.1128/AAC.03420-14.

(78)   Mercorelli, B.; Oreste, P.; Sinigalia, E.; Muratore, G.; Lembo, D.; Palù, G.; Loregian, A. Sulfated Derivatives of Escherichia Coli K5 Capsular Polysaccharide Are Potent Inhibitors of Human Cytomegalovirus. *Antimicrob. Agents Chemother.* **2010**, *54* (11), 4561–4567. https://doi.org/10.1128/AAC.00721-10.

(79)   Christensen, N. D.; Reed, C. A.; Culp, T. D.; Hermonat, P. L.; Howett, M. K.; Anderson, R. A.; Zaneveld, L. J. D. Papillomavirus Microbicidal Activities of High-Molecular-Weight Cellulose Sulfate, Dextran Sulfate, and Polystyrene Sulfonate. *Antimicrob. Agents Chemother.* **2001**, *45* (12), 3427–3432. https://doi.org/10.1128/AAC.45.12.3427-3432.2001.

(80)   Astrup, T.; Alkjaersig, N. Polysaccharide Polysulphic Acids as Antihyaluronidases. *Nature* **1950**, *166*, 568–569.

(81)   Halpern, V.; Ogunsola, F.; Obunge, O.; Wang, C. H.; Onyejepu, N.; Oduyebo, O.; Taylor, D.; McNeil, L.; Mehta, N.; Umo-Otong, J.; Otusanya, S.; Crucitti, T.; Abdellati, S. Effectiveness of Cellulose Sulfate Vaginal Gel for the Prevention of HIV Infection: Results of a Phase III Trial in Nigeria. *PLoS One* **2008**, *3* (11), 1–7. https://doi.org/10.1371/journal.pone.0003784.

(82)   Van Damme, L.; Govinden, R.; Mirembe, F. M.; Guédou, F.; Solomon, S.; Becker, M. L.; Pradeep, B. S.; Krishnan, A. K.; Alary, M.; Pande, B.; Ramjee, G.; Deese, J.; Crucitti, T.; Taylor, D. Lack of Effectiveness of Cellulose Sulfate Gel for the Prevention of Vaginal HIV Transmission. *N. Engl. J. Med.* **2008**, *359* (5), 463–472. https://doi.org/10.1056/NEJMoa0707957.

(83)   Bezerra, F. F.; Vignovich, W. P.; Aderibigbe, A. O.; Sharp, J. S.; Doerksen, R. J.; Pomin, V. H. Conformational Properties of L -Fucose and the Tetrasaccharide Building Block of the Sulfated L -Fucan from Lytechinus Variegatus. *J. Struct. Biol.* **2019**, No. June, 107407. https://doi.org/10.1016/j.jsb.2019.107407.

(84)   Peng, M. Outbreak of COVID-19: An Emerging Global Pandemic Threat. *Biomed. Pharmacother.* **2020**, *129*, 11049.

(85)   Stadnytskyi, V.; Bax, C.; Andinrud, P. The Airborne Lifetime of Small Speech Droplets and Their Potential Importance in SARS-CoV-2 Transmission. *Proc. Natl. Acad. Sci.* **2020**, *117*, 11875–11877.

(86)   Echternach, M.; Gantner, S.; Peters, G.; Westphalen, C.; Benthaus, T.; Jakubaß, B.; Kuranova, L.; Döllinger, M.; Kniesburges, S. Impulse Dispersion of Aerosols during Singing and Speaking: A Potential COVID-19 Transmission Pathway. *Am. J. Respir. Crit. Care Med.* **2020**, *202*, 1584–1587.

(87)   Singh, A. K.; Singh, A.; Singh, R.; Misra, A. Molnupiravir in COVID-19: A Systematic Review of Literature. *Diabetes Metab. Syndr. Clin. Res. Rev.* **2021**, *15* (6), 102329.

(88)   Vandyck, K.; Deval, J. Considerations for the Discovery and Development of 3-Chymotrypsin-like Cysteine Protease Inhibitors Targeting SARS-CoV-2 Infection. *Curr. Opin. Virol.* **2021**, *49*, 36–40.

(89)   Moghaddar, M.; Radman, R.; I. Macreadie. Severity, Pathogenicity and Transmissibility of Delta and Lambda Variants of SARS-CoV-2, Toxicity of Spike Protein and Possibilities for Future Prevention of COVID-19. *Microorganisms* **2021**, *9*, 2167.

(90)   Ramesh, S.; Govindarajulu, M.; Parise, R. S.; Neel, L.; Shankar, T.; Patel, S.; Lowery, P.; Smith, F.; Dhanasekaran, M.; Moore, T. Emerging SARS-CoV-2 Variants: A Review of Its Mutations, Its Implications and Vaccine Efficacy. *Vaccines* **2021**, *9*, 1195.

(91)   Shang, J.; Wan, Y.; Luo, C.; Ye, G.; Geng, Q.; Auerbach, A.; Li, F. Cell Entry Mechanisms of SARS-CoV-2. *Proc. Natl. Acad. Sci.* **2020**, No. 117, 11727–11734.

(92)   Li, F. Receptor Recognition Mechanisms of Coronaviruses: A Decade of Structural Studies. *J. Virol.* **2015**, *89*, 1954–1964.

(93)   Kuhn, J.; Li, W.; Choe, H.; Farzan, M. Angiotensin-Converting Enzyme 2: A Functional Receptor for SARS Coronavirus. *Cell. Mol. Life Sci.* **2004**, *61*, 2738–2743.

(94)   Li, F.; Li, W.; Farzan, M.; Harrison, S. C. Structure of SARS Coronavirus Spike Receptor-Binding

Domain Structure of SARS Coronavirus Spike Receptor-Binding Domain Complexed with Receptor. *Science (80-.).* **2005**, *309*, 1864–1868. https://doi.org/10.1126/science.1116480.

(95)   Clausen, T. M.; Sandoval, D. R.; Spliid, C. B.; Pihl, J.; Perrett, H. R.; Painter, C. D.; Narayanan, A.; Majowicz, S. A.; Kwong, E. M.; McVicar, R. N.; Thacker, B. E.; Glass, C. A.; Yang, Z.; Torres, J. L.; Golden, G. J.; Bartels, P. L.; Caradonna, T. M.; Kellman, B. P.; Martino, C.; Gordts, P. L. S. M.; Chanda, S. K.; Schmidt, A. G.; Godula, K.; Leibel, S. L.; Jose, Jo.; Corbett, K. D.; Ward, A. B.; Carlin, A. F.; Esko, J. D. SARS-CoV-2 Infection Depends on Cellular Heparan Sulfate and ACE2. *Cell* **2020**, *183*, 1–15. https://doi.org/10.1016/j.cell.2020.09.033.

(96)   Wan, Y.; Shang, J.; Graham, R.; Baric, R. R. S.; Li, F. Receptor Recognition by the Novel Coronavirus from Wuhan: An Analysis Based on Decade-Long Structural Studies of SARS Coronavirus. *J. Virol.* **2020**, *94* (7), e00127-20.

(97)   Lan, J.; Ge, J.; Shan, S.; Zhou, H.; Fan, S.; Zhang, Q.; Wang, Q.; Zhang, L.; Wang, X. Structure of the SARS-CoV-2 Spike Receptor-Binding Domain Bound to the ACE2 Receptor. *Nature* **2020**, *581*, 215–220.

(98)   Tandon, R.; Sharp, J. S.; Zhang, F.; Pomin, V. H.; Ashpole, N. M.; Mitra, D.; McCandless, M. G.; Jin, W.; Liu, H.; Sharma, P.; Linhardt, R. J. Effective Inhibition of SARS-CoV-2 Entry by Heparin and Enoxaparin Derivatives. *Virology* **2021**, *95*, e01987-20.

(99)   Mycroft-West, C. J.; Su, D.; Pagani, I.; Rudd, T. R.; Elli, S.; Guimond, S. E.; Miller, G.; Meneghetti, M. C. Z.; Nader, H. B.; Li, Y.; Nunes, Q. M.; Procter, P.; Mancini, N.; Clementi, M.; Bisio, A.; Forsyth, N. R.; Turnbull, J. E.; Guerrini, M.; Fernig, D. G.; Vicenzi, E.; Yates, E. A.; Lima, M. A.; Skidmore, M. A. Heparin Inhibits Cellular Invasion by SARS-CoV-2: Structural Dependence of the Interaction of the Surface Protein (Spike) S1 Receptor Binding Domain with Heparin. *Blood Cells, Inflamm. Infect.* **2020**, *120* (12), 1700–1715.

(100) Li, J.; Zhang, Y.; Pang, H.; Li, S. Heparin Interacts with the Main Protease of SARS-CoV-2 and Inhibits Its Activity. *Spectrochim. Acta Part A Mol. Biomol. Spectrosc.* **2022**, *267*, 120595.

(101) Warkentin, T. E.; Levine, M. N.; Hirsh, J.; Horsewood, P.; Roberts, R. S.; Gent, M.; Kelton, J. G. Heparin-Induced Thrombocytopenia in Patients Treated with Low-Molecular-Weight Heparin or Unfractionated Heparin. *N. Engl. J. Med.* **1995**, *332*, 1330–1336.

(102) Hirsh, J.; AnandJ, S. S.; Halperin, J. L.; Fuster, V. Guide to Anticoagulant Therapy: Heparin : A Statement for Healthcare Professionals from the American Heart Association. *Circulation* **2001**, *103*, 2994–3018.

(103) King, D.; Kelton, J. Heparin-Associated Thrombocytopenia. *Ann. Intern. Med.* **1984**, *100*, 535–540.

(104) Warkentin, T.; Kelton, J. Heparin-Induced Thrombocytopenia. *Annu. Rev. Med.* **1989**, *40*, 31–44.

(105) Ginsberg, J.; Hirsh, J. Use of Anticoagulants during Pregnancy. *Chest.* **1989**, *95*, 156S-160S.

(106) Ginsberg, J. S.; Kowalchuk, G.; Hirsh, J.; Brill-Edwards, P.; Burrows, R.; Coates, G.; Webber, C. Heparin Effect on Bone Density. *Thromb. Haemost.* **1990**, *64*, 286–289.

(107) Curry, N.; Bardana, E.; Pirofsky, B. Heparin Sensitivity. Report of a Case. *Arch. Intern. Med.* **1973**, *132*, 744–745.

(108) O'Kelly, R.; Magee, F.; McKenna, T. Routine Heparin Therapy Inhibits Adrenal Aldosterone Production. *J. Clin. Endocrinol. Metab.* **1983**, *56*, 108–112.

(109) Salih, A. E. M.; Thissera, B.; Yaseen, M.; Hassane, A. S. I.; El-Seedi, H. R.; Sayed, A. M.; Rateb, M. . Marine Sulfated Polysaccharides as Promising Antiviral Agents: A Comprehensive Report and Modeling Study Focusing on SARS CoV-2. *Mar. Drugs.* **2021**, *19*, 406.

(110) Chen, X.; Han, W.; Wang, G.; Zhao, X. Application Prospect of Polysaccharides in the Development of Anti-Novel Coronavirus Drugs and Vaccines. *Int. J. Biol. Macromol.* **2020**, *164*, 331–343. https://doi.org/10.1016/j.ijbiomac.2020.07.106.

(111) Jin, W.; Zhang, W.; Mitra, D.; McCandless, M. G.; Sharma, P.; Tandon, R.; Zhang, F.; Linhardt, R. J. The Structure-Activity Relationship of the Interactions of SARS-CoV-2 Spike Glycoproteins with

Glucuronomannan and Sulfated Galactofucan from Saccharina Japonica. *Int. J. Biol. Macromol.* **2020**, *163* (1649–1658).

(112) Ray, B.; Schütz, M.; Mukherjee, S.; Jana, S.; Ray, S.; Marschall, M. Exploiting the Amazing Diversity of Natural Source-Derived Polysaccharides: Modern Procedures of Isolation, Engineering, and Optimization of Antiviral Activities. *Polymers (Basel).* **2020**, No. 13, 136.

(113) Aranda, P.; Wicklein, B.; Ruiz-Garcia, C.; Martín-Sampedro, R.; Darder, M.; Real, G. Del; Ruiz-Hitzky, E. Research and Patents on Coronavirus and COVID-19: A Review. *Recent Pat. Nanotechnol.* **2020**, *14*, 328–350.

(114) Grubaugh, N.; Petrone, M.; Holmes, E. We Shouldn't Worry When a Virus Mutates during Disease Outbreaks. *Nat. Microbiol.* **2020**, *5*, 529–530.

(115) Ferron, F.; Subissi, L.; Morais, A. T. S. De; Le, N. T. T.; Sevajol, M.; Gluais, L.; Decroly, E.; Vonrhein, C.; Bricogne, G.; Canard, B.; Imbert, I. Structural and Molecular Basis of Mismatch Correction and Ribavirin Excision from Coronavirus RNA. *Proc. Natl. Acad. Sci.* **2018**, *115*, E162-171.

(116) Shahhosseini, N.; Babuadze, G. G.; Wong, G.; Kobinger, G. P. Mutation Signatures and in Silico Docking of Novel SARS-CoV-2 Variants of Concern. *Microorganisms* **2021**, *9* (5), 926.

(117) Geddes, L. From Alpha to Omicron: Everything you need to know about coronavirus variants of concern https://www.gavi.org/vaccineswork/alpha-omicron-everything-you-need-know-about-coronavirus-variants-concern.

(118) Huang, H.; Zhu, Y.; Niu, Z.; Zhou, L.; Sun, Q. SARS-CoV-2 N501Y Variants of Concern and Their Potential Transmission by Mouse. *Cell Death Differ.* **2021**, *28*, 2840–2842.

(119) Fujino, T.; Nomoto, H.; Kutsuna, S.; Ujiie, M.; Suzuki, T.; Sato, R.; Fujimoto, T.; Kuroda, M.; Wakita, T.; Ohmagari, N. Novel SARS-CoV-2 Variant in Travelers from Brazil to Japan. *Emerg. Infect. Dis.* **2021**, *27* (4), 1243–1245.

(120) de Siqueira, I. C.; Camelier, A. A.; Maciel, E. A. P.; Nonaka, C. K. V.; Neves, M. C. L. C.; Macêdo, Y. S. F.; de Sousa, K. A. F.; Araujo, V. C.; Paste, A. A.; Souza, B. S. de F.; Gräf, T. Early Detection of P.1 Variant of SARS-CoV-2 in a Cluster of Cases in Salvador, Brazil. *Int. J. Infect. Dis.* **2021**, *108*, 252–255.

(121) Romano, C. M.; Felix, A. C.; de Paula, A. V.; de Jesus, J. G.; Cerdeira; Andrade, P. S.; Faria; Cândido, D.; de Oliveira, F. M.; Ribeiro, A. C.; da Silva, F. C.; Inemami, M.; Costa, A. A.; Leal, C. O. D.; Figueiredo, W. M.; Pannuti, C. S.; Souza, W. M. de; Faria, N. R.; Sabino, E. C. SARS-CoV-2 Reinfection Caused by the P.1 Lineage in Araraquara City, Sao Paulo State, Brazil. *Rev. Inst. Med. Trop. Sao Paulo* **2021**, *63*, e36.

(122) Prajapat, M.; Handa, V.; Sarma, P.; Prakash, A.; Kaur, H.; Sharma, S.; Bhattacharyya, A.; Kumar, S.; Sharma, A. R.; Avti, P.; Medhi, B. Update on Geographical Variation and Distribution of SARS-NCoV-2: A Systematic Review. *Indian J. Pharmacol.* **2021**, *53* (4), 310–316.

(123) Greaney, A. J.; Loes, A. N.; Crawford, K. H. D.; Starr, T. N.; Malone, K. D.; Chu, H. Y.; Bloom, J. D. Comprehensive Mapping of Mutations to the SARS-CoV-2 Receptor-Binding Domain That Affect Recognition by Polyclonal Human Serum Antibodies. *Cell Host Microbe* **2021**, *29* (3), 463–476.

(124) Baum, A.; Fulton, B. O.; Wloga, E.; Copin, R.; Pascal, K. E.; Russo, V.; Giordano, S.; Lanza, K.; Negron, N.; Ni, M.; Wei, Y.; Atwal, G. S.; Murphy, A. J.; Stahl, N.; Yancopoulos, G. D.; Kyratsous, C. A. Antibody Cocktail to SARS-CoV-2 Spike Protein Prevents Rapid Mutational Escape Seen with Individual Antibodies. *Science (80-.).* **2020**, *369* (6506), 1014–1018.

(125) Liu, Z.; VanBlargan, L. A.; Rothlauf, P. W.; Bloyet, L.-M.; Chen, R. E.; Stumpf, S.; Zhao, H.; Errico, J. M.; Theel, E. S.; Ellebedy, A.; Fremont, D.; Diamond, M. S.; Whelan, S. P. J. Landscape Analysis of Escape Variants Identifies SARS-CoV-2 Spike Mutations That Attenuate Monoclonal and Serum Antibody Neutralization. *bioRxiv* **2021**, *22* (6), 372037.

(126) Pomin, V. H.; Mahdi, F.; Jin, W.; Zhang, F.; Linhardt, R. J.; Paris, J. J. Red Algal Sulfated Galactan Binds and Protects Neural Cells from HIV-1 Gp120 and Tat. *Pharmaceuticals* **2021**, *14*, 714.

(127) Marques, J.; Vilanova, E.; Mourão, P. A. S.; Fernàndez-Busquets, X. Marine Organism Sulfated Polysaccharides Exhibiting Significant Antimalarial Activity and Inhibition of Red Blood Cell Invasion by Plasmodium. *Sci. Rep.* **2016**, *6*, 24368.

(128) Glauser, B.; Mourao, P.; Pomin, V. Marine Sulfated Glycans with Serpin-Unrelated Anticoagulant Properties. *Adv. Clin. Chem.* **2013**, *62*, 269–303.

(129) Melo, F.; Mourao, P. An Algal Sulfated Galactan Has an Unusual Dual Effect on Venous Thrombosis Due to Activation of Factor XII and Inhibition of the Coagulation Proteases. *Thromb. Haemost.* **2008**, *9*, 531–538.

(130) Farias, W. R. L.; Valente, A.-P.; Pereira, M. S.; Mourão, P. A. S. Structure and Anticoagulant Activity of Sulfated Galactans. *J. fo Biol. Chem.* **2000**, *275*, 29299–28307.

(131) Melo, F. R.; Pereira, M. S.; Foguel, D.; Mourão, P. A. S. Antithrombin-Mediated Anticoagulant Activity of Sulfated Polysaccharides: Different Mechanisms for Heparin and Sulfated Galactans. *J. Biol. Chem.* **2004**, *279* (20), 20824–20835. https://doi.org/10.1074/jbc.M308688200.

(132) Dwivedi, R.; Pomin, V. Marine Antithrombotics. *Mar. Drugs* **2020**, *18* (10), 514.

(133) Carvalhal, F.; Cristelo, R. R.; Resende, D. I. S. P.; Pinto, M. M. M.; Sousa, E.; Correia-da-Silva, M. Antithrombotics from the Sea: Polysaccharides and Beyond. *Mar. Drugs* **2019**, *17*, 170.

(134) Mourao, P. Perspective on the Use of Sulfated Polysaccharides from Marine Organisms as a Source of New Antithrombotic Drugs. *Mar. Drugs* **2015**, *13*, 2770–2784.

(135) Zucker, S.; Buttle, D. J.; Nicklin, M. J. H.; Barrett, A. J. The Proteolytic Activities of Chymopapain, Papain, and Papaya Proteinase III. *Biochem. Biophyc. acta.* **1985**, *828*, 196–2004.

(136) Tsou, C. Cytochrome c Modified by Digestion with Proteolytic Enzymes. 1. Digestion. *Biochem. J.* **1951**, *49*, 362–367.

(137) Farndale, R. W. R. W.; Sayers, C. A. C. A.; Barrett, A. J. A. J. A Direct Spectrophotometric Microassay for Sulfated Glycosaminoglycans in Cartilage Cultures. *Connect. Tissue Res.* **1982**, *9* (4), 247–248.

(138) Pomin, V. V. H.; Valente, A. A. P.; Pereira, M. S. M.; Mourao, P.; Mourão, P. A. S. Mild Acid Hydrolysis of Sulfated Fucans: A Selective 2-Desulfation Reaction and an Alternative Approach for Preparing Tailored Sulfated Oligosaccharides. *Glycobiology* **2005**, *15* (12), 1376–1385. https://doi.org/10.1093/glycob/cwj030.

(139) Queiroz, I. N. L. I. N. L.; Vilela-Silva, A.-C. E. S. A. C. E. S.; Pomin, V. H. V. H. Oligosaccharides from the 3-Linked 2-Sulfated Alpha-L-Fucan and Alpha-L-Galactan Show Similar Conformations but Different Dynamics. *Glycobiology* **2016**, *26* (11), 1257–1264. https://doi.org/10.1093/glycob/cww080.

(140) Pomin, V. H.; Park, Y.; Huang, R.; Heiss, C.; Sharp, J. S.; Azadi, P.; J.H., P. Exploiting Enzyme Specificities in Digestions of Chondroitin Sulfates A and C: Production of Well-Defined Hexasaccharides. *Glycobiology* **2012**, *22*, 826–838.

(141) Queiroz, I. N. L. I. N.; Wang, X.; Glushka, J. N. J. N.; Santos, G. R. C. G. R.; Valente, A. P. A. P.; Prestegard, J. H. J. H. J. H.; Woods, R. J. R. J.; Mourão, P. A. S. P. A. P. A. S.; V.H., P.; Pomin, V. H. Impact of Sulfation Pattern on the Conformation and Dynamics of Sulfated Fucan Oligosaccharides as Revealed by NMR and MD. *Glycobiology* **2015**, *25* (5), 535–547. https://doi.org/10.1093/glycob/cwu184.

(142) Albano, R. M.; Pavão, M. S.; Mourão, P. A.; B., M. Structural Studies of a Sulfated L-Galactan from Styela Plicata (Tunicate): Analysis of the Smith-Degraded Polysaccharide. *Carbohydr. Res.* **1990**, *208*, 163–174.

(143) Castro, M. O.; Pomin, V. H.; Santos, L. L.; Vilela-Silva, A.-C. E. S.; Hirohashi, N.; Pol-Fachin, L.; Verli, H.; Mourão, P. A. S. A Unique 2-Sulfated β-Galactan from the Egg Jelly of the Sea Urchin Glyptocidaris Crenularis. *J. fo Biol. Chem.* **2009**, *284*, 18790–18800.

(144) Bezerra, F.; Pomin, V. Structural Mechanisms Involved in Mild-Acid Hydrolysis of a Defined

Tetrasaccharide-Repeating Sulfate Fucan. In *Enzymatic Technologies for Marine Polysaccharides*; CRC Press, 2019; pp 111–128.

(145) Dwivedi, R.; Samanta, P.; Sharma, P.; Zhang, F.; Mishra, S. K.; Kucheryavy, P.; Kim, S. B.; Aderibigbe, A. O.; Linhardt, R. J.; Tandon, R.; Doerksen, R. J.; Pomin, V. H. Structural and Kinetic Analyses of Holothurian Sulfated Glycans Suggest Potential Treatment for SARS-CoV-2 Infection. *J. fo Biol. Chem.* **2021**, *297* (4), 101207.

(146) Farias, W.; Nazareth, R.; Mourão, P. Dual Effects of Sulfated D-Galactans from the Red Algae Botryocladia Occidentalis Preventing Thrombosis and Inducing Platelet Aggregation. *Thromb. Haemost.* **2001**, *86*, 1540–1546.

(147) Sampaio, T. B. P.; Costa, B. B.; Moreira, T. A.; Cabral, L. M.; Silva, L. C. R. P.; Mourão, P. A. S.; Vilanova, E.; Cinelli, L. P. Insights on Chemical-Biological Correlations Learned from Investigations on the Sulfated Galactan from the Marine Alga Bothryocladia Occidentalis. *Int. J. Biol. Marcomolecules* **2020**, *158*, 471–476.

(148) Fonseca, R. J. C.; Oliveira, S.-N. M. C. G.; Melo, F. R.; Pereira, M. G.; Benevides, N. M. B.; Mourão, P. A. S. Slight Differences in Sulfation of Algal Galactans Account for Differences in Their Anticoagulant and Venous Antithrombotic Activities. *Thromb. Haemost.* **2008**, *99*, 439–545.

(149) Ryu, W.-S. New Emerging Viruses. In *Molecular Virology of Human Pathogenic Viruses*; 2016; pp 289–302.

(150) Bhave, S.; Elford, H.; McVoy, M. A. Ribonucleotide Reductase Inhibitors Hydroxyurea, Didox, and Trimidox Inhibit Human Cytomegalovirus Replication in Vitro and Synergize with Ganciclovir. *Antiviral Res.* **2013**, *100* (1), 151–158. https://doi.org/10.1016/j.antiviral.2013.07.016.

(151) Crawford, K. H. D. K. H. D.; Eguia, R.; Dingens, A. S. A. S.; Loes, A. N. A. N. A. N.; Malone, K. D. K. D.; Wolf, C. R. C. R.; Chu, H. Y. H. Y.; Tortorici, M. A. A.; Veesler, D.; Murphy, M.; Pettie, D.; King, N. P. N. P.; Balazs, A. B. A. B.; Bloom, J. D. J. D. Protocol and Reagents for Pseudotyping Lentiviral Particles with SARS-CoV-2 Spike Protein for Neutralization Assays. *Viruses* **2020**, *12* (5), 513. https://doi.org/10.3390/v12050513.

(152) Kim, S. Y.; Jin, W.; Sood, A.; Montgomery, D. W.; Grant, O. C.; Fuster, M. M.; Fu, L.; Dordick, J. S.; Woods, R. J.; Zhang, F.; Linhardt, R. J. Characterization of Heparin and Severe Acute Respiratory Syndrome-Related Coronavirus 2 (SARS-CoV-2) Spike Glycoprotein Binding Interactions. *Antiviral Res.* **2020**, *181*, 104873.

(153) Luo, M. Influenza Virus Entry. *Adv. Exp. Med. Biol.* **2012**, *726*, 201–221. https://doi.org/10.1007/978-1-4614-0980-9_9.

(154) Kim, M.; Han, J.; Kim, S.; Kim, H. S.; Lee, W. G.; Kim, S. J.; Kang, P.-S.; Lee, C.-K. In Vitro Inhibition of Influenza A Virus Infection by Marine Microalga-Derived Sulfated Polysaccharide p-KG03. *Antiviral Res.* **2012**, *93*, 253–259. https://doi.org/10.1016/j.antiviral.2011.12.006.

(155) Yim, J. H.; Kim, S. J.; Ahn, S. H.; Lee, C. K.; Rhie, K. T.; Lee, H. K. Antiviral Effects of Sulfated Exopolysaccharide from the Marine Microalga Gyrodinium Impudicum Strain. *Mar. Biotechnol.* **2004**, *6*, 17–25. https://doi.org/10.1007/s10126-003-0002-z.

(156) Li, J.; Li, S.; Yan, L.; Ding, T.; Linhardt, R. J.; Yu, Y.; Liu, X.; Liu, D.; Ye, X.; Chen, S. Fucosylated Chondroitin Sulfate Oligosaccharides Exert Anticoagulant Activity by Targeting at Intrinsic Tenase Complex with Low FXII Activation: Importance of Sulfation Pattern and Molecular Size. *Eur. J. Med. Chem.* **2017**, *139*, 191–200. https://doi.org/10.1016/j.ejmech.2017.07.065.

(157) Pacheco, R. G.; Vicente, C. P.; Zancan, P.; Mourão, P. A. Different Antithrombotic Mechanisms among Glycosaminoglycans Revealed with a New Fucosylated Chondroitin Sulfate from an Echinoderm. *Blood Coagul. Fibrinolysis* **2000**, *11*, 563–573.

(158) Wang, D.; Shenk, T. Human Cytomegalovirus UL131 Open Reading Frame Is Required for Epithelial Cell Tropism. *J. Virol.* **2005**, *79* (16), 10330–10338. https://doi.org/10.1128/jvi.79.16.10330-10338.2005.

(159) McVoy, M. A.; Mocarski, E. S. Tetracycline-Mediated Regulation of Gene Expression within the Human Cytomegalovirus Genome. *Virology* **1999**, *258* (2), 295–303. https://doi.org/10.1006/viro.1999.9724.

(160) Cui, X.; Adler, S. P.; Davison, A. J.; Smith, L.; Habib, E. S. E.; McVoy, M. A. Bacterial Artificial Chromosome Clones of Viruses Comprising the Towne Cytomegalovirus Vaccine. *J. Biomed. Biotechnol.* **2012**, *2012*, 428498. https://doi.org/10.1155/2012/428498.

(161) Xiao, K.; Allison, D. F.; Buckley, K. M.; Kottke, M. D.; Vincent, P. A.; Faundez, V.; Kowalczyk, A. P. Cellular Levels of P120 Catenin Function as a Set Point for Cadherin Expression Levels in Microvascular Endothelial Cells. *J. Cell Biol.* **2003**, *163* (3), 535–545. https://doi.org/10.1083/jcb.200306001.

(162) He, T.-C.; Zhou, S.; da Costa, L. T.; Yu, J.; Kinzler, K. W.; Vogelstein, B. A Simplified System for Generating Recombinant Adenoviruses. *PNAS* **1998**, *95* (March), 2509–2514.

(163) Mulloy, B.; Ribeiro, A. C.; Alves, A. P.; Vieira, R. P.; Mourão, P. A. S. Sulfated Fucans from Echinoderms Have a Regular Tetrasaccharide Repeating Unit Defined by Specific Patterns of Sulfation at the 0-2 and 0-4 Positions. *J. Biol. Chem.* **1994**, *269* (35), 22113–22123.

(164) Rogers, T. F.; Zhao, F.; Huang, D.; Beutler, N.; Burns, A.; He, W.; Limbo, O.; Smith, C.; Song, G.; Woehl, J.; Yang, L.; Abbott, R. K.; Callaghan, S.; Garcia, E.; Hurtado, J.; Parren, M.; Peng, L.; Ramirez, S.; Ricketts, J.; Ricciardi, M. J.; Rawlings, S. A.; Wu, N. C.; Yuan, M.; Smith, D. M.; Nemazee, D.; Teijaro, J. R.; Voss, J. E.; Wilson, I. A.; Andrabi, R.; Briney, B.; Landais, E.; Sok, D.; Jardine, J. G.; Burton, D. R. Isolation of Potent SARS-CoV-2 Neutralizing Antibodies and Protection from Disease in a Small Animal Model. *Science (80-.).* **2020**, *369* (6506), 956–963.

(165) Patel, M.; Giddings, A. M.; Sechelski, J.; Olsen, J. C. High Efficiency Gene Transfer to Airways of Mice Using Influenza Hemagglutinin Pseudotyped Lentiviral Vectors. *J Gene Med* **2017**, *15* (1), 51–62. https://doi.org/10.1002/jgm.2695.High.

Chapter 6: Conclusion

Through the years, our understanding of PPCs has evolved from a DNA-targeting potential cancer chemotherapy to a DNA- *and* HS-targeting multifunctional therapeutic. In this work, we expanded PPCs' application to infectious disease, namely viral infections. Collectively, we identified cationic platinum, cobalt, and ruthenium coordinated compounds with antiviral activity against a number of viruses, however not all compounds acted with the same mechanism of action or spectra of activity. This disparity underlines an intriguing balance between DNA and HS affinity and binding.

These relationships are most prominently illustrated by DiplatinNC, RuRed, and WC; each compound has a +6 charge and a number of ammines for hydrogen bonding, but they differ in their geometry (square planar or octahedral, linear or nonlinear). Each compound varies in its DNA and HS affinity and each compound has a different antiviral activity: DiplatinNC inhibits HS-dependent viral attachment across a number of viruses and there is evidence that DiplatinNC binds HCMV virion itself to inhibit infection; RuRed inhibits sialic acid-dependent viruses; and WC inhibits HCMV through a late-acting mechanism, but may inhibit other viruses such as SARS-CoV-2 via HS metalloshielding. These differences clearly demonstrate that the antiviral activity and mechanism of an inorganic compound is not determined by charge alone.

The distinct mechanisms of action highlight a balance between extracellular (HS or SA) and intracellular (DNA) binding affinities and effects, recalling the analogies drawn between the phosphate clamp and arginine fork in DNA and the sulfate clamp in HS.[1–3] Although HS plays a number of roles on the cell surface, it is also implicated in the cellular accumulation of cationic molecules and their transport within the cell or nucleus; this is well demonstrated by the transport of cationic antibodies and polyarginine-based cell penetrating peptides.[4] In the case of PPCs and CCCs generally, it is essential to decipher the contentions between HSPG-mediated cellular accumulation, high-affinity HS binding, and DNA binding, as well as virion binding in HCMV and EV71 in order to establish a method to design inorganic broad-spectrum antivirals with specific mechanisms of action, whether they be DNA or HS/SA centered.

In the future, there are three major issues to decipher: WC mechanism of action in HCMV, sialic acid affinity of PPCs, and an animal model for antiviral activity of PPCs and WC. The comparison of DiplatinNC and RuRed reveals that CCCs have preferences for specific glycans, overruling the previous thought that the glycan-metal interaction was generic and charge dependent. While RuRed has a demonstrated affinity for sialic acids, PPCs have yet to be assessed for sialic acid affinity. Structure-activity relationships between compound structure, SA affinity, and HS affinity will further expand bioinorganic chemistry and display the potential medicinal use of inorganic compounds.

PPCs' largest barrier to development is the perceived toxicity issues associated with platinum compounds. Cisplatin, a covalently binding platinum cancer chemotherapy, has a large number of off-target toxicities, limiting its dosage and patient compliance. The series of PPCs studied here are substitution-inert and therefore should not see the same level of toxicity; however, this has not been formally assessed in a viral animal model. Unfortunately, CMVs are species specific so HCMV cannot be tested in an animal model. PPCs were too cytotoxic in guinea pig cells, eliminating GPCMV as an option. RhCMV crosses the placenta to infect the fetus, similar to HCMV, however the expense of rhesus macaques is limiting. MCMV does not cross the placenta but the brain development of newborn mice

parallels human fetal brain development; thus, MCMV is a reasonable option for an animal model.[5,6] Additionally, testing WC in MCMV may aide in determining its mechanism of action.

While this work demonstrated that WC has a late-acting mechanism, allows HCMV gene expression, and displays a unique viral packaging phenotype, we have yet to determine the mechanism of action. Possibilities include, but are not limited to, an inhibition of topoisomerase I or II, or condensation of viral DNA within the capsid. Testing in MCMV will reveal if WC's mechanism of action is HCMV specific or general to all CMVs; a lack of MCMV activity would rule out generic mechanism such as DNA condensation, however it would complicate finding an animal model. It is also important to investigate the metabolites of WC in biological media; although formally inert, it remains to be seen if WC remains intact or if it has the potential to covalently bind to biological targets. Additionally, we cannot forget that WC is a chiral compound and therefore should be examined as its separated enantiomers; both the antiviral activity and mechanism of action of each enantiomer should be compared to that of racemic mixture, used in this work.

Overall, our study demonstrates the utility of the metalloglycomics concept – the study of the interaction of metal ions and coordination compounds with biologically relevant oligosaccharides and, in particular, GAGs and proteoglycans – in design of new antiviral chemotypes.[7] The inhibition of viral attachment is an attractive target, particularly in light of emerging viruses like SARS-CoV-2; yet, targeting HS or the binding viral glycoprotein is underexploited. This work combines glycan targeting and medicinal inorganic chemistry into a new innovative field of high clinical relevance, expanding both areas of research into hitherto unexplored territory.

6.1 References

(1)   Komeda, S.; Moulaei, T.; Woods, K. K.; Chikuma, M.; Farrell, N. P.; Williams, L. D. A Third Mode of DNA Binding: Phosphate Clamps by a Polynuclear Platinum Complex. *J. Am. Chem. Soc.* **2006**, *128* (50), 16092–16103. https://doi.org/10.1021/ja062851y.

(2)   Komeda, S.; Qu, Y.; Mangrum, J. B.; Hegmans, A.; Williams, L. D.; Farrell, N. P. The Phosphate Clamp as Recognition Motif in Platinum–DNA Interactions. *Inorganica Chim. Acta* **2016**, *452*, 25–33. https://doi.org/10.1016/j.ica.2016.04.052.

(3)   Calnan, B. J.; Tidor, B.; Biancalana, S.; Hudson, D.; Frankel, A. D. Arginine-Mediated RNA Recognition: The Arginine Fork. *Science (80-.).* **1991**, *252* (5009), 1167–1171.

(4)   Naik, R. J.; Chatterjee, A.; Ganguli, M. Different Roles of Cell Surface and Exogenous Glycosaminoglycans in Controlling Gene Delivery by Arginine-Rich Peptides with Varied Distribution of Arginines. *Biochim. Biophys. Acta - Biomembr.* **2013**, *1828* (6), 1484–1493. https://doi.org/10.1016/j.bbamem.2013.02.010.

(5)   Reddehase, M. J.; Lemmermann, N. A. W. Mouse Model of Cytomegalovirus Disease and Immunotherapy in the Immunocompromised Host: Predictions for Medical Translation That Survived the "Test of Time." *Viruses* **2018**, *10* (12), 693. https://doi.org/10.3390/v10120693.

(6)   Fisher, M. A.; Lloyd, M. L. A Review of Murine Cytomegalovirus as a Model for Human Cytomegalovirus Disease—Do Mice Lie? *Int. J. Mol. Sci.* **2021**, *22* (1), 1–19. https://doi.org/10.3390/ijms22010214.

(7)   Farrell, N. P.; Gorle, A. K.; Peterson, E. J.; Berners-Price, S. J. Metalloglycomics. In *Metallo-Drugs: Development and Action of Anticancer Agents*; Sigel, A., Sigel, H., Freisinger, E., Sigel, R. K. O., Eds.; Walter de Gruyter, GmbH: Belrin, Germany, 2018; pp 109–136.

Vita

Mary E Zoepfl was born in Beaufort, South Carolina. She receives her Bachelors of Science in Biochemistry from the University of Virginia in 2018. She enrolled in the Chemical Biology PhD program at Virginia Commonwealth University in 2018.

PUBLICATIONS

Shoup, M., Ourahmane, A., Ginsburg, E.P., Farrell, N.P., Mcvoy, M.A., 2020. Substitution-inert polynuclear platinum compounds inhibit human cytomegalovirus attachment and entry. Antiviral Res. 184, 104957.

Zoepfl, M., Dwivedi, R., Taylor, M.C., Pomin, V.H., McVoy, M.A., 2021. Antiviral activities of four marine sulfated glycans against adenovirus and human cytomegalovirus. Antiviral Res. 190, 105077.

Paiva, R.E.F., Peterson, E.J., Malina, J., Zoepfl, M., Hampton, J.D., Johnson, W.E., Graminha, A., Ourahmane, A., McVoy, M.A., Brabec, V., Berners-Price, S.J., Farrell, N.P., 2021. On the Biology of Werner's Complex. Angew. Chemie Int. Ed. 60, 17123–17130.

Kim, S.B., Zoepfl, M., Samanta, P., Zhang, F., Xia, K., Thara, R., Linhardt, R.J., Doerksen, R.J., McVoy, M.A., Pomin, V.H., 2022. Fractionation of sulfated galactan from the red alga Botryocladia occidentalis separates its anticoagulant and anti-SARS-CoV-2 properties. J. Biol. Chem. Accepted M.

Drafted:

Anil K. Gorle, Mary Zoepfl, Mark von Itzstein, Susan J. Berners-Price, and Nicholas P. Farrell. Metalloglycomics. Therapeutic Applications from Novel Approaches to Targeting Glycosaminoglycans. To be submitted to Frontiers Journal.

Mary Zoepfl, Anton Chestukhin, Victor Pomin, and Michael McVoy. Selective antiviral inhibition of marine sulfated glycans. To be submitted to Antiviral Research.

Mary Zoepfl, Anton Chestukhin, Eric Ginsburg, Nicholas Farrell, and Michael McVoy. Polynuclear platinum compounds selectively inhibit HS-dependent viruses. To be submitted to Antiviral research.